

LIBRARY
U. S. GEOLOGICAL SURVEY
BUREAU OF MINES
U. S. GOVERNMENT PRINTING OFFICE
ST. LOUIS, MISSOURI 63132

BUREAU OF MINES
LIBRARY
SEATTLE, WASH.
MARCH 1987
SUSAN MCGOWAN
PC LIBRARY

Recent Reverse Faulting in the Transverse Ranges, California

U. S. GEOLOGICAL SURVEY PROFESSIONAL PAPER 1339



**RECENT REVERSE FAULTING
IN THE TRANSVERSE RANGES,
CALIFORNIA**



View west along front of eastern San Gabriel Mountains. Steepest slopes at right are underlain by Mesozoic and older basement rocks and generally average about 35 percent (19°); lower slopes are benched and basement rocks are overlain by locally thick patches of late Pleistocene surficial deposits having well-developed, deep red textural-B soil horizons, for example the isolated flat with roads in right center. Scarps of Cucamonga fault across Day Canyon fan just right of center (see Morton and Matti, this volume). The lowland surface at left is underlain by several late Pleistocene and Holocene alluvial units that lack red textural-B horizons. This surface extends almost continuously from San Bernardino (about 20 km behind viewer) to Pasadena (near Los Angeles), a distance of about 85 km; it underlies much of the Los Angeles-San Bernardino urbanized area. Photograph taken in 1960 by John S. Shelton; copyrighted, used with permission.

Recent Reverse Faulting in the Transverse Ranges, California

U. S. GEOLOGICAL SURVEY PROFESSIONAL PAPER 1339



UNITED STATES GOVERNMENT PRINTING OFFICE, WASHINGTON : 1987

DEPARTMENT OF THE INTERIOR
DONALD PAUL HODEL, *Secretary*

U.S. GEOLOGICAL SURVEY
Dallas L. Peck, *Director*

Library of Congress Cataloging-in-Publication Data

Recent reverse faulting in the Transverse Ranges, California.

(U.S. Geological Survey Professional Paper 1339)

Includes Bibliographies.

Supt. of Docs. no.:I 19.16:1339

1. Thrust faults (Geology)—California—Transverse Ranges. 2. Geology, stratigraphic—Recent. 3. Geology—California—Transverse Ranges. I. Series: Geological Survey Professional Paper 1339.

QE606.5.U6R43 1987

551.8'7'09794

86-600150

**For sale by the Books and Open-File Reports Section,
U.S. Geological Survey, Federal Center, Box 25425, Denver, CO 80225**

CONTENTS

	Page
Introduction, by Douglas M. Morton and Robert F. Yerkes	1
1. Seismicity and tectonics of the Cucamonga fault and the eastern San Gabriel Mountains, San Bernardino County, by Chris H. Cramer and John M. Harrington	7
2. Quaternary geology and seismic hazard of the Sierra Madre and associated faults, western San Gabriel Mountains, by Richard Crook, Jr., C.R. Allen, Barclay Kamb, C.M. Payne, and R.J. Proctor	27
3. Exploratory trenching of the Santa Susana fault in Los Angeles and Ventura Counties, by Richard Lung and R.J. Weick	65
4. Late Quaternary deformation in the western Transverse Ranges, by R.F. Yerkes and W.H.K. Lee	71
5. Reverse-fault system bounding the north side of the San Bernardino Mountains, by Fred K. Miller	83
6. Tectonic implications of small earthquakes in the central Transverse Ranges, by James C. Pechmann	97
7. Seismicity and tectonics of the Santa Monica-Hollywood-Raymond Hill fault zone and northern Los Angeles Basin, by Charles R. Real	113
8. Recurrent Holocene displacement on the Javon Canyon fault—A comparison of fault-movement history with calculated average recurrence intervals, by A.M. Sarna-Wojcicki, K.R. Lajoie, and R.F. Yerkes	125
9. Late Cenozoic structure of the Santa Susana fault zone, by Robert S. Yeats	137
10. Geology and seismicity of the eastern Red Mountain fault, Ventura County, by Robert S. Yeats, W.H.K. Lee, and Robert F. Yerkes	161
11. Geology and Quaternary deformation of the Ventura area, by R.F. Yerkes, A.M. Sarna-Wojcicki, and K.R. Lajoie	169
12. The Cucamonga fault zone: Geological setting and Quaternary history, by Douglas M. Morton and Jonathan C. Matti	179

PLATES

(In Pocket)

- PLATE 2.1 Geologic map of the Sierra Madre fault zone, Big Tujunga Canyon to the Arroyo Seco
2.2 Geologic map of the Sierra Madre fault zone, the Arroyo Seco to Santa Anita Canyon
2.3 Geologic map of the Sierra Madre fault zone, Santa Anita Canyon to Glendora
2.4 Geologic map of the Raymond fault, the Arroyo Seco to Arcadia
2.5 Trench logs at the Sunny Slope Reservoir and San Marino High School
2.6 Geologic map and cross sections of the Jet Propulsion Laboratory area, Pasadena
4.1 Faults and selected fault-plane solutions, western Transverse Ranges, California
5.1 Geologic map of the fault zone bounding the north side of the San Bernardino Mountains, California
9.1 Geologic map of the Santa Susana fault zone and vicinity, California
11.1 Geologic map of the Ventura area, Ventura County, California
12.1 Geologic map of the Cucamonga fault zone, southern California

Any use of trade names is for descriptive purposes only and does not imply endorsement by the USGS.

RECENT REVERSE FAULTING IN THE TRANSVERSE RANGES, CALIFORNIA

INTRODUCTION

By DOUGLAS M. MORTON and ROBERT F. YERKES

The Transverse Ranges province is characterized by reverse faults that strike eastward across most of southern California, transecting all the northwest-trending faults of the San Andreas system except the San Andreas itself (see figure below). The damaging 1971 San Fernando earthquake ($M_L = 6.4$), which occurred on one of the reverse faults, focused interest on that fault and others of the Transverse Ranges. Before the 1971 earthquake, the location and geologic history of the reverse faults were poorly known and their seismic potential not appreciated, even though it was at least the fourth damaging earthquake during historical time to originate on a Transverse Range fault.

The province extends about 500 km eastward from Point Arguello on the west and averages about 50 km in width. The San Andreas fault cuts obliquely across the province about 300 km east of Point Arguello and separates the San Gabriel Mountains on the west from the San Bernardino Mountains on the east. The east-west physiographic and structural trends, as expressed for example in the steep south flank of the San Gabriel Mountains (frontispiece), contrast markedly with the northwest trends of the provinces to the north and south. Bailey and Jahns (1954) identify and describe 13 major east-trending topographic-structural units that make up the province; the largest are the San Bernardino and San Gabriel Mountain ranges. Both ranges are distinctive for their size, more than 100 km long; their elevation, more than 3,000 m; and their exposure of Mesozoic and older rocks. West of the San Gabriel Mountains, the Transverse Ranges consist chiefly of diverse Cretaceous and Cenozoic sedimentary rocks, both marine and nonmarine, and local bodies of middle Miocene volcanic rocks, as in the Santa Monica Mountains. A unique and prominent feature is the Santa Barbara Channel-Ventura basin, a long, narrow, east-trending, exceptionally deep structural-depositional trough that locally contains more than 2,000 m of marine Pleistocene sediment.

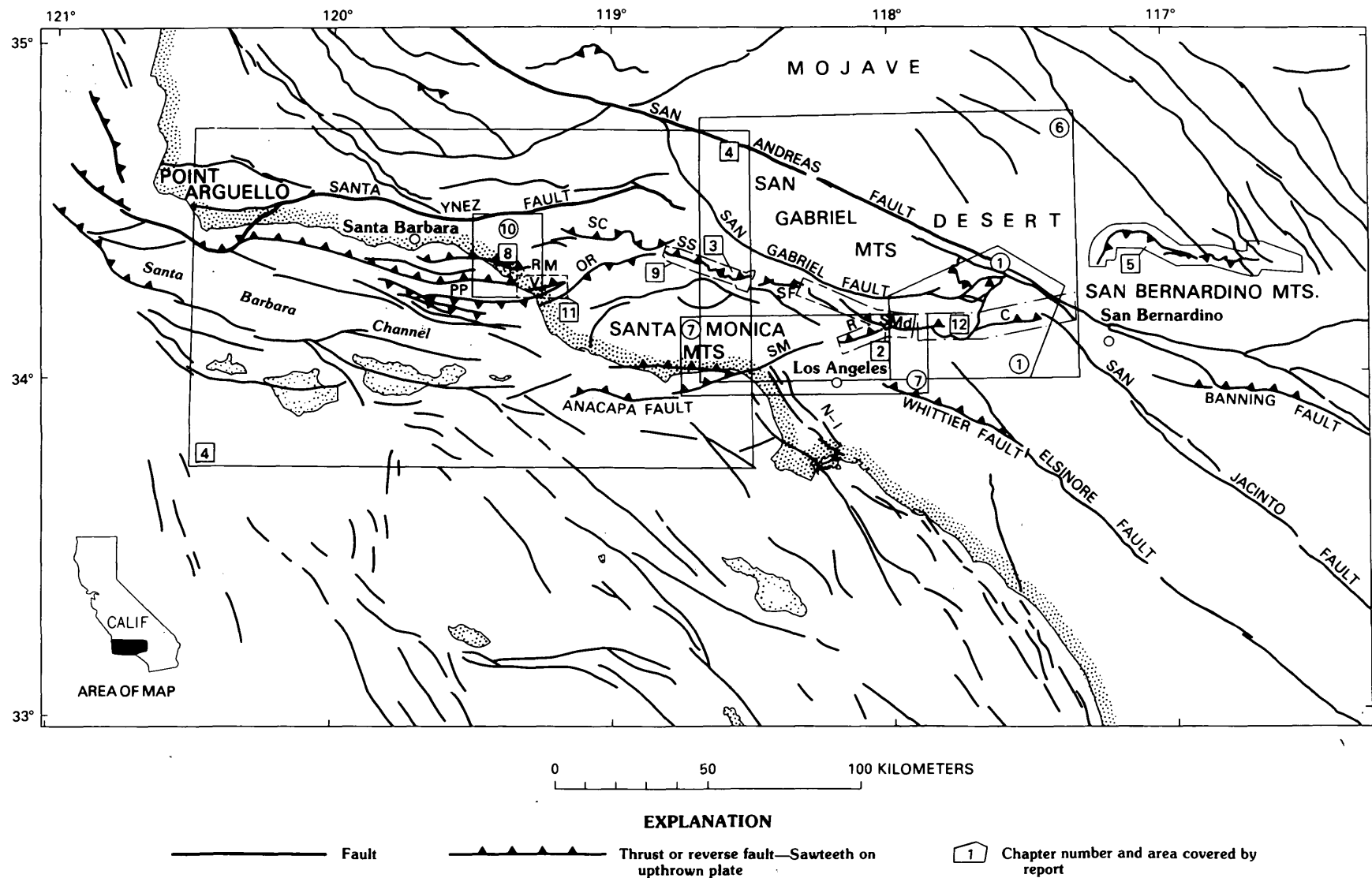
The distinctive structural style of the Transverse Ranges is dominated by the effects of north-south compressive deformation, which is attributed to convergence between the "big bend" of the San Andreas fault north of the San Gabriel Mountains and motion of the Pacific plate (Wentworth and Yerkes, 1971; Savage and others,

1978; Thatcher, 1981). Such effects include (1) active mountain building as shown by about 2 m of absolute uplift during the 1971 San Fernando earthquake (Oliver and others, 1975); (2) reverse or reverse-oblique displacement on the numerous east-trending faults and compatible fault-plane solutions for well-recorded earthquakes throughout the western part of the province (Whitcomb and others, 1973; Yerkes and Lee, 1979; Yerkes and others, 1981); (3) the extremely deep, long, narrow, east-trending Santa Barbara Channel-Ventura basin, filled with young sediment and having overturned, reverse-faulted flanks (Bailey and Jahns, 1954); (4) widespread, uplifted reverse-faulted marine and stream terrace deposits, locally rising at long-term rates of 5-10 mm/yr (Lajoie and others, 1979); (5) a generally north-south compressive stress field extending over much of southern California as shown by horizontal survey data (Savage and others, 1981; Thatcher, 1981); and (6) the southern California uplift, an intermittent, contemporary topographic bulge detected by comparison of precise level surveys; the uplift is of regional extent and its south flank is co-extensive with that of the Transverse Ranges province (Castle, 1978).

Following the comprehensive investigations of the San Fernando earthquake (see U.S. Geological Survey, 1971; Whitcomb and others, 1973; Oakeshott, 1975), the Geological Survey greatly expanded its research efforts on earthquake hazards and expanded geophysical instrument networks throughout southern California; in addition it funded numerous related investigations by others. This volume presents the results on 12 investigations of important faults in the Transverse Ranges (see figure below) and provides estimates of their activity (summarized in table below). Two general types of investigations are reported: (1) detailed geologic mapping and trenching studies of Quaternary deposits and (2) analyses of seismicity; the latter studies include most of the Transverse Ranges west of long 117.5° W.

The investigations indicate that faults with geologic evidence of Holocene activity are generally associated with relatively high present-day seismicity, and that displacements are compatible with fault-plane solutions of associated earthquakes. Relatively active segments are the Javon Canyon-Red Mountain and Pitas Point-Ventura faults northeast of Santa Barbara Channel—the area

RECENT REVERSE FAULTING IN THE TRANSVERSE RANGES, CALIFORNIA



Reports are shown by chapter number and type of investigation: circles for seismologic studies; squares for detailed mapping and (or) trenching studies.

- ① Cramer and Harrington, Seismicity and tectonics of the Cucamonga fault and eastern San Gabriel Mountains
- ② Crook, Allen, Kamb, Payne, and Proctor, Quaternary geology and seismic hazard of the Sierra Madre and associated faults, western San Gabriel Mountains
- ③ Lung and Weick, Exploratory trenching of the Santa Susana fault in Los Angeles and Ventura Counties
- ④ Yerkes and Lee, Late Quaternary deformation in the western Transverse Ranges
- ⑤ Miller, Reverse-fault system bounding the north side of the San Bernardino Mountains
- ⑥ Pechmann, Tectonic implications of small earthquakes in the central Transverse Ranges
- ⑦ Real, Seismicity and tectonics of the Santa Monica-Hollywood-Raymond Hill fault zone and northern Los Angeles Basin
- ⑧ Sarna-Wojcicki, Lajoie, and Yerkes, Recurrent Holocene displacement on the Javon Canyon fault
- ⑨ Yeats, Late Cenozoic structure of the Santa Susana fault zone
- ⑩ Yeats, Lee, and Yerkes, Geology and seismicity of the eastern Red Mountain fault, Ventura County
- ⑪ Yerkes, Sarna-Wojcicki, and Lajoie, Geology and Quaternary deformation of the Ventura area
- ⑫ Morton and Matti, The Cucamonga fault zone: geologic setting and Quaternary history

where the greatest uplift rates of marine terrace deposits were measured—and the San Fernando fault, locus of the 1971 earthquake and uplift. The Cucamonga and Raymond segments show convincing evidence of Holocene rupture, but only minor or ambiguous evidence of present-day seismicity. Faults for which evidence of Holocene rupture is lacking or precluded are the San Cayetano, Santa Susana, Sierra Madre east of the San Fernando, and the north boundary zone of the San Bernardino Mountains. These relatively inactive faults also appear to be historical seismic gaps in the system of frontal fault zones. The south frontal zone of the Santa Monica Mountains, which includes the offshore Anacapa fault—locus of the 1973 ($M_L = 5.9$) Point Mugu earthquake—and the onshore Santa Monica and associated faults west of the Los Angeles River, is not reported here in detail. Hill and others (1977) report extensive investigations of the onshore faults; Ellsworth and others (1973), Boore and Stierman (1976), and Stierman and Ellsworth (1976) report on the 1973 Point Mugu earthquake and aftershocks. No conclusive evidence of Holocene surface rupture is known for the onshore faults west of Los Angeles River, but all show evidence of late Pleistocene movement. Real (this volume) includes interpretations of small earthquakes just west of the river that might be associated with the zone.

The estimates of fault activity (see table below) are based on a variety of geologic data and represent only long-term averages. Slip rates and recurrence intervals range over almost three orders of magnitude, estimates of average displacement per event agree more closely, and the estimates of effective fault (earthquake-associated surface rupture) length and maximum earthquake are generally consistent. If the maximum single-event rupture length is assumed to be 15 km, an upper-bound earthquake of about $M_L = 7$ is implied for the recently active south-boundary faults west of the San Andreas fault—a value that has not been exceeded during historical time.

Although our understanding of the Transverse Ranges has expanded greatly during the last decade, much additional work is needed to approach a satisfactory working-model synthesis. Accurate quantitative estimates of local earthquake hazard depend critically on defining contemporary—rather than long-term average—recurrence intervals and slip rates for specific faults. Even when contemporary rates are available for some specific fault—as they appear to be for segments of the San Andreas fault—the faults must be understood in terms of a regional seismotectonic synthesis. In addition to refining preliminary geophysical and seismic-risk models (Anderson, 1979; Bird and Rosenstock, 1984) to account for both horizontal and vertical components of deformation, such a synthesis should account for the known distribution of Franciscan-type (Catalina Schist) and oceanic basement rocks relative to continental-type basement and predict their distribu-

Estimates of activity for selected reverse faults

Fault	Slip rate (mm/yr) ¹	RI ² (yr)	Surface rupture ³		Maximum earthquake ⁴	Reported by
			D (m)	L(km)		
Javon Canyon--	1.1	700	0.8	5	---	Sarna-Wojcicki and others ⁵
Red Mountain--	1.8	---	---	15	---	Yeats and others ⁵
Ventura	.5	---	---	10	---	Yerkes and others ⁵
San Cayetano	2	---	---	---	6-7	Keller and others (1980)
San Fernando, 1971	3-4	200	1.4	15	6.4	Bonilla (1973); Sharp (1981)
Sierra Madre	---	5,000	---	15	7	Crook and others ⁵
Raymond	.14	3,000	.4	15	6.7	Crook and others ⁵
Cucamonga	4-5.6	625-1000	2	-15	7	Morton and others ⁵

¹Vertical component only; long-term average from geologic evidence.²RI, recurrence interval for major slip events inferred from geologic evidence.³Maximum vertical displacement on a single strand (D) and rupture length (L) associated with single major slip event.⁴ M_L , local (Richter) magnitude.⁵This volume.

tion beneath the Cenozoic cover of the western Transverse Ranges. Also to be explained are such features as the patch of persistent seismicity in eastern Santa Barbara Channel; the general area of the destructive ($M_L \geq 7$) December 21, 1812, earthquake, and the location of the destructive ($M_L = 6.3$) 1925 and locally damaging ($M_L = 5.9$) 1941 and ($M_L = 5.1$) 1978 Santa Barbara earthquakes. A successful synthesis also should predict the subsurface configuration of the east-trending zones of reverse faults and explain their origin, their apparently contrasting degrees of activity, and their relations to the several northwest-trending right-lateral faults that they transect. In considering the compressive structures of the Transverse Ranges and their relations to the adjacent provinces, the origin—and persistence through much of late Quaternary time—of the surprisingly widespread, generally north-south compressive stress field also should be explained.

REFERENCES CITED

- Anderson, J. G., 1979, Estimating the seismicity from geological structure for seismic-risk studies: Seismological Society of America Bulletin, v. 69-1, p. 135-158.
- Bailey, T. L., and Jahns, R. H., 1954, Geology of the Transverse Range province, southern California, pt. 6, Chap. 1 of Jahns, R. H., ed., Geology of southern California: California Division of Mines Bulletin 170, p. 83-106.
- Bird, Peter, and Rosenstock, R. W., 1984, Kinematics of present crust and mantle flow in southern California: Geological Society of America Bulletin, v. 95, no. 8, p. 946-957.
- Bonilla, M. G., 1973, Trench exposures across surface fault ruptures associated with San Fernando earthquake, in San Fernando, California, earthquake of February 9, 1971, V. III, Geological and Geophysical Studies, edited by N. A. Benfer, J. L. Coffman, and J. R. Bernick: U.S. Department of Commerce, National Oceanic and Atmospheric Administration, Environmental Research Laboratory, Washington, D.C., p. 173-182.
- Boore, D. M., and Stierman, D. J., 1976, Source parameters of the Pt. Mugu, California, earthquake of February 21, 1973: Seismological Society of America Bulletin, v. 66-2, p. 385-404.
- Castle, R. O., 1978, Leveling surveys and the southern California uplift: Earthquake Information Bulletin, v. 10, no. 3, p. 88-92.
- Ellsworth, W. L., Campbell, R. H., Hill, D. P., Page, R. A., Alewine, R. W., Hanks, T. C., Heaton, T. H., Hileman, J. A., Kanamori, H., Minister, B., and Whitcomb, J. H., 1973, Point Mugu, California, earthquake of 21 February 1973 and its aftershocks: Science, v. 182, p. 1127-1129.
- Hill, R. L., Sprotte, E. C., Bennett, J. H., Chapman, R. H., Chase, G. W., Real, C. R., and Borchardt, G., 1977, Santa Monica-Raymond Hill fault zone study, Los Angeles County, California: California Division of Mines and Geology, Final Technical Report, U.S. Geological Survey Contract 14-08-0001-15858.
- Keller, E. A., Johnson, D. L., Clark, M. N., and Rockwell, T. K., 1980, Tectonic geomorphology and earthquake hazard, north flank central Ventura basin, California: unpub. report to U.S. Geological Survey, contract 14-08-0001-17678, 167 p., 9 pls., 48 figs.
- Lajoie, K. R., Kern, J. P., Wehmiller, J. F., Kennedy, G. L., Mathieson, S. A., Sarna-Wojcicki, A. M., Yerkes, R. F., and McCrary, P. A., 1979, Quaternary marine shorelines and crustal deformation, San Diego to Santa Barbara, California, in Abbott, P. L., ed., Geological excursions in the southern California area, original papers and field trip: Roadlogs prepared for the Geological Society of America Annual Meeting, California State University, San Diego, California, November 1979, p. 3-15.
- Oakeshott, G. B., ed., 1975, San Fernando, California, earthquake of 9 February 1971: California Division of Mines and Geology Bulletin 196, 33 articles, 463 p., 5 pls.
- Oliver, H. W., Robbins, S. L., Grannell, R. B., Alewine, R. W., and Biehler, S., 1975, Surface and subsurface movements determined by remeasuring gravity, in Oakeshott, G. B., ed., San Fernando, California, earthquake of 9 February 1971: California Division of Mines and Geology Bulletin 196, p. 195-211.
- Savage, J. C., Prescott, W. H., Lisowski, M., and King, N. E., 1978, Strain in southern California—Measured uniaxial north-south regional contraction: Science, v. 202, p. 883-885.
- Savage, J. C., Prescott, W. H., Lisowski, M., and King, N. E., 1981, Strain accumulation in southern California, 1973-1980: Journal of Geophysical Research, v. 86, no. B8, p. 6991-7001.
- Sharp, R. V., 1981, Displacements on tectonic ruptures in the San Fernando earthquake of February 9, 1971—discussion and some implications: U.S. Geological Survey Open-File Report 81-668, 14 p., 2 figs.
- Stierman, D. J., and Ellsworth, W., 1976, Aftershocks of the February 21, 1973, Pt. Mugu, California earthquake: Seismological Society of America Bulletin, v. 66-6, p. 1931-1952.

- Thatcher, Wayne, 1981, Crustal deformation studies and earthquake prediction research, *in* Simpson, D. W., and Richards, P. G., eds., *Earthquake prediction, an international review*: American Geophysical Union, Washington, D.C., p. 394-410.
- United States Geological Survey and National Oceanic and Atmospheric Administration, 1971, The San Fernando, California, earthquake of February 9, 1971: U.S. Geological Survey Professional Paper 733, 56 articles, 253 p.
- Wentworth, C. M., and Yerkes, R. F., 1971, Geologic setting and activity of faults in the San Fernando area, California: U.S. Geological Survey Professional Paper 733, p. 6-16.
- Whitcomb, J. H., Allen, C. R., Garmany, J. D., and Hileman, J. A., 1973, San Fernando earthquake series, 1971—Focal mechanisms and tectonics: *Reviews of Geophysics and Space Physics*, v. 11, no. 3, p. 693-730.
- Yerkes, R. F., and Lee, W. H. K., 1979, Late Quaternary deformation in the western Transverse Ranges: U.S. Geological Survey Circular 799-B, p. 27-37.
- Yerkes, R. F., Greene, H. G., Tinsley, J. C., and Lajoie, K. R., 1981, Seismotectonic setting of the Santa Barbara Channel area, southern California: U.S. Geological Survey Miscellaneous Field Studies Map MF-1169, 27 p., 16 figures, 2 plates.

1. SEISMICITY AND TECTONICS OF THE CUCAMONGA FAULT AND THE EASTERN SAN GABRIEL MOUNTAINS, SAN BERNARDINO COUNTY

By CHRIS H. CRAMER¹ and JOHN M. HARRINGTON²

ABSTRACT

During the spring of 1977, the California Division of Mines and Geology conducted a microearthquake investigation of the Cucamonga fault in San Bernardino County. An array of eight portable seismographs was deployed between Lytle Creek and San Antonio Canyon in the eastern San Gabriel Mountains from mid-March to early July. Three months of usable records were obtained, and more than 200 microearthquakes ($M = -1.0\text{--}3.0$) were located.

Microearthquake activity having focal depths of less than 10 km occurs beneath much of the easternmost San Gabriel Mountains, but microearthquake activity down to focal depths of 17 km occurs along the margins of the San Gabriel Mountains, beneath the Pomona Valley (Fontana and Chino area), and in the San Jose Hills. The San Jacinto fault is presently active, and the Cucamonga, Red Hill, San Antonio Canyon, Walnut Creek, and San Jose faults have associated seismic activity suggesting that they are active features. Activity from 1900 to 1974 has been high for this region.

Twenty-seven focal-mechanism determinations provide new information about the tectonics of the eastern San Gabriel Mountains. Strike-slip mechanisms dominate the region; thrust-type mechanisms are mainly confined to the interior of the eastern San Gabriel Mountains. Fault motions indicated by these focal-mechanism determinations show that the San Gabriel Mountains east of San Antonio Canyon have been detached from the rest of the range and are being actively forced northward and uplifted from the south by the north edge of the Peninsular Ranges province.

INTRODUCTION

Between March 16 and July 8, 1977, the California Division of Mines and Geology (CDMG) monitored the Cucamonga fault and the easternmost San Gabriel Mountains for microearthquake activity (fig. 1.1). Interest in the Cucamonga fault stems from the presence of Quaternary fault scarps along much of its length, indications obtained from the regional seismograph network of the California Institute of Technology (CIT) of earthquake activity beneath the eastern San Gabriel Mountains, and the proximity of the fault to the Pomona Valley—a region of rapid urbanization. This study is the first detailed microearthquake investigation of the Cucamonga, the Red Hill, and other faults between Lytle Creek and San Antonio

Canyon. The resulting microearthquake locations and focal mechanisms indicate that many of these faults are active and also provide insight into the tectonics of the region.

ACKNOWLEDGMENTS

The following people and institutions made this monitoring project possible: First, those who granted us permission to install our seismographs on private or federal land, especially Mr. George B. Banchard, Jr., Cucamonga County Water District, Mr. Kenneth Dykeman, Glendora Ranger Station, Angeles National Forest and Mr. Allen Hess, Lytle Creek Ranger Station, San Bernardino National Forest; second, the Earth Science Department at California State Polytechnic University, Pomona, for their assistance in maintaining the portable seismograph network and setting off calibration shots—Dr. Lawrence J. Herber, Mr. Steven Ryland, Doug Cook, Matt Mahronich, Jon Luksch, David Weaver, and Grayce Teal; and finally, the Seismological Laboratory, California Institute of Technology, and the U.S. Geological Survey for allowing access to data and seismograms from their telemetered regional seismograph stations near our study area.

PREVIOUS WORK

Geologic investigations and mapping by Morton (1976) show the Cucamonga as a system of fault scarps between Lytle Creek and San Antonio Canyons. Jennings (1975) maps the Cucamonga as a Quaternary fault, and Morton (oral commun., 1977) believes the two scarps on the Day Canyon fan range in age from about 1,000 yr for the younger to about 10,000 yr for the older. Thus, the more recent movements along the Cucamonga fault were of Holocene age. The two Day Canyon scarps show large cumulative vertical offsets of 5 m on the younger and 40 m on the older; thrust movement is indicated on shallow-dipping ($\sim 35^\circ$) outcrops at the mouth of Etiwanda Canyon.

Previous earthquake monitoring consists of regional

¹California Division of Mines and Geology, Sacramento, California.

²Geology Department, University of California Davis, Davis, California.

Manuscript received for publication on October 7, 1980.

coverage by CIT (Hileman and others, 1973; Friedman and others, 1976; Fuis and others, 1977) and a short microearthquake study of the adjacent San Bernardino area by Hadley and Combs (1974). Figure 1.2 shows historical seismicity from 1900 through 1974 (Real and others, 1978). Seismic activity has been high along the San Jacinto fault near the Cucamonga fault, in the easternmost San Gabriel Mountains, under Pomona Valley, and in the San Jose Hills. Activity decreases to the west, and

this trend continues along the Santa Monica-Raymond Hills trend (Real, this volume). Hadley and Combs (1974) also located a cluster of activity near Fontana during five two-week recording sessions in 1972 and 1973.

Seismicity from 1972 to 1976 recorded by CIT is shown in figure 1.3. As a result of improved station coverage, the seismicity trends are more sharply defined, although the seismicity pattern is very similar to that of figure 1.2. Again, earthquakes are concentrated along the San Jacin-

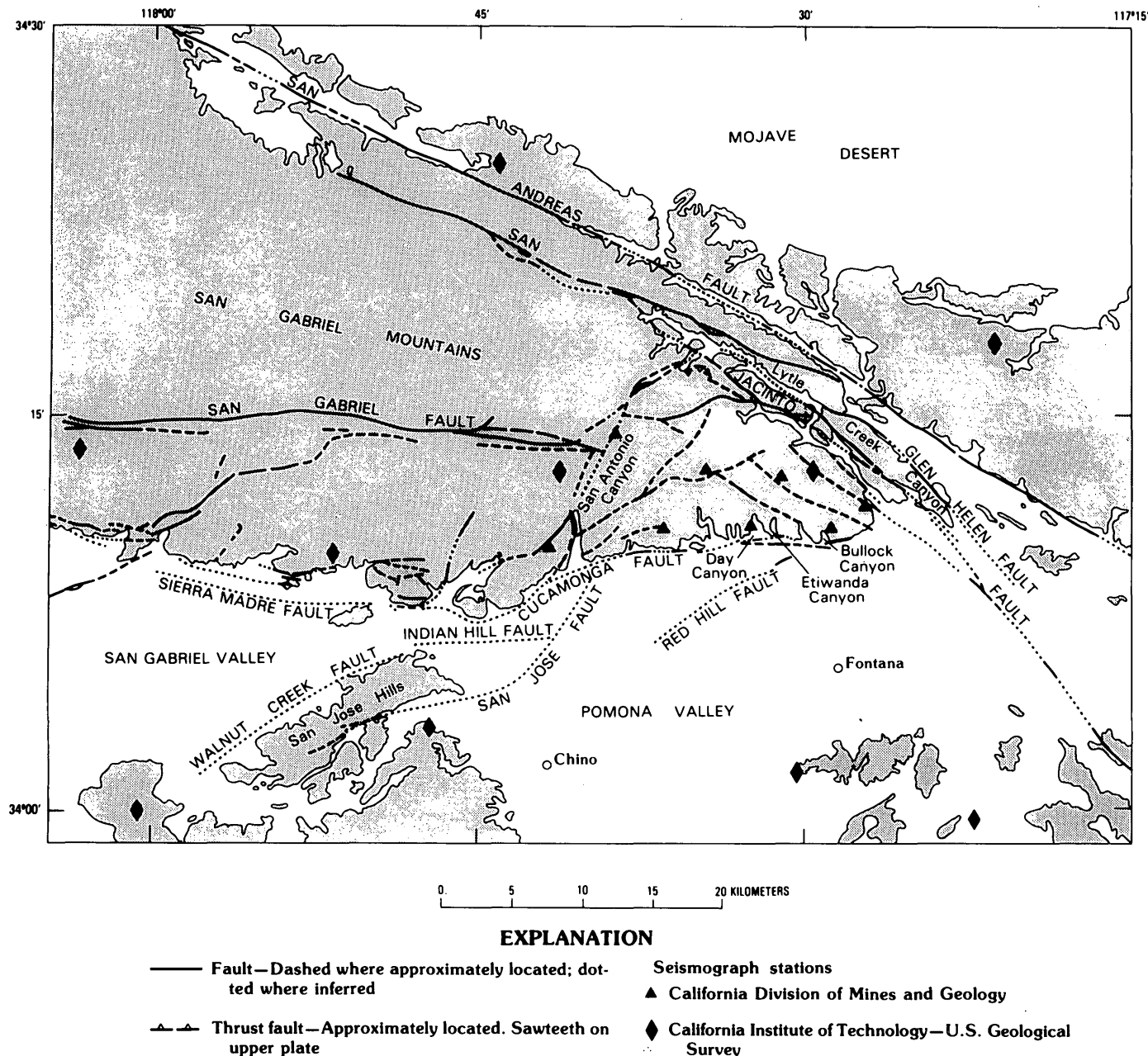


FIGURE 1.1.—Eastern San Gabriel Mountains, California, showing CDMG portable seismograph stations, CIT-USGS telemetered stations, major faults, and the contact between basement rocks (shaded) and alluviated valleys.

to fault, north of the Cucamonga fault, near Fontana and Chino, and at the western edge of the Pomona Valley. Activity decreases dramatically to the west and north.

INSTRUMENTATION AND DATA REDUCTION

Eight portable seismograph systems (Sprengnether MEQ-800s with Mark Products L-4C, 1 Hz, seismometers) were employed in this study. Amplifier gains were typical-

ly 78 or 84 dB, with a high-cut filter of 10 Hz. The overall system response is shown in figure 1.4. Time and amplitude calibrations were applied every other day when records were changed.

Figure 1.1 shows the location of the CDMG portable seismograph sites. Six of the eight seismographs were installed on March 15 and 16, 1977. The installation of the last two seismographs was delayed until April 26, 1977, because of snow at higher elevations (table 1.1). Once in-

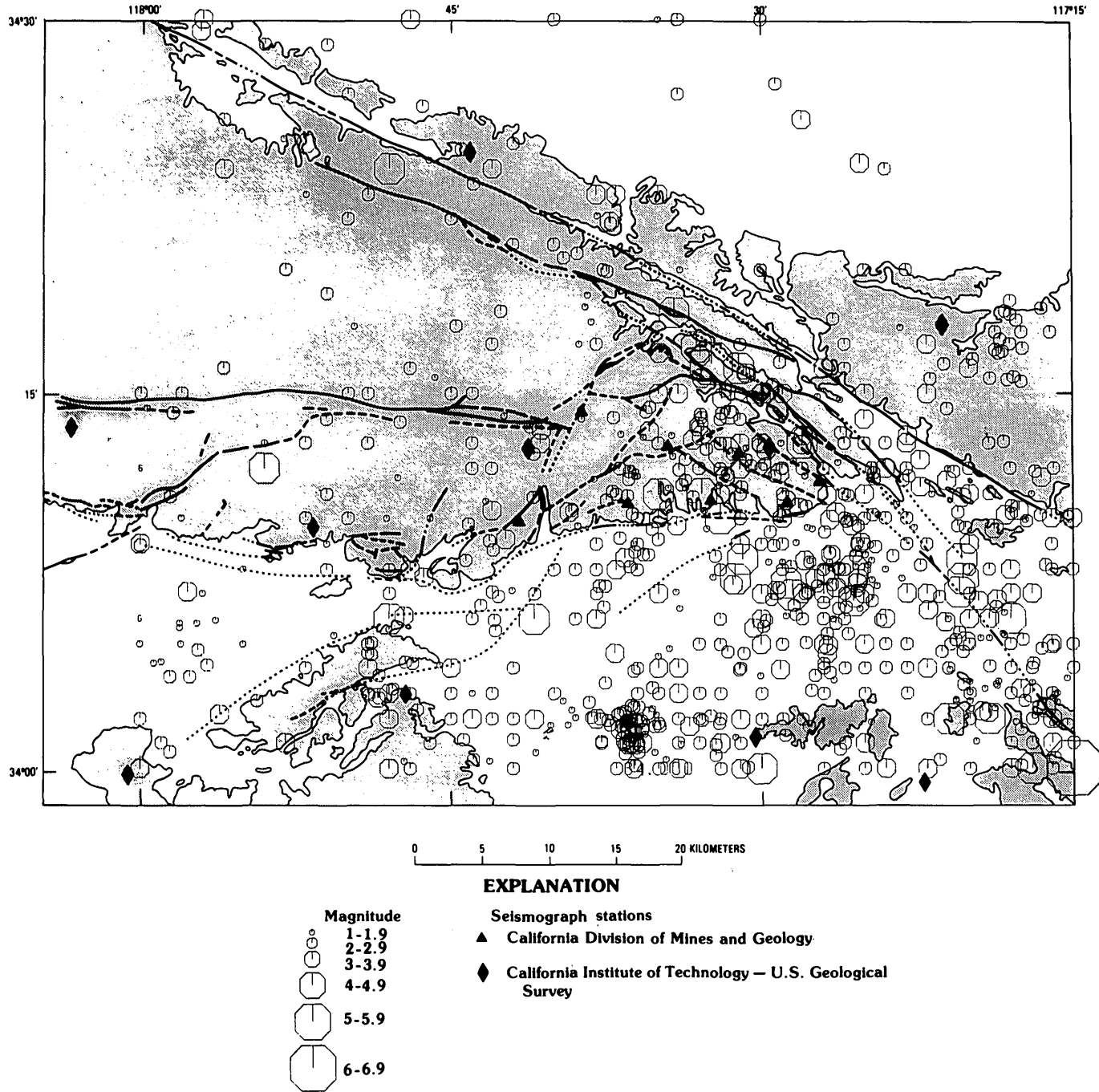


FIGURE 1.2.—Historical seismicity from 1900 to 1974 (Real and others, 1978) for the eastern San Gabriel Mountains. Geology same as in figure 1.1.

stalled, all CDMG stations were operational until July 8, 1977, except during spring snowstorms. More than 3 months of usable records were obtained. Data from these records have been augmented with data from seismographs of the CIT-USGS regional telemetered network. Locations of the nearby CIT-USGS seismographs are also shown in figure 1.1.

Seismograms were read to the nearest 0.05 s, and locations were determined by using Lahr's (1980) HYPOELLIPE computer program. Final locations were determined by applying a pseudo-master-event technique to improve relative locations among events. The pseudo-master-event technique employed was to use the weighted mean of a station's residuals as a station correction in order to reduce systematic errors due to site geology or consistent mispicking of arrivals. Only arrival times at sta-

tions within 50 km of the epicenter were used in the final hypocenter determinations.

The velocity model employed in the final location process is shown in table 1.2. This model is taken principally from that of Hadley and Kanamori (1977) for the Transverse Ranges. The Hadley and Kanamori velocity model has been modified in the upper 5 km by the results of two small calibration shots. The CDMG calibration shots near the east and west ends of the portable seismograph array provided the very shallow velocity control for this model. A V_p/V_s ratio of 1.75 was used to incorporate the S-wave data. Elevation corrections were applied to the arrival-time data by assuming a 4.0 km/s P -wave velocity for the material above sea level.

Magnitudes have been determined from maximum amplitude measurements as suggested by Eaton and

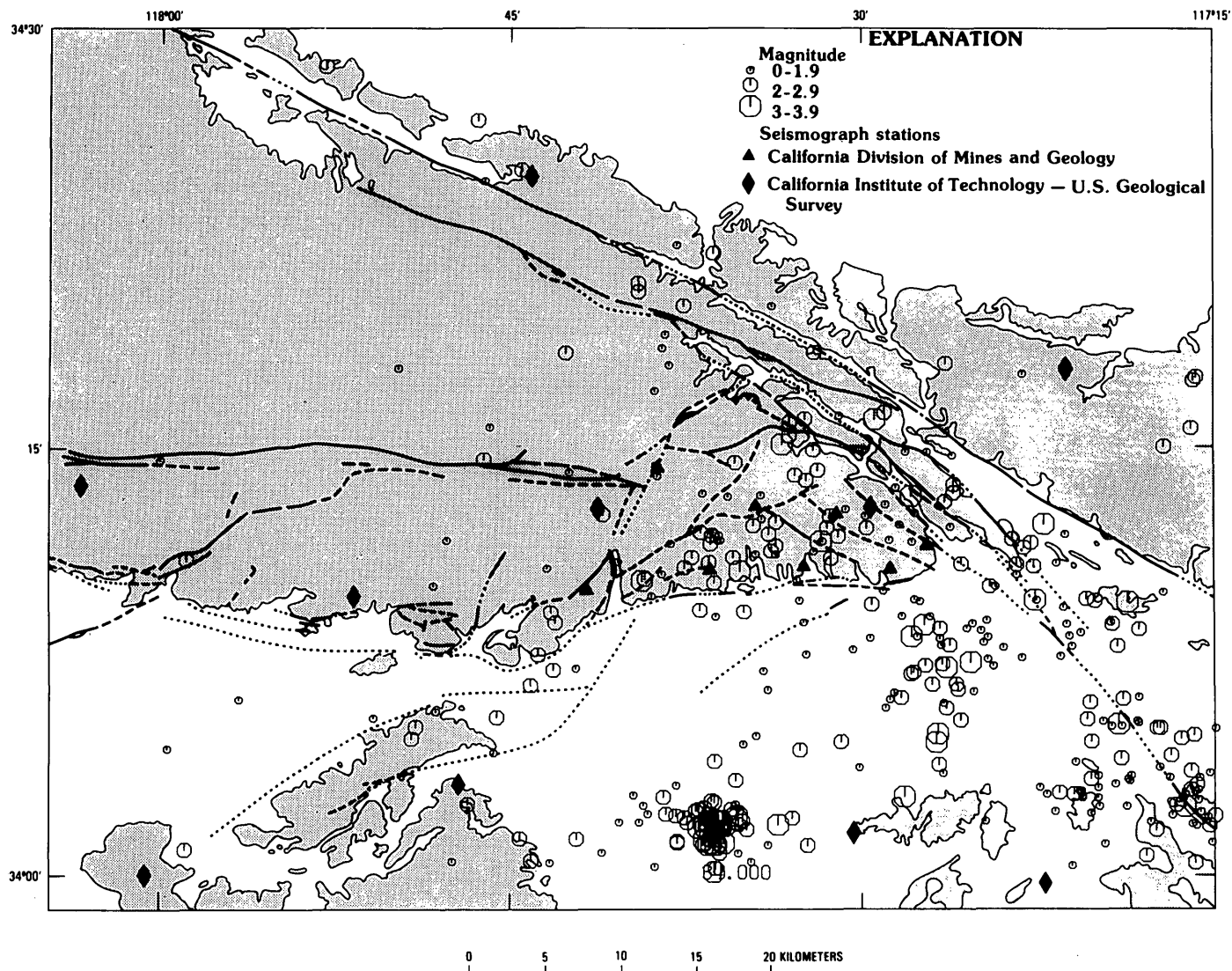


FIGURE 1.3.—Seismicity from 1972 to 1976 for the eastern San Gabriel Mountains. Geology same as in figure 1.1.

TABLE 1.1.—*California Division of Mines and Geology portable seismograph stations*

Sta	Lat (N.)	Long (W.)	Elev (m)	Installed yr mo d	Removed yr mo d
CBUL	34°10.77'	117°29.01'	824	77 03 15	77 07 08
C DAY	34°10.81'	117°32.36	860	77 03 15	77 07 08
CEVY	34°10.16'	117°41.77'	902	77 03 16	77 07 08
CGVR	34°11.75'	117°27.25'	799	77 03 16	77 07 08
CICE	34°14.96'	117°38.07	1,530	77 03 16	77 07 08
CSSW	34°12.78'	117°31.16	1,725	77 04 26	77 07 08
CUCC	34°10.78'	117°36.59'	1,183	77 03 16	77 07 08
CUCP	34°12.89'	117°34.29'	1,750	77 04 26	77 07 08

others (1970). For those events with amplifier-clipped seismograms, magnitudes have been estimated from the duration (Lee and others, 1972) using constants determined for central California. Listed magnitudes (table 1.3) must be considered as relative, because the magnitude-estimation techniques employed have not been calibrated to the Richter magnitude scale in this study area. The exceptions are those events with magnitudes above 2.0 which have been assigned preliminary Richter magnitudes by CIT as indicated by the letter P (for Pasadena) following the listed magnitude.

SEISMICITY

Figure 1.5 displays the 218 epicenters of the events detected and located during this study. The symbol plotted at the epicenter indicates that event's focal depth. Magnitudes for these events range from -1.0 to 2.9. Only events inside the study area boundary are shown, and other events to the southeast along the San Jacinto trend have been eliminated. Table 1.3 lists the origin time, location, magnitude, and location-quality information of the events plotted in figure 1.5.

Seismic activity occurs in a diffuse pattern under most of the San Gabriel Mountains between San Antonio Canyon and Lytle Creek. Concentrations of epicenters occur along the San Jacinto fault and portions of the Glen Helen fault, and beneath Fontana in the eastern Pomona Valley. A few events are located to the west of San Antonio Canyon, in the western Pomona Valley, and in the San Jose Hills.

Almost all focal depths within the San Gabriel Mountains are less than 10 km. On the periphery of the San Gabriel Mountains and under the Pomona Valley and San Jose Hills, focal depths extend below 10 km and reach a maximum depth of 17 km beneath Fontana. These depths suggest that the eastern San Gabriel Mountains are a relatively shallow tectonic feature.

This observed pattern of seismicity is very similar to the historical and recent seismicity patterns displayed on

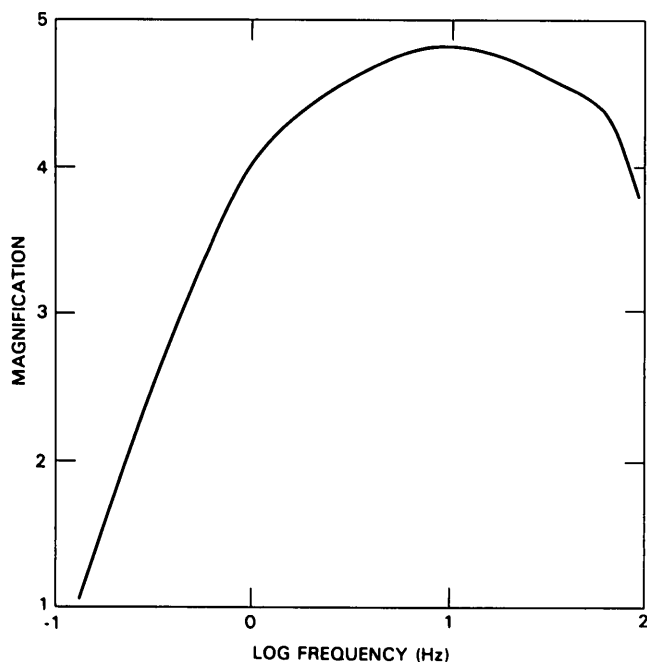


FIGURE 1.4.—Typical seismograph response curve for instrumentation and sites used in Cucamonga fault study.

TABLE 1.2.—*Velocity model* used in eastern San Gabriel Mountain study*

Layer	Depth-to-top (km)	P-velocity (km/s)	S-velocity ⁺ (km/s)
1	0.0	5.90	3.37
2	4.5	6.20	3.54
3	15.0	6.70	3.83
4	33.0	7.80	4.46
5	42.0	8.30	4.74

*Modified from Hadley and Kanamori (1977).

⁺Vp/Vs ratio taken as 1.75.

TABLE 1.3.—Final hypocenter solutions, eastern San Gabriel Mountains, March 16 to July 8, 1977

#	1977	HR	MN	SEC	LAT (N.)	LONG (W.)	DEPTH	MAG	NO	GAP	DMIN	RMS	ERH	ERZ	Q
1	MAR 18	8	58	41.48	34-17.18	117-35.68	2.43	2.2P	25	71	11.9	0.14	0.6	1.7	B
2	MAR 18	16	30	8.03	34-14.90	117-31.61	8.14	.5	8	302	8.6	0.03	1.9	1.9	C
3	MAR 18	20	28	48.00	34-15.75	117-30.92	14.10	.4	8	279	9.7	0.04	1.1	1.3	C
4	MAR 19	0	0	42.94	34-17.85	117-45.15	4.27	.2	9	154	15.1	0.05	0.6	1.5	B
5	MAR 19	8	28	46.15	34-12.17	117-37.78	2.13	.2	15	94	5.6	0.09	0.5	1.9	B
6	MAR 19	8	42	49.22	34- 7.46	117-27.30	1.19*	-.1	7	293	9.9	0.05	1.1	7.9	D
7	MAR 20	4	38	23.94	34- 8.29	117-26.76	4.62	.2	15	173	9.2	0.19	2.6	5.5	C
8	MAR 20	10	59	21.97	34-14.54	117-33.35	7.73	.5	20	160	7.3	0.18	1.0	2.4	C
9	MAR 20	21	25	42.47	34- 7.63	117-28.08	6.74	1.9	33	59	8.8	0.11	0.4	1.2	A
10	MAR 20	22	22	43.49	34- 6.03	117-26.33	0.06	-.1	7	321	12.8	0.02	0.7	19.0	D
11	MAR 21	0	21	11.49	34-10.97	117-29.32	6.99	-.3	9	86	3.5	0.17	4.2	4.3	B
12	MAR 21	0	39	58.53	34- 7.92	117-26.26	10.24	.0	5	312	10.8	0.01	52.9	40.5	D
13	MAR 21	1	15	52.31	34-16.08	117-33.19	6.59	.2	11	237	11.1	0.05	0.8	1.8	C
14	MAR 21	4	45	38.70	34- 9.73	117-29.13	4.80	-.3	6	254	5.3	0.02	1.5	0.7	C
15	MAR 21	8	49	30.33	34- 6.12	117-30.36	0.05	.1	9	287	11.4	0.06	1.2	56.4	D
16	MAR 21	9	14	13.79	34-17.08	117-35.55	4.32	.2	13	177	12.1	0.13	1.4	2.4	C
17	MAR 21	10	17	58.93	34-13.31	117-30.52	6.68	.3	13	212	5.4	0.10	1.2	1.4	C
18	MAR 21	11	17	14.33	34-13.34	117-25.65	13.65	.8	25	102	7.0	0.11	0.5	0.9	B
19	MAR 22	5	19	22.99	34-12.51	117-35.46	5.39	.3	10	132	6.1	0.04	0.5	1.0	B
20	MAR 22	5	22	30.16	34-12.37	117-35.32	4.79	-.3	7	130	6.4	0.01	0.3	0.9	B
21	MAR 22	15	17	51.97	34-10.30	117-28.21	11.61	.8	24	87	6.4	0.09	0.5	0.7	A
22	MAR 30	23	53	9.66	34-14.56	117-29.21	6.57	.2	9	237	7.0	0.05	1.5	2.0	C
23	MAR 31	3	0	35.91	34-15.67	117-30.86	7.26	.2	8	278	9.5	0.06	3.2	4.1	D
24	MAR 31	3	45	5.87	34- 8.91	117-26.92	5.57	.0	10	208	8.1	0.08	1.5	2.3	C
25	APR 01	12	13	56.39	34-13.85	117-43.14	4.46	-.2	5	315	11.6	0.01	13.4	9.4	D
26	APR 01	13	59	34.60	34-12.65	117-24.57	9.11	.2	9	326	18.8	0.05	1.1	0.8	C
27	APR 02	10	0	10.65	34- 9.37	117-31.85	11.54	.0	8	230	7.7	0.32	6.3	7.0	D
28	APR 02	18	18	4.56	34-13.47	117-27.76	14.44	.1	9	276	5.4	0.10	2.4	2.2	D
29	APR 02	19	42	1.49	34- 8.21	117-34.09	9.78	.4	16	119	10.1	0.17	1.3	2.0	B
30	APR 03	3	0	57.32	34- 7.57	117-28.14	4.08	-.3	9	212	9.5	0.14	1.7	4.4	C
31	APR 03	6	7	12.25	34-10.23	117-26.29	4.67	-.3	9	257	9.4	0.20	5.2	3.1	D
32	APR 03	7	16	36.44	34-13.21	117-30.13	3.84	-.4	6	274	5.6	0.02	1.1	1.7	C
33	APR 03	7	17	19.11	34-11.99	117-29.96	4.56	.1	10	150	4.3	0.09	1.6	1.8	C
34	APR 03	7	17	49.19	34-13.76	117-30.51	2.21	-.3	6	278	6.2	0.03	1.3	1.9	C
35	APR 03	9	45	42.12	34- 7.38	117-26.48	2.33	-.1	7	240	12.9	0.02	0.4	1.1	C
36	APR 04	0	51	46.22	34- 7.57	117-27.27	3.58	-.2	8	229	9.9	0.08	1.9	3.6	C
37	APR 04	3	53	52.39	34- 7.53	117-27.11	3.47	-.3	9	232	10.1	0.10	1.8	4.2	C
38	APR 04	22	28	48.09	34- 7.38	117-27.19	4.63	.6	15	189	10.3	0.13	1.2	2.4	C
39	APR 05	22	35	3.05	34-11.75	117-32.35	7.37	.3	7	195	6.8	0.06	10.4	3.4	D
40	APR 06	4	43	14.80	34- 0.81	117-34.49	9.32	1.2	21	82	18.7	0.11	0.5	1.9	A
41	APR 07	5	28	31.45	34-13.72	117-24.59	9.17	.2	8	155	8.7	0.08	3.5	3.2	C
42	APR 07	5	28	33.04	34-12.99	117-23.99	11.05	1.4	30	53	9.3	0.39	1.6	4.2	B
43	APR 05	8	57	24.46	34- 5.98	117-28.55	2.94	.0	4	316	10.9	0.00	99.0	99.0	D
44	APR 07	10	45	6.39	34-10.57	117-34.67	5.97	.2	17	179	8.0	0.15	0.9	1.8	C
45	APR 07	12	50	43.77	34-11.97	117-22.45	13.55	.3	8	343	11.6	0.05	0.7	1.8	C
46	APR 07	13	57	26.54	34- 8.53	117-34.82	7.40	.0	5	339	13.1	0.08	99.0	57.7	D
47	APR 07	23	25	13.37	33-53.50	117-42.67	5.37	1.0	19	126	30.8	0.18	1.5	6.3	C
48	APR 08	5	26	3.25	34- 7.32	117-27.32	0.32*	-.4	8	205	10.3	0.05	1.1	35.7	D
49	APR 08	11	10	46.86	34- 6.62	117-29.17	0.05	-.2	11	192	9.9	0.12	0.7	73.3	D
50	APR 08	16	16	59.20	34- 7.42	117-27.60	1.66	.0	9	199	9.6	0.11	2.9	9.6	D
51	APR 08	22	50	12.69	34-13.60	117-31.74	3.61	-.4	6	286	7.7	0.05	5.9	10.3	D
52	APR 10	0	10	24.38	34- 5.24	117-31.54	1.10*	-.1	7	183	10.9	0.04	1.8	7.9	D
53	APR 10	0	19	16.98	34-11.63	117-34.90	5.66	.6	16	127	7.7	0.12	0.9	1.5	B
54	APR 10	10	4	19.37	34-13.93	117-31.19	6.42	-.1	6	249	7.3	0.07	8.6	9.3	D
55	APR 10	18	10	29.83	34- 8.37	117-26.77	2.84	.4	15	212	9.0	0.14	1.4	3.1	C
56	APR 10	20	1	41.81	34-15.83	117-29.53	6.54	.2	8	286	10.2	0.06	4.9	8.1	D
57	APR 12	3	1	49.90	34- 4.47	117-48.67	13.47	.6	10	263	27.7	0.03	0.6	0.6	C
58	APR 13	4	34	52.27	34- 7.61	117-26.62	2.19*	-.3	6	311	10.4	0.06	1.8	6.2	D
59	APR 13	11	40	51.72	34- 7.06	117-28.20	6.86	.2	11	191	9.4	0.08	0.9	1.8	C
60	APR 13	16	52	58.92	34-13.86	117-29.23	3.43	-.2	6	298	5.7	0.06	3.6	5.9	D
61	APR 14	18	24	30.12	34-14.15	117-25.17	15.24	.8	24	97	8.6	0.13	0.7	0.8	B
62	APR 15	6	43	41.15	34-10.42	117-36.90	9.08	.0	12	179	8.6	0.07	0.7	1.1	B
63	APR 15	6	51	23.16	34-12.56	117-31.91	9.30	.4	14	200	5.6	0.16	2.2	1.7	C
64	APR 15	10	50	26.99	34-11.15	117-37.66	5.72	-.2	9	141	7.1	0.09	1.6	1.6	C
65	APR 17	2	53	15.31	34- 7.03	117-29.41	10.20	.8	13	88	10.7	0.08	0.6	1.3	A
66	APR 17	13	12	44.28	34- 8.39	117-27.37	6.41	-.1	6	277	14.0	0.03	1.5	2.6	C
67	APR 18	2	12	3.10	34- 7.87	117-28.87	16.62	1.9	28	60	12.4	0.13	0.5	1.1	A
68	APR 18	12	41	37.17	34- 7.62	117-28.38	7.47	1.0	25	57	12.2	0.15	0.6	2.0	B

TABLE 1.3.—*Final hypocenter solutions, eastern San Gabriel Mountains, March 16 to July 8, 1977—Continued*

#	1977	HR	MN	SEC	LAT (N.)	LONG (W.)	DEPTH	MAG	NO	GAP	DMIN	RMS	ERH	ERZ	Q
69	APR 18	17	7	57.85	34-11.68	117-27.74	7.88	.4	4	182	12.2	0.01	99.0	86.9	D
70	APR 18	17	47	17.98	34-10.33	117-34.92	10.87	.4	7	191	11.0	0.06	1.0	3.0	C
71	APR 20	3	56	23.99	34-15.48	117-31.73	5.20	.0	10	274	9.7	0.09	4.0	7.0	D
72	APR 20	8	0	52.96	34-15.36	117-34.68	12.24	.2	7	255	9.1	0.06	2.7	1.7	D
73	APR 20	14	22	50.60	34-13.79	117-29.94	7.18	.1	10	212	5.8	0.05	1.3	1.2	C
74	APR 20	22	27	53.03	34-16.81	117-30.99	6.43	.7	22	121	11.3	0.08	0.4	1.3	B
75	APR 22	7	10	8.57	34-13.10	117-29.45	2.77	-.6	5	315	4.4	0.02	15.7	14.8	D
76	APR 23	4	26	17.39	34- 7.74	117-32.36	0.87*	-.2	10	264	8.6	0.18	3.4	30.3	D
77	APR 23	8	34	17.63	34-15.46	117-31.31	10.59	.4	9	233	9.4	0.04	1.7	1.4	C
78	APR 23	12	47	48.51	34-16.51	117-27.53	11.01	.6	10	277	12.9	0.04	1.4	1.5	C
79	APR 24	4	40	2.93	34-16.45	117-32.84	12.09	.2	7	285	12.0	0.05	1.6	2.1	C
80	APR 24	4	59	33.85	34-16.67	117-32.67	10.91	.2	6	320	12.4	0.01	0.8	0.9	C
81	APR 26	3	36	27.44	34-12.58	117-40.31	0.38*	.2	9	227	12.6	0.18	1.6	49.8	D
82	APR 26	4	56	19.52	34-21.10	117-33.10	5.10	.4	7	317	19.5	0.06	3.9	36.2	D
83	APR 26	11	44	6.49	34-16.50	117-28.41	12.70	.3	7	315	12.1	0.04	4.4	4.0	D
84	APR 26	15	12	41.63	34-10.80	117-25.22	9.05	.3	9	330	7.9	0.08	5.2	1.8	D
85	APR 27	3	50	55.76	34-15.92	117-31.12	11.42	-.1	8	261	10.1	0.13	15.6	11.7	D
86	APR 27	6	24	8.73	34- 5.52	117-29.53	0.03*	-.1	6	360	15.5	0.16	8.0	99.0	D
87	APR 27	21	31	37.99	34-13.40	117-41.67	5.96	-.1	9	241	9.2	0.03	0.6	0.8	C
88	APR 28	1	24	58.13	34- 5.88	117-31.61	3.79	-.1	14	139	9.9	0.20	1.9	6.4	C
89	APR 28	2	58	0.55	34-12.46	117-23.61	14.03	.3	13	337	9.8	0.09	1.6	1.7	C
90	APR 28	16	10	56.79	34-12.41	117-28.83	4.10	.1	7	200	3.0	0.06	1.8	2.0	C
91	APR 29	8	18	32.51	34-10.01	117-26.59	15.52	.6	24	159	6.9	0.12	0.6	1.1	B
92	APR 29	10	38	54.11	34- 8.34	117-26.36	3.72	.2	13	290	9.4	0.09	0.8	2.3	C
93	APR 29	20	7	23.80	34-14.27	117-26.91	15.69	.3	16	292	7.1	0.09	1.2	1.2	C
94	APR 30	7	20	35.00	34- 6.21	117-28.93	5.78	1.4	28	84	10.0	0.12	0.5	2.0	B
95	APR 30	8	36	21.88	34- 8.51	117-27.84	5.99	-.3	9	325	8.0	0.12	2.1	2.7	C
96	APR 30	12	28	23.99	34- 6.46	117-28.82	0.37*	-.2	13	183	9.9	0.09	0.9	28.7	D
97	MAY 01	6	35	56.83	34- 5.61	117-28.83	10.92	1.1	28	74	11.0	0.42	2.0	3.7	B
98	MAY 01	12	18	45.00	34-12.55	117-24.86	6.93	.1	12	332	9.7	0.11	2.1	2.6	C
99	MAY 03	14	26	15.85	34- 7.33	117-25.81	4.26	.3	12	183	11.4	0.07	0.9	0.8	C
100	MAY 03	19	4	47.57	34-15.36	117-30.99	10.51	.5	15	233	6.8	0.10	1.2	1.2	C
101	MAY 06	5	27	11.35	34-10.39	117-37.97	6.78	.5	20	179	7.0	0.09	0.5	1.0	B
102	MAY 06	6	15	22.71	34-13.78	117-25.49	13.26	.5	13	166	7.8	0.06	0.9	1.3	C
103	MAY 07	13	40	17.24	34- 7.71	117-28.02	4.07	.1	15	284	8.8	0.15	1.4	4.0	C
104	MAY 07	13	56	36.00	34- 7.97	117-28.35	1.81	.3	14	262	8.1	0.09	0.9	6.4	D
105	MAY 08	23	22	12.41	34-15.18	117-33.32	5.34	.6	12	232	10.5	0.05	0.9	2.0	C
106	MAY 11	3	45	38.56	34-13.63	117-31.20	6.32	.3	7	219	7.0	0.03	1.0	1.2	C
107	MAY 11	17	42	57.10	34-15.15	117-31.96	5.59	.4	8	237	9.6	0.10	3.2	6.6	D
108	MAY 13	8	13	38.41	34-12.76	117-37.07	4.03	.3	13	120	8.7	0.07	0.8	2.2	B
109	MAY 14	17	33	23.94	34-10.62	117-20.46	12.33	.5	6	345	18.3	0.01	1.6	0.9	C
110	MAY 15	21	2	44.26	34-12.15	117-34.62	7.69	.0	9	139	7.4	0.05	0.9	1.4	B
111	MAY 15	22	42	26.71	34-14.43	117-34.02	7.35	1.7	21	110	7.2	0.15	0.8	2.2	B
112	MAY 16	3	13	46.06	34- 7.09	117-27.54	2.10	.5	15	94	10.6	0.05	0.4	1.6	B
113	MAY 16	16	17	49.18	34-12.04	117-26.98	1.97	.1	7	290	4.7	0.06	2.0	3.4	C
114	MAY 16	22	31	53.88	34- 9.88	117-25.16	4.69	.3	11	252	8.8	0.12	1.4	2.7	C
115	MAY 17	0	23	42.26	34-14.61	117-31.03	5.47	.0	9	262	7.3	0.03	0.9	1.2	C
116	MAY 17	3	57	53.45	34-11.77	117-27.83	2.48	-.1	10	162	3.5	0.07	1.1	1.3	C
117	MAY 17	8	34	14.88	34- 6.95	117-29.06	7.42	.3	14	177	9.3	0.05	0.6	0.9	B
118	MAY 17	14	37	32.83	34-14.25	117-26.62	4.34	.1	8	303	7.4	0.21	11.8	9.4	D
119	MAY 18	2	12	47.33	34-13.81	117-30.95	5.94	-.1	8	283	6.4	0.04	1.4	1.1	C
120	MAY 18	10	2	22.81	34- 4.10	117-27.53	0.33*	.1	5	331	18.6	0.11	18.8	99.0	D
121	MAY 18	13	22	36.67	34-12.20	117-27.73	3.74	.1	11	210	3.5	0.05	0.8	0.9	C
122	MAY 20	8	0	8.29	34- 8.60	117-27.40	8.98	-.2	10	284	8.2	0.07	1.0	1.7	C
123	MAY 20	9	23	42.25	34-11.32	117-28.14	7.70	.0	11	172	6.5	0.09	2.7	1.5	C
124	MAY 21	2	50	2.12	34-12.03	117-33.84	6.84	.0	15	122	4.8	0.09	1.5	1.9	B
125	MAY 21	9	13	5.51	34-13.08	117-30.77	2.68	-.3	9	230	4.9	0.08	1.9	1.5	C
126	MAY 21	15	30	22.61	34-15.11	117-28.30	6.50	-.1	8	288	8.1	0.05	1.9	1.3	C
127	MAY 22	9	48	18.31	34- 6.60	117-29.17	1.82*	.2	15	177	10.0	0.12	0.9	7.0	C
128	MAY 23	7	31	54.14	34- 8.41	117-26.83	5.97	.0	13	211	9.6	0.09	1.4	2.3	C
129	MAY 23	10	50	23.58	34-12.42	117-26.68	10.81	.0	7	300	6.9	0.03	2.0	1.8	C
130	MAY 23	23	13	13.60	34- 4.89	117-25.98	0.92*	.4	10	301	14.7	0.13	1.1	18.4	D
131	MAY 24	18	7	35.23	34-13.61	117-31.54	8.19	.3	8	194	7.4	0.01	0.2	0.3	C
132	MAY 24	18	28	48.51	34-13.43	117-41.14	3.36	1.0	18	90	8.5	0.13	0.8	1.5	A
133	MAY 24	23	36	40.65	34-13.52	117-41.02	3.44	.2	11	108	8.5	0.06	0.7	1.1	B
134	MAY 25	3	53	9.83	34- 2.49	117-33.08	8.22	.9	19	152	17.1	0.29	2.0	4.8	C
135	MAY 25	5	34	58.64	34- 7.76	117-32.69	1.95*	-.1	4	323	15.7	0.06	22.7	49.7	D
136	MAY 27	3	43	15.71	34- 9.34	117-49.96	13.51	.9	14	174	14.9	0.11	1.5	1.4	C

TABLE 1.3.—*Final hypocenter solutions, eastern San Gabriel Mountains, March 16 to July 8, 1977—Continued*

#	1977	HR	MN	SEC	LAT (N.)	LONG (W.)	DEPTH	MAG	NO	GAP	DMIN	RMS	ERH	ERZ	Q
137	MAY 27	8	17	45.59	34-12.50	117-23.65	13.91	.6	16	160	13.7	0.06	0.5	1.1	B
138	MAY 28	22	28	28.03	34-11.08	117-26.25	8.29	.1	12	252	6.3	0.18	3.6	3.6	D
139	MAY 29	2	49	40.08	34-18.02	117-29.30	5.68	.1	6	325	14.1	0.05	13.0	42.4	D
140	MAY 29	3	5	23.56	34-14.57	117-29.79	5.92	.2	8	294	7.1	0.06	2.4	3.3	C
141	MAY 31	6	19	56.55	34-17.21	117-32.31	11.46	.3	11	274	11.8	0.06	1.8	2.0	C
142	MAY 31	14	29	48.10	34-13.91	117-30.68	8.64	-.3	9	236	6.3	0.08	2.7	2.4	D
143	JUN 01	10	18	21.10	34-16.78	117-32.43	12.02	.7	15	257	8.8	0.08	1.2	1.6	C
144	JUN 03	2	47	25.62	34- 6.65	117-29.71	0.88*	.0	16	167	9.9	0.13	1.3	14.2	C
145	JUN 03	7	36	32.88	34-13.91	117-24.64	13.76	.3	16	322	8.9	0.07	1.6	1.0	C
146	JUN 03	11	50	20.80	34-12.94	117-35.14	7.89	-.1	9	245	5.8	0.05	1.6	1.1	C
147	JUN 03	14	10	41.94	34- 5.85	117-27.56	6.00	.3	8	319	11.8	0.05	2.3	3.8	C
148	JUN 05	18	54	25.95	34-19.92	117-42.70	3.10	.4	7	327	19.3	0.03	1.6	4.9	D
149	JUN 06	4	50	42.49	34-11.15	117-37.52	9.49	-.1	7	160	7.1	0.03	0.7	0.7	B
150	JUN 06	21	9	39.51	34-13.94	117-37.04	8.99	.3	9	144	10.1	0.05	1.4	1.4	C
151	JUN 07	9	45	39.09	33-54.50	117-41.28	12.76	1.5	28	106	20.6	0.17	0.7	1.8	B
152	JUN 07	18	15	41.11	34- 7.33	117-28.06	2.84	.8	19	92	9.2	0.11	0.6	1.7	B
153	JUN 12	13	4	36.29	34-18.64	117-35.26	9.65	.5	15	186	12.5	0.07	1.2	2.1	C
154	JUN 12	14	15	5.07	34- 1.86	117-34.94	7.55	2.7P	26	77	18.6	0.22	0.9	3.9	B
155	JUN 13	1	14	10.01	34- 3.58	117-51.56	4.68	.9	18	259	19.4	0.29	2.2	5.3	D
156	JUN 13	6	46	22.10	34- 3.20	117-50.91	5.41	.9	15	255	19.1	0.07	0.8	1.8	C
157	JUN 13	12	2	25.93	34- 4.87	117-50.18	5.93	1.0	19	175	16.2	0.29	1.8	5.0	C
158	JUN 14	6	59	20.43	34- 7.11	117-26.87	0.69*	.6	16	131	10.9	0.22	2.0	35.4	C
159	JUN 16	10	23	33.19	34-15.43	117-30.38	10.90	.6	13	239	7.6	0.07	1.0	1.7	C
160	JUN 16	23	51	10.31	34-14.79	117-30.48	7.23	.8	21	149	7.5	0.10	0.6	1.1	B
161	JUN 17	2	29	31.11	34-13.44	117-32.60	8.88	.3	14	182	4.4	0.08	1.5	1.5	C
162	JUN 17	2	42	18.77	34-11.83	117-33.71	5.99	.1	9	124	5.9	0.06	1.4	1.7	B
163	JUN 17	11	57	53.13	34-13.20	117-27.77	6.60	.5	7	262	4.9	0.05	2.9	3.3	C
164	JUN 18	10	26	25.06	34-17.74	117-36.39	4.78	.2	6	314	12.9	0.03	1.2	2.5	C
165	JUN 18	16	20	39.28	34-15.00	117-39.01	2.46	.7	22	92	8.6	0.09	0.4	1.0	B
166	JUN 18	18	0	49.37	34-12.79	117-24.01	14.06	.4	12	333	9.2	0.06	2.0	1.6	C
167	JUN 19	8	1	21.54	34-15.11	117-39.39	1.84	-.1	9	138	9.1	0.09	0.7	2.9	C
168	JUN 19	16	16	53.24	34-11.62	117-45.25	3.12	.1	10	138	12.6	0.07	1.0	2.4	C
169	JUN 19	21	35	54.53	34- 7.10	117-26.60	2.35	.5	15	173	11.2	0.08	0.8	3.4	C
170	JUN 20	6	27	28.13	34-12.84	117-23.98	9.54	.6	15	162	9.3	0.10	0.7	1.2	B
171	JUN 20	7	19	51.70	34- 2.36	117-33.88	6.41	.5	15	186	17.3	0.14	1.1	2.0	C
172	JUN 20	9	56	19.12	34- 2.45	117-33.79	6.69	.5	14	206	17.0	0.08	1.0	1.5	C
173	JUN 20	18	38	9.40	34-13.64	117-40.86	4.63	.8	18	99	10.2	0.10	0.5	1.5	B
174	JUN 20	23	28	20.61	34-14.50	117-39.49	2.84	.1	7	137	8.8	0.06	1.5	3.5	C
175	JUN 21	4	36	9.83	34-15.67	117-31.22	8.49	.3	10	277	7.0	0.05	1.4	1.3	C
176	JUN 21	7	47	42.18	34-14.92	117-39.01	4.91	.6	18	109	9.8	0.09	0.6	1.1	B
177	JUN 21	8	56	31.60	34- 6.69	117-43.35	2.94	.6	17	108	17.3	0.08	0.6	2.3	B
178	JUN 22	4	32	53.30	34- 8.28	117-26.77	5.76	.3	15	212	9.2	0.09	1.1	1.7	C
179	JUN 22	17	47	55.42	34-15.15	117-30.44	12.02	.7	16	153	7.2	0.06	0.8	1.0	B
180	JUN 23	4	56	50.96	34- 8.41	117-27.78	5.54	.9	29	75	8.2	0.10	0.5	1.1	A
181	JUN 24	11	7	9.70	34-12.20	117-28.52	11.93	.3	9	188	2.7	0.05	1.2	2.1	C
182	JUN 24	16	45	4.09	34-14.59	117-27.03	7.84	.2	9	271	7.2	0.05	2.1	2.5	C
183	JUN 25	4	49	51.85	34-16.12	117-31.37	11.87	.7	12	301	9.9	0.08	1.7	1.7	C
184	JUN 27	20	59	43.58	34- 6.82	117-57.17	10.83	2.9P	24	54	15.6	0.13	0.8	2.3	B
185	JUN 29	0	51	37.83	34-12.36	117-28.46	4.24	-.4	7	205	6.6	0.04	2.8	2.5	D
186	JUN 29	17	54	46.85	34-14.18	117-25.61	5.02	.4	12	265	8.2	0.04	0.7	1.3	C
187	JUN 30	1	7	29.25	34-13.73	117-26.08	11.62	1.9	38	56	7.1	0.13	0.4	1.0	A
188	JUN 30	6	35	36.09	34-10.15	117-25.56	9.09	1.0	26	94	8.0	0.16	0.9	1.0	B
189	JUN 30	10	22	5.05	34- 7.72	117-28.04	7.56	.9	26	92	8.8	0.08	0.4	0.8	B
190	JUL 01	12	51	0.83	34- 8.23	117-24.08	5.30	.3	11	336	12.0	0.09	1.4	3.7	C
191	JUL 02	2	2	9.21	34-11.34	117-22.02	1.00*	.6	17	318	12.4	0.14	1.5	11.2	D
192	JUL 02	13	39	33.04	34-12.39	117-20.36	5.00*	.4	3	360	12.3	0.02	99.0	99.0	D
193	JUL 02	20	40	10.63	34- 6.09	117-28.18	1.26	.3	16	196	10.6	0.09	0.7	6.4	D
194	JUL 02	21	12	15.17	34-11.07	117-21.43	0.23*	.4	6	346	13.4	0.05	8.1	72.9	D
195	JUL 03	3	13	52.41	34-13.80	117-34.53	7.34	.2	7	217	6.4	0.02	0.5	0.5	C
196	JUL 03	21	34	59.55	34- 6.85	117-26.10	2.86	.6	13	178	12.1	0.09	0.8	1.8	B
197	JUL 04	3	21	24.70	34-12.66	117-34.93	5.88	-.1	4	181	12.1	0.01	99.0	99.0	D
198	JUL 04	10	18	22.50	34-12.38	117-34.21	4.07	.0	7	173	7.6	0.06	2.5	2.3	C
199	JUL 05	0	51	51.67	34-12.18	117-34.28	5.15	-.2	4	181	7.6	0.01	99.0	99.0	D
200	JUL 05	1	17	16.18	34-13.02	117-23.31	13.76	.7	12	330	14.5	0.09	1.6	1.8	C
201	JUL 05	2	59	35.47	34- 2.78	117-33.18	7.00	.9	13	151	18.9	0.09	0.8	2.0	C
202	JUL 05	10	52	5.72	34- 7.94	117-28.10	3.67	.0	7	299	8.8	0.05	0.8	2.7	C
203	JUL 06	2	35	20.38	34-10.21	117-36.54	6.66	.0	7	189	9.1	0.03	0.5	1.3	C
204	JUL 06	9	57	55.46	34-12.51	117-27.41	5.67	-.2	6	244	17.0	0.05	3.0	2.8	D

TABLE 1.3.—*Final hypocenter solutions, eastern San Gabriel Mountains, March 16 to July 8, 1977—Continued*

#	1977	HR	MN	SEC	LAT (N.)	LONG (W.)	DEPTH	MAG	NO	GAP	DMIN	RMS	ERH	ERZ	Q
205	JUL 06	11	44	28.53	34- 9.53	117-45.30	13.94	.3	7	282	20.0	0.07	2.5	1.7	D
206	JUL 06	23	26	34.66	34-11.50	117-28.49	10.58	.0	4	181	20.0	0.02	99.0	99.0	D
207	JUL 07	12	46	0.69	34- 9.04	117-25.59	2.80	.9	26	63	16.3	0.09	0.3	0.9	B
208	JUL 08	4	34	30.09	34-17.13	117-28.75	4.78	-.1	5	345	12.9	0.00	53.2	99.0	D
209	JUL 08	9	9	36.97	34-12.69	117-26.72	5.00*	-.7	3	341	6.8	0.00	99.0	99.0	D
210	JUL 08	10	56	30.50	34-10.49	117-24.70	0.05*	-.6	6	331	10.8	0.03	0.7	24.6	D
211	JUL 08	10	59	52.60	34-14.54	117-25.83	8.11	.4	13	259	12.2	0.12	1.7	2.3	C
212	JUL 08	11	50	1.31	34-12.44	117-26.33	5.00*	-.8	3	360	12.2	0.06	99.0	99.0	D
213	JUL 08	13	4	49.42	34-10.67	117-24.52	1.00*	-.0	7	335	12.0	0.03	2.0	4.3	C
214	JUL 08	13	39	46.74	34-11.04	117-24.53	5.00*	-.3	3	360	12.0	0.16	99.0	99.0	D
215	JUL 08	13	56	8.22	34-12.43	117-25.95	5.00*	-.7	3	360	12.0	0.07	99.0	99.0	D
216	JUL 08	14	17	19.77	34-12.91	117-25.16	0.67	-.8	4	360	12.0	0.13	99.0	99.0	D
217	JUL 08	14	43	7.23	34-12.74	117-25.37	5.00*	-.7	3	359	12.0	0.55	99.0	99.0	D
218	JUL 08	15	2	3.54	34-10.29	117-24.51	1.24	.0	7	332	11.2	0.01	0.3	0.8	C
219	JUL 08	15	14	19.89	34-10.83	117-24.85	1.87*	-.2	6	334	10.3	0.07	1.3	2.0	C
220	JUL 08	19	23	25.75	34-12.61	117-25.68	4.29	-.7	4	360	10.3	0.06	99.0	99.0	D

Note, for each event in the above table the following information is given:

Origin time in Greenwich mean time: date, hour (HR), minute (MN), and second (SEC).

Epicenter in degrees and minutes of north latitude (LAT (N.)) and west longitude (LONG (W.)).

DEPTH= depth of focus, in kilometers. Assumed depth is indicated by "*".

MAG= estimated earthquake magnitude (see text for methods used). P after magnitude indicates CIT Richter magnitude.

NO= number of P and S arrival times used in locating the earthquake.

GAP= largest azimuthal separation, in degrees, between stations.

DMIN= epicentral distance, in kilometers, to the nearest station.

RMS= root-mean-square error of the travel-time residuals. RMS= $\sqrt{\text{sum}(\text{R}_i \times \text{R}_i / \text{NO})}$, where R_i is the observed seismic-wave arrival time minus the computed time at the i th station.

ERH= standard error of the epicenter, in kilometers. ERH= $\sqrt{\text{SDX}_2 + \text{SDY}_2}$, where SDX_2 and SDY_2 are the square of the standard errors in latitude and longitude, respectively, of the epicenter.

ERZ= standard error of the focal depth, in kilometers.

Q= solution quality of the hypocenter. This measure is intended to indicate the general reliability of each solution:

Q	Epicenter	Focal Depth
A	Excellent	Good
B	Good	Fair
C	Fair	Fair
D	Poor	Poor

See Lahr and Ward (1978) for complete description of Q.

figures 1.2 and 1.3. However, the microearthquake survey provides better spatial resolution and depth control for events that occurred near the array. Also, the following discussion of the focal mechanisms from this study permits new insight into the tectonics of the area because of new data that can only be provided by a detailed micro-earthquake study.

FOCAL MECHANISMS

Figure 1.6 shows 27 individual and composite focal mechanisms for the study area. Each focal mechanism is reproduced with its first-motion data in figure 1.7. The focal mechanisms reveal that the entire region is undergoing deformation under north-south compression. The

dominant mode of deformation is along strike-slip faults, particularly in the areas surrounding the San Gabriel Mountains. Thrust faulting seems confined to the interior of the San Gabriel Mountains; some thrust and oblique thrust faulting occurs across the San Jacinto and Glen Helen faults. The dominance of strike-slip faulting agrees with the focal-mechanism observations of Johnson (1977) for the region surrounding the San Bernardino Mountains. The next section is a detailed presentation of individual focal mechanisms and associated fault movements.

FAULT MOVEMENTS

CUCAMONGA FAULT

Because of the prominent scarps along the Cucamonga fault, the question arises as to whether any microearth-

quake activity is occurring there at present. Although there is no inclined plane of hypocenters dipping from the surface trace of the Cucamonga fault, a cluster of activity with thrust-type focal mechanisms occurs about 7 km beneath Cucamonga Peak. Focal mechanism j (figure 1.6) indicates a fault plane dipping about 50° N. From the spatial position of this pocket of activity, these events could lie on a fault dipping 50°–60° from the surface trace of the Cucamonga. If the observed 35° surface dips on the Cucamonga fault steepen to 50°–60° at depth, as has been observed on other faults in the Transverse Ranges (Butler and others, 1977; Yeats and others, 1978), then the activity beneath Cucamonga Peak could lie on the Cucamonga fault.

The epicenters of a few events do fall near the surface trace of the Cucamonga fault, but their focal depths (6–12

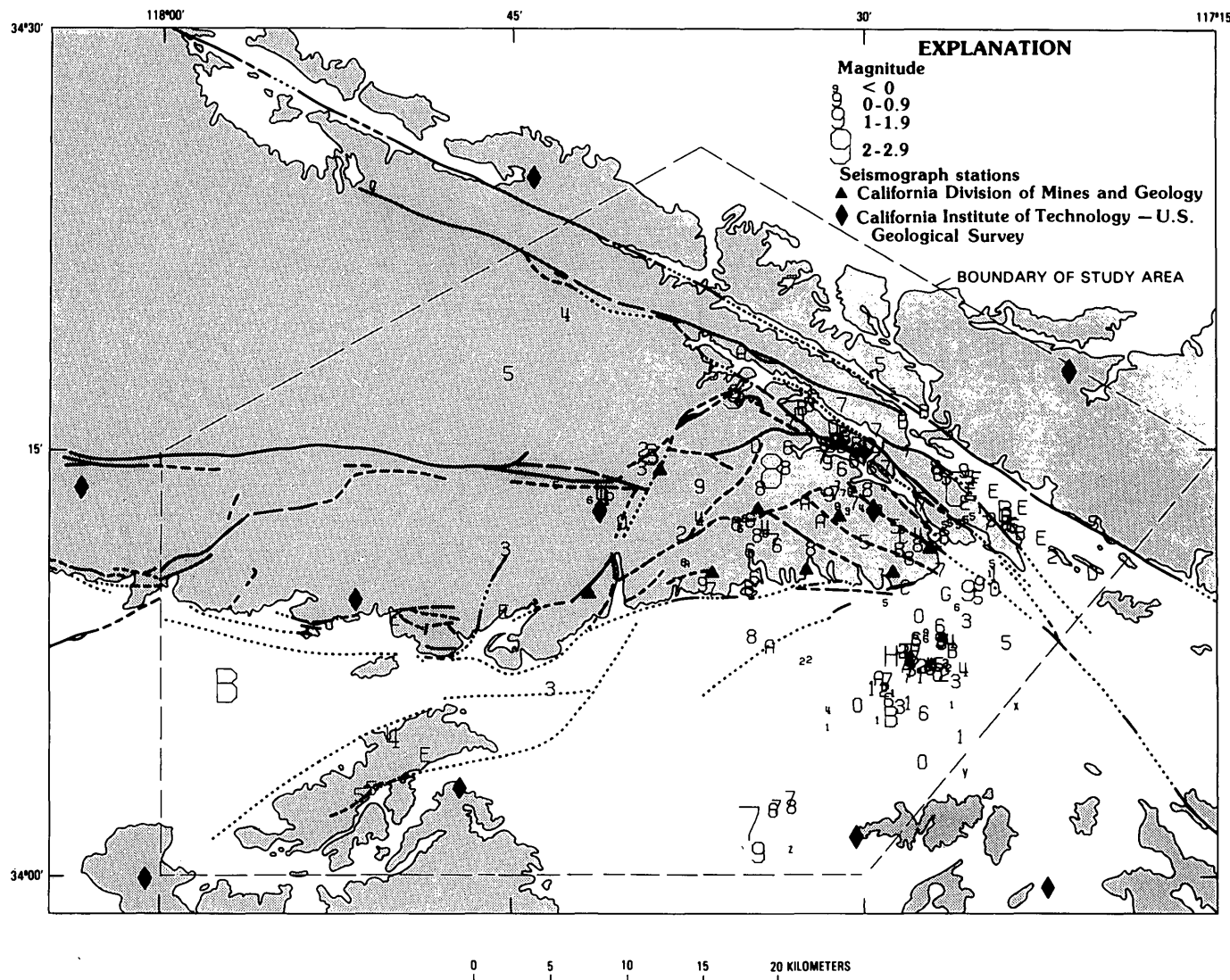


FIGURE 1.5.—Microearthquake locations for activity recorded between March 16 and July 8, 1977. Geology same as in figure 1.1. Numbers indicate focal depth to nearest kilometer; events deeper than 9 km indicated by letters: A, 10 km; B, 11; C, 12; D, 13; E, 14; F, 15; G, 16; H, 17.

km) are too deep for this activity to be on the Cucamonga fault. Also, focal mechanisms i and p (fig. 1.6) indicate strike-slip movement on vertical faults for these events. The compression axis for focal mechanism i is rotated to the northwest, indicating the possibility of thrusting having developed across northeasterly trending faults in the vicinity of San Antonio Canyon.

RED HILL FAULT

Three microearthquake epicenters appear to fall on the Red Hill fault just south of the Cucamonga fault. A composite focal mechanism (h) indicates left-lateral strike-slip movement on a northeast-trending fault plane that

parallels the Red Hill fault. The fact that these deeper events (7–12 km) lie very close to the Red Hill fault also suggests vertical faulting. The Red Hill fault may be a seismically active vertical strike-slip fault.

It is curious that the trend of the Cucamonga fault changes from east to northeast at the point where the Red Hill fault would intersect the Cucamonga. This alignment suggests that a relationship exists between the Red Hill fault and the orientation of the Cucamonga fault between Bullock's Canyon and Lytle Creek.

SAN JACINTO FAULT SYSTEM IN LYITLE CREEK

Much of the microearthquake activity detected during the present study occurred in Lytle Creek Canyon, which

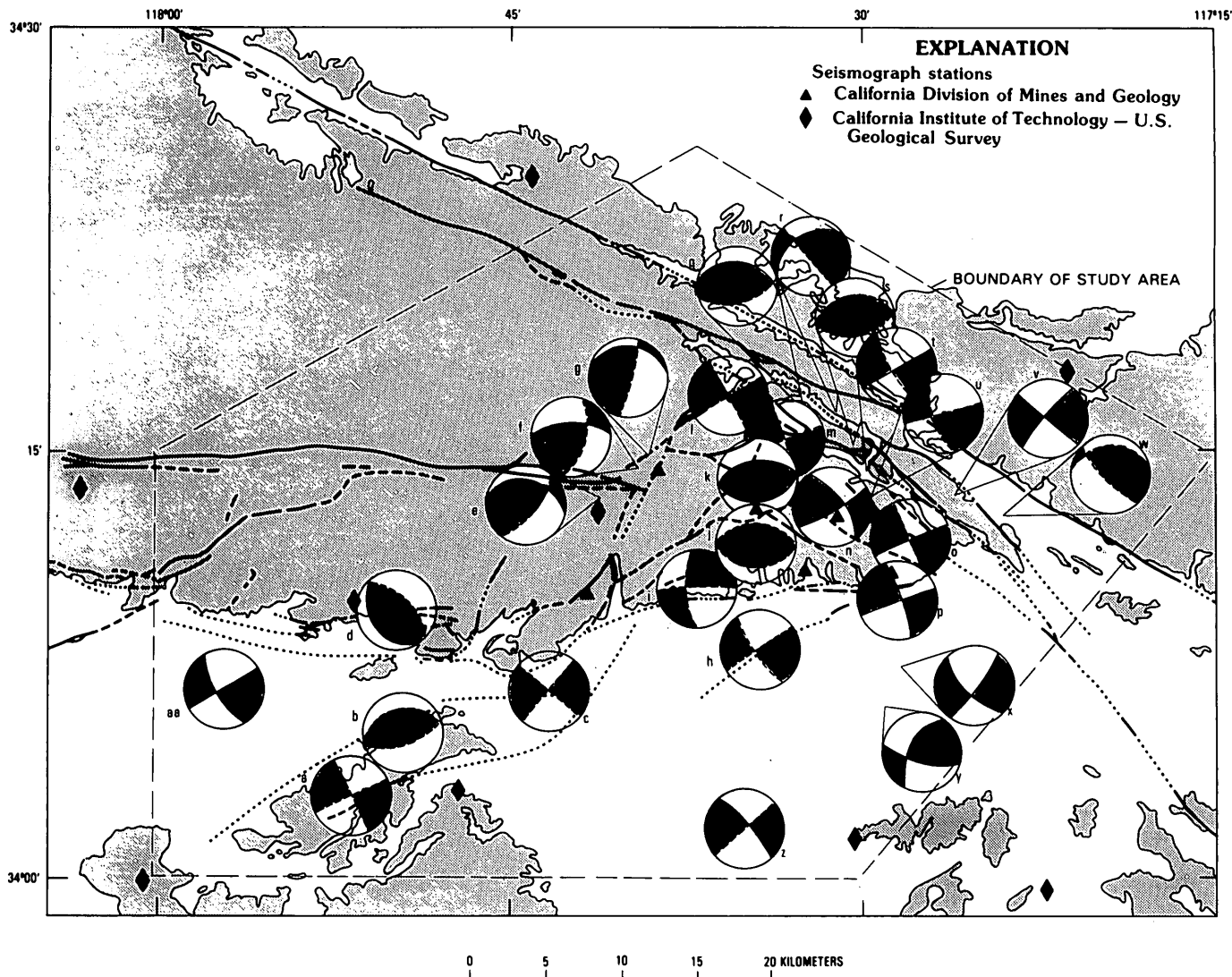


FIGURE 1.6.—All focal mechanisms from the study superimposed on geologic map. All mechanisms are lower hemisphere equal area projections with compressional quadrants shaded. Dashed nodal lines indicate poorly constrained fault planes. Lowercase letters refer to text and table 1.3. Detailed mechanisms are presented in figure 1.7. See figure 1.1 for explanation of geology.

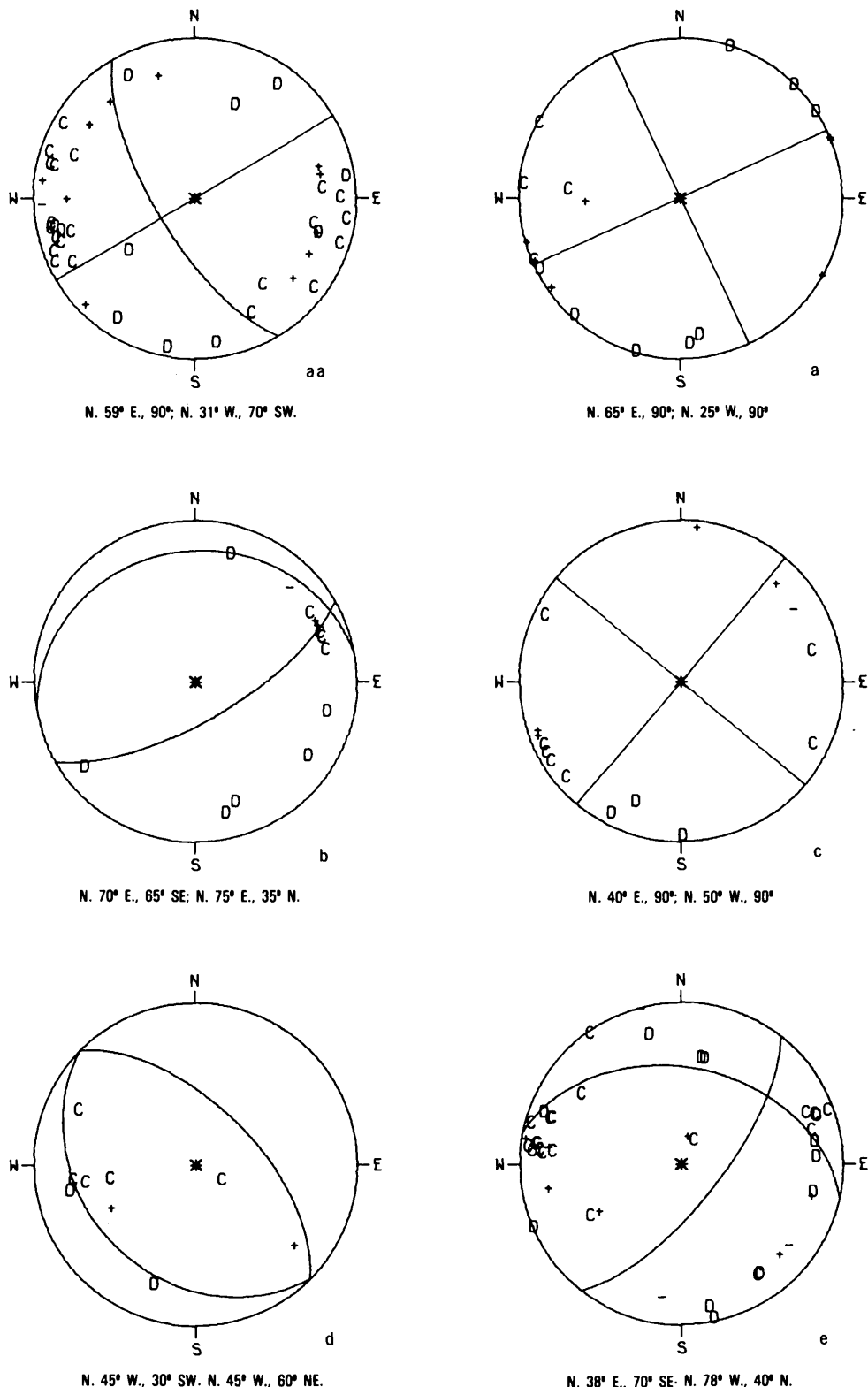


FIGURE 1.7.—Detailed plots of the 27 single and composite focal mechanisms shown on figure 1.6 and discussed in the text. Each plot is labeled aa-z to agree with corresponding plot on figure 1.6. Strikes and dips of the two fault planes of each mechanism are given below each plot. All focal mechanisms are lower-hemisphere equal-area projections. C and + represent compressional first motions; D and - represent dilatational first motions.

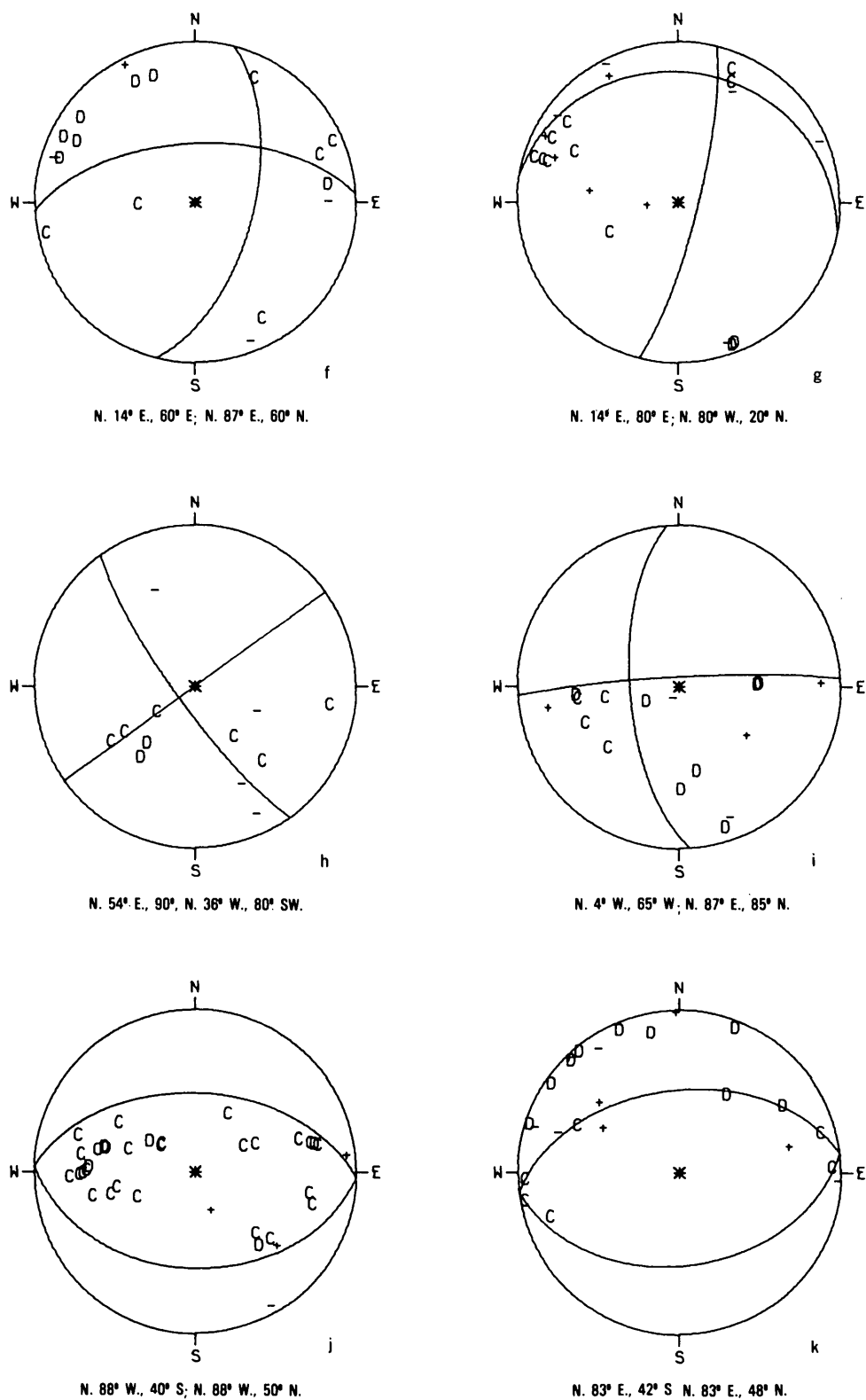


FIGURE 1.7.—Continued.

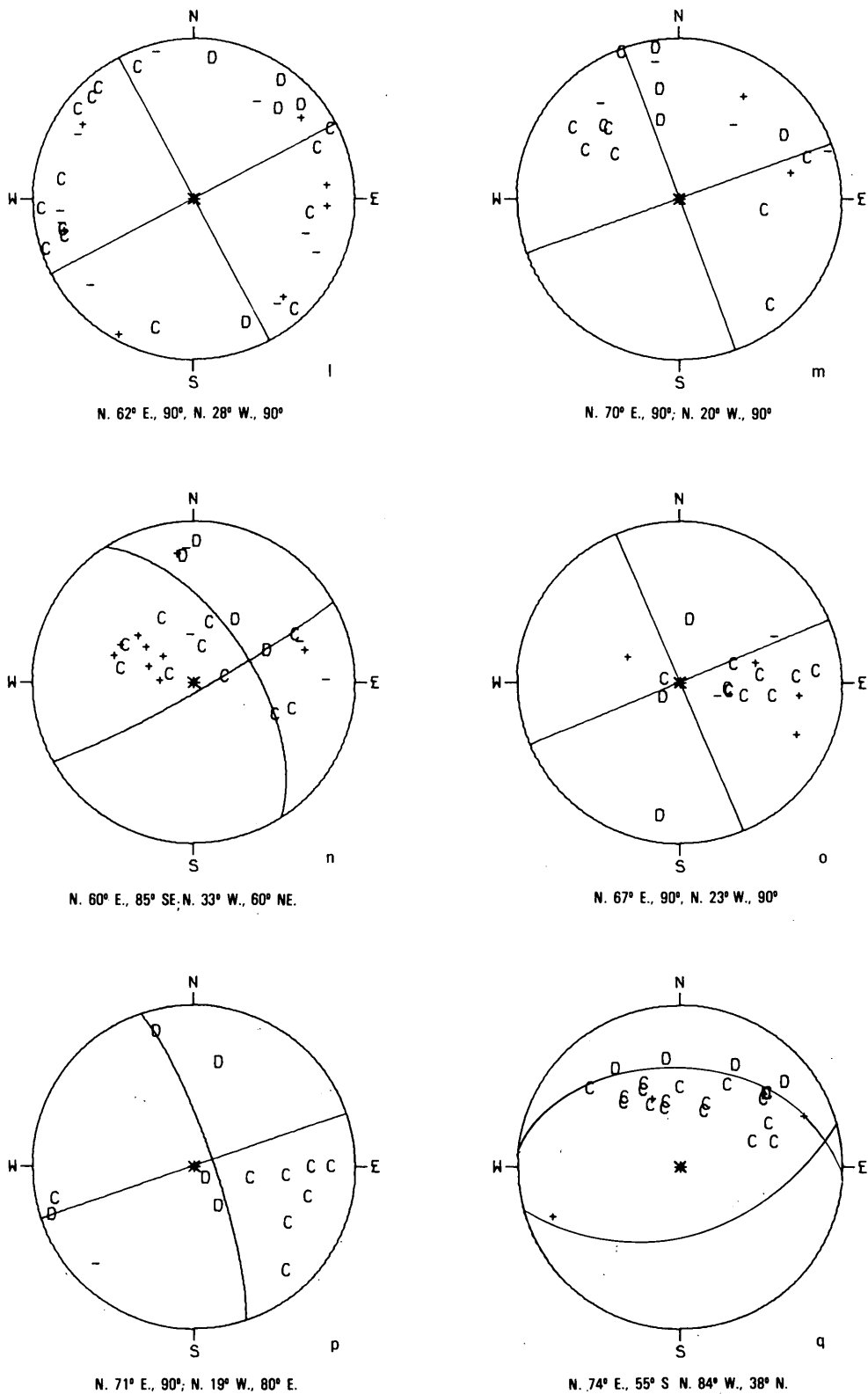


FIGURE 1.7.—Continued.

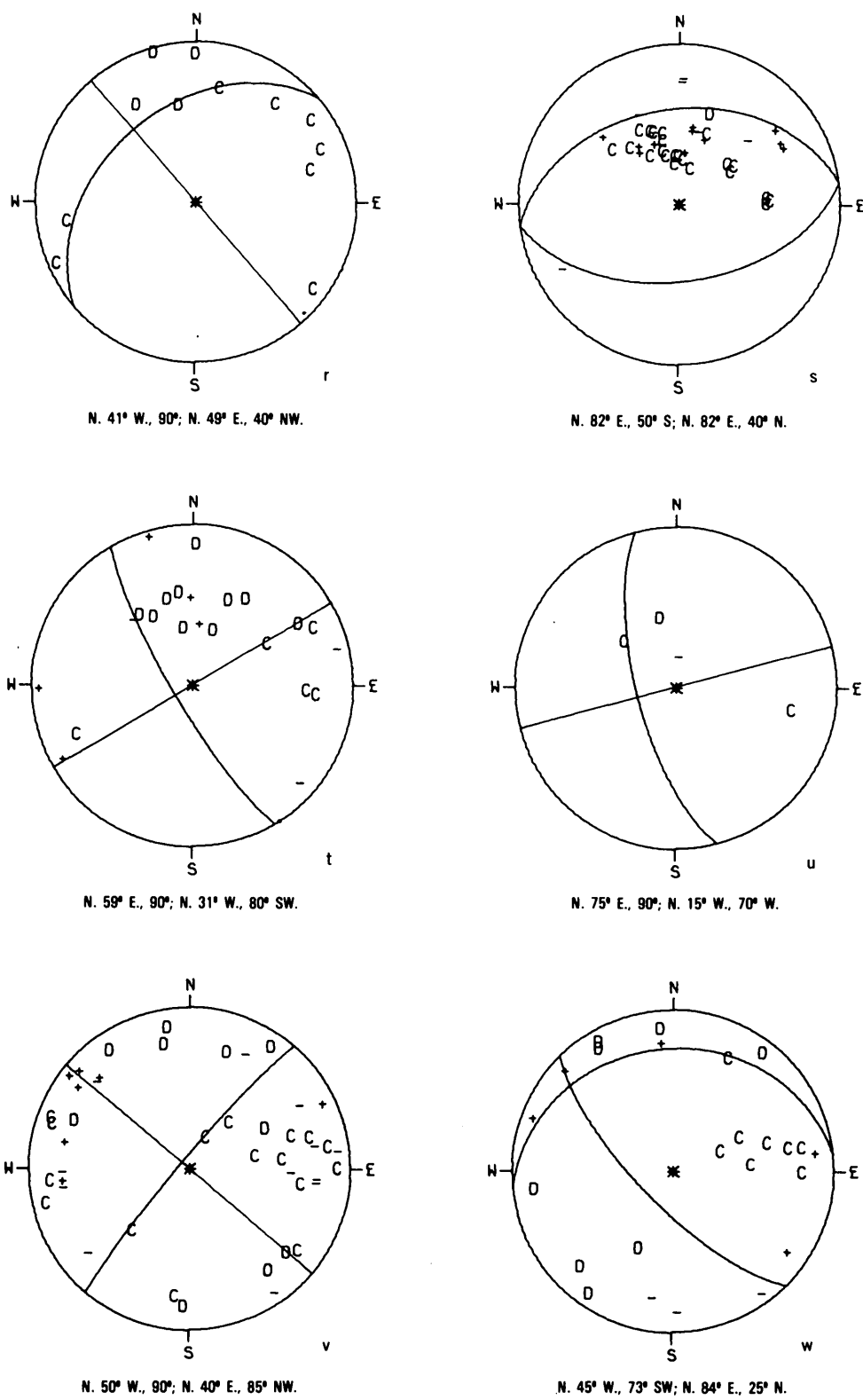


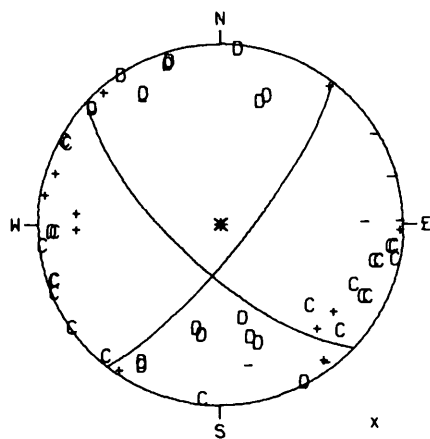
FIGURE 1.7.—Continued.

lies on the northwest-trending San Jacinto fault system. Except at the eastern end of the portable network, focal depths are not always well constrained, but the epicentral location is generally good for events with magnitudes greater than zero. The several focal mechanisms along this trend (o, q-u) indicate right-lateral strike-slip movement on northwest-trending vertical fault planes.

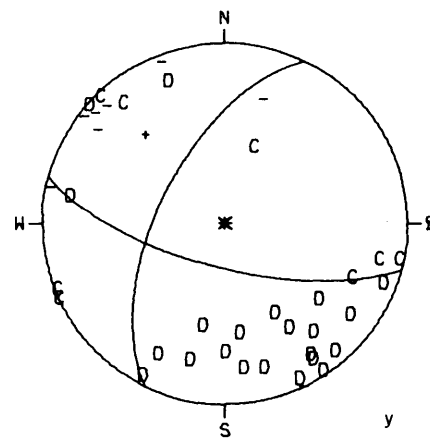
Two of these mechanisms do show north-south thrusting, indicating a region of compression at the north end of Lytle Creek Canyon where the San Jacinto approaches the San Andreas fault and where the San Jacinto changes to a more west-northwesterly trend and parallels the San Andreas. Thrust mechanisms, however, are not unusual along the San Andreas in central and southern California. In fact, recent swarm activity along the San Andreas fault system about 100 km to the northwest shows dominantly thrust-type mechanisms during this same period (McNally and others, 1978).

The September 12, 1970, magnitude 5.4 Lytle Creek earthquake occurred on a branch of the San Jacinto fault just northeast of focal mechanism q in figure 1.6. The main-shock focal mechanism has a preferred fault plane striking 313° and dipping 56° NE. and an auxiliary fault plane striking 81° and dipping 48° S. (D. Hadley, written commun., 1978). The sense of motion on the preferred plane is right lateral and reverse on a northwest-trending fault, which is compatible with the motions observed during this study.

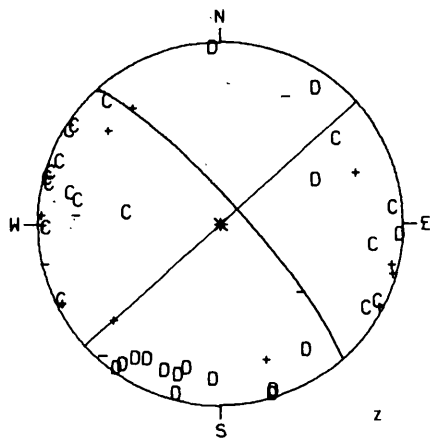
Microearthquake activity within the San Gabriel Mountains immediately adjacent to Lytle Creek Canyon also has strike-slip focal mechanisms (l-n, p). This activity suggests that the easternmost end of the San Gabriel Mountains is being sheared under the influence of the right-lateral San Jacinto fault system. Some northwest-trending faults have been mapped to the west of the Lytle Creek Canyon.



N. 38° E., 78° SE; N. 47° W., 70° SW.



N. 75° W., 70° S.; N. 26° E., 60° NW.



N. 48° E., 90° ; N. 42° W., 80° NE.

FIGURE 1.7.—Continued.

GLEN HELEN FAULT

A northwest trend of epicenters is located on the Glen Helen fault east of Lytle Creek. Focal mechanisms v and w indicate right-lateral motion similar to that on the San Jacinto fault system.

SAN ANTONIO CANYON

Two distinct clusters of microearthquake activity were detected in San Antonio Canyon near its juncture with the eastern end of the San Gabriel fault. Focal depths are shallow (2-5 km, good depth control), and three focal mechanisms (e-g) indicate oblique-reverse movement. The preferred fault plane is a northeast-trending near-vertical plane that parallels the trend of these two clusters of activity and the mapped faults in the canyon. The oblique-reverse sense of motion suggests that the east side of the San Antonio Canyon is being pushed up and northward relative to the west side.

EASTERN SIERRA MADRE FAULT

Little activity occurred on the portion of the range front fault west of San Antonio Canyon. This lack of activity is consistent with the low seismicity in this region noted from the CIT catalog (figs. 1.2 and 1.3). However, two deep microearthquakes (14 km) occurred in the San Gabriel Mountains west of San Antonio Canyon. Focal mechanism d suggests a northeast-southwest thrust motion for one of these deep events. It is difficult to determine, without further monitoring, whether or not these events occurred on the eastern Sierra Madre fault.

The largest event detected, a magnitude 2.9 earthquake, has its epicenter in the eastern San Gabriel Valley. This strike-slip event (focal mechanism aa) appears to have occurred on an unmapped fault beneath the San Gabriel Valley.

SAN JOSE-WALNUT CREEK FAULTS

Five epicenters are located near the San Jose and Walnut Creek faults. Focal mechanisms a and c plus one by Real (this volume) indicate left-lateral strike-slip movement on these northeast-trending faults. Focal mechanism b suggests the possibility of some compression and thrusting near the northern end of the San Jose Hills where the Walnut Creek fault turns more east-west. Further

monitoring with a portable network will be required to determine whether microearthquakes are actually occurring on these two faults, although this study and epicenters determined from the CIT regional seismograph network (figs. 1.2 and 1.3) suggest present activity.

FONTANA AND CHINO ACTIVITY

A pronounced concentration of microearthquake epicenters occurs beneath Fontana and the eastern Pomona Valley. This concentration of activity was first noticed by Hadley and Combs (1974). Focal mechanisms x and y indicate strike-slip movement. Although it is unclear what fault or faults these events lie on, a strong overall northeast-southwest lineation and several possible short northwest-southeast cross-cutting trends appear in the epicenter pattern. Future work using one or two strategically placed downhole seismometers in the eastern Pomona Valley in conjunction with portable surface seismographs could greatly improve resolution and the understanding of this seismic trend.

Another concentration of microearthquake activity occurs near Chino just northeast of the 1971-74 Chino swarm of magnitude 3+ earthquakes. Focal mechanism z indicates strike-slip movement similar to that observed beneath the rest of the Pomona Valley. A focal mechanism from the east side of the Chino swarm indicates strike-slip movement similar to focal mechanism z with a small component of dip-slip motion, but two focal mechanisms from the west side of the swarm show normal faulting on northeast-trending faults (D. Hadley, written commun., 1978). Perhaps, coincidentally, the Chino activity lies along the same overall northeast-southwest trend observed for the Fontana epicenters. Future work with downhole seismometers near Chino could prove useful in obtaining a better understanding of this activity.

TECTONIC SIGNIFICANCE

The inferred movements along the major faults in the study area based on focal mechanisms are shown in figure 1.8. Of primary interest are the tectonic forces acting on the easternmost tip of the San Gabriel Mountains, which we will refer to as the Cucamonga block. Although the complex interactions occurring in the study area are simplified in the diagram, it serves to highlight the general pattern of deformation in the area.

As discussed above and presented on figure 1.8, the triangular-shaped Cucamonga block exhibits relative

northward movement along its western and eastern boundaries, but shows relative southward movement along its southern boundary. Such movements appear contradictory considering the north-south compressive stresses throughout the region. In reality, the Cucamonga block has been detached from the rest of the San Gabriel Mountains and is being actively pushed northward and thrust up from the south.

Within the larger tectonic framework of southern California, the San Andreas fault system, particularly the San Jacinto fault, appears to be a major plate boundary. High rates of deformation and seismic-strain release, particularly on the San Jacinto to the south, support this concept. Continued northward movement of the Pacific plate forces the Peninsular Ranges province northward into the

Transverse Ranges—a major resistive element to movement along the plate boundary. The northern edge of the Peninsular Ranges province is being thrust under the San Gabriel Mountains. Because the Cucamonga block forms the easternmost point of the San Gabriel Mountains and is next to the active plate boundary, it has been sheared off from the rest of the San Gabriel Mountains along the faults in San Antonio Canyon and is presently being forced northward.

Internal deformation is also occurring in the Cucamonga block because of the tectonic forces acting upon it and because it is adjacent to an active plate boundary. The eastern part of the block is actively being sheared by internal right-lateral faults, as discussed in the previous section. Internal thrusting on a fault or faults north of the

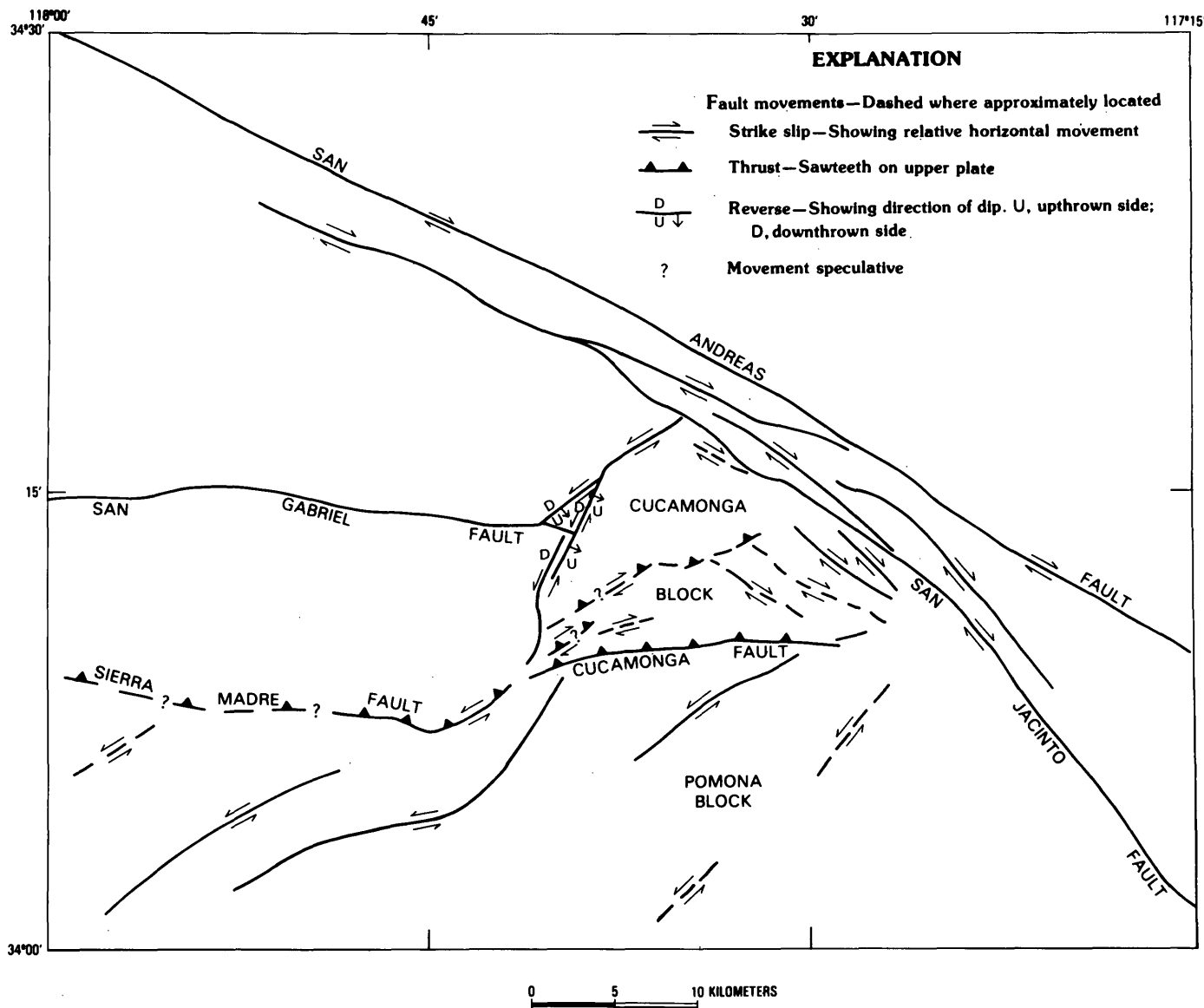


FIGURE 1.8.—Fault movements inferred from focal mechanisms in figure 1.7. See text for tectonic implications.

Cucamonga fault is suggested by composite focal mechanism k. Thus the east end of the block is accommodating the northward movement by horizontal shearing, whereas the central and western parts are meeting greater horizontal resistance to northward movement and hence are accommodating by vertical uplift. Such movements would explain why the greatest topographic relief is in the western part of the block and why the topographic relief decreases to the east within the block.

West of San Antonio Canyon the range front is farther south than along the south edge of the Cucamonga block. Also, topographic elevations and frequency of seismicity in historic times are lower here than in the Cucamonga block (figs. 1.2 and 1.3). These factors, as well as a greater distance from the major plate boundary represented by the San Jacinto fault, point to lower rates of tectonic deformation in the San Gabriel Mountains west of San Antonio Canyon than farther to the east.

The truncation of the San Gabriel fault at San Antonio Canyon is also explained by this tectonic model of the eastern San Gabriel Mountains. The recent northward movement and uplift of the Cucamonga block has cut off the older San Gabriel fault. Although several fault zones can be suggested as eastern extensions of the old San Gabriel fault within the Cucamonga block, more recent deformation and movement within the Cucamonga block has probably eliminated that older trace.

South of the San Gabriel Mountains, the dominant sense of motion is left lateral strike slip. Differential movements along these left-lateral faults are occurring in the northern Peninsular Ranges province as it forces its way northward and then adjusts to the movements of the Cucamonga block. Accordingly, the San Jose and Walnut Creek faults are major active tectonic features, movement along which corresponds with the northward yielding of the Cucamonga block. This concept is supported by both the historical and current seismicity near these faults. The high rate of seismicity near Fontana and Chino indicates a similar pattern of deformation closer to the major plate boundary where there is less resistance to the northward movement of the Peninsular Ranges block. The left-lateral sense of the Red Hill fault is thus explained. Also the alignment of the Red Hill fault with the eastern end of the Cucamonga fault may indicate that (1) movement along the Red Hill fault is controlling the orientation of the eastern end of the Cucamonga fault or (2) the left-lateral Red Hill fault truncates the Cucamonga fault at Bullock's Canyon.

CONCLUSIONS

This microearthquake survey of the eastern San Gabriel Mountains in the vicinity of the Cucamonga fault has provided new insight into the seismicity and tectonics of the

region. The data show a diffuse seismicity pattern under the San Gabriel Mountains between San Antonio Canyon and Lytle Creek. Concentrations of microearthquake activity occur along San Jacinto fault system and beneath Fontana—less activity occurring near Chino and beneath the San Jose Hills. Focal mechanisms indicate dominantly strike-slip fault movements except for thrust-fault movements in the core of the eastern San Gabriel Mountains. Focal depths within the San Gabriel Mountains are less than 10 km, but on the margins and in the surrounding areas, focal depths extend below 10 km, the deepest (17 km) occurring beneath Fontana. The deeper microearthquakes generally seem to be associated with strike-slip faults.

Microearthquake activity suggests that several faults may be active besides the San Andreas and San Jacinto faults. The Cucamonga fault appears to have had thrust-type microearthquakes on it about 7 km beneath Cucamonga Peak. Three microearthquakes suggest that the Red Hill fault is an active left-lateral strike-slip fault. Microearthquakes on the faults in San Antonio Canyon show oblique-reverse (left-lateral) movement. Several microearthquakes in the San Jose Hills indicate that the Walnut Creek fault and possibly the San Jose fault are active left-lateral faults. The microearthquake activity beneath Fontana and near Chino indicate the possibility of buried left-lateral faults beneath Pomona Valley at those two locations.

The fault movements indicated by our study of focal mechanisms provides a detailed picture of the tectonics of the eastern San Gabriel Mountains. The eastermost triangular tip (Cucamonga block) has been broken off the main body of the San Gabriel Mountains and is being forced northward and thrust up by the northward tectonic movement of the Peninsular Ranges province. Such movement fits the larger tectonic framework of the province, which apparently is being forced northward into the Transverse Ranges by plate-tectonic motion with the northern edge of the province being thrust under the San Gabriel Mountains. Internal deformation is occurring within the Cucamonga block. In the western part internal deformation is largely vertical, while in the eastern part it is largely horizontal shearing under the influence of the San Jacinto fault system. This picture explains the greater topographic relief to the west within the Cucamonga block. The observed northward movement of the Cucamonga block has truncated the older San Gabriel fault at San Antonio Canyon. West of the San Antonio Canyon, little seismicity and hence tectonic activity seems to be occurring in the San Gabriel Mountains. South of the San Gabriel Mountains, the northeast edge of the Peninsular Ranges province appears to be adjusting to the northward yielding of the Cucamonga block by left-lateral strike-slip movements on northeast-trending faults

such as the Red Hill, Walnut Creek, and San Jose faults, and a fault beneath the Fontana area. It seems that the movements along the Walnut Creek and San Jose faults, which trend into the faults in San Antonio Canyon, must be related to the northward movement of the Cucamonga block.

REFERENCES CITED

- Butler, J. L., Norris, D. O., and Yeats, R. S., 1977, A mechanical analysis of Santa Susana-San Fernando-type reverse faults, Transverse Ranges, California [abs.]: Eos (American Geophysical Union Transactions), v. 58, p. 1121-1122.
- Easton, J. P., O'Neill, M. E., and Murdock, J. N., 1970, Aftershocks of the 1966 Parkfield-Cholame, California, earthquake: A detailed study: Seismological Society of America Bulletin, v. 60, p. 1151-1197.
- Friedman, M. E., Whitcomb, J. H., Allen, C. R., and Hileman, J. A., 1976, Seismicity of the southern California region, 1 January 1972 to 31 December 1974: Pasadena, California, California Institute of Technology, Seismological Laboratory, 93 p.
- Fuis, G. S., Friedman, M. E., and Hileman, J. A., 1977, Preliminary catalog of the earthquakes in southern California July 1974-September 1976: U.S. Geological Survey Open-File Report 77-181, 107 p.
- Hadley, David, and Combs, James, 1974, Microearthquake distribution and mechanisms of faulting in the Fontana-San Bernardino area of southern California: Seismological Society of America Bulletin, v. 64, p. 1477-1499.
- Hadley, D., and Kanamori, H., 1977, Seismic structure of the Transverse Ranges, California: Geological Society of America Bulletin, v. 88, p. 1469-1478.
- Hileman, J. A., Allen, C. R., and Nordquist, J. M., 1973, Seismicity of the southern California region, 1 January 1932 to 31 December 1972: Pasadena, California, California Institute of Technology, Seismological Laboratory, 489 p.
- Jennings, C. W., 1975, Fault map of California: California Division of Mines and Geology, California Geologic Data Map No. 1, scale 1:750,000.
- Johnson, T. L., 1977, Seismicity of the eastern Transverse Ranges [abs.]: Eos, (American Geophysical Union Transactions), v. 58, p. 1121.
- Lahr, J. C., 1980, HYPOELLISE, a computer program for determining local earthquake hypocentral parameters, magnitude, and first motion pattern: U.S. Geological Survey Open-File Report 80-59, 65 p.
- Lee, W. H. K., Bennet, R. E., and Meagher, K. L., 1972, A method of estimating magnitude of local earthquakes from signal duration: U.S. Geological Survey Open-File Report, 29 p.
- McNally, K. C., Kanamori, Hiroo, Pechmann, James, and Fuis, Gary, 1978, Seismicity increase along the San Andreas fault, southern California: Science, v. 201, p. 814-817.
- Morton, D. M., 1976, Geological map of Cucamonga fault zone between San Antonio Canyon and Cajon Creek, San Gabriel Mountains, southern California: U.S. Geological Survey Open-File Report 78-728, scale 1:24,000.
- Real, C. R., Toppozada, T. R., and Parke, D. L., 1978, Earthquake catalog of California, 1900-1974: California Division of Mines and Geology (magnetic tape and microfiche).
- Yeats, R. S., Lee, W. H. K., and Yerkes, R. F., 1978, Geology and seismicity of the Red Mountain fault, Ventura County, California [abs.]: Eos (American Geophysical Union Transactions), v. 59, p. 385.

2. QUATERNARY GEOLOGY AND SEISMIC HAZARD OF THE SIERRA MADRE AND ASSOCIATED FAULTS, WESTERN SAN GABRIEL MOUNTAINS

By RICHARD CROOK, JR., C. R. ALLEN, BARCLAY KAMB, C. M. PAYNE, and R. J. PROCTOR¹

ABSTRACT

This detailed study of a 40-km-long section of the Sierra Madre and associated fault zones in the central Transverse Ranges, along the south side of the San Gabriel Mountains, is aimed at providing information for evaluating the seismic hazard that these faults pose to the heavily populated area immediately to the south. Evidence on the location of fault strands and the style and timing of fault movements during the Quaternary was obtained from detailed geologic mapping, aerial-photograph interpretation, alluvial stratigraphy, structural and stratigraphic relations in some 33 trench excavations at critical localities, and subsurface data.

We present a time-stratigraphic classification for the Quaternary deposits in the study area, based on soil development, geomorphology, and contact relations among the alluvial units. We distinguish four units, with approximate ages, as follows: unit 4, about 200,000 yr to middle Quaternary; unit 3: about 11,000 to 200,000 yr; unit 2: about 1,000 to 11,000 yr; and unit 1; younger than about 1,000 yr. We use this classification to evaluate on a semiquantitative basis the evidence for fault activity in the study area and to infer the relative seismicity of different segments of the Sierra Madre fault zone during the Quaternary. Alluvial-fan development (particularly fanhead incision and the ages of alluvial-fan deposits) also gives clues as to relative seismicity.

The most active segment of the Sierra Madre fault zone within the study area is the westernmost section, adjacent to the faults that broke during the 1971 San Fernando, Calif., earthquake. The age of activity, as indicated by the occurrence of Holocene faulting, decreases toward the east. Along the Sierra Madre fault, through La Cañada, Altadena, Sierra Madre, and Duarte, is abundant evidence of late Pleistocene faulting. Total vertical displacement is more than 600 m, but there is no evidence for Holocene fault movement. These observations suggest that the presently applicable recurrence interval between major earthquakes in the central and eastern sections of the Sierra Madre fault zone is longer than about 5,000 yr. The local magnitude (M_L) of the largest credible earthquake that could occur on the Sierra Madre fault zone in the study area is estimated at 7, on the grounds that the fault zone is probably limited mechanically by subdivision into separate arcuate segments about 15 km long.

The Raymond fault, which branches southwestward from the Sierra Madre fault in the eastern part of the study area, shows well-defined evidence of a late Quaternary history of repeated fault movements. Displacements of alluvial strata observed in trench excavations across the fault give evidence of five major seismic events, whose times of occurrence can be estimated from radiometric dating at approximately 36,000, 25,000, 10,000–2,200 (two events), and 2,200–1,500 yr B.P. Further evidence suggests at least three more faulting events in the past

29,000 yr, for which specific dates cannot be determined. Because some additional events probably remain undetected, we infer that an average recurrence interval of about 3,000 yr, with an average vertical displacement of 0.4 m per event, is applicable to the Raymond fault in its present state, as indicated by its history of movement over the past 36,000 yr. This level of activity is distinctly higher than that found for the Sierra Madre fault zone in the central and eastern parts of the study area. If the entire 15-km length of the Raymond fault would rupture in a single event, as seems likely, a maximum credible earthquake of $M_L 6\frac{1}{4}$ can reasonably be assumed.

INTRODUCTION

PURPOSE AND SCOPE

The purpose of this study is to understand better the seismic hazard posed by the frontal-fault system of the San Gabriel Mountains of southern California along a 40-km-long segment from the mouth of Big Tujunga Canyon to the mouth of San Gabriel Canyon. This segment of the fault system, known locally as the Sierra Madre fault, lies adjacent to or within the foothill communities of Sunland, Tujunga, La Crescenta, Glendale, La Cañada-Flintridge, Altadena, Pasadena, San Marino, Sierra Madre, Arcadia, Monrovia, Bradbury, Duarte, Azusa, and Glendora; the total combined population of these communities is approximately 350,000. Although it has long been recognized that this area shares a relatively high seismic exposure with the rest of southern California, particular impetus was given to this study by the 1971 San Fernando earthquake because the fault zone whose displacement caused this earthquake lies immediately adjacent west of, and is approximately continuous with, the Sierra Madre fault zone (fig. 2.1). The major question is whether or not these two areas share a similar seismic hazard. Indeed, it has even been suggested that because strain has already been relieved in the San Fernando segment, faults of the same system to the east and west are the most likely candidates for future earthquakes.

The investigative technique used in this study was primarily a field investigation of faults to determine their precise locations, subsurface configurations, seismic histories, and present activity. There is abundant evidence

¹All authors: California Institute of Technology, Pasadena, California.

Manuscript received for publication on October 1, 1981.

from worldwide experience that those faults that have had displacements most often in the recent geologic past—particularly the past 11,000 yr—are most likely to slip during significant earthquakes in the near future. Thus, in this study, we placed special emphasis on the determination of recent fault movement. To determine this movement required detailed and systematic mapping of the fault zones, mapping and interpretation of Quaternary alluvial and physiographic features, compilation of various kinds of information on subsurface fault configuration and displacements, and excavation of numerous trenches across faults suspected of being active. Most of our conclusions are based on the dating of faulted and unfaulted strata exposed in 33 trenches that were excavated as part of this study. This dating involved the use of standard radiometric techniques as well as the development of a time-stratigraphic classification for the Quaternary alluvial units exposed in the study area.

Historical seismicity is also an important clue to under-

standing seismic hazard; however, both the historical and instrumental records of earthquakes in southern California are so brief that extreme caution must be used in interpreting these statistically inhomogeneous data (Allen and others, 1965). The primary contribution of the present study is in looking farther back into the recent geologic history than is possible with the historical and instrumental data, so as to obtain a more meaningful statistical data base from which to extrapolate into the future. The current seismicity of the San Gabriel Mountains, particularly in terms of the focal mechanisms and tectonic implications of contemporary earthquakes, is discussed by Pechmann (this volume).

METHODS OF STUDY AND SOURCES OF INFORMATION

The basic method of study involved three principal elements: (1) delineation of fault traces by geologic mapping based on surface inspection, trenching, and inter-

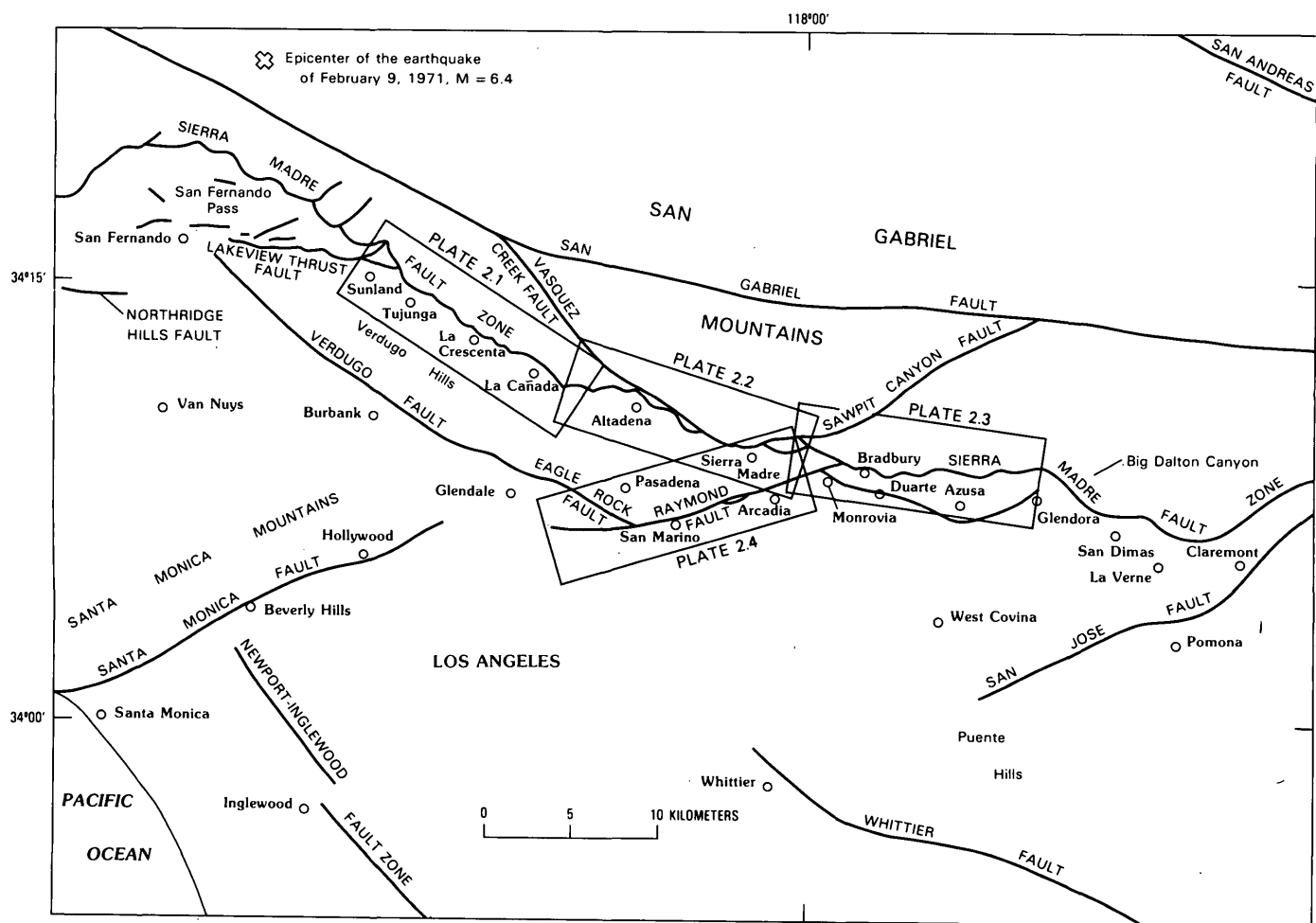


FIGURE 2.1.—Index map of study area in southern California, showing faults studied in this investigation (pls. 2.1-2.4) and their relation to other major fault systems in the Los Angeles area.

interpretation of aerial photographs; (2) determination of subsurface fault locations, configurations, and displacements from exploratory-borehole and water-well logs, from water levels, and from various geophysical data; and (3) deduction of the local history of fault movement by the use of chronologic information on the Quaternary deposits associated with fault traces.

GEOLOGIC MAPPING

Geologic mapping of the fault zones was done in the field at a scale of 1:12,000 on topographic base maps prepared from U.S. Geological Survey 7½-minute quadrangle sheets. The results, edited for presentation at a scale of 1:24,000, are presented in plates 2.1 though 2.4. Plates 2.1 through 2.3 cover the Sierra Madre fault zone in three segments from Big Tujunga Canyon on the west to the San Gabriel River on the east. The Raymond fault zone is shown in plate 2.4; its limits were chosen so as to include only those sections of the Raymond fault showing evidence for, or suspected of, Quaternary faulting.

Mapping was carried out during 1976 and 1977 with the assistance of Richard Lewis, Raymond Durkan, and Thomas Anderson. Where available, mapping by other workers was field checked and either used intact or altered where our opinions differed or where new exposures exist. Use was made of maps prepared by the following authors and agencies: Eaton (1957) and Beattie (1958), at the southwest and extreme west ends of plate 2.1; the Metropolitan Water District of Southern California (unpub. data, 1964–74), on plates 2.2 and 2.3; Morton (1973), in the east half of plate 2.2 and on plate 2.3; Saul (1976), central portion of plate 2.2; California Division of Mines and Geology (1964), at the extreme east end of plate 2.3; Buwalda (1940) on plate 2.4; and Lamar (1970) at the extreme west end of plate 2.4. Stratigraphic nomenclature and age assignments of stratigraphic units may not necessarily be those adopted by the U.S. Geological Survey.

AERIAL PHOTOGRAPHS

Extensive use was made of the oldest available aerial photographs. These are the Spence oblique aerial photograph collection (1922–52) at the University of California, Los Angeles (UCLA), Geography Department, and the Fairchild aerial photograph collection (1928–60) at the Whittier College Geology Department, Whittier, Calif. More recent aerial photographs were also examined. Special photographs for this study were taken on January 8, 1976, by I. K. Curtis, who provided a set of 48 vertical photographs at a scale of 1:12,000. Ground-view photographs dating back to the 1880's were also examined at the Henry E. Huntington Library in San Marino.

TRENCHING

A total of 33 trenches were excavated and logged during this project (table 2.1). The important features observed and conclusions reached are summarized below in the supplementary section entitled "Trenching." In addition, trenching by other workers helped to define the Raymond fault at localities 64, 67, and 68 (pl. 2.4).

DRILLING

A series of 14 exploratory boreholes were drilled at the Jet Propulsion Laboratory (JPL) of the California Institute of Technology (CIT) in 1977; the drilling and logging were done by Le Roy Crandall & Associates under contract to JPL. We selected 11 of the borehole sites in an effort to delineate the number and location of the branches of the Sierra Madre fault zone beneath JPL; The results of this study are described below (see pls. 2.2 and 2.6).

RADIOCARBON DATING

All materials penetrated in trenches or exposed in outcrops and suspected of containing carbonaceous remains were sampled for radiocarbon dating. A total of 13 samples were deemed significant enough in placement and rich enough in carbon to be dated (see table 2.2).

SEISMIC-REFRACTION AND MAGNETOMETER SURVEYS

Unpublished information obtained from surveys by the Envicom Corp. and by Le Roy Crandall & Associates was utilized in the Duarte-Azusa area to help locate buried fault traces at localities 30 and 32 through 34 (pl. 2.13).

CLAST SOUND-VELOCITY MEASUREMENTS

We developed and tested a new method for ascertaining on a quantitative basis the relative ages of alluvial units. The extent of weathering of clasts of a definite, recognizable lithology was determined by measuring the seismic-wave velocity of the clasts, which decreases with increasing weathering. Seismic velocity was measured with a portable instrument used commercially for measuring the speed of sound in concrete (see appendix entitled "Measurement of Progressive Clast Weathering").

BOREHOLE-LOG AND WATER-LEVEL DATA

We searched the water-well files of the Los Angeles County Flood Control District for pertinent information contained in driller's logs and for water levels as they per-

RECENT REVERSE FAULTING IN THE TRANSVERSE RANGES, CALIFORNIA

TABLE 2.1.—Summary of data from trenches excavated across the Sierra Madre and Raymond faults

[CDMG, California Division of Mines and Geology; CIT, California Institute of Technology; LA, Leighton & Associates, Inc.; LRCA, Le Roy Crandall & Associates; USGS, U.S. Geological Survey]

Trench	Fault	Location of excavation*	Property owner	Excavation method	Fault exposed	Mapped by	Map scale	Photographs taken	No. of samples taken for ^{14}C dating	Date excavated
1	Raymond	Foothills Junior High School athletic field, Arcadia	City of Arcadia	Backhoe	No	CIT	1:60	Yes	3	12/22/76
2	Sierra Madre	Arroyo Seco channel, N. of JPL bridge, Pasadena	City of Pasadena Water Department	--do--	Yes	--do--	1:24, 1:60	Yes	0	12/29/76
3	--do--	Eaton Canyon toll road, west of bridge	City of Pasadena	--do--	Yes	--do--	1:60, 1:300	Yes	0	1/5/77
3A	--do--	--do--	--do--	--do--	No	--do--	Not mapped	No	0	2/1/78
4	--do--	East of Pasadena Glen, west of Hastings Canyon Pasadena	City of Pasadena and Natural U.S. Forest Service	Backhoe	Yes	--do--	not mapped	Yes	0	1/5/77
5	Raymond	Clairbourn School, south of athletic field, San Marino	Clairbourn School, San Marino	Backhoe	No	CIT, LA	1:60	No	0	2/4/77
6, 6A	Raymond	Toe of slope on north side of ridge, Los Angeles County Arboretum, Arcadia	Los Angeles County	--do--	No (?)	CIT	1:48 (6A not mapped)	Yes	0	2/2/77
7	--do--	Sunnyslope Reservoir, near southeast corner of reservoir	Sunny Slope Water Co.,	--do--	Yes	--do--	1:24	Yes	7 (15 paleo-magnetic)	2/16- 2/18/77
8	--do--	Lacy Park, northwest corner near tennis courts	City of San Marino	--do--	No	--do--	1:24, 1:48	Yes	2	3/2/77
9	Sierra Madre	JPL northwest of Building 32	JPL, Pasadena	Backhoe and natural exposure	Yes	CIT, LRCA	1:24	Yes	Calcite crust on cobble in gouge, 1,000-2,000 yr (USC)	2/23/77
10	--do--	Behind JPL Building 150	--do--	Hand	Yes	CIT	Sketch	Yes	0	2/77
11	--do--	Monastery north of Sunnyside, Sierra Madre	U.S. Forest Service	--do--	Yes	--do--	1:24	Yes	2	3/77
12	--do--	Gould Canyon	--do--	--do--	Yes	--do--	Sketch	No	1	4/13/77
13	--do--	Duarte, west of Van Tassel Canyon	Emblem Homes	Backhoe	No	--do--	1:24	No	1	6/20/77
13A	--do--	--do--	--do--	--do--	No	--do--	1:24	No	1	7/20/77
14	Raymond	San Marino High School	San Marino City Schools	--do--	Yes	CDMG, CIT, LRCA	1:24	Yes	6	8/19- 8/22/77
14A	--do--	--do--	--do--	--do--	Yes	--do--	1:24	No	2	8/29- 8/30/77
15	--do--	Edison right-of-way, Chapman Woods	Southern California Edison Co.	--do--	Yes	CIT, USGS	1:24	Yes	3	10/19- 10/21/77
16,	Sierra Madre	Debris basin behind Rubio Dam, east side	Los Angeles County Flood Control District	Tracked front-end loader	No	Sketched by CIT	--	Yes	0	11/22/77
16A	--do--	East of spreading grounds, Santa Anita Wash	Metropolitan Water District	--do--	No	Not mapped	--	No	0	11/30/77

TABLE 2.1.—Summary of data from trenches excavated across the Sierra Madre and Raymond faults—Continued

Trench	Fault	Location of excavation*	Property owner	Excavation method	Fault exposed	Mapped by	Map scale	Photographs taken	No. of samples taken for ^{14}C dating	Date excavated
18A	--do--	Spoil area west of Dunsmore Dam	Los Angeles County Flood Control District	--do--	Yes	CIT	1:24	Yes	1	1/18-1/20/78
18B	--do--	--do--	--do--	--do--	Yes	--do--	1:24	Yes	0	1/18-1/20/78
18C	--do--	--do--	--do--	--do--	Yes	--do--	1:24	Yes	0	1-18-1/20/78
19	--do--	Bradbury-Duarte boundary, south of mesa	Allen E. Bostwick	Backhoe	No	--do--	1:120	Yes	0	12/20/77
20A	--do--	North of Sierra Madre Villa Dam	Coast Federal Savings and Loan Association	--do--	Yes	--do--	1:24	Yes	0	1/25/78
20B	--do--	--do--	--do--	--do--	Yes	--do--	1:24	Yes	0	1/25/78
20C	--do--	--do--	--do--	--do--	Yes	--do--	1:24	Yes	1	1/26/78
21A	--do--	JPL, Northwest of Building 32	JPL, Pasadena	--do--	No	--do--	1:60	No	0	7/10-7/11/78
21B	--do--	--do--	--do--	--do--	No	--do--	1:60	No	0	7/11-7/12/78
21C	--do--	--do--	--do--	--do--	No	Not mapped	--	No	0	7/13/78
22	Raymond	Sunny Slope Reservoir, Pasadena	Sunny Slope Water Co.	Poplain excavator	Yes	CDMG, CIT	1:24	Yes	3	9/78

*See Appendix 1 for more precise locations.

tain to ground-water barriers or buried faults. Additional borehole-log information was supplied by the Metropolitan Water District of Southern California. Information gathered from this search that proved to be important is noted on the geologic maps (pls. 2.1-2.4).

CONSULTANT GEOTECHNICAL REPORTS

Locally, in La Cañada-Flintridge, Arcadia, and Duarte, we obtained information on fault locations from geotechnical reports and geologic maps prepared by private consultants.

ACKNOWLEDGMENTS

In the course of this study, we benefited from the help and cooperation of many individuals and organizations. Workers who made geologic and geophysical information available to us are acknowledged specifically in the preceding section. In addition, we thank the following people and organizations for help in carrying out our work:

Donald Asquith of the Envicom Corp.; Glenn Brown, of Le Roy Crandall & Associates; Greg Davis, of the University of Southern California; Michael Hart, of the Sunny Slope Water Co., Pasadena; Robert Hill and Drew Smith of the California Division of Mines and Geology; Harry Kues and Michael Johnson of the Los Angeles County Flood Control District; Clarence Levoe and Frederick Springate of JPL; James McCalpin, Douglas Morton, John Tinsley, and Robert Yerkes of the U.S. Geological Survey; Kerry Sieh and James Westphal of CIT; Robert Sydnor of Leighton & Associates, Inc.; Thomas Underbrink of the Pasadena Water and Power Department; and Converse Consultants, Pasadena. Landowners in the study area, too numerous to acknowledge individually, were helpful in allowing access to their properties.

This study was supported by U.S. Geological Survey Contract 14-08-0001-15258; the drilling program at JPL was supported by the U.S. National Aeronautics and Space Administration. This report was previously published as Contribution No. 3191, Division of Geological and Planetary Science, California Institute of Technology, Pasadena, CA 91125.

TABLE 2.2.—Radiocarbon samples and ages

[All ages based on the Libby half-life of carbon-14 of $5,570 \pm 30$ yr. n.a., not analyzed]

Sample (laboratory No.)	Locality	^{14}C age (yr)	Sample type	Depth of burial	Sedimentation rate (mm/yr)
Raymond fault					
C-3 (WSU 1834)	Sunny Slope trench 7	¹ $25,400 \pm 700$	Organic silty clay	3.7	0.15
C-4 (WSU 1835)	--do--	¹ $25,500 \pm 590$	Peat	3.3	.13
C-5 (WSU 1836)	--do--	¹ $25,500 \pm 640$	Organic silty clay	3.3	.13
C-6 (WSU 1837)	--do--	¹ $2,160 \pm 105$	Soil	(²)	--
C-9 (WSU 1838)	--do--	¹ $20,990 \pm 440$	Organic silty clay	(²)	--
C-16 (USGS 407)	San Marino trench 14	³ $35,800 \pm 1,300$	Clayey peat	3.8	.11
C-17 (USGS 403)	--do--	³ $29,100 \pm 400$	Peat	3.0	⁴ .10
C-18 (WSU 1849)	--do--	¹ $10,600 \pm 160$	Organic silt	1.9	.18
C-19 (WSU 1850)	San Marino trench 14	¹ $6,060 \pm 110$	Soil	.9	.15
C-20 (WSU 1851)	San Marino trench 14A	¹ $3,575 \pm 100$	--do--	.8	.22
C-21 (WSU 1852)	--do--	¹ $1,630 \pm 100$	--do--	.5	⁵ --
CDA (GX 3239)	Sunny Slope trench (1973)	⁶ $2,920 \pm 180$	--do--	(²)	--
Sierra Madre Fault					
C-23 (UCLA 2079A)	Eaton Canyon	⁷ 200 ± 80	Charcoal	n.a.	--
C-24 (UCLA 2079B)	Pasadena Glen trench 20C	⁷ $2,200 \pm 80$	Wood	n.a.	--

¹Analyst, J. C. Sheppard, Washington State University, Pullman.²Sample out of place owing to faulting.³Analyst, Stephen Robinson, U.S. Geological Survey, Menlo Park, Calif.⁴Rate between samples C-16 and C-17 is 0.12 mm/yr.⁵Rate between samples C-20 and C-21 is 0.14 mm/yr.⁶Analyst, Geochron Laboratories, Cambridge, Mass.⁷Analyst, C. R. Berger, University of California, Los Angeles.

LITHOLOGIC UNITS

PRE-TERTIARY ROCKS

The rocks that make up the crystalline basement of the San Gabriel Mountains have been described in detail by Miller (1934), Morton (1973), Ehlig (1975), and Saul, (1976), and are described only briefly here. The rocks are a highly complex mixture of materials of metamorphic and igneous origin, ranging in age from 19 m.y.B.P. to at least 1.4 b.y.B.P. (Hsu and others, 1963; Silver and others, 1963).

GNEISS

The oldest and most complex unit in the study area is the gneiss that occurs throughout the study area (pls. 2.1-2.4). This gneiss is complex in both structure and

metamorphic facies. It is generally well banded and moderately well to well foliated; both features trend northwest, transverse to the mountain front. The rock is composed predominantly of quartzofeldspathic gneiss containing local patches of amphibolite and biotite schist. Locally, metasedimentary units (for example, marble and calcsilicates) occur in the Monrovia outlier and in Fish Canyon. The gneiss is pre-Cretaceous in age.

RUBIO DIORITE OF MILLER (1934)

The Rubio Diorite of Miller (1934) intruded the gneiss and now occurs as discontinuous bodies in the gneiss and as xenoliths in the Cretaceous intrusive rocks between Millard and Santa Anita Canyons (pl. 2.2). The unit occurs in close proximity to, or is encompassed within, the Vasquez Creek fault zone between Millard and Eaton

Canyons and is associated with the Sierra Madre fault zone east of Eaton Canyon. The diorite is characteristically very dark and is rich in hornblende, biotite, and plagioclase. Locally it is very coarse grained (pegmatitic); hornblende crystals are several centimeters long. The Rubio Diorite is pre-Cretaceous in age.

LOWE GRANODIORITE OF MILLER (1934)

The Lowe Granodiorite of Miller (1934) is one of the most distinctive rock types in the San Gabriel Mountains. Characteristically it is light gray to white and contains large black phenocrysts of hornblende and biotite and, commonly, large gray phenocrysts of potassium feldspar. Silver (1971) dated the rock at 220 ± 10 m.y.B.P. (Triassic).

This unit does not crop out within the study area but occurs in the upper reaches of all the major and most of the smaller drainages between the Arroyo Seco and Santa Anita Canyon. Therefore, clasts of this unit are found in nearly all the Quaternary alluvial units. We have developed a quantitative method of measuring the degree of weathering of these clasts to determine the relative ages of the Quaternary units (see appendix entitled "Measurement of Progressive Clast Weathering").

WILSON DIORITE OF MILLER (1934)

The Wilson Diorite of Miller (1934) is the most widespread rock type in the study area and the most consistent lithologically. It is exposed nearly continuously along the mountain front from Big Tujunga Canyon to San Gabriel Canyon. The Wilson Diorite is a gray medium- to coarse-grained biotite-hornblende quartz diorite, generally massive but locally foliated. It intrudes all of the previously described units. The Wilson Diorite was dated by Larson and others (1958) at 122 m.y.B.P. (Cretaceous).

QUARTZ MONZONITE AND GRANODIORITE

Another widespread plutonic unit is a gray to tan fine- to medium-grained quartz monzonite and granodiorite that occurs as small lenticular bodies and dikes. This unit intrudes all the previously described units.

TERTIARY ROCKS

INTRUSIVE ROCKS

Unmetamorphosed hypabyssal intrusive dikes of various compositions are common in several areas along the mountain front. Only the larger dikes are shown on the maps (pls. 2.1-2.3); they are presumably Miocene in age.

VOLCANIC AND SEDIMENTARY ROCKS

Volcanic and sedimentary rocks of Tertiary and inferred Tertiary age are exposed at the west and east ends of the study area. All these rocks are moderately to highly deformed and faulted, and all are unconformably overlain by deposits of Quaternary age.

In the Sunland-Tujunga area (pl. 2.1), these deposits consist of volcanic flows and sandstone—the middle Miocene Topanga Formation; shale and siltstone—the upper Miocene Modelo Formation; sandstone and conglomerate—commonly called the Pliocene Pico Formation by some workers; and upper Pliocene(?) conglomerate composed mainly of volcanic clasts. All these units are highly deformed and dip steeply, and all are faulted. All contacts with the pre-Tertiary basement are faulted.

In the Bradbury area (pl. 2.3), the Tertiary deposits consist of middle Miocene conglomerate and sandstone, as well as small amounts of shale and volcanic flows—the Topanga Formation (Shelton, 1955); the Pliocene(?) Duarte Conglomerate (Shelton, 1946); and Pliocene and Pleistocene sandstone, siltstone, and conglomerate—the Saugus Formation.

The Duarte Conglomerate is a relatively massive moderately well consolidated conglomerate containing well-rounded clasts as large as 1 m in diameter. The presence of clasts of the Pelona Schist, mylonitic augen gneiss, and the Lowe Granodiorite, indicates that the source of the clasts was the San Gabriel River drainage. The Duarte Conglomerate unconformably overlies or is faulted against the older Topanga Formation (pl. 2.3; fig. 2.13) and is unconformably overlain by and faulted against the younger unit 4 alluvium.

A distinctive sedimentary unit consisting of alternating beds of relatively clean sandstone, pebble- to cobble-size conglomerate, and red siltstone occurs in the Ruby Canyon-Monrovia Canyon area (pl. 2.8; fig. 2.12). This unit is very similar in appearance to the Pliocene and Pleistocene Saugus Formation in the Sunland area of northern San Fernando Valley.

QUATERNARY DEPOSITS

Among the most striking features in the study area are the large, sweeping alluvial-fan surfaces at the foot of the steep mountain front in the La Cañada-La Crescenta and San Gabriel Valleys (fig. 2.2). These large fans consist of hundreds of meters of sand and gravel deposits derived from the San Gabriel Mountains since middle Pleistocene time. These deposits are important to this study because they reflect the tectonic history of the San Gabriel Mountains.

We recognized at the outset of this study that a means of classifying the Quaternary deposits according to age

is necessary to determine the faulting history and to evaluate the seismicity of the Sierra Madre and Raymond fault zones. We here propose an informal four-part classification that can be applied to all the Quaternary deposits studied. The four units are classified on the basis of geomorphic relations, topographic position, stratigraphic position, and degree of soil development, as shown diagrammatically in figure 2.3. Other, less tangible but equally important criteria are color, grain size, clay content, degree of consolidation, and degree of clast weathering (as determined by both visual and clast-sound-velocity methods). This classification is similar to that of Buwalda (1940), although he used only three designations.

The basic differences between the four units are best indicated by the criteria listed above. These differences result from processes that are dependent upon time, temperature, water content, parent material, and geomorphic position. A basic assumption made in this classification is that time is the most significant variable. More detailed discussions of the classification criteria are presented in the sections on the individual units below.

UNIT 4

The oldest alluvium mapped in the study area, unit 4, is age correlative with the Pleistocene San Dimas Formation of Eckis (1928), but because this name has been used by other workers to include units we consider to be much younger, we prefer our informal designation. Within the study area, this unit consists of poorly consolidated to well-consolidated fine to coarse alluvial sand, silty sand and gravel, gravelly sheetflood deposits (McGee, 1897), and minor amounts of coarse debris-flow or mudflow deposits. These deposits are generally distinguished by

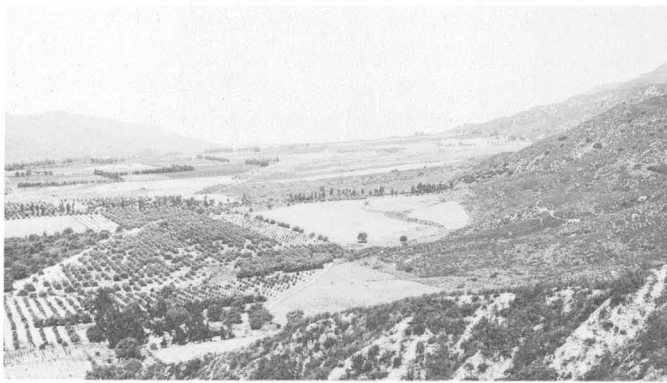


FIGURE 2.2.—Alluvial fans in La Cañada-La Crescenta area. Buried branch of Sierra Madre fault zone lies approximately at break in slope between fan surfaces and mountain front. Steeper slopes (upthrown block) consist of unit 4 alluvium (foreground) and crystalline basement (background); fans consist of unit 1 alluvium (foreground), unit 3 alluvium (center), and unit 4 alluvium (skyline). View westward from Gould Mesa above JPL. Photograph courtesy of Huntington Library collection.

having several or all of the following properties: red to reddish-yellow (2.5YR to 5YR) hues, low to high clay content, chalky-white feldspar sand grains, highly weathered clasts of all rock types, and fractures or joints with or without cementation. These properties are most obvious where a soil profile has developed but are also found throughout the deposits. Pedogenic processes apparently intensify the development of these characteristics, but they seem to continue to develop in deposits removed from the soil zone by burial.

Almost the entire Sunland-Tujunga-La Crescenta area is devoid of exposures of unit 4. The unit probably exists below younger alluvial deposits, but at the surface it is restricted to one small fan at the mouth of Rowley Canyon and several small remnants between Haines and Cooks Canyons (pl. 2.1).

The west half of the city of La Cañada is built on a composite unit 4 fan surface. This surface, the ancient La Cañada fan, formed from coalescing fans from Snover, Hall Beckley, Winery, and Hay Canyons and probably was once continuous with the Gould Mesa surface but has been displaced from it along the Sierra Madre fault zone.

Unit 4 of the La Vina fan extends from Gould Mesa eastward almost to Lake Avenue in Altadena (pl. 2.2). These deposits, which have been extensively eroded by both large and small drainages, offer excellent exposures. Below Gould Mesa, on the west side of the Arroyo Seco is a continuous exposure, more than 90 m thick. Here, the deposits consist of discontinuous beds and lenses of poorly to moderately well sorted fine to coarse sand and pebble, cobble, and boulder gravel; clasts are generally subrounded to rounded. Boulders as much as half a meter in diameter are common, and some exceed a meter in diameter. Clast lithologies vary considerably but are typical of those found in recent alluvium of the Arroyo Seco. All the clasts are highly weathered; the clasts of the Lowe Granodiorite in this unit have the lowest seismic velocity of such clasts in all the alluvial units (see supplementary section below entitled "Measurement of Progressive Clast Weathering"). This exposure also contains a buried soil (B horizon), approximately 15 m above the canyon bottom; remnants of a buried B horizon are also exposed in a small canyon southeast of La Vina Sanitarium.

A nearly complete profile of the highly developed soil typical of unit 4 is exposed on a housing pad on the ridge south of the La Vina Sanitarium. This soil is also evident on the Gould Mesa surface and continues, unfaulted, down over the south face of the mesa to the base of the slope near JPL Building 251.

At Monk Hill, approximately 3.5 km south of the frontal-fault system, a small patch of unit 4, exposed at the surface, surrounds a small outcrop of quartz-rich metasedimentary rock.

Several small fault-bounded unit 4 blocks, exposed between Rubio and Eaton Canyons, have been raised above the Altadena fan surface along a branch of the Sierra Madre fault zone. The highest surfaces have a moderately well developed soil, though not so highly developed as that on the La Vina-Gould Mesa surfaces.

Unit 4 between Eaton and Santa Anita Canyons consists mainly of the coarse alluvial facies; the finer sheet-flood facies crops out between Pasadena Glen and Hastings Canyon. In this reach, most of the original unit 4 fan surface has been removed by erosion and covered by younger alluvial units or faulted basement. A few isolated original depositional surfaces are exposed in Eaton Canyon, Little Santa Anita Canyon, and high on a ridge east of Bailey Canyon.

The Eaton Canyon deposit is unusual in that unit 4 appears to be composed of two subunits separated by an erosional surface. Both subunits consist of fine- through coarse-grained sand containing a few layers and lenses of pebble-cobble gravel and a few scattered boulders. Although the lower subunit has been eroded, the remnants of the B horizon appear more highly developed than the B horizon of the upper subunit. Both subunits and the erosional contact are visible beneath the transmission towers just north of the Civil Defense Center on New York Drive.

In the Pasadena Glen-Hastings Canyon area, the unit 3 fan surface is underlain at a depth of 2 to 3 m by a unit 4 fan with a paleosol at its upper surface that appears equivalent in development to the soil on the upper unit 4 unit in Eaton Canyon. These deposits are the sheetflood facies, with thick (max 3 m) sequences of massive fine-grained silty sand containing a few boulders as much as 2 m in diameter.

Unit 4 on the ridge above Bailey Canyon consists of a 15-m-thick section of crudely bedded silty sand containing numerous angular to subrounded pebbles and cobbles. The upper surface includes a reddish-brown soil containing abundant clay. This is the highest occurrence (elev, 762 m) of alluvial deposits within the study area.

Unit 4 exposed in Little Santa Anita Canyon is the coarse alluvial facies, containing numerous rounded boulders of the Lowe Granodiorite and the Wilson Diorite, all highly weathered. Small remnants of the original fan surface remain on the east side of the canyon, but most of the surface has been stripped by erosion.

The Monrovia outlier between Santa Anita and Monrovia Canyons contains numerous small remnants of unit 4, once part of a fan surface that covered the entire low-lying block of crystalline basement (pl. 2.3). This surface, here named the "Alta Vista surface," can be traced nearly

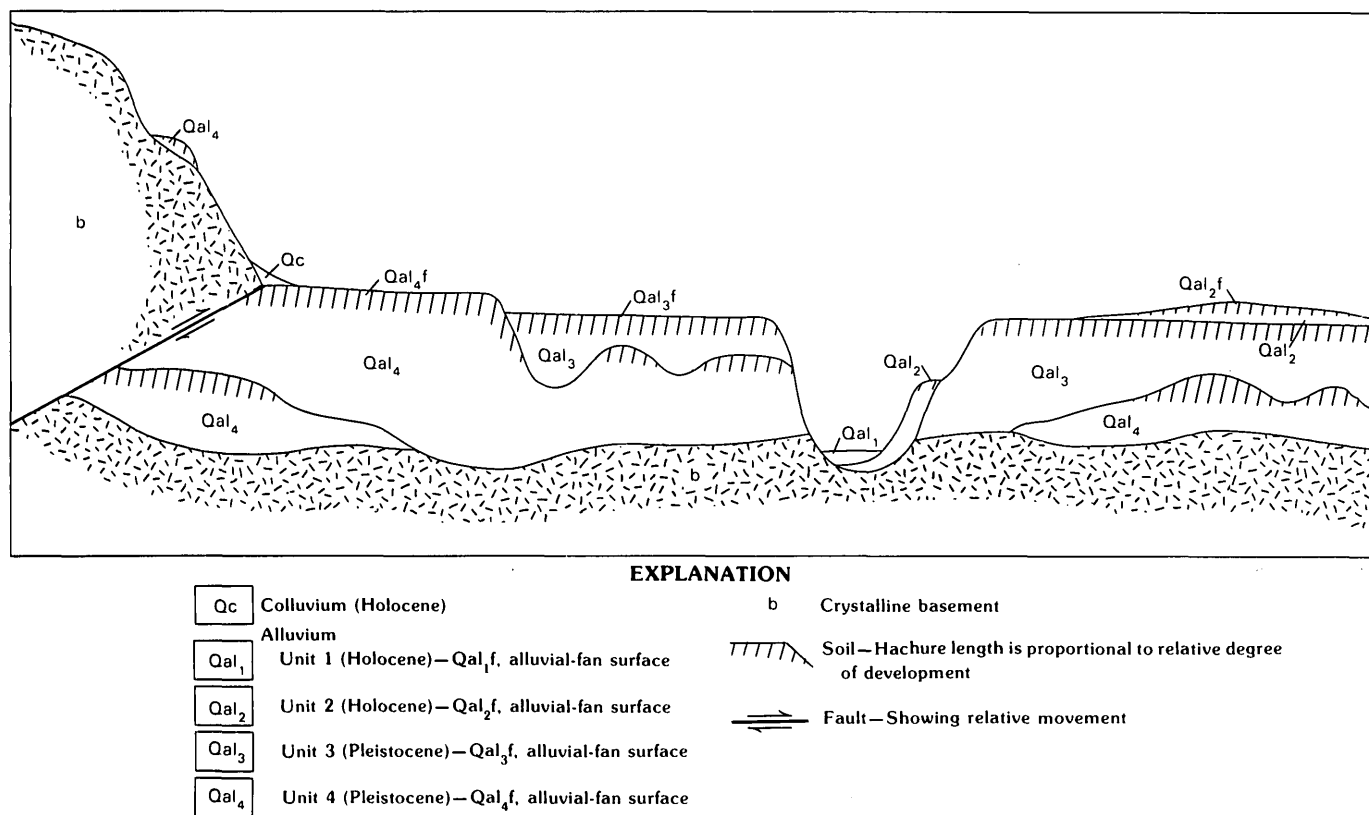


FIGURE 2.3.—Diagrammatic cross section of Quaternary alluvial units and geomorphic surfaces.

continuously for about 1.6 km up Monrovia Canyon, but nearly all of the surface along Santa Anita Canyon has been eroded away.

Most of unit 4 in this area consists of moderately well consolidated medium to coarse sand and pebble and cobble gravel, with a few boulders 1.5 m in diameter. Clasts range from subangular to rounded and all are highly weathered. All the deposits have a highly developed soil at their upper surface, although erosion has removed the upper part from most of the small remnants. The deposits underlying the surface along Alta Vista Drive are finer grained, have a sheetflood-mudflow origin, and include a more highly developed soil than elsewhere on the surface. The higher degree of soil development may be due in part to the fine-grained texture of the deposit.

The Bradbury area contains extensive deposits of unit 4, as well as remnants of the original fan surfaces. These deposits consist of both the coarse-grained alluvial sand and gravel and the finer grained sheetflood deposits. Some unusually fine-grained deposits in the Norumbega Drive area west of Bradbury are composed of silty fine-grained sand, silt, and some clay. All remnants of the original fan surfaces have a highly developed soil on them. The distribution of unit 4 east of the San Gabriel River was taken from the maps by Streitz (1964) and Morton (1973) by correlating the units that were mapped by them as the San Dimas Formation with our unit 4.

UNIT 3

By far the most abundant of the exposed Quaternary deposits mapped in the study area is unit 3. Most earlier workers lumped unit 3 with our unit 4 and called them earlier alluvium (Mendenhall, 1908) or older alluvium (Eckis, 1934). It was not until Buwalda's (1940) study of the Raymond Basin that these deposits were recognized as a separate unit, which he designated "old alluvium" as distinct from "recent alluvium" and "ancient alluvium."

The unit 3 deposits form most of the alluvial fans between the Arroyo Seco and Santa Anita Canyon, and a few of the fans between Big Tujunga Canyon and the Arroyo Seco. These deposits, in addition to the typical coarse-grained alluvial sand and gravel and sheetflood deposits, include a facies of very large boulders. This facies generally consists of 80 percent or more of cobbles and boulders, many with diameters of more than a meter; 2- to 3-m sizes are common. These deposits occur at the mouths of the present larger drainages; a good exposure is along the Mount Wilson Toll Road at the mouth of Eaton Canyon (pl. 2.2).

Distinguishing characteristics of unit 3 are: yellow through yellowish-brown to pale-brown hues (7.5YR to 10YR), unconsolidated to moderately consolidated, little to no clay, unaltered feldspar sand grains, no fractures

or joints such as are common in unit 4, moderately to highly weathered clasts with moderate to high biotite content, relatively fresh and hard clasts with little or no biotite, and moderately high seismic velocities in clasts of the Lowe Granodiorite. Where undisturbed, surfaces of unit 3 have a poorly developed soil profile. Near the fan heads this profile generally consists of an A horizon and a cambic B horizon (Soil Survey Staff, 1975). The older surfaces on distal parts of the larger fan surfaces may have a poorly to moderately developed textural B horizon, examples of which are visible in Interstate Highway 210 roadcuts in western Pasadena. This more advanced development is probably due in part to the older age and in part to the finer parent material that occurs in distal parts of the fan (Eckis, 1938).

In the area between Big Tujunga and Blanchard Canyons, unit 3 consists of isolated remnants of fan heads and stream terraces along the lower parts of the larger drainages. The original fan surfaces are still recognizable in a few localities, for example, above Sunland and in Cooks Canyon, but most of the deposits have been removed by erosion subsequent to uplift along the frontal-fault system.

Most of the fans between Blanchard and Pickens Canyons are composed of unit 3. All except the Dunsmore fan are incised at their heads and offer good exposures. Some fans, such as in Shields and Pickens Canyons, appear to be offset near their heads by the frontal faults (locs. [3] - [6], pl. 2.1).

The Altadena fan, the largest example of a unit 3 fan (pl. 2.2), is actually a composite feature formed by a series of coalescing fans. The Altadena fan is bounded on the west and east by the incised Arroyo Seco and Eaton Canyon, and on the north and south by the Sierra Madre and Raymond fault zones. Excellent exposures of the deposits are afforded in both the Arroyo Seco and Eaton drainages. Along the Arroyo Seco the deposits consist of crudely bedded moderately consolidated to loose sand and gravel containing boulders as much as half a meter in diameter; locally, some of the finer sand layers contain minor amounts of red clay. Near the mouth of Eaton Canyon the deposits are the large-boulder facies. Farther downstream, this facies gives way to the normal coarse-grained sand and gravel, which is visible unconformably overlying unit 4 about 750 m north of New York Drive.

Profiles drawn radially down the Altadena fan surface show it to be a segmented fan, typical of an area undergoing periodic uplift (Bull, 1964). A comparison of the surface soil at the fan head at Las Flores Canyon and the lower fan surface along Interstate Highway 210 indicates that the lower fan surface is distinctly older.

The Arroyo Seco and Millard Canyon contain remnants of stream-cut terraces covered with thin deposits of unit 3. Most of these deposits are on crystalline basement, but

a few are on surfaces cut in unit 4, for example, the high surface at the confluence of Millard Canyon and the Arroyo Seco. The Kinneloa and Sierra Madre fans are mapped as unit 3, although their soil development, clast weathering, and stage of dissection indicate they probably consist of older deposits of unit 3. The Hastings fan also contains unit 3 deposits, but their stratigraphic position, high seismic velocities of clasts, and the more youthful appearance of the fan suggest that these deposits represent some of the youngest unit 3.

A small remnant of the unit 3 fan that once extended southward from the mouth of Santa Anita Canyon is exposed along the access road to Arcadia Wilderness Park. This is the large-boulder facies, which has been overthrust by crystalline basement (loc. ④8, pl. 2.2).

Between Santa Anita Canyon and the San Gabriel River, unit 3 consists of three remnants of a fan surface in Monrovia Canyon. These deposits are the large-boulder facies and are exposed along both canyon walls and in the east wall of Ruby Canyon. Apparently most of this area north of the frontal-fault system never had unit 3 deposited on it.

UNIT 2

Unit 2 consists of fluvial and alluvial-fan deposits of unconsolidated gray through olive to pale brown (5YR to 10YR), fine to coarse sand and pebble, cobble, and boulder gravel. The clasts are subangular to rounded, as much as 2 m in diameter, and generally unweathered, although some of the biotite-rich rock types are moderately weathered. Soil development on this material is restricted to poorly developed A horizons. These deposits also form numerous stream terraces both within the mountain front and within incised drainages on the older fan surfaces.

In the Sunland-Tujunga area, most of unit 2 forms alluvial fans. The surface designated "Old Zachau fan" on plate 2.1 appears to be uplifted and was once continuous with the distal parts of the composite fan underlying the western part of the city of Sunland; the intervening area has been covered by younger deposits. Approximately 20 m upstream from the mouth of Haines Canyon, an uplifted unit 2 fan head is perched 50 m above the present channel.

Dunsmore Canyon has a unit 2 fan that has buried most of a larger unit 3 fan. The unit 2 fan has two prominent scarps on its surface (loc. ⑦, pl. 2.1) whose upper surfaces probably correspond to two unit 2 terraces upstream from the fan. The deposits of this fan were exposed in three bulldozer trenches across the lower, most prominent scarp (fig. 2.4). A soil with an unusually thick A horizon has developed across the fault scarp, but it is thinner above and 10 m south of the scarp (fig. 2.5).

Many of the drainages incised in the older fans in this area contain remnants of unit 2 along them. In the Cooks

and Pickens drainages they are deposited on unit 3, and in Hall Beckley Canyon they are on unit 4. There are several unit 2 terraces in the Arroyo Seco—just downstream from the JPL bridge on the east side of the wash, in Oak Grove Park (pl. 2.1), and just above the present stream channel upstream from the canyon mouth.

The Las Flores and Rubio Canyon drainages (pl. 2.2), which have incised the upper part of the Altadena fan surface, have built a moderate-size unit 2 fan on the middle part of the Altadena surface south of the Altadena Golf Club.

Unit 2 makes up most of the fans between the Santa Anita and San Gabriel Canyon drainages. The deposits are designated as unit 2 on the basis of their stratigraphic and geomorphic position, shape, and size. They were deposited after uplift of unit 3 and have subsequently been buried in part by Holocene deposits from numerous small drainages.

UNIT 1

Unit 1 underlies the channels and flood plains of all drainages, as well as several fan surfaces. These deposits consist of unconsolidated, poorly sorted, white to gray coarse sand and pebble, cobble, and boulder gravel. Typical exposures are visible in the numerous gravel-pit operations in most of the major drainages. None of these deposits has a soil developed on it.

Zachau, Haines, and Blanchard Canyons in Tujunga (pl. 2.1) all have well-developed unit 1 alluvial fans at their mouths. Early aerial photographs indicate that these fans were actively building before flood control channels were built and the area developed. Also, in Gould Canyon, a unit 1 fan was actively building on the eastern part of the ancient La Cañada fan.

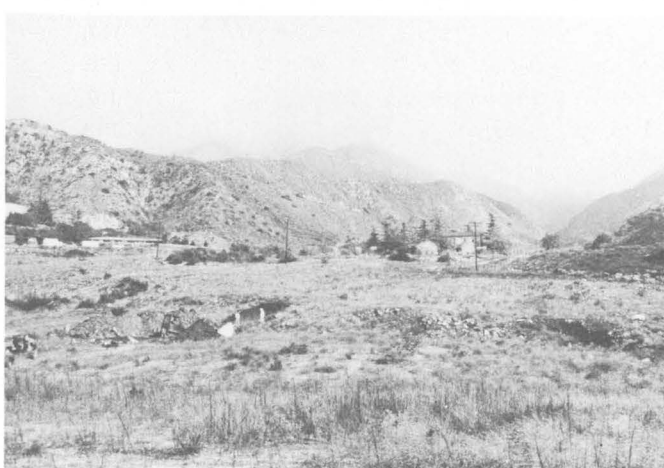


FIGURE 2.4.—South scarp on unit 2 Dunsmore fan. Scarp trace is indicated by line of boulders to right of excavation in center of photograph. Three trenches were excavated across the scarp, all of which exposed the fault.

In the Bradbury-Duarte area (pl. 2.3) several small unit 1 fans have formed at the mouths of intermediate-size drainages, where they cross a buried trace of the Sierra Madre fault zone. A very large composite fan of unit 1 has formed where the Eaton, Little Santa Anita, and Santa Anita Washes cross the Raymond fault (pls. 2.2, 2.4). A small unit 1 fan has been deposited in Eaton Wash by the Hastings Canyon drainage.

AGES OF QUATERNARY UNITS

Although no radiometric dates are available for most of the units classified as Quaternary (except for a single ¹⁴C date on unit 2 alluvium in the Pasadena Glen-Hastings Canyon area), their Quaternary age can be established with confidence. These units are identical in appearance and similar in origin to the Pacoima Formation in the San Fernando Valley (Oakeshott, 1958), where

they overlie the Pliocene and Pleistocene Saugus Formation. A similar relation is visible in the Monrovia Canyon area. Additionally, Eckis (1928) reported that parts of a skeleton of *Elephas imperator*(?) of Pleistocene age were found approximately 20 m below a fan surface in the San Dimas Formation, which is equivalent to our unit 4.

With no absolute dates for unit 4 available, other methods must be used to estimate its upper time boundary. Because this unit everywhere appears to show effects of fan-surface stabilization and concurrent soil development, we attempt to use rates of soil development to estimate its age.

All unit 4 alluvium that was not immediately buried by younger deposits has a moderately well developed to well-developed soil at its surface. This soil was mapped by the Soil Conservation Service (Eckman and Zinn, 1917) as either the Placentia or Ramona series; the Placentia is the more highly developed. The Placentia and Ramona

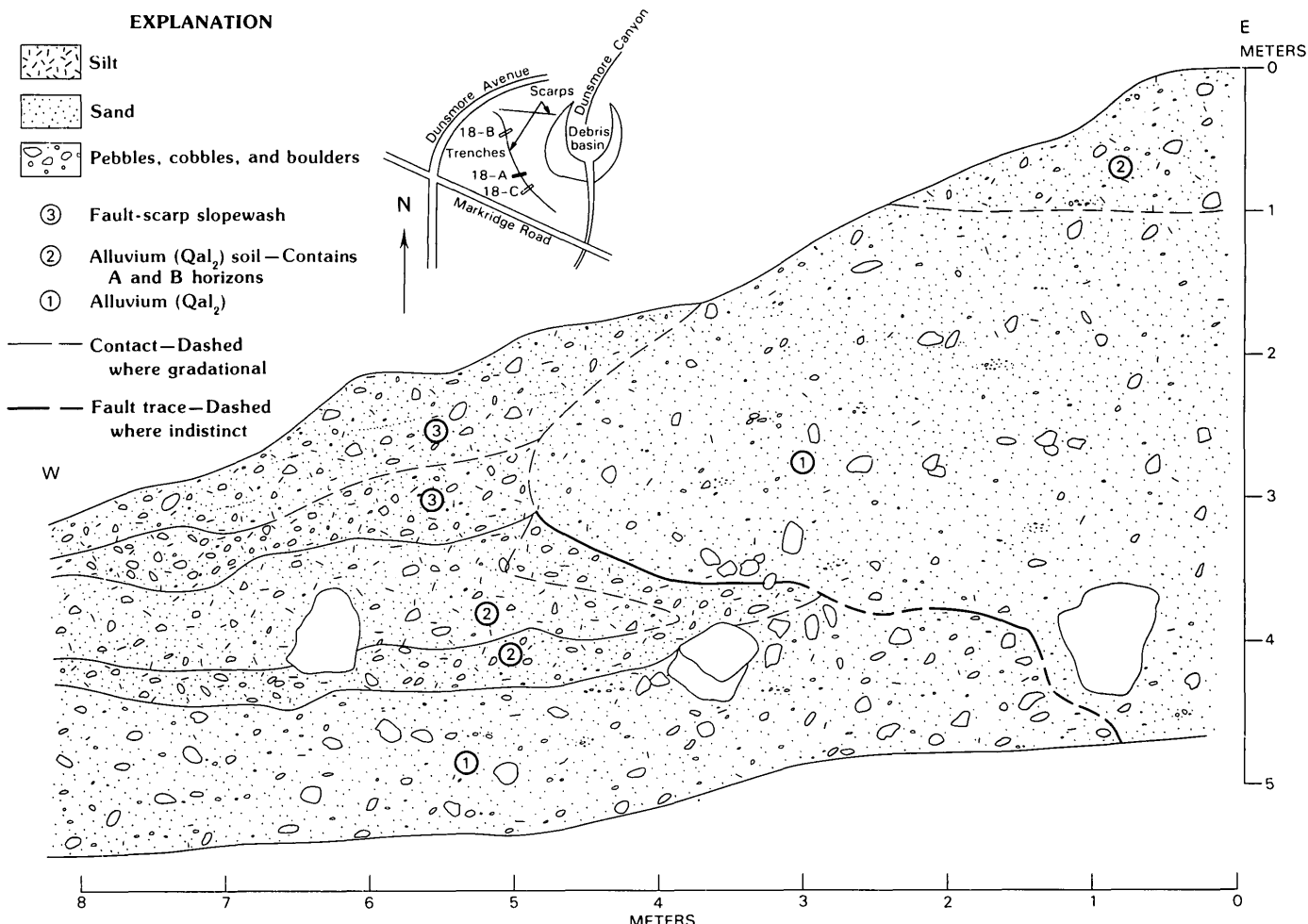


FIGURE 2.5.—Log of trench 18-A (bearing, N. 75° E.) on unit 2 Dunsmore fan, in Dunsmore Canyon, Glendale. Fault surface is indicated by differences in color of deposits or, locally, by sheared highly weathered biotite-rich clasts; fault trends N. 20° W. Thick soil here is due to local accumulation of debris washed from upper fan surface; soil was much thinner at other two excavation sites.

soils appear similar in parent material and degree of development to the Montpellier and Snelling soils mapped by Marchand (1977) in the northeastern San Joaquin Valley. Marchand tentatively assigned ages of 300,000 to 500,000 yr to the Montpellier soil developed on the upper surface of the Turlock Lake Formation, and of 100,000 years to the Snelling soils on the Riverbank Formation. Roy Shlemon (oral commun., 1978) indicated that 100,000 yr is the minimum time required in southern California to develop a strong argillic B horizon with 2.5YR to 5YR hues.

The most highly developed unit 4 soils (Placentia) occur on the La Vina, Gould Mesa, Alta Vista, and Older Spinks fan surfaces. These soils have been at the surface since their formation; they are probably at least 200,000 yr old, but more likely are closer to the 300,000-year age assigned by Marchand to the Montpellier soil. The unit 4 surfaces that were buried by unit 3 deposits some time after their formation exhibit less well developed (Ramona) soils, probably 100,000 yr old or younger. This age suggests that the oldest unit 4 soils have been exposed approximately 200,000 years longer than the buried unit 4 soils and would put the upper age boundary of unit 4 at about 200,000 yr.

Unit 3 appears to range in age from 11,000 to 200,000 yr, on the basis of several lines of evidence. The 200,000-yr lower age boundary discussed above is substantiated by the Ramona-type soils (Eckman and Zinn, 1917) found on the lower parts of the Altadena fan (~100,000 yr old) that overlie an unknown thickness of unit 3. An upper age boundary of about 11,000 yr is suggested by the Hanford series soils that occur on the heads of the Altadena fan, which resemble the Hanford series soils in the San Joaquin Valley considered to be Holocene by Marchand (1977). W.B. Bull (oral commun., 1978) also considered one of the soils mapped as Hanford in the Altadena area—believed by us to be the youngest unit 3—to be Holocene.

The following reasoning indicates to us that the upper boundary of unit 3 coincides with the Pleistocene-Holocene boundary. Bull and others (1979) proposed that a 50-m-thick terrace in San Gabriel Canyon represents a rapid aggradation cycle caused by climatic change; they suggested that the cycle occurred during the Holocene, on the basis of ^{14}C dating of two samples collected near the base of the terrace (W. B. Bull, oral commun., 1980). Deposits of Holocene age suggesting similar aggradational cycles are found in the Arroyo Seco and Eaton Canyon (pls. 2.1, 2.2; see also subsection above entitled "Unit 2"), and in Cajon Pass (45 km northeast of Glendora) (R.J. Weldon, oral commun., 1981), all of which might be correlative with the San Gabriel Canyon terrace. The Arroyo Seco, Eaton Canyon, and Cajon Pass aggradation cycles, however, were preceded by a major

erosional cycle that, at least in Cajon Pass, occurred approximately 11,000 to 10,000 yr B.P. (R.J. Weldon, oral commun., 1981). We propose that this cycle caused the major incision of the large unit 3 fans (for example, the Altadena fan). Additionally, a statistically significant clustering of ^{14}C dates around 10,000 yr B.P. in the southern California area (J.C. Tinsley, oral commun., 1981) suggests a major change in the depositional-erosional process that may also be attributable to the climatic change at the Pleistocene-Holocene boundary (Ericson and others, 1961).

Unit 2 is considered to be Holocene. This unit has a single ^{14}C age of $2,200 \pm 80$ yr in the Pasadena Glen-Hastings Canyon area (fig. 2.10; table 2.2). The boundary between units 2 and 1 is placed at 1,000 years B.P.

GEOMORPHOLOGY

Only those aspects of geomorphology are discussed here that pertain directly to fault activity: (1) Alluvial-fan development, particularly fan-head incision, may reflect differences in the degree of fault activity along the range front; and (2) landslides may represent prehistoric earthquakes, especially those that originate as thrust faults ("thrust-rooted slides"). The continuity from thrust fault to landslide indicates continuing tectonic deformation.

ALLUVIAL FANS

The most obvious geologic evidence of activity along faults, such as the Sierra Madre zone, comes from fault scarps and related features that are directly caused by surficial displacements. Alluvial-fan development, however, can also give significant clues to the rate and periodicity of movements along faults whose displacements have caused the uplift that, in turn, has caused deposition of the alluvial fans. In particular, Bull (1964) suggested that segmented fans generally reflect episodic uplift and that when uplift ceases for a sufficiently long period, fan heads tend to become incised and active deposition occurs farther down the fan surface. Thus, varying degrees of fan-head incision along a given mountain front may indicate different degrees of activity along the bounding fault system, as appears to be the case along the front of the San Gabriel Mountains.

Generally speaking, fan heads in the area of the San Fernando earthquake, west of the study area, are incised to a lesser degree than those in the La Cañada-Pasadena area—for example, the relatively untrenched fans of Pacoima and Little Tujunga Canyons, in the San Fernando area, in comparison with the deeply incised fan heads of the Arroyo Seco and Eaton Canyon in Pasadena. Similarly, fans at the east end of the San Gabriel Mountains, such as at Day and Deer Canyons (Eckis, 1928), are

far less incised than those near Pasadena. Thus, on the basis of this evidence alone, we might conclude that the present rate of uplift along the Sierra Madre fault is less in the study area than to the east and west. Other geologic factors, however, also influence the relative degree of fan-head incision. For example, the incision in the Arroyo Seco, was, at least in part, caused by drainage piracy near the foot of the fan. Nevertheless, one conclusion of this study, based primarily on other, nongeomorphic lines of evidence, is that the degree of activity along the Sierra Madre fault zone is less in this area than to the east and west; the geomorphic evidence supports this conclusion.

Within the study area, detailed examination of fan geomorphology reveals possible differences in present uplift rates. Starting at the west end in the Tujunga area (pl. 2.1), Fairchild aerial photographs taken in 1928 show that the fans at the mouths of Zachau, Haines, and Blanchard Canyons were actively building before human intervention. The fact that the more distal parts of these fans are composed of older unit 2 deposits suggests continuing uplift, at rates exceeding the rates of incision by the streams—a reasonable relation, as evidenced by the nearby 1971 San Fernando earthquake. It is unlikely that such fault features as scarps, lineaments, or depressions would last long in such depositionally active areas. Indeed, careful study of the 1928 aerial photographs fails to reveal any such features on the Zachau, Haines, or Blanchard fans except for a single lineament near the west edge of the Haines fan (loc. [2], pl. 2.1). Fans in this area are being built with geologic rapidity. Not only have some of the world's highest short-period rainfalls been recorded in the San Gabriel Mountains (for example, 66.34 cm in 24 hours in 1943, at Santa Anita Canyon), but also major floods occur here at far higher recurrence rates than do major earthquakes, as was locally demonstrated by the 1934 La Crescenta-Montrose flood (Chawner, 1934) and similar episodes in 1916 (McGlashan and Ebert, 1918), 1926 (Jahns, 1971), and 1938 (Troxell, 1942).

Eastward for the next 5 km, most fan surfaces are composed of unit 3 deposits except at Dunsmore and Shields Canyons; these two drainages have unit 2 deposits on the fan heads that are only slightly incised. These features suggest a lower degree of fault activity than in the Haines Canyon area, although the unit 2 deposits have been faulted, as shown in the trenches across the more prominent of the two scarps preserved on the Dunsmore fan (see fig. 2.6). This faulting is the youngest that has been documented along the Sierra Madre fault zone (in the study area) east of the 1971 breaks (pl. 2.1).

The Cooks, Shields, and Pickens unit 3 fan heads are deeply incised, and the area of active deposition here is on the lower parts of the fans, as demonstrated by the 1934 New Year's Day flood (Chawner, 1934). The presence on these fans of what appear to be scarps (locs.

[3—6], pl. 2.1) in varying states of degradation indicates displacement of unit 3. These facts suggest that in this area little, if any, faulting (uplift) has occurred since the beginning of Holocene time.

Still farther east, between Snover and Hay Canyons, the fan surface is underlain by unit 4. This surface is deeply incised by all but the smallest drainage, and, in addition, several drainages have eroded headward from the toe of the fan. Recent deposition mainly on the lower parts of the fan suggests local, relatively minor uplift associated with seismic activity since the deposition of unit 4.

The conclusion from the foregoing evidence is that the most recently active section of the Sierra Madre fault zone within the study area is in the Sunland-Tujunga segment, adjacent to the 1971 San Fernando earthquake zone. The interval since the last period of fault activity (uplift) appears to increase progressively eastward and is greatest in the La Cañada Section.

In the Pasadena-Altadena-Sierra Madre area, these criteria indicate relatively little seismic activity since the deposition of unit 3. In fact, there is little evidence that any but the older unit 3 has been faulted, as discussed below. East of the juncture of the Sierra Madre and Raymond fault zones, in the Monrovia Canyon-Bradbury area, the criteria indicate that faulting has taken place more recently here than west of the juncture, and the existence of the large unit 1 fan south of the Raymond fault in Arcadia strongly suggests recent and continued activity for this fault.



FIGURE 2.6.—Dunsmore Canyon and head of unit 2 Dunsmore fan, showing two distinct fault scarps (arrows). Several unit 2 terrace surfaces, visible on right (east) side of canyon above building probably correspond to segments of the fan surface separated by the fault scarps. Oblique aerial photograph courtesy of UCLA Spence collection.

LANDSLIDES

Landslides are common throughout the San Gabriel Mountains, particularly close to the range front, where the shattered and highly weathered rock is especially susceptible to mass movement. Most of the slides observed in the study area, however, appear to be shallow "skin" failures of only local extent, rather than large rotational blocks such as are present elsewhere in the range. No direct evidence of massive earthquake-triggered slides was observed, although numerous rock falls were seen to take place at the time of the 1971 San Fernando earthquake. A possible exception is the Henninger Flats landslide (Eaton Canyon area), which Saul (1976) suggested may have been triggered by a prehistoric earthquake. This particular slide is a highly complex feature of undetermined size and extent; one frontal fault cuts the base of the slide in Moist Canyon (loc. ④1, pl. 2.2). We do not anticipate that massive landsliding will be a major problem in the area of this study during future local earthquakes; instead, we expect that numerous shallow failures and rock slides will occur, somewhat analogous to those reported in the San Fernando area in 1971 (Morton, 1975).

An unusual but important form of landsliding along the mountain front occurs downhill from various segments of the Sierra Madre fault zone. These features, here termed "thrust-rooted slides," consist of highly fractured masses of crystalline basement rock that have moved downhill on slide planes effectively continuous with the thrust planes above and behind them, so that the slide-thrust surface takes on an antiform configuration. The slide mass is derived directly from the upthrown block of the thrust, so that there is no clear dividing line between the part of the mass that should be termed a slide and the part that represents the upthrown block. A somewhat similar phenomenon, on a much larger scale, was described along the Alpine fault of New Zealand by Wellman (1955). He mapped shallow nappe-like structures of Alpine schist overlying glacial moraines in front of the locally thrusted Alpine fault in the South Island. We suspect that there may be many more of these thrust-rooted slides along the front of the San Gabriel Mountains than have generally been recognized. Probably the best exposure of these slides in the study area is in Gould Canyon (see section below entitled "Sierra Madre Fault Zone").

SIERRA MADRE FAULT ZONE

REGIONAL STRUCTURAL PATTERN

The southern boundary of the Transverse Ranges tectonic province is characterized by east-west-trending structural elements that are strikingly anomalous within the otherwise northwest-trending structural grain of coastal California. The tectonic environment of the

province has been discussed by numerous workers (for example, Bailey and Jahns, 1954; Morton and Baird, 1975) and is not described further here except to emphasize that the reason for the anomalous trend is not well understood. This trend is probably related to the mechanics of the "great bend" of the San Andreas fault in southern California, although the Transverse Ranges extend considerably farther to the east and west than does the bent segment of the fault. The present regional stress system is, however, presumably dominated by the plate boundary represented in California by the northwest-trending San Andreas fault.

The San Gabriel Mountains constitute one of the principal tectonic blocks within the Transverse Ranges, bounded on the north by the San Andreas fault and on the south by the Sierra Madre fault zone. The steep south face of the range was recognized as a fault scarp early in the 20th century (Arnold and Strong, 1905; Mendenhall, 1908), but the delineation and naming of the bounding structure as the Sierra Madre fault was by Kew (1924). Kew and subsequent workers, including Davis (1927), interpreted the mountain front as due to normal faulting; however, Hill (1930) effectively demonstrated the dominant reverse or thrust nature of the faulting, at least in the western section near San Fernando. The most striking evidence for low-angle thrusting has come from major tunneling operations in the foothill area, as described by Proctor and others (1970), who also pointed out 11 specific exposures between Altadena and Glendora where crystalline rocks of the range front are thrust southward over Quaternary gravel lying at the base of the escarpment. The same relations were confirmed by the 1971 San Fernando earthquake, which was associated with a maximum of about 2.5 m of combined thrust and left-lateral surface displacements on faults having an average dip of about 40° N. (Kamb and others, 1971; Sharp, 1975).

Although rocks within the San Gabriel Mountains are as old as Precambrian and have a complex history (Ehligh, 1975), the present range is the result of tectonism that has occurred in coastal California throughout much of late Mesozoic and Cenozoic time. Some parts of the range were sufficiently elevated to have shed coarse detritus into adjacent basins during Oligocene time, although the principal uplift of the mountain block in its present configuration appears to have been an abrupt middle Pleistocene event (Oakeshott, 1958). On the basis of evidence from a deep well near San Fernando, the total post-Pliocene uplift on bounding members of the Sierra Madre fault zone may be about 4 km. Continuation of this uplift is indicated by numerous earthquakes in the area, including the 1971 event, as well as by geodetic observations (Castle and others, 1976).

Recognition many years ago that the Sierra Madre fault is by no means a single break (Miller, 1928; Eckis, 1934)

has led to some confusion in its nomenclature. Today, however, the term "Sierra Madre fault zone" is generally applied to the entire 100-km-long complex zone of mechanically related faults that grossly demarcate the base of the San Gabriel Mountains from San Fernando Pass on the west to Cajon Pass on the east; some workers (Proctor and Payne, 1972; Wesson and others, 1974) extend the zone of thrust faults farther west to include members of the Santa Susana fault system.

In contrast to the reconnaissance mapping carried out by earlier workers, detailed geologic mapping within the study area was recently carried out by Morton (1973) and Saul (1976) in the Mount Wilson and Azusa quadrangles. Although we have independently restudied the fault zone in these same areas, we have been greatly influenced by these earlier investigations.

In addition to pointing out the complexity of faulting at individual localities along the mountain front, several investigators have noted that the Sierra Madre fault zone appears to be segmented into a series of arcuate salients, convex toward the valley (for example, Proctor and others, 1972, fig. 1). Ehlig (1975) argued that each of these 15- to 25-km-long segments may have behaved as a structural unit, and he pointed to the association of the 1971 San Fernando earthquake with a single salient; he postulated that the maximum sizes of earthquakes elsewhere along the mountain front may be controlled by the dimensions of individual salients. We discuss the evidence for this view in the subsection below entitled "Fault Activity and Recurrence Interval Between Major Earthquakes."

DETAILED DESCRIPTION OF THE FAULT ZONE

Many places where direct evidence of faulted Quaternary alluvium can be demonstrated are shown on the geologic maps (pls. 2.1-2.4). In addition, 60 localities with indirect evidence of faulted alluvium are listed. The following sections describe the most noteworthy evidence and the localities where these features are most easily visible, from west to east.

BIG TUJUNGA TO GOULD CANYONS

Immediately east of the 1971 fault trace in Big Tujunga Canyon (Proctor and others, 1972; Barrows and others, 1975), the Sierra Madre fault zone begins one of its characteristic arcuate salients, convex toward the valley. The fault zone in this area is composed of at least two separate traces, which converge eastward in the vicinity of Haines Canyon. The northern trace skirts the east side of Big Tujunga Canyon, where it has displaced the surface of a unit 3 fan but has not cut the unit 2 fan to the north. The southern trace has cut the unit 2 Old Zachau fan (map and cross section A-A', pl. 2.1) and joins an east-

west-trending segment which moved during the 1971 earthquake, a relation implying that the southern trace is the presently active one.

The fault trace for the next 2 km eastward is inferred to be at the base of the break in slope. The geomorphic evidence for this inference—the truncated ridges and hanging drainages shown on the 1933 Fairchild aerial photographs (flight 2878)—is convincing, even though no actual fault traces are presently visible.

The fault is well exposed in the west wall of Cooks Canyon, where it dips 40° N. and thrusts diorite over alluvium (unit 3). A high scarp is visible just west of this exposure at the mouth of the canyon, and a lower scarp existed on the east side of the canyon before grading for homes obscured it.

Two distinct fault scarps, one 4 and the other 2 m high, were visible on the unit 2 Dunsmore fan before spring 1978 (fig. 2.6). The more southerly, more prominent of the two was trenched and logged (fig. 2.5) in January 1978; the scarps were subsequently buried by debris hauled from local debris basins. This locality is the east limit for confirmed Holocene faulting on the Sierra Madre fault zone within the study area.

Between Dunsmore and Pickens Canyons, a distance of 2.7 km, the fault trace is inferred both from the present geomorphology and from its appearance before development. Both Shields and Pickens fans appear to have scarps in unit 3 alluvium. A second trace to the south is postulated across Shields fan on the basis of an exposure of crystalline basement; however, this outcrop may be part of the shallow rock ridge shown by the California Water Rights Board (1961) south of the fault.

Unit 3 alluvium was seen to be faulted in three places in Pickens Canyon. The northernmost locality (loc. ⑧, pl. 2.1) has a 4-m vertical offset of the basement-alluvium contact; the other two traces have displacements exceeding the 7-m height of the exposures. The total displacement of unit 3 is unknown but must exceed 18 m of vertical slip.

At least 10 additional exposures of the Sierra Madre fault zone between Snover Canyon and the Arroyo Seco involve thrusting of crystalline basement over the oldest alluvium (unit 4). Multiple traces are inferred near Snover and Winery Canyons and just east of Hay Canyon on the basis of scarp-like features, in addition to the exposed traces.

On the west side of Hall Beckley Canyon the upper plate of the thrust fault is seen as a lobe draped over the nose of a ridge. Gravitational forces have caused the distal edge of the lobe to dip downhill to the southeast. Two features similar to this thrust-rooted slide (see subsection entitled "Landslides" in preceding section) are found in Gould Canyon and are described below.

At Winery Dam, basement rocks are clearly thrust over unit 4; however, just 250 m west the contact is deposi-

tional. This is one of the few places in La Cañada where the observed unit 4-basement contact is not a fault.

In the unnamed canyon between Hay and Gould Canyons, just east of Haskell Street (loc. ⑯, pl. 2.1), diorite is thrust over unit 4, as was noted during grading operations in 1964. To the west, the same fault can be seen in the Haskell Street cut, totally within basement rocks.

Just west of Gould Canyon, the Sierra Madre fault zone splits into two separate traces. The northern trace swings northeastward into the mountains and forms the east end of the Tujunga-La Cañada salient; the southern trace swings southeastward and forms the beginning of the Arroyo Seco-to-Santa Anita Canyon salient.

The Gould Canyon thrust fault, here named, is the best exposed and best studied example of a thrust-rooted slide. Immediately north and west of Lone Grove Way in Gould Canyon, diorite can be seen overlying unit 4 and unit 3 alluvium. Here, the contact dips 15°–25° S. toward the valley. Traced northward, the fault surface can be seen to level off; 400 m farther upcanyon, it dips sharply 20°–30° N., still with diorite over unit 4 (cross section *B-B'*, pl. 2.1).

In 1969, heavy rains caused reactivation of part of the south-dipping gravity part of the thrust plate. A bucket-auger borehole was drilled by private consultants through the projected slide plane between the Southern California Edison Co. transmission towers. The borehole log revealed 16 m of diorite overlying old alluvium, separated by 3 cm of gouge. Mapping during the present study revealed that the "slide" is part of the upper plate of a major thrust, of which two distinct lobes form the ridges on either side of Gould Canyon. The feature is well exposed along the Southern California Edison Co.'s access road on the west side of the canyon.

The main thrust can be traced northward to Aqua Canyon, where the fault is exposed in a roadcut on the Angeles Crest Highway. Here, basement overlies unit 3 alluvium along a 35°-N. dipping plane. The fault was traced eastward into the Arroyo Seco, where it cuts only basement rocks.

GOULD CANYON TO ARROYO SECO

The Gould Canyon-Arroyo Seco area is cut by several east-west-trending north-dipping faults between the frontal fault at the mouth of the Arroyo Seco and the Gould Canyon thrust fault, 2 km north. Considerable attention has been given to the area of JPL in northwesternmost Pasadena, west of the Arroyo Seco (fig. 2.7, pls. 2.1, 2.6) because the present study coincided with an independent review of local seismic hazards by JPL itself, so that parts of these two studies were meshed. In particular, we had access to information derived from boreholes drilled

to determine the local subsurface fault geometry, and we assisted in locating additional boreholes. In addition, we excavated four trenches in the area and participated in examining other excavations. As a result, more is known about the subsurface geometry of the Sierra Madre fault zone in the vicinity of JPL than at any other locality along the mountain front.

During excavation in 1971 for a bridge across the Arroyo Seco adjacent to JPL, a fault was revealed that appeared to thrust crystalline basement southward over Holocene stream alluvium, with a postalluvium throw of at least 10 m (Converse Consultants, written commun., 1971). This fault, here termed the "Bridge fault" of the Sierra Madre fault zone, projected along the base of the steep escarpment through JPL and appeared to be one member, if not the major member, of the Sierra Madre fault zone in this area.

As part of the present study, the Bridge fault was again trenched in about the same place (loc. ⑭, pls. 2.2, 2.6). Although the search for datable materials in the trench walls was unsuccessful, the fault geometry was apparent, and it became clear that the gravel beneath the thrust is not Holocene alluvium but the older more consolidated unit 3 alluvium. Natural but poor exposures of the same fault are visible on the terrace riser to the east (loc. ⑮, pls. 2.2, 2.6), and trench 9, excavated by Le Roy Crandall & Associates 200 m southwest (loc. ⑯, pls. 2.1, 2.7; fig. 2.8) revealed a similar thrust relation. An additional 150 m of trench was excavated in unit 2 deposits of the small fan underlying the facility between trench 9 and borehole 4 in an attempt to ascertain whether or not faulting has occurred on the Bridge fault since the beginning of Holocene time. The trenches (21A, 21B, 21C) were located on the projected strike of the fault (pl. 2.6), but no evidence was found to indicate that the unit 2 deposits had been faulted. One other exposure within the JPL property, showing basement rocks thrust over Quaternary gravel, is visible north of Building 150 (loc. ⑰, pls. 2.1, 2.6), but it was uncertain whether this fault represented the main break, inasmuch as it strikes into the mountain front rather than along its base. As a result of these and other concerns about the precise positions of fault traces throughout the JPL property, 14 boreholes were drilled, 5 of which penetrated the fault plane. The fault traces shown on the geologic map of the area (pl. 2.6) are based on the resulting borehole data, together with information on surface exposures.

The cross sections based on the surface and borehole data (pl. 2.6) are generally self-explanatory in demonstrating the fault geometry. Of particular interest is cross section *C-C'* because not only is the attitude of the fault well documented by the two boreholes that penetrate it (and one that must barely "miss"), but also a throw of at least 244 m is indicated by borehole 4, which penetrated

244 m of gravel without reaching basement. Clearly the fault is not minor.

From the many exposures and boreholes within the JPL area, it appears that the fault zone consistently dips about 45° N. and crops out near the base of the escarpment. No conclusions can be drawn concerning possible changes of dip with depth. In the western part of the property, the Bridge fault splits into at least three branches, although the southernmost trace shown on the geologic map (pl. 2.6) is inferred entirely from the topography. In interpreting this map, it should be borne in mind that the

dotted lines represent extrapolated traces at the ground surface, but in some areas the control is so poor that the actual trace could be as much as 100 m from the dotted trace shown. The three branches probably reconverge to the northwest and form a single trace that bounds the west side of Gould Mesa.

Gould Mesa is the most conspicuous remnant of the once-extensive unit 4 fan formed by the Arroyo Seco. It is now bounded on the north, west, and south by branches of the Sierra Madre fault zone. The southern or Bridge fault branch has displaced the fan surface approximately



FIGURE 2.7.—Arroyo Seco and site of JPL in 1934. Bridge fault (BF) is exposed in bluff just east of bridge at mouth of canyon; borehole data indicate that fault trace is north of road west of trench 9 (pl. 2.6), near second bush along road west of bridge, which also exposed fault. Unit 2 fan deposits (Qal₂f) have not been faulted. Geologic and geomorphic evidence suggests that main branch of fault crosses west end of road and bends sharply northwestward. Two unit 4 fan surfaces (Qal₄f) were once con-

tinuous; unit 3 and unit 4 fan surfaces (Qal₃f and Qal₄f, respectively) at lower right are separated by a fault scarp (loc. 20, pl. 2.2). Qal₁, unit 1 alluvium. Note thrust-rooted slides (arrows) of Gould Canyon thrust fault (GCT) in upper left corner. Fault lines solid where location certain; dashed where approximately located; dotted where concealed. Oblique aerial photograph courtesy of UCLA Spence collection.

220 m vertically, on the basis of "red clay" encountered at depth in water wells south of the fault. The discrepancy between this displacement and the minimum of 244 m given previously can be explained by faulting contemporaneous with deposition.

A second fault (loc. ②1, pl. 2.1) approximately 760 m north of the Bridge fault has offset the Gould mesa surface approximately 30 m vertically, north side up. This fault can be traced through the unit 4 alluvial deposits and exhibits associated sedimentary features which suggest that faulting was contemporaneous with deposition.

The fault mapped on the north side of Paradise Canyon appears to have displaced the mesa surface vertically an additional 30 m. The total offset is difficult to estimate here, because the unit 4 alluvium north of the fault has been removed by erosion.

The northernmost branch of the Sierra Madre fault zone in this area is the eastward extension of the Gould Canyon thrust fault. The probable minimum throw of this fault, 300 m, suggests a total of more than 660 m for this series of faults (cross section *B-B'*, pl. 2.1).

ARROYO SECO TO CHIQUITA CANYON

None of the faults just described can be traced more than a few hundred meters east of the Arroyo Seco. The Bridge fault appears to have formed a small scarp (loc. ⑯3, pl. 2.2) on the Altadena fan surface northwest of Audubon School. It then is inferred to trend along, and possibly be the contact between, the Altadena fan unit 3 and the older La Vina surface unit 4 north of Loma Alta Drive. Two more scarps are visible just west of Lincoln Avenue and north of Loma Alta Drive (loc. ⑯29, pl. 2.2).

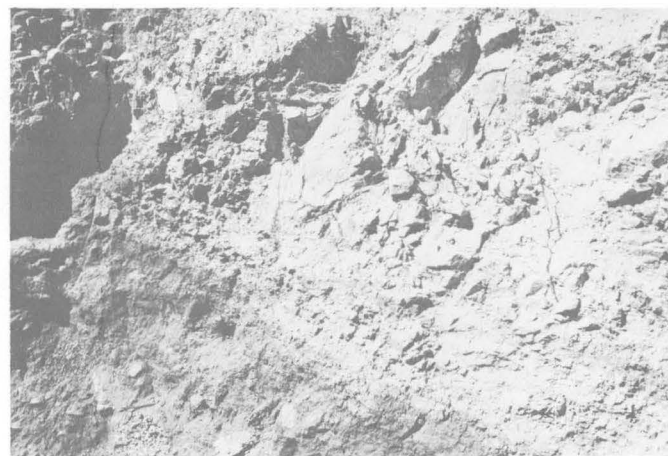


FIGURE 2.8.—Exposure of a thrust fault in trench 9 at JPL, showing light-colored granitic rocks thrust over unit 3 alluvium. Note weathering of several clasts in unit 3 that were broken off by the backhoe. Fault is overlain by unfaulted colluvial deposits, visible in upper left corner. Field of view, approximately 2 m square. Photograph courtesy of JPL.

The northernmost scarp appears to be the contact between units 3 and 4 and probably marks the trace of a significant fault, but it cannot be traced westward into the Arroyo Seco. Eastward, it probably converges with the Bridge fault.

Near the north boundary of the La Vina Sanitarium, another east-west-trending branch of the Sierra Madre fault zone appears near, or becomes the contact between, basement rocks and the unit 4 La Vina surface (loc. ⑯30, pl. 2.2). Here, diorite is thrust over unit 4 alluvium; the fault dips 23°–30° N. Displacement on this branch is probably small, because the depositional contact between unit 4 and basement rocks is seen in close proximity on both the hanging wall and the footwall. Furthermore, the fault cannot be traced for a distance of more than 1 km, even though excellent exposures occur in Millard Canyon to the west and along the Chaney Trail to the east.

CHIQUITA CANYON TO EATON CANYON

In the vicinity of Camp Chiquita in Altadena (northwest corner, pl. 2.2), the Vasquez Creek fault zone (Miller, 1928; Jahns and Proctor, 1975), which is a branch of the San Gabriel fault, and the Sierra Madre fault zone merge in a complex zone of anastomosing faults, 0.6 to 1.2 km wide. Traces of this combined zone can be followed to the Rubio-Eaton Canyons area and, possibly, for another 4.8 km still farther east. This merging of zones is indicated by the presence of the Rubio Diorite, which occurs as long dikelike features, xenoliths, and fault slivers in and along the Vasquez Creek fault zone. Most of these bodies have a northwestward strike and a steep northerly to vertical dip. In the complexly faulted Eaton Canyon area (center, pl. 2.2), the Vasquez Creek fault zone appears to die out, and the Rubio Diorite becomes associated with the frontal-fault system. The outcrop pattern indicates a change in attitude to a shallow northward dip subparallel to the thrust faults of the Sierra Madre fault zone. This change in attitude, also suggested by the gneiss-diorite contact northeast of the Kinneloa fan, may indicate that stresses in the crystalline basement have been relieved in part by folding. Such folding must have occurred early in the fault history of the Sierra Madre fault zone because unit 4 deposits in the area are not similarly folded.

Near the mouth of Chiquita Canyon (north of Altadena), the frontal fault swings abruptly from a northeastward to a southeastward trend and parallels the Vasquez Creek fault zone to the north. The frontal fault is well exposed for about 460 m from near the top of Cañon Boulevard northward to where it appears to merge with one of the traces of the Vasquez Creek fault zone. The trace is highly sinuous as it winds in and out of several local drainages; the fault dips 13°–15° N. Basement rock is thrust over unit 4 alluvium and is highly crushed and weathered as

far as 10 m above the fault plane. Here, a small spur fault from this trace thrusts alluvium over basement—the only place where this condition was observed in the entire study area.

From the Arp property southeastward to Rubio Canyon, the frontal fault is nowhere exposed and, therefore, has been projected along the toe of the slope as a buried trace; a considerable amount of grading and natural alluviation have obliterated the surface trace in this area. A seismic-refraction survey was carried out near the top of Lake Avenue in an attempt to locate the projected main frontal fault. Seismic lines totaling 180 m were run transverse to the projected fault trace on the fan surface on the west side of Las Flores Canyon (Cobb estate). The absence, to a depth of 30 m, of anomalous conditions suggestive of faulting indicates either that the fault is deeply buried or that there is little or no velocity contrast between the rock and (or) soil materials presumably displaced by the fault. Another possibility is that the fault trace is more than 90 m north or south of the projected trace.

Near the Las Flores debris basin, the frontal fault bifurcates. One trace continues southeastward along the main break in slope of the mountain front, where basement has been thrust over unit 4 alluvium along a plane dipping 18° - 40° N.; the other trace is inferred to bound the low basement outlier between Rubio and Gooseberry Dams, and then swing southeastward to Eaton Canyon. A bore-hole near the intersection of Allen Avenue and Altadena Drive penetrated basement rocks at a depth of 42 m; this observation suggests that, owing to the shallow depth of bedrock, the fault trace lies south of this site. Outcrops of gneiss exposed on either side of Eaton Canyon (pl. 2.2) suggest that the fault probably lies to the south. Additional evidence for this fault is provided by the log of a recently drilled Pasadena Water Department well (C-115; see pl. 2.2) in Eaton Canyon, which indicates basement rock between depths of 10 and 24 m, in turn underlain by alluvial sand and gravel.

EATON CANYON TO PASADENA GLEN

In the Eaton Canyon area, the high-angle nearly linear faults of the Vasquez Creek fault zone give way to the low-angle sinuous thrust faults of the Sierra Madre fault zone. Here, a series of five thrust faults are exposed that provide evidence suggesting a trend of progressively younger faulting from south to north. The three southernmost faults have thrust diorite and gneiss over unit 4 alluvium, units 4 and 3, and unit 3, respectively, from south to north (map and cross section $C-C'$, pl. 2.2). This series of faults cannot be traced laterally owing to the presence of artificial fill and younger alluviation, but they

may be manifested eastward by two low scarps on the Kinneloa fan. The fourth fault can be traced nearly continuously from Eaton Canyon, where unit 3 alluvium is faulted, eastward to Hastings Canyon, where unit 4 alluvium is faulted. The fifth trace is entirely within crystalline basement except that it has faulted the basal part of a large landslide that overlies unit 3 deposits 150 m to the south (cross section $C-C'$, pl. 2.2). To the west this fault can be traced to the mouth of Eaton Canyon, where it has thrust quartz monzonite over unit 3 alluvium, as exposed in trench 3, but appears not to have faulted unit 2 alluvium, as exposed in trench 3A. This fault can be traced only a short distance to the east, where it appears to die out in a splay of several faults in Pasadena Glen.

Minimum vertical displacement on the low-angle faults is approximately 152 m, as estimated from the displacement of the base of unit 4. Minimum displacement on the basement trace is unknown but may be 30 m, on the basis of the offset of the nearly horizontal diorite-gneiss contact north of the Kinneloa West Debris Dam.

Most of the movement on these faults probably occurred before deposition of the upper part of unit 3 alluvium because the Altadena fan surface adjacent to Eaton Canyon does not appear deformed or disrupted, and the correlative fan surface across Eaton Canyon has the same elevation. In addition, the fault exposed in trench 3 cannot be traced upward through unit 3 alluvium, and there is no offset of the fan surface to correspond to a projected trace.

Saul (1976) showed most of this area (south of Henninger Flats landslide, pl. 2.2) as the "Henninger Flats landslide complex," with its head in upper Eaton Canyon and its toe buried by unit 1 alluvium in Eaton Canyon. In our opinion, it is unlikely that this slide either is so extensive or is rotational, as shown in his cross section $B-B'$. The Rubio Diorite associated with the low-angle faults retains its structural continuity through this area, and the units 3 and 4 alluviums contained within this supposed complex have not been rotated but, instead, retain the original shallow southward dip.

PASADENA GLEN TO BAILEY CANYON

In this segment, the Sierra Madre fault zone consists of several separate traces—two low-angle thrusts involving alluvial units that lie at the base of the mountain front, and two high-angle faults to the north within the basement complex. The two low-angle thrusts are nearly parallel and less than 100 m apart (fig. 2.9). The upper fault thrusts gneiss over unit 4 alluvium and can be traced nearly continuously from the Eaton Canyon area to the Sunnyside debris basin, where it becomes much steeper

and more complex. The lower trace is not nearly so well defined. It is exposed at the surface in two localities separating diorite from unit 4 alluvium and was exposed

at two localities in CIT trenches 20A, 20B, and 20C, where it was seen to have disrupted colluvium overlying unit 4. The fault could not be traced into the valley fill, which

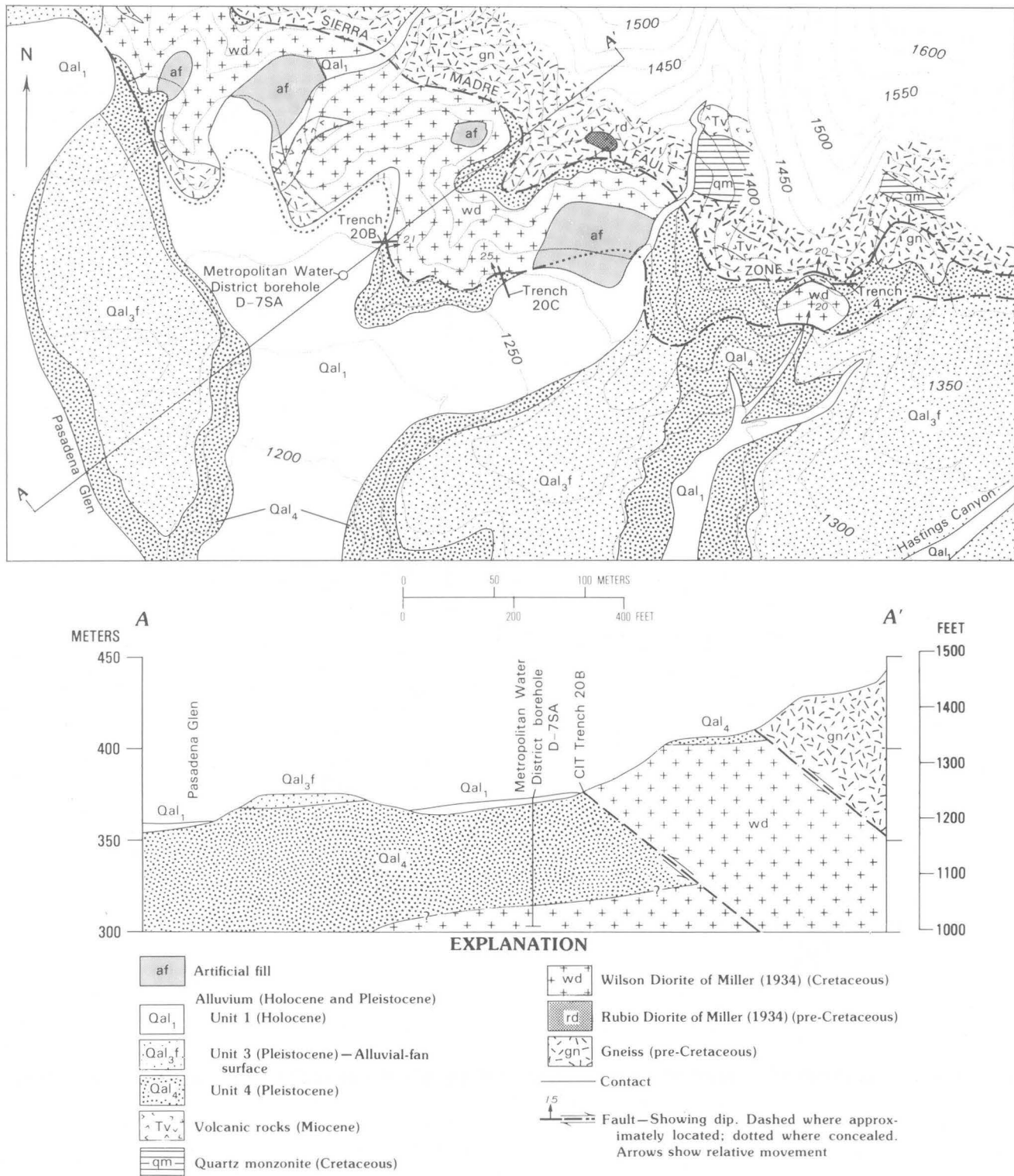


FIGURE 2.9.—Detailed geologic map and cross section of Pasadena Glen-Hastings Canyon area, showing traces of two thrust faults and locations of CIT trenches 20B and 20C (see fig. 2.10 for cross section of trench 20C and pl. 2.2 for locations).

is probably unit 2 alluvium. In trench 20C, the fault is overlain by 0.6 m of unfaulted bedded silty sand with a Holocene soil (fig. 2.10). This unit contained an in-place root that yielded a ^{14}C age of $2,200 \pm 80$ yr B.P.

The lower fault could not be traced into Pasadena Glen or Hastings Canyon, although it must have moved recently enough to have cut the Kinneloa fan surface (loc. 19, pl. 2.2), as indicated by the fact that the faulted colluvium is younger than the incision of unit 3 surfaces. The sides of the incised channel are mantled by the faulted colluvium.

The positions of the two high-angle faults in most of this reach are inferred from two series of aligned canyons and notches in ridges. The lower fault is exposed in Bailey

Canyon, and further evidence is provided by the patches of unit 4 alluvium high on a ridge on the east side of the canyon.

In this area, a minimum total vertical displacement of approximately 330 m has occurred since deposition of unit 4—210 m along the high-angle fault in the basement and 120 m along the thrust faults. This conclusion is based on displacement of the unit 4 alluvium-basement depositional contact.

Both Pasadena Glen and Hastings Canyon contain mutually exclusive, distinctive rock types in outcrop—the Lowe Granodiorite in Pasadena Glen and porphyritic andesite in Hastings Canyon. This unique feature allows a distinction between alluvial deposits from each of the

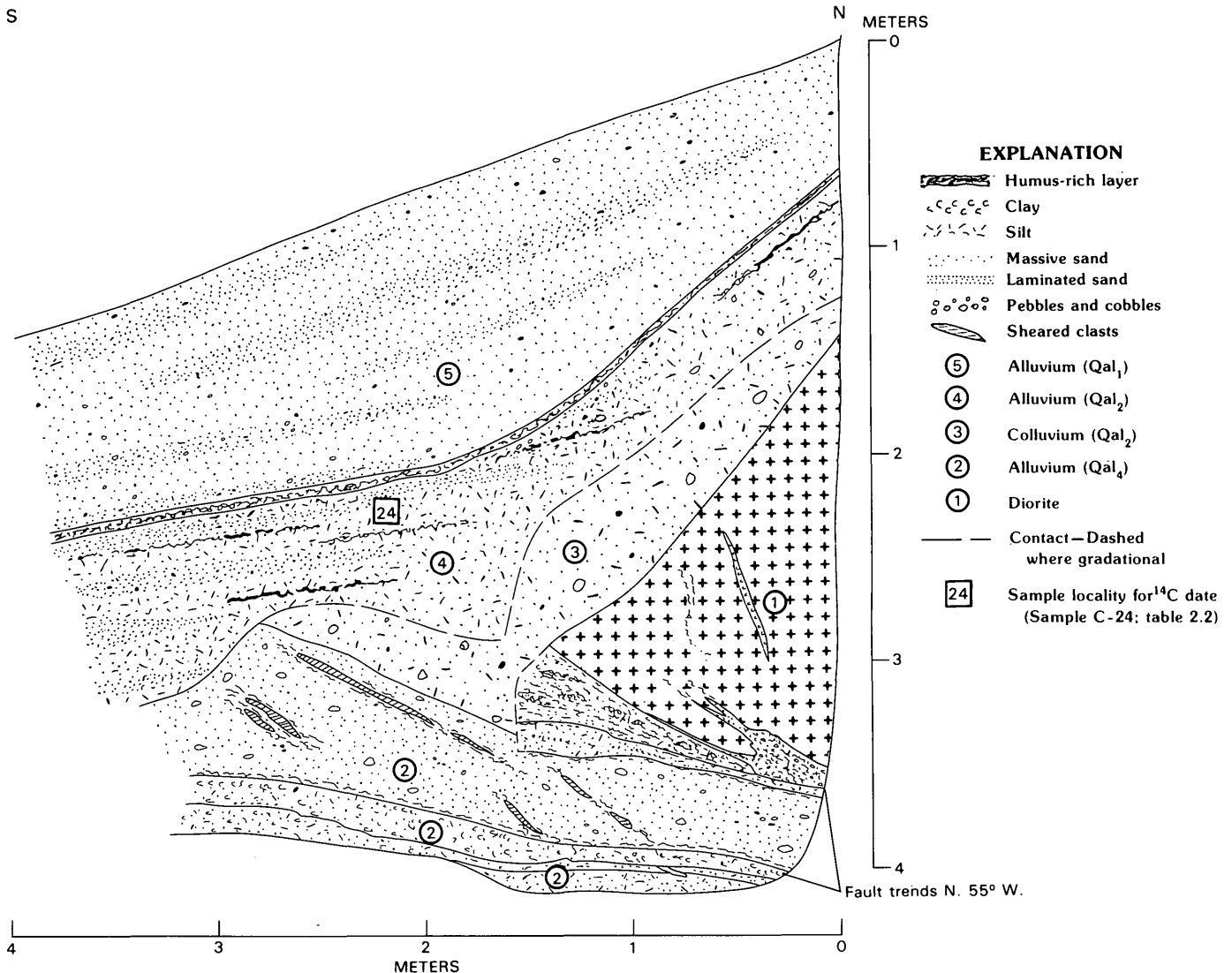


FIGURE 2.10.—Log of west wall of CIT trench 20C (bearing, N. 23° E.) in Pasadena Glen, Pasadena, showing a branch of Sierra Madre fault (see fig. 2.9 for location).

two adjacent drainages. Thus, left-lateral offset of these distinctive unit 4 deposits cannot be more than 1.2 km from their source drainage.

BAILEY CANYON TO SANTA ANITA CANYON

Between Bailey Canyon and Santa Anita Canyon, evidence for faulting along the mountain front is only suggestive. Aligned notches in ridges indicate two high-angle faults in the basement, one of which is exposed behind the Carter Dam; Buwalda (1940, p. 35) mentioned a steep fault with "ancient alluvium" (unit 4) against diorite in the vicinity of the high-angle fault north of the Sturtevant Dam. A thrust fault is postulated at the base of the scarplike feature between the Sierra Madre and Lannan fans. The upthrown block consists of units 3 and 4 deposits resting on crystalline basement; minimum vertical displacement of the unit 3 deposits across this trace is 20 m.

SANTA ANITA CANYON TO MONROVIA CANYON

At Santa Anita Canyon, the Sierra Madre fault zone enters what is here called the Monrovia outlier, where it becomes the most complex system of frontal faults in the study area (map and cross section *D-D'*, pl. 2.3). Part of the system branches off to the northeast as the Clamshell-Sawpit fault zone (Morton, 1973), whereas the rest of the system continues easterly across the outlier to emerge at the mouth of Monrovia Canyon. To further complicate the

picture, the Raymond fault joins the Sierra Madre fault zone at the southeast corner of the outlier.

At the west side of Arcadia Wilderness Park (loc. 48, pl. 2.2) is one of the most impressive exposures of a thrust fault in the Sierra Madre fault zone (fig. 2.11). Banded gneiss is thrust over the large-boulder facies of unit 3 alluvium. This fault consists of several feet of gouge and crushed rock generated from the gneiss. The fault cannot be traced into the upper part of the unit 3 alluvium and probably has been inactive since the faulted part was deposited. The fault continues to the northeast and becomes part of the Clamshell-Sawpit fault zone.

Numerous east-west-trending north-dipping thrust faults cross the central part of the Monrovia outlier. Many of these faults were seen in the Metropolitan Water District's water tunnel, but because of the heavy cover of chapparal and poison oak in this area, surface continuity of these traces was not proved. They clearly do not cut the unit 4 remnants, nor do they appear to have displaced them vertically relative to each other. One of the thrust faults, exposed in Ruby Canyon (loc. 51, pl. 2.3; fig. 2.12), is visibly overlain by unfaulted unit 4 alluvium. In Monrovia Canyon (loc. 52, pl. 2.3), faulting has displaced Quaternary deposits; here, quartz monzonite has been thrust over the large-boulder facies of unit 3 alluvium. Morton (1973) showed the San Dimas Formation (equivalent to our unit 4) as faulted against basement 0.8 km northwest of Ruby Dam. Closer examination indicates, however, that the faulted material is the Saugus Formation, which has steep dips, and that the fault appears to be overlain by nearly flat-lying unit 4 deposits that make up the Alta Vista fan.

Whereas faulting within the outlier appears to have preceded the deposition of alluvial unit 4, the elevations of the unit 4 remnants suggest a subsequent uplift of the entire block and northward tilting by as much as 2°. This tilting is also indicated by gentle northward dips in some of the deposits.

MONROVIA CANYON TO SAN GABRIEL CANYON

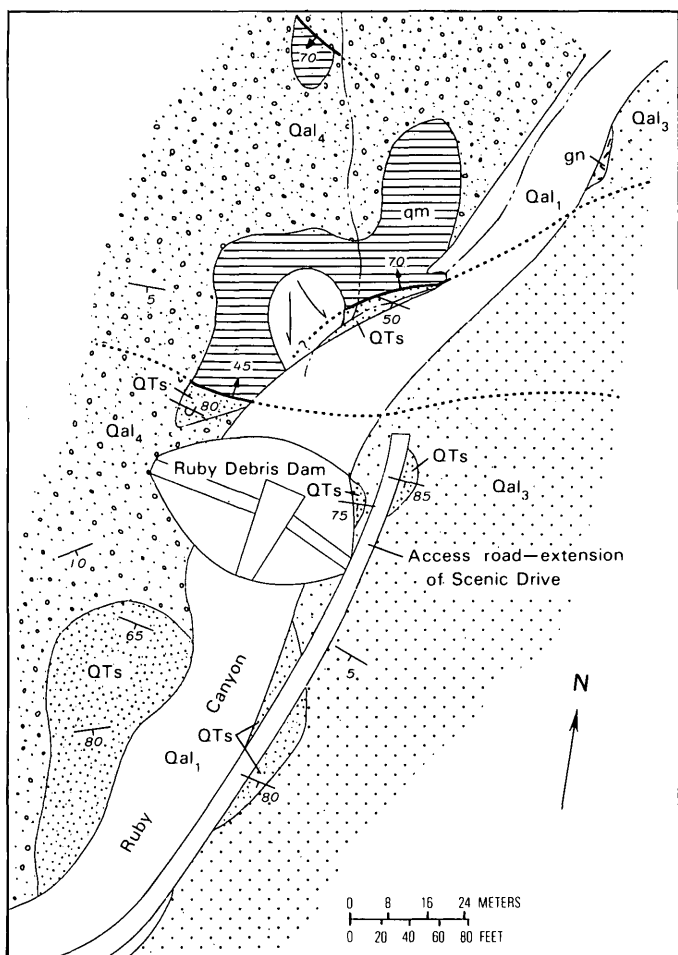
East of Monrovia Canyon and throughout the Bradbury area, the Sierra Madre fault zone appears simpler than to the west in terms of the number of fault traces, but more complex in terms of the number and age of sedimentary units involved. Exposures are insufficient to allow a completely satisfactory explanation for the complex relations between the folded and faulted units, and we can make only broad generalizations concerning the history of faulting in this area.

Evidence for the earliest faulting and deformation along the Sierra Madre fault zone within the study area is found here. Exposures of the Miocene Topanga Formation southeast of the Spinks Dam (pl. 2.3) show that the



FIGURE 2.11.—Thrust fault exposed in Arcadia Wilderness Park. Fault surface is just below man's arms. Photograph courtesy of Metropolitan Water District of Southern California.

Topanga Formation was already highly deformed before deposition of the Pliocene(?) Duarte Conglomerate. An



EXPLANATION

	Unit 1 alluvium (Holocene)
	Unit 3 alluvium (Pleistocene)
	Unit 4 alluvium (Pleistocene)
	Saugus (?) Formation (Pleistocene and Pliocene)
	Quartz monzonite (Cretaceous)
	Gneiss (pre-Cretaceous)
	Contact—Approximately located
	Fault—Showing direction of dip. Dotted where concealed; queried where doubtful
	Strike and dip of beds
	Strike and dip of overturned beds
	Landslide—Showing direction of movement

FIGURE 2.12.—Geologic map of Ruby Debris Dam area, Monrovia, showing an old branch of Sierra Madre fault. Unfaulted unit 4 alluvium of Alta Vista surface overlies faulted crystalline basement and the Saugus (?) Formation (see pl. 2.3 for location).

angular discordance of 110° can be seen here between the south-dipping Duarte Conglomerate and the overturned north-dipping Topanga Formation. Just west of the Bradbury Dam (fig. 2.13), two exposures of the contact between the Duarte and the Topanga can be seen—one is a fault contact, and the other a conformable depositional contact. These relations, in addition to the fact that the two units are everywhere dipping at moderate to high angles, indicate continued faulting and folding along this zone up to the time of deposition of unit 4 alluvium, as substantiated by the tilting of the Pliocene and Pleistocene Saugus (?) Formation in Monrovia Canyon and the steep dips on the Saugus Formation beneath nearly flat-lying unit 4 deposits in Ruby Canyon.

The great discordance between the Topanga Formation and the Duarte Conglomerate raises an interesting question concerning the Sierra Madre fault zone in this area. Jahns (1973) suggested that the ancestral right-lateral San Gabriel fault was active in this area, as the deformed Tertiary sediment may indicate. The common occurrence of calc-silicate units and marble beds in gneiss in the Monrovia outlier and in the Fish Canyon area may also indicate right-lateral displacement, as do the fault-bounded slivers of the Duarte Conglomerate near Monrovia Canyon that were derived from the San Gabriel River drainage. The Sierra Madre fault zone has subsequently become active in this zone of weakness.

There is little evidence for faulting on the northernmost fault trace in the Bradbury area since the deposition of unit 4 alluvium. The surface of the Older Spinks fan has not been faulted, although it does appear to have been warped slightly upward in the vicinity of the buried fault. To the northwest, deformation of unit 4 alluvium becomes progressively greater, as evidenced by the steepening dips, but the age of these deposits is believed to increase in this direction, and they probably grade into the Saugus(?) Formation that underlies unit 4 alluvium in Ruby Canyon.

Two fault exposures near the mouth of Monrovia Canyon (loc. 52, 54, pl. 2.3) appear to contradict the idea of minor post-unit-4-alluvium movement on the northern fault trace. Movement here may occur sympathetically with that on the Duarte and Raymond faults in a manner similar to that of the Veterans fault and the main fault zone in the 1971 San Fernando earthquake (Kamb and others, 1971).

The most recent faulting in this area has occurred along the Duarte fault, since deposition of unit 3 alluvium (California Department of Water Resources, 1966), perhaps as recently as the youngest unit 2 alluvium. A scarplike feature on the older Monrovia fan and a lineament seen on aerial photographs south of Bradbury (locs. 24, 25, pl. 2.3) indicate that the unit 2 fan surfaces may be faulted. Also, two small unit 1 alluvial fans at the mouths of Bradbury and Spinks Canyon suggest relatively recent uplift.

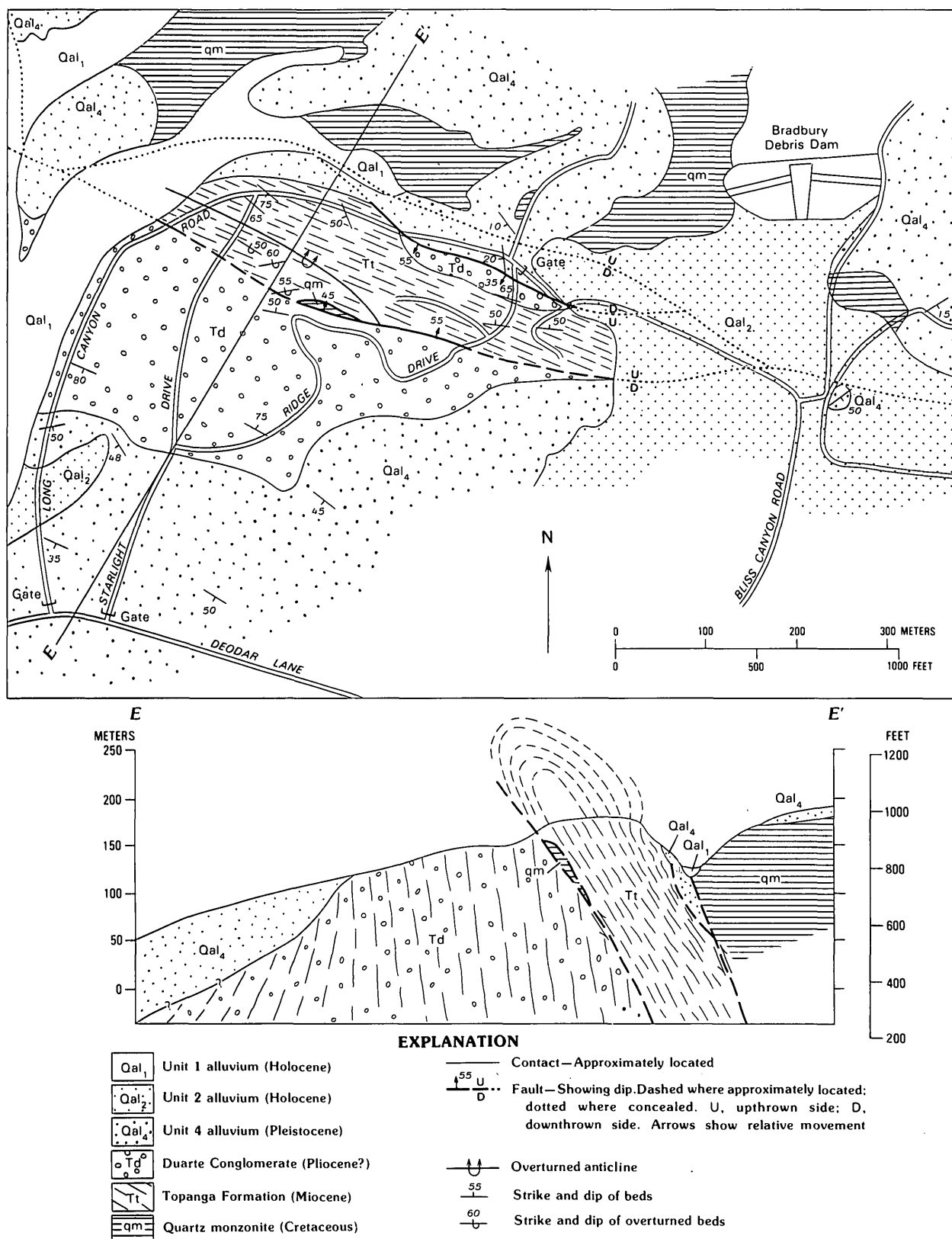


FIGURE 2.13.—Geologic map and cross section of Bradbury Dam area, Bradbury, showing complexity of faulting in upper branch of Sierra Madre fault zone. The highly deformed Topanga Formation is overlain by and faulted against the Duarte

Conglomerate, which, in turn, is somewhat less deformed and is overlain by still less deformed unit 4 alluvium, which is also faulted. These relations suggest that faulting here was nearly continuous from at least Pliocene through late Quaternary time.

Although the Duarte fault trace is not exposed, its topographic expression is evident in the Bradbury area as a mesalike feature north of Foothill Boulevard, where a minimum vertical displacement of 60 m is indicated, assuming that the analog of the unit 4 surface on the mesa top lies just below the surface south of the fault.

AZUSA AREA

East of Bradbury, the Sierra Madre fault zone is inferred to split into at least three separate traces, mainly on the basis of geophysical surveys and water-level data. Seismic-refraction and magnetometer surveys carried out by several private consulting firms (Envicom Corp., Evans-Goffman and McCormick, Leighton & Associates, Inc., and Le Roy Crandall & Associates) indicate anomalies in several localities that are interpreted as faults (locs. [30], [32]-[34], pl. 2.3).

A small scarp on the lower part of the Maddock fan and a lineament formed by vegetation observed on a 1928 aerial photograph in the Holocene San Gabriel River gravels (locs. [27], [31], pl. 2.3) seem to substantiate one of these traces. Anomalous ground-water levels in numerous water wells in the Azusa fan indicate ground-water barriers that coincide with the faults inferred from the geophysical data. Although the age of faulting cannot be determined from these data, the scarp, vegetation lineament, and ground-water levels only 2 to 3 m below the surface (loc. [36], pl. 2.3) in the eastern part of the city of Azusa suggest that Holocene sediment has been faulted.

Trenches 13 and 13A (table 2; see supplementary section below entitled "Trenching") along the upper trace of the Sierra Madre fault zone between Maddock and Van Tassel Canyons (loc. [32], pl. 2.3) indicate that movement along this trace has not occurred since the upper 4 m of alluvium was deposited.

FAULT ACTIVITY AND RECURRENCE INTERVAL BETWEEN MAJOR EARTHQUAKES.

The 1971 San Fernando earthquake dramatically illustrated that for at least a part of the Sierra Madre fault zone, the seismic hazard is far from negligible. However, the extent to which the same degree of activity extends eastward into the area of this study is subject to debate because, although the fault system as a whole extends along the entire 100-km-long mountain front, it is not clear that all parts of the frontal fault necessarily have the same extent of late Quaternary displacement. Many workers have pointed out that abrupt fault scarps in alluvium are not obvious along the mountain front in the Pasadena-Azusa area except along the Raymond fault (discussed in the next section below), although most of the foothill area has been urbanized to such an extent that diagnostic

physiographic features might well have been removed or concealed. Thus, the primary focus of this study is to determine the recency of faulting in this area and its implication for seismic-hazard evaluation.

Although old aerial photographs have been extensively studied and the Sierra Madre fault zone has been systematically trenched, we are unable to positively identify either fault scarps or displaced strata in units younger than late Pleistocene anywhere east of Dunsmore Canyon (between Tujunga and La Crescenta). Some subdued scarplike features and ground-water barriers in the Duarte-Azusa area could represent breaks in Holocene deposits, but the evidence is marginal. This situation contrasts sharply with that in the area of the 1971 San Fernando earthquake, where units correlative with our unit 2 alluvium were clearly broken even before 1971. Thus, although the escarpment represented by the mountain front is continuous across the entire area, the recency of displacement along the bounding fault zone apparently decreases toward the east. To our knowledge, it is only as far away as Cucamonga Canyon, 30 km east of the study area, that abrupt scarps again occur in units as young as unit 2 alluvium (Eckis, 1928; Morton, 1976). It is particularly anomalous that the part of the range front opposite the very highest peaks of the range should be the segment where the evidence for recent displacements is least persuasive. This relation is the exact opposite of that seen along the east face of the Sierra Nevada.

In view of the absence of significant displacement in unit 2 alluvium throughout most of the study area, again except for the Raymond fault, we conclude that major earthquakes have not occurred in this segment of the Sierra Madre fault zone for several thousand years, perhaps as long as 11,000 years (the oldest age tentatively assigned to unit 2). This conclusion is unexpected, inasmuch as our initial working hypothesis was that the seismic hazard should be considered relatively uniform along the entire mountain front, including the San Fernando area.

In addition to the recurrence interval between major shocks, another important problem in the evaluation of seismic hazard is specification of the maximum earthquake that is realistically possible here under present tectonic conditions—what we term the "maximum credible earthquake." Certainly it must be as large as the $M=6.4$ event in 1971. Wesson and others (1974) postulated a "maximum expectable earthquake" of magnitude $7\frac{1}{2}$ to $7\frac{3}{4}$ for the same general area. Their estimate was based on an assumed rupture of half the total length of the fault zone, which they put at 130 km, as well as on comparisons with the 1952 Kern County $M=7.7$ earthquake, which occurred on a somewhat similar thrust-fault system 100 km to the north.

In contrast, Ehlig (1975) pointed out that the Sierra Madre fault zone comprises several distinct arcuate salients, each 15 to 20 km long and convex toward the

valley. He proposed that these individual salients are mechanically coherent and that a single earthquake might be expected to involve no more than a single salient, as was in fact observed during the 1971 San Fernando earthquake, particularly in Big Tujunga Canyon, where the breaks terminated in a major cusp between adjacent arcuate salients. No such individual salients or sectors are present along the White Wolf fault, where movement over the entire 50-km length caused the 1952 Kern County earthquake.

Within and adjacent to the study area, four individual salients can be identified, separated by cusps pointing toward the mountains; these salients extend: (1) from San Fernando Pass to Big Tujunga Canyon (20 km), (2) from Big Tujunga Canyon to the Arroyo Seco (15 km), (3) from the Arroyo Seco to Monrovia Canyon (18 km), and (4) from Monrovia Canyon to Big Dalton Canyon (16 km). We agree with Ehlig (1975) that these sectors are so distinct in their structural patterns that a single earthquake involving more than one of them would come as a surprise, although we hesitate to label such an event as "incredible." Examples can be found elsewhere in the world of several distinct segments of a fault zone breaking at the same time, such as in Japan (Allen, 1975). Assuming that two salients broke at once, the total length of 32 km would suggest an average causative earthquake of $M = 6.9$ (Slemmons, 1977), although errors in such extrapolations can be great (Bolt, 1978).

On the basis of the faulting that occurred during the 1952 Kern County earthquake, generally assumed to have been of $M = 7.7$, some investigators have proposed that an event at least as large should be expected on the Sierra Madre fault zone because it has an even greater total length than the White Wolf fault, whose rupture caused the 1952 event. We disagree with such a direct comparison for three reasons: (1) As argued above, the segmentation of the Sierra Madre fault is quite unlike the relatively continuous geometry of the White Wolf fault; (2) field studies by Cotton and others (1977) along the White Wolf fault showed evidence of pre-1952 faulting of probable Holocene age, in contrast to the absence of such evidence along much of the Sierra Madre fault; (3) recent work by Kanamori and Jennings (1978) showed that the $M = 7.7$ assigned to the 1952 event by Gutenberg (1955) is approximately comparable to the surface-wave magnitude (M_S) rather than to the local magnitude (M_L) which is commonly assigned to local southern California earthquakes and is measured at a frequency that is most appropriate to the evaluation of engineering damage. Using strong-motion accelerograms from the 1952 earthquake, Kanamori and Jennings (1978) proposed that the equivalent M_L for this earthquake should be about 7.2.

In our opinion, the maximum credible earthquake for the segment of the Sierra Madre fault that we have studied should be about magnitude (M_L) 7, and the

average recurrence interval between major shocks longer than 5,000 yr. Although such a recurrence interval is long relative to those of such very active faults as the San Andreas, it is certainly not too long to be of concern in the siting and planning of critical structures. Furthermore, the recent study by Sieh (1978) of prehistoric large earthquakes on the San Andreas fault demonstrated the large variations in the intervals between individual events. Although the average recurrence interval over the past 1,500 yr is 160 yr, the intervals between major events on this section of the San Andreas fault during the same period have ranged in length from about 50 to 300 yr.

RAYMOND FAULT ZONE

REGIONAL STRUCTURAL PATTERN

Just as several branches of the Sierra Madre fault system diverge into the range, several other branches diverge out into the valley floor in front of the range. Probably the most important of these branches is the Raymond fault, which diverges southwestward from the range front near Monrovia and represents the southernmost element of the Transverse Ranges in the study area. Still farther west, other faults on the continuation of the Raymond trend mark the boundary between the Santa Monica Mountains on the north and the Los Angeles basin on the south. There is some doubt, however, that the Raymond fault itself is continuous with individual breaks in this western area (Lamar, 1970).

The Raymond fault has long been recognized as a significant ground-water barrier in the Pasadena-San Marino area and was first described as a dike or buried ridge of impervious rock (Mendenhall, 1908; Conkling, 1927). The first recognition that the alluvial gravel is truly offset was apparently by Miller (1928), who considered the feature to be a basinward extension of the Sawpit fault, which trends northeast into the range north of Monrovia. It was subsequently termed the "Raymond fault" by Eckis (1934) and was the subject of an extensive investigation by Buwalda (1940) in connection with litigation over water rights (California Division of Water Resources, 1941). In recent years, it has been termed both the "Raymond fault" and the "Raymond Hill fault" on State geologic maps (Jennings and Strand, 1969; Jennings, 1977). We prefer the simpler terminology in recognition of Eckis' (1934) first usage of the name as applied to a demonstrated fault.

FAULT CHARACTERISTICS

The Raymond fault is a high-angle reverse fault that also shows significant left-lateral displacement. Its recent activity is attested to by numerous geomorphic features along its entire length. The fault trace is defined by a

scarp that is continuous between Monrovia Canyon and the Arroyo Seco, except where it passes through Holocene alluvium in Santa Anita and Eaton Canyons.

Between Monrovia Canyon and Santa Anita Canyon, the Raymond fault is the frontal fault, and, although it cannot be seen, it is presumed to thrust basement rocks over alluvium. Westward from Santa Anita Canyon to Raymond Hill, alluvium is faulted against alluvium. From Raymond Hill to the Arroyo Seco and beyond, the Miocene Topanga Formation is thrust over alluvium.

EVIDENCE FOR FAULTING

Much clear evidence for recent movement on the Raymond fault was documented by Buwalda (1940), including: (1) a nearly continuous fault scarp, (2) closed depressions, (3) springs and a high ground-water table, (4) backtilted fan surfaces, (5) displaced drainages, (6) pressure ridges, (7) recent surface cracking, and (8) surface exposures.

SCARPS

The most prominent feature of the fault is the continuous scarp from the Arroyo Seco eastward to San Marino High School in San Marino. East of the school to the Los Angeles County Arboretum (Arcadia), the scarp has been nearly obliterated by erosion from Eaton Wash and subsequent fan development along the Raymond trace (map and cross section $G-G'$, pl. 2.4). Two elongate pressure ridges, trending parallel to the fault trace at the Arboretum and immediately north of the Santa Anita Race Track, are separated by a prominent fault scarp. Between the Santa Anita Race Track and the Monrovia outlier, the fault scarp has been obliterated by the active Santa Anita Canyon. The south boundary of the Monrovia outlier is believed to be the fault scarp, although the fault itself is not seen along this segment.

The scarp is most prominent through the San Marino-South Pasadena area and attains a maximum height of more than 30 m north of Lacy Park. It is a linear feature except for the sharp S-curve northwest of Lacy Park at the inferred juncture with the Eagle Rock fault (Buwalda, 1940, p. 64). The scarp does not appear to indicate a highly active fault, such as the San Andreas, because the average slope of the scarp face is less than 20° and the numerous small canyons eroded across it and into the upthrown block have maintained relatively low gradients (Wallace, 1977). Additionally, Buwalda, (1940, p. 48, 49) says the movement causing "a 4-foot scarplet crossing the floor of the mouth of the Kewen Canyon***must therefore have transpired many centuries ago." This observation could not be substantiated because the site is now covered with houses.

In western Arcadia, a low scarp and two lineaments show clearly on 1929 Fairchild airphoto K-363. These

features are significant because they are in the unit 1 alluvium of Eaton Wash.

CLOSED DEPRESSIONS

Buwalda (1940) recognized six closed depressions along the Raymond fault (pl. 2.4), of which at least Lacy Park and Baldwin Lake (Los Angeles County Arboretum) are sag ponds fed by springs north of the fault. An excavation dug into Lacy Park (Wilson Lake) "revealed at least 20 feet of interbedded clay, peat, [and] tule stems" (Buwalda, 1940, p. 47). It is not known whether the other depressions have similar sediments rich in organic material.

SPRINGS AND HIGH GROUND-WATER TABLE

The Raymond fault is an effective ground-water barrier and was first recognized as such (Mendenhall, 1908) because of the numerous springs, marsh deposits, high ground-water table, and artesian pressure in wells north of the barrier. All these springs have since stopped flowing because of lowering of the ground-water table except for those at Baldwin Lake and two perennial springs along the east bank of the Arroyo Seco. The latter two springs may each define a separate trace of the Raymond fault (loc. [3], pl. 2.4).

Additional evidence of a high ground-water table is provided by the black poorly drained soils, rich in organic materials, mapped as the Chino loam on the 1917 Pasadena area soil survey (Eckman and Zinn, 1917). These soils, which occur between trench 7 and Baldwin Lake north of the Raymond fault trace (east center, pl. 2.4), apparently are the result of abundant decayed vegetation in perennial marshes.

BACKTILTED FAN SURFACES

Buwalda (1940, pl. 1) showed many areas along the Raymond fault zone "that originally sloped south, now slope north or are horizontal." Most of these surfaces are north of the fault and are the lower parts of the Altadena and Sierra Madre fans; several surfaces are south of the fault, the largest of which contains the Lacy Park sag pond. Most of the backtilting is attributed to the vertical component of movement on the Raymond fault.

DISPLACED DRAINAGES

Abundant evidence for the position of the Raymond fault is provided solely by its effect on the numerous drainage systems that cross it. Many small drainage channels either terminate or begin at the fault; many others cross the fault with a jog that generally suggests left-

lateral movement, although in most places it is impossible to prove offset of the channel as opposed to diversion parallel to the fault trace. One example of an offset channel is visible adjacent to trench 7 (pl. 2.4), and Alhambra Wash is an example of a diverted drainage (Buwalda, 1940, p. 46).

PRESSURE RIDGES

Two 18-m-high hills, elongate parallel to the Raymond fault, are visible at the Arboretum and Santa Anita Park. These hills are considered to be pressure ridges squeezed up between several branches of the fault.

Two trenches (6, 6A) were excavated at the base of the north slope of the Arboretum ridge (table 2.1; see supplementary section below entitled "Trenching"). Although the fault was not seen, a south-dipping lithologic contact of undetermined origin was exposed downslope from north-dipping alluvial deposits that may be of unit 4. The fault probably is north of the end of the trenches and inaccessible. Another trace presumably bounds the south side of the hill.

RECENT SURFACE CRACKING

Several localities were noted where pavement or structures showed cracking along the trace of the Raymond fault. Although these cracks were first thought to suggest fault creep (Payne and Wilson, 1974; Proctor, 1974), they are now considered to be largely the result of subsidence due to ground-water withdrawal. Tension cracks commonly form along basin boundaries as fluid is removed from unconsolidated alluvium within it. One unusual feature here, however, is that the cracks at the Sunny Slope Reservoir in Pasadena suggest a horizontal component of movement.

SURFACE EXPOSURES

The only known surface exposure of the Raymond fault is on the east side of Alhambra Wash in a manmade cut (loc. 59, pl. 2.4). Buwalda (1940, p. 44) also described what appear to be other breaks north of this site. The existing outcrop exposes the north-dipping main break(?) at the toe of the scarp. The fault plane juxtaposes unit 3 alluvium to the north against unit 2 or, possibly, unit 1 alluvium to the south. The fault is 5 to 10 cm wide and is iron stained. No gouge or other fault-generated debris is apparent.

LITHOLOGIC UNITS

Surficially, the Raymond fault displaces only alluvial deposits except in the Monrovia outlier, where crystalline

basement is presumed to be the upthrown block, at Raymond Hill, and at Grace Hill, where the Topanga Formation forms the upthrown block (map and cross section F-F', pl. 2.4).

The Topanga Formation, as exposed at Raymond and Grace Hills and along the Arroyo Seco north of the Raymond fault, consists of interbedded conglomerate, siltstone, and sandstone. All the exposed deposits are highly deformed by both folding and faulting. A more complete description of these units was given by Lamar (1970).

The area north of the fault zone between the Arroyo Seco and the Eaton Canyon flood plains is regarded as the southernmost part of the Altadena fan. This area is underlain by unit 3 deposits, consisting predominantly of massive poorly sorted fine-grained alluvial sand and sandy silt and lesser amounts of fluvial sand and gravel. These deposits appear to be very thin just north of the fault scarp because unit 4 alluvium crops out in several of the canyons that cross the scarp. Unit 4 alluvium has also been exposed in several excavations for foundation footings on the upper surface of the scarp.

Within and south of the fault zone in this same area, the alluvial deposits are younger and generally different in composition from those north of the fault (pl. 2.5; see subsection below entitled "Fault Displacement"). The topography indicates that fan building has occurred south of the fault; the fan heads are at the base of the scarp. Exposures in trenches 7, 14, 14A, and 15 showed that these deposits generally are much better sorted and bedded than those north of the fault (pl. 2.5).

In the past, faulting created ponds or small lakes large enough to allow accumulation of massive fine-grained silty sand and clayey sandy silt to a thickness of several meters. North of the fault, deposits of this type are associated with unit 4 gravel on the Patton estate west of the Huntington Library, and with unit 3 deposits at the Sunny Slope Reservoir, where they grade upward into Holocene marsh deposits rich in organic material (sample C-6, table 2.2). Eastward from the Eaton Wash concrete-lined channel, nearly all the surficial deposits along the Raymond fault zone are of unit 1 and consist of fluvial sand and gravel derived from the Eaton, Little Santa Anita, and Santa Anita drainages.

SEISMIC HISTORY

Careful examination of sedimentary features and deposits, as exposed in trenches 7, 14, and 14A (pl. 2.4; trench logs 7 and 14, pl. 2.5), has revealed significant new information on the seismic history of the Raymond fault zone. This information, along with ^{14}C ages on 11 samples collected from these trenches (pl. 2.5; table 2.2), allows an age or age limit to be assigned to the seismic events recognized.

Five events have been identified in the three trenches. In only one place—the southern break in trench 7 (pl. 2.5)—can the faulting features and ^{14}C ages be confidently combined to date the seismic event. In all other places, either a ^{14}C -dated feature is thought to record a seismic event (although it could have been from an earthquake on another fault), or faulting is recognized that can only be bracketed by dated units deposited an unknown period before or after the event.

Trench 7 at the Sunny Slope Reservoir exposed two separate faults (see trench log, pl. 2.5). The southern fault, which comes to within 3.3 m of the present ground surface and has a vertical displacement of only 6 cm, appears to record a single seismic event. The shaking that accompanied the event is indicated by the contorted and discontinuous silty-clay layers, which were probably still saturated and unconsolidated at the time of the event. The three $25,500 \pm 600$ -yr ages on samples C-3, C-4, and C-5 (table 2.2) precisely date this event.

The northern fault, which can be traced to within 1.3 m of the surface, terminates just short of a series of fingerlike fissures extending down from and filled with black marsh deposits rich in organic material. Sample C-6 (table 2.2), taken from one of these cracks, gave an age of $2,160 \pm 105$ yr B.P. Although this fissure could not be proved to be caused by faulting, this sample age is close to the age of $2,920 \pm 180$ yr B.P. on a similar sample collected from a fissure within the fault zone by Converse Consultants in a nearby trench (Payne and Wilson, 1974). The absence of correlatable units on both sides of the northern fault and the grossly different lithologies on either side indicate that multiple events have occurred along this fault.

San Marino High School trench 14 (see trench log, pl. 2.5), excavated by Le Roy Crandall & Associates, exposed two separate branches of the Raymond fault, 4 m apart. The considerably greater detail exposed in this trench adds significantly to the data on the seismic history of this fault. An age of $35,800 \pm 1,300$ yr B.P. was obtained on highly distorted clayey peat (sample C-16, table 2.2) at a depth of 3.8 m. The peat and surrounding deposits have the appearance of having been deformed by liquefaction (Sims, 1973, 1975; K.E. Sieh, oral commun., 1977) and by faulting. An age of $29,100 \pm 400$ yr B.P. was obtained on another deformed clayey peat with flame structures (sample C-17), 80 cm above sample C-16; the deformation of this layer also has the appearance of being due to liquefaction. This peat bed may record an event that occurred shortly after its deposition, or it may have been deformed during the event that caused the liquefaction features in the deposits 15 cm higher in the section. This upper set exhibits flame structures, slump structures, and a possible sandblow, 1.5 m south of the fault, that was

ejected from below and that also deformed and dislocated the surrounding silt beds.

An age of $10,600 \pm 160$ yr B.P. was obtained on a peaty silt (sample C-18, table 2.2) 1.9 m below the ground surface south of the southern fault trace. The reverse faulting of this layer records an event that occurred after its deposition but before deposition of the overlying 1.1 m of fluvial deposits, which record a subsequent normal-faulting event that dropped a fault-bounded wedge of these deposits downward to the north (pl. 2.5).

Sample C-19 (table 2.2), collected from the faulted lower part of the thick A horizon of the Holocene soil, yielded an age of $6,060 \pm 110$ yr B.P. This age and the age of 10,600 yr B.P. on sample C-18 bracket at least two events along the southern fault trace. The age of $6,060 \pm 110$ yr B.P. also places a maximum limit on the date of the event that displaced sample C-19.

Trench 14A, also excavated by Le Roy Crandall & Associates, 200 m west of trench 14, exposed a single branch of the Raymond fault. An age of $1,630 \pm 100$ yr B.P. was obtained on an apparently unfaulted paleosol (sample C-21, table 2.2) overlying the fault. A second sample (C-20) from a faulted paleosol, 30 cm lower than sample C-21 and south of the fault trace, yielded an age of $3,575 \pm 100$ yr B.P. These two ages appear to bracket the last movement at this locality and are consistent with the date associated with the youngest event seen in trench 7 (pl. 2.5).

FAULT DISPLACEMENT

Determination of the sense and extent of displacement on the Raymond fault has proved difficult, owing to the absence of exposures and of reliable subsurface data. That the Raymond is a high-angle reverse fault with considerable vertical slip is indicated by its high scarp and by its exposures in trenches; however, assessment of the total extent of vertical slip is more difficult.

Well logs were used to construct two cross sections across the Raymond Basin (pl. 2.4). The log of the Standard Oil Co. Live Oak Well No. 1, located 2.8 km south of the fault in San Gabriel, and logs from deep water wells in the central part of the basin were utilized to draw cross section G-G' (pl. 2.4), which shows the relations across the fault. The Live Oak well log indicates that the base of the alluvium is at a depth of 1,180 m; basement was penetrated at 2,460 m, with 1,280 m of intervening Tertiary sediment. Wells do not extend deep enough north of the fault to penetrate basement rock in the vicinity of cross section G-G'. A few driller's logs from wells north of the fault suggest Tertiary sediment at a depth of 230

m, but this information is questionable. Assuming south-dipping basement surfaces on either side of the fault, as much as 775 m of vertical displacement is possible. The gravity data of Sanford (1958) and Kingsley (1963) suggest that 190 m of post-Miocene displacement has occurred.

In the western part of the Raymond basin, however, evidence for vertical displacement is equivocal and somewhat contradictory. Three coreholes drilled by the California Department of Transportation (loc. 40; cross section *F-F'*, pl. 2.8) indicate diorite within 73 m of the surface south of the Raymond fault but no basement rocks within 107 m of the surface north of the fault. This relation is difficult to explain unless a significant amount of lateral displacement has also occurred.

Contrary to these data is some evidence that unit 4 alluvium north of the fault has been displaced vertically about 135 m, north side up. This evidence consists of notations of red clay and sand beds in drillers' logs for three wells south of the Raymond fault—beds considered to be equivalent to the unit 4 alluvium exposed at the top of the scarp.

We estimated the extent of vertical displacement during the past 36,000 years in the San Marino area as follows. Sedimentation rates were calculated from the ^{14}C ages on the deposits in trenches 7, 14, and 14A (table 2.2). We assumed that the sedimentation rate south of the fault equals the vertical slip rate, so that a constant gradient is maintained on the ground surface across the fault. The value used for the sedimentation/slip rate was 0.13 mm/yr—a weighted average from the data listed in table 2.2. Thus, at this rate, the estimated total vertical displacement during the past 36,000 yr is 4.7 m. This extent of displacement would indicate 0.58 m per seismic event, assuming eight events, or 0.39 m per event, assuming a 3,000-yr recurrence interval (see subsection below entitled "Fault Activity and Recurrence Interval Between Major Earthquakes"). This value is corroborated by the 0.66-m vertical offset of a sand bed (north side up) along what appeared to be a single break exposed in a Sunny Slope Water Co. pipeline trench (22, table 2.1).

Lateral displacement along the Raymond fault is much more difficult to assess. As noted above, the basement-surface relations across the west end of the fault suggest an unknown but significant amount of lateral slip, as do the apparent left-lateral displacements of small drainages. Lateral slip is also suggested by the drag features seen in trench 15 and by the variations in thickness of correlatable beds across several minor faults.

In summary, the total extent of displacement along the Raymond fault is unknown. The vertical displacement may range from 135 to 775 m, and the lateral displacement is unknown.

FAULT ACTIVITY AND RECURRENCE INTERVAL BETWEEN MAJOR EARTHQUAKES

We derived recurrence intervals and displacement rates for the Raymond fault from ^{14}C ages with analytical uncertainties ranging from ± 80 to $\pm 1,300$ years (at one standard deviation). All these ages were obtained from silt, clay, or soil, rich in organic material (table 2.2). The ages obtained on the soil samples are not the true ages of the soil but determinations of the mean residence time of the contained organic materials and thus are too young by an indeterminable amount. Thus, the dates for some events are minimums.

Even with no radiometric dates, the Raymond fault would appear to be considerably more active than the strands of the Sierra Madre fault zone along the range front. This greater activity is indicated by the abruptness of the Raymond fault scarp, the presence of several closed depressions along it, and the clear involvement of relatively young deposits. All these features contrast sharply with those at the base of the main mountain front. It might be argued, of course, that in the Pasadena area the Raymond fault is currently taking up the north-south compression that would otherwise be expressed in more activity along the Sierra Madre fault zone, but this hypothesis does not explain the seeming absence of Holocene activity along either fault zone for some distance eastward from Monrovia.

More definitive evidence for fault activity along the Raymond fault zone comes from the numerous radiocarbon ages obtained on materials from within the deformed zone, as discussed in detail in the preceding section. These trench data suggest as many as eight individual seismic events along the Raymond fault within the past 36,000 yr. Five of these events are reasonably well documented, whereas evidence for the remaining three is only suggestive; moreover, additional events might well have occurred for which evidence does not remain or has not been found.

Sample C-16 suggests a seismic event at 35,800 yr B.P., which we term event 1. Event 2, at 25,500 yr B.P., is demonstrated by samples C-4 and C-5. Sample C-17 may also record event 2. Samples C-18 and C-19 bracket events 3 and 4 between 10,600 and 6,060 yr B.P., and sample C-19 also places a maximum date of 6,060 yr B.P. on event 5. We assume that event 5 is also the event that affected samples C-6, C-20, and CDA-1, which is bracketed at between 2,160 and 1,630 yr B.P. by samples C-6 and C-21.

There is some indication that the event that disturbed sample C-17 predated event 2; this event is here termed "event 1A." An additional event, 2A, may be recorded in the possible liquefaction and faulting of the organic

clayey silt 1 m below sample C-18. Another event, 4A, may be recorded in the inclined fault above sample C-18, bounding the south side of the downdropped wedge and subsequent to event 4 on the vertical fault bounding the north side of the wedge.

Thus, the eight suggested events, from the oldest to youngest, are as follows:

Event	Date (yr B.P.)
1	$35,800 \pm 1,300$
1A	$29,100 \pm 400$
2	$25,500 \pm 600$
2A	$29,100 \pm 400$ to $10,600 \pm 160$
3	$10,600 \pm 160$ to $6,060 \pm 110$
4	$10,600 \pm 160$ to $6,060 \pm 110$
4A	—
5	$2,160 \pm 105$ to $1,630 \pm 100$

If these eight events represent all the major earthquakes during this 36,000-yr period, then the average recurrence interval between such events is 4,500 yr. Assuming that some events were undetected in our study, the true recurrence interval is probably somewhat less, possibly 3,000 years. In comparison with the Sierra Madre fault zone to the north, it is particularly significant that at least three events occurred within Holocene time—the most recent about 2,200–1,500 yr B.P. Before jumping to the conclusion that the Raymond fault is highly active, however, we note that the apparent recurrence interval between major earthquakes on the adjacent segment of the San Andreas fault, 35 km to the north, is about 160 years (Sieh, 1978), perhaps only a 20th of the interval on the Raymond fault.

Estimation of the maximum credible earthquake on the Raymond fault must be based almost entirely on maximum rupture length, inasmuch as we have no other realistic basis for judgement. Assuming a fracture length of 15 km from Monrovia to the Arroyo Seco, and using the regression relation of Slemmons (1977), we derive an average magnitude of 6.5. The regression analysis of Mark and Bonilla (1977) gives a magnitude of 6.9 for that same fault length that illustrates the uncertainties in this type of approach. We prefer the basic data set of Slemmons, and, in our judgment, a magnitude (M_L) of $6\frac{3}{4}$ represents a realistic maximum credible earthquake for the Raymond fault—albeit an exceedingly unlikely one.

SUMMARY OF SEISMIC-HAZARD EVALUATION

All the major faults within the study area may be considered active in the sense that they cut Quaternary rocks, and, indeed, the total Quaternary displacement on some breaks may be several kilometers. The very existence of the San Gabriel Mountains and their steep south face testifies to this continuing tectonic activity. Of far greater

relevance to seismic-hazard evaluation, however, is the surprising variation in the fault activity of the various faults within the study area. Furthermore, the current fault activity of many of these faults may differ considerably from that averaged over all of Quaternary time, and so we have concentrated our attention on the Holocene and very latest Pleistocene fault-movement histories in the belief that this very recent history is most relevant to hazard evaluation. Abundant worldwide evidence suggests that faults which have been most active in the recent geologic past are those with which we must be concerned in planning for the near future (Allen, 1975).

Increased awareness of earthquake hazards in the greater Los Angeles area (for example, Environmental Research Laboratories, 1973) has in recent years led to several new Government regulations, such as those of the Alquist-Priolo Act (Hart, 1974) and in the requirements for local seismic-safety elements (Wiggins, 1974; Envicom Corp., 1975). The results of our studies generally reinforce the need for such regulations. In particular, we agree that most of the Raymond fault is sufficiently active and well located that it should be included under the coverage of the Alquist-Priolo Act, and we agree with the current tentative proposal that only parts of the Sierra Madre fault zone should be so designated.

As discussed in detail in the preceding sections, we consider the maximum credible earthquake on the Sierra Madre fault system between Dunsmore and San Gabriel Canyons to be of magnitude (M_L) 7 and to have a recurrence interval between major events of more than 5,000 yr. No demonstrable Holocene displacement has occurred along this segment, in sharp contrast to the San Fernando segment to the west. Also in contrast, the Raymond fault, which lies 5 km south of the Sierra Madre fault in Pasadena but converges with it toward the east, has had at least three displacements associated with significant earthquakes within Holocene time; at least eight such events have occurred within the past 36,000 years. The recurrence interval between major events on the Raymond fault may be 3,000 yr, and we judge the maximum credible earthquake on this fault to be of magnitude (M_L) $6\frac{3}{4}$.

It is interesting to compare our estimates with those of other workers. Greensfelder (1974) proposed a magnitude of 7.5 for the maximum credible earthquake on the "Malibu-Santa Monica-Raymond Hill" fault. However, this large-magnitude assignment results from assuming a total length for the active fault zone that we do not believe is supported by geologic studies, particularly that of Lamar (1970). We see no evidence that the Raymond fault extends westward as an active feature much beyond the Arroyo Seco in Pasadena. For the Sierra Madre fault, Greensfelder (1974) assigned a magnitude of 6.5 to the

maximum credible earthquake, but this value is apparently based on the assumption that the short segment north of Pasadena is independent of segments farther east and west. In contrast, Wesson and others (1974) assigned a magnitude of $7\frac{1}{2}$ to $7\frac{3}{4}$ to the "maximum expectable earthquake" on the Sierra Madre fault, primarily on the basis of the assumed 130-km length of this fault and on comparisons with the 1952 Kern County earthquake, generally assumed to be of magnitude 7.7. We take an intermediate position on the basis of our studies and recognize distinct salients within the fault zone that appear to have limited mechanical independence, partly following Ehlig (1975). Furthermore, as discussed earlier, we consider it inappropriate to directly compare the Sierra Madre fault with the White Wolf fault, whose movement caused the 1952 Kern County earthquake. Although both faults are thrust faults and are, to some degree, mirror images of one another across the "big bend" of the San Andreas fault, they differ significantly in their detailed geometry and in their degree of Holocene activity. Additionally, recent studies by Kanamori and Jennings (1978) indicated an M_L of about 7.2 for the 1952 event and that the magnitude of 7.7 earlier assigned by Gutenberg (1955) is more nearly a surface-wave magnitude (M_S). Not only is M_L the magnitude that should be compared with those of other earthquakes in the southern California catalog (for example, the magnitude of 6.4 for the 1971 San Fernando earthquake), but M_L is measured at frequencies of ground motion much more relevant to the evaluation of engineering damage than is M_S .

Recent reports by engineering consultants concerning earthquake-resistant design for dams in the foothills area have assigned values for the maximum credible (or equivalent) earthquake on the Sierra Madre fault that range from 7.0 to 7.5. Postulated recurrence intervals between such events have been approximately a few hundred years, much less than we now propose on the basis of the absence of demonstrable Holocene displacements along this segment of the fault zone.

A general conclusion from our study is that the magnitudes of the maximum credible earthquakes we propose do not grossly differ from those proposed by earlier workers. On the other hand, the projected recurrence intervals between major earthquakes on these two fault zones are far greater than those proposed earlier, particularly for the Sierra Madre fault zone in this area.

REFERENCES CITED

- Allen, C. R., 1975, Geological criteria for evaluating seismicity: Geological Society of America Bulletin, v. 86, no. 8, p. 1041-1057.
- Allen, C. R., St. Amand, Pierre, Richter, C. F., and Nordquist, J. M., 1965, Relationship between seismicity and geologic structure in the southern California region: Seismological Society of America Bulletin, v. 55, no. 4, p. 753-797.
- Arnold, Ralph, and Strong, A. M., 1905, Some crystalline rocks of the San Gabriel Mountains, California: Geological Society of America Bulletin, v. 16, p. 183-204.
- Bailey, T. H., and Jahns, R. H., 1954, Geology of the Transverse Range province, Southern California, [pt.] 6 of Geology of the natural provinces, chap. 2 of Jahns, R. H., ed., Geology of Southern California: California Division of Mines Bulletin 170, p. 83-106.
- Barrows, A. G., Kahle, J. E., Weber, F. H., Saul, R. B., and Morton, D. M., 1975, Surface effects map of the San Fernando earthquake area, pl. 3 of Oakeshott, G. B., ed., San Fernando, California, earthquake of 9 February 1971: California Division of Mines and Geology Bulletin 196, scale 1:24,000.
- Beattie, R. L., 1958, Geology of the Sunland-Tujunga [Calif.] area: Los Angeles, University of California, M.A. thesis, 102 p.
- Bolt, B. A., 1978, Incomplete formulations of the regression of earthquake magnitude with surface fault rupture length: Geology, v. 6, no. 4, p. 233-235.
- Bull, W. B., 1964, Geomorphology of segmented alluvial fans in western Fresno County, California: U.S. Geological Survey Professional Paper 352-E, p. 89-129.
- Bull, W. B., Menges, C. M., and McFadden, L. D., 1979, Stream terraces of the San Gabriel Mountains, southern California: Final technical report, U.S. Geological Survey Contract 14-08-0001-G-394, 139 p.
- Buwalda, J. P., 1940, Geology of the Raymond Basin: Report to Pasadena Water Department, 131 p.
- , 1948, Geologic faulting in southern California: The process, its effects, and its consequences: Engineering and Science Monthly, February, p. 15-18.
- California Department of Water Resources, 1966, Geohydrology, app. A of Planned utilization of ground water basins: San Gabriel Valley: Bulletin 104-2, 230 p.
- , 1971, Meeting water demands in the Raymond Basin area: Bulletin 104-6, 54 p.
- California Division of Mines and Geology, 1964, Preliminary geologic map of the SW-1/4 Glendora quadrangle, Los Angeles County: Sacramento, scale 1:9,600.
- California Division of Water Resources, 1941, Report of Referee in the Superior Court of the State of California in and for the County of Los Angeles; City of Pasadena vs. City of Alhambra, and others (Raymond Basin): Sacramento, 2 v.
- California Water Rights Board, 1961, Draft of report of Referee in the Superior Court of the State of California in and for the County of Los Angeles; the City of Los Angeles, a municipal corporation, plaintiff, vs. City of San Fernando, a municipal corporation, et al., defendants (No. 650079): Sacramento, 2 v.
- Castle, R. O., Church, J. P., and Elliott, M. R., 1976, Aseismic uplift in southern California: Science, v. 192, no. 4236, p. 251-253.
- Chawner, W. D., 1934, The Montrose-La Crescenta flood of 1934 and its sediments: Pasadena, California Institute of Technology, M.S. thesis, 42 p.
- Conkling, Harold, 1927, San Gabriel investigation: California Department of Public Works, Division of Water Rights Bulletin 5, 640 p.
- Converse Consultants, 1971, Geological investigation of the Jet Propulsion Laboratory, Pasadena, California: Pasadena, Calif., Rept. No. 71-222-H, 150 p.
- Cotton, W. R., Hay, E. A., and Hall, N. T., 1977, Analysis of active thrust-faulting on the White Wolf fault, Kern County, California [abs.]: Geological Society of America Abstracts with Programs, v. 9, no. 4, p. 405.
- Davis, W. M., 1927, The rifts of southern California: American Journal of Science, ser. 5, v. 18, p. 57-72.
- Eaton, G. P., 1957, Miocene volcanic activity in the Los Angeles Basin

- and vicinity; Pasadena, California Institute of Technology, Ph. D. dissertation, 388 p.
- Eckis, R. P., 1928, Alluvial fans of the Cucamonga district, southern California: *Journal of Geology*, v. 36, no. 3, p. 224-247.
- _____, 1934, Geology and groundwater storage capacity of valley fill: California Division of Water Resources Bulletin 45, p. 279.
- Eckmann, E. C., and Zinn, C. J., 1917, Soil survey of the Pasadena area California: U.S. Department of Agriculture, Bureau of Soils, 56 p.
- Ehlig, P. L., 1975, Geologic framework of the San Gabriel Mountains, chap. 2 of Oakeshott, G. B., ed., San Fernando, California, earthquake of 9 February 1971: California Division of Mines and Geology Bulletin 196, p. 7-18.
- Envicom Corp., 1975, Seismic safety element for thirteen cities in the San Gabriel Valley: Sherman Oaks, Calif., 129 p. and 2 appendices.
- _____, 1977, Geologic investigation of tentative tract 33532, Duarte, California: Sherman Oaks, Calif., 6 p.
- Environmental Research Laboratories, 1973, A study of earthquake losses in the Los Angeles, California area: Boulder, Colo., U.S. Department of Commerce, National Oceanic and Atmospheric Administration, 331 p.
- Ericson, D. B., Ewing, Maurice, Wollin, Goesta, and Heezen, B. C., 1961, Atlantic deep-sea sediment cores: Geological Society of America Bulletin, v. 72, no. 2, p. 193-285.
- Greensfelder, R. W., 1974, Maximum credible rock acceleration from earthquakes in California: California Division of Mines and Geology Map Sheet 23, 12 p., scale 1:2,500,000.
- Gutenberg, Beno, 1955, Magnitude determination for larger Kern County shocks, 1952; effects of station azimuth and calculation methods, [chap.] 8 of Seismology, pt. 2 of Oakeshott, G. B., ed., Earthquakes in Kern County California during 1952: California Division of Mines Bulletin 171, p. 171-175.
- Hart, E. W., 1974, Zoning for surface fault hazards in California: The new special studies zones maps: California Geology, v. 27, no. 10, p. 227-230.
- Hill, M. L., 1930, Structure of the San Gabriel Mountains, north of Los Angeles, California, with a Forward by F. S. Hudson: University of California Publications, Department of Geological Sciences Bulletin, v. 19, no. 6, p. 137-170.
- Hsu, K. J., Edwards, George, and McLaughlin, W. A., 1963, Age of the intrusive rocks of the southeastern San Gabriel Mountains, California: Geological Society of America Bulletin, v. 74, no. 4, p. 507-512.
- Jahns, R. H., 1971, Geologic hazards, associated risk, and the decision-making process, in *Earthquake risk*: Joint Committee on Seismic Safety Conference, Carmel, Calif., 1971, Proceedings, p. 39-53.
- _____, 1973, Tectonic evolution of the Transverse Ranges province as related to the San Andreas fault system, in *Proceedings of the conference on tectonic problems of the San Andreas fault system*: Stanford University Publications in the Geological Sciences, v. 13, p. 149-170.
- Jahns, R. H., and Proctor, R. J., 1975, The San Gabriel and Santa Susana-Sierra Madre fault zones in the western and central San Gabriel Mountains, southern California [abs.]: Geological Society of America Abstracts with Programs, v. 7, no. 3, p. 329.
- Jennings, C. W., compiler, 1977, Geologic map of California: Sacramento, California Division of Mines and Geology, scale 1:750,000.
- Jennings, C. W., and Strand, R. G., compilers, 1969, Los Angeles sheet of Geologic map of California: California Division of Mines and Geology, scale 1:250,000.
- Kamb, Barclay, Silver, L. T., Abrams, M. J., Carter, B. A., Jordan, T. H., and Minster, J. B., 1971, Pattern of faulting and nature of fault movement in the San Fernando earthquake, in *The San Fernando, California, earthquake of February 9, 1971*: U.S. Geological Survey Professional Paper 733, p. 41-54.
- Kanamori, Hiroo, and Jennings, P. C., 1978, Determination of local magnitude, M_L , from strong-motion accelerograms: *Seismological Society of America Bulletin*, v. 68, no. 2, p. 471-485.
- Kew, W. S. W., 1924, Geology and oil resources of a part of the Los Angeles and Ventura Counties, California: U.S. Geological Survey Bulletin 753, 202 p.
- Kingsley, John, 1963, Gravity and general geology of the San Gabriel Valley: Los Angeles, University of California, M.A. thesis, 31 p.
- Lamar, D. L., 1970, Geology of the Elysian Park-Repetto Hills Area, Los Angeles County, California: California Division of Mines and Geology Special Report 101, 45 p.
- Larsen, E. S., Jr., Gottfried, David, Jaffe, H. W., and Waring, C. L., 1958, Lead-alpha ages of the Mesozoic batholiths of western North America: U.S. Geological Survey Bulletin 1070-B, p. 35-62.
- Marchand, D. E., 1977, The Cenozoic history of the San Joaquin Valley and adjacent Sierra Nevada as inferred from the geology and soils of the eastern San Joaquin Valley, in Singer, M. I., ed., *Guidebook for joint session of American Society of Agronomy, Soil Science Society of America and Geological Society of America*: Modesto, Calif., p. 39-50.
- Mark, R. K., and Bonilla, M. G., 1977, Regression analysis of earthquake magnitude and surface fault length using the 1970 data of Bonilla and Buchanan: U.S. Geological Survey Open-File Report 77-614, 8 p.
- McGee, W. J., 1897, Sheetflood erosion: Geological Society of American Bulletin, v. 8, p. 87-112.
- McGlashan, H. D., and Ebert, F. C., 1918, Southern California floods of January 1916: U.S. Geological Survey Water-Supply Paper 137, 140 p.
- Mendenhall, W. C., 1908, Foothill belt, southern California: U.S. Geological Survey Water-Supply Paper 219, 180 p.
- Miller, W. J., 1934, Geology of the western San Gabriel Mountains of California: University of California Publications in Mathematics and Physical Sciences, v. 1, no. 1, p. 1-114.
- Morton, D. M., 1973, Geology of parts of the Azusa and Mt. Wilson quadrangles, San Gabriel Mountains, Los Angeles County, California: California Division of Mines and Geology Special Report 105, 21 p.
- _____, 1975, Seismically triggered landslides in the area above the San Fernando Valley, chap. 10 of Oakeshott, G. B., ed., San Fernando, California, earthquake of 9 February 1971: California Division of Mines and Geology Bulletin 196, p. 145-154.
- _____, 1976, Geologic map of the Cucamonga fault zone between San Antonio Canyon and Cajon Creek, San Gabriel Mountains, southern California: U.S. Geological Survey Open-File Report 76-726.
- Morton, D. M., and Baird, A. K., 1975, Tectonic setting of the San Gabriel Mountains, chap. 1 of Oakeshott, G. B., ed., San Fernando, California, earthquake of 9 February 1971: California Division of Mines and Geology Bulletin 196, p. 3-6.
- Oakeshott, G. B., 1958, Geology and mineral deposits of the San Fernando quadrangle, Los Angeles County, California: California Division of Mines and Geology Bulletin 172, 147 p.
- Payne C. M., and Wilson, K. L., 1974, Age dating recent movement on the Raymond fault, Los Angeles County, California [abs.]: Geological Society of America Abstracts with Programs, v. 6, no. 3, p. 234-235.
- Proctor, R. J., 1974, New localities for fault creep in southern California—Raymond and Casa Loma faults [abs.]: Geological Society of America Abstracts with Programs, v. 6, no. 3, p. 238.
- Proctor, R. J., Crook, Richard, Jr., McKeown, M. H., and Moresco, R. L., 1972, Relation of known faults to surface ruptures, 1971 San Fernando earthquake, southern California: Geological Society of America Bulletin, v. 83, no. 6, p. 1601-1618.
- Proctor, R. J., and Payne, C. M., 1972, Evidence for, and engineering consequences of recent activity along the Sierra Madre fault zone, southern California [abs.]: Geological Society of America Abstracts with Programs, v. 4, no. 3, p. 220.
- Proctor, R. J., Payne, C. M., and Kalin, D. C., 1970, Crossing the Sierra Madre fault in the Glendora tunnel, San Gabriel Mountains, Califor-

- nia: *Engineering Geology*, v. 4, no. 1, p. 5-63.
- Sanford, A. R., 1958, Gravity survey of a part of the Raymond and San Gabriel basins: Pasadena, California Institute of Technology, Ph. D. dissertation, 142 p.
- Saul, R. B., 1976, Geology of the west central part of the Mt. Wilson 7-1/2' quadrangle, San Gabriel Mountains, Los Angeles County, California: California Division of Mines and Geology Map Sheet 28, 15 p., scale 1:12,000.
- 1977, Geologic hazards, Mt. Wilson quadrangle: California Geology, v. 30, no. 2, p. 35-36.
- Sharp, R. V., 1975, Displacement on tectonic ruptures, chap. 15 of Oakeshott, G. B., ed., San Fernando, California, earthquake of 9 February 1971: California Division of Mines and Geology Bulletin 196, p. 187-194.
- Shelton, J. S., 1946, Geology of northeast margin of San Gabriel Basin, Los Angeles County, California: U.S. Geological Survey Oil and Gas Investigations Preliminary Map 63, scale 1:24,000.
- 1955, Glendora volcanic rocks, Los Angeles Basin, California: Geological Society of America Bulletin, v. 66, no. 1, p. 45-89.
- Sieh, K. E., 1978, Prehistoric large earthquakes produced by slip on the San Andreas fault at Pallett Creek, California: Journal of Geophysical Research, v. 83, no. B8, p. 3907-3939.
- Silver, L. T., 1971, Problems of crystalline rocks of the Transverse Ranges: Geological Society of America Abstracts with Programs, v. 3, no. 2, p. 193-194.
- Silver, L. T., McKinney, C. R., Deutsch, S. M., and Bolinger, Jane, 1963, Precambrian age determinations in the western San Gabriel Mountains, California: Journal of Geology, v. 71, no. 2, p. 196-214.
- Sims, J. D., 1973, Earthquake induced structures in sediments of Van Norman Lake, San Fernando, California: Science, v. 182, no. 4108, p. 161-163.
- 1975, Determining earthquake recurrence intervals from deformational structures in young lacustrine sediments, in Pavoni, Nazario, and Green, Ronald, eds., Recent crustal movements: Tectonophysics, v. 29, no. 1-4 (special issue), p. 141-152.
- Slemmons, D. B., 1977, Faults and earthquake magnitude: Report 6, Miscellaneous Paper S-73-1, State-of-the-art for assessing earthquake hazards in the United States, U.S. Army Engineer Waterways Experiment Station.
- Soil Survey Staff, 1975, Soil taxonomy: A basic system of soil classification for making and interpreting soil surveys: U.S. Department of Agriculture, Soil Conservation Service Agriculture Handbook 436, 754 p.
- Troxell, H. C., 1942, Floods of March 1938 in southern California: U.S. Geological Survey Water-Supply Paper 844, 399 p.
- Wallace, R. E., 1977, Profiles and ages of young fault scarps, north-central Nevada: Geological Society of America Bulletin, v. 88, no. 9, p. 1267-1281.
- Wellman, H. W., 1955, The geology between Bruce Bay and Haast River, South Westland (2nd ed.): New Zealand Geological Survey Bulletin n.s. 48, 46 p.
- Wesson, R. L., Page, R. A., Boore, D. M., and Yerkes, R. F., 1974, Expectable earthquakes and their ground motions in the Van Norman reservoirs area: U.S. Geological Survey Circular 691-B, p. B1-B9.
- Wiggins, J. H., Co., 1974, Seismic safety study—City of Los Angeles: Redondo Beach, Calif., Technical Report 74-1199-1, 398 p.
- observed and the conclusions reached from each excavation. The initial numbers preceding each description correspond to the trench numbers.
1. *Foothills Junior High School, Arcadia*.—The trench was excavated in the athletic field across an apparent scarp of the Raymond fault as observed on 1929 Fairchild aerial photographs. The site was picked at the break in slope from original grading maps. Observations: A 1-m-high scarp-like feature was noted, and continuity of horizontal bedding was established for the entire length of the trench, although a thin sand lens with an anomalous steep southward dip was observed at the south end. Conclusions: The deposits exposed in the trench are probably unit 2 and are not faulted (loc. 60, pl. 2.4).
2. *Arroyo Seco, north of JPL Bridge, Pasadena*.—The trench was excavated in the stream bottom just north of the east bridge pier. The site was picked to reinterpret relations uncovered previously by Converse Consultants of Pasadena. Observations: A branch of the Sierra Madre fault zone was exposed; Mesozoic basement rock is thrust over unit 3 alluvium. The fault zone consists of 30 cm of clay gouge and as much as 150 cm of crushed rock, with one main and several minor fault surfaces; the zone strikes N. 40° W. and dips 30°-40° N. The unit 3 alluvium contains highly weathered diorite clasts, some of which have been smeared out by faulting. Conclusions: This trench exposes one of the major fault branches at the mountain front. Recent alluvium did not seem to be faulted, as had previously been suspected (loc. 24, pl. 2.2).
3. *Eaton Canyon, Pasadena*.—The trench was excavated along the inside edge of the old Mount Wilson Toll Road, approximately 46 m west of the bridge, between outcrops of unit 3 alluvium and quartz monzonite. Observations: A branch of the Sierra Madre fault zone was exposed; Mesozoic basement rock is thrust over unit 3 alluvium. The fault zone consists of 13 cm of clay gouge and 60 cm of crushed granitic rock. Three separate fault surfaces were observed; the zone strikes N. 70° W. and dips 45° N. The upper several centimeters of unit 3 alluvium is well indurated. The fault contact between granitic rock and unit 3 alluvium is very sharp. Conclusions: This fault branch could not be traced upward in unit 3 alluvium and probably has not been recently active; it is only one of several thrust faults at the mountain front in this area (loc. 35, pl. 2.2).
- 3A. *Eaton Canyon, Pasadena*.—This trench was excavated along the inside edge of a road, 10 m below the southeast end of trench 3 and on the strike of the fault exposed in trench 3. Observations: Unit 2 alluvium, consisting of loose moderately well bedded sand and gravel, was exposed. Continuity of bedding was established for the entire 21 m of trench. Conclusions: Unit 2 alluvium once filled Eaton Wash to an elevation of 8 to 9 m above the present channel. The absence of faulting in these deposits indicates only pre-Holocene movement for this fault branch.
4. *East of Pasadena Glen, west of Hastings Canyon, Pasadena*.—Excavation consisted of scraping off the existing roadcut where a thrust fault had previously been mapped; Mesozoic basement rock is thrust over unit 4 alluvium. Observations: The exposure showed banded gneiss overlying unit 4 alluvium along an indistinct contact. Fault gouge is absent. Conclusions: This thrust fault is one of several along the Sierra Madre fault zone at the mountain front; at least one additional branch lies to the south (loc. 44, pl. 2.2).
5. *Clairbourn School, San Marino*.—A 33-m-long trench was excavated by Leighton & Associates, Inc., perpendicular to an east-west-trending lineament observed on a 1929 Fairchild aerial photograph. Observations: An old filled-in east-west-trending gully was exposed. Continuity of bedding in older alluvium was established along the entire trench length. Conclusions: The southern branch of the Raymond fault probably does not extend westward to this site. The lineament is probably an erosional feature.
- 6 and 6A. *Los Angeles County Arboretum, Arcadia*.—Both trenches were excavated at the base of the north slope of the pressure ridge between two branches of the Raymond fault. Observations: Bedding in the alluvium dips 15° N. Unit 3(?) alluvium and younger colluvium ap-

APPENDIXES

TRENCHING

A total of 33 trenches and pits were excavated for this project: 23 by backhoe, 6 by tracked front-end loader, 1 by Poclain excavator, and 3 by hand (table 2.1). This section summarizes the important features

pear to lie unconformably over unit 4(?) alluvium. Both trenches had a planar feature, striking N. 70° E. and dipping 50° to 75° S., that shows a lithologic and color change only. There was no evidence of displacement or fault-generated debris. Conclusions: Although warping of the sediment is apparent, the main branch of the Raymond fault was not penetrated; it may be beyond the north end of the trenches (loc. ⑥, pl. 2.4).

7. *Sunny Slope Reservoir, Pasadena.*—The trench was excavated across the northern branch of the Raymond fault at a site adjacent to trenches dug previously by other workers. Observations: Two separate fault planes were exposed, both cutting marsh deposits of different ages, rich in organic material. Distinct lithologies were found on either side of the north trace. The fault zone strikes N. 70°–85° E. and dips 30°–80° N. The most recent soil appears to have been affected by faulting. Several samples were collected for ¹⁴C dating. Conclusions: This trench exposed the main branch of the Raymond fault. There is evidence of Holocene faulting, and the lithologic relations observed and ¹⁴C ages obtained have added significantly to our knowledge of the seismic history of this fault (see trench log, pl. 2.5; loc. ⑥, pl. 2.4).

8. *Lacy Park, San Marino.*—A 14.5-m-long trench was excavated on the slope between the fault scarp and the old Wilson Lake site. Observations: A 6-m-thick deposit of colluvium was exposed. No fault features were observed, and continuity of bedding was established along the entire length of the trench at depth. Conclusions: The Raymond fault does not cut these deposits and probably lies a short distance beyond the north end of the trench (loc. ⑧, pl. 2.4).

9. *JPL, northwest of Building 32, Pasadena.*—The trench was excavated by Le Roy Crandall & Associates. Observations: A branch of the Sierra Madre fault zone was exposed, showing Mesozoic basement rock thrust over unit 3 alluvium (fig. 2.8). The fault zone consists of several splay faults; the main fault contains 1 to 2 cm of clay gouge. The basement rock is highly crushed for 3 m above the fault, and the alluvium is moderately indurated for 12 cm below the fault. The fault strikes N. 85°–90° E. and dips 29°–33° N. The fault is overlain by colluvium derived from unit 2 alluvium upslope. Conclusions: This trench exposes the same major branch of the fault as that seen in trench 2. The fault does not cut later Holocene colluvium at this site (loc. ⑨, pl. 2.1).

10. *JPL, Building 150, Pasadena.*—The original exposure was made during construction of Building 150 and was reexposed by hand. Observations: Mesozoic basement rock is thrust over unit 4 alluvium; several fault surfaces and a landslide complicate the picture. Conclusions: This splay of the main fault branch appears to be quite old because the fault does not displace the soil developed on unit 4 alluvium upslope.

11. *Gully west of Passionist Fathers Monastery, Sierra Madre.*—This exposure was excavated by hand. Observations: The excavation exposed Mesozoic basement rock thrust over unit 4 alluvium. The fault plane strikes N. 70° W. and dips 50° N. The upper part of the fault surface dips south, owing to downhill sliding or creep, and is overlain by fresh (unit 1?) colluvium and bedded sand. Conclusion: This is a major branch of the Sierra Madre fault zone, but it has not displaced the overlying slide debris or unit 1(?) alluvium (loc. ⑩, pl. 2.2).

12. *Gould Canyon, La Canada.*—This exposure was excavated by hand in the bottom of Gould Canyon. Observations: The excavation exposed Mesozoic basement (diorite) rock thrust over unit 4 alluvium. The fault surface strikes N. 5° W. and dips 20° W., and consists of 2 to 10 cm of clay gouge. Conclusions: The attitude of the fault surface is anomalous and appears to be part of a gravity-controlled thrust-rooted slide. This fault is a major branch of the Sierra Madre zone (loc. ⑪, pl. 2.1).

13 and 13A. *West of Van Tassel Canyon, Duarte.*—Trenches were excavated parallel to, and within 3 m of, two of seven trenches dug previously by a consulting firm. The logs prepared by the consultant for all seven of these trenches showed one or two traces of the Sierra Madre fault zone displacing alluvium. Our intent was to log the trenches in more detail and to collect soil rich in organic material, shown on the

consultant's logs, for ¹⁴C dating. Observations: No evidence of faulting was seen in either trench, and continuity of bedding was established for the entire length of both trenches. Conclusions: The subtle lithologic changes interpreted by other workers as faulting are probably due to depositional variations. The Sierra Madre fault zone, located in this area on magnetic surveys of other workers, is buried by a minimum of 3.5 m of undisturbed unit 2(?) alluvium (loc. ⑫, pl. 2.3).

14 and 14A. *San Marino High School, San Marino.*—Two trenches near the athletic field were excavated by Le Roy Crandall & Associates. The Raymond fault was exposed in both trenches. Observations: The easternmost trench exposed two separate fault traces within a complex sequence of clay, silt, sand, and gravel rich in organic material. Several faulting events are recognizable; the northernmost trace is the most recently active one and affects the B horizon of the modern soil. Lithologies differ strikingly across this trace: The north side consists of massive sandy clayey silt, and the south side of bedded sand and gravelly sand of fluvial origin. The fault strikes N. 70°–80° E. and dips 60°–90° N. Eight samples of clay and silt rich in organic material were collected for ¹⁴C dating. Conclusions: The main branch of the Raymond fault zone locally consists of more than one fault trace. The most recent movement appears to be predominantly strike-slip. The lithologic relations seen and ¹⁴C dates (table 2.2) obtained have added considerably to our knowledge of the seismic history of the Raymond fault (see trench log, pl. 2.5; loc. ⑬, pl. 2.4).

15. *Edison Company Powerline right-of-way, Chapman Woods, Pasadena.*—A single trench was dug across the Raymond fault under the powerlines and 100 m north of Huntington Drive. Observations: The major fault and several minor faults were exposed in this trench. South of the main fault, the units consist of bedded fluvial sand and gravel, with two interbedded paleosols. North of the fault, similar deposits contain several massive clayey sandy silt beds that are not found south of the fault. Correlation of units across the minor faults is generally possible at shallow depths but impossible in much of the lower half of the trench. Alluvial units within 0.3 m of the surface have been affected by faulting. Both strike-slip and dip-slip movement is evident. The fault zone is 11 m wide at this site; the fault surface strikes N. 50°–85° E. and dips 40°–90° N. Four samples were collected for ¹⁴C dating. Conclusions: The Raymond fault zone is locally quite complex; it commonly consists of several discrete fault surfaces, the most conspicuous of which appears to be the one most recently active. Strike-slip displacement appears to be the predominant sense of movement (loc. ⑭, pl. 2.4).

16 and 16A. *Rubio Canyon, Altadena.*—Two trenches were excavated across a suspected fault trace within the upper part of the Rubio Canyon debris basin. The site was picked on the basis of the report by Saul (1977). Observations: The fault trace was not uncovered. Conclusions: The alluvium in the trenches has not been faulted, and the seeps noted by Saul were probably caused by water flowing on top of silt beds.

17. *Santa Anita Wash, Arcadia.*—A trench was excavated in unit 1 alluvium across the projected trace of a branch of the Sierra Madre fault zone. Observations: The fault was not uncovered; almost the entire trench was in artificial fill.

18A, 18B, and 18C. *Dunsmore Canyon, Glendale.*—Three trenches were excavated across the southernmost of two apparent scarps on the Dunsmore fan surface. The fault was exposed in all three trenches. Observations: The trenched scarp is 4 m high. A single fault plane, in places obscure, was exposed in each trench. There were some indications of multiple fault planes in trench B. The faulted deposits are of unit 2 alluvium. The fault surfaces contain no gouge, and commonly the only evidence of faulting is a color change or smeared clasts. Conclusions: The scarp height suggests multiple faulting events. This alluvium is the youngest for which movement is documented along the Sierra Madre fault zone within the study area east of the 1971 San Fernando earthquake zone. These observations indicate late(?) Holocene movement (see trench log, fig. 2.5; loc. ⑯, pl. 2.1).

TABLE 2.3.—*P*-wave velocities in clasts of Lowe Granodiorite from a sequence of alluvial deposits near the mouth of the Arroyo Seco

Alluvial-deposit sequence	Average clast velocity (km/s)	Standard deviation of mean	Number of clasts measured
A (oldest)	1.20	.06	52
B	1.41	.07	28
C	1.58	.06	36
D	1.77	.06	48
E	1.60	.09	17
F (youngest)	2.01	.05	38

19. *Bradbury*.—A 52-m-long trench was excavated at the bottom of the prominent scarplike feature near the south boundary of the city of Bradbury. Observations: No definite fault features were exposed. Continuity of bedding was verified for the entire trench length. Conclusions: The trenched deposits are not faulted.

20A, 20B, and 20C. *Near Sierra Madre Villa Dam, east of Pasadena Glen, west of Hastings Canyon, Pasadena*.—Three trenches were excavated at two separate sites; the fault was exposed in all three trenches. Observations: In each trench, Mesozoic basement is thrust over unit 4 alluvium and younger colluvium of undetermined age. The fault surface strikes N. 55° W.–30° E. and dips 7°–20° N. The fault plane in trench C is truncated and overlain by 0.6 m of younger alluvium. A piece of wood was collected from the alluvium for ¹⁴C dating. Conclusions: This fault branch is probably the most recently active of the Sierra Madre fault zone in this area; however, it does not cut unit 2 alluvium that yielded an age of 2,200±80 yr (see fig. 2.9 and trench log, fig. 2.10; loc. 43, pl. 2.2).

21A, 21B, and 21C. *JPL, Pasadena*.—Three trenches were excavated in unit 2 alluvium across the projected trace of the fault exposed in trench 9. Observations: No faulting was observed in the exposed deposits. Conclusions: This branch of the Sierra Madre fault zone does not cut unit 2 alluvium and has not been active during Holocene time (see pl. 2.6).

22. *Sunny Slope Reservoir, Pasadena*.—The trench was excavated for a waterline by the Sunny Slope Water Co. Observations: The Raymond fault was crossed at a shallow angle and was difficult to distinguish because lithologies are similar on both sides of the fault surface. One major and several minor faults were exposed. One minor fault is associated with deposits rich in organic material that may be used to date a seismic event. A second minor fault displaces a sand bed 0.66 m vertically (north side up); movement appears to have occurred during a single event. The main fault strikes N. 75° E. and dips nearly vertically. Two samples of tree branches were collected north of the fault at depths of 4.3 and 4.9 m, and a peat sample was collected from the fault zone. Conclusions: This is the main branch of the Raymond fault. The Holocene soil could not be shown to be faulted.

MEASUREMENT OF PROGRESSIVE CLAST WEATHERING

It has long been known that alluvial clasts undergo progressive weathering, so that older alluvial units are distinguishable from younger ones by the greater degree of weathering shown by clasts of a given

lithology. We developed a new method during this study whereby the *P*-wave velocities of clasts (clast sound velocity [CSV]) of a specific lithology are measured. Preliminary results show that the CSV decreases progressively and significantly as a function of alluvial-unit age.

The CSV is obtained from traveltimes measurements made in the field with a DynaMetric Micro Seismic Timer model 217B. The instrument is portable and measures seismic traveltimes for a seismic compressional (*P*) wave generated by a hammerblow on the clast surface. The wave travels a predetermined distance through the clast. To avoid any possible systematic offset of origin time, apparent traveltimes for several different distances—generally four or more—were measured, and distance-time plots of the resulting data were used to determine the seismic velocity. Because of the range of path distances required, clasts had to be larger than 15 cm in greatest dimension. For each distance-time plot, a seismic velocity (slope) was determined by linear regression analysis. Without exception, the indicated correlation coefficient was high (greater than +0.98).

As a test of this method, six alluvial deposits in the Arroyo Seco were chosen that ranged in age from unit 1 (Holocene) through unit 4, as determined from geology and geomorphology. The CSV was measured on a group (17–52) of Lowe Granodiorite clasts from each deposit. All the CSV values from a given deposit were averaged to give an average CSV for the deposit. Statistical tests indicated that deposits corresponding to a single terrace level have the same CSV within the statistical resolution. All the CSV values corresponding to each terrace level were averaged to give an ensemble-average CSV for the deposit; table 2.3 lists the result. Statistical tests show that the separate deposits can be differentiated statistically by these CSV data at confidence levels (*t*-test) of 80 percent or greater.

Table 2.3 shows that the CSV decreases progressively with increasing alluvial age. This correlation holds for all the CSV data except those for deposit E, for which the CSV is low. This discrepancy may represent a statistical fluctuation because only 17 Lowe Granodiorite clasts from unit E could be measured, and so the resulting standard deviation of the mean CSV for that unit is high. The discrepancy may also have resulted from the relatively small sizes of the clasts available for measurement from unit E, compared to those from the other units. Nevertheless, the overall indication of a progressive decrease of CSV with age, as shown by table 2.3, is impressive and gives us reason to think that the CSV method holds promise for the relative-age determination of alluvial units.

3. EXPLORATORY TRENCHING OF THE SANTA SUSANA FAULT IN LOS ANGELES AND VENTURA COUNTIES

By RICHARD LUNG¹ and R. J. WEICK¹

ABSTRACT

Determining the fault-rupture hazard in tectonically active urban areas, especially in many parts of California, is important in land-use regulation. Our exploratory trenching in 1977, comprising 29 excavations at two sites along the Santa Susana fault zone, demonstrated the usefulness and limitations of such fault investigations in locating faults and determining their relative or limiting age, depending upon whether material over the fault can be chronostratigraphically dated. At one site we were successful only in bracketing the fault location, but at another we were able to document the probable age of last movement as greater than 10,000 yr. Because of the complexity of the fault zone, much work remains to be done before the potential hazards associated with it can be fully evaluated.

INTRODUCTION

A subsurface exploration program was conducted in 1977 to study the recency of faulting in the Santa Susana fault zone at selected locations in western Los Angeles and southeastern Ventura Counties. The study complemented the surface and subsurface investigations of Robert S. Yeats and others from Ohio University, Athens, Ohio. Whereas their study concentrated on the late Tertiary history and subsurface structure by utilizing extensive oil-well data and mechanical-modeling techniques, our study focused on the Holocene displacement history and land-use implications associated with potentially active faulting. The two principal sites of field study were located in the Limekiln Canyon area at the northern edge of the Porter Ranch area in Los Angeles County, and in the Tapo Canyon area north of Simi Valley in Ventura County (fig. 3.1).

FIELD INVESTIGATION AND GEOLOGICAL SETTING

STUDY OBJECTIVES AND METHODS

The primary aims of the study were as follows: (1) determine the age of the latest movement and the extent of faulting within the Santa Susana zone by exploratory

trenching, detailed mapping, and sampling of datable materials; (2) evaluate criteria useful in detecting and determining fault activity and recency; and (3) prepare guidelines appropriate for subsurface investigation of proposed developments in potentially active fault zones.

Initial tasks included a review of previous pertinent geologic maps and reports, particularly those by Yeats (1976), Saul (1975), Weber (1975), and various private consultants. Conflicting fault locations, as mapped by others, were noted, and attempts were made to reconcile these by detailed geologic mapping, aided by a study of aerial photographs. After this work was completed, the field investigation proceeded with a two-stage trenching program starting at Limekiln Canyon, followed by trenching at Tapo Canyon. A series of 28 backhoe trenches and pits, plus a preexisting sidehill cut (figs. 3.2 and 3.3), were excavated in the two areas to locate the fault traces, and particularly to locate places where the fault might be covered by relatively recent deposits containing carbonaceous or other age-datable materials.

REGIONAL SETTING

The two localities are approximately 16 km apart, in the east-central and west-central parts of the Santa Susana fault zone. This zone merges with the Oak Ridge fault on the west, and with the San Fernando fault zone on the east. The fault zone consists of a series of convex-upward, moderately steep to low-angle thrusts with the Modelo Formation of Miocene age overriding deposits of Pliocene to Quaternary age on the south. The strip map and cross sections on figure 3.1 are from Yeats (1976) and show the general structural and stratigraphic relations along the fault zone.

LIMEKILN CANYON EXPLORATION

In the initial trenching east of Limekiln Canyon, we attempted to pinpoint the location of the southern trace of the fault zone, which at that time was considered by others to be the more recently active trace (fig. 3.2). Materials found in four trenches, however, indicated that the fault must be farther south than previously thought,

¹Leighton and Associates, 1151 Duryea Avenue, Irvine, CA 92714.

Manuscript received for publication on February 5, 1981.

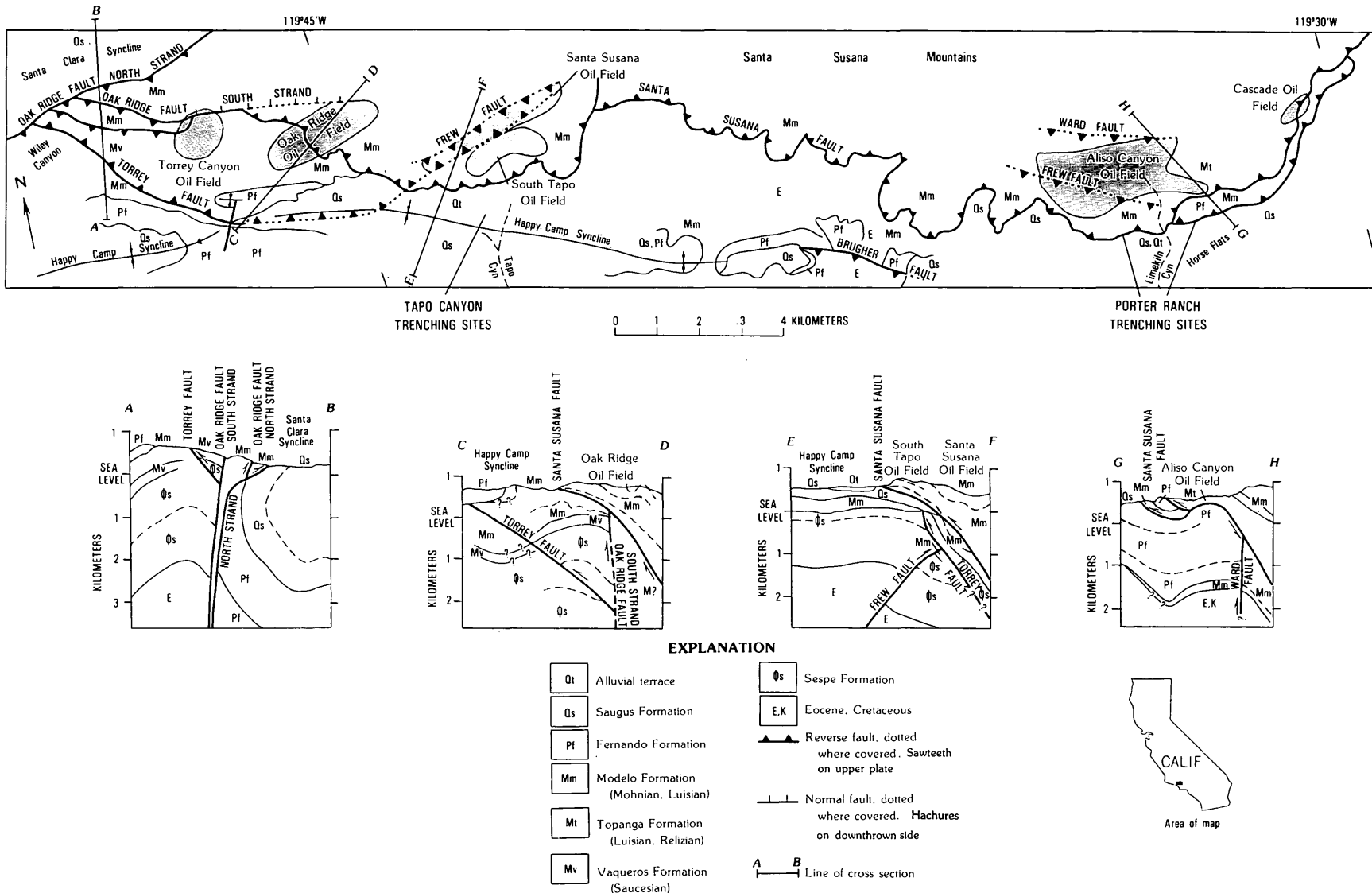


FIGURE 3.1.—Tectonic map and cross sections of Santa Susana fault zone, showing critical age relations for four ages of faulting. Modified after Yeats (1976).

and within an existing tract development. We attempted to expose the fault in a series of 13 pits along the base of the foothills west of Limekiln Canyon. Because of the

extensive overburden, however, the exploration was only successful in restricting the fault location to a zone approximately 53 m wide, slightly north of the location

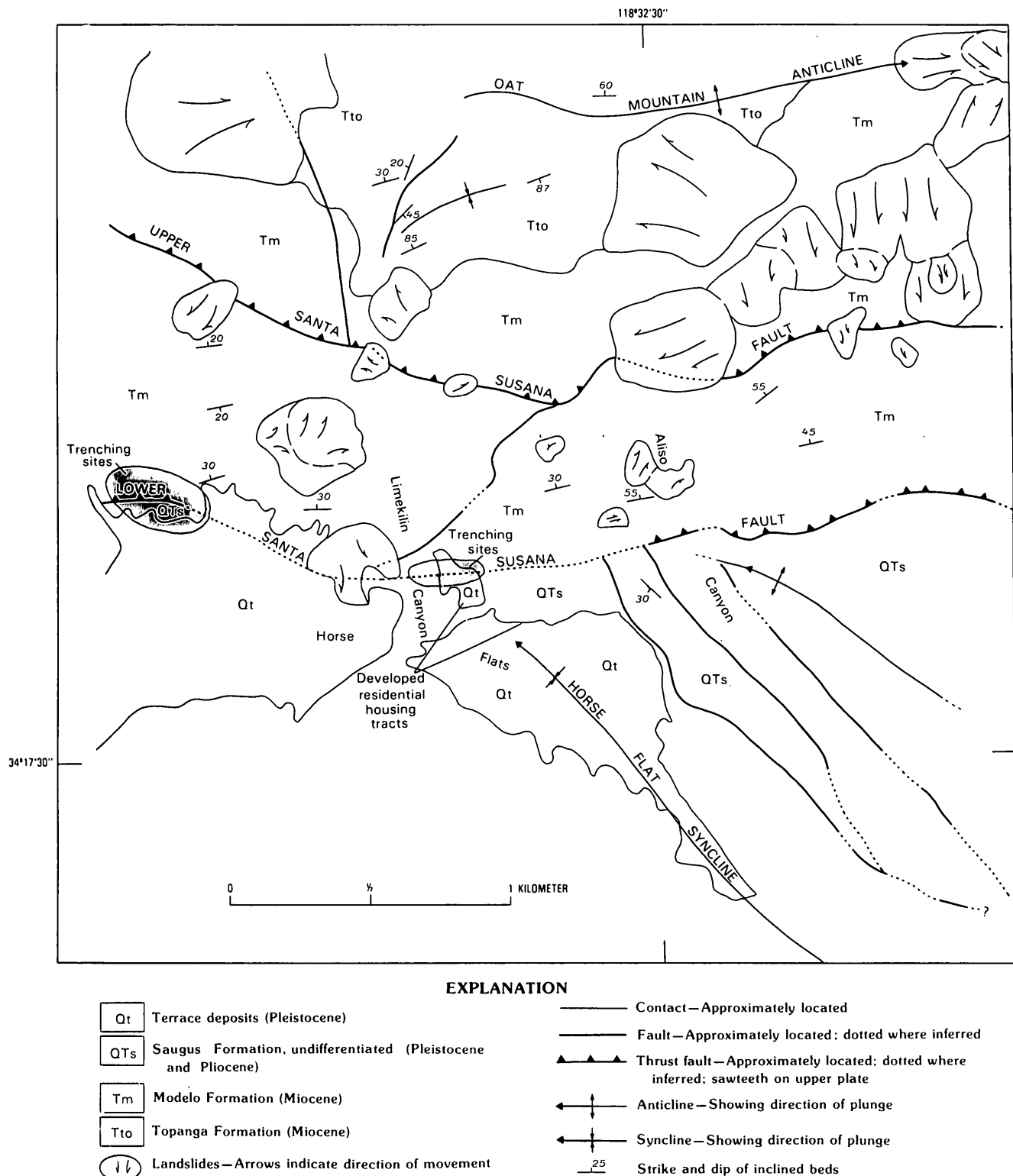


FIGURE 3.2.—Generalized regional geologic map of the Porter Ranch area. Modified after Saul (1975).

previously mapped. Unexpectedly thick, caliche-rich, older landslide debris hampered attempts to expose the fault. No carbonaceous materials for radiometric age dating were found in the surficial deposits.

We considered trenching across the upper Santa Susana fault, some 690 m north; however, based on work by Yeats and a review of the geologic setting of the area, we decided that the likelihood of determining the recency of the fault was minimal, and so we discontinued further trenching in the Limekiln Canyon area.

TAPO CANYON EXPLORATION

We made a total of 12 excavations at two sites in tributary canyons north-west of Tapo Canyon, about 1.8 km north of the Gillibrand sand and gravel quarry (fig. 3.3). At site 1, the main fault trace was well exposed in a sidehill cut. Here the Modelo Formation was juxtaposed against terrace deposits, and both were overlain by unbroken, dissected fan deposits capping the ridge (fig. 3.4). Clearly, the latest movement on the main fault trace at

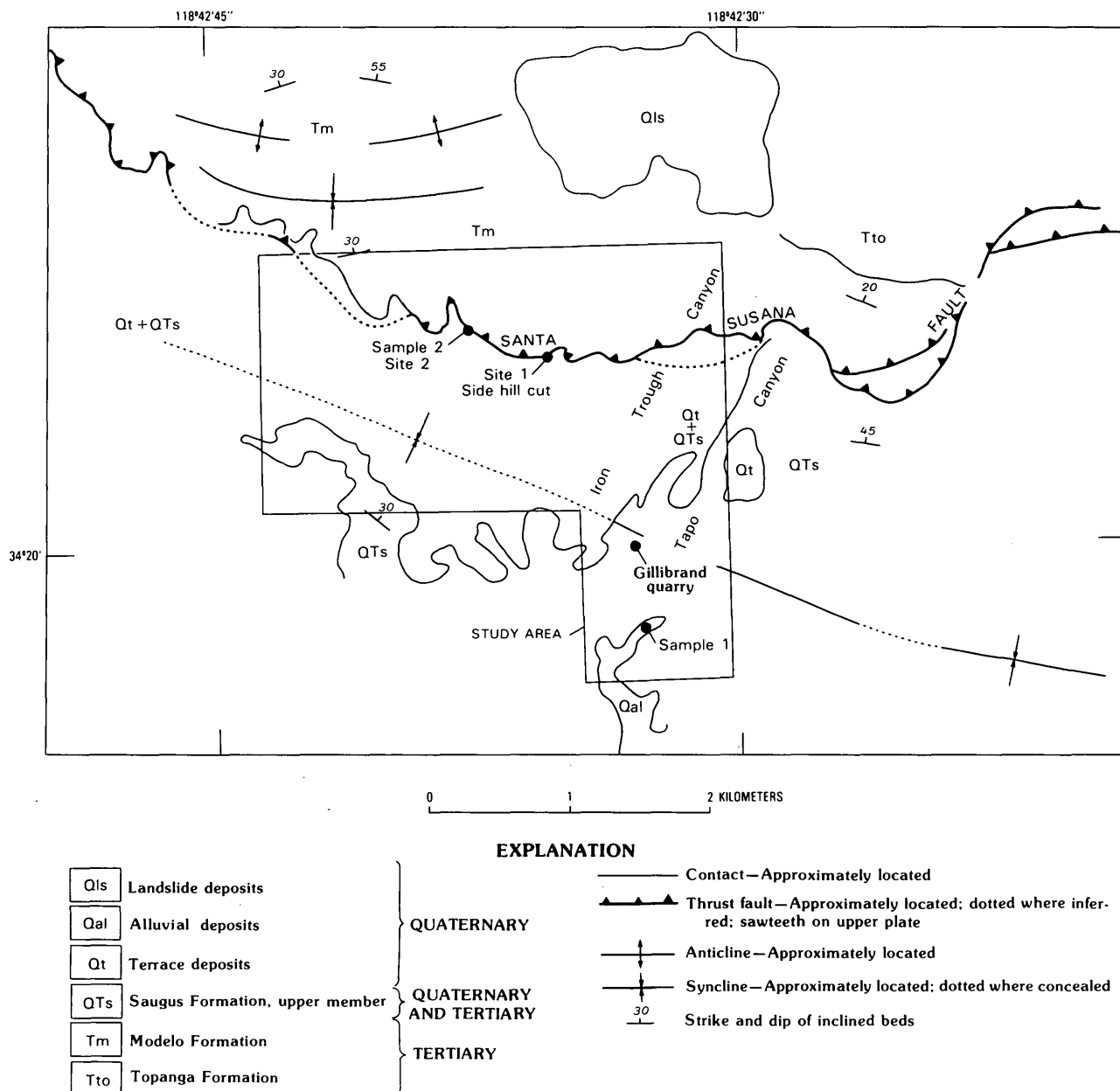


FIGURE 3.3.—Generalized geologic map of the Tapo Canyon area. Modified after Weber and others (1973).

this location predates the fan deposits which geomorphically appear to be relatively old because of the amount of uplift and dissection they have undergone.

Trenches on the east side of site 1 revealed the probability of a lower branch fault, along which a sliver of the Saugus Formation (well-rounded cobble-to-pebble conglomerate) was caught up with the thrust zone. We found a tar seep—a not uncommon occurrence in association with the Santa Susana fault—in one of the trenches exposing the Saugus Formation.

At site 2, to the west, we were unsuccessful in confirming the fault location because of the depth of the overburden. In one of the trenches made in the older alluvium in the upper part of a flat-bottomed canyon, however, a series of peatlike layers at a depth of 4.0 to 5.2 m was exposed, associated with dark-brown paleosols near the bottom of the trench. These materials may be contemporaneous with ancient landslides just to the north, but undoubtedly are younger than the fan deposits at site 1. Radiometric ^{14}C age dating of the organic material from the lowermost layer (fig. 3.3, sample 2) yielded an age of $10,010 \pm 580$ yr B.P.

SUMMARY

On the basis of our field exploration and mapping, we believe the main trace of the west portion of the Santa

Susana fault zone has had no surface displacement in at least $10,010 \pm 580$ yr, and perhaps in as long as 14,000 yr. In the Limekiln Canyon area bordering the Porter Ranch area, the lower thrust plane is apparently folded and is probably inactive. To the north in the Aliso Canyon oil field, a branch of the Santa Susana fault has been active more recently (Yeats and others, 1978, p. 51) and should be considered potentially active.

Although the existence of a younger, more northern branch of the fault in the Tapo Canyon area cannot be ruled out, no evidence of such a trace is apparent. A bedding-plane fault within the Modelo Formation, however, could easily go undetected.

Considerable detailed mapping, correlated with oil-well data, remains to be done before the potentially active portion of the fault zone can be delineated with any certainty over its entire length. Along most traces of the fault, a lack of sites with suitable overlying surficial materials makes their state of activity difficult to determine by trenching.

As is true with any fault trenching study, its success depends in large part upon thorough geologic mapping and review of the available data in advance of the field exploration. Our investigation revealed that even though relatively detailed mapping was obtained, much of the subsurface work was expended on verifying, or at least bracketing, the fault location. The presence of thicker-

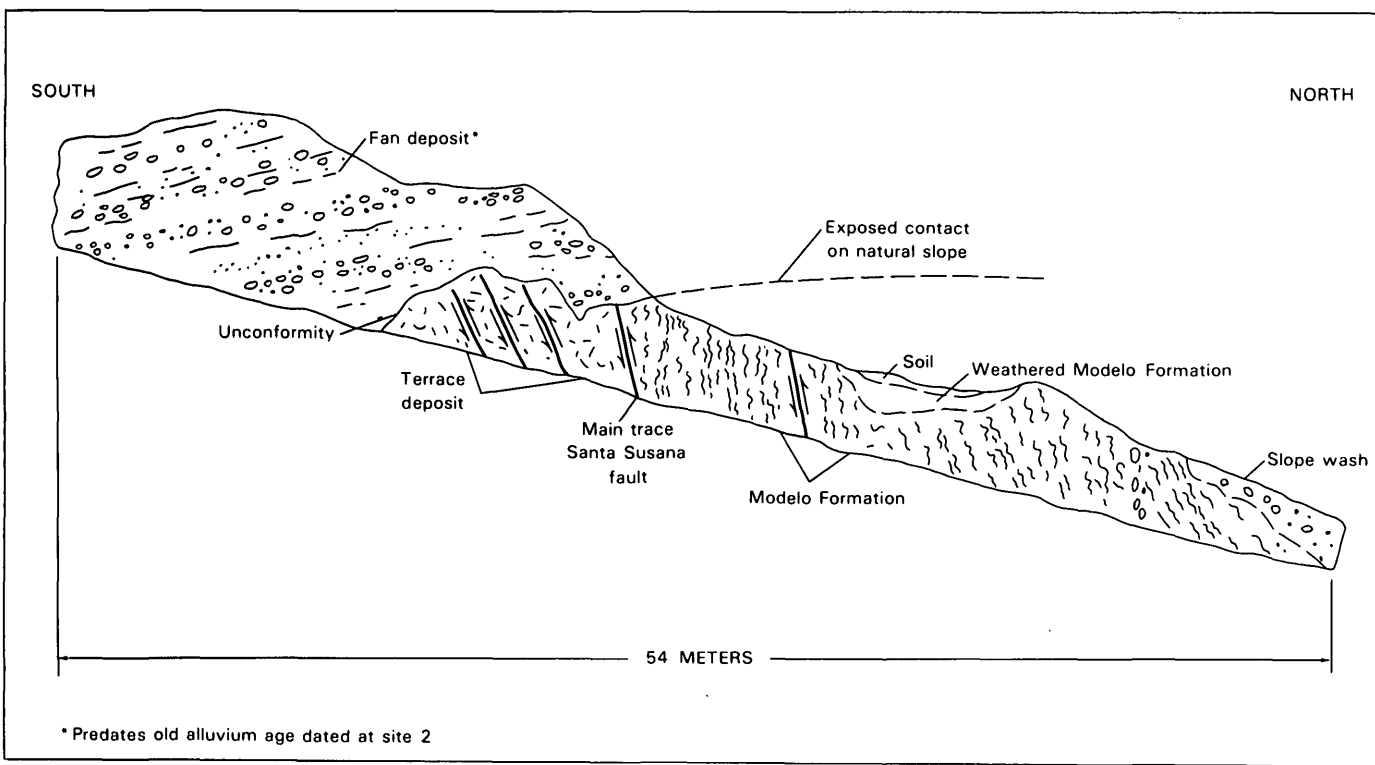


FIGURE 3.4.—Sketch of structures exposed in a sidehill cut, Tapo Canyon area. Arrows on faults indicate direction of relative movement. Horizontal and vertical scales equal.

than-anticipated surficial deposits (including slope wash and landslide debris) necessitated additional excavation or the selection of alternative trenching sites. Age dating of the unfaulted alluvial materials within the fault zone was moderately successful.

REFERENCES CITED

- Saul, R. B., 1975, Geology of the southeast slope of the Santa Susana Mountains and geologic effects of the San Fernando earthquake: California Division of Mines and Geology Bulletin 196, p. 53-70.
- Weber, F. H., Jr., Cleveland, G. B., Kahle, J. E., Kiessling, E. W., Miller, R. V., Mills, M. F., and Morton, D. M., 1973, Geology and mineral resources study of southern Ventura County, California: California Division of Mines and Geology Preliminary Report 14, 102 p.
- Weber, F. H., Jr., 1975, Seismic hazards study of Ventura County, California: California Division of Mines and Geology, Open file report 76-5 LA, p. 191-195.
- Yeats, R. S., 1976, Neogene tectonics of the central Ventura Basin, California; in Fritsche, A. E., Ter Best, H., and Wornardt, W. W., eds., The Neogene symposium: Society of Economic Paleontologists and Mineralogists, p. 19-32.
- Yeats, R. S., Lant, K. J., and Shields, K. E., 1978, Subsurface geology of the Santa Susana fault in the aftershock area downstep of the 1971 San Fernando earthquake (Summaries of Technical Reports, v. 5, p. 49-53): U.S. Geological Survey Contract No. 14-08-0001-15271, under the earthquake hazards reduction program.

4. LATE QUATERNARY DEFORMATION IN THE WESTERN TRANSVERSE RANGES

By R. F. YERKES and W. H. K. LEE

ABSTRACT

A 6-year (1970-75) record of seismicity for a 2° by 2° area of the western Transverse Ranges includes 630 well-located events of M_L 2 to 6 that are associated with zones of east-trending reverse faults. P -wave first-motion plots of 200 events are analyzed, and 50 are of quality adequate for detailed study. Fault-plane solutions together with surface geology and local well data show the reverse faults to be chiefly north dipping with a left-oblique component. Specific segments in eastern Santa Barbara Channel and Ventura basin are active on the basis of geology and seismicity: Red Mountain-San Cayetano, Pitas Point-Ventura, Oak Ridge, Mid-Channel, and Anacapa-Santa Monica. P axes for small-event solutions are oriented the same direction as those of larger earthquakes in the region—near horizontal and generally normal to the big bend of the San Andreas fault. The reverse-fault solution for the 1978 M_L 5.1 Santa Barbara earthquake closely fits those of five others previously located within 15 km.

All available evidence, geodetic, deep well, uplift rate of dated terrace deposits, and fault-plane solutions, is consistent for the rate and sense of deformation on individual faults. The maximum average rate of tectonic uplift along the Santa Barbara-Ventura coast approaches 10 mm/yr over the last 45,000 years—the greatest rate known for the Pacific Coast area excluding Alaska—and has not slowed over the last 2,500 years.

INTRODUCTION

The Transverse Ranges province is distinctive for its east-west trend, the type, age, and history of its exposed basement rocks, its high rate of deformation as indicated by the dramatic fault-controlled mountain fronts and extremely deep basins filled with young, intensely deformed deposits, and, perhaps most of all, its disparate geologic and tectonic history compared with other parts of southern California. A significant step in interpreting southern California geology was the fault-plane solutions of the 1971 San Fernando earthquake (Wesson and others, 1971; Whitcomb, 1971; Whitcomb and others, 1973); those solutions verified not only the structural dominance but also the activity of the several north-dipping reverse faults that characterize the Transverse Ranges west of the San Andreas fault and bound them on the south.

This report concentrates on the seismicity, fault-plane solutions, and structural geology as based on seismic data recorded during 1970-75 in a large part of the western Transverse Ranges. The area covered by the present

study is shown in figure 4.1; it includes most of the Transverse Ranges west of the San Gabriel fault and is approximately bounded on the north by the Santa Ynez fault and on the south by the Anacapa-Santa Monica faults. Also shown in figure 4.1 are the epicenters of historical earthquakes of magnitude 6 or greater. Of these larger earthquakes, the five in the western Transverse Ranges, especially the 1971 San Fernando and 1973 Point Mug, are associated with east-trending north-dipping reverse faults. Fault-plane solutions for the San Fernando and Point Mug earthquakes verify these associations and indicate north- to northeast-trending subhorizontal P axes (Wesson and others, 1971; Whitcomb, 1971; Ellsworth and others, 1973).

SEISMICITY

DISTRIBUTION

Well-located epicenters and focal depths of 630 earthquakes that took place in the 6-year period 1970 through 1975 are plotted on sheet 1 of Yerkes and Lee (1979); fault-plane solutions for 50 of these earthquakes are plotted on plate 4.1 of this report. Location quality of epicenters, derivation of local magnitude, and associated data for the earthquakes are given in Lee and others (1979).

Ninety-seven percent of the epicenters are located south of the Santa Ynez fault; none are obviously associated with the fault. The few events north of the fault were not recorded well enough for fault-plane solutions, and none are obviously associated with mapped faults; the same is true for events northeast of the San Gabriel fault. No attempt was made to relocate earthquakes of the San Fernando earthquake sequence, as this sequence was intensively studied by Whitcomb and others (1973).

Many of the events south of the Santa Ynez fault can be associated with specific faults on the basis of focal mechanisms and hypocentral depths (table 4.1). The best associations are made for the Red Mountain, Pitas Point-Ventura, Mid-Channel, and Anacapa faults. Stratigraphic and geomorphic evidence indicates that all these faults have ruptured the ground surface during late Quaternary

Manuscript received for publication on May 20, 1981.

time (pl. 4.1; Ziony and others, 1974). The Red Mountain and Pitas Point-Ventura faults have probably moved in Holocene time.

The quality of the associations between earthquakes and specific faults is illustrated by examples on plate 4.1. Vertical sections show that projected hypocenters of the 1973 Point Mugu earthquake sequence and the projected trace of the Anacapa fault coincide. Also, the subsurface trace of the Red Mountain fault, located independently on the basis of well data (Yeats and others, this volume) matches the distribution of hypocenters. These and other examples support our procedure (table 4.1) of inferring fault dips on the basis of geometrical associations between surface traces, hypocentral depths, and focal mechanisms.

DEPTH

Within the western Transverse Ranges, the deepest hypocenters are 19 km for an event in the north-central part of Santa Barbara Channel and 17 km for an event in the Oxnard plain; in addition, aftershocks of the 1973

Point Mugu sequence were as deep as 19 km (Yerkes and Lee, 1979b, sheet 2). However, the depths of earthquakes in the band of seismicity that extends from the central and northern Santa Barbara Channel to the east center of the map area generally range from 13 to 16 km. The hypocenters do not delineate any east-west or north-south plunge.

The type and distribution of basement rocks that underlie the Upper Cretaceous and Cenozoic sedimentary rock sequence of the western Transverse Ranges between the Santa Monica and Santa Ynez Mountain are completely unknown. Regional-scale maps showing inferred structure contours on the possible basement rock surface for this area have been published (Curran and others, 1971, fig. 5; Nagle and Parker, 1971, fig. 13). Comparison of the contours shown on these maps with the focal depths of recorded earthquakes suggests that the seismicity is generated within the basement-rock sequence or near its surface, but no strong correlations in trend or plunge are apparent.

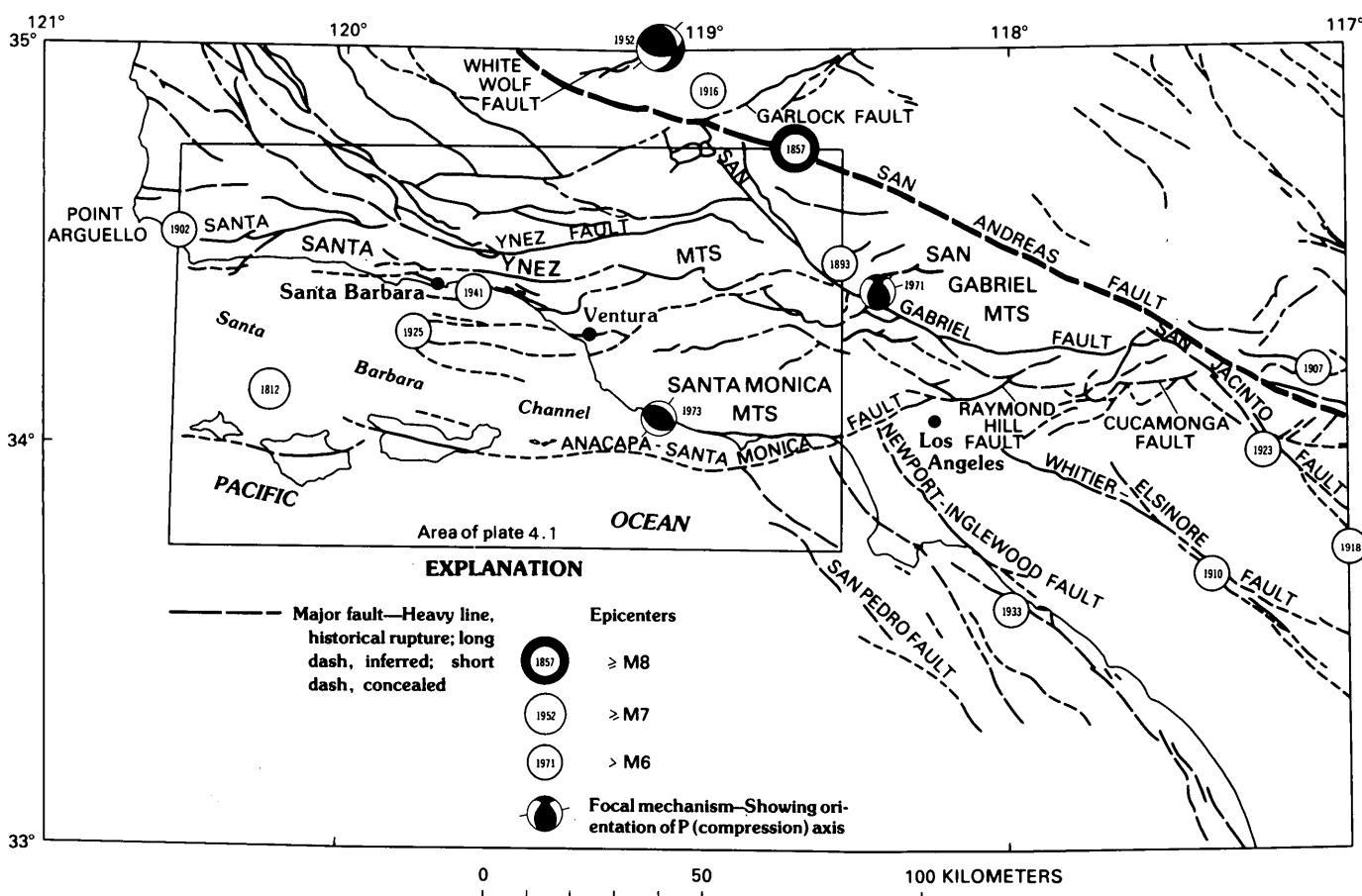


FIGURE 4.1.—Part of southern California showing area investigated, and relation of western Transverse Ranges (bounded by Santa Ynez, San Gabriel, and Anacapa-Santa Monica faults) to major faults and epicenters and fault-plane solutions of large historical earthquakes. Modified from Jennings and others (1973).

TABLE 4.1—*Fault-plane solutions associated with specific faults*

Fault	Category ¹	Event number ²	Depth (km)	Apparent dip
Red Mountain ³	H	158, 396, 397, 505	5 1/2	63° N.
Pitas Point	H, L	8(?), 100, 162(?) 365, 388 391, 618, SB78(?)	12-14	40°-60° N.
Ventura	H	40	4-8	60° N.
San Cayetano	E, L	576(?)	8-16	60-70° N.
Mid-Channel	E	41, 51, 90, 449, 482, 558	8-14	65° N.
Oak Ridge	L	129	11	61° S.
Santa Susana	L	428	5(?)-11	65° N.
San Pedro	P	555, 625	5-11	90°
Anacapa	P	197 + 30 aftershocks	8-16	44° N.
East Santa Cruz basin	E, P	357(?)	13-15	38° N.

¹Letter indicates geologic time span of latest known surface movement; H, Holocene; L, late Pleistocene; E, early Pleistocene; P, late Pliocene.

²Events are tabulated and plotted on plate 4.1. SB78 is the Santa Barbara earthquake of August 13, 1978.

³Subsurface location verified by well data.

FAULT-PLANE SOLUTIONS

QUALITY

A set of 50 fault-plane solutions for earthquakes of local magnitude 2 or larger was selected from a total of about 200 on the basis of quality of location and solution. For most of the events tabulated, location and solution quality are C or better; the location is known to 5 km or less and the orientation of the nodal planes is known to $\pm 11^\circ$ or less. First-motion data for events cited in table 1 have been plotted by Lee and others (1979). Many of the events can be associated with mapped solutions relative to mapped faults as shown in plate 4.1. All of the solutions along and north of the Anacapa-Santa Monica fault indicate reverse displacement and can be associated with reverse faults that show geologic evidence of late Quaternary displacement at the ground surface, especially the Red Mountain fault, the Pitas Point-Ventura fault (which traverses the city of Ventura), the Mid-Channel fault zone, and the Anacapa fault.

Some northwest-trending faults south of the Anacapa-Santa Monica fault are associated with fault-plane solutions: two solutions along or near the San Pedro Escarpment indicate right-lateral movement, whereas the 1973 Anacapa earthquake near Anacapa Island (event 357, pl. 4.1) is best associated geometrically with northeast-dipping reverse movement, perhaps on one of the faults mapped along the southwest flank of Santa Cruz-Catalina Ridge.

P AXES

The trends of *P* axes are inferred to represent those of the maximum compressive stress for the analyzed events (Fig. 4.2). Most (82 percent) are within 15° of

horizontal and 60 percent are within 10° . The two maxima, at due north and N. 50° E., bracket and approximate the normal to the San Andreas fault (at N. 24° E.) as well as the *P* axis for the 1971 San Fernando earthquake.

SLIP VECTORS

The orientation and classification of slip vectors are plotted in figure 4.3. A dominant maximum shows a plunge of about 55° NE., indicating reverse-left-oblique displacement. Subsidiary maxima at 45° N. and 45° E. indicate north-over-south reverse displacement and left-lateral strike slip, respectively. The shaded field defined by these maxima contains 70 percent of the points. This field is dominated by reverse-left-oblique slip, which characterized the 1971 San Fernando earthquake, and north-over-south reverse slip, which characterized the 1973 Point Mugu earthquake. As indicated on figure 4.3 by slip vectors for the 1971 San Fernando (SF) and 1973 Point Mugu (PM) earthquakes, the displacements for the smaller earthquakes in the western Transverse Ranges are fully representative of the larger events with known displacements.

1978 SANTA BARBARA EARTHQUAKE

The Santa Barbara earthquake of August 13, 1978 (event SB78, pl. 4.1), occurred in the same general area as the larger 1925 and 1941 earthquakes; its epicenter perhaps was between those of the earlier events. The distribution of main-shock and after-shock hypocenters describes a surface striking N. 65° - 75° W. toward the shoreline at Goleta (Lee and others, 1978, figs. 3 and 5), where the largest accelerations were measured and the most extensive damage occurred. The fault-plane solution, distribution of aftershocks, and local geology indicate reverse slip on a fault dipping 30° - 60° N. The rupture

surface and fault-plane solution are not clearly associated with a recognized fault but may be associated with the Pitas Point or nearby fault (cross section A-A' pl. 4.1).

SUMMARY

Fault-plane solutions for events in the western Transverse Ranges can be associated with segments of several east-trending north-dipping reverse faults, especially the Red Mountain, Pitas Point-Ventura, Mid-Channel, and Anacapa faults. Geologic evidence indicates that these segments have ruptured the ground surface during late Quaternary time. The solutions indicate near-horizontal P axes oriented generally within 30° of normal to the great bend of the San Andreas fault. The dominant type of displacement indicated by slip vectors varies between north-over-south reverse and reverse-left-oblique. These characteristics pertain to the entire range of magnitudes recorded within the network area, as well as to larger earthquakes such as the 1971 San Fernando and 1973 Point Mugu events.

EFFECTS OF DEFORMATION

In addition to the prominent topographic and geologic effects of the numerous east-trending folds and faults,

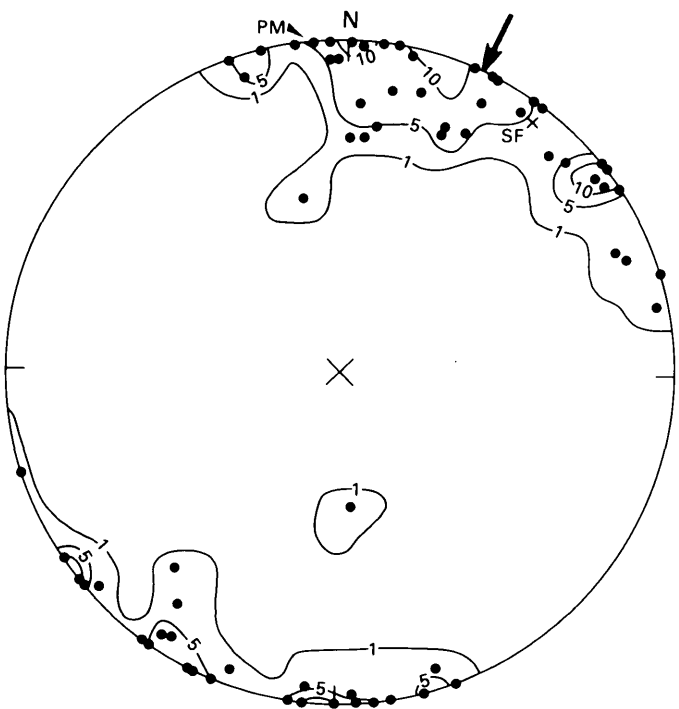


FIGURE 4.2.—Stereoplot showing distribution and orientation of P axes for 51 events, 1970–75, excluding aftershocks of 1973 Point Mugu sequence. PM, Point Mugu main shock; SF, 1971 San Fernando main shock (not contoured). Contours, 1, 5, and 10 percent per 1 percent area; lower hemisphere projection. Arrow at N. 24° E. is normal to San Andreas fault. See table 4.3 for data.

well illustrated on the geologic map of southern Ventura County (Weber and others, 1973), high rates of deformation across east-trending reverse faults of the western Transverse Ranges are evidenced by recurrent Holocene ruptures, geodetic leveling, uplift of dated marine terrace deposits, and stratigraphic separation of dated strata.

RECURRENT HOLOCENE FAULTING

Two known and one probable examples of recurrent Holocene faulting occur in the western Transverse Ranges; all are along, or on trend with, the north margin of the Santa Barbara Channel. This margin is a structural bench underlain by an extensive east-trending zone of north-dipping reverse faults; to the west, the zone coincides with a submarine scarp about 100 m high, and to the east it includes the Pitas Point-Ventura fault (Yerkes

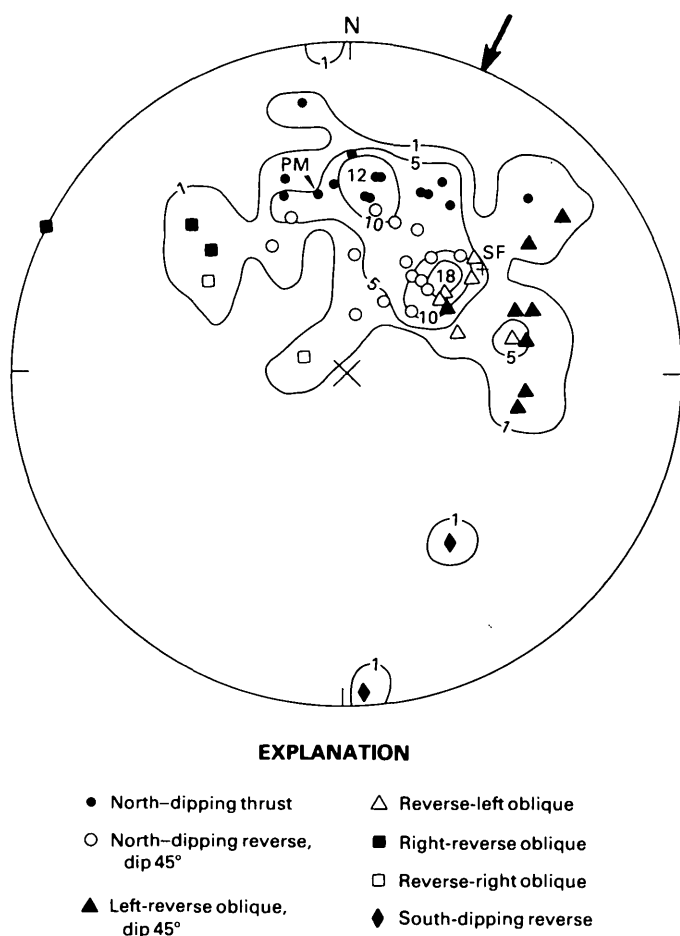


FIGURE 4.3.—Stereoplot showing distribution, orientation, and classification of slip vectors for 51 events, 1970–1975, excluding aftershocks of 1973 Point Mugu sequence. PM, Point Mugu main shock; SF, 1971 San Fernando main shock (not contoured). Contours: 1, 5, 10, and 15 percent per one percent area; lower hemisphere projection. Large area within 5 percent contour contains 70 percent of the points. Arrow at N. 24° E. is normal to trace of San Andreas fault.

and others, 1981). The easternmost locality occurs along the Pitas Point-Ventura fault, which in the eastern channel cuts Holocene deposits with about 25 m stratigraphic separation and onshore cuts fan deposits estimated to be about 6,000 yr old (Greene, 1976; Sarna-Wojcicki and others, 1976).

The second locality (7, pl. 4.1) is near the mouth of Javon Canyon, on the south limb of the Rincon oil field about 10 km west of the Ventura River. The south-dipping Javon Canyon fault displaces stream terrace deposits about 2,500 yr old and nonmarine cover; total separation is about 4 m and includes at least four events (Sarna-Wojcicki and others, this volume).

The third locality was exposed in exploratory trenches cut through terrace deposits into bedrock near the shoreline about 5 km east of Point Conception. The bedrock fault splay upward into several strands in the thick cover and at least one of the strands extends up to the modern soil; maximum displacement in one to five events is 85 cm in deposits less than 12,000 yr old (Rice and others, 1981).

GEODETIC EVIDENCE

Comparison of repeated level lines along the coast from the Ventura River to the Santa Barbara-Ventura County line and northward along the river has confirmed a minimum average tilt up to the north of nearly 13 microrads over the period 1920-68 across the Red Mountain-Pitas Point-Ventura set of faults (Buchanan-Banks and others, 1975); the relative uplift rate is about 5 mm/yr.

Short-term rates of uplift in the Point Conception area are even greater. Comparison of 1900 and 1920 profiles between Ventura and Guadalupe (42 km north of Point Arguello) indicate differential arching over the Point Conception-Gaviota area of more than 240 ± 78 mm. Studies of the development of the southern California uplift indicate that this uplift probably occurred within the interval 1905-1910, for an average rate of at least 37 mm/yr (Yerkes and others, 1981).

Similarly, comparison of 1960 and 1968 level surveys shows that the upper (northern) plate of the west-trending Anacapa-Santa Monica reverse fault rose by 30-40 mm at least as far west as Point Mugu—a rate consistent with continued thrusting along this frontal system of the Transverse Ranges (Castle and others, 1978). Additional warping between 1968 and 1971 indicated left-lateral reverse creep at depth, and 1971-73 (post-1973 earthquake) data indicate additional upper-plate uplift of more than 30 mm.

Regional maps of elevation changes in the western Transverse Ranges east of long $119^{\circ}15'$ (Ventura) based on comparisons of 1960-61, 1968-69 and 1968-69 to 1971 (post San Fernando earthquake) leveling show strong

TABLE 4.2—Elevations and estimated ages of fossil collections from uplifted marine terraces

Map ¹	Collection		Elevation (m)				Uplift rate (mm/yr)	
	No.	Name	Sample loc.	SL ²	At T ₀ ³	Age ⁴ (10 ³ yr)	Max	Min
1	M5790	Goleta	5	15	-39	45	1.73	0.33
2	BSB9-3	Carpinteria	4.6	5	-39	45	.98	.11
3	Y440B	Carpinteria	26	40	-39	(45)	1.76	.89
4	Y440A	Rincon Point	50	N.a.	-39	(45)	1.98	1.11
5	M7245	Punta	146	N.a.	-39	45	4.11	3.24
6	M7229	Punta Gorda	125	N.a.	-39	45	3.64	2.78
7	M7230	Rincon oil field	215	N.a.	-39	45	5.64	4.78
8	M7249	Rincon oil field	226	N.a.	-39	45	5.89	5.02
9	M7283	Rincon oil field	256	N.a.	-39	45	6.56	5.69
10	M7494	Punta-B-13	2.7	N.a.	0	5 ⁵ 2.1	1.29	
11	Y438B	Punta Gorda	2	11	0	5 ⁵ 2.5	5.20	
12	M7295	Punta Gorda	15	N.a.	0	5 ⁵ 5.5	2.73	
13	M7228	Culvert 390.06	6	15	0	5 ⁵ 2.5	8.40	
14	M7477	1 km NW. Pitas Point	36.5	N.a.	0	5 ⁵ 6.5	5.61	
15	M7297	Pitas Point	8	N.a.	0	5 ⁵ 4.2	1.90	
16	M7472	Baptiste Ranch	19	N.a.	0	5 ⁵ 3.8	5.00	
17	M7242	Ventura	117	120	-20	82	1.67	1.43
18	Y413B	Ventura	15	N.a.	-20	82	.43	.18

¹Number shown on plate 4.1.

²SL, shoreline angle; N.a., not available.

³T₀, time of formation (from Bloom and others, 1974).

⁴Age estimates by stereochemical or radiocarbon analysis of mollusks. Estimates in parentheses based on map continuity with dated sample.

⁵Radiocarbon analysis.

gradient changes associated with the Oak Ridge, Santa Rosa, Santa Susana-San Fernando-Sierra Madre, and Malibu Coast (Anacapa?) faults (Castle and others, 1975, figs. 2 and 5). Of these, only the Santa Rosa fault was not associated with recorded seismicity during the 1970-75 interval. The data coverage does not include the San Cayetano fault, but it does show that no prominent gradient changes were associated with the Santa Monica and Raymond Hill faults east of the shoreline.

DEFORMED MARINE TERRACES

Segments of least three deformed marine terraces are exposed along the Santa Barbara-Ventura coast at elevations ranging from 2 m to at least 256 m (fig. 4.4; table 4.2). The ages of mollusks from deposits on the terraces have been estimated by amino-acid stereochemistry and ¹⁴C as 2,500, 45,000, and 82,000 yr B.P. (Lajoie and others, 1979). The 45,000-yr-B.P. terrace is exposed at elevations of 26 m or less along the seafloor for about 7

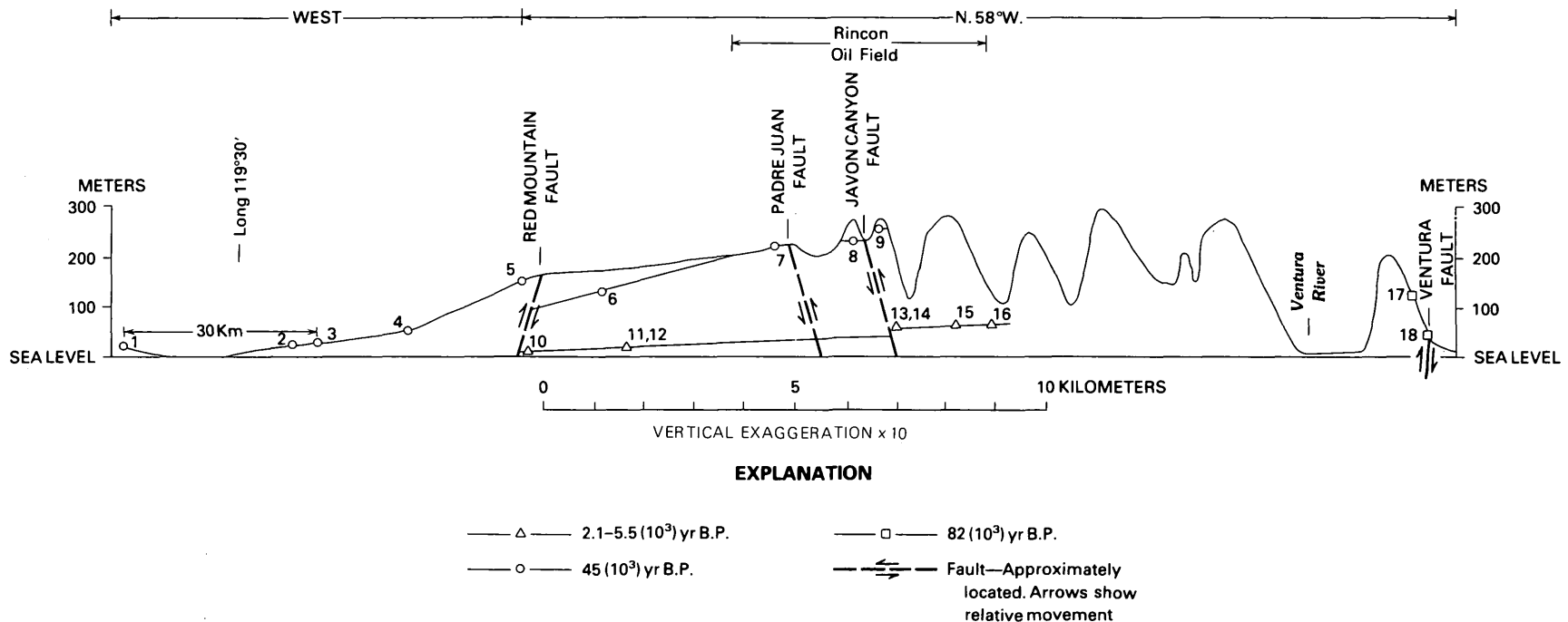


FIGURE 4.4.—Section along Santa Barbara-Ventura coast showing deformation of dated marine terraces. Numbered localities keyed to table 4.2.

km west of long 119°30' near Carpinteria, where the Red Mountain and associated faults intersect the shoreline (pl. 4.1). Southeast of that point all the terraces, including the 2,500-yr-B.P. terrace, are tilted up to the north and east (fig. 4.4). Apparent average rates of uplift in this area for the last 45,000 yr locally exceed 5 mm/yr as referred to present sea level, including the rate for the 2,500-yr-B.P. terrace (table 4.2).

FAULTS

The north-dipping, east-trending Red Mountain, San Cayetano, Santa Susana, Pitas Point-Ventura, and Mid-Channel faults coincide in general with east-trending bands of seismicity that extend across the north half of the area. Detailed surface and subsurface investigations show that very large separations and late Quaternary movements have occurred on the Red Mountain fault, the Pitas Point-Ventura fault, and segments of the San Cayetano and Santa Susana faults.

RED MOUNTAIN FAULT

Well data from the oil fields west of the Ventura River show that upper Eocene and lower Miocene strata are thrust over Pliocene and Pleistocene strata by the Red Mountain fault (Yeats and others, this volume). The age of the youngest strata involved in the faulting is not well defined by the well data. However, the fault truncates a syncline that, east of the Ventura River, involves the San Pedro Formation as used by Weber and others (1973), which has been dated at 200,000–400,000 yr B.P. on the basis of radiometric and stereochemical age estimates (fig. 4.5). On the assumption that the thrust faulting followed the folding, much or all of the 5,500 m of apparent separation on the Red Mountain fault could have occurred during about the last one-half to one million years.

PITAS POINT-VENTURA FAULT

Where crossed by a seismic profile about 2 km offshore in the northeastern part of the Santa Barbara Channel, the Pitas Point fault appears as a north-dipping reverse fault that displaces a late Pleistocene erosion surface about 25 m up on the north; it appears to cut Holocene strata but not the sea floor (Greene, 1976, p. 508-509, figs. 4, 6).¹

Extensive data are available for the Ventura fault (Sarna-Wojcicki and others, 1976). The surface trace is marked by a prominent, linear, south-facing scarp as much as 12 m high and about 10 km long; it is bounded on the

north by an uplifted bench. Except where locally buried by young surficial deposits, the escarpment forms the boundary between old alluvial-fan deposits, deformed marine terrace deposits, or deformed bedrock, all overlain by old soils on the north and young, undeformed surficial deposits overlain by young soils on the south. The gradients of all but the largest streams that cross the escarpment are deflected upward on the north by about 25 m. Test trenches cut in surficial deposits across the escarpment show numerous small soil-filled cracks that commonly are traceable downward into east-trending high-angle faults with separations as large as 40 cm. The southerly dips of strata in the trenches and adjacent boreholes increase downward south of the escarpment. The youngest strata cut by the fault are apparently Holocene.

No direct evidence is available as to the amount of displacement across the Ventura fault. A north-south structure section about 4 km east of the Ventura River shows apparent vertical separation of about 245 m, up on the north, at the base of lower Pleistocene strata (Ogle and Hacker, 1969), although that interpretation may be only an inference. A detailed structure section another

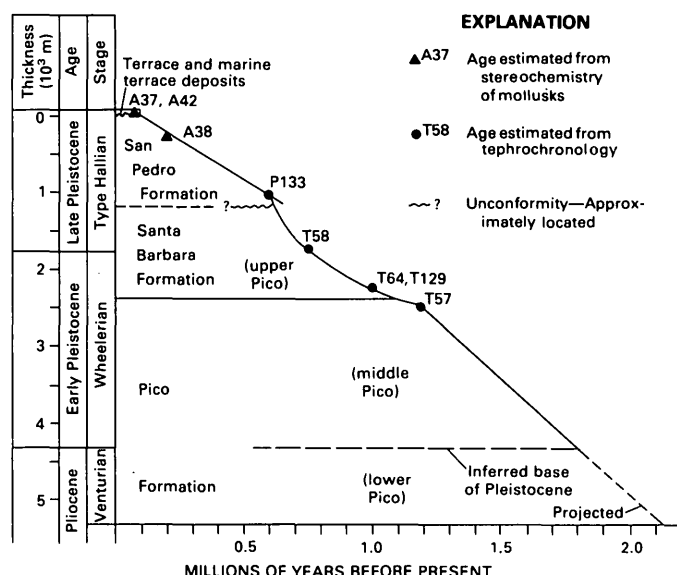


FIGURE 4.5.—Stratigraphic thickness and estimated ages, Pleistocene sequence, south limb of Ventura anticline. Samples A37, A42 represent amino-acid racemization age estimates on mollusks from marine deposits, estimated at 80,000–100,000 yr B.P.; sample A38 represents an amino-acid racemization age estimate on mollusks from San Pedro Formation, estimated at about 200,000 yr B.P. (Lajoie and others, 1979). Sample P133 represents Lava Creek ash 600,000 yr B.P.; T58 represents Bishop ash 730,000 yr B.P.; T64, T129 represent Glass Mountain-D ash 800,000–900,000 yr B.P.; T57 represents Bailey ash (1.2 m.y. B.P.); age estimates and ash correlations from Sarna-Wojcicki and others (1984). Other correlations from Natland (1952, 1953) and Holman (1958). Ages of stage boundaries from Van Eysinga (1975). Stratigraphic nomenclature from Weber and others (1973) except for informal terms (in parentheses) applied to subsurface units.

¹Later work indicates that the Pitas Point fault probably is an element of a zone of north-dipping reverse faults that transects the entire north margin of Santa Barbara Channel (Yerkes and others, 1981).

5 km to the east, based on closely spaced and abundant data, shows an apparent vertical separation of as much as 200 m at the base of upper Pleistocene strata. An unknown component of left-lateral slip is indicated locally by small folds having near-vertical axes in bedrock just north of the fault and by the fault-plane solution of an associated earthquake (No. 40, table 4.3).

SAN CAYETANO FAULT

Apparent stratigraphic separation across segments of the San Cayetano fault diminishes eastward from a maximum of 7,300–9,000 m (vertical, up on the north) at Sespe Creek (6 km east of long 119°) where low scarps in stream terrace deposits of late Quaternary age coincide with the fault trace (Fine, 1954; Cemen, 1977). Ten kilometers east of Fillmore, alluvium of late Quaternary age north of the Santa Clara River is warped along the buried trace of the fault (Cemen, 1977). Youthful geomorphic features and upthrust Quaternary gravel beds at several localities along its trace suggest at least late Quaternary activity at the surface.

SANTA SUSANA FAULT

The apparent stratigraphic separation across faults of the Santa Susana set is at least 4,000 m, which includes about 2,000 m of vertical offset (up on the north) and 3,200 m of left-lateral strike slip (Yeats and others, 1977). The hanging wall locally is expressed topographically; in some places the fault cuts late Pleistocene fan deposits and northeast-trending elements along the west margin of San Fernando Valley ruptured during the 1971 San Fernando earthquake.

MID-CHANNEL FAULT ZONE

Published data on faults of the Mid-Channel fault zone are sparse. A report by Campbell and others (1975) includes an interpretive section (B-B') through the area of most intense seismic activity near long 119°45' W., lat 34°15' N. The section shows a fault-bounded gentle anticline ("12-mile reef") that coincides with the Mid-Channel zone. A medial fault cuts upward to the sea floor, but the bounding fault on the south is truncated by the Holocene part of the undivided Quaternary deposits (unit Q) and the north-bounding fault cuts upward about halfway through the lower Pleistocene part of the lower Pleistocene and upper Pliocene strata (unit Qpl). A vertical separation of about 50 m, up on the north, at the base of the upper Pliocene marine strata (unit Tpu) is shown for the north-bounding fault; a separation of similar amount, down on the north, is shown for the south-bounding fault. No vertical separation is shown on the medial fault.

A possible correlative of the north boundary fault of the zone (the isolated segment at long 119°30' W., lat 34°11' N.) is illustrated in the seismic profile and interpretive section by Greene (1976, fig. 8, "Santa Barbara slope" fault). The section indicates about 120 m of vertical separation, up on the north, and the profile suggests that the fault cuts through lower Pleistocene deposits (unit Qs) to the sea floor. These interpretations, coupled with the spatial association of the focal mechanisms, indicate that the Mid-Channel zone is seismically active, but whether one fault or more is active cannot be determined. The fault-plane solutions associated with the Mid-Channel zone occur in the general area where the Oak Ridge fault, which onshore is known to dip south and to parallel the south flank of the Ventura basin syncline, intersects the Mid-Channel zone. The dip of the mid-channel faults is thus not easily evaluated, and their association with the fault-plane solutions is weak.

OAK RIDGE FAULT

The Oak Ridge fault is a gently to steeply south-dipping reverse fault, the trace of which generally follows the south bank of the Santa Clara River. At South Mountain, just west of long 119°, the fault thrusts lower Miocene and upper Eocene strata over upper Pleistocene strata, for an apparent stratigraphic separation of at least 2,000 m (Baddley, 1954). Near Saticoy, displacement in sediments of late Quaternary age has caused a ground-water barrier. Offshore data from seismic profiles between long 119°15' and 119°30' indicate that Pleistocene strata are upthrown on the south more than 135 m; no surface displacement at the sea floor is known (Greene, 1976).

ANACAPA-SANTA MONICA FAULT

The Anacapa and Santa Monica faults are major elements of an east-trending zone of deformation that marks the southern front of the Transverse Ranges along the south flank of the Santa Monica and San Gabriel Mountains. Other elements of the zone include the Raymond Hill and Cucamonga faults (fig. 4.1); the zone extends east onshore for about 100 km, and all faults are north-dipping reverse-left oblique faults. East of its intersection with the shoreline at Santa Monica, two or more subparallel elements of the zone are recognized. One, generally called Santa Monica, is aligned with a north-dipping reverse fault at the mouth of Potrero Canyon that cuts upper Pleistocene terrace deposits. Other elements locally are associated with a ground-water barrier in Pleistocene deposits; in the Santa Monica area, a topographic scarp in upper Pleistocene deposits is aligned with the barrier (Hill and others, 1977).

TABLE 4.3.—*Data on mapped focal mechanism*

[Mag., magnitude; azi, azimuth, pl, plunge]

Event No.	Map coord	Yr Mo D	Time (G.m.t.) (hr:min:s)	Depth (km)	Mag	Focal Planes				Slip Vector	
						Primary		Auxiliary		P-axis	
						Azi (degrees)	Dip (degrees)	Azi (degrees)	Dip (degrees)	Azi (degrees)	Pl (degrees)
8	C2	70-02-20	7:35:35	12.3	2.4	116	35 N.	116	55 S.	26	0
21	D2	70-04-16	21:55:48	8.9	2.9	108	76 N.	50	24 S.	0	30
30	D3	70-05-25	2:57:54	8.0	2.7	156	44 E.	170	46 W.	72	2
35	B4	70-06-20	15:27:31	8.0	3.1	146	60 E.	146	30 W.	56	0
40	F2	70-08-26	1: 8:59	8.0	3.6	112	60 N.	160	40 S.	42	12
41	D2	70-08-29	8:14:16	8.0	2.3	118	50 N.	164	50 W.	50	0
51	C2	70-12-06	1:19:33	15.5	2.0	98	60 N.	144	40 W.	26	13
64	H2	71-02-16	4:37:3	5.4	3.6	96	50 N.	80	44 S.	0	0
74	H3	71-04-02	5:40:24	3.4	3.8	100	42 N.	78	52 S.	178	3
90	D2	71-05-07	2: 3:21	10.4	2.6	118	50 N.	118	40 S.	28	5
100	C2	71-05-15	16:54:13	13.7	2.7	90	35 N.	138	60 W.	214	15
129	F2	71-11-04	19:17:39	11.1	2.5	88	56 S.	88	34 N.	176	11
144	A2	72-01-17	5:49:58	10.3	2.7	116	76 N.	98	14 S.	26	21
158	D2	72-04-04	5: 2:56	8.7	3.1	108	44 N.	86	48 S.	186	5
162	C2	72-04-17	0:28:38	8.9	3.0	95	57 N.	42	46 S.	340	6
165	H4	72-06-11	11: 5: 4	10.9	2.8	134	84 N.	52	36 S.	21	25
166	C2	72-06-15	16:42: 9	13.4	2.2	130	65 N.	13	45 W.	68	12
172	G3	72-07-14	23: 1:15	6.6	2.7	107	70 N.	134	25 S.	21	21
173	G1	72-07-27	1:12: 4	8.0	3.0	90	85 N.	24	10 E.	346	45
197	F3	73-02-21	14:45:57	12.2	5.9	86	44 N.	86	46 S.	356	0
288	H4	73-03-26	1:27:44	8.0	2.5	100	28 N.	144	70 W.	220	23
297	C2	73-03-29	17:54:16	14.2	3.3	108	45 N.	136	50 W.	213	4
357	E4	73-08-06	23:29:16	13.8	5.0	115	50 N.	130	50 S.	211	5
359	E4	73-08-06	23:53:46	13.7	1.9	150	62 E.	130	30 S.	53	15
365	E2	73-08-15	2:16:21	4.3	3.0	112	40 N.	112	50 S.	202	5
371	F4	73-08-20	14: 1:49	8.0	2.5	104	60 N.	87	30 S.	8	15
376	F2	73-08-24	9: 4:55	13.4	2.4	120	50 N.	158	50 W.	228	2
385	H3	73-09-02	6:28: 3	13.9	2.3	46	44 N.	91	56 S.	162	6
388	E2	73-09-04	9:11:25	11.5	3.4	103	52 N.	72	42 S.	358	6
391	E2	73-09-07	15:18:10	9.9	2.6	98	40 N.	98	50 S.	189	5
396	F2	73-09-13	13: 7:45	12.1	2.2	146	48 E.	136	40 W.	52	6
397	F2	73-09-13	13: 8:37	16.0	2.2	142	50 E.	148	40 W.	42	5
418	H2	73-11-14	17:15:31	13.1	2.2	142	60 E.	142	30 W.	52	0
426	G3	73-12-20	14:23:21	13.3	2.1	152	50 E.	6	44 W.	78	5
428	H2	73-12-25	6: 9: 3	11.3	2.1	120	58 N.	162	36 W.	48	14
449	D2	74-02-27	12:25:36	8.0	2.3	114	52 N.	70	48 S.	2	2
450	H2	74-03-03	16:29: 1	12.9	2.2	158	32 E.	154	66 W.	66	12
472	F3	74-04-25	8:23:53	8.9	2.8	91	72 N.	118	20 S.	6	27
482	D3	74-07-09	0:58:49	10.8	2.0	122	60 N.	122	30 S.	32	15
505	E2	74-09-23	2:22:59	6.5	2.0	128	54 N.	128	36 S.	36	9
553	G4	75-01-11	14:44:18	13.0	2.5	95	45 N.	95	45 S.	5	0
555	H4	75-01-23	3:48:42	8.0	2.8	126	90	24	90	339	0
557	H3	75-01-28	5:22:22	8.0	2.4	52	50 N.	96	50 S.	344	0
558	D2	75-01-28	9:45:49	8.0	2.5	137	54 E.	108	40 S.	33	7
570	H3	75-03-01	5:45: 4	6.6	2.0	128	56 N.	72	52 S.	11	3
575	G1	75-03-24	10:32:25	12.2	2.7	98	60 N.	118	32 S.	15	15
576	G2	75-04-10	21:19:26	6.7	2.0	90	44 N.	126	52 S.	200	4
618	D2	75-10-09	6:16:56	11.8	2.6	77	50 N.	96	42 S.	356	6
625	H4	75-11-03	3:42:17	16.6	1.8	132	84 N.	45	54 S.	20	35
SB78	D2	78-08-13	22:54:52	12.5	5.1	114	40 N.	158	60 S.	229	10
										60	30

The apparent stratigraphic separation across these faults is variable from west to east, according to well data. Northward dips of 40° to 70° and apparent reverse separations of 1,770 to 2,133 m at the top of middle

Miocene strata are reported for the Sawtelle-Beverly Hills oil field area (Knapp, 1962; Eschner and Scribner, 1972; Lang and Dreessen, 1975) 8–15 km east of the shoreline at Santa Monica. Separations at the surface of the buried

basement complex are poorly known, but a structural contour map based on a density-residual gravity model shows vertical separations in the range of 2,400–3,660 m (McCulloh, 1960, fig. 150.1). However, vertical separations at basement may be a relatively small component of displacement across the zone, which is inferred to include a large component of left-lateral strike slip (Campbell and Yerkes, 1976), in part to account for juxtaposition of dissimilar basement rocks and pre-upper Miocene sequences west of the Newport-Inglewood zone. West of the shoreline, the fault zone includes a northern branch, the Malibu Coast fault, and a southern, offshore branch, the Anacapa fault (pl. 4.1). The Anacapa fault is the southern boundary of Transverse Ranges province, as defined by the east-trending structures of Point Dume (Junger and Wagner, 1977, fig. 4), whereas the Malibu Coast fault is a recognized boundary between wholly dissimilar rock sequences (Campbell and others, 1966).

The total vertical separation across the Anacapa fault is unknown. Up-on-the-north separations of 1,000 to 2,000 m are indicated by structure contours on the Miocene-Pliocene unconformity, and 200 to 600 m on lower Pliocene strata, in the area south and southwest of Point Dume (Junger and Wagner, 1977, fig. 7, profiles C-C', D-D'). The seismic profiles indicate that Quaternary sediments in that area are not cut by the fault.

The Malibu Coast fault dips north at 30°–70°, and all evidence indicates reverse dip slip; it marks the zone of deformation along which the Santa Monica Mountains block overrides the low-lying terrane to the south. Stratigraphic separation across the zone is indeterminate, since it juxtaposes unlike rock sequences along its entire length. Topographic relief across the zone is at least 850 m, but very large left-lateral strike slip (60–90 km) in late middle Miocene time has been inferred on regional grounds (Campbell and Yerkes, 1976). Elements of the fault have thrust upper Pleistocene (about 105,000 yr old) marine terrace deposits more than 15 m over upper Miocene strata at one locality near Malibu Creek, and deposits of similar age are cut by faults in the zone at several other localities along its length.

The fault-plane solution for the 1973 Point Mugu earthquake is well constrained and indicates reverse displacement; one of the nodal planes dips about 44° N. and is geometrically and geologically compatible with the Anacapa fault (Ellsworth and others, 1973; Stierman and Ellsworth, 1976; cross sections C-C', D-D', pl. 4.1).

Although the somewhat diverse focal mechanisms and spatial distribution of the aftershocks do not correlate well with the nodal plane of the main shock (fig. 4.6; Stierman and Ellsworth, 1976), they do indicate dominantly reverse faulting on chiefly north-dipping faults in response to northeast-southwest compressive stress, as do other earthquakes along the zone.

A composite fault-plane solution based on five events along, but just south of, the trend of the Santa Monica fault, near the east end of the Santa Monica Mountains about 25 km east of the map area, indicates a steeply north-dipping fault with predominant reverse displacement, a moderate component of left-lateral strike slip, a slip vector plunging about 55° N. 66° E, and a *P* axis plunging about 28° N. 18° E. (Hill and others, 1977, pl. 4, fig. 8). This solution is consistent with those reported from our study.

The segment of the Santa Monica fault between long 118°35' W. and 118°20' W. (15 km east of the present map area) was relatively free of recorded seismicity during the 1970–75 period, whereas many events were recorded throughout the area to the south. The latter area is bounded by the northwest-trending San Pedro escarpment and Newport-Inglewood zones, each of which is characterized by dominantly right-lateral strike slip on the basis of geologic or seismologic evidence or both (see for example Hill and others, 1977, pl. 4, fig. 6; Buika and Teng, 1979). Buika and Teng (1979) note the same concentration of seismicity (during 1973–76) along the northwest-trending faults south of the Santa Monica fault

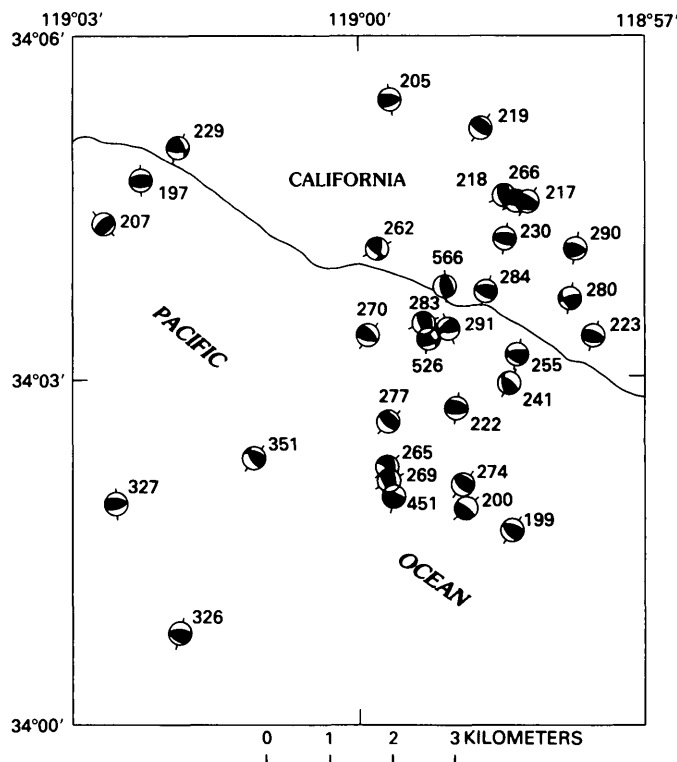


FIGURE 4.6.—Focal mechanisms for 1973 Point Mugu earthquake (No. 197) and aftershocks. Numbers show sequence of events. Lower hemisphere plots, compressional quadrants black, dilatational quadrants blank. Bar shows trend of *P* axis. Symbols located at epicenter of event. Location and area of map shown on plate 4.1.

system and relatively sparse seismicity in the Santa Monica Mountains to the north. They view this as evidence that the northwest-trending faults are terminated by the Santa Monica fault system and that the Santa Monica Mountains are acting as a passive and coherent structural block. They also conclude that the Santa Monica fault system was the locus of chiefly north-over-south reverse-left-oblique slip as a result of compressive stress oriented northeast-southwest.

CONCLUSIONS

Focal mechanisms based on 200 events of M_L 2 to 6 for the period 1970 through 1975 in the western Transverse Ranges reflect the same stress regime as larger earthquakes in the province for which records are available, that is, near-horizontal pressure axes directed generally normal to the great bend of the San Andreas fault. The inferred compressive stress is expressed chiefly by seismicity and reverse displacement along several major zones of east-trending reverse faults (Red Mountain-San Cayetano, Pitas Point-Ventura, Mid-Channel, and Anacapa-Santa Monica); some left-lateral strike slip also is indicated. This type of deformation is entirely typical of the following measurements taken after the 1971 San Fernando earthquake over an area of more than 250 km²:

1. 1.4 m vertical (up on the north) separation across the rupture zone.
2. 1.9 m left-lateral separation.
3. 0.55 m north-south shortening normal to the fault trace.
4. Differential arching and depression of more than 2 m that accentuated preexisting landforms.
5. Horizontal deformation on a regional scale that lengthened northwest-trending control lines.

Most significantly, the following evidence on rate and sense of deformation is mutually consistent for individual faults: geologic data on age and sense of latest displacement and amount and sense of stratigraphic separation, geodetic data on tilting of coastal areas underlain by faults, uplift of dated marine terrace deposits in coastal areas underlain by faults, and associated focal mechanisms. The indicated average rates of vertical deformation (5–10 mm/yr) have been constant at least over the last 45,000 yr.

The east-trending reverse faults that dominate the structure of the western Transverse Ranges are slip surfaces along which many kilometers of north-south shortening and a lesser amount of east-west extension have occurred in late Quaternary time. At the present rates, all the measured compressive deformation within the western Transverse Ranges could have occurred during the last 0.5 to 1 m.y.

REFERENCES CITED

- Baddley, E. R., 1954, Geology of the South Mountain Oil Field, Ventura County, Map Sheet no. 29 of Jahns, R. H., ed., Geology of Southern California: California Department of Natural Resources, Division of Mines Bulletin 170, geologic map (scale about 1:18,000) with text and section.
- Bloom, A. L., Broeker, W. S., Chappell, J. M. A., Matthews, R. K., and Mesolella, K. J., 1974, Quaternary sea level fluctuations on a tectonic coast-New $^{230}\text{Th}/^{234}\text{U}$ dates from the Huon Peninsula, New Guinea: *Quaternary Research*, v. 4, no. 2, p. 185–205.
- Buchanan-Banks, J. M., Castle, R. O., and Ziony, J. I., 1975, Elevation changes in the central Transverse Ranges near Ventura, California: *Tectonophysics*, v. 29, p. 113–125.
- Buika, J. A., and Teng, T. L., 1979, A seismicity study for portions of the Los Angeles basin, Santa Monica basin, and Santa Monica Mountains, California: University Southern California, Technical Report 79-9, 191 p.
- Campbell, R. H., Wolf, S. C., Hunter, R. E., Wagner, H. C., Junger, Arne, and Vedder, J. G., 1975, Geologic map and sections, Santa Barbara Channel region, California: U.S. Geological Survey Open-File Report 75-123, scale 1:250,000.
- Campbell, R. H., and Yerkes, R. F., 1976, Cenozoic evolution of the Los Angeles Basin area—Relation to plate tectonics, in Howell, D. G., ed., Aspects of the geologic history of the California Continental Borderland: American Association of Petroleum Geologists Miscellaneous Publication 24, p. 541–558.
- Campbell, R. H., Yerkes, R. F., and Wentworth, C. M., 1966, Detachment faults in the central Santa Monica Mountains, California: U.S. Geological Survey Professional Paper 550-C, p. C1–C11.
- Castle, R. O., Church, J. P., Elliott, M. R., and Morrison, N. L., 1975, Vertical crustal movements preceding and accompanying the San Fernando earthquake of February 9, 1971—A summary: *Tectonophysics*, v. 29, p. 127–140.
- Castle, R. O., Church, J. P., Elliott, M. R., and Savage, J. C., 1978, Preseismic and coseismic elevation changes in the epicentral region of the Point Mugu earthquake of February 21, 1973: *Seismological Society of America Bulletin*, v. 67, no. 1, p. 219–231.
- Cemen, Ibrahim, 1977, Geology of the Sespe-Piru Creek area, Ventura County, California: Athens, Ohio, Ohio University, M.S. thesis, 69 p.
- Curran, J. F., Hall, K. B., and Herron, R. F., 1971, Geology, oil fields, and future petroleum potential of Santa Barbara Channel area, California: American Association of Petroleum Geologists Memoir 15, p. 192–211.
- Ellsworth, W. L., Campbell, R. H., Hill, D. P., Page, R. A., Alewine, R. W., III, Hanks, T. C., Heaton, T. H., Hileman, J. A., Kanamori, Hiroo, Minster, Bernard, and Whitcomb, J. H., 1973, Point Mugu, California, earthquake of 21 February, 1973, and its aftershocks: *Science*, v. 182, p. 1127–1129.
- Eschner, S., and Scribner, M. K., 1972, The discovery and development of the Sawtelle Field: American Association of Petroleum Geologists—Society of Exploration Geologists, Pacific Section, Annual Meeting, Technical Program Preprint No. 47, 5 p.
- Fine, S. F., 1954, Geology and occurrences of oil in the Ojai-Santa Paula area, Ventura County, Map sheet 28 of Jahns, R. H., ed., Geology of southern California: California Department of Natural Resources, Division of Mines Bulletin 170, scale 1:62,500.
- Greene, H. G., 1976, Late Cenozoic geology of the Ventura basin, California, in Howell, D. G., ed., Aspects of the geologic history of the California Continental Borderland: American Association of Petroleum Geologists Miscellaneous Publication 24, p. 499–529.
- Hill, R. L., Sprotte, E. C., Bennett, J. H., Chapman, R. H., Chase, G. W., Real, C. R., and Borchardt, G., 1977, Seismicity and focal mechanisms of the study area, Pt. 2 of Santa Monica—Raymond Hill fault zone study, Los Angeles County, California: California Division of Mines

- and Geology, Final Technical Report, U.S. Geological Survey Contract 14-08-15858, December 1977, 35 p., 4 pls.
- Holman, W. J., 1958, Correlation of producing zones of Ventura basin oil fields, in Higgins, J. W., ed., A guide to the geology and oil fields of the Los Angeles and Ventura regions: Los Angeles, California, American Association of Petroleum Geologists, Pacific Section, p. 191-199.
- Jennings, C. W., Strand, R. G., Rogers, T. H., Stinson, M. C., Burnett, J. L., Kahle, J. E., and Streitz, 1973, Preliminary fault and geologic map, State of California: California Division of Mines and Geology, Preliminary Report 13-south half, scale 1:750,000.
- Junger, Arne, and Wagner, H. C., 1977, Geology of the Santa Monica and San Pedro basins, California Continental Borderland: U.S. Geological Survey Miscellaneous Field Studies Map MF-820, scale 1:250,000.
- Knapp, R. N., chm., 1962, Cenozoic correlation section across Los Angeles basin from Beverly Hills to Newport, California: American Association of Petroleum Geologists, Pacific Section, Correlation Section 14.
- Lajoie, K. R., Kern, J. P., Wehmiller, J. F., Kennedy, G. L., Mathieson, S. A., Sarna-Wojcicki, A. M., Yerkes, R. F., and McCrory, P. F., 1979, Quaternary marine shorelines and crustal deformation, San Diego to Santa Barbara, California, in Abbott, P. L., ed., Geological excursions in the southern California area. Guidebook for field trips, Geological Society of America Annual Meeting, Nov. 1979: Department Geological Sciences, San Diego State University, San Diego, Calif., p. 3-15.
- Lang, H. R., and Dreessen, R. S., 1975, Subsurface structure of the northwestern Los Angeles basin: California Division of Oil and Gas Technical Papers, TP01, July 1975, p. 15-21.
- Lee, W. H. K., Johnson, C. E., Henyey, T. L., and Yerkes, R. F., 1978, Preliminary study of the Santa Barbara, California, earthquake of August 13, 1978, and its major aftershocks: U.S. Geological Survey Circular 797, 11 p.
- Lee, W. H. K., Yerkes, R. F., and Simirenko, M., 1979, Recent earthquake activity and focal mechanisms in the western Transverse Ranges, California: U.S. Geological Survey Circular 799-A, p. 1-26.
- McCulloh, T. H., 1960, Gravity variations and the geology of the Los Angeles basin of California: U.S. Geological Survey Professional Paper 400-B, p. B320-B325.
- Nagle, H. E., and Parker, E. S., 1971, Future oil and gas potential of onshore Ventura basin, California: American Association of Petroleum Geologists Memoir 15, p. 254-297.
- Natland, M. L., 1952, Pleistocene and Pliocene stratigraphy of southern California: Los Angeles, University of California, Ph.D. thesis, 165 p.
- 1953, Correlation of Pleistocene and Pliocene stages in southern California: Pacific Petroleum Geologist, v. 7, no. 2, p. 2.
- Ogle, B. A., and Hacker, R. N., 1969, Cross section coastal area Ventura County, in Geology and oil fields of coastal areas Ventura and Los Angeles basins, California: American Association of Petroleum Geologists, Society of Exploration Geologists, and Society of Economic Paleontologists and Mineralogists, Pacific Sections, 44th annual Meeting, Los Angeles, 1969, Guidebook, scale 1:48,000.
- Rice, S. J., Treiman, J. A., Borchardt, G. A., Jones, A. L., Mualchin, L., Chapman, R. H., and Sherburne, R. W., 1981, Geologic and seismic hazards evaluation of the proposed Little Cojo Bay LNG terminal site, Point Conception, California: California Division Mines and Geology, Sacramento, California, 68 pp, 5 App., 2 Att.
- Sarna-Wojcicki, A. M., Bowman, H. R., Meyer, C. E., Russell, P. C., Woodward, M. J., McCoy, G., Rowe, J. J., Baedecker, P. A., Asaro, F., and Michael, H., 1984, Chemical analyses, correlations, and ages of upper Pliocene and Pleistocene ash layers of east-central and southern California: U.S. Geological Survey Professional Paper 1293, 40 p.
- Sarna-Wojcicki, A. M., Williams, K. M., and Yerkes, R. F., 1976, Geology of the Ventura fault, Ventura County, California: U.S. Geological Survey Miscellaneous Field Studies Map MF-781, scale 1:6,000.
- Stierman, D. J., and Ellsworth, W. L., 1976, Aftershocks of the February 21, 1973, Point Mugu, California earthquake: Seismological Society of America Bulletin, v. 66, no. 6, p. 1931-1952.
- Van Eysinga, F. W. B., 1975, Geological time table (3d ed.): Amsterdam, Elsevier, 1 sheet.
- Weber, F. H., Jr., Cleveland, G. B., Kahle, J. F., Kiessling, E. F., Miller, R. V., Mills, M. F., Morton, D. M., and Cilweck, B. A., 1973, Geology and mineral resources study of southern Ventura County, California: California Division of Mines and Geology Preliminary Report 14, 102 p., geologic map scale 1:48,000.
- Wesson, R. L., Lee W. H. K., and Gibbs, J. F., 1971, Aftershocks of the earthquake, in The San Fernando, California, earthquake of February 9, 1971: U.S. Geological Survey Professional Paper 733, p. 24-29.
- Whitcomb, J. H., 1971, Fault-plane solutions of the February 9, 1971, San Fernando earthquake and some aftershocks, in the San Fernando, California, earthquake of February 9, 1971: U.S. Geological Survey Professional Paper 733, P. 30-32.
- Whitcomb, J. H., Allen, C. R., Garmany, J. D., and Hileman, J. A., 1973, San Fernando earthquake series, 1971—focal mechanisms and tectonics: Reviews of Geophysics and Space Physics, v. 11, no. 3, p. 693-730.
- Yeats, R. S., Lant, K. J., and Shields, K. E., 1977, subsurface geology of the Santa Susana fault in the aftershock area downstep of the 1971 San Fernando earthquake: Ohio University, Athens, Department of Geology, Final Technical Report, U.S. Geological Survey Contract No. 14-08-0001-15271, 26 p.
- Yerkes, R. F., Greene, H. G., Tinsley, J. C., and Lajoie, K. R., 1981, Seismotectonic setting of the Santa Barbara Channel area, southern California: U.S. Geological Survey Map MF-1169, 1 sheet., text, tables, figs.
- Yerkes, R. F., and Lee, W. H. K., 1979a, Late Quaternary deformation in the western Transverse Ranges, California: U.S. Geological Survey Circular 799-B, p. 27-37, 6 figs., 2 tables.
- Yerkes, R. F., and Lee, W. H. K., 1979b, Faults, fault activity, epicenters, focal depths, focal mechanisms, 1970-75 earthquakes, western Transverse Ranges, California: U.S. Geological Survey Map MF-1032, 2 sheets.
- Ziony, J. I., Wentworth, C. M., Buchanan-Banks, J. M., and Wagner, H. C., 1974, Preliminary map showing recency of faulting in coastal southern California: U.S. Geological Survey Miscellaneous Field Studies Map MF-585, 3 sheets, scale 1:250,000.

5. REVERSE-FAULT SYSTEM BOUNDING THE NORTH SIDE OF THE SAN BERNARDINO MOUNTAINS

By FRED K. MILLER

ABSTRACT

The San Bernardino Mountains form the easternmost part of the Transverse Ranges province. The mountain range is bounded on the north side by a complex system of reverse faults. Displacements on this north-bounding fault system, together with displacements on fault systems within and bounding the south margin of the San Bernardino Mountains, probably account for much, if not the entire, uplift of the range. Individual breaks that make up the north zone dip southward under the range between 10° and 50° . Movement on the zone appears to be in a reverse sense, but could have a small component of strike-slip movement. The time at which faulting began is unknown, but it has continued until recently; the fault zone still may be active.

Along much of the northern frontal zone, crystalline rocks ranging from Precambrian to Cretaceous in age are thrust over similar rocks of the same age. Rocks in the lower plate, however, include sedimentary and volcanic rocks of Tertiary age and Quaternary alluvium in addition to the crystalline rocks. Attitudes of individual breaks within the fault zone suggest that the locus of fault activity may have migrated northward through time.

The frontal fault system has a complex relation with the northwest-trending strike-slip faults of the Mojave Desert. Two of these faults, the Helendale and Old Woman Springs faults, intersect the frontal system. Although the relations are equivocal, it appears that the strike-slip faults cut the lower plate of the reverse system, but have relatively little expression in the upper plate.

INTRODUCTION

GEOLOGIC SETTING

The north flank of the San Bernardino Mountains is bounded by a south-dipping system of reverse faults. This fault zone is important not only because it is a major structural feature, but because the youthful-appearing scarps preserved in alluvium flanking the range suggest that the system may still be active.

The geologic map (pl. 5.1) shows the extent of the fault system where it has surface expression. Beyond the western edge of the mapped area the fault zone probably swings westward, away from its last-observed south strike, and continues concealed along the northern flank of the San Bernardino Mountains to the San Andreas fault. At the east end of the zone, the fault system appears to die out, but it may be distributed over a wide

zone farther back in the range or may be concealed beneath alluvium in front of the range.

The San Bernardino Mountains form the easternmost 90 to 100 km of the Transverse Ranges province. The mountain range is bounded on the north by the system of south-dipping reverse faults described in this report, on the southwest and west by the San Andreas fault, and on the south by the Pinto Mountain fault (fig. 5.1). A system of large east-west-striking, north-dipping reverse faults traverses the central part of the range in the Santa Ana River valley just north of San Gorgonio Mountain. Also, north of San Gorgonio Mountain, but on the south side of the Santa Ana River valley, there may be another fault system, normal or reverse, that drops the Santa Ana River valley down relative to the San Gorgonio Mountain block (Dibblee, 1964b).

Eastward from approximately where the Old Woman Springs fault intersects the mountain front, the elevation of the range decreases progressively to the desert floor at about the longitude of Yucca Valley. Elevations average about 2,000 m, except for the mass centered on San Gorgonio Mountain in the southern part of the range, which rises to about 3,350 m.

Most of the San Bernardino range is underlain by intermediate-composition granitic rocks of Mesozoic age (Miller and Morton, 1980). Precambrian schist and gneiss (Silver, 1971) make up about 20 percent of the basement rock, mostly in the southern part of the range; slightly smaller areas of gneiss occur in the central and north parts. Unconformably overlying the gneiss is relatively unmetamorphosed quartzite, phyllite, and dolomite of late Precambrian age, which in turn is overlain by Paleozoic limestone and dolomite, part of which is believed to be Mississippian (Richmond, 1960; Stewart and Poole, 1975). Other than the granitic plutons, no rocks of Mesozoic or early Tertiary age are present. The youngest rocks in the range consist of several patches of late Miocene basalt, and, in structural depressions, sedimentary rocks that may range in age from Miocene to Pleistocene. The sedimentary rocks range from conglomerate to shale; most units are unconformably overlain by Quaternary gravels, particularly around the flanks of the range.

Manuscript received for publication on December 16, 1980.

PREVIOUS STUDIES

Richmond (1960) included an 8-mile segment of the north-bounding fault zone on his map of the San Bernardino Mountains north of Big Bear Lake, but the faults he shows are somewhat generalized. The entire length of this frontal fault system was mapped by Dibblee (1964a, 1967, 1968), but he also generalized the zone on his maps. Shreve (1968) mapped the area around the Blackhawk landslide, which lies north of the strip map (pl. 5.1); some of the faults that make up the frontal fault system are shown on his map.

DESCRIPTION OF ROCKS IN AND AROUND THE FAULT ZONE

The following lithologic descriptions purposely are brief, because the fault system bounding the range is the primary topic of this report, and because the number of lithologic units shown on the geologic map (pl. 5.1) is too great to permit detailed descriptions of each. In addition, the description of a particular unit as given here may or may not be representative of that unit at other places in the range. Also, considerable variation exists within many of the units even in the area shown on plate 5.1, and the variation for most is even greater within the mountain range as a whole. Therefore, the descriptions apply to the various units only as they occur in the area covered by plate 5.1 unless specifically noted.

PRECAMBRIAN(?) ROCKS

LAYERED GNEISS

Layered gneiss, most of which is highly contorted, occurs at various places along the eastern half of the fault zone. The main masses are centered west of Big Horn Canyon and west, south, and east of Rattlesnake Canyon. Gneiss also occurs in parts of the unit mapped as crystalline rocks undivided, and as inclusions as much as a few hundred meters in length within some of the plutonic units.

Most commonly the gneiss consists of medium-grained light-colored quartzo-feldspathic layers ranging in thickness from a few millimeters to half a meter, separated by biotite-rich layers generally less than 5 cm in thickness. Locally, discontinuous zones as much as several hundred meters thick contain amphibole-bearing dark layers, some of which carry garnet. Andalusite and (or) sillimanite occur locally in the biotite-rich layers in Big Horn Canyon and in gneiss inclusions in granitic rock to the east.

The gneiss has well-developed layering and at many localities a well-developed lineation defined by streaked-out minerals. South of Rattlesnake Canyon the attitude of both layering and lineation is relatively uniform, but at most other localities it is highly contorted and two or more generations of folds have developed.

Most, if not all, of the gneiss is probably correlative with the Baldwin Gneiss of Guillou (1953), dated by Silver

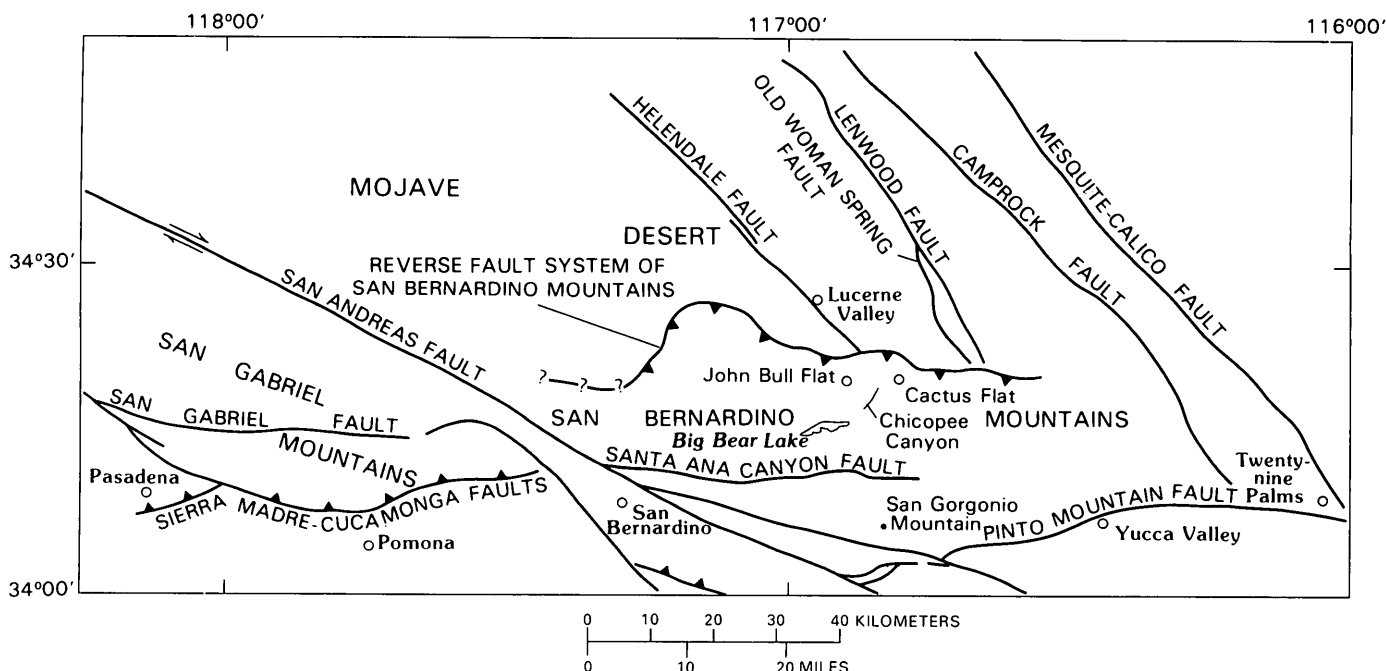


FIGURE 5.1.—Frontal fault system of San Bernardino Mountains relative to other geologic features and geographic locations mentioned in text.

(1971) at 1,750 m.y. B.P. Potassium-argon analyses of the gneiss yield Cretaceous ages because of regional cooling effects or regional resetting (Miller and Morton, 1980).

LEUCOCRATIC GNEISS

South of Rattlesnake Canyon, the layered gneiss grades into leucocratic biotite-bearing quartz-feldspathic gneiss. Most of the rock is medium grained, but bands of aplitic and pegmatitic material are common. A fabric ranging in degree of development from excellent to almost imperceptible is present in the rock. This fabric consists of a faint foliation or crudely developed layering but at some places includes, or consists exclusively of, a poorly to moderately well developed mineral lineation.

The rock in general has a quartz monzonite composition and averages about 3 to 5 percent biotite. No systematic or noticeable variations in composition were noted, but the unit was not studied in detail. The composition and appearance of the rock suggest that it may be a metamorphosed plutonic rock.

Quartz diorite and granodiorite appear to intrude the leucocratic gneiss south of Rattlesnake Canyon. Although the relationship between the granodiorite and gneiss is fairly clear, faulting, or brecciation associated with faults, obscures the contact with the quartz diorite. Because the leucocratic gneiss appears to grade into the layered gneiss and the fabric developed in both rocks is not present in any younger rocks, including those of late Precambrian age, the leucocratic gneiss is considered to be Precambrian.

PALEOZOIC ROCKS—CARBONATE ROCKS, UNDIVIDED

From Arrastre Canyon west to Dry Canyon, limestone and dolomite, previously mapped by Vaughn (1922) and Dibblee (1964a) as the Furnace Limestone, are shown on the map (plate 5.1) as undivided carbonate rocks. Most of these rocks are metamorphosed to marble and dolomitic marble by the numerous Mesozoic plutonic rocks. Bedding is not well preserved because of the metamorphism, although most of the rock contains dark streaks that may or may not be parallel to bedding. The color of the rock ranges from medium to pale gray and pale tan where the metamorphism is not pronounced and is generally white where it is metamorphosed to coarse-grained marble. In the area covered by plate 5.1, no noncarbonate clastic beds were observed, the only obvious impurity being minor lenses of chert.

Most of the carbonate rock is highly brecciated because of its proximity to the system of reverse faults bounding the range. Much of the landslide debris, especially in the vicinity of Blackhawk Mountain, is derived from fault-

brecciated carbonate rock. Because of the lack of stratigraphic control within the Furnace Limestone, faults within this unit farther back in the range may have gone undetected.

Richmond (1960) assigned a Mississippian and possibly early Pennsylvanian age for part of the formation, but the fossils that form the basis for this assignment are from the upper part of an extremely thick section. Stewart and Poole (1975) considered the Furnace Limestone to be Cambrian to Permian(?) and suggested that much of the late Precambrian and Paleozoic section present in the Great Basin is represented in the Furnace Limestone and pre-Furnace Limestone sedimentary rocks of the San Bernardino Mountains.

MESOZOIC ROCKS

The emplacement history and relative ages of the Mesozoic plutonic rocks are poorly understood. Extensive K-Ar dating of both plutonic and metamorphic rocks in the San Gabriel and San Bernardino Mountains and in the southern Mojave Desert has delineated a large region in which K-Ar isotopic systems have undergone extensive resetting (Miller and Morton, 1980). The San Bernardino Mountains fall near the center of this region, so none of the crystalline rocks in the range yield emplacement or even primary metamorphic K-Ar ages. The age of a distinctive hornblende monzonite, however, was well established by Miller (1976) by using the Pb-U method, and relatively good estimates can be made for some groups of plutonic rocks on the basis of correlation with similar rocks that occur outside the reset region in the eastern Mojave Desert.

As a result of the age uncertainties the relative ages as shown in the explanation, and implied by the order of the descriptions, should be considered tentative.

HORNBLENDE MONZONITE

Mafic-rich hornblende monzonite crops out at several places between Grapevine Canyon and Furnace Canyon, the largest mass being located just east of Grapevine Canyon. Several tens of square kilometers are underlain by this rock farther back in the range north, northwest, and west of Big Bear Lake (fig. 5.1).

Although composition of the body ranges from quartz monzonite to monzodiorite, the most common rock type is hornblende monzonite with a color index of 15 to 20. Biotite, which may be the product of contact metamorphism, makes up about 5 percent of the rock in the vicinity of younger plutons. In much of the rock, hornblende has cores of clinopyroxene.

The rock is medium to fine grained and differs considerably in grain size and texture from place to place.

The most obvious textural differences result from the nonuniform development of both foliation and lineation. Even on the scale of an outcrop, the degree of fabric development and the orientations of fabric elements appear to be variable. At many localities, what may have been a primary fabric appears to have been disrupted in a nonuniform manner by late stage, semibrittle deformation in the pluton. Thin discontinuous seams of mylonitized rock that are now epidotized form anastomosing, veinlike features throughout much of the rock.

K-Ar ages on this rock range from 82 m.y. B.P. on biotite to 197 m.y. B.P. on hornblende. Neither of these numbers is indicative of the emplacement age, however, as both reflect cooling history or resetting by later metamorphism. In addition, the hornblende's apparent age may be older than that which would be yielded by pure hornblende, because the dated mineral separate contained inseparable pyroxene. Miller (1976) obtained a Pb-U age of 220 m.y. B.P. (Triassic) on zircon from this rock which he considers an emplacement age.

MAFIC QUARTZ DIORITE

Hornblende-biotite quartz diorite occurs in relatively small patches from one end of the mountain range to the other. Only the larger masses of this rock type are shown on plate 5.1; one is located south of Rattlesnake Canyon, and two others are at the mouth of, and just west of, Grapevine Canyon.

All three of these bodies are internally heterogeneous with respect to both texture and composition. Quartz content is generally 5 to 15 percent, color index 35 to 80, and about 15 to 60 percent of the rock is plagioclase. Hornblende is more abundant than biotite; locally biotite is absent. Biotite has a distinctive habit in this rock type, occurring in relatively large but very thin crystals.

Texturally, these bodies rarely display a fabric, but where they do, it is a crude lineation. The major variation in texture is a pronounced difference in grain size which ranges from fine to coarse. Locally segregations of hornblende or plagioclase form coarse masses that have an orbicular appearance. In places, particularly in the mass south of Rattlesnake Canyon, the rock is extremely coarse grained and contains irregularly shaped mafic pods.

The emplacement age of these bodies is not precisely known, although at least one similar mafic intrusive in the southern Mojave Desert yielded a hornblende K-Ar apparent age of 199 m.y. B.P. (Miller and Morton, 1980). Co-existing biotite yielded an apparent age of 116 m.y. B.P., so the 199 m.y. B.P. figure should be considered minimum for time of emplacement. The quartz diorite intrudes the layered gneiss and is intruded by leucocratic biotite quartz monzonite.

FINE-GRAINED MAFIC GRANODIORITE

A distinctive hornblende-biotite granodiorite occurs in two masses, one at the mouth of Arrastré Creek and the other about 1.5 km to the east. The two masses may be connected farther back in the range. The easternmost body is faulted against the mafic quartz diorite, but dikes of the granodiorite with chilled margins cut the quartz diorite. Near Arrastré Creek, the granodiorite intrudes the Furnace Limestone. The relationship to the two-mica quartz monzonite on the east side of Arrastré Creek is not well established, but the two-mica body appears to intrude the granodiorite.

The composition of the granodiorite is highly variable mainly due to differences in the content of mafic minerals. The color index of the rock ranges from 20 to 60, averaging about 30. The variations between the two extremes occur on an outcrop scale. The ratio of hornblende to biotite ranges from about 5:1 in the darkest rock to about 1:5 in the lightest. Much of the hornblende occurs as radiating masses of prismatic crystals, and the biotite as relatively large but thin tablets.

In places, the more leucocratic parts of the rock have a very subtle foliation, but most of the body has no recognized fabric. All of the rock regardless of color index is medium to fine grained. Inclusions are abundant locally, but show no consistently preferred orientation.

FOLIATED HORNBLENDE-BIOTITE GRANODIORITE

In the eastern quarter of the mapped area, medium- to coarse-grained foliated hornblende-biotite granodiorite forms two discrete masses that may be connected farther back in the range and several smaller masses just north of Rattlesnake Canyon. Although more than one pluton may be represented, they are combined into a single group here because of lithologic similarities.

The mass just east of Bighorn Canyon has a subtle foliation at its east end, which becomes progressively better developed toward Bighorn Canyon. The increase in development of the foliation is accompanied by an increase in color index from about 15 to 25. Locally a poorly developed lineation defined by aligned hornblende and streaked-out biotite crystals is evident. The rock is nonporphyritic and, except for the foliation, hypidiomorphic granular. The mass north of Rattlesnake Canyon is slightly more mafic than the two to the east. In all of these rocks the ratio of hornblende to biotite increases as the color index increases. Potassium feldspar is irregularly distributed in the rock and, in places, is sparse enough to make the rock borderline between granodiorite and quartz diorite. Spheine is abundant in all of the rock.

All of the bodies are characterized by large numbers of inclusions, which range in size from a few centimeters to

several hundred meters. The larger inclusions are irregular in shape and show no preferred orientation, but the smaller ones, 5 to 15 cm in average size, are aligned in the plane of foliation.

The foliated granodiorite intrudes the layered gneiss and is intruded by a porphyritic quartz monzonite, leucocratic biotite quartz monzonite, and the granodiorite of Rattlesnake Canyon.

GRANODIORITE OF RATTLESNAKE CANYON

Hornblende-biotite granodiorite underlies about 5 km², forming an arcuate pluton centering on the lower portion of Rattlesnake Canyon. Except for a local increase in mafic minerals in the vicinity of a small inclusion swarm, the texture, appearance, and modal composition of the rock are remarkably uniform throughout the body.

The rock is medium grained and nonporphyritic. The color index averages 15 to 18 with a hornblende:biotite ratio of about 1:3. Plagioclase is subhedral and potassium feldspar subhedral to anhedral. The potassium feldspar is commonly pink. All minerals are about the same size, giving the rock a very even grained appearance. Sphene is the most common accessory and, though not abundant, is ubiquitous. Locally, the rock contains sparse feldspar phenocrysts up to 2 cm in length, but these occurrences are rare. No foliation or lineation has been observed. Small inclusions and aplite and pegmatite dikes are common, but not abundant.

The rock intrudes the foliated hornblende-biotite granodiorite and the layered gneiss, but appears to be intruded by a leucocratic biotite quartz monzonite that occurs discontinuously around the periphery of the pluton.

GRANODIORITE OF BOUSIC CANYON

Twenty kilometers west of the granodiorite in Rattlesnake Canyon, at the mouth of Bousic Canyon, is a hornblende-biotite granodiorite that is possibly related to the body at Rattlesnake Canyon. The Bousic Canyon body is not described, because it is identical to the Rattlesnake Canyon pluton, except that it consistently contains about 5 modal percent more potassium feldspar than the granodiorite to the east. The only reasons for not mapping them as a single genetic unit are the difference in potassium feldspar and the distance between the bodies. Both could be small parts of much larger bodies (or a single body) as both are bounded by alluvial deposits and the frontal fault system on the north.

HETEROGENEOUS BIOTITE QUARTZ MONZONITE

Two separated bodies of biotite quartz monzonite that may or may not be related occur near the east end of the range. The western of the two bodies, located on both

sides of Rattlesnake Canyon, is actually a series of small masses separated from one another and arranged concentrically around the periphery of the granodiorite of Rattlesnake Canyon. In this area, the intrusive is nearly uniform with respect to composition and texture, except for a few pods of pegmatite and aplite. The rock is medium-grained biotite quartz monzonite with trace amounts of muscovite. It has a color index of 10 or less. Locally the rock has a very faint foliation, but in most of the pluton the minerals show no preferred orientation. Inclusions or inclusionlike masses are common, but most are less than 20 cm long; they consist of streaked concentrations of mafic minerals rather than true inclusions.

The mass at the east end of the range, on the other hand, is a heterogeneous rock that contains large inclusions of gneiss and mafic granitic rock in addition to numerous pods of pegmatitic and aplitic material. The main rock, biotite quartz monzonite, is even grained and very similar to the mass at Rattlesnake Canyon; the chief differences are the more abundant foreign material in it and the slightly coarser grain size. Pegmatite and aplite masses locally make up more than 25 percent of the rock by volume and form irregularly shaped masses up to 50 m long. The combined pegmatite, aplite, and inclusions in places make up at least half of the unit by volume.

The Rattlesnake Canyon mass intrudes gneiss, the foliated hornblende-biotite granodiorite, and possibly the granodiorite of Rattlesnake Canyon. The eastern mass appears to intrude the foliated hornblende-biotite granodiorite and is intruded by the porphyritic quartz monzonite.

TWO-MICA QUARTZ MONZONITE

A small area, of less than half a square kilometer, on the east side of Arrastre Creek is underlain by biotite-muscovite quartz monzonite. The rock is medium- to coarse-grained, nonporphyritic, and hypidiomorphic granular. It is garnet bearing and has a color index of about 10. The muscovite:biotite ratio is about 1:5. The rock appears to be intrusive into the fine-grained mafic granodiorite.

Except for the lack of lineation and foliation, this rock is identical to the two-mica quartz monzonite on Cactus Flat, about 3.5 km to the southwest. Vaughan's (1922) Cactus Granite is not adopted here, because there are at least five separate intrusive bodies on and around the flanks of Cactus Flat. The small two-mica body east of Arrastre Creek is most like the two-mica quartz monzonite pluton on the northeast side of Cactus Flat.

RATTLESNAKE MOUNTAIN PLUTON

A uniform biotite quartz monzonite, designated the Rattlesnake Mountain pluton by MacColl (1964), underlies

a large area in the western part of the mapped area. The rock is porphyritic coarse-grained biotite quartz monzonite and has an average color index of about 5. Pink potassium feldspar phenocrysts average about 2 to 3 cm in length and are in a matrix of plagioclase, quartz, and biotite about half that size. The rock is uniform with respect to composition and texture. It has virtually no fabric, but does contain numerous flattened inclusions and schlieren. These structures are less well developed in the part of the pluton shown on plate 5.1 than they are in the southern part. MacColl (1964) has made a detailed study of the pluton and its emplacement.

K-Ar dating on biotite yields apparent ages of 81 m.y. B.P., 80 m.y. B.P., and 72 m.y. B.P., but the entire Rattlesnake pluton is well within the area of K-Ar isotopic resetting or anomalous cooling ages defined by Miller and Morton (1980). The 81-m.y. B.P. number should be considered a younger limit on the emplacement age.

LEUCOCRATIC BIOTITE QUARTZ MONZONITE

Fine-grained leucocratic biotite quartz monzonite occurs in two small bodies separated by about half a kilometer of carbonate rock between Bousic Canyon and Crystal Creek. The quartz monzonite is distinctive because the feldspars in it are pale gray, and it has a very low color index of 3 to 5. Biotite, the only mafic mineral, occurs in small crystals less than 1 mm across, but characteristically a few are as much as seven times that size. Potassium feldspar is slightly more abundant than plagioclase and, along with quartz, forms an even-grained rock with an average crystal size of about 1.5 mm. Except for the few large biotite crystals, the quartz monzonite is nonporphyritic and has no fabric.

This rock is part of a much larger mass centered on John Bull Flat about 5 km farther south in the range. The rock there is identical to that in the mapped area, except that most of it is coarser grained. Many fine-grained dikes and quartz veins, very limited contact metamorphism, and sparse miarolitic cavities suggest that the whole body was emplaced at a shallow depth. The placer gold in Holcomb Valley, just north of Big Bear Lake (see fig. 5.1) may be related to this plutonic type. The pluton intrudes the carbonate rock and the hornblende monzonite, but there has been no isotopic dating of the rock.

PORPHYRITIC QUARTZ MONZONITE

Porphyritic biotite quartz monzonite occurs in dikes and faulted plutons from the east end of the mapped area to the mouth of Cushenberry Canyon. Some of the plutons extend back into the range and, in the case of the mass at the east end of the area, represent only the northernmost part of a large plutonic body. Although the quartz

monzonite occurs in several widely separated bodies, the compositional and textural similarities are so consistent from place to place that the rock is considered to represent widespread emplacement of a single magma or genetically related magmas.

The rock has a distinctive trimodal grain size that is particularly well developed in the large dikes formed by this intrusive type. Phenocrysts of potassium feldspar average about 2 cm in length, rarely exceeding 4 cm. Concentration of phenocrysts is variable, ranging from about 35 percent of the rock to complete absence. A few areas of nonporphyritic rock at the east end of the range are delineated on plate 5.1. Nearly all of the potassium feldspar occurs as phenocrysts and almost none in the groundmass. The groundmass is made up of plagioclase and quartz with an average grain size of about 0.4 cm. Biotite in small crystals averaging about 0.1 to 0.2 cm make up the third distinct crystal size, giving the rocks a speckled appearance and a color index of about 10. In the few places where phenocrysts are not present, the potassium feldspar occurs as subhedral crystals the same size as the plagioclase and quartz. In places, the grain size is greater than normal, but the trimodal distribution remains essentially intact.

Much of the rock shown as nonporphyritic at the east end of the range may actually be a mixture of the foliated hornblende-biotite granodiorite and a nonporphyritic phase of the quartz monzonite. Everywhere the quartz monzonite is mapped, it contains large included masses of country rock. These masses are generally irregularly shaped, not oriented, and range from tens to hundreds of meters in maximum dimension. They are particularly abundant in the nonporphyritic areas at the east end of the range.

GRANITIC ROCKS, UNDIVIDED

Several areas of plutonic rock have been mapped as undivided granitic rocks either because they are a heterogeneous mixture of different plutonic types or because they are extremely small areas of an indistinctive plutonic type that could not be assigned to other units.

The small mass in Bighorn Canyon is medium-grained leucocratic biotite quartz monzonite that may or may not belong to one of the other plutonic units. The small body on the east side of Crystal Creek is medium- to coarse-grained, slightly foliated biotite quartz monzonite, but also includes many smaller, irregularly shaped, mafic dike-like bodies. A complex mixture of biotite quartz monzonite, pegmatite, alaskite, and aplite makes up the undivided granitic rock in the north-central part of the Rattlesnake Mountain pluton. Some large metamorphic inclusions, particularly of mafic rock, occur at this latter locality.

The age of the undivided granitic rocks could range from Triassic to Cretaceous.

CRYSTALLINE ROCKS, UNDIVIDED

In several areas, particularly in the western half of the mapped area, complexly mixed outcrops of granitic and metamorphic rock are mapped as undivided crystalline rocks. East of the Rattlesnake Mountain pluton, these areas are primarily mixtures of layered gneiss, amphibolite, porphyritic biotite quartz monzonite, and some leucocratic biotite quartz monzonite and pegmatite.

West of the Rattlesnake Mountain pluton, however, some of the rocks include types not present anywhere else in the mapped area. A large part of the northern half of the undivided crystalline rocks west of the Rattlesnake Mountain pluton is underlain by porphyritic hornblende-biotite granodiorite and hornblende monzonite and syenite. The granodiorite contains numerous gray potassium feldspar phenocrysts as much as 4 cm long in a medium- to coarse-grained matrix of plagioclase, quartz, and hornblende, with only minor amounts of biotite. It contains much less quartz than most of the probable Cretaceous plutons and abundant sphene. This rock is widespread in the southern Mojave Desert and has yielded discordant K-Ar apparent ages on coexisting hornblende-biotite of 183 m.y. B.P. and 149 m.y. B.P. The monzonite and syenite are probably related to a hornblende monzonite near Lucerne Valley (fig. 5.1) dated by Miller (1976) at 220 m.y. B.P. using Pb-U methods. These quartz-deficient rocks are intimately mixed with plutonic rocks of more conventional composition, and along with the latter, intrude quartzite, marble, schist, and gneiss derived from sedimentary rocks of late Precambrian or Paleozoic age.

TERTIARY ROCKS

OLD WOMAN SANDSTONE

The Old Woman Sandstone, named by Shreve in Richmond (1960), occurs in numerous small areas from the east end of the range to just west of Crystal Creek. The unit probably extends farther east and west in the subsurface. It is, in all cases, north of the southernmost reverse fault of the fault system bounding the range.

The unit is predominantly tan conglomeratic arkose and mudstone. Beds are irregular, ranging from a few millimeters to several meters in thickness; bedding is commonly defined by pebble layers or by thin beds or lenses of sand. Cross bedding and filled channels are common but vary in abundance throughout the unit. Together with feldspar and quartz, biotite is almost everywhere present in the arkosic matrix. Most larger clasts are fairly well rounded and consist of basalt or andesite, gneiss, schist, granitic rock, and hornfels. Clasts of carbonate rock are present but rare. The rock is poorly indurated and is well exposed only where overlain by more resistant units.

Late Blancan (2-3 m.y. B.P.) vertebrate fossils have been found in the upper middle part of the Old Woman Sandstone (May and Repenning, 1982). Basalt that appears to be interlayered with arkose near the base of the Old Woman Sandstone yielded a whole-rock K-Ar age of 6.2 m.y. B.P. (Janet Morton, U.S. Geological Survey, unpub. data, 1979). The basalt sample was collected where arkose, assigned to the Old Woman Sandstone, is overlain by two distinctly different flows; the dated sample was taken from the upper, younger flow.

BASALTS INTERLAYERED WITH THE OLD WOMAN SANDSTONE

OLDER BASALTS

The lower basalt flows found in the lower part of the Old Woman Sandstone occur in the vicinity of the Old Woman Springs fault. The basal contact was not seen. The basalt is fine grained, medium to dark gray, and locally vesicular. Thickness of the flows is not known, because individual flows are difficult to recognize. At least part of the basalt was extruded subaqueously, as evidenced by locally abundant pillows. Most of the rock is cut by irregular cracks that presumably are related to cooling.

In thin section, the rock shows a pilotaxitic to trachytic texture. Olivine, which forms the only phenocrysts, is uniformly about one-half millimeter across, and mostly altered to iddingsite. The groundmass is a fine-grained mixture of plagioclase, pyroxene, and opaque minerals; almost no glass is present even though the rock is very fine grained.

YOUNGER BASALT

Relatively thin basalt flows overlie the more massive lower basalt. These rocks are very fine grained, weather brown, and are much less broken than the lower basalt. Individual flows average 2 to 4 meters in thickness and are highly vesicular. Mineralogically the upper basalt is identical with the lower, except that it is less altered and contains up to 20 percent partially devitrified glass in the matrix. Texturally the upper and lower flows are similar, except that the upper is finer grained. This rock yields a whole-rock K-Ar age of 6.2 m.y. B.P. (Janet Morton, U.S. Geological Survey, unpub. data, 1979).

QUATERNARY DEPOSITS

FANGLOMERATE AND RIVER-DEPOSITED MATERIAL

This alluvial unit, as shown on plate 5.1, includes much of the gravel that shows some degree of induration. All gravels younger than the Old Woman Sandstone that are not shown as separate units are grouped into this unit. As a result, it includes deposits representing several generations of deposition, spanning a considerable part

of the Quaternary. It is possible that some parts of other alluvial or fanglomerate units are mapped with this unit even though care was taken to avoid this. Also, the relative range in age of parts of this unit may overlap that of some younger alluvial or fanglomerate units.

At most places the unit consists of moderately to poorly indurated boulder and pebble fanglomerate. Bedding is poorly developed or absent in most exposures owing to the large size of the clasts and the high-energy conditions necessary to transport boulder-size clasts. In addition, most exposures are generally more than 90 percent covered by colluvial material derived from the poorly indurated fanglomerate. The boulders are as much as several meters in diameter and are poorly to well rounded. The overall deposit is poorly sorted and is derived entirely from rocks presently exposed in the San Bernardino Mountains. Although no systematic studies were made, at no place were boulders observed that could not have had their source areas immediately upslope. Sorting, degree of rounding, and development of bedding generally increase away from the mountains.

At several localities gravels that unconformably overlie the Old Woman Sandstone are more indurated and more steeply dipping than most of the rest of this unit; specifically, just west of One Hole Spring, on the east side of Blackhawk Canyon, one mile east of the mouth of Cushenberry Canyon, and on the west side of Arctic Canyon. The rocks at those localities may, therefore, be older and may represent a distinctly different cycle of deposition than most of this unit. This is also true for the low northeast-trending ridge at the northwest end of the mapped area. Because of the proximity to the present-day channel, some of the gravels may have been deposited by the ancestral Mojave River. The gravels along the ridge are finer grained and better bedded than most in this unit, and they have been oxidized in part. These relatively fine grained rocks occur from north of the Rattlesnake Mountain pluton to the southwest boundary of the mapped area. Because of the differences in grain size and bedding characteristics between these deposits and those that make up the rest of the unit, it is thought that they represent a depositional environment distinctly different from that of the other rocks of this unit east of the Rattlesnake Mountain pluton.

FANGLOMERATE OF CUSHENBERRY CANYON

A fanglomerate just east of the mouth of the Cushenberry Canyon, even though moderately well indurated, is mapped separately from the unit previously described, because it is almost monolithologic. About 90 percent of the clasts are from the unit called carbonate rocks, undivided; a small proportion of clasts are derived from granitic rock plutons on Cactus Flat and from Precam-

brian quartzite in Chicopee Canyon, (fig. 5.1) both of which are drained by Cushenberry Canyon. The fanglomerate is uniformly gray and is made up of cobble to boulder-size clasts having an average size of 10 cm. About 20 percent of the rock is sand, silt, clay, and caliche matrix. Rounding of the clasts is poor to good.

This unit probably overlaps in age parts of the fanglomerate and river-deposited material just described, even though it locally overlies some of the more indurated parts of that unit.

CARBONATE-CEMENTED FANGLOMERATE

Both the indurated alluvium unit and the fanglomerate of Cushenberry Canyon are unconformably overlain by a relatively thin well-indurated fanglomerate composed chiefly of clasts derived from the undivided rocks. This unit is distinguishable from the other fanglomerates because it is well indurated by carbonate cement and has a nearly uniform brown color. The degree of rounding and sorting of the clasts is about the same as in the other fanglomerates, as is the poor development of stratification.

OXIDIZED ALLUVIUM

Several generations of alluvial-fan material are preserved along the flanks of the range, the oldest of which is a series of fans that have oxidized surface material. Both the surface and upper meter or two of these fans is oxidized to a relatively vivid orange color that can be distinguished from that of all other fans on color aerial photographs. The color is also obvious on the ground, but not as obvious as might be expected from the contrast on the aerial photographs. The lower part of the fan material that is not so obviously oxidized is difficult to distinguish from other fan materials, and if places exist in the mapped area where the oxidized layer is removed, it is possible that parts of these older fans have been included in the younger fan units.

Clast size falls mainly in the boulder range with a matrix of cobbles, sand, and silt. At most places the ratio of boulders to matrix is estimated to be greater than 3:1. Boulders are as much as 5 m across and vary in degree of roundness from poor to good; most are poorly to moderately rounded. Bedding is obvious only where occasional lenses of cobbles or sand are present. The sediments are only slightly indurated.

All of the clast material in any particular fan comes from that part of the mountains directly upslope from that fan. Many of the fans, however, do not head in presently active canyons, but along a portion of the mountain front between the present canyon mouths. The fans are roughly coincident with broad eroded areas within the range that were probably source areas for the sediments but that

have subsequently been modified by later erosion leading to modern-day drainages. The streams from present-day canyons are dissecting all of the fans with oxidized surfaces.

TERRACE-FORMING ALLUVIUM

Thin veneers of alluvial material that were probably derived from sediments forming the oxidized fans are mapped separately, because they display well-developed surfaces at a distinctly lower level than the oxidized fan surfaces. The sediments that form this alluvial unit and their state of preservation are almost indistinguishable from the oxidized fans. However, although the surface of the terrace-forming alluvium is slightly oxidized, it is not nearly to the degree that the older oxidized fans are. Also, the deposits of this unit correlate better with present stream courses and in almost all cases flank and are cut by present-day stream channels.

MIXED ALLUVIUM AND COLLUVIUM

Large deposits of alluvium, most of which are younger than the units showing oxidation and older than recent alluvium, have been grouped into a single unit. This unit may include some of the oxidized alluvium and some recent alluvium, however, because of the difficulties in distinguishing alluvial units from one another at some places. Minor amounts of colluvium, some derived from older alluvial units, are also included.

This unit is generally finer grained than the other units, mainly because much of it is farther from the mountain front and because it is partially derived from erosion of older alluvial units. Boulder-sized clasts are less abundant than in all other units and, to a limited degree, are better rounded. The proportion of sand and cobbles is greater than in other units, although the range in size of all clasts is about the same, because the unit is so extensive and includes such a range of depositional environments.

On color aerial photographs this unit has a smooth textural surface and in places a streaked pale-orange color. This color may be in part oxidation of the surface, but in most places probably comes from the reworked oxidized material of the older oxidized alluvium. The surface of this unit is being eroded at some places and at others younger alluvium is being deposited on it.

GRAY ALLUVIAL FAN MATERIAL

Large plumes of gray alluvium form youthful fans at the mouths of many of the steeper major canyons along the entire length of the range. The heads of these fans are about at grade with, and at the same elevation as, the present stream channels. The overall geomorphic form

of the fans is in most cases well preserved, as is the rilled surface characteristic of young fans. Minor erosion is evident on some fans, and in some cases the distal end of a fan is being covered with modern alluvium from an active stream.

Most of the material that makes up these fans is very coarse, with a boulder to matrix ratio greater than 3:1. As might be expected, the degree of rounding of clasts is generally poor. All of the material is derived from the drainage area at the head of the fans. These fans may be debris flows, but on the basis of their geomorphic expression, they predate the debris flows east of Grapevine Canyon described below.

DEBRIS FLOWS

Three kilometers east of Grapevine Canyon, two debris flows flank a fault-elevated area of oxidized alluvium (fig. 5.2). The flows are made up of unsorted sediments ranging in size from silt to boulders over a meter in diameter. The deposit is generally nonindurated. Both flows head in existing canyons and appear to postdate local fault scarp development. Although dissection by streams exiting from the larger canyons is evident, the form of the flows is well preserved. The steep-fronted lobate ends of both flows show only minor degradation.

LANDSLIDE MATERIAL

All landslide material has been grouped into a single map unit. Shreve (1968) demonstrated that several generations of landslides are separated by periods of fan-glonerate accumulation in the Blackhawk Canyon area. The reader is referred to his treatment of the subject. A few small areas of landslide material are shown south of Rattlesnake Canyon. These are dissected and could be the remnants of much larger landslides farther back in the range. A moderately large slide is shown on the east side of Crystal Creek and is presently being dissected by that creek. The steep north face of the range and the highly brecciated rocks in places create conditions conducive to future landslides.

RECENT ALLUVIUM

Recent alluvium consists of silt to boulder-size alluvium deposited along modern stream channels. All of this material is derived locally, and some of it may be reworked from older alluvial deposits.

ARTIFICIAL FILL

The artificial fill shown on the map results from the mining of limestone and the road building related to that mining.

DESCRIPTION OF THE FAULT SYSTEM

The frontal fault system on the north side of the San Bernardino Mountains appears to be made up of numerous reverse fault segments which in subsurface may or may not form a single throughgoing fault. At places, especially on the east and west ends, the zone appears to be relatively simple, consisting of only one or two breaks that can be traced several kilometers. However, exposures are poor at the west end of the range, and the system may consist of a complex zone of multiple breaks there. At many places faults may exist farther back in the range, but they are difficult to recognize in the more heterogeneous crystalline units. Small discontinuous shear zones are common in these crystalline rocks more than a mile back from the range front. The aggregate movement distributed across these shear zones could make

up a significant proportion of the total offset across the zone.

Along the central two-thirds of the range front, the fault system consists of a complex zone that ranges from about 1 km to as much as 6 km in width. Most of the individual faults in this part of the zone are short and discontinuous, averaging no more than 2 to 4 km in length. A few of the scarps, interpreted on the strip map (pl. 5.1) as fault scarps, may or may not be of tectonic origin. Some short scarp segments are easily confused with the sharply defined distal scarps of debris flows which are present at several places along the range front (fig. 5.2).

At the relatively few localities where the dip of individual faults in the zone can be measured, it is in all cases toward the south, ranging from about 10° to as much as 70° ; the average dip is about 45° . The dip of individual breaks in one part of the system is not constant for very



FIGURE 5.2.—Scarp developed near distal end of alluvial fan about 3 km east of Grapevine Canyon; view is toward the south. Scarp is flanked on both sides by debris flows and may or may not be of tectonic origin. Degree of erosion appears to be about the same as that of scarps at west end of range (fig. 5.5). The aligned series of scarps near the head of the fans is developed along the high-angle fault shown in figure 5.4.

long distances along the strike and may be irregular down-dip as well. Half a kilometer east of One Hole Spring, a large fault belonging to the frontal system is well-exposed in a 25-m-high canyon wall and has a constant dip of about 55° S. (fig. 5.3). About 1 km to the west, however, the measured dip on what appears to be the same fault is 22° S. and 9 km to the east the dip is 10° S. No reliable attitudes have been measured on faults west of Grapevine Canyon. Across the strike of the system, dip measurements on individual faults show no systematic variations, although, in a gross sense, the straighter traces of faults closer to the range front suggest they may be steeper than those farther out.

The relatively straight west-northwest-trending fault segment 6 km east of Grapevine Canyon may or may not be part of the frontal system of faults. This fault, where exposed, is vertical and lies at the base of range-facing scarps in the fanglomerate and oxidized alluvium units (fig. 5.4). These scarps, however, may reflect only the latest movement on the fault (either strike slip or dip slip), as the fault, in general, has brought crystalline rock on the south against alluvium on the north. Numerous short west-northwest-trending fault segments in alluvial material 1-9 km west of the south end of the Helendale fault also form infacing scarps. Most of these range-facing scarps are bounded north and south by scarps facing the valley.

The direction of movement distributed across the system as a whole is up on the south. At many places along the range front, crystalline rocks are thrust northward

over unconsolidated to poorly consolidated alluvial units of different ages. Because of the parallelism between the San Andreas fault and many of the short straight segments, there may be a small component of strike-slip along the zone as a whole. The strike-slip component could not be great, however, because clasts of several distinctive rock types, for example, the Rattlesnake pluton, are found in the older alluvial and fanglomerate units directly downslope from the source areas in the mountains. Such clasts were not identified in gravels below streams not presently draining areas underlain by the Rattlesnake pluton. The same holds true for the easternmost Paleozoic carbonate rocks near Arrastre Canyon. There may or may not be strike-slip movement along the frontal system east of where the Old Woman Springs fault intersects the range front.

No evidence was found to allow estimates of total displacement across the zone. Individual scarps in alluvium are as high as 60 m, and the aggregate height of the three scarps developed on the fan west of Rattlesnake Canyon



FIGURE 5.3.—View east of canyon wall $\frac{1}{2}$ km east of One Hole Spring. Gneissic rock on right is faulted over more easily eroded Old Woman Sandstone. The two units are separated by about 50 m of gouge (between dashed lines) and breccia that dips 55° S. (right). Largest boulders in lower left corner of photo are residual lag from erosion of a relatively young north-facing scarp.



FIGURE 5.4.—Range-facing scarps developed along a vertical fault 6 km east of Grapevine Canyon. This fault is probably not part of the frontal fault system. View is to the west.

is about 80 m. The longest fault segment in this part of the zone, along which an unknown amount of movement has occurred, is at the head of that fan.

If the entire height of the range is attributable to the frontal fault system, then at least 450 m of uplift has occurred at the west end, at least 1,200 m in the central part, and at least 600 m at the east end. It is unlikely that 450 m of uplift has occurred along the single strand in the oxidized alluvium at the west end of the range, because the total thickness of the alluvial unit is probably not that great. At least some of the uplift presumably occurred along the distributed shears in the crystalline rock, or occurred prior to deposition of the oxidized alluvium.

The youthful scarps developed in several of the alluvial units indicate that at least the latest faulting is relatively young (fig. 5.5). No scarps are preserved in the recent alluvium, but this is not conclusive evidence that older parts of this unit are not cut by faults. Any scarps developed in recent alluvium in present-day stream channels could not survive many of the periodic torrential floods that occur this close to such a steep mountain front. The fault shown as a solid line in the recent alluvium at the mouth of Cushenberry Canyon (pl. 5.1) is actually a preexisting scarp mostly covered by a thin veneer of ponded alluvium; the fault does not cut the alluvium as

might be interpreted from the map.

The gray alluvium may or may not be cut by faults of the frontal system. Where faults are shown as solid lines bounding areas of gray alluvium on plate 5.1, the faults are actually pregray alluvium scarps that have acted as topographic barriers in the ponding of alluvium. In the area just west of Blackhawk Canyon, a fault scarp appears to have developed in the gray alluvium, although even there the relationships are not clear enough to rule out the possibility that the scarp predates ponding of alluvium. In addition, this fault is not part of the system of range-front reverse faults, as it dips steeply to the northeast, and may be the southeasternmost expression of one of the northwest-striking Mojave Desert faults. The infacing scarps shown as solid lines on plate 5.1 north of Furnace Canyon have clearly ponded the gray alluvium.

The faults of the frontal system cut all of the older alluvial units and many of the crystalline rock units. The time the faulting began is not clear, but most of the uplift appears to have taken place before deposition of the gray alluvium. That unit, in fact, may have resulted in part from a period of rapid uplift and subsequent deposition due to erosion of oversteepened source areas.

Stout (1975) reported a ^{14}C age of $17,400 \pm 500$ yr B.P. for fresh-water mollusk shells from calcareous mudstone deposited in a closed depression on the morphologically youthful surface of the Blackhawk landslide (upper part only mapped near Blackhawk Canyon, pl. 5.1). Although an earthquake along the frontal fault system would be a plausible initiating mechanism for the slide, the relations of the slide and the fault system are not clear. No strands of the fault system are known to cut the landslide, but since the main part of the slide is north of the fault system, the system could have been active since the slide occurred.

No fossils or other age data are available for any of the alluvial units. The youngest dated rock is the basalt collected near the Old Woman Springs fault about 1 km northwest of the mapped area shown on plate 5.1, which gave a K-Ar whole-rock age of 6.2 m.y. B.P. If the fault at Old Woman Springs ever extended south of the frontal fault system, the evidence has been completely removed by erosion. Basalt from isolated localities within the San Bernardino Mountains has been dated, but these flows, one at an elevation of 2,460 m, are consistently older than the Old Woman Springs sample by more than a million years (Janet Morton, unpub. K-Ar whole-rock data, 1979).

The relatively youthful appearance of many scarps in the older alluvial units suggests that faulting continued until fairly recent times and that the system may still be active. The youngest, least-eroded scarps generally appear to be those farthest from the range, and those most eroded are near the range front. This difference in erosion may be due to an outward migration of fault activity or to the fact that the slopes closer to the range front are



FIGURE 5.5.—Youthful scarps developed in alluvial units. Scarps such as these suggest that the frontal fault system may still be active. Photo shows a north-south segment of fault at west end of area shown on plate 5.1. View toward the south. Note gently sloping accordant surface developed in much of range, and the relatively even, unmodified crest of the mountains.

steeper and, therefore, more susceptible to erosion. The apparent outward migration of fault activity, if real, may be due to a migration of the actual locus of activity or may be due to the migration of all crustal rocks east of the San Andreas fault over a stationary locus that is responsible for fault activity and is coincident with the position of the western Transverse Ranges.

The northwest-trending Helendale and Old Woman Springs faults intersect the range front, but do not appear to extend into the rocks south of the frontal fault system other than to cause minor brecciation. About 40 km northwest of its intersection with the range front, apparent displacement on the Helendale fault is about 6 km right lateral, as indicated by an offset quartz monzonite pluton (Miller and Morton, 1980). Dibblee (1964a) shows the fault entering the San Bernardino Mountains at Cushenberry Canyon and continuing southeast at least another 14 km, beyond which its identity becomes confused with other northwest-trending faults. Recent mapping by the author on and around Cactus Flat, about 5 km into the range, indicates that even though some of the rock is brecciated along the southeastward projection, there is virtually no offset of several plutonic and metamorphic features that cross this zone of brecciated rock.

Movement along the Helendale fault, although reflected in the rocks of the upper plate south of the frontal fault system, is confined almost entirely to the Mojave block north of the frontal faults. Offset along the Helendale may continue beneath the San Bernardino Mountains, but is confined to the block beneath the south-dipping frontal faults. The brecciation, but lack of offset, along the projection of the strike-slip faults in the rocks in the upper plate presumably is caused by movements in the lower plate.

The Old Woman Springs fault does not appear to penetrate the upper plate of the range-front fault system but intersects the reverse faults at a much more acute angle than does the Helendale fault. A slight bend in the reverse fault system at the range front near the intersection makes the two fault systems almost parallel. Because both fault zones are complex and are made up of more than one strand in this area, at several places they are difficult to distinguish from one another. The Old Woman Springs fault intersects the frontal system about 4 km east of Rattlesnake Canyon, at which point the high-angle strike-slip fault is distinct from the moderate-angle reverse fault. The Old Woman Springs fault appears to end at, or go under the upper plate of, the frontal system, but about 2 km to the southeast it re-emerges for about half a kilometer. Past that point, it appears that the strike-slip fault either ends at, merges with, or is overthrust by the frontal system; the latter interpretation is preferred.

No evidence for the magnitude of displacement across the Old Woman Springs fault in the Mojave Desert is

available, nor is there any for the Lenwood fault, with which the Old Woman Springs fault merges 25 km to the northwest. The southernmost expression of the Lenwood fault may be represented by the straight side of a low hill about 1½ km northeast of where the Old Woman Springs fault intersects the range front faults (pl. 5.1). The projection of this probable fault intersects the range front about 1 or 2 km east of where the Old Woman Springs fault emerges from beneath the reverse system. There is no indication of the Lenwood fault anywhere near this projected system in either the upper or lower plate of the range front fault system.

REFERENCES CITED

- Dibblee, T. W., 1964a, Geologic map of the Lucerne Valley quadrangle, San Bernardino County, California: U.S. Geological Survey Miscellaneous Geologic Investigations Map I-426, scale 1:62,500.
- , 1964b, Geologic map of the San Gorgonio Mountain quadrangle, San Bernardino and Riverside Counties, California: U.S. Geological Survey Miscellaneous Geologic Investigations Map I-431, scale 1:62,500.
- , 1967, Geologic map of the Old Woman Springs quadrangle, San Bernardino County, California: U.S. Geological Survey Miscellaneous Geologic Investigations Map I-518, scale 1:62,500.
- , 1968, Geologic map of the Lake Arrowhead quadrangle, San Bernardino County, California: U.S. Geological Survey Open-File Map, scale 1:62,500.
- Guillou, R. B., 1953, Geology of the Johnston Grade area, San Bernardino County, California: California Division of Mines Special Report 31, 18 p.
- MacColl, R. S., 1964, Geochemical and structural studies in the batholith rocks of southern California: Part 1, Structural geology of Rattlesnake Mountain pluton: Geological Society of America Bulletin, v. 75, p. 805-822.
- May, S. R., and Repenning, C. S., 1982, New evidence for the age of the Old Woman Sandstone, Mojave Desert, California: Geological Society of America 78th Annual Meeting, Cordilleran Section Field Trip Guidebook, p. 93-96.
- Miller, C. F., 1976, Alkali rich monzonites, southern and central California—A unique magmatic episode?: Geological Society of America Abstracts with Programs, v. 8, no. 3, p. 395.
- Miller, F. K., and Morton, D. M., 1980, Potassium-argon geochronology of the eastern Transverse Ranges and southern Mojave Desert, southern California: U.S. Geological Survey Professional Paper 1152, 30 p.
- Richmond, J. F., 1960, Geology of the San Bernardino Mountains north of Big Bear Lake, California: California Division of Mines Special Report 65, 65 p.
- Shreve, R. L., 1968, The Blackhawk landslide: Geological Society of America Special Paper 108, 47 p.
- Silver, L. T., 1971, Problems of crystalline rocks of the Transverse Ranges: Geological Society of America Abstracts with Programs, v. 3, no. 2, p. 193-194.
- Stewart, J. H., and Poole, F. G., 1975, Extension of the Cordilleran miogeosynclinal belt to the San Andreas fault, southern California: Geological Society of America Bulletin, v. 86, p. 205-212.
- Stout, M. L., 1975, Age of the Blackhawk landslide, southern California: Geological Society of America Abstracts with Programs, v. 7, no. 3, p. 378.
- Vaughan, F. W., 1922, Geology of the San Bernardino Mountains north of San Gorgonio Pass: University of California Publications in Geological Sciences, Berkeley, California, v. 13, p. 319-411.

6. TECTONIC IMPLICATIONS OF SMALL EARTHQUAKES IN THE CENTRAL TRANSVERSE RANGES

By JAMES C. PECHMANN¹

ABSTRACT

Fault-plane solutions for 22 small (local magnitude (M_L) ≤ 4.6) earthquakes in the central Transverse Ranges were determined using an azimuthally varying crustal model. The dominant type of faulting observed is reverse faulting on east-striking planes, which suggests a regional stress field characterized by north-south compression. Some strike-slip faulting also occurs. There is some indication that strike-slip earthquakes may be more common than reverse-slip earthquakes during episodes of crustal dilatation. The rate of north-south crustal shortening attributable to small-earthquake deformation during 1974–76 is two orders of magnitude smaller than the north-south contraction of 0.3 parts per million per year measured at the surface. The scatter in earthquake hypocenters and the general inconsistency of focal mechanisms with geologically determined motions on nearby major faults indicate that the small earthquakes in this region are not associated with large-scale block movements along major fault systems. Rather, they appear to represent fracturing along random minor zones of weakness in response to the regional stress field or, alternatively, small-scale block movements that are below the resolution of this study. Earthquakes in the San Gabriel Mountains north of the Santa Susana-Sierra Madre-Cucamonga frontal fault system tend to concentrate near the eastern and western ends of the range, where good evidence for late Quaternary movement along the frontal faults has been found. Seismicity is markedly lower north of the central section of the frontal fault system, where evidence for late Quaternary movement is lacking.

INTRODUCTION

The Transverse Ranges province of southern California is a complex east-trending geomorphic and structural unit that interrupts the northwest-trending tectonic grain of the Pacific-North American plate boundary (Bailey and Jahns, 1954; Jahns, 1973). In this region the San Andreas fault turns sharply from its general southeast orientation to strike east-southeastward across the Transverse Ranges before splintering into several major branches and continuing southeastward to the Gulf of California (Allen, 1968). South of this San Andreas “big bend” is a broad zone of roughly east-trending, north-dipping thrust and reverse faults including the Santa Monica, Santa Susana, Sierra Madre, and Cucamonga frontal fault systems (fig. 6.1), along which mountain blocks of the central and

western Transverse Ranges have been thrust upward and southward.

Interest in the tectonics of the central Transverse Ranges has increased since 1970 because of several developments, notably the following five: (1) The documentation of right-lateral shear-strain accumulation along the locked “big bend” segment of the San Andreas fault (Prescott and Savage, 1976; Savage and others, 1981a, b) contemporaneous with at least partial strain release along the fault system to the northwest and southeast by creep and moderate earthquakes (Allen, 1968, 1982; Harsh and others, 1978; Burford and Harsh, 1980). (2) The occurrence of the 1971 San Fernando earthquake (local magnitude (M_L) = 6.4) along the western end of the Sierra Madre fault system (U.S. Geological Survey, 1971; Murphy, 1973; Oakeshott, 1975). (3) The reported formation between 1959 and 1974 of a vertical crustal uplift throughout most of the Transverse Ranges province (Castle and others, 1976). Leveling data indicate that this uplift, the so-called Palmdale bulge, reached a maximum of 35 cm within the study area (fig. 6.1) and then partially subsided between mid-1974 and mid-1976 (Bennet, 1977; Mark and others, 1981). However, serious questions have been raised regarding the accuracy of the leveling data which define the uplift (Jackson and Lee, 1979; Strange, 1981), and the Palmdale bulge is currently a matter of great controversy (Kerr, 1981). (4) The occurrence from 1976 to 1977 of an earthquake swarm along the locked section of the San Andreas fault (fig. 6.1). This swarm was the first observed along this section of the San Andreas since cataloging of instrumental data began in 1932 (McNally and others, 1978). (5) Abrupt changes in the horizontal strain accumulation patterns in southern California that were detected in 1978 and 1979. The measured changes were particularly large on geodetic networks in the Transverse Ranges (Savage and others, 1981a, b).

Vastly improved data on earthquakes in southern California have become available through the increase in the number of stations in the California Institute of Technology/U.S. Geological Survey seismographic network from 39 stations in 1972 to nearly 150 stations in 1978 (Whitcomb, 1978) to over 200 stations in 1983.

¹Seismological Laboratory, California Institute of Technology, Pasadena, California 91125; present address: Department of Geology and Geophysics, University of Utah, Salt Lake City, Utah 84112.

Studies of southern California crustal structure using the expanded array (Kanamori and Hadley, 1975; Hadley and Kanamori, 1977; Hadley, 1978) have made possible more accurate interpretations of the earthquake data. Previous studies of earthquakes in the central Transverse Ranges have dealt primarily with the San Fernando earthquake and its aftershocks (Whitcomb and others, 1973; Hadley and Kanamori, 1978) and with microearthquake data from small temporary arrays (Hadley and Combs, 1974; Murdock, 1979; Cramer and Harrington, this volume).

The purpose of this report is to present seismicity and focal-mechanism data for the entire central Transverse Ranges area and to discuss their tectonic significance in terms of the geologic evidence concerning long-term deformation and also in terms of the available geodetic evidence pertaining to short-term deformation. The first three sections present a regional study of seismicity and focal mechanisms completed in January 1979. The following section summarizes some results of a later study by Sauber and others (1983), which suggest that changes in

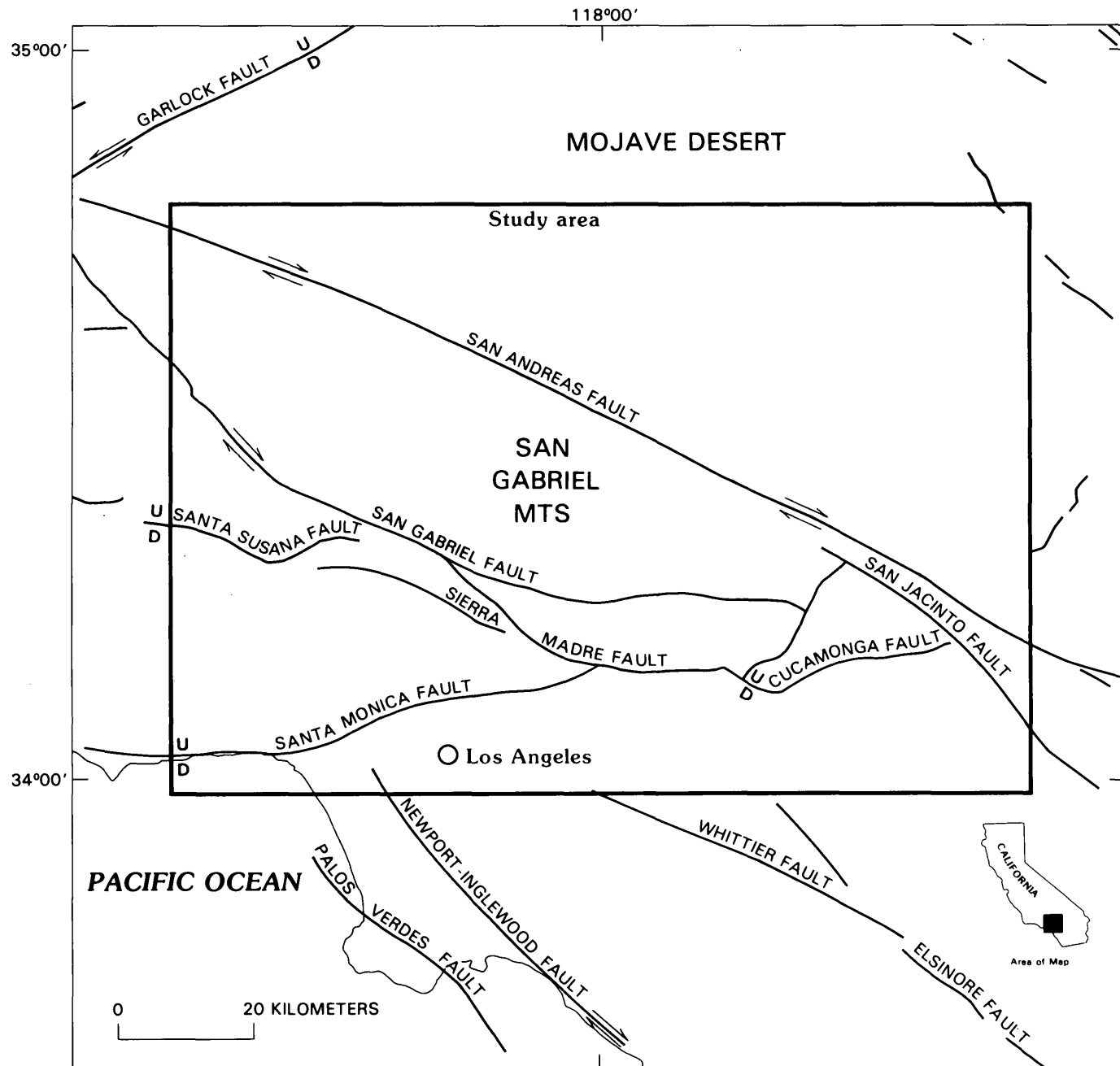


FIGURE 6.1.—Locations and senses of motion of major fault systems within the central Transverse Ranges, generalized from Jennings and others (1975). Arrows show relative horizontal (strike-slip) movement. U and D indicate upthrown and downthrown sides of dip-slip faults.

the regional strain accumulation pattern that took place in late 1978-79 triggered changes in focal mechanisms and in the level of small earthquake activity near Palmdale. These two studies suggest a model for the relationship of small earthquakes in the central Transverse Ranges to strain accumulation on the San Andreas and frontal fault systems that is outlined in the concluding section.

ACKNOWLEDGMENTS

I would like to thank Clarence Allen for suggesting this research and providing encouragement and advice. Dave Hadley, Carl Johnson, and Jim Whitcomb supplied computer programs and many helpful suggestions. Discussions with Karen McNally, Bernard Minster, John Cipar, Hiroo Kanamori, Tracy Johnson, and many others at the California Institute of Technology Seismological Laboratory were also of great benefit. This research was supported in part by the United States Geological Survey, Contract No. 14-08-0001-15258, and by the NASA Office of Applications Grant #NSG5224. This report is Contribution Number 3198, Division of Geological and Planetary Sciences, California Institute of Technology, Pasadena, California 91125.

SEISMICITY, 1933-1977

Epicenter locations are shown in figures 6.2 and 6.3 for all earthquakes located by the California Institute of Technology (Caltech) between 1933 and 1977 within the study area shown in figure 6.1. Faults shown in figure 6.1 are generalized from Jennings and others (1975). Epicenters and magnitudes are taken directly from the Caltech/U.S. Geological Survey southern California earthquake catalog (Hileman and others, 1973; Friedman and others, 1976; Whitcomb and others, 1978). Since location techniques and the density of seismographic stations have changed greatly through the years, these maps must be interpreted with care. Prior to 1961 epicentral determinations were done graphically and reported to the nearest minute. This explains the tendency of epicenters to line up in north-south and east-west directions on the earlier maps. Because the preliminary 1977 catalog was used, hypocentral locations for 1977 are subject to slight modification, quarry blasts have not been removed, and magnitude determinations for the smaller events are incomplete. Quarry locations are indicated by a "Q" in figure 6.3. Earthquakes in 1977 for which magnitudes had not yet been determined are plotted as having $M_L \leq 2$ in figure 6.3 but may lie in the range $2 < M_L \leq 3$.

Examination of figure 6.3 shows that despite a much-improved detection capability and greater location accuracy, the epicenters still do not show much tendency

to cluster near the surface traces of faults. The only exceptions are along the San Jacinto fault and along a northeast-trending feature south of the Cucamonga fault previously identified by Hadley and Combs (1974) on the basis of a microearthquake survey. Hadley and Combs actually found two northeast-trending clusters 5 km apart in this area, the northern one being coincident with the Fontana water barrier. Several aftershock sequences and localized swarms show up very well on the seismicity maps in figures 6.2 and 6.3. The San Fernando aftershock zone is a prominent feature north of the Sierra Madre fault system in the western half of both the 1971-73 and 1974-77 maps. The 1972 Ontario swarm shows up very clearly as a dense cluster near the southeastern corner of the 1971-73 map. The epicenters in figure 6.3 near the western end of the surface trace of the Santa Susana fault are mostly aftershocks from a magnitude 4.6 event on April 8, 1976. This event is noteworthy because of its large number of aftershocks and its unusually great depth of 18 km. The 1976-77 swarm just to the south of the San Andreas fault in the center of figure 6.3 has been studied by McNally and others (1978). The subsequent increase in seismicity here and to the northwest along the San Andreas fault has been shown to be real. However, it is not clear whether the apparent increase in seismicity after 1973 in the Mojave Desert to the northeast of the San Andreas fault (compare figs. 6.2 and 6.3) is real or merely an artifact of improved station coverage.

The scatter in the epicenters of $M_L < 6.0$ shocks in southern California and the general lack of clear spatial relationships between these shocks and recognized faults have often been noted (Richter, 1958; Allen and others, 1965). Important exceptions to the rule are the concentrations of seismicity to the southeast of the study area associated with the Imperial, Brawley, and San Jacinto faults (Friedman and others, 1976; Whitcomb and others, 1978). All of these faults are dominantly strike-slip faults which are known to be creeping (Johnson and Hadley, 1976; Goult and others, 1978; Keller and others, 1978). Although the San Jacinto fault and its zone of seismicity extends into the southeastern corner of the study area (figs. 6.1 and 6.3), creep has not been demonstrated along this segment of the San Jacinto but only along sections to the southeast. The general scattering of epicenters throughout most of the central Transverse Ranges is perhaps not surprising, given the large number of Quaternary dip-slip faults in the area, most of which are either known or presumed to be of shallow dip (Jennings and others, 1975). Although most recent (post-1974) determinations of epicentral locations are probably accurate to within 2-3 km in this area, comparable accuracy in the hypocentral depth is difficult to obtain. The available data are of sufficient quality to rule out a concentration of hypocenters along a single great megathrust cropping out

along the frontal fault system and dipping northward beneath the mountains. However, careful relocations using a master-event technique may in the future serve to delineate and characterize a series of separate faults, as has been done for the western Transverse Ranges (Lee and others, 1979).

A noteworthy feature of the 1974–77 seismicity map (fig. 6.3) is that in the mountains north of the Santa Susana-Sierra Madre-Cucamonga frontal fault systems most of the seismicity is concentrated to the west and to

the east, with comparatively few epicenters located in the central part of the San Gabriel mountains between the eastern Sierra Madre and San Andreas fault zones. This same pattern has been present at least since 1961, when computer location of earthquakes began at Caltech (fig. 6.2). Relocation of selected earthquakes before 1961 using arrival times on file at Caltech has shown that additional work is necessary in order to extend this analysis farther back in time. Available geologic evidence concerning the long-term seismicity correlates well with these observa-

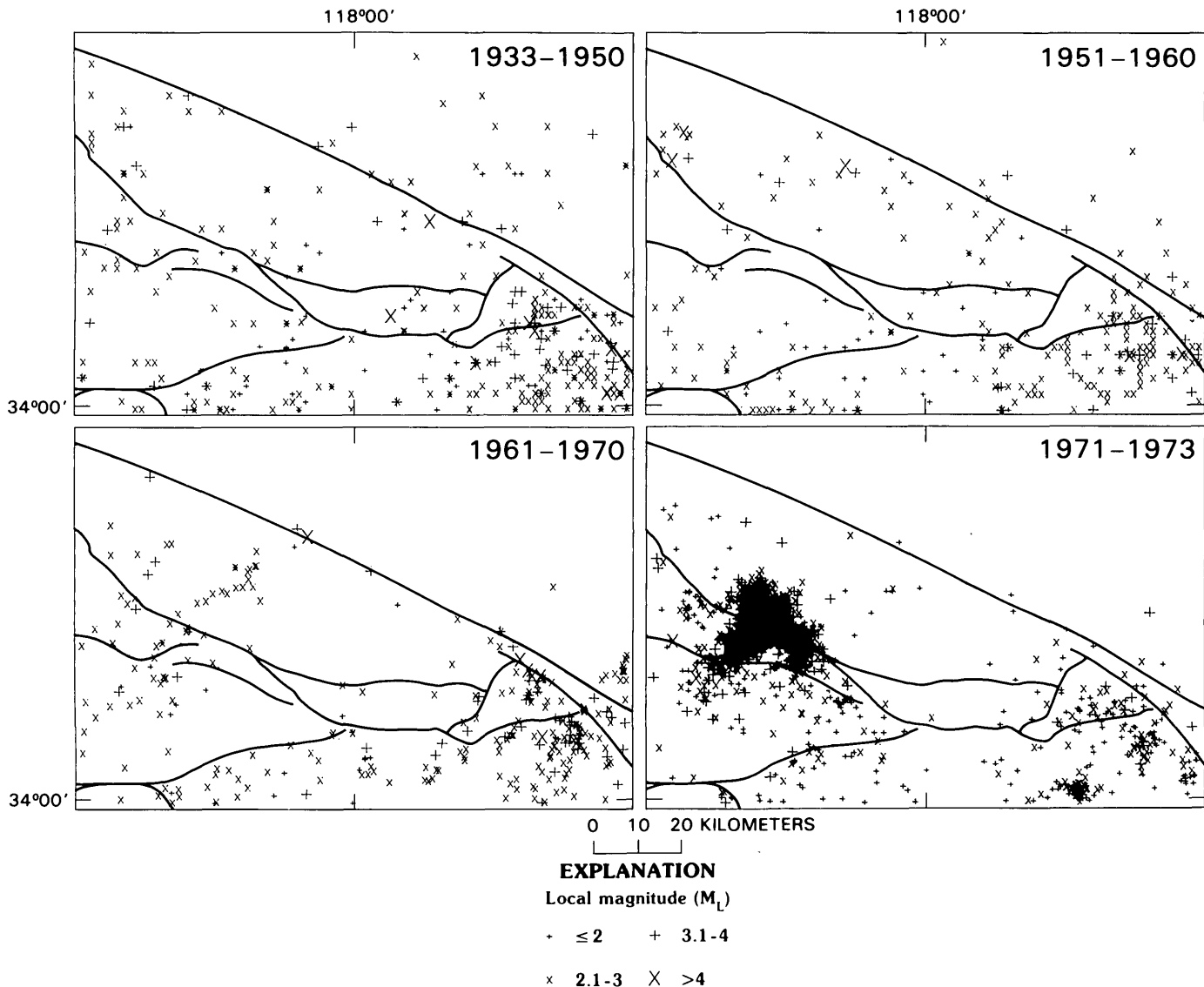


FIGURE 6.2.—Epicenters of all earthquakes located by the California Institute of Technology within the study area for various time intervals. Different symbols indicate local magnitude (M_L) as shown. See figure 6.1 for fault names.

tions. Crook and others (this volume) have found that evidence for late Quaternary movement is lacking in the central part of the San Gabriel frontal fault system south of this gap but is present to the east and to the west. Since geodolite measurements by Savage and others (1978; 1981a, b) indicate that the post-Miocene north-south

crustal shortening of the Transverse Ranges (Jahns, 1973) is still occurring, it appears that within the central San Gabriel mountains this deformation must at present be taking place aseismically. This may mean that the deformation here is taking place at a greater depth than elsewhere.

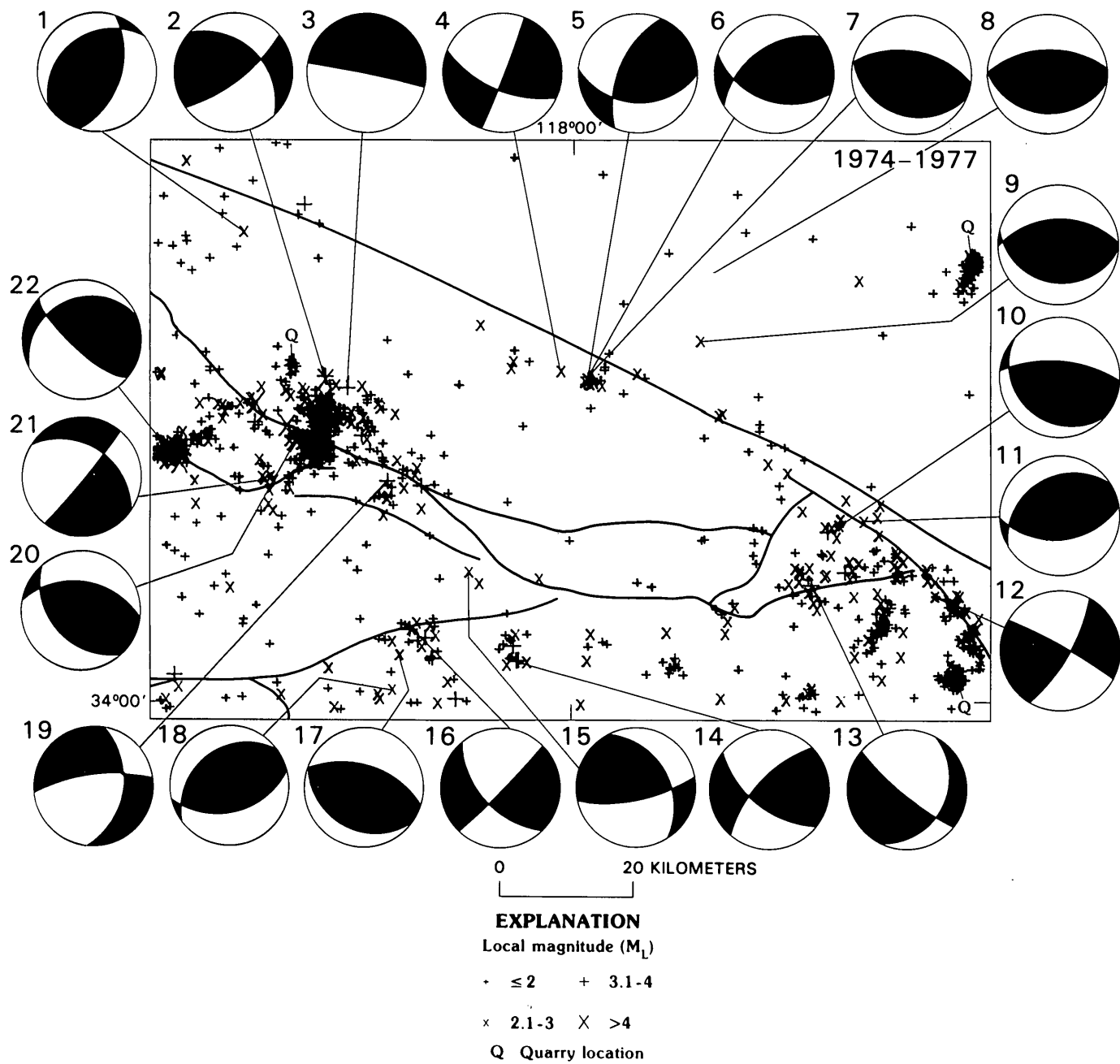


FIGURE 6.3.—Locations of focal mechanisms of figure 6.5 and epicenters of all earthquakes located by the California Institute of Technology within the study area for the time interval 1974–77. Shaded quadrants are compressional. See figure 6.1 for fault names.

TABLE 6.1.—*Events selected for regional focal mechanism study*

[For locations and fault-plane solutions of events, see figs. 6.3 and 6.5, respectively]

Event	Date (mo/d/yr)	Origin time (G.m.t.)	M_L	Caltech catalog location			Revised depth ¹ (km)
				Lat (N)	Long (W)	Depth (km)	
1	11/07/76	1421	2.6	34° 40.20'	118° 33.10'	8.0	7.5
2	12/08/76	0213	3.3	34° 28.13'	118° 24.52'	12.4	13.3
3	10/17/76	0538	3.9	34° 27.16'	118° 22.26'	14.9	11.2
4	12/13/76	0826	2.2	34° 28.56'	118° 0.60'	5.9	8.2
5	01/01/77	0100	2.8	34° 27.49'	117° 57.69'	5.4	8.7
6	03/07/77	1104	3.0	34° 27.68'	117° 58.18'	8.0	9.1
7	09/06/77	0508	3.0	34° 27.95'	117° 57.93'	7.2	8.7
8	06/19/78	0741	3.0	34° 37.07'	117° 45.02'	6.7	7.6
9	11/03/76	1741	2.6	34° 31.11'	117° 46.40'	8.0	10.1
10	12/30/76	0225	2.6	34° 15.64'	117° 32.37'	5.0	10.2
11	05/29/76	2038	3.0	34° 15.93'	117° 29.86'	4.7	13.3
12	11/05/75	0237	3.0	34° 9.66'	117° 22.70'	7.2	8.0
13	01/13/75	2328	3.3	34° 10.64'	117° 35.16'	3.6	8.0
14	12/19/74	1236	3.5	34° 4.38'	118° 4.80'	9.2	6.4
15	11/06/74	0038	3.0	34° 11.71'	118° 9.96'	1.0	3.4
16	03/15/77	0801	2.2	34° 6.94'	118° 15.73'	8.8	10.1
17	11/30/76	2355	2.5	34° 4.76'	118° 16.93'	8.0	8.0
18	06/27/76	2211	2.9	34° 1.86'	118° 17.67'	10.4	8.0
19	12/27/75	2108	3.1	34° 19.37'	118° 18.14'	2.1	4.7
20	08/12/77	0219	4.5	34° 22.78'	118° 27.52'	9.5	10.1
21	08/09/76	1054	2.8	34° 19.62'	118° 30.97'	8.0	0.4
22	04/08/76	1521	4.6	34° 20.81'	118° 39.34'	14.5	17.9

¹The changes in epicentral (horizontal) locations averaged 2.2 km and in all cases were less than 6 km.

FOCAL-MECHANISM DETERMINATIONS

In determining focal mechanisms of local earthquakes from P -wave first-motion diagrams, the principal uncertainty is calculating the takeoff angles for first-arrival ray paths. These angles are highly dependent upon the assumed crustal structure and hypocentral depth. For this study a four-layer crustal model based on the work of Hadley and Kanamori (1977) and Hadley (1978) was used. The model consists of a 5-km-thick surface layer (5.5 km/s) underlain successively by upper crust, (6.1–6.3 km/s), lower crust, (6.6–6.8 km/s), and an upper-mantle halfspace (7.8 km/s) beginning at a depth of 33 km (inset, fig. 6.4). The interface between the low-velocity upper crust and the high-velocity lower crust, the Conrad discontinuity, is located at a depth of about 15 km in the central part of the study area. To the northeast in the Mojave Desert this discontinuity is much deeper, only about 5 km above the Mohorovičić discontinuity (Moho), but in the southwest corner of the study area in the Santa Monica Mountains it shallows to a depth of perhaps 10 km. Although in general the Conrad discontinuity appears to dip to the northeast in the central Transverse Ranges, the details of its geometry are poorly known. This creates particular problems in locating earthquakes and determining focal mechanisms, especially since in some areas the discontinuity is located within the seismic zone, which here extends to a depth of about 15 km. One approach to this problem is to employ a model consisting of many horizon-

tal layers, so that the Conrad discontinuity can be smoothed out into a gradient over a depth of 10 km. This technique was used by Hadley and Kanamori (1978). The advantage of this technique is that it reduces the sensitivity of the focal mechanism to changes in the depth of the source. In this study a different, and hopefully more accurate, method is used.

Events for the regional focal-mechanism study were chosen more or less at random, although some attempt was made to obtain a representative geographical distribution within the study area. Twenty-two events ranging in magnitude from 2.2 to 4.6 were selected for study from the time period 1974 to 1978 (table 6.1). To determine the focal mechanisms, arrival times and first motions were first read from 16-mm Developocorder film viewed at a scale of 1 cm/s. These data were supplemented in many cases by readings from Helicorder paper records, films from temporary trailer stations, and computer-stored seismographic traces from the Caltech Earthquake Detection and Recording (CEDAR) system (Johnson, 1979). The 22 earthquakes were then relocated using the computer program HYPO71 (Lee and Lahr, 1975) and a horizontally layered version of the model shown in figure 6.1. Only stations within 60 km of the epicenter were used in order to maximize the depth resolution and minimize the use of arrival times from the dipping Conrad discontinuity, placed at a depth of 15 km in the location model. The average number of stations used for each relocation was 12. Reduced traveltimes, $T - \Delta/6.0$, was then plotted

against distance, Δ , for various azimuth ranges. An interpretation of each plot was made in terms of the Hadley-Kanamori model, and then traveltime information was used to assign takeoff angles individually for each station. An example of this method is shown in figure 6.4 for event number 20 (table 6.1), a local magnitude 4.5 event that occurred on August 12, 1977, at a depth of about 10 km. The reduced-travelttime plots for azimuth ranges I and IV clearly show two branches. Arrivals labelled P_g are interpreted as direct waves with an apparent velocity near 6.2 km/s beyond about $\Delta = 50$ km. The branch labelled

P_n corresponds to critically refracted waves from the Moho with an apparent velocity of about 7.8 km/s. Refracted waves from the lower crust called P^* are not observed as first arrivals in regions I and IV because the Conrad discontinuity deepens too quickly in these directions. However, to the south of the source in region III, where the Conrad discontinuity shallows, the reduced traveltimes show an apparent velocity close to 6.6 km/s, indicating that all of the arrivals in this azimuth range are probably P^* . The reduced-travelttime plot for azimuth range II, which is roughly along the strike of the Conrad

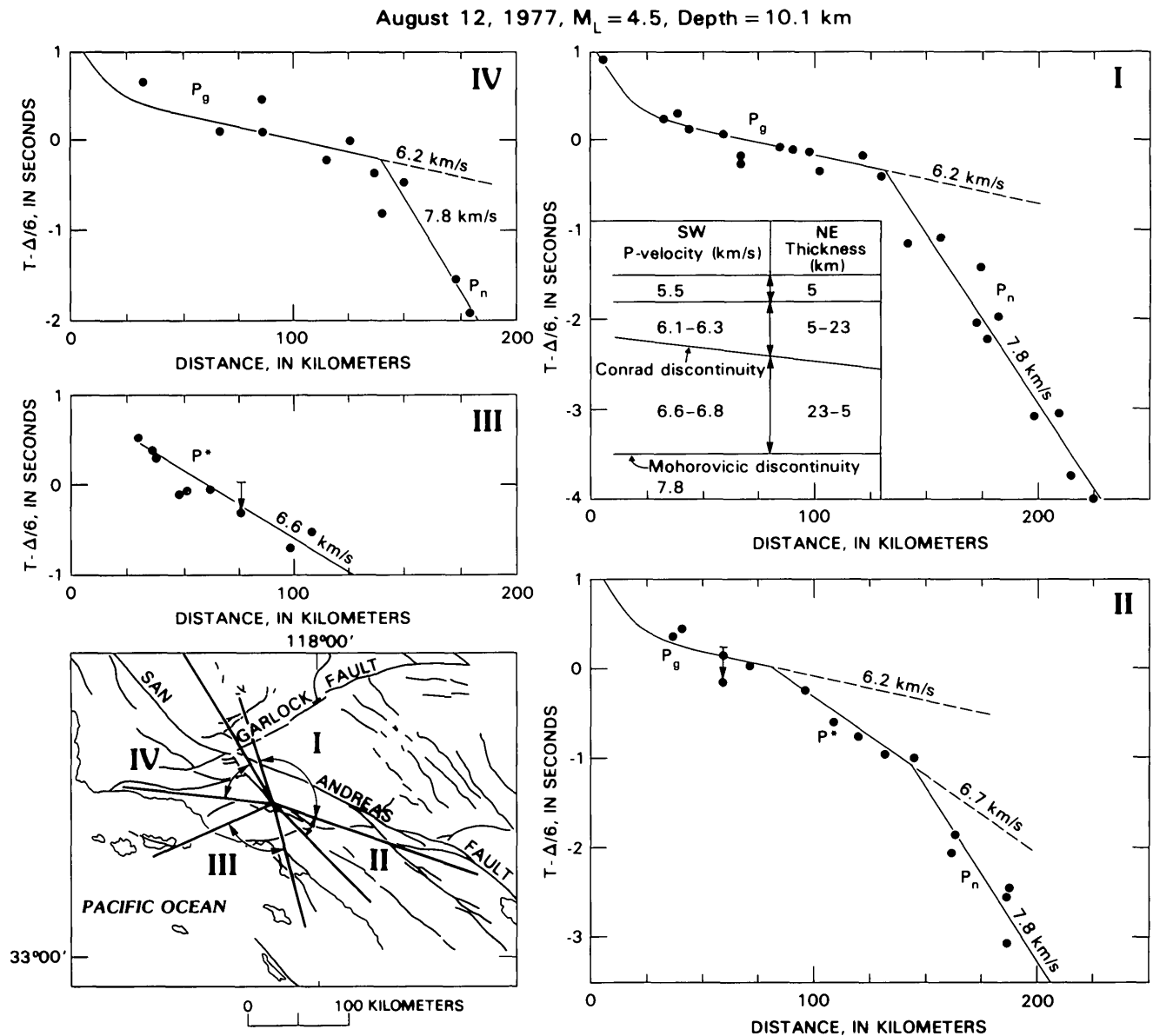


FIGURE 6.4.—Plots of reduced travelttime, $T - \Delta/6$, versus distance, Δ , for event number 20 (table 6.1) for the four azimuth ranges shown in the map at lower left. Vertical arrows above some points show deep-sediment corrections determined by Raikes (1978). P_g , P^* , and P_n

identify different seismic arrivals discussed in the text. Inset shows the velocity model used to interpret the plots (Hadley and Kanamori, 1977; Hadley, 1978). Dip on the Conrad discontinuity is exaggerated.

RECENT REVERSE FAULTING IN THE TRANSVERSE RANGES, CALIFORNIA

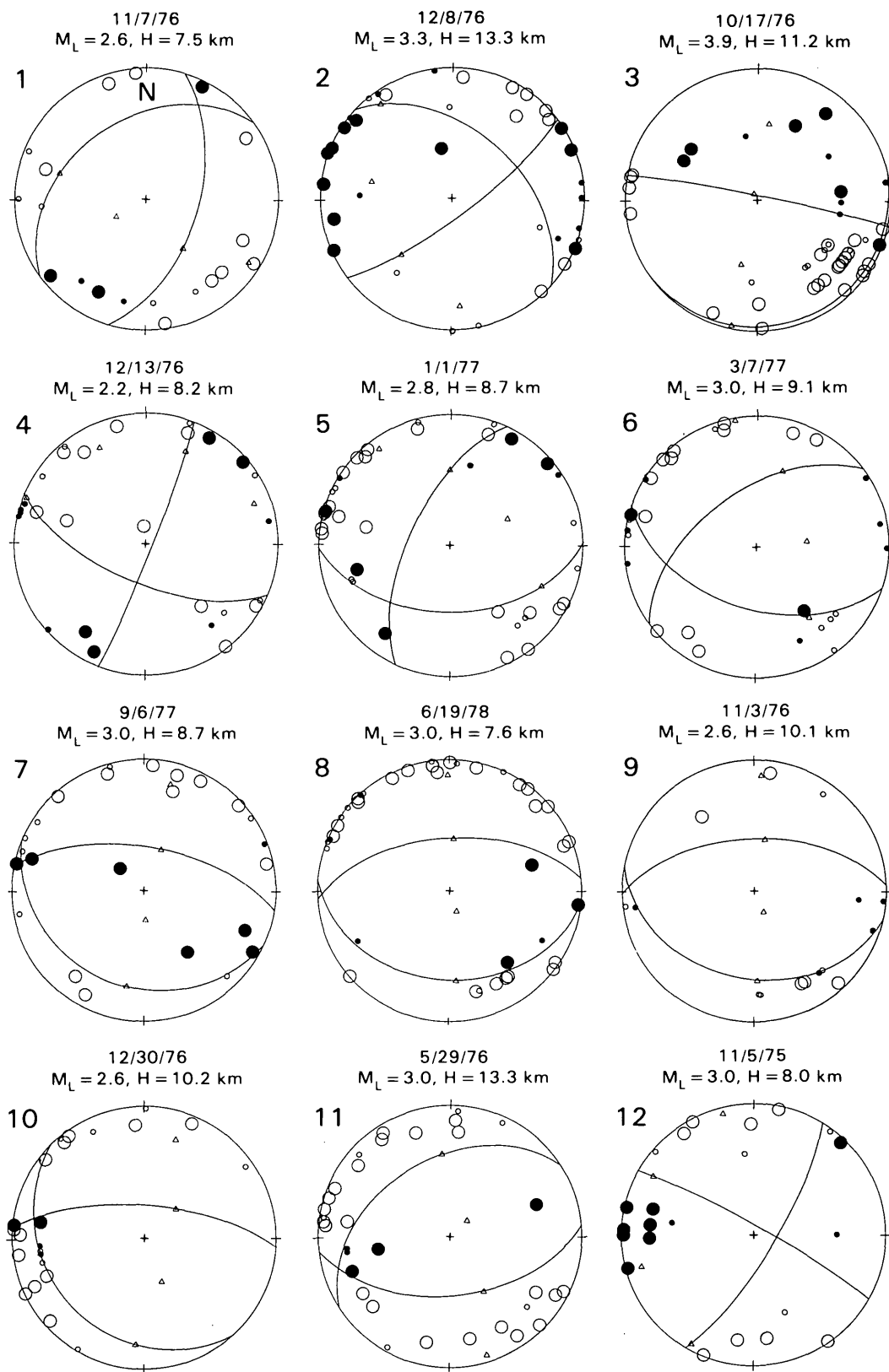


FIGURE 6.5.—Lower hemisphere P -wave fault-plane solutions for 22 events in the central Transverse Ranges. Dots indicate compressional first motions; circles indicate dilatational first motions. Good-quality readings of first motions shown by large symbols; fair-quality readings by small symbols. Slip vectors, compression axes, and tension axes are shown with triangles. The date, local magnitude (M_L) and depth (H) are given for each event. Event numbers correspond to those in figure 6.3.

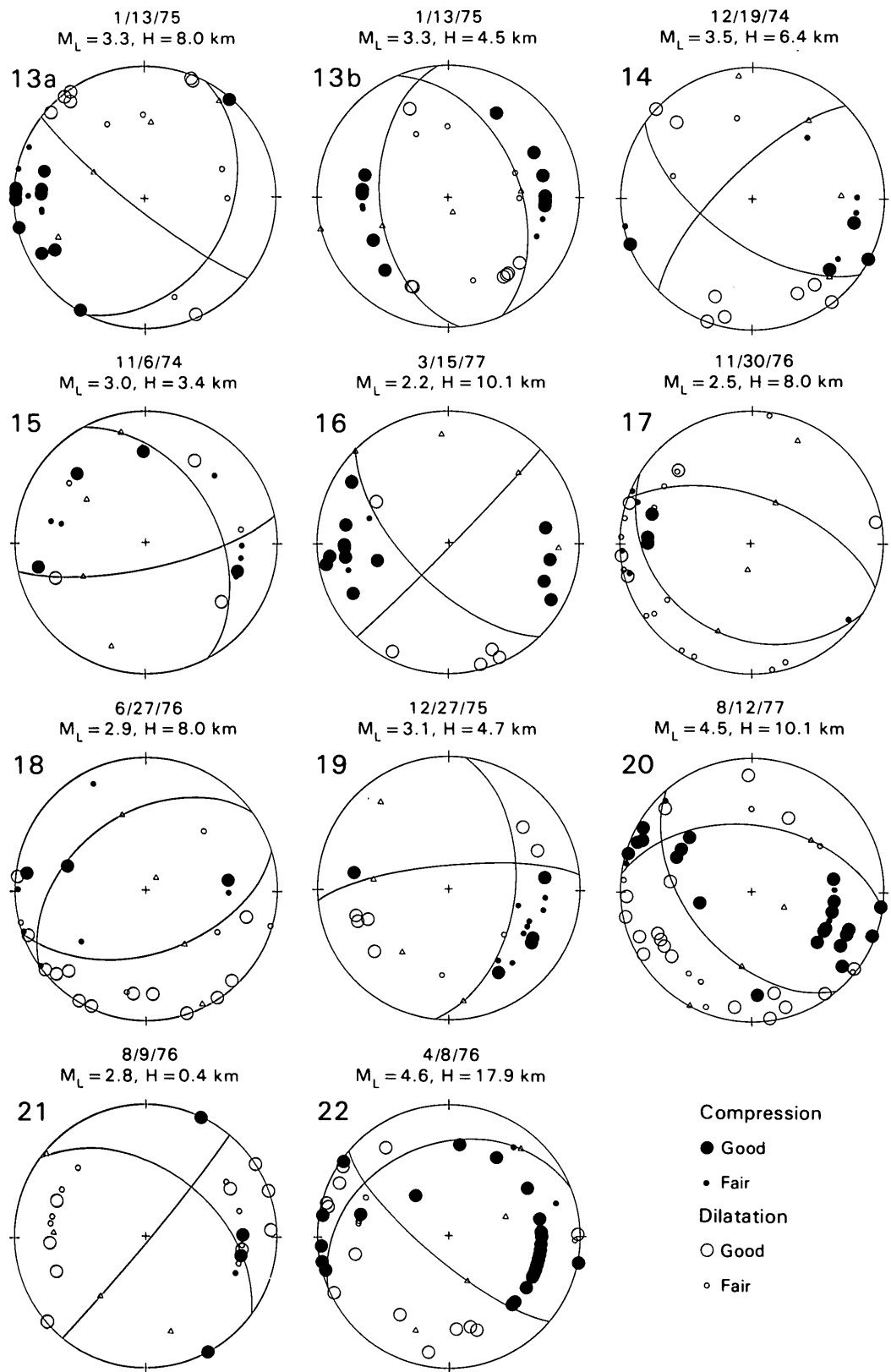


FIGURE 6.5.—Continued.

discontinuity, shows three branches corresponding to P_g , P^* , and P_n . Since the dip on the Conrad discontinuity is not well known but is probably small, the takeoff angles for all three branches of the traveltimes were calculated using the horizontally layered location model. The resultant P -wave first-motion plot is shown in figure 6.5 (focal mechanism 20).

Use of the technique just described eliminates much of the uncertainty in determining takeoff angles when the source depth is not well constrained. A problem still remains, however, if the event is located near a discontinuity in the velocity model, because the traveltimes for a source located just above a discontinuity are nearly identical to those for a source located just below it, but the takeoff angles are quite different. When this problem was encountered, the mechanisms were determined for sources located on both sides of the discontinuity, and the mechanism with the fewest stations in error was chosen. Only in one instance were the two mechanisms significantly different and of equal quality, and for this event (focal mechanism 13, fig. 6.5) both solutions are shown.

RESULTS OF REGIONAL FOCAL-MECHANISM STUDY

Figure 6.5 shows the P -wave first-motion plots for the events studied. The nodal planes were determined with the aid of the computer program FOCPLT developed by Whitcomb and Garmany (Whitcomb, 1973). This program tests a grid of trial mechanisms spaced at approximately 5-degree intervals on the focal sphere and then chooses a mechanism which minimizes the number of first-motion readings in error. Less reliable readings are given half the weight of other readings, and a linear function is used to downweight stations within 3 degrees of a nodal plane. Most of the focal mechanisms shown in figure 6.5 are well-constrained. The numbers are keyed to figure 6.3, which shows the location of each mechanism.

Examination of figure 6.3 shows that there is little systematic variation in mechanism from place to place within the study area. Most of the solutions show strike-slip faulting, reverse faulting, or a combination of strike-slip and reverse faulting. In general, the fault-plane orientations and senses of motion do not agree very well with those of the major faults shown. Along the San Jacinto fault, mechanism 12 is consistent with geologic evidence for right-lateral strike-slip motion on a northwest-trending fault. However, 20 km to the northwest along the same fault zone, thrusting is observed. Mechanisms 4, 5, 6, and 7 are especially interesting because master-event relocations for these events by McNally and others (1978) show that they all cluster within a small volume 3 km in maximum dimension, centered 2 km southwest of the mapped surface trace of the San Andreas fault at a depth of about 8 km. Although mechanism 4 is consistent with the long-

term sense of motion on the San Andreas fault, the others are not and, furthermore, show systematic changes in mechanism with time. This swarm may be associated with the San Andreas fault or with one of several subparallel faults that splay southward from the main fault at this point. Focal mechanisms for events 3, 20, and 22 agree well with those determined independently by Hadley and Kanamori (1978). Two of these, events 3 and 22, are consistent with motion on either nearly vertical or nearly horizontal planes. Hadley and Kanamori argue on the basis of these mechanisms and other evidence that regional horizontal decollements may exist within the central Transverse Ranges. If the horizontal plane in mechanisms 3 and 22 is chosen as the fault plane, then movement of the upper block is towards the south or southwest.

Although the fault-plane solutions in figure 6.5 show considerable diversity, the compression axes for most of them are oriented nearly north-south and horizontal. Other investigators have obtained similar results in the central Transverse Ranges (Whitcomb and others, 1973; Cramer and Harrington, this volume). In the western Transverse Ranges the compression axis is still the most stable parameter, but the preferred orientation is closer to north-northeast—south-southwest and horizontal (Stierman and Ellsworth, 1976; Corbett and Johnson, 1982; Yerkes and Lee, this volume). Earthquakes in the eastern Transverse Ranges have focal mechanisms characterized by north-south compression axes and east-west tension axes (Webb and Kanamori, 1985).

To produce a combined plot of the compression axes that reflected the degree of constraint of the mechanisms, I used the grid of scores calculated by FOCPLT for each event. Positions of the compression axes corresponding to best-fit solutions with the minimum numbers of stations in error were assigned a weight of 3. Positions that allowed less than one additional good-quality reading or two additional fair-quality readings to be in error were assigned a weight of 2. Positions with the number of stations in error beyond the minimum lying in the range 1–2 good or 2–4 fair were given a weight of 1. Scores worse than this were given zero weight. The weights for all the events were added up at each focal-sphere grid point and the results contoured to give the plot shown in figure 6.6. A similar diagram for the tension axes is also shown.

Figure 6.6 clearly demonstrates that focal mechanisms in the central Transverse Ranges are characterized by a horizontal north-south compression axis and a nearly vertical tension axis. The dominant type of faulting is, therefore, reverse faulting on east-striking planes with dip near 45°. Even though compression and tension axes for individual earthquakes do not necessarily reflect the actual tectonic stress field (McKenzie, 1969), the well-defined maxima in figure 6.6 suggest that these parameters have

physical significance in a statistical sense. The north-south compression suggested by the fault-plane solutions is consistent with the north-northwest orientations for maximum horizontal compressive stress measured in boreholes in this region (Flaccus and others, 1980; Zoback and others, 1980). There is, in addition, abundant geologic evidence to suggest strong north-south compression in the Transverse Ranges province during post-Miocene times. This north-south compression has resulted in folding along east-west axes, thrust and reverse faulting with some components of strike-slip, and major uplift of several crustal blocks (Jahns, 1973).

A more direct conclusion that can be drawn from figure 6.6 is that the average deformation resulting from small earthquakes in this region is north-south crustal shortening and vertical extension, at least for the time period 1974 to 1978. Since this is permanent deformation, it constitutes a form of elastic strain relief. Geodolite measurements of horizontal strain accumulation by Savage and others (1978) in the interval from 1972 to 1978 indicate a remarkably consistent uniaxial north-south contraction of about 0.2–0.3 parts per million per year (ppm/yr) throughout southern California. This strain apparently accumulated uniformly with time. The amount of north-south contraction attributable to faulting during small earthquakes is therefore relevant to the rate of stress ac-

cumulation across both the San Andreas and frontal fault systems.

Kostrov (1974) derives an expression to describe how movements in separate earthquakes along numerous randomly located fractures can be summed in a quasi-plastic deformation process. The expression is

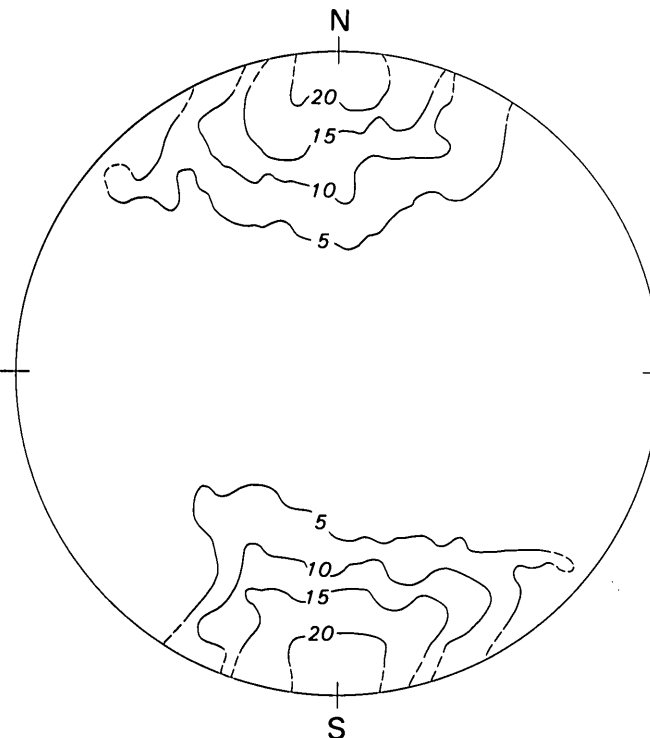
$$\dot{\varepsilon}_{ij} = \frac{1}{2\mu\Delta v\Delta t} \sum_{\kappa} M_{0ij}^{(\kappa)}$$

where $\dot{\varepsilon}_{ij}$ is the mean tensor of the rate of deformation due to the seismic flow of rock masses, Δv and Δt are the volume and time interval, respectively, over which the $M_{0ij}^{(\kappa)}$ are summed, μ is the rigidity, and $M_{0ij}^{(\kappa)}$ is the ij 'th component of the moment tensor of the κ th earthquake. If M_0 is the moment,

$$M_{0ij} = M_0 (b_j n_i + b_i n_j),$$

where \vec{b} is a unit vector in the displacement direction and \vec{n} is a unit vector perpendicular to the fault plane. To estimate the mean tensor of the rate of seismic deformation in the central Transverse Ranges, we assume that the average \vec{b} and \vec{n} vectors are those corresponding to the average mechanism indicated by figure 6.6. In a coordinate system with the X_1 -axis directed eastward, the

COMPRESSION AXES



TENSION AXES

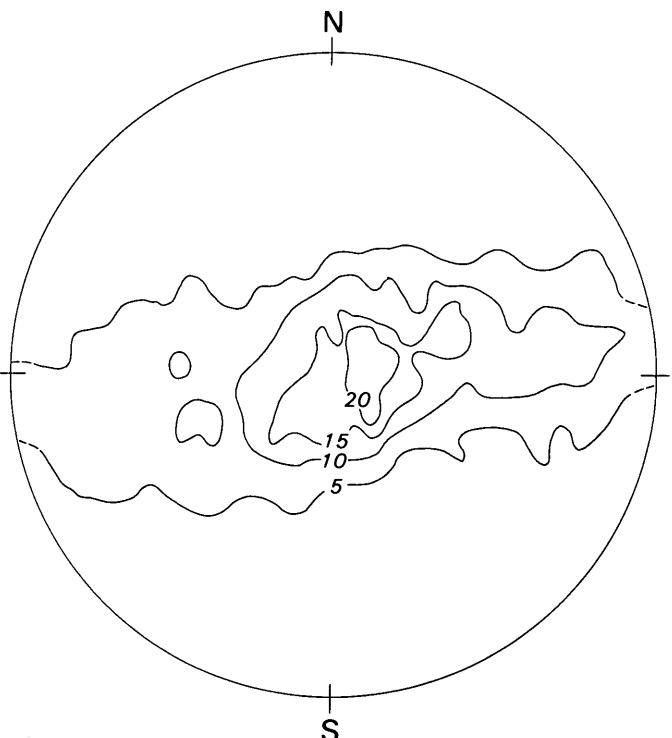


FIGURE 6.6.—Orientation of compression and tension axes on the focal sphere, taking into account variation of quality of mechanisms in figure 6.5. See text for explanation.

X_2 -axis northward, and the X_3 -axis upward, the expression for $\dot{\epsilon}_{ij}$ reduces to

$$\dot{\epsilon}_{33} = -\dot{\epsilon}_{22} = \frac{1}{2\mu\Delta v\Delta t} \sum_{\kappa} M_0^{(\kappa)}$$

with all other components zero. Since the mechanisms were determined for earthquakes during the time period 1974–1978, but post-1976 magnitudes were incomplete, we calculated $\dot{\epsilon}_{33}$ for the three-year period 1974–1976. Define $n(M)$ to be the number of events with local magnitude greater than or equal to M during this period within the boxed area of figure 6.1. Since all earthquakes that occurred during this time were less than magnitude 5.0, and earthquakes of magnitude less than 0.0 have negligibly small moments, we can write

$$\dot{\epsilon}_{33} \approx \frac{-1}{6\mu\Delta v} \int_0^{5.0} M_0(M) \frac{dn(M)}{dM} dM$$

where $M_0(M)$ is an empirical moment-magnitude relationship. On the basis of Wyss and Brune (1968), Thatcher and Hanks (1973), Bakun (1984), and Hanks and Boore (1984), we use the following relationship for $M_0(M)$

$$\log M_0 = 1.5M + 16.0 \quad 3.3 \leq M \leq 5.0$$

$$\log M_0 = 1.2M + 17.0 \quad 0.0 \leq M \leq 3.3$$

The function $n(M)$ was found to be given to a good approximation by

$$\log n = 4.5 - 1.0M.$$

Since most earthquakes in the study area occur at depths less than 15 km, we set the volume Δv equal to the area of the box in figure 6.1 times 15 km. This gives $\Delta v = 1.7 \times 10^{20} \text{ cm}^3$. Assuming $\mu = 2 \times 10^{11} \text{ dynes/cm}^2$ and substituting into the above expression, the result is $\dot{\epsilon}_{33} = -\dot{\epsilon}_{22} \approx 1 \times 10^{-9}/\text{year}$.

This number is two orders of magnitude smaller than the rate of north-south contraction determined geodetically at the surface for the same time period. We conclude that seismic faulting during 1974–76 within the study area can account for only a negligibly small amount of the measured north-south contraction. Hence, most of the contraction must represent either elastic strain accumulation or aseismic deformation.

EVIDENCE FOR TEMPORAL CHANGES IN FOCAL MECHANISMS

Shortly after this regional focal-mechanism and seismicity study presented above was completed in January 1979, changes were detected in the horizontal strain accumulation patterns in southern California through two different geodetic monitoring techniques: interferometry measurements using extraterrestrial radio sources (P. F. MacDoran, unpub. data from the Aries Project, 1980) and ground-based trilateration with a laser-ranging device (Savage and others, 1981a, b). The horizontal-strain accumulation across all three of the U.S. Geological Survey trilateration networks that lie within or partially within the central Transverse Ranges was a uniaxial north-south contraction of 0.2–0.3 ppm/yr from 1971–74, when measurements began, through 1978 (Savage and others, 1978). Between late 1978 and 1979, an episode of both north-south and east-west extension was observed over a region that encompassed at least the northwestern part of the study area. The largest amount of dilatation observed, about 2 ppm, was on the Palmdale trilateration network, which spans a 20-km-long section of the San Andreas fault within the study area (Savage and others, 1981a, b).

The remarkable agreement between the principal strain directions determined from trilateration measurements at the surface and the principal axes of the deformation tensor inferred from small-earthquake mechanisms during the period 1974–78 (fig. 6.6) suggests that small-earthquake mechanisms may accurately reflect the regional strain field even though their contribution to the regional deformation is quite minor. A question therefore arises as to whether or not the 1978–79 strain anomalies were accompanied by changes in the dominant faulting mechanism. In order to search for such changes, a systematic study of focal mechanisms of earthquakes during 1976–80 in the “big bend” region of the San Andreas fault was undertaken by several workers including the author (Sauber and others, 1983). The results of this study are summarized briefly below.

The 26 focal mechanisms (including 7 from this study) analyzed by Sauber and others (1983) generally showed reverse faulting, strike-slip faulting, or a combination of the two and were consistent with north-south compression. Reverse faulting on northeast- to southeast-striking planes was the most common faulting mechanism observed, as was found also for the regional study reported here (figs. 6.5 and 6.6). Around the time of the crustal dilatation episode, however, there appeared to be an unusually large number of strike-slip events. This observation suggests that a change in focal mechanism accompanied the strain changes, but the correlation must be considered tentative because of the limitations of the data (see Sauber and others, 1983).

The change in mechanism from reverse to predominant strike slip observed by Sauber and others (1983) during the period from mid-1978 to mid-1979 is at least qualitatively consistent with the measured horizontal strain changes and may reflect a change in the tectonic stress field. Within the study area, the most compressive principal stress is roughly north-south. Anderson's (1951) theory of faulting predicts reverse faulting for this region if the least principal stress is vertical and strike-slip faulting if the least principal stress is east-west. Therefore, the change in mechanism from reverse to strike-slip suggests that the least principal stress rotated from near vertical to approximately horizontal and east-west. The east-west extension that began in 1978-79 could have caused such a rotation, depending on the pre-existing stress and the magnitude and sign of any changes in the vertical stress component. Although north-south extension was also observed at this time, it was smaller in magnitude than the north-south compressive strain accumulated over the previous 7 years, and hence the orientation of the most compressive principal stress probably remained approximately north-south.

The maximum linear strain change observed on the Palmdale network was 1.5 ppm. Assuming a linear relation between stress and strain and an elastic modulus of 3×10^{11} dynes/cm², this strain change corresponds to a stress change of only half a bar. Thus, changes in the dominant type of faulting mechanism might occur as a result of small changes in stress.

CONCLUSIONS

The overall seismicity within the central Transverse Ranges can best be described as diffuse. Focal mechanisms for recent small earthquakes in this region similarly indicate that most of the seismicity is not directly related to the major Quaternary faults (fig. 6.3). The dominant mechanism of faulting at present appears to be reverse faulting on east-striking planes. Less commonly, strike-slip faulting on generally northwest- or northeast-striking planes is observed. Most mechanisms represent a combination of these two principal fault types, which correspond to the major categories of active fault systems found in this region.

Horizontal-strain accumulation across geodetic networks in the central Transverse Ranges appears to consist of 0.2-0.3 ppm/year of approximately north-south compression, occasionally interrupted by episodes of both north-south and east-west extension. The average deformation resulting from small earthquakes in this region is very similar to the pattern of strain accumulation inferred from surface measurements: north-south crustal shortening, vertical extension, and a lesser amount of east-west extension. However, calculations show that the

small earthquakes ($M \leq 5$) are relieving only a negligible amount of the accumulating strain. There is some evidence to suggest that strike-slip earthquakes are more common than reverse-slip earthquakes during periods of dilatation. If this is true, faulting in small earthquakes may be sensitive to small changes in the applied stress.

The above observations suggest that a reasonable physical model for the deformation between large earthquakes in this region is quasi-homogeneous north-south crustal shortening accompanied by vertical and east-west extension, which involves elastic-strain accumulation and brittle seismic fracturing near the surface together with viscous or viscoelastic flow at depth. Most of the small earthquakes appear to be part of this quasi-homogeneous deformation process and are not associated with large-scale block movements along major faults. Detailed studies may in some cases serve to identify small earthquakes with small-scale block movements. However, it seems likely that a wide variety of pre-existing zones of weakness exist throughout the region and that slip occurs on those most favorably oriented to the local stress field.

The central Transverse Ranges stress field inferred from fault-plane solutions and near-surface measurements appears to be dominated by north-south compression with the least principle stress axis near vertical. However, the origin of this stress field is not well understood. Simple dislocation models of the San Andreas fault system predict north-northwest to north-northeast compression in the central Transverse Ranges, with an equal amount of horizontally directed tension perpendicular to the compression (Rodgers and Chinnery, 1973; Prescott and Savage, 1976). Bird and Piper (1980) have developed a plane-stress finite-element nonlinear tectonic flow model for southern California that includes a weakened zone along the San Andreas fault. This model comes closer to reproducing the observed stress field, but fails in other respects. Even more puzzling than the origin of the stress field is the cause of the fluctuations in the isotropic strain that occur despite the nearly uniform shear-strain accumulation. Inasmuch as earthquakes are the only source of information about stress conditions deep within the earth, their continued study should prove useful in investigating the above problems.

REFERENCES CITED

- Allen, C. R., 1968, The tectonic environments of seismically active and inactive areas along the San Andreas fault system, in Dickinson, W. R., and Grantz, Arthur, eds., Proceedings of the conference on geologic problems of the San Andreas fault system: Stanford University Publications in Geological Sciences, v. 11, p. 70-82.
—, 1982, Creep and strain studies in southern California, in Summaries of technical reports, National Earthquake Hazards Reduction Program: U.S. Geological Survey Open-File Report 82-65, v. 13, p. 225-227.

- Allen, C. R., St. Amand, Pierre, Richter, C. F., and Nordquist, J. M., 1965, Relationship between seismicity and geologic structure in the southern California region: Seismological Society of America Bulletin, v. 55, p. 753-797.
- Anderson, E. M., 1951, The dynamics of faulting: Edinburgh, Oliver and Boyd, 206 p.
- Bailey, T. L., and Jahns, R. H., 1954, Geology of the Transverse Range province, southern California, in Jahns, R. H., ed., Geology of southern California: California Division of Mines Bulletin 170, p. 83-106.
- Bakun, W. H., 1984, Seismic moments, local magnitudes, and coda-duration magnitudes for earthquakes in central California: Seismological Society of America Bulletin, v. 74, p. 439-458.
- Bennet, Jack, 1977, Palmdale "bulge" update: California Geology, v. 30, p. 187-188.
- Bird, Peter, and Piper, K., 1980, Plane-stress finite-element models of tectonic flow in southern California: Physics of the Earth and Planetary Interiors, v. 21, p. 158-175.
- Burford, R. O., and Harsh, P. W., 1980, Slip along the San Andreas fault in central California from alignment array surveys: Seismological Society of America Bulletin, v. 70, p. 1233-1261.
- Castle, R. O., Church, J. P., and Elliott, M. R., 1976, Aseismic uplift in southern California: Science, v. 192, p. 251-253.
- Corbett, E. J., and Johnson, C. E., 1982, The Santa Barbara, California, earthquake of 13 August 1978: Seismological Society of America Bulletin, v. 72, p. 2201-2226.
- Flaccus, C. E., Richardson, R. M., Sbar, M. L., Engelder, T., and Yale, D., 1980, Tectonic stress near the San Andreas fault from strain relief measurements [abs.]: Eos (American Geophysical Union Transactions), v. 61, p. 1118.
- Friedman, M. E., Whitcomb, J. H., Allen, C. R., and Hileman, J. A., 1976, Seismicity of the southern California region, 1 January 1972 to 31 December, 1974: California Institute of Technology, Division of Geological and Planetary Sciences, Contribution 2734.
- Goultby, N. R., Burford, R. O., Allen, C. R., Gilman, Ralph, Johnson, C. E., and Keller, R. P., 1978, Large creep events on the Imperial fault, California: Seismological Society of America Bulletin, v. 68, p. 517-521.
- Hadley, D. M., 1978, Geophysical investigations of the structure and tectonics of southern California: Pasadena, California Institute of Technology, Ph.D. dissertation, 167 p.
- Hadley, David, and Combs, J., 1974, Microearthquake distribution and mechanisms of faulting in the Fontana-San Bernardino area of southern California: Seismological Society of America Bulletin, v. 64, no. 5, p. 1477-1499.
- Hadley, David, and Kanamori, Hiroo, 1977, Seismic structure of the Transverse Ranges, California: Geological Society of America Bulletin, v. 88, p. 1469-1478.
- 1978, Recent seismicity in the San Fernando region and tectonics in the west-central Transverse Ranges, California: Seismological Society of America Bulletin, v. 68, no. 5, p. 1449-1457.
- Hanks, T. C., and Boore, D. M., 1984, Moment-magnitude relations in theory and practice: Journal of Geophysical Research, v. 89, p. 6229-6235.
- Harsh, P. W., Burford, R. O., and Kinugasa, Y., 1978, Rates of fault slip during historic time in central California [abs.]: Eos (American Geophysical Union Transactions), v. 59, p. 1209-1210.
- Hileman, J. A., Allen, C. R., and Nordquist, J. M., 1973, Seismicity of the southern California region, 1 January 1932 to 31 December 1972: California Institute of Technology, Division of Geological and Planetary Sciences, Contribution no. 2385.
- Jackson, D. D. and Lee, W. B., 1979, The Palmdale bulge—An alternate interpretation [abs.]: Eos (American Geophysical Union Transactions), v. 60, p. 810.
- Jahns, R. H., 1973, Tectonic evolution of the Transverse Ranges province as related to the San Andreas fault system, in Kovach, R. L., and Nur, Amos, eds., Proceedings of the conference on tectonic problems of the San Andreas fault system: Stanford University Publications in Geological Sciences, v. 13, p. 149-170.
- Jennings, C. W., Strand, R. G., Rogers, T. H., Stinson, M. G., Burnett, J. L., Kahle, J. E., Streitz, R., and Switzer, R. A., 1975, Fault map of California with locations of volcanoes, thermal springs and thermal wells: California Division of Mines and Geology, California Geologic Data Map 1, scale 1:750,000.
- Johnson, C. E., 1979, I, CEDAR—an approach to the computer automation of short-period local seismic networks, II, Seismotectonics of the Imperial Valley of southern California: Pasadena, California Institute of Technology, Ph.D. dissertation, 343 p.
- Johnson, C. E., and Hadley, D. M., 1976, Tectonic implications of the Brawley earthquake swarm, Imperial Valley, California, January 1975: Seismological Society of America Bulletin, v. 66, p. 1133-1144.
- Kanamori, Hiroo, and Hadley, David, 1975, Crustal structure and temporal velocity change in southern California: Pure and Applied Geophysics, v. 113, p. 257-280.
- Keller, R. P., Allen, C. R., Gilman, Ralph, Goultby, N. R., and Hileman, J. A., 1978, Monitoring slip along major faults in southern California: Seismological Society of America Bulletin, v. 68, p. 1187-1190.
- Kerr, R. A., 1981, Palmdale Bulge doubts now taken seriously: Science, v. 214, p. 1331-1333.
- Kostrov, V. V., 1974, Seismic moment and energy of earthquakes and seismic flow of rock (Translated by F. Goodspeed): Izvestija, Earth Physics, no. 1, p. 23-40.
- Lee, W. H. K., and Lahr, J. C., 1975, HYP071 (revised): A computer program for determining hypocenter, magnitude, and first motion pattern of local earthquakes: U.S. Geologic Survey Open-File Report 75-311, 114 p.
- Lee, W. H. K., Yerkes, R. F., and Simirenko, M., 1979, Recent earthquake activity and focal mechanisms in the western Transverse Ranges, California: U.S. Geological Survey Circular 799A, p. A1-A26.
- Mark, R. K., Tinsley, J. C., Newman, E. B., Gilmore, T. D., and Castle, R. O., 1981, An assessment of the geodetic measurements that define the southern California uplift: Journal of Geophysical Research, v. 86, p. 2783-2808.
- McKenzie, D. P., 1969, The relation between fault plane solutions for earthquakes and the directions of the principal stresses: Seismological Study of America Bulletin, v. 59, p. 591-601.
- McNally, K. C., Kanamori, Hiroo, Pechmann, J. C., and Fuis, Gary, 1978, Earthquake swarm along the San Andreas fault near Palmdale, southern California, 1976 to 1977: Science, v. 201, p. 814-817.
- Murdock, J. N., 1979, A tectonic interpretation of earthquake focal mechanisms and hypocenters in Ridge Basin, southern California: Seismological Society of America Bulletin, v. 69, p. 417-425.
- Murphy, L. M., ed., 1973, San Fernando, California, earthquake of February 9, 1971: U.S. Department of Commerce, National Oceanic and Atmospheric Administration, v. 3, 432 p.
- Oakeshott, G. B., ed., 1975, San Fernando, California, earthquake of 9 February, 1971: California Division of Mines and Geology Bulletin 196, 463 p.
- Prescott, W. H., and Savage, J. C., 1976, Strain accumulation on the San Andreas fault near Palmdale, California: Journal of Geophysical Research, v. 81, p. 4901-4908.
- Raikes, S. A., 1978, Regional variations in upper mantle compressional velocities beneath southern California: Pasadena, California Institute of Technology, Ph.D. dissertation (part I), 209 p.
- Richter, C. F., 1958, Elementary seismology: San Francisco, W. H. Freeman and Co., 768 p.
- Rodgers, D. A., and Chinnery, M. A., 1973, Stress accumulation in the Transverse Ranges, southern California in Kovach, R. L., and Nur, Amos, eds., Proceedings of the conference on tectonic problems of

- the San Andreas fault system; Stanford University Publications in Geological Sciences, v. 13, p. 70-79.
- Sauber, Jeanne, McNally, Karen, Pechmann, J. C., and Kanamori, Hiroo, 1983, Seismicity near Palmdale, California, and its relation to strain changes: *Journal of Geophysical Research*, v. 88, p. 2213-2219.
- Savage, J. C., Prescott, W. H., Lisowski, M., and King, N. E., 1978, Strain in southern California: measured uniaxial north-south regional contraction: *Science*, v. 202, p. 883-885.
- _____, 1981a, Strain accumulation on the San Andreas fault near Palmdale, California: Rapid, aseismic change: *Science*, v. 211, p. 56-58.
- _____, 1981b, Strain accumulation in southern California, 1973-1980: *Journal of Geophysical Research*, v. 86, p. 6991-7002.
- Stierman, D. J., and Ellsworth, W. L., 1976, Aftershocks of the February 21, 1973, Point Mugu, California, earthquake: *Seismological Society of America Bulletin*, v. 66, p. 1931-1952.
- Strange, W. E., 1981, The impact of refraction correction on leveling interpretations in southern California: *Journal of Geophysical Research*, v. 86, p. 2809-2824.
- Thatcher, Wayne, and Hanks, T. C., 1973, Source parameters of southern California earthquakes: *Journal of Geophysical Research*, v. 78, no. 35, p. 8547-8576.
- U.S. Geological Survey, 1971, The San Fernando, California, earthquake of February 9, 1971: U.S. Geological Survey Professional Paper 733, 254 p.
- Webb, T. H., and Kanamori, Hiroo, 1985, Earthquake focal mechanisms in the eastern Transverse Ranges and San Emigdio Mountains, southern California, and evidence for a regional decollement: *Seismological Society of America Bulletin*, v. 75, no. 3, p. 737-757.
- Whitcomb, J. H., 1973, The 1971 San Fernando earthquake series focal mechanisms and tectonics: Pasadena, California Institute of Technology, Ph.D. dissertation (part II).
- _____, 1978, P and S-phase data from local earthquakes in southern California for 1966 to 1975: *Seismological Society of America Bulletin*, v. 68, p. 523-525.
- Whitcomb, J. H., Allen, C. R., Blanchard, A. C., Fisher, S. A., Fuis, G. S., Hutton, L. K., Jenkins, D. J., Johnson, C. E., Reed, B. A., and Richter, K. J., 1978, Southern California array for research on local earthquakes and teleseisms (SCARLET), Caltech-USGS monthly preliminary epicenters for January 1977 to March 1978: California Institute of Technology, Division of Geological and Planetary Sciences.
- Whitcomb, J. H., Allen, C. R., Garmany, J. D., and Hileman, J. A., 1973, San Fernando earthquake series, 1971: focal mechanisms and tectonics: *Reviews of Geophysics and Space Physics*, v. 11, p. 693-730.
- Wyss, Max, and Brune, J. N., 1968, Seismic moment, stress, and source dimensions for earthquakes in the California-Nevada region, *Journal of Geophysical Research*, v. 73, no. 14, p. 4681-4694.
- Zoback, M. D., Tsukahara, Hiroaki, and Hickman, Stephen, 1980, Stress measurements at depth in the vicinity of the San Andreas fault: implications for the magnitude of shear stress at depth: *Journal of Geophysical Research*, v. 85, no. 11, p. 6157-6173.



7. SEISMICITY AND TECTONICS OF THE SANTA MONICA-HOLLYWOOD-RAYMOND HILL FAULT ZONE AND NORTHERN LOS ANGELES BASIN

By CHARLES R. REAL¹

ABSTRACT

A study of the seismicity along the frontal fault system forming the southern boundary of the Transverse Ranges province has strengthened the correlation between earthquakes and specific fault zones in the vicinity of the northern Los Angeles basin. Combined phase data from the California Institute of Technology and the University of Southern California seismograph stations have been used to relocate and obtain first-motion patterns for 39 earthquakes ranging in magnitude from 1.1 to 4.0 that have occurred since 1972. The revised hypocenter locations generally have standard errors less than 1.5 and 2.5 km, respectively, in the horizontal and vertical dimensions.

Composite focal mechanisms show that displacement is reverse left-lateral oblique along the Santa Monica-Hollywood-Raymond Hill fault zone, normal right-lateral oblique along the Newport-Inglewood and Whittier fault zones, and left-lateral along the San Jose fault zone. Azimuths of the principal compression axes vary from N. 22° W. to N. 25° E, with plunges ranging from 0° to about 80°.

Northwesterly movement of the Pacific plate along the San Andreas fault system is interrupted by the westerly bend in the San Andreas fault along the northern boundary of the Transverse Ranges block. Large-scale oblique convergent wrenching generates a regional north-south compressive strain across the block that is partially absorbed along its southern boundary by the frontal fault system.

It is concluded that the frontal fault system is seismically active in the vicinity of the northern Los Angeles basin, and that there is a high probability that the Santa Monica-Hollywood-Raymond Hill fault zone is capable of generating damaging earthquakes.

INTRODUCTION

The Santa Monica-Hollywood-Raymond Hill fault zone forms the central portion of a major tectonic boundary separating the east-west-trending Transverse Ranges structural province to the north from the northwest-trending Peninsular Ranges province to the south. This boundary, hereafter referred to as the frontal fault system, continues east along the Sierra Madre and Cucamonga faults, and west along the Malibu Coast and Santa Cruz Island faults.

Although the Transverse Ranges have a complex structural history, much of which is poorly understood, development since Miocene has resulted from north-south crustal

shortening characterized by folding and predominant reverse or thrust faulting along east-west-trending structures (Jahns, 1973). Continuation of this mode of deformation into recent historic time is evidenced by the mechanisms of the local magnitude $M_L = 6.4$, February 9, 1971, San Fernando earthquake (Whitcomb and others, 1973) and the $M_L = 6.0$, February 21, 1973, Point Mugu earthquake (Ellsworth and others, 1973; Stierman and Ellsworth, 1976), and by geodetic measurements and analyses of crustal strain (Castle and others, 1976; Thatcher, 1976; Savage and Prescott, 1977). Although it is evident that the Transverse Ranges are still undergoing structural development, it is unclear which faults within and bounding the province are presently involved in continuing tectonic processes.

Because it passes through heavily urbanized portions of the greater Los Angeles metropolitan area, the Santa Monica-Hollywood-Raymond Hill fault zone is of particular concern from the standpoint of public safety. Conventional field mapping of the hazard potential and associated risk, however, is generally not possible because of the dense urbanization. Although geomorphic features indicating recent movement have generally been obliterated, many old photographs of the area show well-defined linear scarps and ridges, closed depressions, sag ponds, springs, and other features characteristic of active faults, and borehole data show a well-defined ground-water barrier (Hill and others, 1979).

Evidence of such recent activity prompted a multiyear interdisciplinary study, funded by a grant under the Earthquake Hazard Reduction Program of the U.S. Geological Survey, to define the location, extent, and probable recency of faulting along the Santa Monica-Hollywood-Raymond Hill fault zone (fig. 7.1). As a part of this study during 1976-77, the seismicity of the area was examined to determine the mechanisms and recent level of seismic-strain release along the primary and associated faults under study and to examine their interrelations and roles in the current pattern of regional deformation. The results of this seismologic investigation are presented here.

¹California Division of Mines and Geology, 630 Bercut Drive, Sacramento, California 95814.

Manuscript received for publication on October 7, 1980.

PREVIOUS WORK

Some 60 years of reports of felt earthquakes (Holden, 1897; Wood, 1916; Townley and Allen, 1939; Toppozada and others, 1978) and a subsequent 45 years of instrumental recording (Hileman and others, 1973; Friedman and others, 1976; Fuis and others, 1977) of earthquakes have clearly demonstrated that the area of this study is seismically active (fig. 7.2). Studies of large earthquakes accompanied by ground rupture show that such activity represents seismic-strain release resulting from displacements along fault zones (Allen and others, 1965), although this is not apparent on figure 7.2. The diffuse pattern of epicenters on figure 7.2 results primarily from inaccuracy in locating them and does not serve to distinguish seismically active faults.

Recent concern for seismic safety in southern California has led to a marked increase in the density of the regional and local seismograph network (Allen and others, 1977; Teng and others, 1977) and consequently to improvement in locating the hypocenters, as can be seen by examining the epicenters of earthquakes that have occurred since 1972 (fig. 7.3). Considerably higher resolution is evident from distinct pockets of activity near Baldwin Hills along the Newport-Inglewood fault zone,

near Repetto Hills along the Whittier fault zone, and in the Elysian Hills near the junction of the Hollywood-Raymond Hill fault and the trend of the Whittier fault zone. It is worth noting that these active areas coincide with areas where anticlinal hills have formed in response to stresses and deformation along the fault zones.

Owing to the high ambient ground noise characteristic of urban areas, high-gain microearthquake surveys near Los Angeles have been limited to outlying areas. Lamar (1972) conducted a short-term microearthquake survey along the Whittier fault near the town of Whittier and found that noise levels limited the lower threshold of locatable events to about $M_L = 1.0$. Teng and others (1973) report locations of earthquakes down to about that same threshold along the Newport-Inglewood fault. Oil-recovery operations in the many fields associated with faulting in the Los Angeles basin further compound the noise problem. Consequently, downhole seismometers have been placed deep in the ground to improve detection of events (Teng and others, 1977).

The present study uses available phase data from these existing regional and local seismograph networks to help define the relation between earthquake activity and faulting in the study area. Phase data from well-recorded events are combined with a regional and local crustal

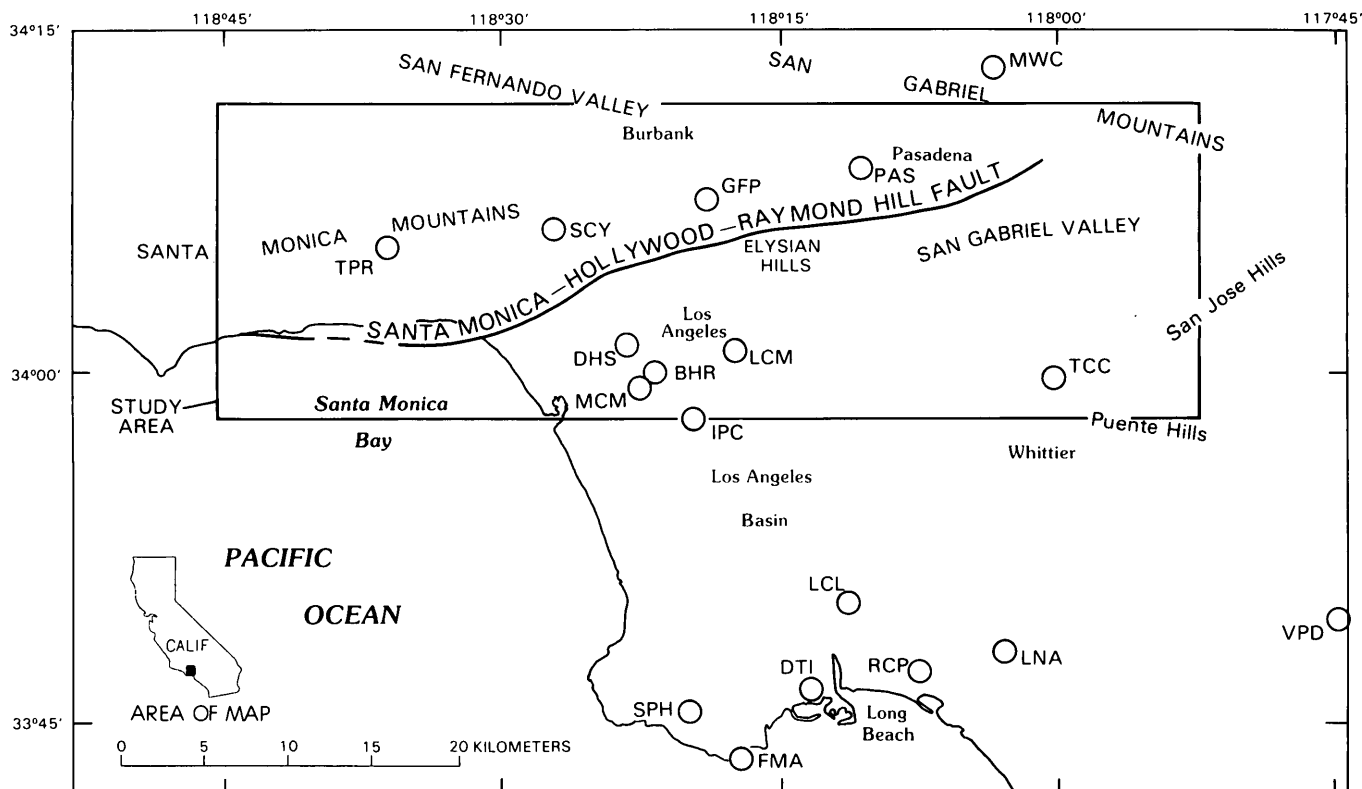


FIGURE 7.1.— Location of study area and local seismograph stations (circles) in southern California.

model to produce revised hypocenter and fault-plane solutions. Only data from well-recorded events have been used. It should be stressed that the earthquake data base is from existing permanent seismograph stations and that the present study demonstrates both the usefulness and the limitations of these data.

Recently, Buika and Teng (1978) carried out a similar study over a much larger area covering the western Los Angeles basin, Santa Monica Bay, and the Santa Monica Mountains. The present study concentrates on the northern Los Angeles basin east of the Santa Monica Bay to the Puente Hills (fig. 7.1).

ACKNOWLEDGMENTS

The author wishes to thank T. L. Teng (University of Southern California) and J. H. Whitcomb (California Institute of Technology), who kindly arranged for the availability of phase data. Well velocity sonic logs were provided by the oil industry. The author also wishes to acknowledge the leadership of R. L. Hill, who ably coor-

dinated the interdisciplinary study of the Santa Monica-Hollywood-Raymond Hill fault zone. This research was supported by the U.S. Geological Survey under USGS grant No. 14-08-0001-15858.

ANALYSIS OF DATA

Reliable fault-plane solutions require a wide spatial distribution of recorded first motions and well-determined hypocenters. Patterns of radiated first motions are particularly sensitive to changes in focal depth. Accurate depth control in turn requires a detailed crustal model and seismograms recorded near the epicenter. With these restrictions in mind, the southern California earthquake catalog has been searched for those events for which sufficient data exist to yield potential fault-plane solutions. Thirty-nine earthquakes from the California Institute of Technology catalog that occurred in the study area from 1972 through 1976, ranging in magnitude from $M_L = 1.1$ to 4.0, were chosen for relocation and a first-motion study based on high record quality and abundance of recordings. P- and S-wave phase data were collected for each event

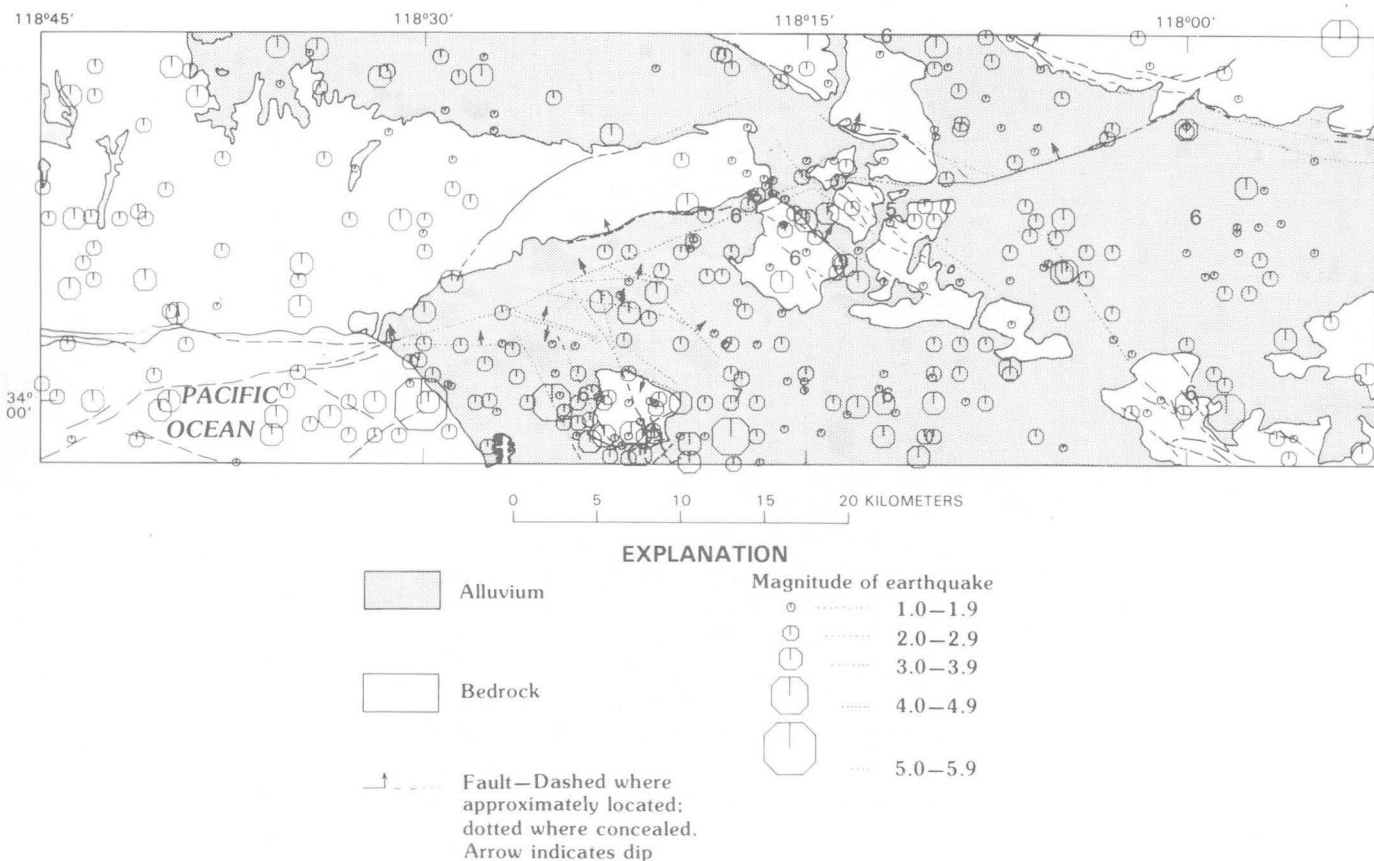


FIGURE 7.2.—Locations and magnitudes of earthquakes in the study area from 1877 to 1976.

from the California Institute of Technology and the University of Southern California local seismograph networks. These data are available in machine readable form in the standard HYPO71 format (Lee and Lahr, 1975). Original seismograms have not been reinterpreted for this study.

Chosen earthquakes are relocated by using the computer program HYPOELLIPE (Lahr, 1979). This program allows for the use of different crustal models for the various stations. A particular model is assumed to hold from the source to the station to which it is assigned, thereby allowing for some lateral variation in crustal structure from station to station.

The distribution of regional seismograph stations used primarily for first-motion study is shown in figure 7.4. Local stations within or near the study area used for both relocation and first-motion study are shown in figure 7.1. In addition to weights already assigned by the seismogram reader, arrival times from stations within 20 km of the epicenter are assigned a secondary weighting factor of unity while those more than 40 km distant are given zero weight. Weighting for station arrivals of intermediate distance follows a ramp function joining the two extremes. In this manner, the data of generally superior quality from nearby stations govern the hypocenter solution. *P*- and *S*-wave data are used in the process of locating the hypocenter. *S*-wave crustal structure is obtained by assuming a *P*- to *S*-wave velocity ratio of 1.78.

CRUSTAL MODEL

Crustal models for the southern California region (Press, 1960; Hileman and others 1973; Kanamori and Hadley, 1975) and for the Los Angeles basin (Teng and others 1973) have been published, but the present availability of additional velocity information from numerous oil fields throughout the basin has made it desirable to modify these models. Two models were found that define crustal structure sufficiently well to permit precise locations of events in the study area.

The first model is regional and applies to seismograph stations on bedrock or to those that lie outside the Los Angeles basin. This model is based on crustal refraction and *P*-delay studies (Kanamori, 1976) and is composed of three layers over a half-space (table 7.1). The second model is local and applies to seismograph stations located within the Los Angeles basin. It is identical to the first except that its uppermost layer is replaced by eight layers of increasing velocity representing basin structure (table 7.2). This structure is based on interval velocity curves computed from 18 sonic logs taken in oil wells located throughout the interior of the Los Angeles basin. Coverage of these logs ranges over intervals of a few hundred to several thousand meters at various depths within the basin. Interval velocity curves were computed from each sonic log and their composite used to produce average

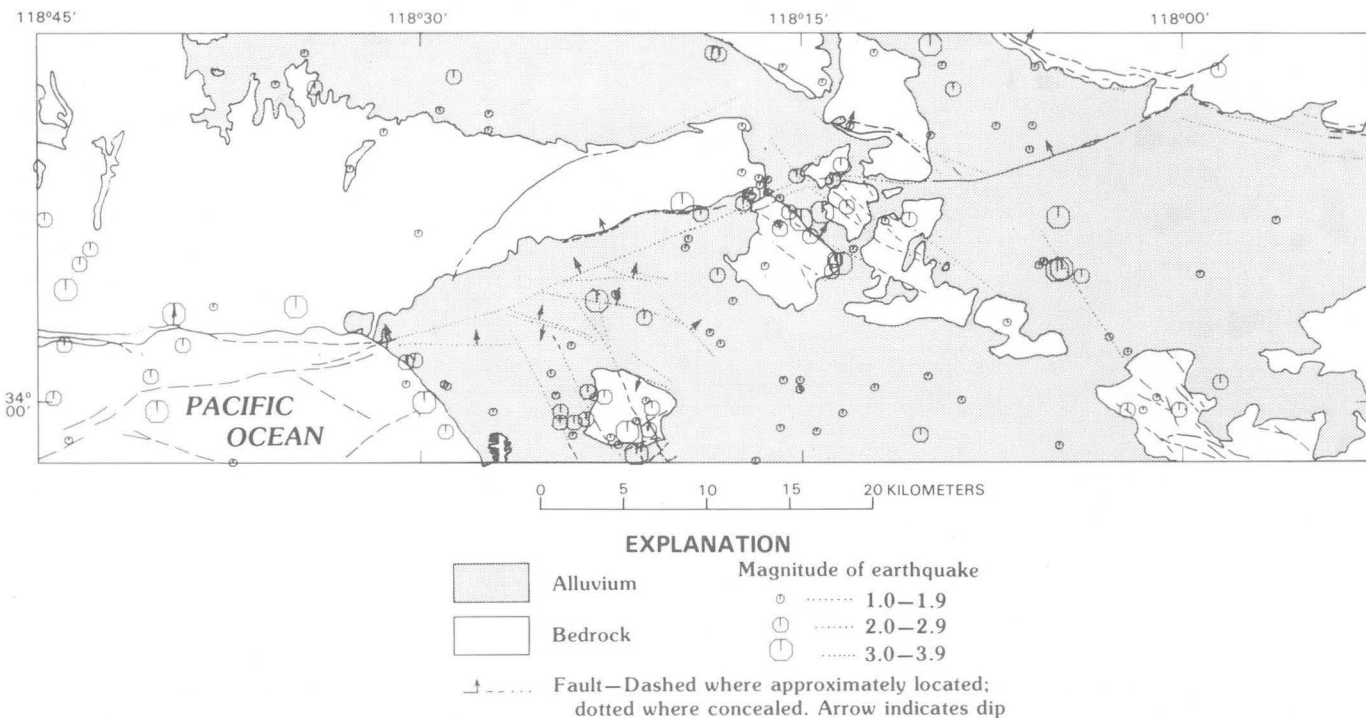


FIGURE 7.3.—Locations and magnitudes of earthquakes in the study area from 1972 to 1976.

TABLE 7.1.—*Crustal velocity model I*

Layer	Velocity (km/s)	Depth (km)	Thickness (km)
1	5.5	0.000	6.000
2	6.2	6.000	14.000
3	6.7	20.000	10.000
4	7.8	30.000	1,000.000

interval velocities ranging from near surface to a depth of about 5 km (fig. 7.5).

With crustal structure so defined, detailed variations in upper crustal velocity are accounted for by station delays. The technique employed iteratively introduces average station residuals by adding them to the station delays for the next successive run. This procedure is repeated until the station residuals are minimized, whereby final station delays compensate for discrepancies between the simplified model and the true velocity structure.

FIRST-MOTION STUDY

Each hypocenter solution produces a lower-hemisphere, equal-area plot of first motions. Despite the care taken in selecting the events, most lacked sufficient data to definitively constrain the fault planes. Consequently, data have been combined to form composite focal-mechanism solutions.

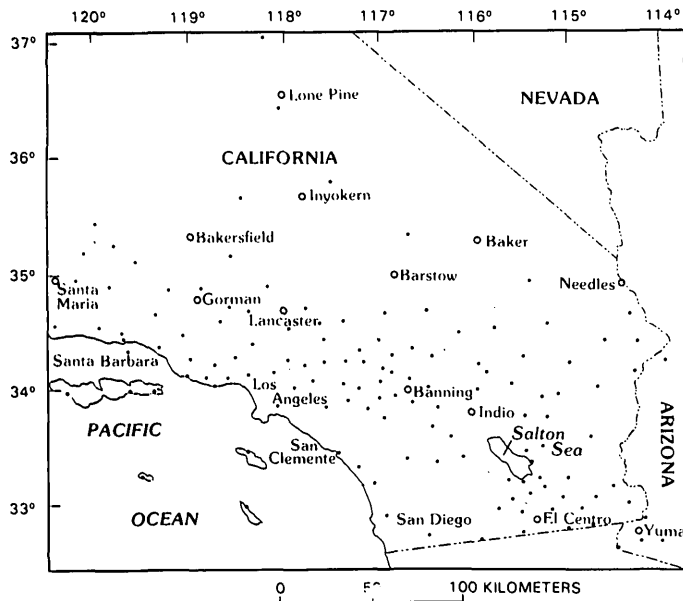


FIGURE 7.4.—Seismograph stations of the joint California Institute of Technology-U.S. Geological Survey regional southern California seismograph network, January 1, 1977 (After Allen and Whitcomb, 1977).

TABLE 7.2.—*Crustal velocity model II*

Layer	Velocity (km/s)	Depth (km)	Thickness (km)
1	1.8	0.0	0.305
2	2.1	0.305	0.305
3	2.5	0.610	0.610
4	2.8	1.219	0.488
5	3.2	1.707	0.488
6	3.6	2.195	0.853
7	4.0	3.048	0.952
8	5.5	4.000	2.000
9	6.2	6.000	14.000
10	6.7	20.000	10.000
11	7.8	30.000	1,000.000

The procedure used selects as initial trial solutions individual mechanisms of the larger events that have reasonably well constrained solutions. Additional first-motion data from nearby events are then added and tested for compatibility. Only data from hypocenter solutions having station gaps less than 180° are used. If the first-motion patterns are contradictory, the data are tested with a different trial solution. If the data are in general

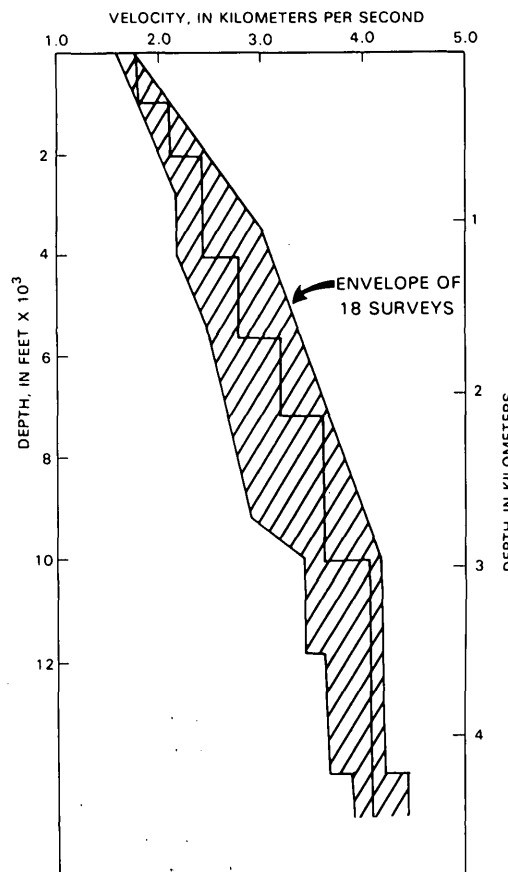


FIGURE 7.5.—Composite interval velocity curve based on 18 sonic log surveys taken in oil wells throughout the Los Angeles basin.

agreement, the nodal planes are adjusted as necessary. This procedure maximizes data use in determining composite fault-plane solutions without serious loss of objectivity.

RESULTS

Revised locations for the 39 earthquakes studied are listed in table 7.3. Focal depths range from 1.2 to 16.0 km. Twenty-seven solutions are of "A" quality. This quality is based on the length of the longest axis (L) of the

error ellipsoid: A, $L \leq 2.5$ km; B, $2.5 < L \leq 5.0$ km; C, $5.0 < L \leq 10.0$ km. Table 7.4 shows the average root-mean-square of the traveltimes residuals and the average standard errors in the horizontal and vertical dimensions for each quality class.

One individual ($M_L = 4.0$) fault-plane solution and four composite fault-plane solutions were determined for the primary and associated fault zones under study (fig. 7.6). Only 22 of the 39 events are used in deriving these mechanisms. The remaining events either have first-motion radiation patterns that conflict with the general

TABLE 7.3.—Revised hypocenters

[Headings explained in notes at end of table]

EVENT	YEAR	MON	DY	HR	MN	SEC	LAT	N.	LONG	W.	DEPTH	MAG	NO	GAP	D3	RMS	ERH	ERZ	QH
1	1972	5	7	13	13	44.2	33-59.6		118-28.4		4.8	2.4	9	186	30.1	0.16	1.9	2.2	A
2		6	29	2	1	52.1	34-	0.7	118-21.2		7.7	1.6	7	161	22.7	0.10	4.3	6.8	C
3		8	27	8	49	26.5	34-	2.8	118-22.9		1.3	3.2	13	142	9.4	0.22	1.2	1.6	A
4		9	10	5	19	5.8	34-	2.8	118-21.2		5.3	1.1	14	128	20.2	0.15	1.3	1.3	A
5		10	2	15	46	24.0	34-	7.2	118-16.1		11.5	1.4	10	144	22.4	0.18	2.9	2.9	B
6	1973	3	29	21	35	34.2	34-	2.1	118-25.5		9.5	3.3	15	176	8.3	0.42	4.0	8.7	C
7		5	13	1	52	34.3	33-	60.0	118-19.9		4.6	2.5	22	53	3.3	0.25	1.2	1.6	A
8		6	7	10	38	12.6	34-	0.8	118-23.1		4.8	2.2	12	274	24.9	0.23	4.4	2.6	B
9*		7	2	15	48	53.9	34-	5.2	118-18.6		1.9	3.2	18	71	10.8	0.09	0.9	0.8	A
10		7	3	2	32	0.6	34-	6.6	118-19.0		1.6	2.7	16	153	14.1	0.17	1.2	9.5	C
11		7	29	10	30	27.1	34-	6.7	118-16.5		8.5	2.0	12	109	16.5	0.13	1.5	3.5	B
12		9	2	6	28	7.3	34-	1.0	118-26.8		2.9	2.5	7	195	31.6	0.37	2.6	6.5	C
13*		11	18	7	29	59.7	33-58.3		118-21.4		4.6	3.2	23	139	3.5	0.15	0.7	1.1	A
14*		11	29	11	25	19.8	34-	0.9	118-23.6		2.8	2.5	23	158	5.1	0.25	1.2	1.0	A
15		12	9	6	59	3.3	34-	5.9	118-11.9		8.3	2.3	20	148	6.2	0.10	1.5	0.8	A
16*		12	9	15	36	14.9	34-	1.1	118-22.7		2.1	2.5	29	81	6.6	0.25	0.8	1.1	A
17*	1974	2	11	12	20	56.8	34-	6.1	118-16.0		9.5	3.4	10	83	17.3	0.05	0.5	1.4	A
18*		2	15	18	56	36.0	34-	6.2	118-16.1		8.5	2.1	13	154	10.3	0.10	1.9	1.6	A
19*		2	20	23	21	32.2	34-	4.4	118-15.9		5.8	2.4	25	87	12.0	0.28	1.5	1.4	A
20*		2	27	5	41	17.7	34-	4.1	118- 5.9		16.0	2.5	15	120	11.4	0.08	0.8	2.3	A
21*		3	6	1	52	34.4	34-	5.7	118-15.9		8.9	2.4	21	74	10.6	0.13	0.9	1.9	A
22		3	9	3	41	36.9	34-	7.4	118-19.9		4.2	2.1	13	78	12.5	0.20	1.3	3.5	B
23*		3	12	7	35	45.2	34-	3.6	118-14.1		2.0	3.1	17	68	11.4	0.06	0.7	0.6	A
24*		3	12	7	38	43.7	34-	6.0	118-14.8		6.1	2.0	15	153	8.8	0.14	2.7	2.2	B
25*		3	12	10	13	42.8	34-	5.2	118-15.2		3.7	1.9	29	88	10.3	0.23	0.9	1.4	A
26*		10	22	12	13	38.7	33-57.8		118-21.8		3.0	3.0	18	163	9.3	0.30	1.5	1.6	A
27*		12	19	12	36	16.9	34-	3.2	118- 6.5		4.8	3.5	16	113	12.0	0.13	1.5	2.3	A
28*		12	19	12	39	50.3	34-	2.8	118- 7.2		2.3	3.2	16	104	12.4	0.10	1.0	1.0	A
29*		12	19	15	15	19.6	34-	3.8	118- 6.5		8.7	1.6	11	193	11.6	0.05	0.6	1.4	A
30*		12	19	15	31	11.8	34-	4.0	118- 6.3		8.7	1.9	11	189	11.7	0.07	0.8	1.9	A
31	1975	1	28	5	22	22.9	34-	9.8	118-36.0		9.6	2.9	9	229	14.8	0.09	3.5	3.7	B
32		2	10	12	54	28.7	34-	7.8	118-14.6		9.5	2.0	23	58	7.0	0.57	2.5	6.5	C
33		4	12	8	23	24.7	34-	2.6	118-18.7		5.7	1.8	10	197	17.5	0.06	0.9	0.7	A
34		6	27	15	41	27.0	34-	7.1	118-14.5		8.9	2.1	11	211	20.5	0.07	0.7	0.9	A
35		7	22	12	24	34.0	33-59.8		118-24.6		8.6	2.0	14	205	11.7	0.13	2.3	2.0	A
36*		10	11	16	55	1.2	34-	6.3	118- 6.7		7.7	3.0	21	114	7.5	0.17	0.9	2.7	B
37*		10	11	19	12	52.3	34-	5.9	118- 6.2		8.3	2.9	10	128	8.4	0.06	0.8	2.2	A
38*	1976	1	1	17	20	12.9	34-	0.8	117-52.5		1.2	4.0	16	84	24.3	0.20	1.8	1.8	A
39*		9	29	7	0	51.5	34-	5.6	118-17.9		5.1	2.0	19	95	11.7	0.11	0.7	1.1	A

The following data are given for each earthquake event:

EVENT identification number for each event. An asterisk indicates the event is used in a focal mechanism solution.

observed pattern in that area or they are located in areas separated from the main clusters of events. In either case, there are insufficient data to determine their mechanisms definitively.

The revised epicenters, location and orientation of fault-plane solutions, and the resulting event groups for each solution, are shown in figure 7.7. The new epicenters have generally shifted less than 2 or 3 km from their former positions. Consequently, areas of concentrated activity have remained unchanged from those shown in figure 7.3. The strikes of the nodal planes, however, are significant when compared to those of the mapped surface fault traces.

Although fault-plane solutions are not unique, inasmuch as displacement along either plane can produce the observed first motions, the predominant patterns of observed faulting provide some constraints on the orientation of the preferred plane. Those planes closely paralleling the observed trends are chosen as the preferred solutions. Sense and direction of displacements from these mechanisms generally agree with observed or inferred displacements along the associated fault zones.

Along the Newport-Inglewood fault trend, the fault plane is nearly vertical, dipping slightly southwest, and

is characterized by predominant right-lateral strike slip with a secondary component of normal dip-slip ground displacement (fig. 7.6). This solution closely resembles that determined by Teng and others (1977), except the preferred plane in their solution dips slightly toward the northeast.

The focal mechanisms from the Elysian Park-Repetto Hills extension of the Whittier fault zone show a steep northeast-dipping fault plane with nearly equal components of normal dip-slip and right-lateral strike-slip ground displacement (fig. 7.6). Immediately to the north, near the junction with Santa Monica-Hollywood-Raymond Hill fault trend, the interpretation is more complex. Either fault plane is possible, as both lie subparallel to existing faults. However, in the case of the northwest-trending plane, the solution trend is more northward than the observed fault trend. Furthermore, use of this plane would call for a reversal in dip along the observed trend from south to north, as indicated by the preceding mechanism, thereby demanding greater structural complexity.

The preferred solution is the northeast-trending fault plane, which lies nearly parallel to the Santa Monica-Hollywood-Raymond Hill fault trend. This solution is in better agreement with the observed fault trend than the

TABLE 7.3.—Revised hypocenters—Continued

Origin time in Greenwich Civil Time (GCT):

YEAR, MON (month), DY (day), HR (hour), MN (minute), and SEC (second).

Epicenter in degrees and minutes of north latitude (LAT N) and west longitude (LONG W).

DEPTH, depth of focus in kilometers.

MAG, Richter local magnitude (M_L) of the earthquake.

NO, number of stations used in locating earthquake.

GAP, largest of azimuthal separation in degrees between stations.

D₃, epicentral distance in kilometers to the third nearest station.

RMS, root-mean-square error of the time residuals: $RMS = [\sum_i (R_i^2 / NO)]^{1/2} \cdot R_i$ is the observed seismic-wave arrival time minus the computed time at the i^{th} station.

ERH, standard error of the epicenter in kilometers: $ERH = [SDX^2 + SDY^2]^{1/2}$.

SDX and SDY are the standard errors in latitude and longitude, respectively, of the epicenter.

ERZ, standard error of the focal depth in kilometers.

QH, solution quality of the hypocenter. This measure is intended to indicate the general reliability of each solution and is based on the longest axis (L) of the error ellipsoid:

QH	L (km)
A	L ≤ 2.5
B	2.5 < L ≤ 5.0
C	5.0 < L ≤ 10.0
D	L > 10.0

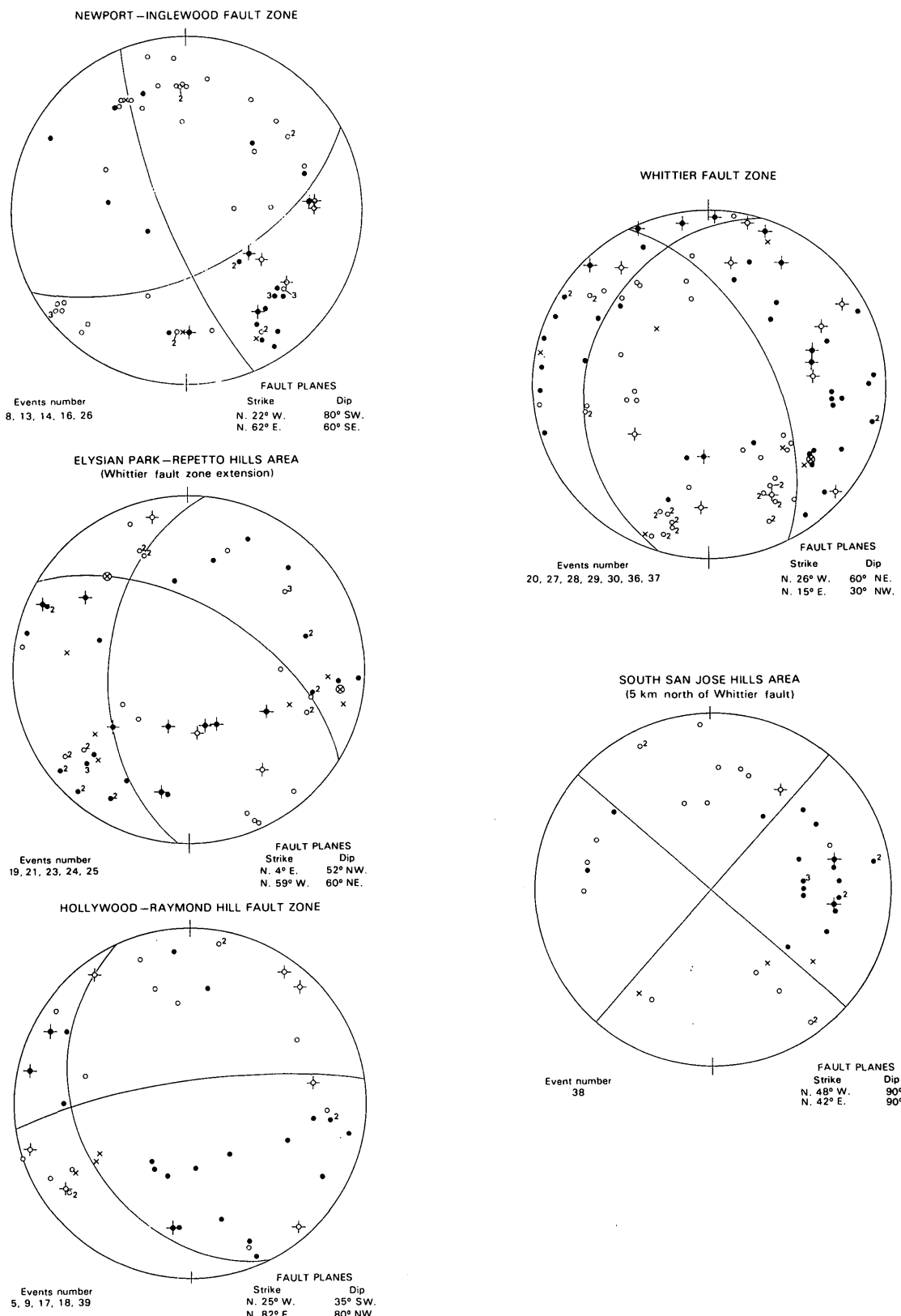


FIGURE 7.6.—Lower hemisphere equal-area projections of first-motion data and fault-plane solutions. Circle, dilatation; dot, compression; multiple readings indicated by numbers; X, nodal point; cross superimposed on symbol indicates emergent (poor) arrival. Listed with each diagram are identification numbers, found in table 7.3, of the events used in each composite solution; see also figure 7.7.

northwest-trending plane and shows a steep north-dipping fault plane with predominant reverse dip-slip and a secondary component of left-lateral strike-slip displacement. Worth noting, however, is that the earthquake epicenters tend to lie south of the mapped fault trace. Associated subsurface fault strands that lie to the south of the main trace are evident from borehole data.

Along the Whittier fault zone and the Workman Hill fault extension, the preferred mechanism (fig. 7.6) shows a fault plane dipping steeply northeast with predominantly normal displacement and a minor component of right-lateral slip. This is in contrast to the predominant reverse displacement observed to the southeast along the Whittier fault.

Farther east in the south San Jose Hills the largest event in the data set ($M_L = 4.0$) shows a strike-slip displacement, if oriented parallel to the Whittier trend. The epicenter, however, lies about 5 km northeast of the Whittier fault zone. The complementary plane lies subparallel to the San Jose fault and, therefore, ground displacement may be purely left-lateral along this fault. This solution appears likely, as focal mechanisms determined for events farther east along this trend are very similar (Cramer and Harrington, this volume).

DISCUSSION AND CONCLUSIONS

As pointed out by McKenzie (1969), fault-plane solutions do not necessarily reveal the orientation of the current regional stress field responsible for the observed seismic activity. Preexisting faults may strongly influence the failure pattern that might otherwise have developed in a more homogeneous medium. But knowledge of the senses and directions of displacements along principal fault trends does provide some insight into the general form of regional deformation.

All principal compression axes (P -axes) of the focal mechanisms are oriented between N. 22° W. and N. 25° E., suggesting a strong north-south component of regional compression. Consistent with the pronounced lateral component of displacement indicated by focal mechanisms, plunge of the P -axes is shallow, ranging from 0° (San Jose Hills) to about 30° (Newport-Inglewood and Santa Monica-Hollywood-Raymond Hill faults). The P -axes plunge much more steeply (50° – 70°) along the northern extension of the Whittier trend, where nearly horizontal east-west tensional stresses give rise to normal displacement (fig. 7.6).

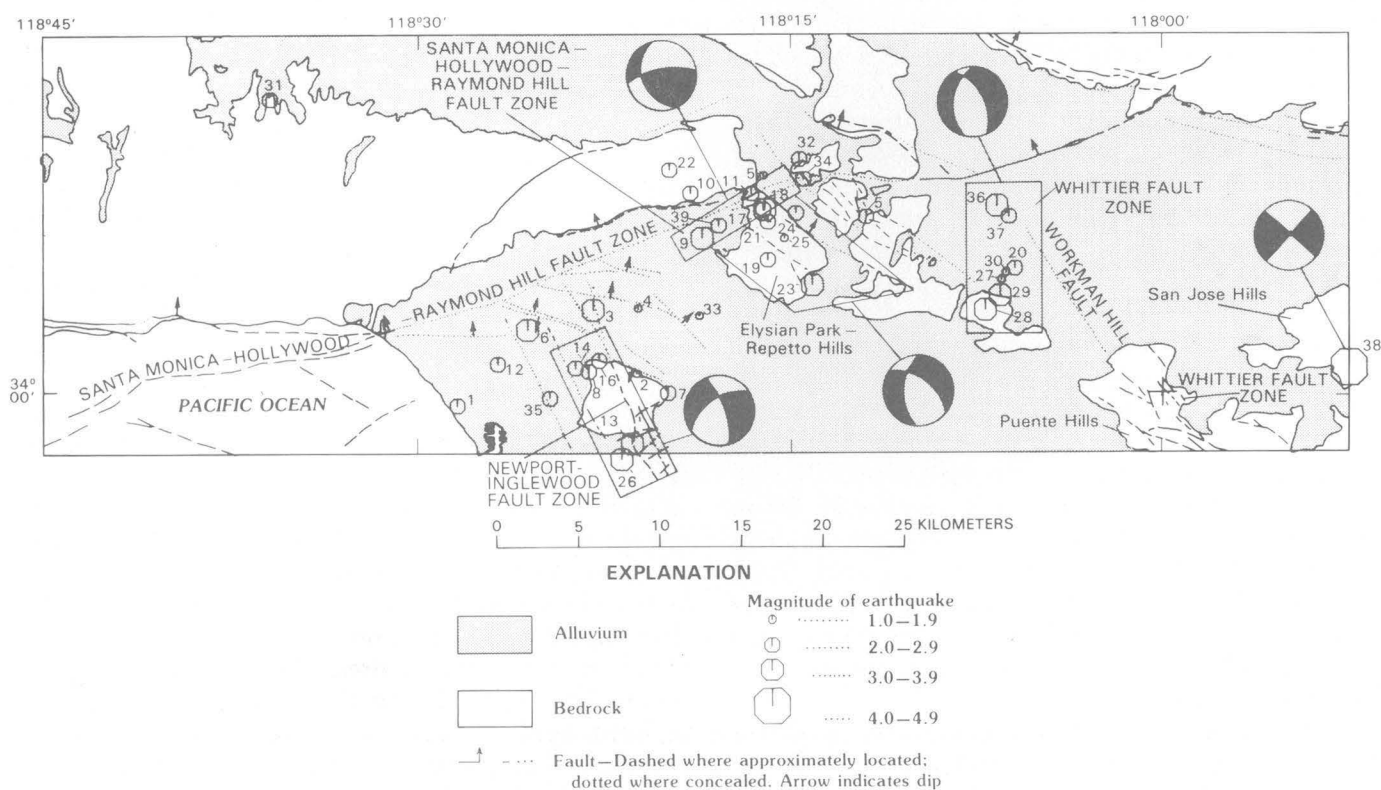


FIGURE 7.7.—Revised earthquake locations and focal mechanisms.

TABLE 7.4.—Average root-mean-square (RMS) time residuals and standard distance (ERH) and depth (ERZ) errors for relocated events according to quality class

Quality class	RMS	ERH	ERZ	Number of events
A	0.14	1.13	1.44	27
B	0.16	2.46	3.01	7
C	0.33	2.88	7.66	5

Deformation along the Newport-Inglewood and Whittier fault zones has been attributed to right-lateral wrench-style faulting (Harding, 1973; Wilcox and others, 1973). This structural style is characterized by a series of en echelon anticlines and synthetic faults. Fault strands within a wrench zone are often anastomosing, giving rise to strike-slip, normal, and reverse displacements.

Dip-slip movements result from local tensional or compressional stresses acting across the fault zone when the trend of a strike-slip fault changes. For a right-lateral strike-slip fault, deviation of the fault trend toward the right imparts a tensional stress across the fault, resulting in oblique divergent wrenching, whereas deviations toward the left impart a compressional stress, characterized by oblique convergent wrenching (Wilcox and others, 1973).

Normal displacements can also arise from keystone faulting on the anticlinal crests. Microearthquakes associated with this type of faulting would probably have shallow focal depths (1–2 km). Antithetic faults also develop along wrench zones, but generally are subdued since they are opposed to the regional tectonic grain. Their oblique trend across the regional stress field may result in a significant component of reverse displacement.

The focal mechanisms determined from this study, and their associated fault zones, mutually conform to right-lateral wrenching. In fact, much of the gross structure in the northern Peninsular Ranges and Transverse Ranges can be attributed to wrenching, if one assumes that the regional stress field is generated by movement along the San Andreas fault system.

Over much of its length the San Andreas fault trends N. 30° – 40° W. Across the eastern edge of the Transverse Ranges, this trend deviates to the west to about N. 70° W. The north-south compressional stresses acting across the Transverse Ranges have been attributed to this bend (Benioff, 1955; Rodgers and Chinnery, 1969, 1973; Rodgers, 1975). Thus, recent tectonism in this region probably represents crustal yielding from large-scale oblique convergent wrenching along the North American-Pacific plate boundary.

Other faults in the Peninsular Ranges, subparallel to the general trend of the San Andreas fault, are responding to the relative plate motion in a similar manner on

a smaller scale. As their trends turn westward, a reverse component of displacement arises, while northward shifts in the fault azimuths give rise to a normal component of displacement.

The Newport-Inglewood and Whittier fault zones both veer north at their northern extremities, which probably accounts for the observed normal components of microearthquake mechanisms along these zones (fig. 7.6). Where faults of the Whittier zone trend more to the north, such as the Workman Hill fault, the focal mechanism is predominantly normal.

Consistent with this pattern, the expected sense of displacements along northeast-trending faults such as the frontal system, including the Santa Monica, Hollywood, and Raymond Hill faults, is reverse left oblique. The reverse component of faulting might reasonably be expected to predominate, accommodating crustal shortening resulting from the regional north-south compressive stress. The mechanism of the February 21, 1973, Point Mugu earthquake, 40 km west of the study area (Ellsworth and others, 1973), and its aftershocks (Stierman and Ellsworth, 1976) and the focal mechanism of microearthquakes along the Santa Monica-Hollywood-Raymond Hill fault zone (fig. 7.6) and Cucamonga fault zone 20 km east of the study area (Cramer and Harrington, this volume), support this predominant sense of displacement.

The regional pattern of deformation in the study area can be summarized by the relative motions of major fault blocks. Responding to northward movement of the Pacific plate, fault blocks in the northern Peninsular Ranges are moving northwest along a series of northwest-trending, right-lateral, strike-slip faults. Most of the relative movement between the Pacific and North American plates is occurring along the San Jacinto and San Andreas faults, with increasingly smaller relative block displacements westward along the Whittier and Newport-Inglewood faults. A broad region of north-south compression across the Transverse Ranges results from a westward shift in the trend of the San Andreas fault. The frontal fault system forms a principal southern boundary along which the Transverse Ranges block is being elevated and forced westward in response to this crustal shortening.

Because of the much smaller region over which the com-

pressive stresses act, crustal strain is more concentrated at the eastern end of the Transverse Ranges block. This is supported by the relatively higher seismic-strain release and physiographic relief at the eastern extent of the frontal fault system (Allen and others, 1965; Hileman and others, 1973; Cramer and Harrington, this volume). Farther west, other thrust faults to the north, such as the San Fernando-Sierra Madre, are helping to accommodate the compressive strain.

What appears clear is that the frontal fault system plays an active role in crustal deformation in this region. Although the likelihood of large fault displacements appears greater along the eastern extremity, the February 21, 1973, Point Mugu earthquake manifests the potential for generating a damaging earthquake along the western extent. Situated between these extremes, the Santa Monica-Hollywood-Raymond Hill fault zone, in view of its proximity to metropolitan Los Angeles and the associated hazard potential, cannot be ignored. Results of this study indicate the probability that segments of this fault zone are seismically active and, considering their extent and relationship to regional crustal deformation, that they may be capable of generating damaging earthquakes.

REFERENCES CITED

- Allen, C. R., St. Amand, Pierre, Richter, C. F., and Nordquist, J. M., 1965, Relationship between seismicity and geologic structure in the southern California region: *Seismological Society of America Bulletin*, v. 55, no. 4, p. 753-797.
- Allen, C. R., and Whitcomb, J. H., 1977, Second quarterly and semi-annual report summary, 1 October 1976 to 31 March 1977: U.S. Geological Survey Summaries of Technical Reports, v. IV, p. 35-38.
- Benioff, Hugo, 1955, Relation of the White Wolf fault to the regional tectonic pattern, in Oakeshott, G. B., ed., *Earthquakes in Kern County, California, during 1952*: California Division of Mines and Geology Bulletin 171, p. 203-204.
- Buika, J. A., and Teng, T. L., 1978, Recent seismicity and fault-plane solutions of the Santa Monica Mountains, Santa Monica Bay, and northern Los Angeles basin: Geologic guide and engineering geology case histories Los Angeles metropolitan area, in Association of Engineering Geologists First Annual California Section Conference: p. 64-72.
- Castle, R. O., Church, J. P., and Elliott, N. R., 1976, Aseismic uplift in southern California: *Science*, v. 192, p. 251-253.
- Ellsworth, W. L., Campbell, R. H., Hill, D. P., Page, R. A., Alewine, R. W., III, Hanks, T. C., Heaton, T. H., Hileman, J. A., Kanamori, H., Minster, B., and Whitcomb, J. H., 1973, Point Mugu, California, earthquake of 21 February 1973 and its aftershocks: *Science*, v. 182, p. 1127-1129.
- Friedman, M. E., Whitcomb, J. H., Allen, C. R., and Hileman, J. A., 1976, Seismicity of the southern California region, 1 January 1972 to 31 December 1974: California Institute of Technology Seismological Laboratory, 397 p.
- Fuis, G. S., Friedman, M. E., and Hileman, J. A., 1977, Preliminary catalog of earthquakes in southern California, July 1974-September 1976: U.S. Geological Survey Open File Report 77-181, 107 p.
- Harding, T. P., 1973, Newport-Inglewood trend, California, an example of wrenching style of deformation: *American Association of Petroleum Geologists Bulletin*, v. 57, p. 97-116.
- Hileman, J. A., Allen, C. R., and Nordquist, J. M., 1972, Seismicity of the southern California region 1, January 1932 to 31 December 1972: California Institute of Technology, Seismological Laboratory, 397 p.
- Hill, R. L., Sprotte, E. C., Chapman, R. H., Chase, G. W., Bennett, J. H., Real, C. R., Slade, R. C., Borchardt, G., and Weber, F. H., Jr., 1979, Earthquake hazards associate with faults in the greater Los Angeles metropolitan area, Los Angeles County, California, including faults in the Santa Monica-Raymond, Verdugo-Eagle Rock, and Benedict Canyon fault zones: California Division of Mines and Geology Open-File Report 79-16 LA, p.
- Holden, E. S., 1897, Catalog of earthquakes on the Pacific coast, 1796-1897: Smithsonian Miscellaneous Collection no. 1087 (v. 37, no. 5), 253 p.
- Jahns, R. H., 1973, Tectonic evolution of the Transverse Ranges province as related to the San Andreas fault system, in Kovach, R. L., and Nur, A., eds., *Proceedings of the Conference on Tectonic Problems of the San Andreas Fault System*, Stanford University Publications, Geological Sciences, v. XIII, p. 149-170.
- Kanamori, H., 1976, Earthquake prediction studies in southern California; Research in progress: U.S. Geological Survey Open-File Report 76-456, p. 80-91.
- Kanamori, H., and Hadley, D., 1975, Crustal structure and temporal velocity change in southern California: *Pure and Applied Geophysics*, v. 113, p. 257-380.
- Lahr, J. C., 1979, HYPOELLIPSE: A computer program for determining local earthquake hypocentral parameters, magnitude, and first motion pattern: U.S. Geological Survey Open-File Report 79-431, 232 p.
- Lamar, D. L., 1972, Microseismicity and recent tectonic activity in Whittier fault area, California: *Earth Science Research Corporation*, 44 p.
- Lee, W. H. K., and Lahr, J. C., 1975, HYPO71 (revised): A computer program for determining hypocenter, magnitude, and first motion pattern for local earthquakes: U.S. Geological Survey Open-File Report 75-311, 113 p.
- McKenzie, D. P., 1969, The relation between fault plane solutions for earthquakes and the directions of the principal stresses: *Seismological Society of America Bulletin*, v. 59, no. 2, p. 591-601.
- Press, Frank, 1960, Crustal structure in the California-Nevada region: *Journal of Geophysical Research*, v. 65, p. 1039-1051.
- Rodgers, D. A., 1975, Deformation, stress accumulation, and secondary faulting in the vicinity of the Transverse Ranges of southern California: *Providence*, R. I., Brown University, Ph. D. dissertation.
- Rodgers, D. A., and Chinnery, M. A., 1969, Displacements and strains associated with a curved strike-slip fault: *Eos (American Geophysical Union Transactions)*, v. 50, p. 238.
- , 1973, Stress accumulation in the Transverse Ranges, southern California, in Kovach, R. L., and Nur, A., eds., *Proceedings of the Conference on Tectonic Problems of the San Andreas Fault System*, Stanford University Publications, Geological Sciences, v. XIII, p. 70-79.
- Savage, J. C., and Prescott, W. P., 1977, Geodimeter measurements on the Palmdale Bulge, 1959-1977: *Eos (American Geophysical Union Transactions)*, v. 58, n. 12, p. 1121.
- Stierman, D. J., and Ellsworth, W. L., 1976, Aftershocks of the February 21, 1973 Point Mugu, California, earthquake: *Seismological Society of America Bulletin*, v. 66, no. 6, p. 1931-1952.
- Teng, T. L., Henyey, R. L., Manov, D., and Lo, C., 1977, Seismic network development and monitoring in the greater Los Angeles basin and its offshore area: U.S. Geological Survey Summaries of Technical Reports, v. IV, p. 195-199.
- Teng, T. L., Real, C. R., and Henyey, R. L., 1973, Microearthquakes and water-flooding in Los Angeles: *Seismological Society of America Bulletin*, v. 63, p. 859-875.
- Thatcher, W., 1976, Episodic strain accumulation in southern California: *Science*, v. 194, p. 691-695.

- Toppozada, T. R., Higgins, C. H., and Parke, D. L., 1978, Earthquake catalog of California 1900-1981: California Division of Mines and Geology Special Report 135.
- Townley, S. D., and Allen, M. W., 1939, Descriptive catalog of earthquakes of the Pacific coast of the United States 1769-1928: Seismological Society of America Bulletin, v. 29, p. 1-297.
- Whitcomb, J. H., Allen, C. R., Garmany, J. D., and Hileman, J. A., 1973, San Fernando earthquake series, 1971 focal mechanisms and tectonics: Review of Geophysics and Space Physics, v. 11, no. 3, p. 693-730.
- Wilcox, R. E., Harding, T. P., and Seely, D. R., 1973, Basic wrench tectonics: American Association of Petroleum Geologists, v. 57, no. 1, p. 74-96.
- Wood, H. O., 1916, California earthquakes: Seismological Society of America Bulletin, v. 6, p. 55-180.

8. RECURRENT HOLOCENE DISPLACEMENT ON THE JAVON CANYON FAULT—A COMPARISON OF FAULT-MOVEMENT HISTORY WITH CALCULATED AVERAGE RECURRENCE INTERVALS

By A. M. SARNA-WOJCICKI, K. R. LAJOIE, AND R. F. YERKES

ABSTRACT

The Javon Canyon fault is an east-trending, south-dipping, high-angle reverse fault well exposed in Javon Canyon northwest of Pitas Point in the western Transverse Ranges of California. The fault offsets a stream terrace and bedrock channel graded to a low emergent Holocene marine terrace and platform dated at about 3,500 yr B.P. by ^{14}C . The fault also offsets a higher late Pleistocene marine terrace and platform dated at about 45,000–50,000 yr B.P. by amino-acid racemization and uranium-series methods on mollusk shells. By dividing total vertical displacement (throw) of each offset platform by its age, similar rates of about 1.1 mm/yr are obtained for long-term vertical displacement, suggesting that the average strain rate on this fault has been relatively constant from about 50,000 to 3,500 yr B.P. Structural-stratigraphic relations of the units in the footwall of the fault in Javon Canyon indicate that at least four, and probably five, displacement events occurred on this fault within the last 3,500 yr. A history of late Holocene activity is derived for this fault from individual measured throws associated with each of the five inferred events, total measured throw, the long-term strain rate, and the 3,500-yr age of the stream-terrace platform. This history is compared to a calculated average recurrence interval, throw, and estimated upper-bound magnitude, a common approach in other fault recurrence studies where single-event displacements are not known. The calculated average recurrence interval, throw, and magnitude underestimate the maximum capability of the fault derived from its history of individual events.

INTRODUCTION

In many studies of active faults, the amount of movement during individual prehistoric slips related to discrete seismic events cannot be determined. Instead, a more generalized analysis of the past movement history of an active fault usually is all that can be determined on the basis of available data. In order to assess the activity of a fault, stratigraphic and geomorphic offsets representing several events are measured to determine total displacement over a specific amount of time—usually measured by radiometric or other age determinations of offset markers. An average recurrence interval can be obtained by dividing a representative single-event displacement, commonly one recorded in historical time for the fault in

question, into the total measured offset to obtain an estimate of the number of events occurring during the measured time. This number is then divided into the previously determined interval of time to obtain an average recurrence interval. In the absence of other evidence regarding the detailed past history of a fault, this information is used in assessing the anticipated future potential of a fault. Such assessments may include estimates of expected upper-bound magnitudes of earthquakes determined from relations between fault displacements, lengths, and magnitudes compiled from worldwide data (for example, by using curves of Bonilla and Buchanan, 1970).

This approach can lead to erroneous conclusions regarding the anticipated behavior of a fault if (1) the single-event displacement used in the calculation is not representative of the fault's behavior, (2) displacements for individual events range widely, (3) the long-term rate of strain on the fault in question has changed through time, or (4) aseismic creep is involved in fault movement.

The purpose of this report is (1) to document recurrent prehistoric Holocene displacements on the Javon Canyon fault, and (2) to compare the derived fault-movement history with a calculated average recurrence interval, displacement, and estimated upper-bound magnitude.

The Javon Canyon fault is an east-trending, south-dipping, high-angle reverse fault, well exposed in Javon Canyon, about half a kilometer northeast (inland) of the Santa Barbara Channel coastline, northwest of Pitas Point, in the western Transverse Ranges of California (fig. 8.1). A long-term, average rate of displacement on this fault is determined from measured offsets of two independently dated reference planes cut by the fault: namely, a Holocene stream terrace graded to an emergent marine-terrace platform, and a late Pleistocene marine-terrace platform. In Javon Canyon, evidence of recurrent Holocene movement is obtained from several superposed debris aprons produced at the ground surface by repeated collapse of the hanging wall of the fault after fault movement. Intervals between fault movements are estimated

Manuscript received for publication on September 3, 1980.

by using the following criteria: (1) the long-term average rate of displacement derived from offset of dated terrace platforms; (2) the total measured offset of the Holocene stream terrace; (3) estimated throws for individual events; and (4) the age of the marine terrace platform to which the Holocene stream terrace is graded. These intervals and events represent a history of displacement on the fault. The calculated intervals have been compared to an average recurrence interval calculated solely from the number of events and total displacement over the same period of time. The inferred history of movement,

amounts of displacement, and associated magnitudes differ substantially from the calculated average recurrence interval, displacement, and inferred magnitude.

REGIONAL GEOLOGIC SETTING

The western Transverse Ranges, in which the Javon Canyon fault is located, are characterized by structures indicating north-south crustal compression. Faults generally trend eastward, have reverse displacements, and dip to both the north and the south. Fold axes trend

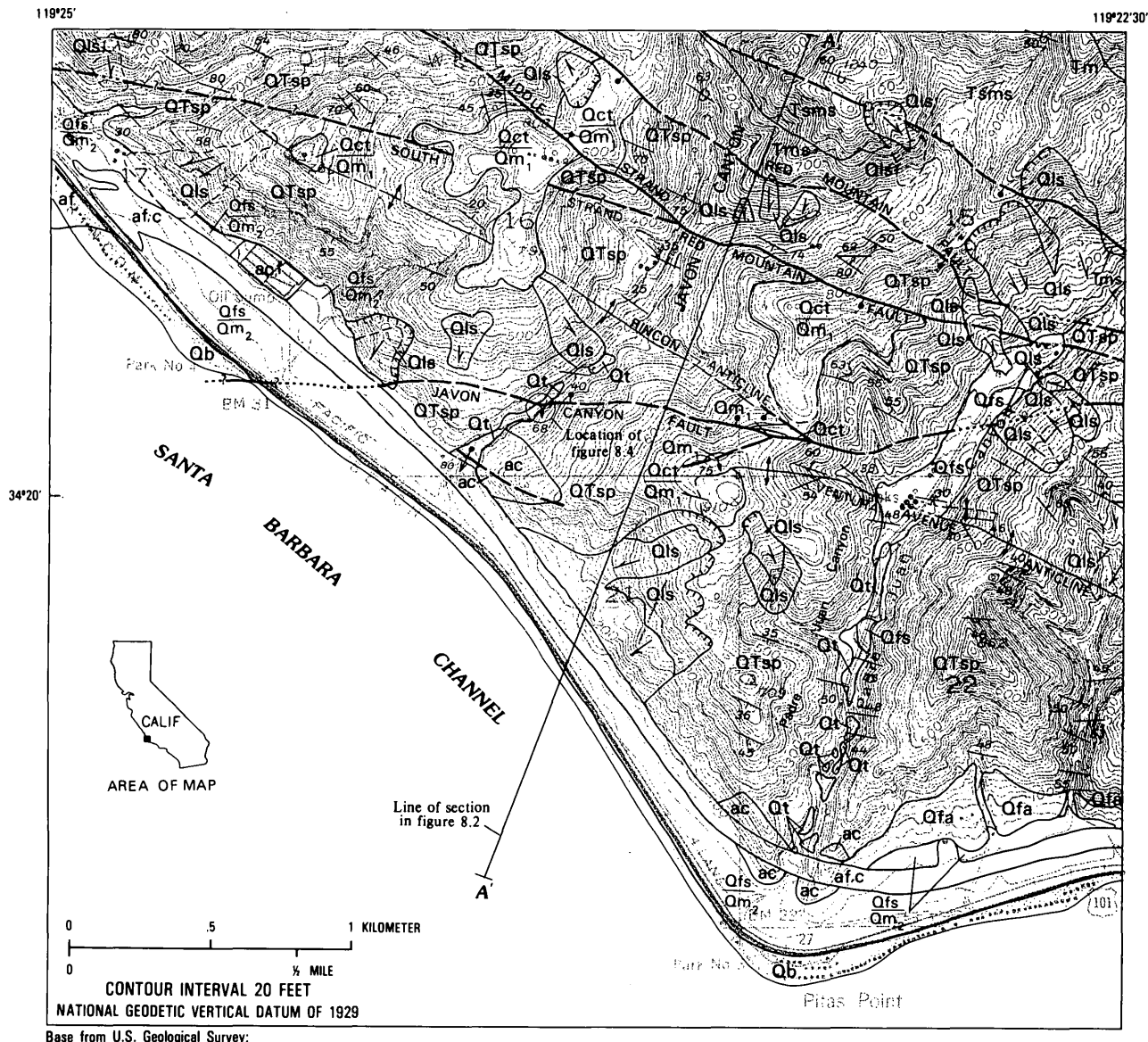
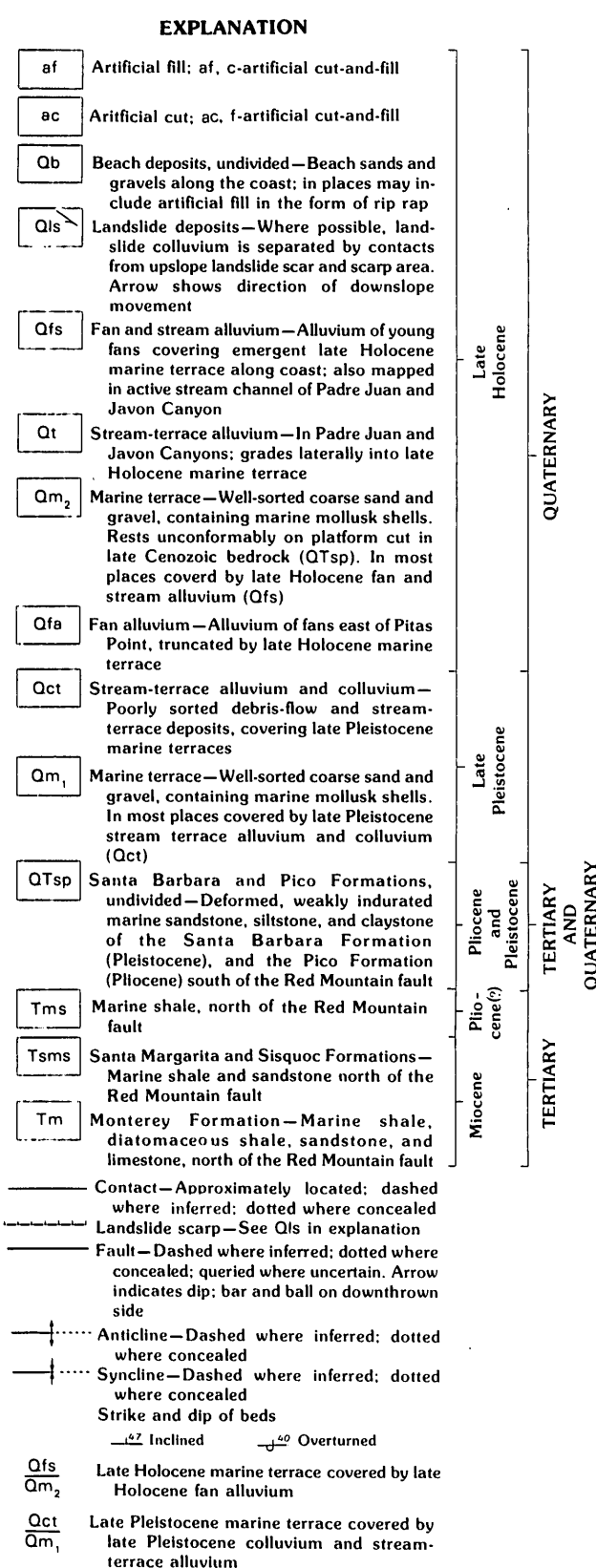


FIGURE 8.1.—Geology of the Pitas Point area in the vicinity of Javon Canyon. Quaternary geology mapped by Sarna-Wojcicki, 1976–78. Bedrock geology, faults, and landslides modified in part from Weber and others (1973). Stratigraphic nomenclature and age assignments from Weber and others (1973).

Base from U.S. Geological Survey;
Pitas Point, 1950, 1:24,000



easterly. The region is seismically active, and first-motion studies of earthquake hypocenters within the region indicate predominantly reverse motion on north-dipping, high-angle reverse faults, with a subordinate left-lateral component (Lee and others, 1979; Yerkes and Lee, 1979). Geodetic studies indicate that the region is undergoing rapid vertical uplift of as much as 10 mm/yr (Buchanan-Banks and others, 1975). This uplift rate is comparable with rates calculated from uplift of dated marine-terrace platforms (Yerkes and others, this volume; Wehmiller and others, 1978) and with rates calculated from deformation of late Cenozoic bedrock (Yeats, 1977; Sarna-Wojcicki and others, 1979). This high uplift rate probably indicates a vertical component accompanying rapid north-south crustal compression.

LOCAL GEOLOGIC SETTING OF THE JAVON CANYON FAULT AND OFFSETS OF LATE PLEISTOCENE AND HOLOCENE TERRACES

Within the study area (fig. 8.1), the Javon Canyon fault cuts late Cenozoic bedrock of the Pliocene and Pleistocene marine Pico Formation and Pleistocene marine Santa Barbara Formation (Weber and others, 1973; Sarna-Wojcicki, unpub. data, 1980). These bedrock units are folded into the east-plunging Rincon anticline, and the Ventura Avenue anticline. The Javon Canyon fault separates the Rincon from the Ventura Avenue anticlines (fig. 8.1). Structurally, the bedrock of this area is bounded on the north by the Red Mountain fault, a north-dipping, seismically active reverse fault which separates Pico and younger strata on the south from older Tertiary sedimentary formations to the north. To the south, this block is bounded by several high-angle, east-trending faults in the Santa Barbara Channel (Greene, 1976; Hoyt, 1976), the largest of which is the Pitas Point fault (not shown). The Pitas Point fault is an offshore extension of the north-dipping, high-angle reverse Ventura fault mapped onland in the area of Ventura (Sarna-Wojcicki and others, 1976; Yerkes and others, this volume). The upper Cenozoic bedrock is also cut by a number of smaller southeast-trending faults, the most prominent of which are the south and middle strands of the Red Mountain fault (fig. 8.1).

The Javon Canyon fault may be the onshore continuation of one of two offshore faults (not shown) mapped in the Santa Barbara Channel by Hoyt (1976), either the North fault, or a smaller, unnamed fault about 1½ km south of the North fault. Both faults have the same up-on-the-south sense of movement as the Javon Canyon fault, but would require some change in trend to connect with it.

The Javon Canyon fault is best exposed (1) in Javon Canyon, about half a kilometer northeast of the Santa Barbara Channel, and (2) at the ridgeline between Padre

FIGURE 8.1.—Continued.

Juan and Javon Canyons, about a kilometer east of the mouth of Javon Canyon (fig. 8.1). It is concealed between these two localities by soil creep, landslides, and vegetation. The fault is also obscured by soil and landslides to the east of the ridge. West of Javon Canyon, the fault shows up as a faint lineation on aerial photographs in a landslide and in bedrock in the valley wall northwest of Javon Canyon. It cannot be traced farther west in the flatlands adjacent to the coast, because it is covered by young alluvial fans derived from the steep hillside adjoining the flatlands. The fault apparently trends out into the Santa Barbara Channel in the vicinity of BM 31 (fig. 8.1), where Holocene marine terrace gravels exposed in a low roadcut along the coastal highway terminate abruptly and are bounded on the north by nonmarine fan alluvium. Good exposures at this locality are lacking owing both to recent alluviation and to extensive grading for coastal highways.

Two prominent marine-terrace platforms are cut into the steeply dipping upper Cenozoic bedrock within the study area (fig. 8.1). Remnants of a late Pleistocene marine terrace (Qm_1) cap ridgecrests between Punta Gorda, northwest of the area of figure 8.1, and Pitas Point. The terrace platform rises from an elevation of about 120 m at Punta Gorda to about 210 m at a point 5 km to the southeast on the Javon-Padre Juan ridge above Pitas Point. About a kilometer east of Padre Juan Canyon lag boulders from this terrace are found at an elevation of 363 m above sea level on a ridgecrest. To the northwest of Punta Gorda this terrace may be correlative to the Carpinteria terrace (Putnam, 1942), which descends from about 60 m above Rincon Point to beneath sea level 5 km to the northwest of Carpinteria. Maximum elevations of this terrace in the vicinity of Padre Juan Canyon roughly coincide with the anticlinal axis in the upper Cenozoic bedrock and indicate continued folding in late Pleistocene time. Fossil mollusk shells collected from the basal marine sands and gravels of this terrace at several localities in the study area yield amino-acid age estimates of about 45,000 yr (Wehmiller and others, 1978). Kaufman and others (1971) published U-series data on mollusks from one of these localities that yield an age of about 50,000 yr. The cool-water types of molluscan fauna from this terrace (Putnam, 1942) are consistent with the middle Wisconsinan age implied by the amino-acid and U-series data. We correlate this fauna and terrace with the 40,000–50,000-yr old middle Wisconsinan sea-level highstand recorded by coral reefs on New Guinea and the Barbados (Bloom and others, 1974).

This 45,000-yr-old marine terrace is offset by a number of faults: the Red Mountain, the Padre Juan, and several unnamed smaller faults, as well as the Javon Canyon fault. The Javon Canyon fault offsets the terrace platform

(Qm_1) vertically by 42 to 49 m (fig. 8.2). Dividing this throw by the 45,000-yr age of the marine platform, we obtain a minimum average long-term displacement rate of 0.9 to 1.1 mm/yr.

A second, younger marine-terrace platform (Sea Cliff bench of Putnam, 1942) is incised into the upper Cenozoic bedrock along the coast between Pitas Point and Punta Gorda, at elevations of 6 m to about 35 m above sea level, south of the older terrace (fig. 8.1). Six radiocarbon ages on marine mollusk shells from littoral to sublittoral sand and gravel on this terrace platform, and from shells of *Pholas* extracted from bored boulders in this terrace deposit (Qm_2) range from 1,820 to 5,535 yr and average about 3,500 yr (table 8.1). These data indicate that this part of the coast has been rising rapidly relative to sea level since about 5,000 yr B.P., when sea level reached its present position following the post-Wisconsinan rise. These observations are independently confirmed by historical geodetic data which indicate uplift rates of about 10 mm/yr along the coast (Buchanan-Banks and others, 1975). Stream terraces in Javon and Padre Juan Canyons grade to this emergent Holocene marine terrace, and are consequently coeval. Aggradation of stream-terrace alluvium in Javon and adjacent canyons was a response to the rapid rise of sea level in post-Wisconsinan time. Incision of streams into stream-terrace alluvium in these canyons occurred sometime after the rate of sea-level rise decreased significantly relative to the tectonic uplift rate of the coast.

In Javon Canyon, the Javon Canyon fault offsets the stream-terrace platform and gravel about 4 m (figs. 8.3 and 8.4). Dividing this displacement (4 m) by the approximate age of the marine terrace (3,500 yr; average of six ^{14}C age determinations) gives an average displacement rate of 1.1 mm/yr. The close agreement in average long-term displacement rates calculated from offsets of the two terrace platforms (0.9 to 1.1 mm/yr, and 1.1 mm/yr, respectively) suggests that strain accumulation on the Javon Canyon fault has been fairly constant over roughly the last 50,000–3,500 yr. In addition to the strain rate calculated for the Javon Canyon fault from offset of the two independently dated marine terraces, an assumption of a constant strain accumulation on the fault seems reasonable if the faulting is a response to constant crustal compression.

Evidence for constant crustal compression is obtained from another line of evidence. The rate of folding on the Venura Avenue anticline in the vicinity of the study area, as expressed by the vertical component of uplift, has been fairly constant over the last 50,000 yr. This rate was calculated from rates of uplift of the late Pleistocene (45,000–50,000 yr) and Holocene (1,800–5,500 yr) marine-terrace platforms in the vicinity of the anticlinal axis

TABLE 8.1.—Radiocarbon ages on mollusks from emergent late Holocene terrace in vicinity of Javon Canyon between Pitas Point and Punta Gorda

[All dates have been corrected for -700-yr reservoir effect]

Sample No.	Lab. No.	Age (yr B.P.)	Material dated	Locality
M7300	UM-1585 ¹	2,740±75	Pholad	Punta Gorda
M7295	UM-1586	5,535±110	Tivela	Punta Gorda
M7228	USGS-400 ²	1,820±40	Tivela	Near mouth of Javon Canyon
M7228	USGS-401	3,090±40	Pholad	Near mouth of Javon Canyon
M7297	UM-1465	4,155±90	Pholad	Pitas Point
M7472	UM-1800	3,790±95	Protothaca	East of Pitas Point
Bag 1	UM-1084	1,805±345	Carbonized wood and plants	Holocene terrace in Javon Canyon

¹University of Miami Radiocarbon Laboratory.

²U.S. Geological Survey Radiocarbon Laboratory, Menlo Park.

(Sarna-Wojcicki and others, 1979). Maximum rates of uplift obtained on the basis of both geologic and geodetic measurements are about 10–15 mm/yr.

EVIDENCE FOR RECURRENT HOLOCENE DISPLACEMENT ON THE JAVON CANYON FAULT IN JAVON CANYON

The excellent natural exposure of the Javon Canyon fault in Javon Canyon (fig. 8.3) reveals a history of recurrent movement in late Holocene time. The exposure is at the bottom of the canyon, in the wall of an incised meander of the stream. Figure 8.4 is a profile of the fault exposure in Javon Canyon. The fault strikes N. 82° W. and dips 68° S. The fault plane is clearly expressed and juxtaposes stream-terrace gravels and sands against poorly indurated, sheared, sandy and clayey bedrock of the Pico or Santa Barbara Formations. A clayey gouge, 1 to 4 cm thick, is smeared out along the fault plane. Striations exposed on the fault plane are parallel to the dip, but may record only the last displacement—or possibly postfaulting

backsliding of the hanging wall. Total vertical separation of the stream-terrace gravels and bedrock platform on which they rest is 4 m.

Three or four superposed aprons of angular bedrock debris lie in the footwall of the fault directly beneath the hanging wall. We interpret these debris aprons as being composed of material derived by collapse of the hanging wall following discrete displacement events on the fault. We adopt this interpretation for several reasons. The debris aprons are composed of chaotically jumbled unsorted, angular clasts and matrix of bedrock, both sandstone and claystone. The superposed debris aprons are separated from each other by thin, roughly horizontal beds and lenses of terrace sand, gravel, or colluvium, indicating that periods of debris-apron formation were separated by episodes of stream erosion and deposition. From this we conclude that activity on the fault was sporadic rather than continuous (as in creep). The bedrock material in the hanging wall of the fault—sheared, poorly indurated sandstone and claystone—is so poorly consolidated that it could not support a wall overhanging at 68°. We infer that each

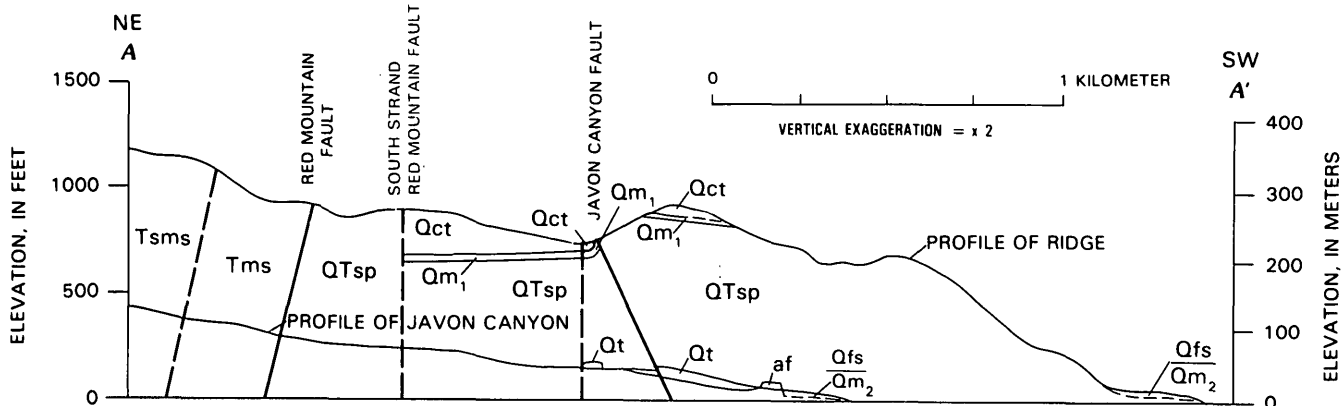


FIGURE 8.2.—Relationships of faults to Quaternary terraces. Profiles of Javon Canyon and of the ridge just to the southeast are projected onto a vertical plane represented by line A-A' on figure 8.1. Faults and formation contacts exposed along these two profiles are also projected onto this plane. Formation symbols are shown in figure 8.1.

debris apron was formed immediately after fault movement by collapse of the overthrust hanging wall.

We estimate that four or five events have taken place on this fault within the last 3,500 yr. The first event, represented by unit 1 in figure 8.4, is inferred from the small fault offset of the bedrock platform northeast of the main fault. This small fault can be traced only in the lower half meter of the terrace gravel and does not appear to reach the level of the lowest debris apron (unit 2 in fig. 8.3). Consequently, event 1 probably predates event 2. Event 2 is represented by truncated bedrock debris overlain by thin beds of sand and gravel. These beds in turn are overlain by the large debris apron (unit 3) that represents event 3. This apron is composed of both sandstone and claystone debris. We infer that it represents a single event because the two lithologies are not separated by intervening sediments. This large apron is overlain by a thin gravel lens that separates it from the overlying debris apron of unit 4. The debris apron corresponding to event 4 in turn is overlain by mixed alluvium and colluvium that separates it from the bedrock debris (unit 5) representing event 5. It is not clear whether the debris aprons of events 4 and 5 were produced by a single event or by two separate ones. We prefer the interpretation that they represent two events, because this interpretation is more consistent with a constant average rate of strain accumulation of about 1.1 mm/yr on the Javon Canyon fault calculated from displacement of the two terrace platforms (see following section).

Because sense of movement on the Javon Canyon fault was up on the south, or downstream side, stratigraphic and structural relations in this exposure suggest that the faulting that offset the stream channel and preexisting stream gravels caused the stream channel to aggrade against the natural bedrock and debris dam formed by

the fault. This damming is evidenced by the buttressing of colluvium and alluvium against debris aprons 3–5. Subsequently, the stream incised the stream-terrace gravel and bedrock dam, exposing the stratigraphic-structural relationships shown in figure 8.3. A decrease in the stream gradient upstream of the fault and a knickpoint (sudden steepening of stream gradient) near the fault may be the topographic expression of displacement on the fault in the stream channel. Other knickpoints are found farther upstream in Javon Canyon and may be related to the several strands of the Red Mountain fault (fig. 8.2).

HISTORY OF HOLOCENE ACTIVITY ON THE JAVON CANYON FAULT

A history of Holocene activity on the Javon Canyon fault can be inferred by combining three items of information: (1) the long-term average rate of fault displacement of about 1.1 mm/yr determined from offsets of two independently dated terrace platforms, (2) the approximate 3,500-yr age of the stream-terrace bedrock platform (assumed to be coeval with the dated emergent Holocene marine-terrace platform), and (3) the estimated vertical throws associated with each of the five inferred displacement events. The amount of vertical displacement associated with each event is estimated from the heights of individual debris aprons, based on our assumption that the height of the apron represents a minimum throw associated with each event. The throw for event 1 (fig. 8.4), represented by the small fault displacement northeast of the main fault, was measured directly. The throw for event 2, an event inferred from a partially eroded debris apron, was determined by summing the estimated throws for the other four events and subtracting from the total throw of 4 m, assuming that the sums of the throws for individual events must equal the total measured throw. The throw for event 5 was estimated by the vertical height between the top of unit 4 and the projected extension of the bedrock and terrace-gravel contact in the hanging wall (fig. 8.4).

There is some uncertainty associated with estimates of throw for each inferred event. The height of each debris apron represents a minimum throw, since each debris pile is derived by collapse of the hanging wall at the surface. Postfaulting erosion might also decrease the height of a debris apron. Furthermore, because sense of faulting is high-angle reverse, there also may have been some relaxation or backsliding of the hanging block relative to the footwall block after each event. These uncertainties cannot be fully evaluated, other than that the total offset of the bedrock-terrace contact should equal the sum of individual throws. A total uncertainty of about 0.6 m is left—the estimated throw for event 2, divided among the four or five events.

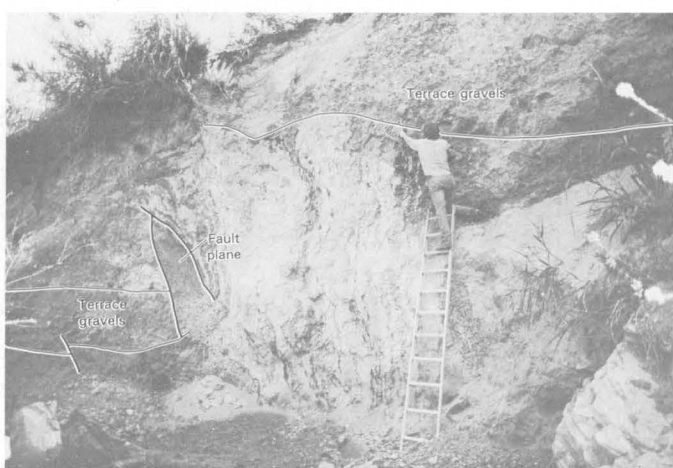


FIGURE 8.3.—Exposure of Javon Canyon fault in Javon Canyon, about half a kilometer northeast of the coast. View is to the southeast.

Figure 8.5A is a diagram showing the inferred fault history derived from this analysis. The diagram was constructed using the following assumptions: event 1 was assigned the age of 3,500 yr, the average of ^{14}C ages on the late Holocene marine terrace to which the stream terrace in Javon Canyon is graded. Event 1 was preceded by stress accumulation until instantaneous rupture of 0.5 m occurred at 3,500 yr. At that time, accumulated excess stress was presumably released; consequently, a line representing the long-term strain ($4 \text{ m}/3,500 \text{ yr} = 1.14 \text{ mm}/\text{yr}$) was drawn through the point representing 3,500 yr and 0.5 m of throw. Throws for each successive event were plotted in succession so that each event represented a return from a condition of excess stress to the long-term strain line. Individual throws on the diagram sum up to the total throw of 4 m. The ages of each event, and intervals between events, can be read directly from the diagram and are tabulated in table 8.2. It follows from figure 8.5A that an event of undetermined throw must have preceded event 1 at around 3,950 yr B.P.—a con-

clusion necessitated by the constant-strain assumption we have made. No stratigraphic or structural evidence for this event was found at the Javon Canyon exposure, and if such an event did take place, it preceded aggradation of stream-terrace alluvium in Javon Canyon at the location where it is crossed by the fault.

The time at which the sequence of faulting events began is uncertain because the emergent late Holocene marine terrace to which the offset stream terrace in Javon Canyon is graded does not yield a discrete age, but a range of ages (about 1,800 to 5,500 yr, table 8.1). This range suggests that either there is considerable analytical error in the ages or, more likely, that the terrace has been rising, continuously or sporadically, relative to present sea level since the worldwide eustatic sea level became stabilized at its present position about 5,000 yr ago, following the post-Wisconsinan sea-level rise.

We cannot choose the youngest age on this marine terrace as a starting point for the sequence of events because stream-terrace aggradation in Javon Canyon was at least

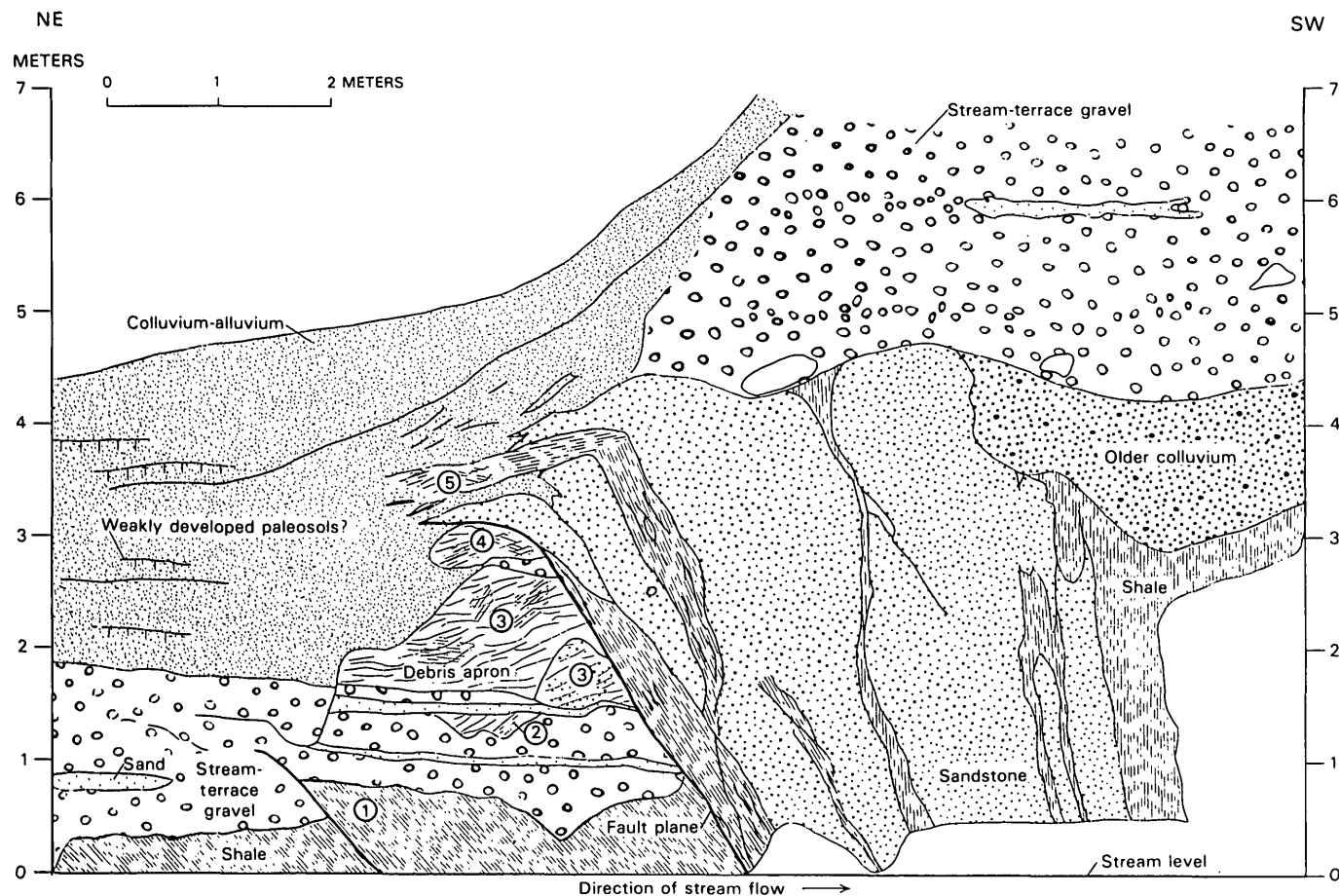


FIGURE 8.4.—Profile of fault exposure shown in figure 8.3. Circled numbers represent seismic events inferred from stratigraphic-structural relations. (1) Small offset of basal part of stream-terrace gravel; (2) debris derived from bedrock and planed off by subsequent stream erosion; (3) debris apron. Smaller, lower right is composed

of sandstone blocks; larger, overlying part is composed of shale and siltstone blocks; (4) debris apron of shale and siltstone; (5) debris apron of shale, siltstone, and sandstone. Debris apron may have slumped or rotated down to the left by downslope motion.

TABLE 8.2.—*History of late Holocene activity on the Javon Canyon fault compared to average calculated recurrence interval, throw, and estimated upper-bound magnitude.*

Event	Maximum estimated age of event (yr) ¹	Interval between events (yr)	Throw on fault (m)	Maximum estimated magnitude ²
History of activity on the Javon Canyon fault				
1	3,500		0.5	5.4
2	2,975	525	.6	5.6
3	1,830	1,145	1.3	6.5
4	1,475	355	.4	5.2
5	425	1,050	1.2	6.4
Average, \bar{x}		769	0.8	5.8
Sample standard deviation, s		± 388	$\pm .4$	$\pm .6$
2x sample standard deviation		± 776	$\pm .8$	± 1.2
Average calculated recurrence interval, throw and magnitude				
1	3,500		0.8	5.9-6.0
2	2,800	700	.8	5.9-6.0
3	2,100	700	.8	5.9-6.0
4	1,400	700	.8	5.9-6.0
5	700	700	.8	5.9-6.0

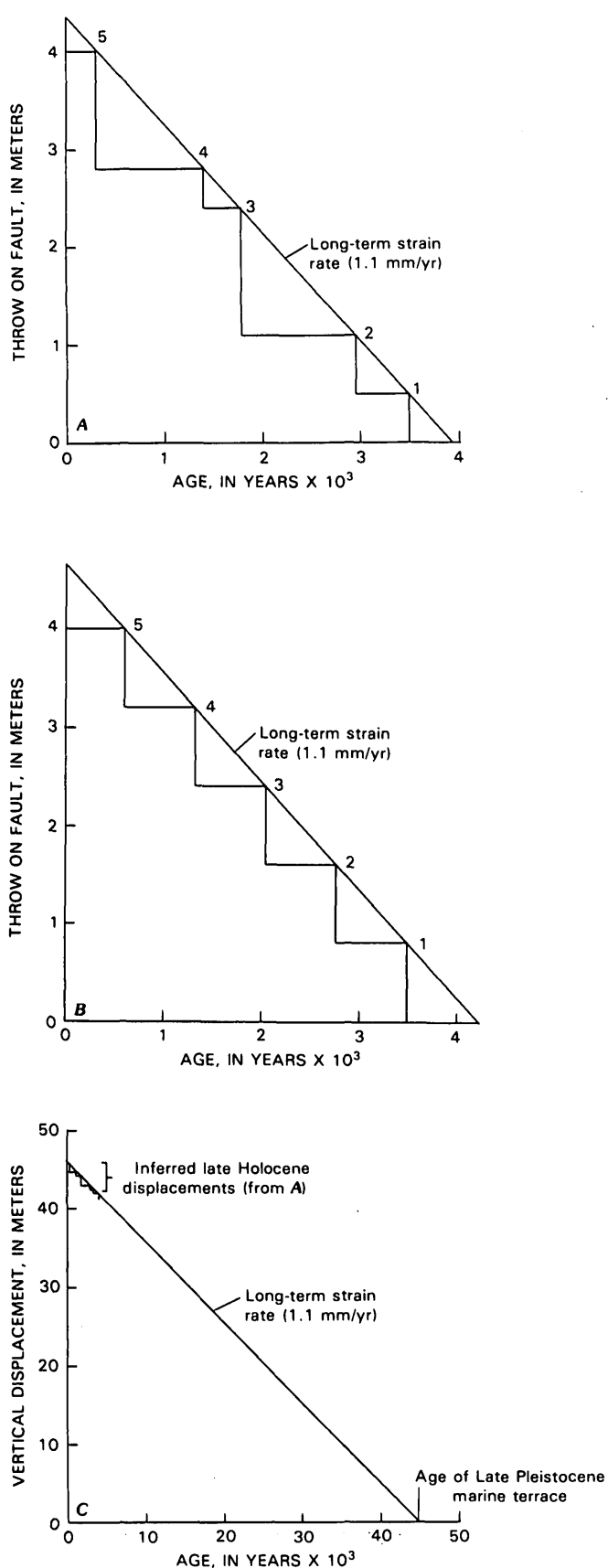
¹Event 1 is assigned the maximum age, equivalent to the 3,500-yr average of six radiocarbon ages on the emergent Holocene marine-terrace platform.

²Estimated upper-bound magnitude from curve for shallow reverse faults (Yerkes and others, 1974) based on worldwide data (Bonilla and Buchanan, 1970). Curve extrapolated to lower magnitude values.

partly contemporaneous with this sequence. Debris aprons associated with events 2 and 3 are partly or wholly interbedded with stream-terrace deposits. Events 4 and 5 may have taken place prior to or after stream incisions had begun. An age of about 1,800 yr B.P. (^{14}C) (table 8.1) has been obtained on charred wood and plant fragments collected from the stream-terrace alluvium about 100 m downstream from the fault exposure shown in figure 8.3. The sample was collected about 1.5 to 2.5 m above the level of the stream. We do not know how the terrace alluvium from this sampling locality relates stratigraphically or structurally to the terrace alluvium at which the fault offset is exposed. Based on our analysis, the 1,800-yr age would place the dated interval of stream-terrace alluvium close in time to event 3 (figs. 8.4 and 8.5). The 1,800-yr age confirms our general observation that the aggradation in Javon Canyon began sometime after about 5,000 yr B.P., but does not help to define the beginning of this sequence. We use the average age of 3,500 yr for the emergent Holocene marine terrace as the beginning age for the sequence of faulting events because it is representative of the age of the marine terrace, and because it yields a strain rate which is similar to that calculated from offset of the older, 45,000-yr marine terrace.

Despite the uncertainty for the beginning of the faulting sequence, the intervals between events and the magnitude of each throw are internally consistent within the assumptions we have stated. Furthermore, there are well-defined limits to how far this sequence can be shifted forward or backward in time.

Event 5, for example, falls at 425 yr B.P., A.D. 1554. This event could not have occurred later than 167 yr B.P., A.D. 1812, the year a particularly strong earthquake of uncertain epicenter occurred in the western Transverse Ranges, as noted in the records of several missions (Wood and others, 1961; Townley and Allen, 1939). On the basis of historical records, subsequent strong earthquakes cannot be attributed to the Javon Canyon fault. Consequently, event 1 could probably not be younger than about 3,200 yr—it certainly could not be younger than about 3,000 yr because this would shift event 5 into the future. On the other hand, if we use the oldest radiocarbon date of 5,535 yr B.P. on the emergent Holocene marine terrace as the age for event 1, event 5 would fall around 2,470 yr B.P. Under these conditions, the average long-term strain rate would be lower (0.7 mm/yr) than that calculated from offset of the 45,000-yr marine terrace, and from offset of the late Holocene stream terrace using the 3,500-yr average age for the late Holocene marine terrace. Furthermore, at a 1.1 mm/yr long-term strain rate, the fault would have accumulated sufficient stress to produce an offset of 2.3 m at present—an offset much greater than any recorded in the terrace deposits discussed here. Although such an offset may not be impossible, it seems unlikely, because it exceeds the mean of displacements, meager as the sample may be, by 2.5 standard deviations. Perhaps a reasonable maximum age for event 5 would be about 1,100 yr which would, under our assumptions, represent the accumulated stress required to produce a throw of 1.3 m, equivalent to the largest throw observed from the geologic data and one which lies close to one



standard deviation from the mean of five throws (table 8.2). These conditions would put event 1 at 4,200 yr B.P. Consequently, the range of uncertainty for the beginning of the entire sequence, under the stated assumptions, would be from 3,200 to 4,200 yr B.P.

In summary, there is some uncertainty in all the assumptions we have made. Certainly, the number of events and precise amounts of throw associated with each event are not established. Furthermore, although the evidence for a constant average long-term strain rate is good, the rate may fluctuate over shorter periods of time. Nevertheless, the evidence seems conclusive that multiple events with variable amounts of displacement have occurred on this fault in late Holocene time.

COMPARISON OF HISTORY OF ACTIVITY WITH AN AVERAGE RECURRENCE INTERVAL, THROW, AND MAGNITUDE FOR THE JAVON CANYON FAULT

The inferred history of late Holocene displacement on the Javon Canyon fault (fig. 8.5A) is compared with an estimate of the average recurrence interval calculated if the number of events, but not their magnitudes, were known (fig. 8.5B). The latter is a much more common case in fault-recurrence-interval studies based on information obtained from stratigraphic or geomorphic evidence. Commonly the character of movement, single-event displacements, and associated magnitudes must be inferred from meager historical information, and prehistoric displacements of individual events cannot be measured. In figure 8.5B, the total displacement is divided by the number of events (5), and an interval between events is calculated using the average strain rate (1.1 mm/yr) determined from offsets of the 45,000- and 3,500-yr-old marine-terrace platforms. In this instance, the earliest event (event 1) is again assigned the average age of about 3,500 yr. The comparison is summarized in table 8.1.

Earthquake magnitudes shown in table 8.1 were estimated by using a plot of vertical component of displacement relative to magnitude of upper-bound events on reverse-slip and oblique-slip faults, based on worldwide

FIGURE 8.5.—Comparison of inferred history of activity on the Javon Canyon fault with calculated average recurrence interval and throw. Events indicated by numbers on line representing long-term strain rate. A, Late Holocene history of seismic activity inferred from individual throws, total throw, long-term strain rate, and 3,500-yr age of stream-terrace platform. B, Late Holocene average recurrence interval and throw calculated from number of events, total throw, long-term strain rate, and 3,500-yr age of stream-terrace platform. C, Long-term strain calculated from offset (46 m) of late Pleistocene marine-terrace platform (45,000 yr B.P.). Magnitude of late Holocene offsets is shown to scale at upper left.

data (Bonilla and Buchanan, 1970; Yerkes and others, 1974). Estimates for magnitudes lower than 6 were obtained by extrapolating the curve for the vertical component of displacement to lower magnitude values. As expected, maximum throws (1.2, 1.3 m), and associated maximum estimated magnitudes (6.4, 6.5) are greater for the inferred seismic history of this fault than they are for the calculated average throw (0.8 m) and associated average magnitude (5.9–6.0). Intervals between events range from 75 percent to 164 percent of the estimated average interval of 700 yr. These data indicate that calculations of average recurrence intervals or average upper-bound magnitudes do not give an accurate estimation of the maximum potential of a fault with respect to displacement, magnitude, and intervals between events. This conclusion is valid even if our interpretation of the exact number of events, magnitudes of associated throws, and value of the long-term strain rate is not. Where data on multiple offsets can be obtained, a one standard deviation from the mean might be a better estimate of the range of commonly expectable displacements, magnitudes, and intervals between events, while two standard deviations would probably encompass most of the expectable effects (see table 8.1). Unfortunately, prehistoric data on amplitude of multiple offsets is lacking for most active faults, while historic data are meager for faults with long recurrence intervals.

When viewed from a long-term time perspective, the late Holocene events inferred for the Javon Canyon fault (fig. 8.5C) appear as small-amplitude "background noise" about the assumed long-term strain rate. This "noise" probably represents the effects of variable amounts of friction along the fault plane or zone which need to be overcome by build-up of stress in order to return to the long-term strain level. The variability from one event to the next is probably at least in part a result of juxtaposition of variable lithologies and roughness elements across the fault plane.

THE JAVON CANYON FAULT INTERPRETED AS A BEDDING-PLANE FAULT

The Javon Canyon fault may be considered a bedding-plane fault, since its attitude is subparallel to regional dip in the bedrock on the south flank of the plunging anticline, and subparallel to the plunging anticlinal axis. Thus one may argue that faulting is a minor secondary effect of folding on the anticline and that sufficient strain could not be accumulated on an apparently shallow structure such as this to cause strong or even moderate-magnitude earthquakes. Several lines of evidence argue against this interpretation. First, the attitude of the fault is steeper (68°) than regional dips (36° – 55°) in the same area on the south flank of the Ventura Avenue anticline. Second, the

fault is subparallel, not parallel, to bedding and to the anticlinal axes of the Rincon and Ventura Avenue anticlines; the fault separates the anticlinal axes of the two folds in the vicinity of the ridge just northwest of Padre Juan Canyon. Consequently, the fault probably is an independent structure, not a secondary effect of anticlinal folding. Third, stratigraphic-structural relations in Javon Canyon indicate that discrete, rapid displacements of up to 1.3 m or greater have taken place on the fault, suggesting associated magnitudes of at least about 6.5 from upper-bound relations between displacements versus magnitude for worldwide historic data for this type of fault.

These observations suggest the following possible interpretations: (1) The Javon Canyon fault is deep seated and not simply a shallow bedding-plane fault, or (2) a shallow bedding-plane fault is capable of generating sudden displacements of up to 1.3 m, or (3) such displacements as documented for the Javon Canyon fault were induced by movements on larger neighboring faults such as the Red Mountain fault or Pitas Point fault (south of mapped area). In the last instance, two major implications for seismic hazard zonation should be noted. For rupture hazard zonation the threat to structures remains the same. For ground response accompanying an earthquake, the hazards would probably be the same or greater, because a larger magnitude earthquake on neighboring master faults would be required to cause sympathetic displacements of 1.2–1.3 m on the Javon Canyon fault, owing to attenuation of ground-shaking effects away from the master faults.

CONCLUSIONS

The Javon Canyon fault has experienced recurrent displacement in late Holocene time. Stratigraphic and structural relations between superposed debris aprons and the fault indicate at least four, and probably five, events within late Holocene time (approximately the last 3,500 yr). The average long-term rate of displacement (strain) on this fault has been about 1.1 mm/yr, as determined from two independent measurements—offset of a Holocene and a late Pleistocene marine-terrace platform. Using the average strain rate, estimates of individual throws, total measured throw, and the correlated age of the Holocene stream-terrace platform, a seismic history is derived for the fault, including a range of displacements (0.5–1.3 m), a range of intervals between events (350–1,000 yr), and a range of estimated upper-bound magnitudes (5.5–6.5). A comparison of the inferred seismic history with a calculated average recurrence interval (700 yr), average displacement (0.8 m), and average magnitude (5.9–6.0) for the Javon Canyon fault indicates that the average values underestimate its maximum capability.

The same conclusion probably applies to other active faults. Lastly, the argument that the Javon Canyon fault may be a bedding-plane fault is not well substantiated and, furthermore, is irrelevant to its hazard potential.

REFERENCES CITED

- Bloom, A. L., Broecker, W. S., Chappell, J. M. A., Matthews, R. K., and Mesolella, K. J., 1974, Quaternary sea level fluctuations on a tectonic coast: New $^{230}\text{Th}/^{234}\text{U}$ dates from the Huon Peninsula, New Guinea: *Quaternary Research*, v. 4, p. 185-205.
- Bonilla, M. G., and Buchanan, J. M., 1970, Interim report on worldwide historic faulting: U.S. Geological Survey open-file report, 32 p.
- Buchanan-Banks, J. M., Castle, R. O., and Ziony, J. I., 1975, Elevation changes in the central Transverse Ranges near Ventura, California: *Tectonophysics*, v. 29, p. 113-125.
- Greene, H. G., 1976, Late Cenozoic geology of the Ventura basin, in Howell, D. G., ed., *Aspects of the geologic history of the California Continental Borderland*: American Association of Petroleum Geologists Miscellaneous Publication 24, p. 499-529.
- Hoyt, H. H., 1976, Geology and recent sediment distribution from Santa Barbara to Rincon Point, California: San Diego State University, MS thesis.
- Kaufman, A., Broecker, W. S., Ku, T. L., and Thurber, D. L., 1971, The status of U-series methods of mollusk dating: *Geochimica et Cosmochimica Acta*, v. 35, p. 1155-1183.
- Lee, W. H. K., Yerkes, R. F., and Simirenko, M., 1979, Recent earthquake activity and focal mechanisms in the western Transverse Ranges, California: U.S. Geological Survey Circular 799-A, p. 1-26.
- Putnam, W. C., 1942, Geomorphology of the Ventura region, California: *Geological Society of America Bulletin*, v. 53, p. 691-754.
- Sarna-Wojcicki, A. M., Lajoie, K. R., Robinson, S. W., and Yerkes, R. F., 1979, Recurrent Holocene displacement on the Javon Canyon fault, rates of faulting, and regional uplift, western Transverse Ranges, California [abs.]: *Geological Society of America, Abstracts with Programs, Cordilleran Section*, v. 11, p. 125.
- Sarna-Wojcicki, A. M., Williams, K. M., and Yerkes, R. F., 1976, Geology of the Ventura fault, Ventura County, California: U.S. Geological Survey Miscellaneous Field Studies Map MF-781, scale 1:6,000, 3 sheets.
- Townley, S. D., and Allen, M. W., 1939, Descriptive catalogue of earthquakes of the Pacific Coast of the United States, 1769 to 1928: *Seismological Society of America Bulletin*, v. 29, no. 1, p. 1-297.
- Weber, F. H., Jr., Cleveland, G. B., Kahle, J. F., Kiessling, E. F., Miller, R. V., Mills, M. F., Morton, D. M., and Cilweck, B. A., 1973, Geology and mineral resources study of southern Ventura County, California: *California Division of Mines and Geology Preliminary Report* 14, 102 p., geological map scale 1:48,000.
- Wehmiller, J. F., Lajoie, K. R., Sarna-Wojcicki, A. M., Yerkes, R. F., Kennedy, G. L., Stephens, T. A., and Kohl, R. F., 1978, Amino-acid racemization dating of Quaternary mollusks, Pacific Coast United States, in Zartman, R. E., ed., *Short Papers of the Fourth International Conference, Geochronology, Cosmochronology, Isotope Geology*: U.S. Geological Survey Open-file Report 78-701, p. 445-448.
- Wood, H. O., Heck, N. H., and Eppley, R. A., 1961, Earthquake history of the United States, Part II, Stronger earthquakes of California and western Nevada: U.S. Coast and Geodetic Survey Report No. 41-1, revised edition (through 1960).
- Yeats, R. S., 1977, High rates of vertical crustal movement near Ventura, California: *Science*, v. 196, p. 295-298.
- Yerkes, R. F., and Lee, W. H. K., 1979, Late Quaternary deformation in the western Transverse Ranges, California: U.S. Geological Survey Circular 799-B, 10 p.
- Yerkes, R. F., Bonilla, M. G., Youd, T. L., and Sims, J. D., 1974, Geologic environment of the Van Norman Reservoir area: U.S. Geological Survey Circular 691-A, 35 p.

9. LATE CENOZOIC STRUCTURE OF THE SANTA SUSANA FAULT ZONE

By ROBERT S. YEATS¹

ABSTRACT

The Santa Susana fault extends along the southern edge of the Santa Susana Mountains from the San Fernando Valley in Los Angeles County 28 km west-northwest into Ventura County. It marks an older hinge line between a thick, continuous middle Miocene to Pliocene sequence on the north and a thin, discontinuous sequence of the same age on the south. The Frew reverse-fault system, south-side up, was overridden by the north-side-up Torrey and Roosa faults that formed before deposition of the Saugus Formation and are precursors to the Santa Susana fault. The Santa Susana fault overrides the Saugus and older formations together with alluvial-fan deposits that unconformably overlie the Saugus; younger alluvial-fan deposits overlie the fault trace. The fault is low dipping and lobate near the surface but steepens at depth to a uniform 55°–60° to maximum well control at ~1.5 km. Comparisons with aftershocks of the 1971 San Fernando earthquake suggest that the fault maintains this dip to depths greater than 12 km. Minimum separation varies from zero west of Oak Ridge oil field, where the Santa Susana apparently becomes a bedding fault, to more than 4 km near Aliso Canyon oil field; true displacement is probably much larger. Comparison of separation on the Santa Susana fault and on the older Torrey and Frew systems suggests that fault displacements have been accelerating since the initiation of the Frew fault during deposition of the Pico Formation. Modern seismicity on the fault is relatively low, although the April 4, 1893, Pico Canyon earthquake may have occurred on the fault. The Santa Susana fault trace steps left and steepens in dip at Gillibrand Canyon and at the west end of Sylmar basin; both steps (lateral ramps) are seismically active. The Gillibrand step is outlined by aftershocks of an $M = 4.6$ event on April 8, 1976, and the Sylmar (San Fernando) step is outlined by aftershocks of the February 9, 1971, earthquake. The Santa Susana fault is part of a discontinuous north-dipping thrust-fault system that extends from the Red Mountain and San Cayetano faults east to the San Fernando, Sierra Madre, and Cucamonga faults, all of which lie on the south-facing margin of the Palmdale uplift.

INTRODUCTION

The southern edge of the Santa Susana Mountains is marked by the Santa Susana reverse fault of Quaternary age. This fault extends from the San Fernando Valley in Los Angeles County 28 km west-northwest into Ventura County (fig. 9.1; pl. 9.1). The fault is traced eastward into the northern margin of the San Fernando Valley (Sylmar basin), where it may merge with the Sierra Madre fault at the southern edge of the San Gabriel Mountains. The easternmost segment of the fault, at the southern

margin of the San Gabriel Mountains north of Sylmar basin, is unconstrained by well data and is not described here; readers are referred to Barrows and others (1975) and Weber (1975) for details and for references to earlier work in this area. Westward, in Ventura County, the Santa Susana fault dies out or changes into a bedding thrust east of the Santa Clara Valley. Strata of Miocene and Pliocene age are continuous across the westward projection of the fault and are not cut by the fault (pl. 9.1).

The Santa Susana fault dips north—gently near the surface and more steeply at depth. At Gillibrand Canyon (fig. 9.2) and at the western edge of the Sylmar basin (pl. 9.1), the fault steps left, forming a lateral ramp, and steepens in dip; the Sylmar (San Fernando) left step was marked by aftershocks of the 1971 San Fernando earthquake, and the Gillibrand Canyon left step was marked by aftershocks of an $M = 4.6$ earthquake in 1976 (Pechmann, 1983; Simila and others, 1983).

The fault separates two contrasting sedimentary sequences. On the north side, the Santa Susana Mountains are part of the folded and uplifted trough sequence of the east Ventura basin, comprising thick deposits of middle Miocene to Pliocene age. On the south side, a discontinuous sequence of Late Cretaceous to late Tertiary age is cut by north-dipping and south-dipping reverse faults. This faulted sequence is overlain unconformably by the Saugus Formation, which is largely of Pleistocene age, and the Saugus is itself overridden by the Santa Susana fault. The contrast between sequences north and south of the Santa Susana fault is due to the superposition of the fault along an older depositional hinge line that marked the southern edge of the east Ventura basin in Miocene and Pliocene time.

The paleogeographic and paleotectonic setting of the Santa Susana fault has been described elsewhere (Yeats, 1979). This paper concentrates on the reverse faults of the Santa Susana fault zone—the pre-Saugus Frew, Ward, Torrey, and Roosa faults, the Santa Susana fault itself, and other post-Saugus (late Quaternary) structures related to it.

PREVIOUS WORK

The area was mapped in reconnaissance by Kew (1924). More detailed surface mapping was done by graduate

¹Department of Geology, Oregon State University, Corvallis, Oregon 97331.

Manuscript received for publication on February 17, 1981.

students at the University of California at Los Angeles (Levorsen, 1947; Bishop, 1950; Bain, 1954; Hetherington, 1957; Jennings, 1957; Jesters, 1958; Martin, 1958; Seiden, 1972) and the California Institute of Technology (Cabeen, 1939; Lewis, 1940), and by Cushman and LeRoy (1938), Oakeshott (1958), Winterer and Durham (1962), Saul (1975, 1979), and Evans and Miller (1978). All these reports were consulted during the study, and most required reinterpretation on the basis of field checking by my students and myself. Surface geology reported by Cabeen (1939), Winterer and Durham (1962), Saul (1975, 1979), and Evans and Miller (1978) was found to be ade-

quate for this study. Modifications were based upon the perspective gained from extensive well control and from road cuts, trenches, test pits, and shallow bore holes not available to the earlier workers.

Nine oil fields are found in the vicinity of the Santa Susana fault (fig. 9.3). Five of these (Aliso Canyon, Cascade, Oak Ridge, Santa Susana, and South Tapo Canyon oil fields) produce oil from beds beneath the Santa Susana fault, permitting detailed mapping of the fault surface using well control. All oil fields have been described briefly in the literature, and published references for each field are listed in table 9.1. These reports were consulted

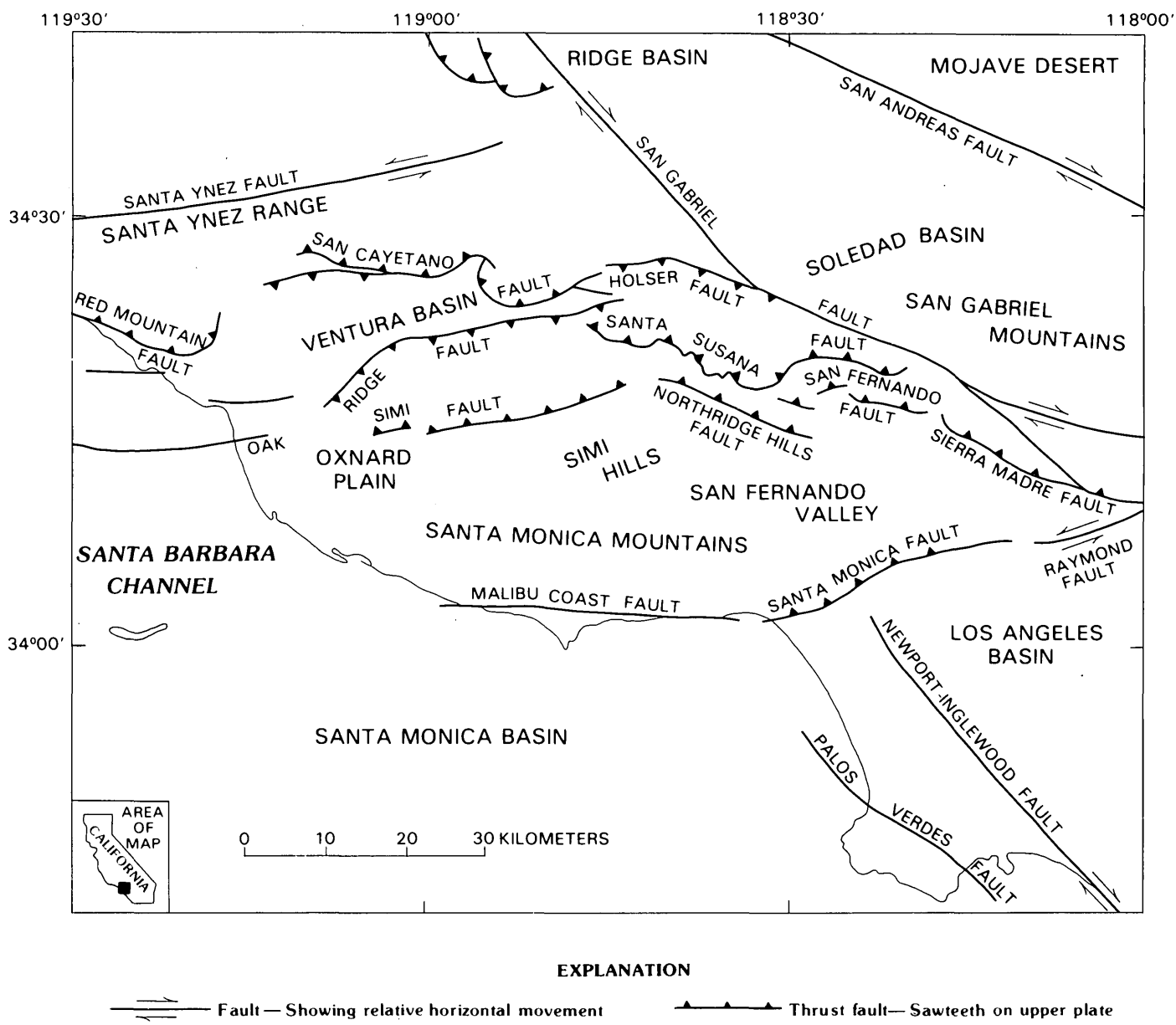


FIGURE 9.1.—Central Transverse Ranges showing location of Santa Susana and other faults. Map and fault traces from Jennings (1977).

along with Nagle and Parker (1971), but it was necessary to remap the subsurface geology for this study.

PRESENT STUDY

My students and I began the study of the Santa Susana fault in 1972. We remapped the surface trace of the Santa

Susana fault from its west end near Torrey Canyon oil field east to Aliso Canyon oil field (pl. 9.1). Field mapping from Gillibrand Canyon to Aliso Canyon oil field was done on color aerial photographs to a scale of 1:18,000; west of Gillibrand Canyon, black-and-white photographs at about the same scale were used. Mapping was transferred to USGS topographic maps enlarged to a scale of 1:12,000.

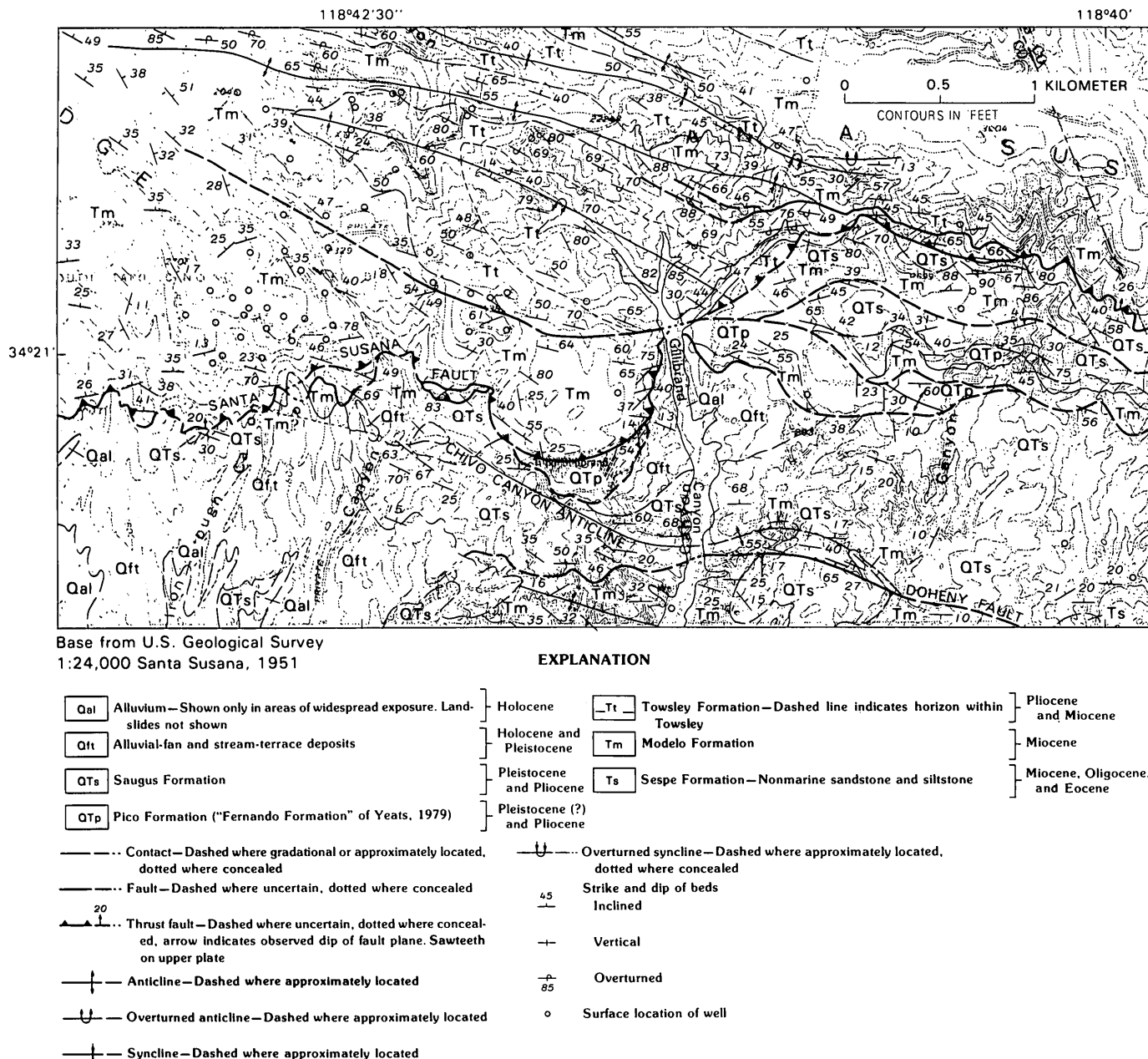


FIGURE 9.2.—Gillibrand Canyon lateral ramp, Santa Susana fault zone. West of Gillibrand Canyon, the Santa Susana fault is a single strand with slices of the Modelo, Pico (Fernando Formation as used by Yeats, 1979), or Saugus Formation. Fault overrides most alluvial fan material (Qft), but locally this material overlies the fault trace. Several localities of the alluvial fan material over the fault at west end of map are too

small to show at this scale (see Leighton and others, 1977). Three subsidiary faults extend west from Gillibrand Canyon, and one dies out in a southward-verging fold. Another three subsidiary faults extend east from Gillibrand Canyon causing repetition of the Modelo to Saugus sequence; the Pico Formation occurs in all but the northernmost slice. These faults rejoin the main fault east of this map (see pl. 9.1).

TABLE 9.1.—Published references on oil fields in the vicinity of the Santa Susana fault

Oil field	References
Aliso Canyon	Hanson and Saunders (1962). Hodges and Murray-Aaron (1943). Ingram (1959). Leach (1948).
Cascade	Ingram (1963). Roth and Sullwold (1958).
Horse Meadows	Cordova (1965). Stewart (1952).
Las Llajas	Levorsen (1947). Tudor (1963).
Mission	Mefferd and Cordova (1961).
Oak Ridge	Hall and others (1958, 1975). Schultz (1955).
Santa Susana	Hall and others (1975). Mitchell and Wolff (1971).
South Tapo Canyon	Hall and others (1975). Hardoin (1958).
Torrey Canyon	Hall and others (1975).

About seven man-months were spent in fieldwork by M. L. Butler, K. J. Lant, J. C. Schlueter, K. E. Shields, K. R. Whaley, and R. S. Yeats.

This paper primarily summarizes studies presented in greater detail in unpublished reports. The northwestern third of the Santa Susana fault from the Oak Ridge fault east to Gillibrand Canyon was described by Ricketts and Whaley (1975). The central segment from Gillibrand Canyon east to Mormon and Browns Canyons at the western end of Aliso Canyon oil field was described by Yeats and others (1977a). Aliso Canyon oil field was described by Lant (1977), and the eastern end of the Santa Susana fault at the edge of the San Fernando Valley and Sylmar basin was described by Shields (1977; see also Yeats and others, 1977b). These reports show the surface geology on a topographic base that includes the Oat Mountain, Piru, San Fernando, Santa Susana, Simi, and Val Verde 7½-minute quadrangles. Cross sections in these reports include electric logs and dipmeter, paleontologic, and lithologic data from wells; geologic interpretations take into consideration both surface and well data. This paper shows surface geology on a planimetric base (pl. 9.1) and cross sections (fig. 9.4); two illustrations (figs. 9.4D, 9.4F) include electric logs because they document critical relations.

Subsurface data from 463 wells drilled by the petroleum industry were acquired principally from the California Division of Oil and Gas. Data so obtained include electric logs, well histories, core and sidewall sample descriptions, and, in some cases, dipmeter and directional surveys. Where the Division of Oil and Gas files are incomplete, well data were acquired directly from oil companies holding proprietary interest. All biostratigraphic data

were obtained from oil companies. In many cases, cores and ditch samples on which the biostratigraphic assignments were made are available from the California Well Sample Repository at Bakersfield (1980) or from the oil company that drilled a particular well. Maps at a scale of 1:12,000 were constructed to show surface locations of wells based on well histories and aerial photographs and to show subsurface locations based on directional surveys. Electric logs were reduced to a working scale of 1:6,000 for cross sections, which were further reduced to 1:12,000 for the reports by Ricketts and Whaley (1975), Lant (1977), and Yeats and others (1977a, b). At least one cross section was constructed through every well to reflect the interpretations in the subsurface maps; only those critical to the interpretations were included in the reports cited above.

Age assignments are based mainly on the microfaunal stages of Kleinpell (1938) and Mallory (1959), although I recognize that these stages are inherently time transgressive over long distances and across facies (Poore, 1976; Crouch and Bukry, 1979.)

ACKNOWLEDGMENTS

Study of the Santa Susana fault was supported by contracts 14-08-0001-15271 and 14-08-0001-15886 from the Earthquake Hazards Program, U.S. Geological Survey, and by the National Science Foundation. Oil-well data were provided by California Division of Oil and Gas and by oil companies in the area. Unpublished maps by R. B. Saul and J. Evans of California Division of Mines and Geology, by oil company geologists, and by geotechnical firms were made available. Discussions with Edward A. Hall, Siegfried Hamann, Allan Hanson, Ben Jones, Beach Leighton, Richard Lung, Richard Saul, Richard Squires, and Robert Yerkes were useful in resolving geological problems. Drew Reed's trailer was used as field headquarters for part of the summer of 1976. The work of Ohio University graduate students Mark Butler, Kevin Lant, Robert Reiser, Edward Ricketts, James Schlueter, Kermit Shields, and Keith Whaley constitutes the foundation on which this paper is based.

REGIONAL GEOLOGIC SETTING

The following is a summary of relations described in more detail by Yeats (1979), who summarizes studies by Canter (1974), Ricketts and Whaley (1975), Lant (1977), Shields (1977), and Yeats and others (1977a, b).

FOOTWALL BLOCK

The area below and south of the Santa Susana fault is part of a subprovince that extends from the Oak Ridge

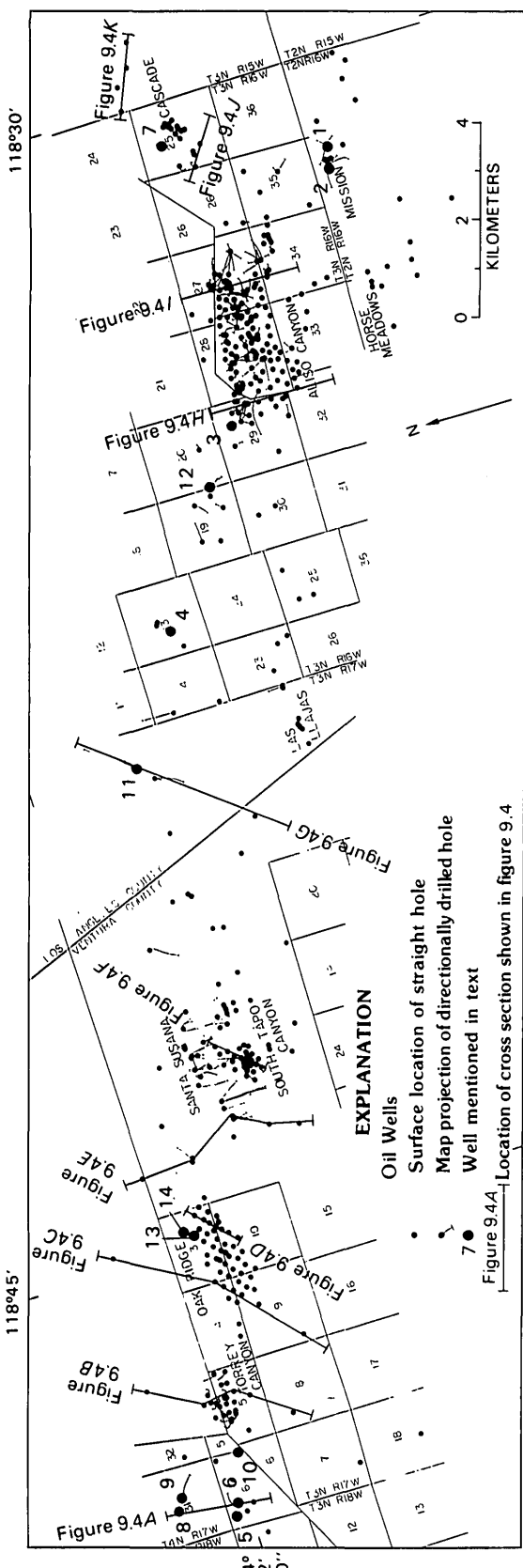


FIGURE 9.3.—Location of oil fields, wells, and lines of structure sections near the Santa Susana fault zone. For greater detail, see Ricketts and Whaley (1975), Lant (1977), Shields (1977), and Yeats and others (1977a). Cross sections are identified by figure number. Numbered wells mentioned in text are: 1, Chevron Mission 5-1; 2, Chevron Mission 6-1; 3, Chevron Roosa 1; 4, Gulf Brady Estates 1; 5, Gulf Hunter 1-6; 6, Gulf Hunter 2-6; 7, Mobil Macson-Mission 1; 8, Texaco Baker-Hunter 1; 9, Texaco Baker-Hunter 2; 10, Texaco Hunter 1; 11, Union Blue Sage 1; 12, Union Gardett 1-20; 13, Union Oak Ridge 11-3; 14, Union Oak Ridge 41-3.

fault south to the northern margin of the Santa Monica Mountains (fig. 9.1) and includes the San Fernando Valley, Simi Hills, and Oxnard Plain. Oldest rocks known from outcrop or from wells are a sequence of deep-water sandstone, siltstone, and conglomerate of Late Cretaceous age. This sequence has a minimum thickness of 1,341 m in the Aliso Canyon oil field (Yeats, 1979) and 2,000 m in the Simi Hills. In the western Simi Hills, the Cretaceous strata are overlain by Paleocene nonmarine and marine beds, but in the present area near the Santa Susana fault, the Paleocene sequence is overlain by the marine Paleocene and Eocene Santa Susana Formation of Clark (1924) and Nelson (1925), such that the Santa Susana rests directly upon Cretaceous rocks (Seedorf, 1983; figs. 9.4G–9.4I). The Santa Susana is overlain by marine Llajas Formation of late and early middle Eocene age (Schenck, 1931; Filewicz and Hill, 1983; Squires, 1983) which in turn is overlain by the nonmarine, variegated Sespe Formation (Kew, 1924), which contains vertebrate fossils of late Eocene to late Oligocene age (Durham and others, 1954; Lander, 1983). The Sespe interingers with and is overlain by shallow-marine sandstone and siltstone of the Vaqueros Formation, which appears to be of late Oligocene and early Miocene age in this area (Hamlin, 1904; Kew, 1924; Cushman and LeRoy, 1938; Canter, 1974; Blake, 1983).

This sequence was tilted westward about 6° and eroded to a low-relief surface before deposition of the Modelo Formation of middle and late Miocene age. For this reason, the Modelo rests on the Vaqueros Formation east to Santa Susana oil field (pl. 9.1; figs. 9.4A–9.4E), on the Sespe Formation from there east to the Las Llajas oil field, (figs. 9.4F, 9.4G), on the Llajas Formation east to Aliso Canyon oil field (pl. 9.1), and on Paleocene or Cretaceous strata at the eastern edge of Aliso Canyon oil field (Yeats and others, 1977b). The Modelo contains a basal, shallow-marine sandstone overlain by dark-brown siltstone, dark-brown shale, white-weathering chert, diatomaceous shale, and thin interbeds of sandstone and volcanic ash. The Modelo contains foraminifera of the Luisian and Mohnian Stages of Kleinpell (1938), with the Luisian-Mohnian boundary about 30 m above marker S-1 in Aliso Canyon oil field (figs. 9.4H, 9.4I; Lant, 1977). The Modelo is overlain with angular unconformity by marine gray siltstone interbedded with sandstone, pebbly sandstone, and conglomerate with Pliocene and Pleistocene(?) fossils. South of the Frew fault, this formation, the Pico Formation ("Fernando Formation" as used by Yeats, 1979), is thin and shallow marine; north of this fault it is as much as 2,070 m thick, possibly deposited as a submarine fan (fig. 9.4H). This sequence may have once been laterally continuous with beds of similar age and lithology north of the Santa Susana fault in the east Ventura basin (Pico Formation). The Frew reverse fault formed in part as this formation was being deposited.

Before the deposition of the overlying Saugus Formation, the older strata underwent reverse faulting (pl. 9.1; fig. 9.4E, 9.4G). The Frew and Ward faults, which are north side down, are truncated by the Torrey and Roosa fault with north side up (fig. 9.4H, 9.4I). The Saugus Formation (Kew, 1924; Winterer and Durham, 1958, 1962) is divided into a lower member (Sunshine Ranch Member) consisting of interfingering marine and nonmarine deposits of Pliocene age and an upper member consisting of marine deposits of Pleistocene age. Thickness varies from a few meters in the Oak Ridge oil field (pl. 9.1; fig. 9.3) to more than 3,000 m in the Sylmar basin east of Cascade oil field (fig. 9.4K; Weber, 1975). Highly fossiliferous sandstone and conglomerate of the Saugus Formation rest unconformably on older strata and on the eroded traces of the Torrey, Frew, and other faults. The Saugus contains conglomerate with an assemblage of crystalline rock clasts except for the upper 60–90 m at Horse Flats, south of Aliso Canyon oil field, where the

clast composition changes upsection to sandstone concretions and shale fragments of the Towsley and Modelo Formations similar to exposures in the Santa Susana Mountains. Saul (1975) deduced that the change in clast composition marked the beginning of uplift of the Santa Susana Mountains, which blocked off more distant source areas underlain mainly by crystalline rocks. The Saugus is overlain unconformably by fan deposits that are described in more detail in the structure section.

HANGING-WALL BLOCK

Near the Cascade oil field, the Mobil Macson-Mission 1 well (well 7, fig. 9.3) penetrated highly sheared gray-green biotite-bearing hornblende-plagioclase-quartz gneiss with subordinate amounts of marble. These rocks are similar to diorite gneiss with screens of metasediments—the pre-Cretaceous Placerita Formation—described by Oakeshott (1958) from exposures in the western San

FIGURE 9.4.—Cross sections through the Santa Susana fault zone. No vertical exaggeration. See figure 9.3 for location of cross sections.
A, Wiley Canyon area west of Torrey Canyon oil field. North strand of Oak Ridge fault is lobate near surface and apparently truncates middle strand of Oak Ridge fault. South strand of Oak Ridge fault truncates Torrey fault. Both north and south strands of Oak Ridge fault have very large separations.

B, Torrey Canyon oil field. Oak Ridge fault has vertical dip, as constrained by Union Torrey 97 and 99 wells. Torrey fault truncated by south strand of Oak Ridge fault. Variable dips in the Modelo Formation near Union Simi 25 well indicate ductile folding; underlying Vaqueros and Sespe Formations folded into broad anticline. Pre-Llajas strata in Torrey 92 well may be in part Cretaceous in age (Seedorf, 1983).
C, Oak Ridge oil field. The Modelo Formation may include some Topanga Formation between Santa Susana fault and south strand of Oak Ridge fault. Oak Ridge fault has normal separation and is overridden by Santa Susana fault. The location of the Oak Ridge fault in this cross section is constrained by Union-Oak Ridge 41-3 well. Ductile folding and faulting in the Modelo Formation is not shared by the underlying, broadly folded Vaqueros and Sespe Formations.

D, Oak Ridge oil field. The Modelo and Topanga Formations are thrust over the Modelo Formation; relatively small separation on Santa Susana fault. The Modelo is folded disharmonically above and below Santa Susana fault. Skootch fault of Hall and others (1975) is a decollement surface within the Modelo separating strongly folded strata above and broadly folded strata below. Modelo rests on Topanga Formation above Santa Susana fault and on Vaqueros Formation below this fault.

E, West of South Tapo Canyon and Santa Susana oil fields. South-dipping Frew fault truncated by north-dipping Torrey fault, the surface trace of which is overlain unconformably by the Saugus Formation. Santa Susana fault overrides the Saugus and some fan deposits. Modelo rests on Topanga Formation north of Santa Susana fault, on Vaqueros Formation between Santa Susana and Torrey faults, and on Sespe Formation south of Torrey fault.

F, South Tapo Canyon oil field. The Modelo Formation with Luisian and Mohnian microfossils is in thrust contact with the Saugus Formation; fault transects bedding at low angle. The Saugus rests unconformably on the Modelo Formation, which itself rests unconformably on the Sespe Formation.

G, East of Gillibrand Canyon lateral ramp. Apparent offset of Frew fault in Union Simi 23 well due to projection of well into section (See fig. 9.3). Frew and Torrey fault traces overlain unconformably by the Saugus Formation, which is itself overridden by Santa Susana fault. South of Doheny fault, Modelo overlies Llajas, and Sespe is absent owing to pre-Modelo erosion. Sespe is present north of Doheny fault, but pre-Modelo erosion removed more Sespe north of Frew fault than south of it.

H, West end of Aliso Canyon oil field. Ward fault truncated by Roosa fault; Frew fault and older strand of Santa Susana fault truncated by younger strand of Santa Susana fault. A relatively thick section of Pico Formation rests on Modelo Formation north of Frew fault, whereas a thin section of Pico rests on Santa Susana Formation south of this fault. Frew fault is more steeply dipping upward, suggesting broad-scale drag near the Santa Susana fault.

I, East end of Aliso Canyon oil field. Ward fault truncated by Roosa fault, which is itself truncated by younger strand of Santa Susana fault. Younger strand offsets older strand with small separation. Older strand, together with the overlying Topanga and Modelo Formations, folded into Oat Mountain anticline, thereby dating the anticline as younger than the older strand of Santa Susana fault but older than the younger strand of this fault.

J, San Fernando lateral ramp at south edge of Cascade oil field. Steeply dipping Santa Susana fault is controlled by well data for more than 2 km vertically.

K, San Fernando Pass north of Cascade oil field. This is the easternmost section in which the Santa Susana fault is controlled by well data; it shows a lobate fault near the surface. Note thick section of the Saugus Formation in Sylmar basin comparable to that in Santa Clara syncline (figure 9.4A). Separation on the Santa Susana fault is relatively low compared to sections farther west.

Gabriel Mountains south of the San Gabriel fault. The top of this unit is weathered, and it is apparently overlain by 335 m of biotitic locally carbonaceous gray siltstone and sandstone questionably assigned to the Topanga Formation (Miocene) by Winterer and Durham (1962). The Topanga Formation crops out in the core of the Oat Mountain anticline in Aliso Canyon oil field and in a north-dipping homocline west of the field and north of Mormon

Canyon and Browns Canyon (pl. 9.1); it also occurs in the subsurface throughout the length of the Santa Susana fault (Yeats, 1979) (fig. 9.4D, 9.4E, 9.4G–9.4J). West of Aliso Canyon, the Topanga contains 30–60 m of extrusive basalt (Yeats, 1979) radiometrically dated at 14.1 ± 1 Ma (Turner, 1970). In the western half of the area, the formation consists of micaceous sandstone interbedded with black to dark-brown foraminiferal siltstone. Minimum

EXPLANATION FOR FIGURES 9.4A-K

Qal	Alluvium (Holocene)	Ttp	Topanga Formation (Miocene)
Qls	Landslide (Holocene)	Ttpb	Basalt
Qft	Alluvial fan and stream-terrace deposits (Holocene and Pleistocene)	Tv	Vaqueros Formation (Miocene to Oligocene)
QTs	Saugus Formation (Pleistocene and Pliocene)	Ts	Sespe Formation (Oligocene to Eocene)
QTp	Pico Formation (Pleistocene? and Pliocene) ("Fernando Formation" as used by Yeats, 1979)	TI	Llajas Formation (Eocene)
Tt	Towsley Formation (Pliocene and Miocene)	Tss	Santa Susana Formation (Eocene and Paleocene) (Clark, 1924; Nelson, 1925)
Tm	Modelo Formation (Miocene)	Ks	Sedimentary rocks (Upper Cretaceous)
Tms	Basal sandstone		

—?— Contact—Approximately located; queried where uncertain

—?— Fault—Dashed where inferred, queried where uncertain; arrows indicate relative movement

~~~~~ Unconformity

—LS-0— Dash-dot line within unit shows electric-log marker, bedding plane (may be numbered)

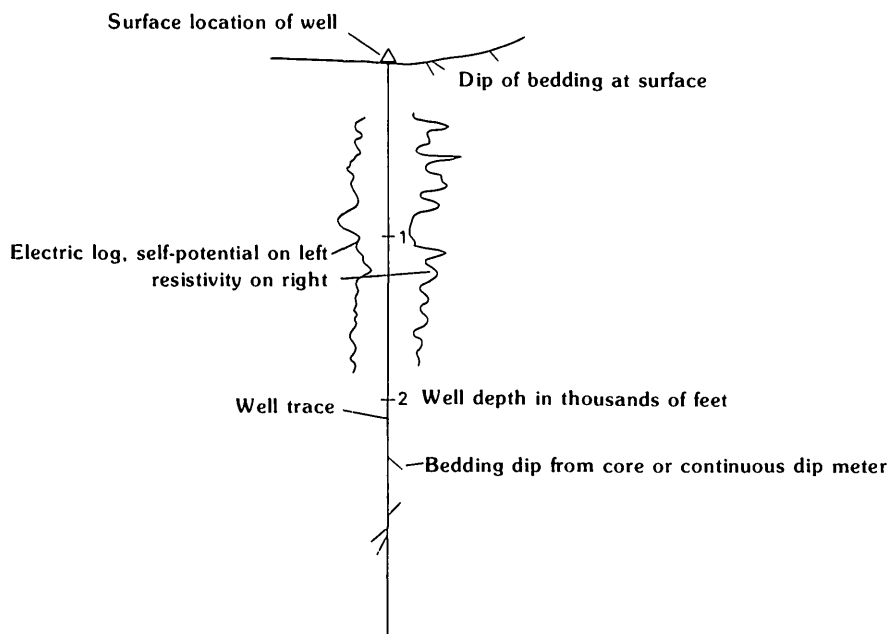
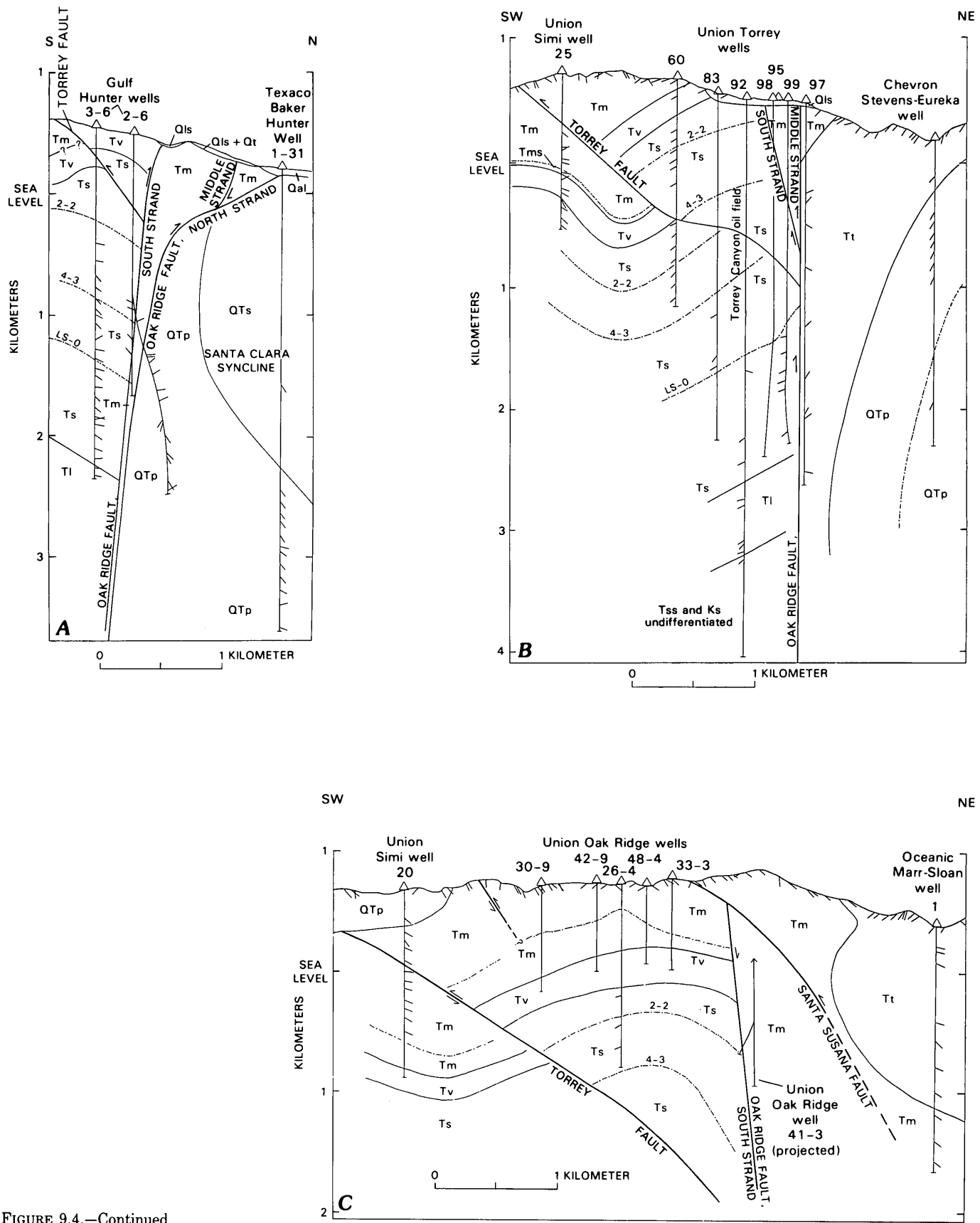


FIGURE 9.4.—Continued.



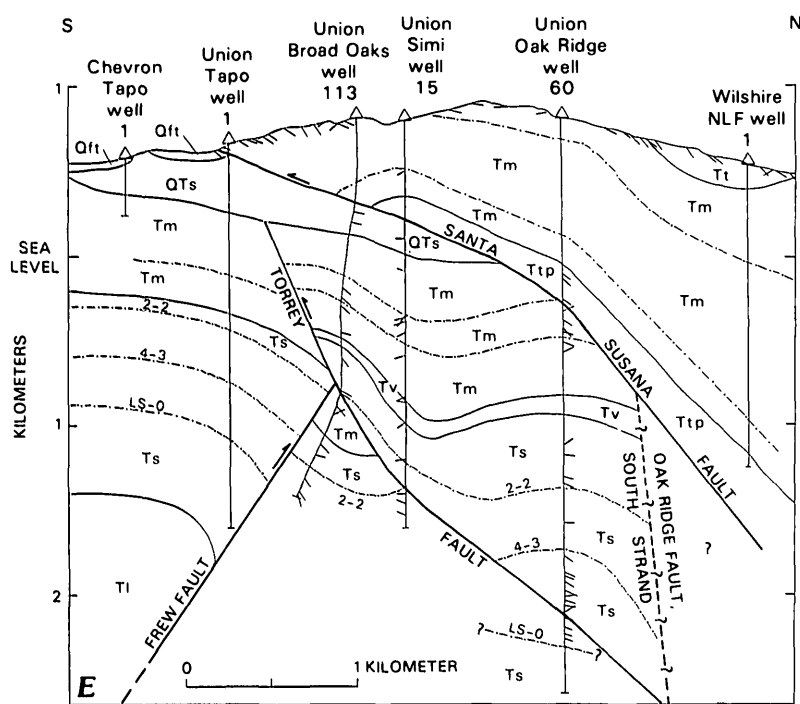
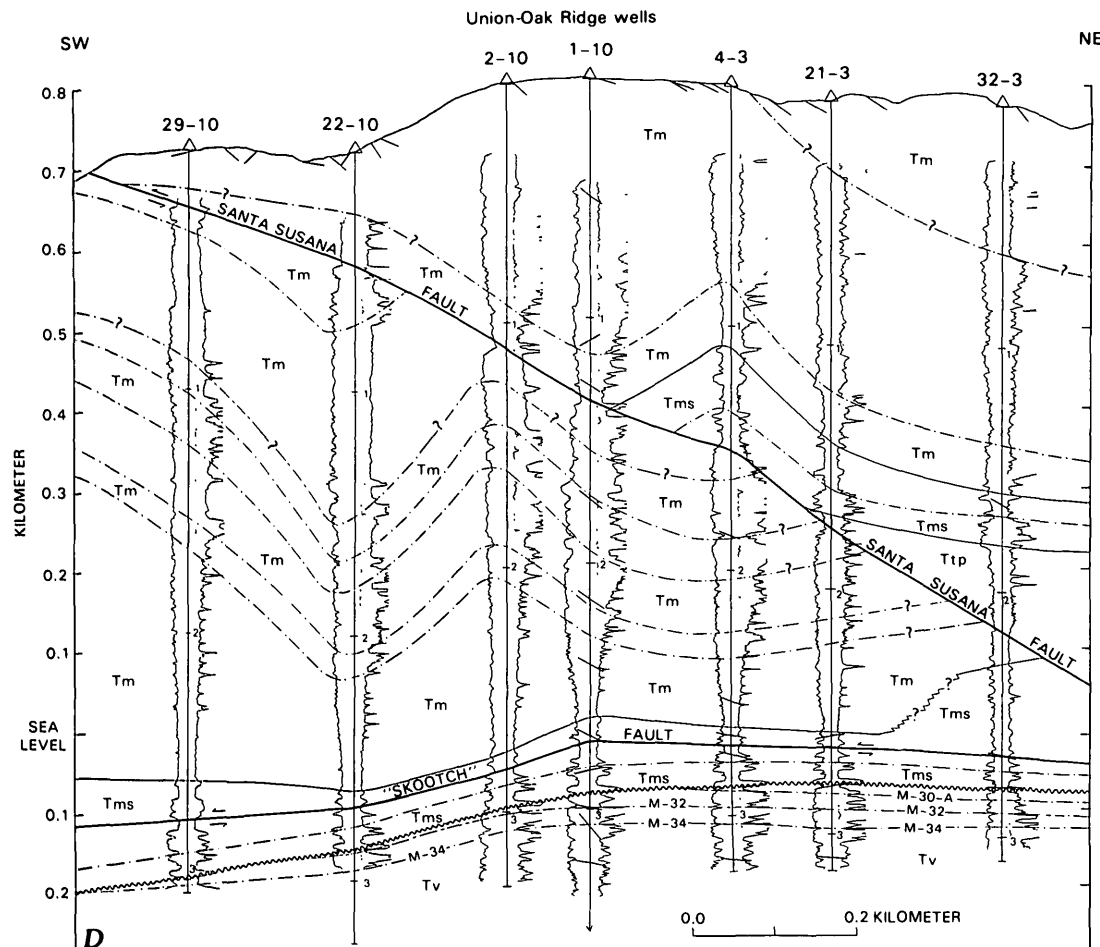


FIGURE 9.4.—Continued.

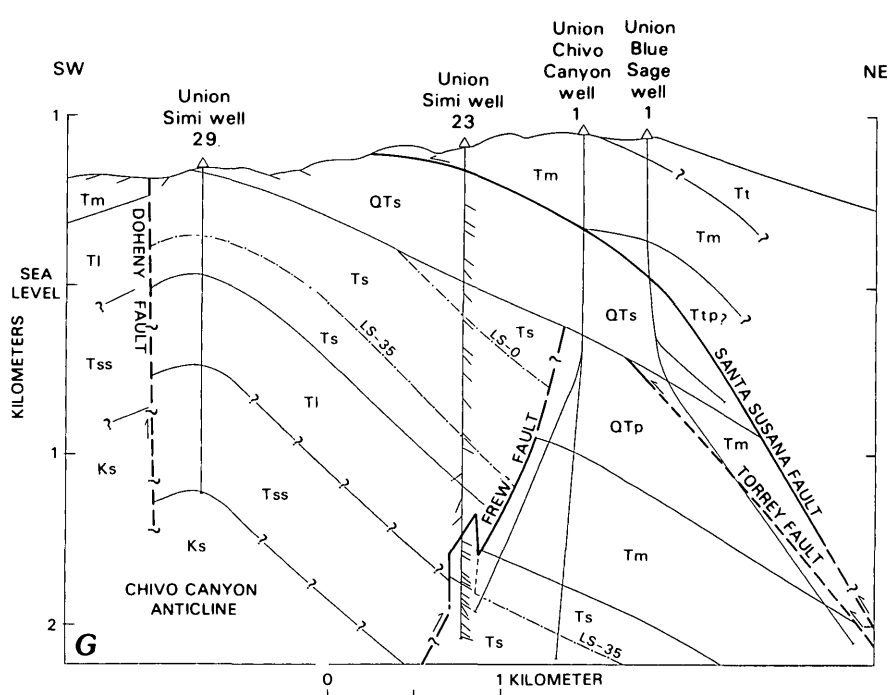
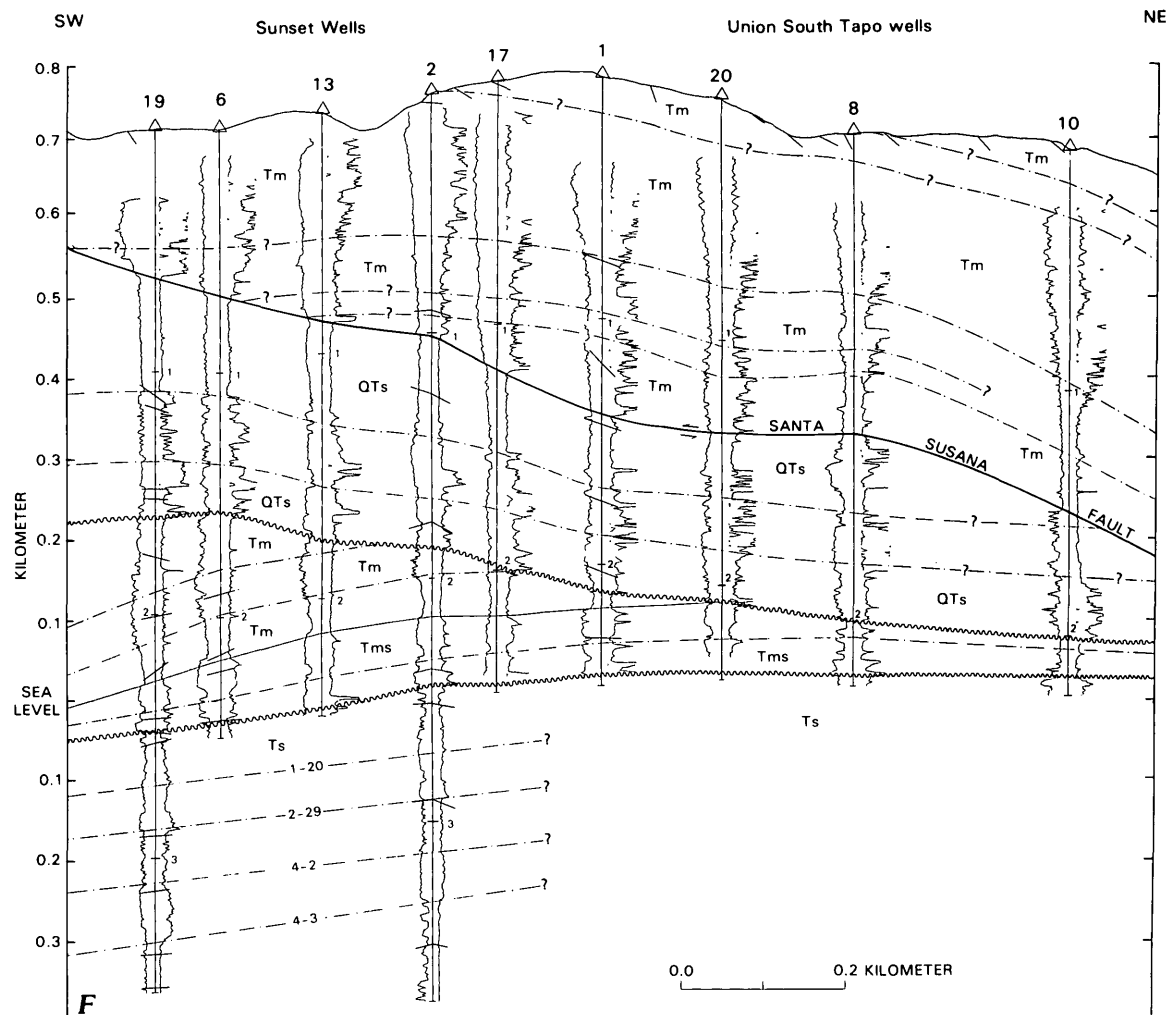


FIGURE 9.4.—Continued.

9. LATE CENOZOIC STRUCTURE OF THE SANTA SUSANA FAULT ZONE

147

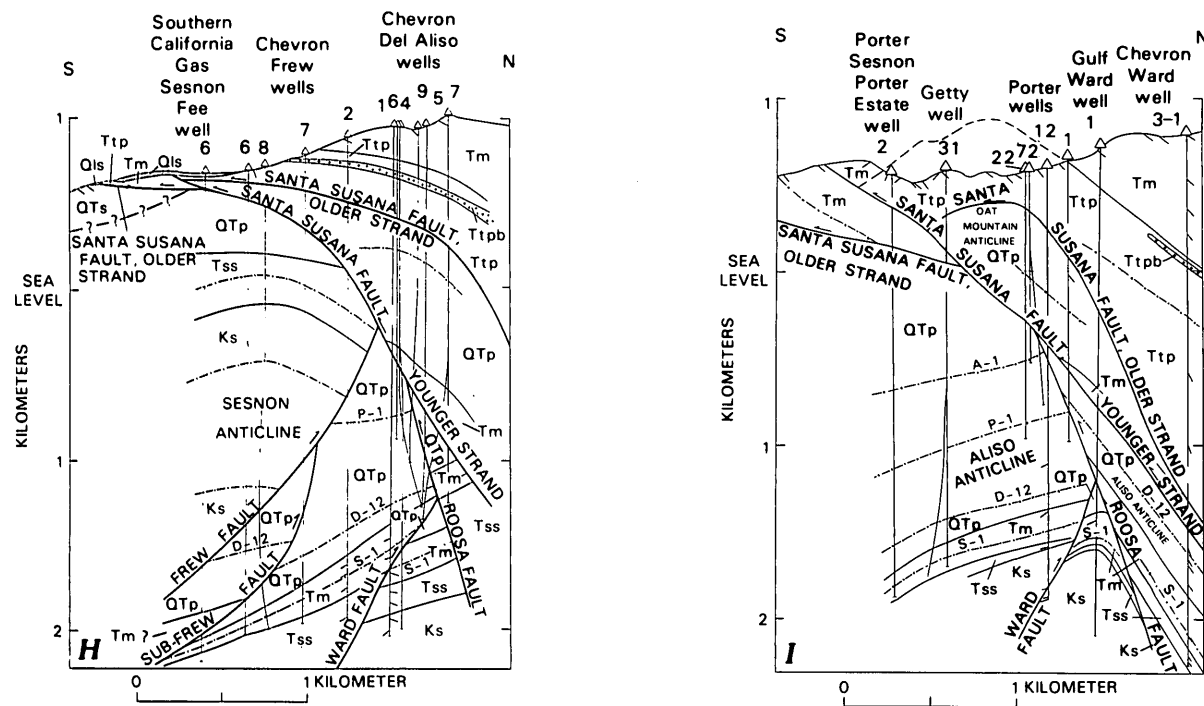


FIGURE 9.4.—Continued.

thickness is 762 m in Aliso Canyon oil field and 180 m in Oak Ridge oil field.

The contact with the overlying Modelo Formation is conformable. Boundaries of the Modelo Formation in the Santa Susana Mountains were described by Winterer and Durham (1958, 1962). A lower part with Luisian microfossils, about 40 m thick at Aliso Canyon oil field, consists of very fine grained sandstone interbedded with and overlain by gray to black siltstone and shale. An upper part with Mohnian microfossils consists of siliceous shale, impure chert, and siltstone with concretions and lentils of limestone. East of Gillibrand Canyon, the upper part of the formation contains rhythmically bedded sandstone, probably deposited by turbidity currents. Thickness of the Modelo is as much as 2,000 m. The Modelo is overlain by the Towsley Formation (Winterer and Durham, 1958). The Towsley, of Miocene and Pliocene age, consists of 1,070–1,250 m of thin-bedded gray to chocolate-brown siltstone interbedded with turbidity-current sandstone with distinctive red-brown concretions of calcite-cemented sandstone. The Towsley is also found in the Sylmar basin east of the Santa Susana fault (fig. 9.4I) where it is 460 m thick near Cascade oil field.

Younger strata of the hanging wall block include the Pico Formation and Saugus Formation. These occur north of the area described except for an area northwest of the Sylmar basin (pl. 9.1).

## STRUCTURAL GEOLOGY

The pre-Pliocene angular unconformities and normal faults of the area have been described elsewhere (Yeats, 1979). This paper concentrates on the compressional tectonism that has dominated the region from Pliocene until the present day. The oldest reverse fault in the area is the Frew fault, which is cut by all other reverse faults and is overlain unconformably by the Saugus Formation (fig. 9.4G). Other faults overlain by the Saugus include the Ward, Roosa, Torrey, and Brugher faults. The Saugus is itself cut by the Santa Susana fault and by the north strand of the Oak Ridge fault (pl. 9.1). The middle and south strands of the Oak Ridge fault (pl. 9.1) are not in contact with the Saugus; hence, their age relations with the Saugus cannot be determined.

### FREW FAULT

The Frew fault (fig. 9.5) is nowhere exposed at the surface. It was discovered in the subsurface in Aliso Canyon oil field (fig. 9.4H), where it brings Cretaceous and Paleogene rocks on the southwest against the Pico Formation ("Fernando Formation" of Yeats, 1979) on the northeast. In Aliso Canyon oil field, the fault dips 60° SW. at depth and steepens upward to 75° near its intersection

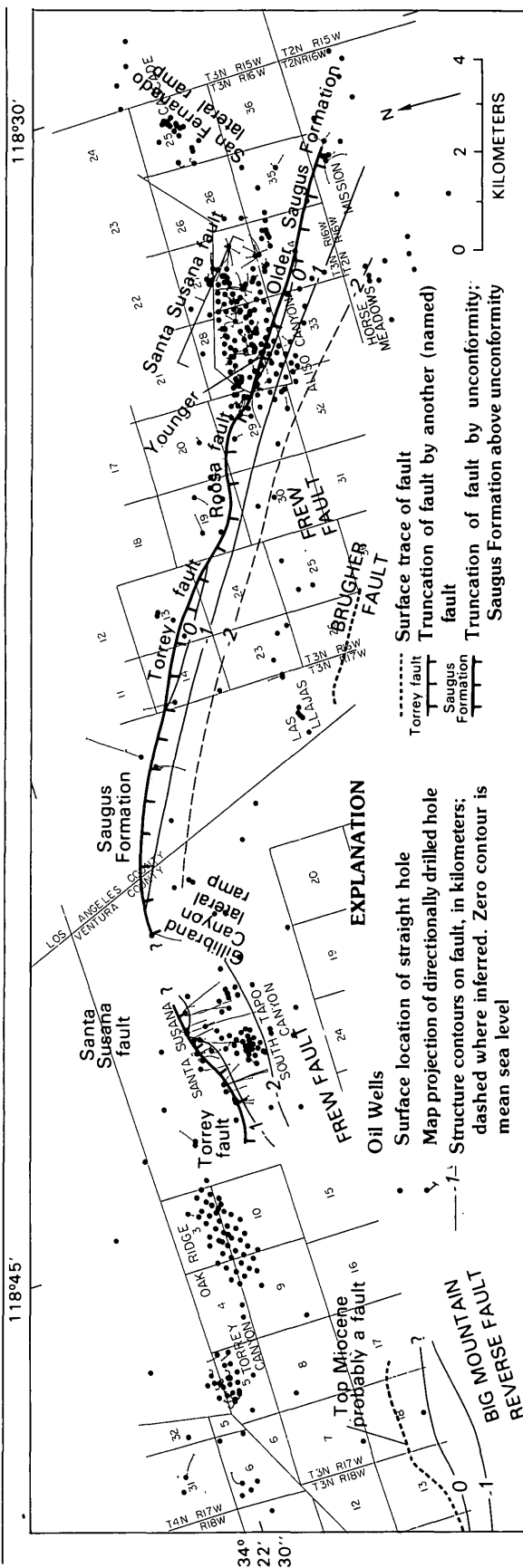


FIGURE 9.5.—Structure contours on Frew fault and Big Mountain reverse fault. Frew fault changes strike and dip across Gillibrand Canyon lateral ramp; connection across lateral ramp unclear. Frew fault apparently affected by San Fernando lateral ramp. Big Mountain reverse fault (Canter, 1974) may be an extension of Frew fault. A zone of overturned strata at the contact of the Modelo and Pico Formations (Canter, 1974) is shown as the

surface expression of the Big Mountain fault. The Frew fault is not exposed at the surface. The Brugher fault, exposed at the surface (see plate 9.1), has its north side down and is overlain by Saugus; it is part of the same fault set as the Frew and the Big Mountain reverse faults.

with the Santa Susana fault, suggesting that the Frew fault has been deformed during movement on the younger Santa Susana fault. The fault is sharply defined in some wells in which Cretaceous sandstone is in contact with Pliocene siltstone and sandstone, but in other wells a zone of gray massive siltstone and shale separates known Cretaceous and Pliocene rocks. Ingram (1959) stated that the Frew fault zone comprises numerous faults in a zone 90–275 m thick, but this is mainly the effect of the sub-Frew fault, which is structurally below the Frew and generally parallel to it. The sub-Frew fault has a separation of 170–200 m and marks the southwestern limit of the Aliso Canyon oil field. The Frew fault in Aliso Canyon oil field has a separation of 1,830–2,120 m (fig. 9.4H); separation diminishes southeastward along strike.

Farther southeast, the Frew fault is traced across a data gap of 4 km to the Mission oil field (fig. 9.5), where two faults in the Chevron Mission 6-1 well (well 2, fig. 9.3) have a combined reverse separation of the Miocene-Pliocene unconformity of 900 m. A still lower fault with similar trend and sense of separation cuts the Chevron Mission 5-1 well (well 1, fig. 9.3) and has nearly 600 m of vertical separation of the Miocene-Pliocene unconformity (Yeats and others, 1977b). These faults are cut by the northeast-dipping Granada Hills-Mission Hills reverse fault, but only the fault in the Chevron-Mission 5-1 well is found in the hanging-wall block of the Granada Hills-Mission Hills fault. All three faults are apparently pre-Saugus, and so they do not extend to the surface. The Frew fault set has not been recognized southeast of Mission oil field.

Northwest of Aliso Canyon oil field, the Frew fault continues without change of strike or dip to Gillibrand Canyon (fig. 9.5). The fault cuts the north limb of the Chivo Canyon anticline and is itself truncated by the Roosa and Torrey faults and by the unconformity at the base of the Saugus (fig. 9.4G). The Frew apparently formed during the time of deposition of the Pico Formation, because the thick sequence of the Pico on the downthrown side of the fault has no counterpart on the upthrown side. Shallow-water Pico beds on the upthrown side described by Squires (1977) may correspond to beds high in the Pico section on the downthrown side.

In the Santa Susana oil field west of Gillibrand Canyon (fig. 9.4E), a south-dipping reverse fault in the same structural position as the Frew fault of Aliso Canyon is correlated to the Frew fault. This correlation was considered questionable by Ricketts and Whaley (1975) because of the difference in trend—the Frew fault of Santa Susana oil field strikes west rather than northwest and does not line up well with the Frew fault east of Gillibrand Canyon (figs. 9.5, 9.6). In the Santa Susana oil field, the Frew fault dips 50° S., and the dip decreases upsection to 20° near the intersection with the Torrey fault (fig. 9.5). Separation is about 610 m. The Frew is cut by the Torrey fault,

which is itself overlain unconformably by the Saugus Formation (pl. 9.1). The difference in trend across Gillibrand Canyon can be explained in several ways: (1) An unmapped fault in Gillibrand Canyon with northwest trend and a large component of left slip offset the Frew fault before the formation of the Santa Susana fault, (2) the Frew fault changes strike at Gillibrand Canyon in a manner comparable to and possibly related to the change of strike of the south strand of the Oak Ridge fault at Wiley and Torrey Canyons (pl. 9.1; fig. 9.6; Ricketts and Whaley, 1975), and (3) the Frew fault west of Gillibrand Canyon is a different fault. I favor the second explanation combined with the first. The Frew fault is related to the Oak Ridge fault set and follows the same curved trend convex to the north. Left slip in the Gillibrand Canyon area before or during movement on the Santa Susana fault made this change in strike more abrupt than it would have been otherwise.

The total mapped length of the Frew fault between the South Tapo Canyon and Mission oil fields is 24 km. This is an exceptionally great distance, considering the fact that the fault is not exposed at the surface anywhere along its length.

West of South Tapo Canyon oil field, the west-trending Big Mountain reverse fault (Canter, 1974) is on trend with the Frew fault and has 100–230 m of separation (fig. 9.5). Canter (1974) believed that the fault cuts Pleistocene beds, but his work predicated the recognition of a major unconformity at the base of the Saugus Formation. Canter (1974) presented clear evidence that the Big Mountain fault cuts beds as young as the Modelo Formation and probable evidence that overturning of the Pico Formation in Happy Camp Canyon is related to drag on the Big Mountain reverse fault. In general, the Big Mountain reverse fault separates a thick sequence of the Pico and Saugus on the north from a thin sequence of the Saugus, including the marine basal member, on the south, the same structural relations that characterize the Frew fault at Aliso Canyon oil field. It seems likely that the overturned Pico at Happy Camp Canyon is overlain unconformably by the Saugus in the Happy Camp syncline, although subsurface and surface data are not sufficient to confirm this. There is no evidence that the Big Mountain reverse fault extends much farther than is shown in figure 9.5, based upon the subsurface control presented by Canter (1974).

#### BRUGHER FAULT

South of the Frew fault and Las Llajas Canyon, the Brugher fault dips 50°–60° S. and brings the Llajas Formation in the hanging wall against the Pico Formation (pl. 9.1). As described by Cabeen (1939), the fault zone is marked by a narrow zone of Modelo Formation. The

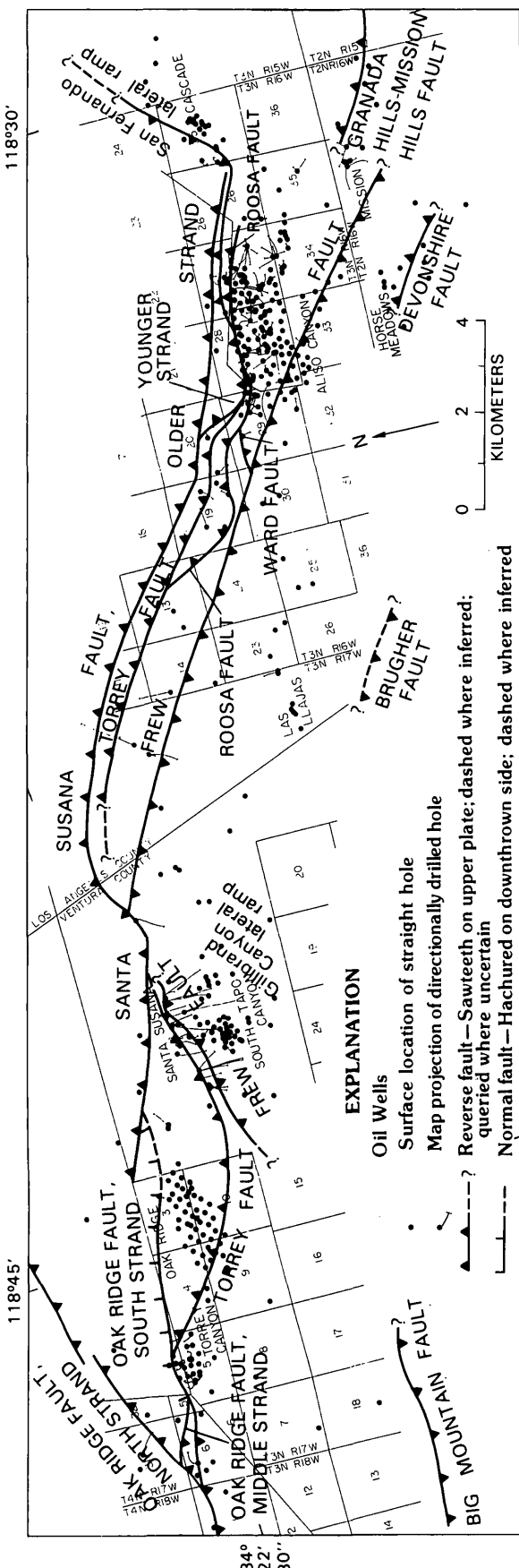


FIGURE 9.6.—Horizontal cross section of Santa Susana fault zone at -1 km. Lateral ramp refers to those parts of fault where dip steepens abruptly and strike changes to northeast. Note that Torrey fault is truncated by south strand, Oak Ridge fault, which is itself overridden by Santa Susana fault. Frew and Torrey faults may bend at Gillibrand Canyon fault or be cut by a younger fault; Torrey fault contains a broad, southward-convex lateral ramp or be cut by a younger fault; Torrey fault is a splay of Frew fault or is truncated by Frew; Roosa fault may be a splay of Torrey fault. Frew fault may extend west toward Big Mountain fault of Canter (1974).

fault is overlain unconformably by the fossiliferous Sunshine Ranch Member of the Saugus Formation. The outcropping Brugher fault is parallel to the Frew fault, has the same sense of separation, and is the same age as the subsurface Frew fault set, and thus Cabeen (1939) was the first to describe the geometry and age relations of a member of this fault set.

#### WARD FAULT

The Ward fault strikes west (fig. 9.6) and dips 60° S. in Aliso Canyon oil field (figs. 9.4H, 9.4I). Like the Frew fault, it has reverse separation with the south side up; separation is 180–210 m. The fault does not crop out, and it is noted in only 10 wells. It is the updip seal for the Sesnon and Frew zones of Aliso Canyon oil field. To the west, the Ward fault is either truncated by the Frew fault, or it is a divergent branch of the Frew fault. To the east, the Ward fault is truncated by the north-dipping Roosa fault.

The southeast-plunging Aliso anticline (fig. 9.4I) involves strata as young as the Pico Formation and is truncated by the Ward and sub-Frew faults. In the central part of Aliso Canyon field, the anticline changes trend from northwest to west. This change in trend occurs at about the same longitude north and south of the Ward and Roosa faults, suggesting that there was no appreciable strike slip along these faults (Lant, 1977). Electric-log correlations are excellent directly across the Ward fault, further supporting the interpretation of dip slip.

#### ROOSA FAULT

In Aliso Canyon oil field, the Roosa fault strikes N. 80°–90° W. (fig. 9.6) and dips 75° N., with some dip variation along strike (figs. 9.4H, 9.4I); separation is 305–365 m. The fault strikes approximately parallel to the younger Santa Susana fault, which truncates it. West of Aliso Canyon field, the Roosa fault changes strike to northwest between the Chevron Roosa 1 and Union Gardett 1–20 wells (wells 3 and 12, respectively, fig. 9.8), and farther west the strike changes back to west. Even farther west, the fault is nearly vertical near the Gulf Brady Estates 1 well (well 4, fig. 9.3), and beyond that, the fault either extends north of the Union Blue Sage 1 well (well 11, fig. 9.3) or it loses separation and dies out. The Roosa is truncated by the Torrey fault, or it is a splay of the Torrey fault (fig. 9.6).

#### TORREY FAULT

The Torrey fault (fig. 9.7) is a north-dipping reverse fault discovered in Torrey Canyon oil field (fig. 9.4B), where a deep test well found the oil-producing Sespe Formation to be repeated by the Torrey fault. Stratigraphic

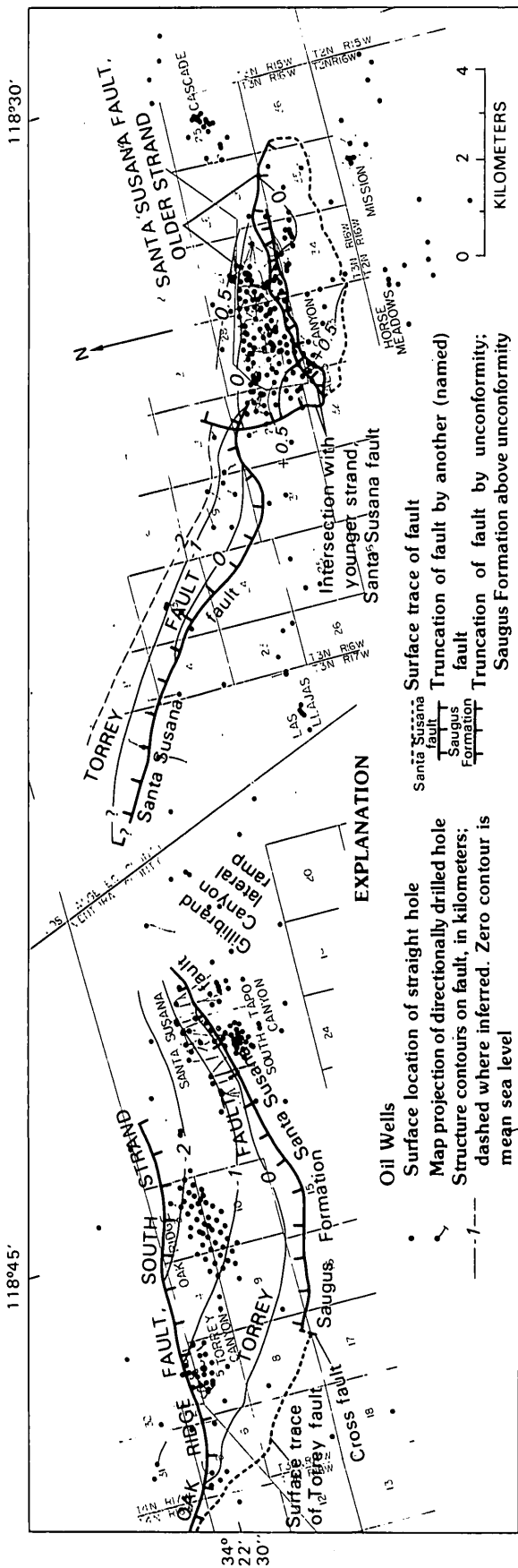


FIGURE 9.7.—Structure contours on Torrey fault and older strand of Santa Susana fault. Torrey fault bends eastward toward Gillibrand Canyon lateral ramp; connection across lateral ramp unclear. Older strand of Santa Susana fault is offset by younger strand.

separation is less than 305 m west of Torrey Canyon oil field (fig. 9.4A), 500 m in Oak Ridge oil field (fig. 9.4C), and 450 m in the Santa Susana oil field below the Frew fault (fig. 9.4E). The fault dips 10°–50° in the Torrey Canyon field, 30°–40° in the Oak Ridge field, and up to 60° in the Santa Susana oil field. West of Gillibrand Canyon, it is broadly arcuate and convex southward in map view (fig. 9.7), changing strike from southeast west of Torrey Canyon oil field to east-northeast in the Santa Susana oil field. Eastward thinning of isopachs of an intra-Sespe interval above and below the Torrey fault shows no measurable strike-slip component (Ricketts and Whaley, 1975). The fault is at the surface southwest of Torrey Canyon oil field, where upright lower Mohnian beds of the hanging wall are juxtaposed against overturned upper Mohnian beds of the footwall (pl. 9.1). The fault is marked by a zone of gouge and pulverized rock. West of Torrey Canyon oil field, the fault is difficult to trace because of extensive landslides. East of the surface exposures, the fault passes unconformably beneath folded Saugus Formation in the Happy Camp syncline (pl. 9.1). The Torrey is truncated downdip by the south strand of the Oak Ridge fault on the northwest and by the Santa Susana fault near Santa Susana oil field.

East of Gillibrand Canyon, a north-dipping reverse fault, which is truncated at the base of the Saugus (fig. 9.4G), is correlated with the Torrey fault, although it is not directly aligned with it (figs. 9.6, 9.7). The strike of the –1-km structure contour in the Santa Susana oil field west of Gillibrand Canyon (fig. 9.7) is such that the contour could join the –1-km contour east of Gillibrand Canyon by a northward-convex curve in the zone of no control. This could be interpreted as a broadly curving left step, a precursor to the sharply curved left step at Gillibrand Canyon displayed by the Santa Susana fault. Because the fault predates the Saugus, the Gillibrand Canyon step is also dated as pre-Saugus, if this interpretation is correct. Farther east, at the western edge of Aliso Canyon oil field, the Torrey fault dips 75° N. and has 305 m of separation. It may truncate the Roosa fault. It is truncated by the younger Santa Susana fault, and so it does not continue eastward into the Aliso Canyon field.

#### OAK RIDGE FAULT, SOUTH AND MIDDLE STRANDS

The Oak Ridge fault (figs. 9.6, 9.8) forms the southern boundary of the deep Ventura trough from the Santa Barbara Channel east to the Santa Susana fault (fig. 9.1). East of Wiley Canyon, the fault divides into north, middle, and south strands (pl. 9.1; figs. 9.6, 9.44). West of Torrey Canyon oil field, the south strand dips 78°–90° S. except near its intersection with the north strand west of the Gulf Hunter wells (wells 5, 6, fig. 9.3) where the near-surface

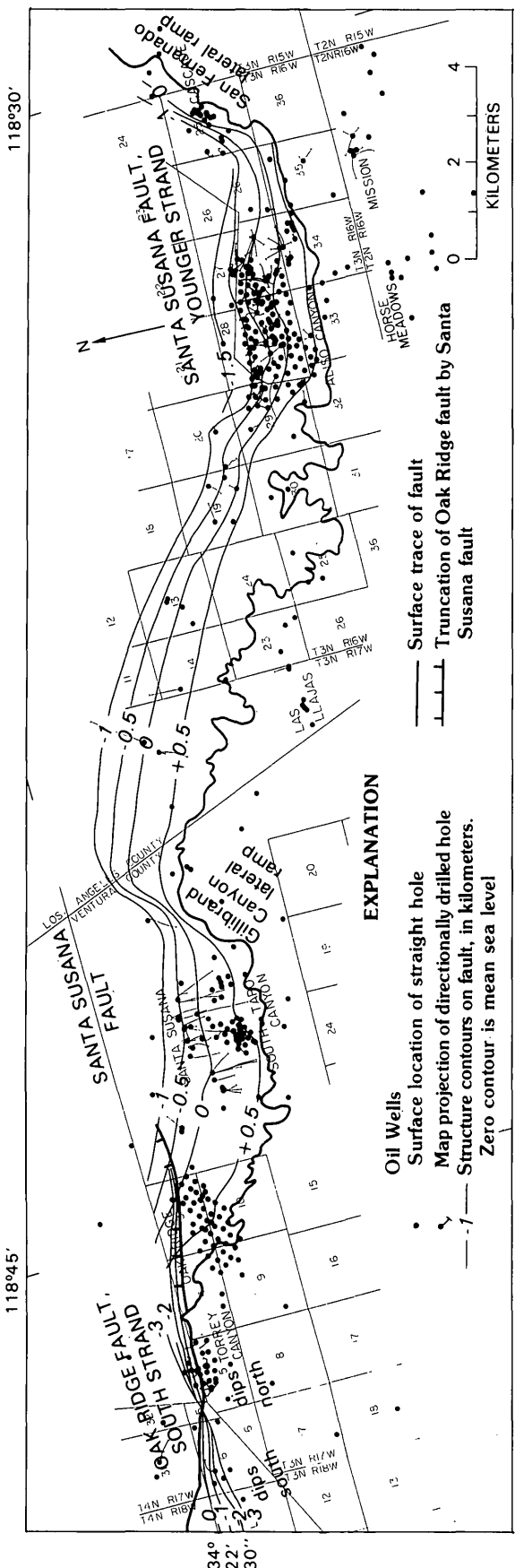


FIGURE 9.8.—Structure contours on Santa Susana fault and south strand of Oak Ridge fault. In Aliso Canyon oil field, contours are on younger strand, Santa Susana fault. In Torrey Canyon oil field, Oak Ridge fault changes eastward from south dip and reverse separation to north dip and normal separation. Santa Susana fault changes strike and dip abruptly at Gillibrand Canyon and San Fernando lateral ramp. Near-surface dip of Santa Susana fault is low compared to dip below sea level at greater depths.

portion of the fault is lobate, dipping gently south (fig. 9.8). In the Gulf-Hunter wells, the north strand turns to the east-northeast, whereas the south strand separates from the north strand and continues its eastward strike (fig. 9.8), separating a wedge of overturned and contorted Modelo Formation on the north from an upright sequence of Vaqueros Formation and Sespe Formation on the south (fig. 9.4B). Between the Texaco Hunter 1 well (well 10, fig. 9.3) and the west end of Torrey Canyon oil field, the fault dip changes from 80° S. to 80° N., and separation changes from reverse to normal at the intersection of the Oak Ridge fault, south and middle strands (fig. 9.8). The normal separation is documented by five wells in the Torrey Canyon field; separation there is more than 6 km (fig. 9.4B, 9.4C). East of Torrey Canyon, the south strand is overridden by the Santa Susana fault (pl. 9.1). Farther east, the fault may be traced in the subsurface along the northern edge of Oak Ridge oil field where it passes between the Union Oak Ridge 11-3 and 41-3 wells (wells 13, 14, fig. 9.3). The south strand of the Oak Ridge fault clearly truncates the Torrey fault in and west of Torrey Canyon oil field (fig. 9.4A, 9.4B). The youngest formation in contact with the fault is the Towsley Formation, but an overturned fold involving the Pico Formation is truncated by the south strand (fig. 9.4B). There is no evidence to demonstrate the age of the south strand with respect to the Saugus Formation.

The middle strand of the Oak Ridge fault is a high-angle reverse fault that dips 80° S. It separates from the north strand east of the Gulf-Hunter 2-6 well (well 6, fig. 9.3, 9.6) and intersects the south strand in the subsurface at the west end of Torrey Canyon oil field. The intersection at the surface is obscured by landslides. The middle strand separates two wedges of the overturned Modelo Formation. It differs from the south and north strands in that it is not lobate near the surface.

## OAK RIDGE FAULT, NORTH STRAND

The north strand of the Oak Ridge fault is a reverse fault that dips 77°–84° S. at depth but is a low-angle fault above 300 m below sea level (fig. 9.4A). The fault separates a wedge of overturned Modelo and Towsley Formations from a thick sequence of Pico and Saugus Formations in the Santa Clara Valley. North of Torrey Canyon oil field, the fault at the surface marks the contact of the Towsley Formation and the Pico (pl. 9.1). In general, it is a range-front fault, marking the southern edge of the Santa Clara Valley. Farther east, Cemen (1977) showed that the north strand dies out, and displacement is taken up by the overturned south limb of the Santa Clara Valley syncline. The fault cuts the Saugus Formation, but does not appear to cut a stream terrace near the Texaco Baker-Hunter 1 and 2 wells (wells 8, 9,

fig. 9.3). However, it may cut a stream terrace northeast of Torrey Canyon oil field.

#### SANTA SUSANA FAULT

The north-dipping Santa Susana reverse fault (fig. 9.8) is the largest and youngest fault in the area. It brings a thick sequence of the cherty facies and sandstone facies of the Modelo Formation over a thin sequence of the largely diatomaceous Modelo Formation. In the northern, hanging-wall block, the Modelo lies on the Topanga Formation and is overlain by the Towsley Formation (pl. 9.1). In the footwall block, the Modelo lies with angular unconformity on strata as old as Late Cretaceous and is itself overlain with angular unconformity by the Pico Formation. Because of these great contrasts in facies across the fault, it is difficult to estimate fault displacement. Stratigraphic separation of the base of the Modelo near Aliso Canyon field is at least 4 km (fig. 9.4G, 9.4I); true displacement is probably much larger owing to extensive slip parallel to bedding. Northwest of Gillibrand Canyon, stratigraphic separation of the base of the Modelo Formation is 1.4 km in the Santa Susana oil field (fig. 9.4E) and near zero west of the Oak Ridge oil field where the Santa Susana apparently becomes a bedding-plane fault (Ricketts and Whaley, 1975). Farther northwest, the contact between the Modelo and Towsley Formations cuts across the projection of the Santa Susana fault, indicating that the Santa Susana fault does not reach the Santa Clara Valley.

The change in clast type in the uppermost part of the Saugus Formation from a provenance of San Gabriel Mountains basement rocks upward to a local provenance of the Towsley and Modelo Formations is interpreted as evidence for the beginning of uplift of the Santa Susana Mountains (Saul, 1975) and the beginning of movement on the Santa Susana fault (Lant, 1977). The age of the uppermost part of the Saugus in the east Ventura basin is estimated at about 0.5 to 0.2 m.y. B.P. based on the presence of the Bishop tuff and the Brunhes-Matuyama chron boundary (Levi and others, 1983). South of the Santa Susana fault, the age of the Saugus is not established more closely than Pleistocene; an age of 0.5 m.y. is assumed arbitrarily for the purpose of calculating displacement rates. An accumulation of 4 km of offset in 0.5 million years would give a displacement rate of 8 mm/yr; the true displacement rate would be larger because the 4 km represents stratigraphic separation, not slip, and is a minimum figure.

Just west of Gillibrand Canyon (fig. 9.2), the Santa Susana fault overrides Modelo-chip fan material which itself overlies the Saugus Formation with angular unconformity. This fan material passes upsection into lithologically similar fan material that overlies the fault trace

unconformably (Leighton and others, 1977). The flat, constructional surface of this fan slopes southward and is itself dissected by streams, which have cut down as much as 35 m below the surface. At least part of this entrenchment occurred in Tapo Canyon (located on plate 9.1) in historical time (Scott and Williams, 1978). The geometric similarity of the fault to the seismically active San Fernando fault to the east and the Red Mountain fault to the west (Yeats and others, this volume) suggests that the fault may also be seismically active.

Below sea level, except for the Gillibrand and San Fernando lateral ramps, the fault has a relatively uniform dip of 55°–60° (fig. 9.8), comparable to the Red Mountain, San Cayetano, and San Fernando faults (fig. 9.1). Closer to the surface, the fault is lobate and dips at a low angle; locally the dip is gentle and to the south (Yeats and others, 1977a). At Aliso Canyon oil field, there are two major strands of the Santa Susana fault, one older than the other (Lant, 1977), but elsewhere there is only one major fault strand. However, subsidiary fault strands divide from the main strand and can be traced for short distances. West of Gillibrand Canyon, a subsidiary strand gives way westward to an overturned fold in the Towsley and Modelo Formations (fig. 9.2). At Gillibrand Canyon, where the Santa Susana fault steps left, there are at least six of these subsidiary strands; all terminate a few kilometers away from the step. The left step itself is marked by the change in fault contours to a more northerly strike and a steeper dip at Gillibrand Canyon, forming a lateral ramp (fig. 9.2, 9.8). The ramp is similar geometrically and in sense of displacement to a left step in the aftershock area of the 1971 earthquake on the San Fernando fault, called a downstep by Whitcomb and others (1973). The Gillibrand Canyon step is not a tear fault, for the northeast zone clearly bends east and west into the west-northwest strike and shallow dip more generally characteristic of the Santa Susana fault (fig. 9.2). Folds in the Modelo Formation north of the step and in the Saugus and Modelo Formations south of the lateral ramp are not offset directly by extensions of the ramp.

In the eastern portion of the Oak Ridge oil field, the contours on the Santa Susana fault define a flexure trending N. 50° E. from the surface at 700 m above sea level to the depth of well control at about 140 m above sea level (seen as a slight wobble on the +0.5 km contour in fig. 9.8; for more detail, see Ricketts and Whaley, 1975). The flexure is defined by 28 well-control points and by a convex-southward bend in the surface trace of the fault. The amplitude of the flexure is 45 m near the surface and 90 m at depth; the flexure is narrower at depth. Above the flexure, the Modelo Formation of the upper plate is folded into a shallow, northeast-plunging syncline with its axis parallel to that of the flexure (pl. 9.1). Below the flexure, the Modelo Formation is folded into an east-west-

trending anticline apparently unrelated to the flexure (Ricketts and Whaley, 1975). The flexure is interpreted as an irregularity in the fault surface which may be indicative of slip direction, analogous to slickensides. The slip direction based on trend of the flexure is more north-easterly than that based on focal mechanisms of the 1971 San Fernando earthquake series (Whitcomb and others, 1973) and on focal mechanisms of earthquakes in the Central Transverse Ranges in 1974-77 (Pechmann, 1983).

The Modelo Formation is folded disharmonically above and below the Santa Susana fault in the Oak Ridge oil field (fig. 9.4D), whereas in the Santa Susana and South Tapo Canyon oil fields, the Modelo beds are involved in broad, gentle folds (fig. 9.4F). In Oak Ridge oil field, the "Skootch" fault of Hall and others (1975) is a bedding thrust which follows the top of the basal Modelo sandstone and locally truncates bedding above and below the fault (fig. 9.4D).

Above sea level, west of Gillibrand Canyon, the fault gradually decreases in dip upward to about  $16^{\circ}$ , and at several localities close to the surface between Oak Ridge and South Tapo Canyon oil fields, the dip locally flattens to zero. The strike of the fault changes gradually from S.  $50^{\circ}$  E. at Oak Ridge to east at South Tapo Canyon oil field, similar to the change in strike of the underlying Torrey fault except that the Torrey changes to an east strike farther west, at Oak Ridge field. North of South Tapo Canyon oil field, the strike of the Torrey fault is N.  $70^{\circ}$  E.

At Sulphur Canyon, north of the Joughin fault and east of the Los Angeles County line (pl. 9.1), there are several imbricate slices along the fault, one of which brings Modelo deep-water sandstone over Modelo diatomaceous shale and the Saugus Formation. The sandstone is a klippe resting on a fault which dips gently south; it is different in lithology from the Modelo chert immediately north of the fault. The sandstone is itself overridden by Modelo diatomaceous shale. Farther east, there are imbrications of Modelo diatomaceous shale, Modelo chert, Pico sandstone, and Saugus conglomerate; the main trace appears to override fan material. In Browns and Mormon Canyons, the near-surface trace of the fault is nearly horizontal and locally dips south; a poorly exposed plate of Modelo chert overlies the Pico, the Saugus, and fan material. Possibly this flat-lying thrust plate is in part an old landslide later dissected by Mormon and Browns Canyons (two northward reentrants in the Santa Susana fault trace shown on plate 9.1). In the area immediately west of Aliso Canyon oil field, the deeper portion of the fault is stepped to the right, opposite in sense to downsteps at Gillibrand Canyon and the western margin of the Sylmar basin (note -1-km contour of the fault in fig. 9.8).

At Aliso Canyon, the Santa Susana fault bifurcates into an older and a younger strand (figs. 9.4H, 9.4I, 9.7, 9.8). These were believed previously to be two parallel strands (Leach, 1948; Hanson and Saunders, 1962; Slosson and Barnhart, 1967; Saul, 1975), but it can be shown that the younger strand, north of the older strand on the surface, has displaced the older strand so that the offset continuation of the older strand is structurally higher in the subsurface (fig. 9.4H, 9.4I). Thus it is necessary to describe three faults: the younger strand, the older strand in the footwall block of the younger strand, and the older strand in the hanging-wall block of the younger strand.

The older strand in the footwall block is defined by surface exposures, by 25 well-control points, and by near-surface boreholes (Slosson and others, 1964, 1965; Leighton and others, 1977). Fault dip is almost horizontal near the surface, increasing as the fault approaches the younger strand. The older strand brings the Modelo and Topanga formations in contact with the Saugus and Pico; the fault itself is marked by a thin zone of brown to black gouge containing Mohnian foraminifers. At Horse Flats (pl. 9.1), terrace deposits overlie the fault trace unconformably, leading Saul (1975) to conclude that the Santa Susana fault has not moved since the middle Pleistocene. The fault at Horse Flats is the older strand, and Saul's conclusion applies only to that strand.

The older strand in the hanging-wall block of the younger Santa Susana fault does not crop out but is defined by 190 well-control points. In the main part of Aliso Canyon oil field, the older strand is folded into a west-trending, doubly plunging antiform (fig. 9.4I) that is similar in trend and plunge to the Oat Mountain anticline in the Topanga and Modelo Formations at the surface, providing evidence that the Topanga and Modelo Formations and the fault were folded at the same time. In the southwest part of Aliso Canyon field, the fault and the overlying beds are folded into an open syncline plunging southwest (note curve in +0.5-km contour on older strand, fig. 9.7). The Topanga is cut by two high-angle faults which do not offset the older strand.

Separation on the older strand is based on the offset of the Mohnian-Luisian contact in the Modelo Formation, which is found on both sides of the fault in the hanging-wall block of the younger Santa Susana fault. Only a minimum figure for dip separation is possible in the Aliso Canyon field because much of the older strand and part of the younger strand are bedding faults in the area of well control. Minimum dip separation is close to 2 km.

The younger strand of the Santa Susana fault is simple in geometry, in contrast to the older strand. The fault is slightly lobate near the surface in the Aliso Canyon field (fig. 9.4H, 9.8), and it steepens gradually to a dip of  $60^{\circ}$  N. The fault truncates all folds and all other faults. Dip

separation of the Modelo-Pico contact is 800 m in figure 9.4H, and dip separation of the older strand is about 100 m in figure 9.4H and 250 m in figure 9.4I. The small displacement of the older strand by the younger compared with the large displacement on the older strand suggests that the younger strand formed relatively late in the Quaternary. The presence of the two strands may be related to the left step in the fault east of Aliso Canyon oil field (San Fernando lateral ramp, fig. 9.8). The younger strand cuts off the corner of the older fault as it bends sharply northeast. The younger fault is itself affected by the step, however, because it gradually changes in strike from southeast to east within Aliso Canyon oil field.

East of Aliso Canyon oil field, the strike of the Santa Susana fault bends to the northeast, and the dip increases from 60° to 85° (fig. 9.4J). The strike change at depths shallower than 600 m below sea level is gradual; strike is easterly in Aliso Canyon and only turns to the northeast at Cascade oil field (fig. 9.8). The fault strike at greater depths, 1,000–1,900 m below sea level, is southeasterly almost to Cascade field where the strike turns to the northeast. In the Cascade oil field, the fault flattens in dip abruptly at a depth of 150 m above sea level and is lobate and low angle from there to the surface at about 425 m above sea level (fig. 9.4J). The fault brings the Modelo and Towsley formations over the Pico Formation and the Sunshine Ranch Member of the Saugus Formation. A deeper fault branches from the Santa Susana and brings the Pico over the Sunshine Ranch Member of the Saugus. This fault does not crop out and may be older than the Santa Susana fault. In the northeast-trending segment, the Santa Susana fault forms the northwestern margin of the Sylmar basin, filled with a thick sequence of the Towsley, Pico, and Saugus Formations. Presumably the Modelo is present but is below well control. The most easterly well control is at Interstate Highway 5 near San Fernando Pass (Active Well, fig. 9.4K). The fault is mapped at the surface farther east (Barrows and others, 1975), but well data are not available.

The left step in the Santa Susana fault at Cascade oil field is in the same area as the lateral ramp or "downstep" marked by aftershocks of the 1971 earthquake—after-shocks which contained a large component of left slip in focal-mechanism solutions (Whitcomb and others, 1973). However, the Santa Susana fault is north of the active 1971 San Fernando thrust fault, which is on trend with the Granada Hills-Mission Hills fault (pl. 9.1) east of the lateral ramp. West of the lateral ramp, aftershocks appear to be downdip from the Northridge Hills fault (fig. 9.1) rather than the Santa Susana fault (Shields, 1977). Whereas the Santa Susana fault is the only potentially active fault in the Santa Susana Mountains, several faults geometrically similar to the Santa Susana appear to be

equally active in the San Fernando Valley, including the Santa Susana fault north of the Sylmar basin, the Granada Hills-Mission Hills fault, and the Northridge Hills fault (Shields, 1977).

## CONCLUSIONS

### HISTORY OF REVERSE FAULTING ALONG THE SANTA SUSANA FAULT ZONE

The Santa Susana fault zone follows an old depositional hinge line which separates a thin discontinuous sequence on the south from a thick continuous sequence on the north. The hinge line began to form during deposition of the Topanga Formation, slightly earlier than 14 m.y. B.P., as indicated by the radiometric age of volcanic rocks interbedded with the Topanga Formation near the Santa Susana fault (Turner, 1970) and radiometric control on the age of the Luisian Stage of Kleinpell (D. L. Turner and R. H. Campbell, in Yerkes and Campbell, 1979). The hinge line became inactive at the end of deposition of the Pico Formation. The Pico contains Repettian Stage (Natland and Rothwell, 1954) microfossils in Aliso Canyon oil field, giving it an age of 4 m.y. or less (Obradovich and Naeser, 1981) and greater than 1.5 m.y., because the Repettian is older than the Olduvai event at the Saticoy oil field in the central Ventura basin (Yeats, 1977). However, the provincial and time-transgressive nature of Repettian faunas reduces the validity of estimating the age of the Pico at Aliso Canyon, which is far from the type locality of the Repettian in the Los Angeles basin, where there is radiometric age control, and far from paleomagnetic age control in the central Ventura basin.

The original facies boundary between the thick sequence north of the Santa Susana fault zone and the thin discontinuous sequence to the south is not preserved because of the large displacement on the Santa Susana fault accompanied by uplift and erosion. If the Pico Formation (Fernando Formation of Yeats, 1979) of the footwall block was originally continuous with the Pico Formation (Winterer and Durham, 1962) north of the Santa Susana fault, as suggested by Yeats (1979), then the Pico hinge line is marked by the Frew reverse fault, which underwent movement during the deposition of the Pico.

The Torrey and Roosa faults truncate the Frew and Ward faults and constitute the first evidence of north-over-south reverse faulting—the same sense of displacement as the Santa Susana fault. The Torrey fault bends northward near the Gillibrand Canyon lateral ramp of the Santa Susana fault, suggesting that the Gillibrand Canyon lateral ramp occupies the site of an older left step that was active before deposition of the Saugus Formation. Displacement on the Torrey fault apparently was not ac-

accompanied by significant uplift of the Santa Susana Mountains, because the Saugus Formation, which overlies the Torrey, contains clast assemblages derived from crystalline basement and not sedimentary rocks of the Santa Susana Mountains.

The age of the Saugus in the east Ventura basin ranges from late Pliocene to late Pleistocene on the basis of vertebrate fossils (Winterer and Durham, 1962) and the presence of the Bishop tuff and the Brunhes-Matuyama chron boundary (Levi and others, 1983). South of the Santa Susana fault, the marine beds of the Saugus contain a fauna similar to that of the San Diego Formation (Cabeen, 1939), which is believed to be Pliocene at San Diego. Conglomerate beds in the Saugus contain a crystalline-rock-clast assemblage except for the upper 60–90 m of the upper nonmarine member at Horse Flats, near Aliso Canyon, which contains clasts derived in large part from the Towsley and Modelo Formations (Saul, 1975; Yeats, 1979). This upward change in clast assemblage from a dominance of crystalline rocks to a dominance of sedimentary rocks signals the uplift of the Santa Susana Mountains (Saul, 1975), which shut off the crystalline rock source. This uplift may have coincided with the beginning of motion on the Santa Susana fault.

As displacement on the Santa Susana fault progressed, the Saugus and older strata south of the fault were uplifted, folded, and overridden by the Santa Susana fault. Fan deposits unconformably overlying the Saugus were also overridden by the fault. However, the fault trace is overlain by younger fan deposits that are lithologically similar to those overridden by the fault. Bedding in these younger deposits slopes southward parallel to the flat, southward-sloping original depositional surface of the fan. These fans are dissected by streams which have cut down as much as 35 m below the surface of the fans (Leighton and others, 1977). In Tapo Canyon, downcutting of 3–11 m below remnants of paired terraces was recognized by Scott and Williams (1978). At least 3 m of the downcutting occurred in the last 50 years (Scott and Williams, 1978).

Yeats (1979) showed the evolution of the Santa Susana fault zone in a series of paleogeologic cross sections beginning with the end of deposition of the Modelo Formation and ending today. These cross sections suggest that the basalt flow in the Topanga Formation at Aliso Canyon oil field has been displaced toward the hanging-wall block of the Frew fault a horizontal distance of at least 6.8 km. The distance could be greater, depending on reconstruction of the eroded Oak Mountain anticline. The Frew and Ward faults account for only 1.1 km of horizontal transport, and the Roosa fault accounts for less than 0.5 km. Thus most of the horizontal shortening occurs on the Santa Susana fault, suggesting that an acceleration of horizontal shortening occurred in the Pleistocene—an ac-

celeration possibly related to acceleration of displacement on the San Andreas fault (Dickinson and others, 1972) and acceleration of subsidence in the Ventura basin (Yeats, 1978).

#### PREDICTED FAULT GEOMETRY AT DEPTH

The Santa Susana fault is irregular and low dipping near the surface, possibly in response to the topographic relief in the region which would cause considerable lateral variation in load stress. At depth, the fault dips uniformly at 55°–60°; deepest control is at 1 km below sea level in the Santa Susana and Cascade oil fields and 1.5 km below sea level in the Aliso Canyon oil field. The change from a low-dipping fault near the surface to a moderately dipping fault at depth is analogous to that defined for the 1971 San Fernando fault, based on hypocenter distribution and focal mechanisms (Whitcomb and others, 1978). At greater depths, at the base of brittle crust, the fault may flatten into a horizontal decollement (Hadley and Kanamori, 1978; Yeats, 1981).

#### RELATION TO OTHER STRUCTURES IN THE HANGING-WALL BLOCK

North of the Santa Susana fault, the rocks of the Santa Susana Mountains and east Ventura basin (fig. 9.9) are extensively folded and faulted (Winterer and Durham, 1962; Cemen, 1977; Nelligan, 1978). Much of this deformation may have occurred at the same time as displacement on the Santa Susana fault and would thus have as much potential for future activity as that fault.

The Oat Mountain anticline is a doubly plunging fold at the Aliso Canyon oil field, which exposes the Topanga Formation in its core. Structure contours on the base of the Modelo Formation are parallel to structure contours of the older strand of the Santa Susana fault. This is taken as evidence that the folding of the Topanga-Modelo contact and the folding of the older strand of the Santa Susana fault took place at the same time, probably during displacement on the younger strand of the Santa Susana fault in late Quaternary time.

Several anticlines and synclines extend west from the Gillibrand Canyon lateral ramp; some of these are overturned and verge toward the south (figs. 9.2, 9.9). One of these folds contains a north-dipping thrust fault on its flank. The thrust faults die out westward. The overturned folds change westward to upright folds which die out 6 km west of Gillibrand Canyon. These folds and associated thrust faults appear to be related to the Gillibrand Canyon lateral ramp of the Santa Susana fault. At Gillibrand Canyon, the Santa Susana fault cuts fan deposits which overlie the Saugus Formation unconformably; this relationship may set a younger limit to the age of folding west of Gillibrand Canyon.

The Gillibrand Canyon lateral ramp is a northeast-trending bend in the Santa Susana fault, not a northeast-trending tear fault cutting the Santa Susana. Nonetheless, a projection of the step northeast across the Santa Susana Mountains marks a structural discontinuity with respect to folds and faults on either side (fig. 9.9). The Del Valle fault and Newhall-Potrero anticline appear to terminate eastward against this discontinuity, and the Pico anticline and Oak Mountain syncline terminate westward against it. Aftershocks of a 1976 earthquake described by Pechmann (1983) and Simila and others (1983) follow the northeast extension of the Gillibrand Canyon downstep at least as far as the San Gabriel fault.

North of the San Fernando lateral ramp, the Pico anticline and Oat Mountain syncline terminate eastward, and the Pico anticline is replaced eastward by the Weldon, Beacon, and Legion reverse faults, each with south side up (Nelligan, 1978) (fig. 9.9). These structures are interpreted as a near-surface response to steps in the Santa Susana fault at depth.

#### SEISMIC AND GROUND-RUPTURE HAZARD

The San Fernando lateral ramp of the Santa Susana fault was seismically active during and after the 1971 San Fernando earthquake as a step of the San Fernando fault (Whitcomb and others, 1973). The epicenter of a  $M=4.6$  earthquake on April 8, 1976, at a depth of 18 km according to Pechman (1983) and 20 km according to Simila and others (1983) was near Gillibrand Canyon; a map showing the zone of aftershocks for the period 1974–77 shows both the Gillibrand Canyon and San Fernando left steps. The Gillibrand Canyon aftershocks are traced northeast at least as far as the San Gabriel fault and the San Fernando events are traced across the San Gabriel fault. Focal-mechanism solutions for 1970–75 earthquakes show predominant thrusting with  $P$ -vectors trending north to northeast (Yerkes and Lee, 1979; Simila and others, 1983); however, Pechmann (1983) indicates that the  $P$ -vector trends north. However, the Santa Susana fault

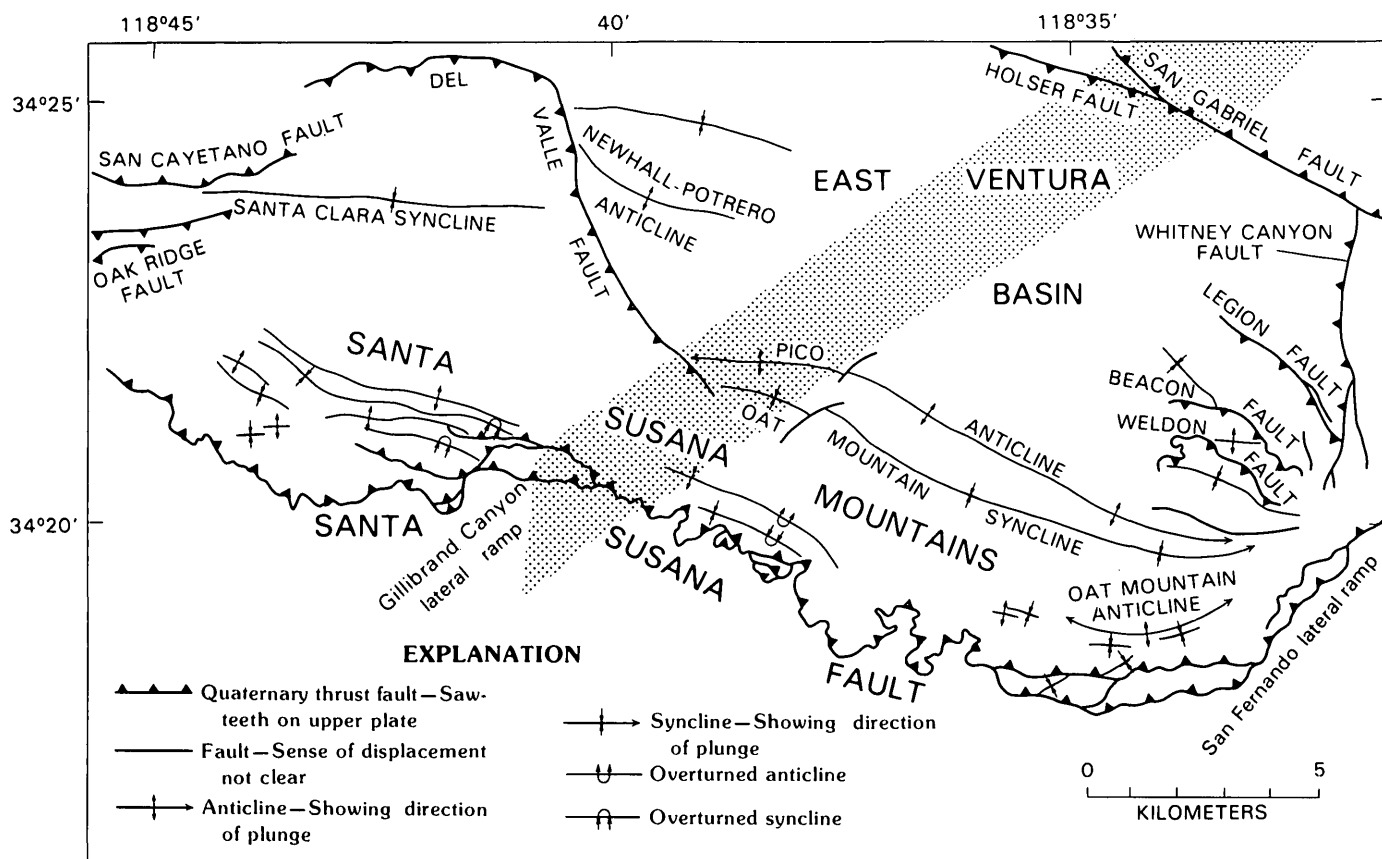


FIGURE 9.9.—Tectonic map of Santa Susana Mountains and East Ventura basin. Geology north of Santa Susana fault trace modified from Winterer and Durham (1962), Cemen (1977), and Nelligan (1978). Newhall-Potrero anticline, adjacent syncline to north, and Del Valle

fault based upon unpublished subsurface data. Patterned area marks aftershock zone of April 8, 1976, earthquakes as located by Pechmann (1983) and zone of high seismicity during the period 1932–81 (Simila and others, 1983).

itself, aside from its downsteps, has relatively low seismicity.

The Pico Canyon earthquake of April 4, 1893 (Richter, 1973), may have occurred on the Santa Susana fault. Local shaking was probably not as intense as in the 1971 San Fernando earthquake (Richter, 1973).

There is no evidence of Holocene ground rupture on the Santa Susana fault except for that mapped by Barrows and others (1975) near the Aliso Canyon oil field associated with the 1971 earthquake. Oil-well casings in the Aliso Canyon and Cascade oil fields were not sheared off by faulting in 1971. At Tapo Canyon, alluvial-fan materials overlie the fault trace and are themselves dissected by streams, suggesting a long interval of time since the last surface rupture.

The southern margin of the southern California (Pomona) uplift has a steep southward gradient across the Santa Susana, Sierra Madre, San Cayetano, and Red Mountain faults (Castle, 1978, fig. 3), suggesting that this zone is the site of a crustal discontinuity across which movement has taken place at depth. However, the leveling data on which the evidence for the southern California uplift is based has been questioned by Jackson and Lee (1979) and Strange (1981). The presence of seismicity along the lateral ramps despite a lack of evidence for Holocene ground rupture, suggests that displacement takes place by brittle faulting at depth and is propagated to the surface at intervals measured in thousands of years.

#### REFERENCES CITED

- Bain, R. J., 1954, Geology of the Eureka Canyon area, Ventura County, California: Los Angeles, University of California, M.A. thesis, 39 p.
- Barrows, A. G., Kahle, J. E., Saul, R. B., and Weber, F. H., Jr., 1975, Geologic map of the San Fernando earthquake area: California Division of Mines and Geology Bulletin 196, pl. 5, incl. map, scale 1:18,000.
- Bishop, W. C., 1950, Geology of southern flank of Santa Susana Mountains, County Line to Limekiln Canyon, Los Angeles County, California: Los Angeles, University of California, M.A. thesis, 115 p.
- Blake, G. H., 1983, Benthic foraminiferal paleoecology and biostratigraphy of the Vaqueros Formation, Big Mountain area, Ventura County, California, in Squires, R. L., and Filewicz, M. V., eds., Cenozoic geology of the Simi Valley area, southern California: Los Angeles, Pacific Section, Society of Economic Paleontologists and Mineralogists, volume and guide book, p. 173-181.
- Cabeen, W. R., 1939, Geology of the Aliso and Browns Canyons area, Santa Susana Mountains, California: Pasadena, California Institute of Technology, M.S. thesis, 36 p.
- California Well Sample Repository, 1980: California Geology, v. 32, p. 42-43.
- Canter, N. W., 1974, Paleogeology and paleogeography of the Big Mountain area, Santa Susana, Moorpark, and Simi quadrangles, Ventura County, California: Athens, Ohio University, M.S. thesis, 58 p.
- Castle, R. O., 1978, Leveling surveys and the southern California uplift: Earthquake Information Bulletin, v. 10, p. 88-92.
- Cemen, I., 1977, Geology of the Sespe-Piru Creek area, Ventura County, California: Athens, Ohio University, M.S. thesis, 69 p.
- Clark, B. L., 1924, A summary of work in progress on the Tertiary and Quaternary of western North America: Pan-Pacific Science Congress, Australia, 1923, Proceedings, v. 1, p. 874-879.
- Cordova, S., 1965, Horse Meadows oil field: California Division of Oil and Gas Summary of Operations, California Oil Fields, v. 52, no. 1, p. 61-65.
- Crouch, J. K., and Bukry, D., 1979, Comparison of Miocene provincial foraminiferal stages to coccolith zones in the California Continental Borderland: Geology, v. 7, p. 211-215.
- Cushman, J. A., and LeRoy, L. W., 1938, A microfauna from the Vaqueros Formation, lower Miocene, Simi Valley, Ventura County, California: Journal of Paleontology, v. 12, no. 2, p. 117-126.
- Dickinson, W. R., Cowan, D. S., and Schweikert, R. A., 1972, Test of new global tectonics: Discussion: American Association of Petroleum Geologists Bulletin, v. 56, p. 375-384.
- Durham, J. W., Jahns, R. H., and Savage, D. E., 1954, Marine-nonmarine relationships in the Cenozoic section of California: California Division of Mines Bulletin 170, chap. 3, p. 59-71.
- Eldridge, G. H., and Arnold, Ralph, 1907, The Santa Clara Valley, Puente Hills and Los Angeles oil district, southern California: U.S. Geological Survey Bulletin 309, 266 p.
- Evans, J. R., and Miller, R. V., 1978, Geology of the southwestern part of the Oat Mountain quadrangle, Los Angeles County, California: California Division of Mines and Geology Map Sheet 33, scale 1:12,000.
- Filewicz, M. V., and Hill, M. E., 1983, Calcareous nannofossil biostratigraphy of the Santa Susana and Llajas Formations, north side Simi Valley, in Squires, R. L., and Filewicz, M. V., eds., Cenozoic geology of the Simi Valley area, southern California: Los Angeles, Pacific Section, Society of Economic Paleontologists and Mineralogists, volume and guide book, p. 45-60.
- Hadley, D. M., and Kanamori, H., 1978, Recent seismicity in the San Fernando region and tectonism in the west-central Transverse Ranges, California: Seismological Society of America Bulletin, v. 68, p. 1449-1457.
- Hall, E. A., Barker, C. T., and Rutherford, V. E., 1975, Geology of the Torrey Canyon, Oakridge, Santa Susana, South Tapo, and Tapo Ridge oil fields, and the nearby area: Pacific Section, American Association of Petroleum Geologists Spring Field Trip, 12 p.
- Hamlin, Homer, 1904, Water resources of the Salinas Valley, California: U.S. Geological Survey Water Supply Paper 89, 91 p.
- Hanson, A. C., and Saunders, J. M., 1962, Aliso Canyon oil field: Pacific Section, American Association of Petroleum Geologists Spring Field Trip Guidebook, p. 4-5.
- Hardoin, J. L., 1958, South Tapo Canyon oil field: California Division of Oil and Gas Summary of Operations, California Oil Fields, v. 44, no. 1, p. 35-45.
- Hetherington, G. E., 1957, Geology of the South Tapo Canyon area, Santa Susana Quadrangle, Ventura County, California: Los Angeles, University of California, M.A. thesis, 93 p.
- Hodges, F. C., and Murray-Aaron, E. R., 1943, Newhall-Potrero, Aliso Canyon, Del Valle, and Oak Canyon oil fields: California Division of Oil and Gas Summary of Operations, California Oil Fields, v. 29, no. 1, p. 5-29.
- Ingram, W. L., 1959, Aliso Canyon oil field: California Division of Oil and Gas Summary of Operations, California Oil Fields, v. 45, no. 1, p. 65-73.
- \_\_\_\_\_, 1963, Cascade oil field: California Division of Oil and Gas Summary of Operations, California Oil Fields, v. 49, no. 1, p. 47-51.
- Jackson, D. D., and Lee, W. B., 1979, The Palmdale bulge—an alternative interpretation: Eos, Transactions American Geophysical Union, v. 60, p. 810.
- Jennings, C. W., 1977, Geologic map of California: California Division of Mines and Geology Geologic Data Map Series, scale 1:750,000.

- Jennings, R. A., 1957, Geology of the southeastern part of the Oat Mountain quadrangle and adjacent parts of the San Fernando quadrangle, Los Angeles County, California: Los Angeles, University of California, M.A. thesis, 105 p.
- Jestes, E. C., 1958, Geology of the Wiley Canyon area, Ventura County, California: Los Angeles, University of California, M.A. thesis, 45 p.
- Kew, W. S. W., 1924, Geology and oil resources of Los Angeles and Ventura Counties, California: U.S. Geological Survey Bulletin 753, 202 p.
- Kleinpell, R. M., 1938, Miocene stratigraphy of California: Tulsa, Oklahoma, American Association of Petroleum Geologists, 450 p.
- Lander, E. B., 1983, Continental vertebrate faunas from the upper member of the Sespe Formation, Simi Valley, California, and the terminal Eocene event, in Squires, R. L., and Filewicz, M. V., eds., Cenozoic geology of the Simi Valley area, southern California: Pacific Section, Society of Economic Paleontologists and Mineralogists, Los Angeles, volume and guide book, p. 142-153.
- Lant, K. J., 1977, Structure of the Aliso Canyon area, eastern Ventura basin, California: Athens, Ohio University, M.S. thesis, 79 p.
- Leach, C. E., 1948, Geology of Aliso Canyon field, Los Angeles County, California, in Howell, J. W., ed., Structure of typical American oil fields: Tulsa, Oklahoma, American Association of Petroleum Geologists, v. 3, p. 24-34.
- Leighton, F. B., Lung, R., and Cann, L. R., 1977, Geologic investigation by surface trenching of active faulting on the Santa Susana faults, Los Angeles and Ventura Counties, California: Final Technical Report to U.S. Geological Survey, Contract No. 14-08-0001-15863, 23 p.
- Levi, Shaul, Schultz, D. L., Yeats, R. S., Stitt, L. T., and Sarna-Wojcicki, A. M., 1983, Paleomagnetism of the Saugus Formation, Los Angeles County, California [abs.]: Geological Society of America Abstracts with Programs, v. 15, no. 5, p. 391.
- Levorsen, R. I., 1947, Geology of the Las Llajas Canyon area, California: Los Angeles, University of California, M.A. thesis, 59 p.
- Lewis, W. D., 1940, The geology of the upper Las Llajas Canyon area, Santa Susana Mountains, California: Pasadena, California Institute of Technology, M.S. thesis, 73 p.
- Mallory, V. S., 1959, Lower Tertiary biostratigraphy of the California Coast Ranges: Tulsa, Oklahoma, American Association of Petroleum Geologists, 416 p.
- Martin, D. R., 1958, Geology of the western part of the Santa Susana Mountains, Ventura County, California: Los Angeles, University of California, M.A. thesis, 75 p.
- Mefferd, M. G., and Cordova, S., 1961, Mission oil field: California Division of Oil and Gas Summary of Operations, California Oil Fields, v. 47, no. 1, p. 79-86.
- Mitchell, W. S., and Wolff, M., 1971, Santa Susana oil field: California Division of Oil and Gas Summary of Operations, California Oil Fields, v. 57, no. 1, p. 77-89.
- Nagle, H. E., and Parker, E. S., 1971, Future oil and gas potential of onshore Ventura basin, California: American Association of Petroleum Geologists Memoir 15, p. 254-296.
- Natland, M. L., and Rothwell, W. T., Jr., 1954, Fossil foraminifera of the Los Angeles and Ventura regions, California, in Geology of southern California: California Division of Mines Bulletin 170, Chap. 3, p. 33-42.
- Nelligan, F. M., 1978, Geology of the Newhall area of the eastern Ventura and western Soledad basin, California: Athens, Ohio University, M.S. thesis, 117 p.
- Nelson, R. N., 1925, A contribution to the paleontology of the Martinez Eocene of California: University of California Department of Geological Sciences Bulletin, v. 15, no. 11, p. 397-466.
- Oakeshott, G. B., 1958, Geology and mineral deposits of San Fernando quadrangle, Los Angeles County, California: California Division of Mines Bulletin 172, 147 p.
- Obradovich, J. D., and Naeser, C. W., 1981, Geochronology bearing on the age of the Monterey Formation and siliceous rocks in California, in Garrison, R. E., and others, eds., The Monterey Formation and related siliceous rocks of California: Los Angeles, Pacific Section, Society of Economic Paleontologists and Mineralogists, p. 87-95.
- Pechmann, J. C., 1983, The relationship of small earthquakes to strain accumulation along major faults in southern California: Pasadena, California Institute of Technology, Ph.D. dissertation, 175 p.
- Poore, R. Z., 1976, Microfossil correlations of California lower Tertiary sections: a comparison: U.S. Geological Survey Professional Paper 743-F, 8 p.
- Richter, C. F., 1973, Historical seismicity of San Fernando earthquake area, in Murphy, L. M., coordinator, San Fernando, California, earthquake of February 9, 1971: U.S. Department of Commerce, National Oceanic and Atmospheric Administration, v. 3, p. 5-11.
- Ricketts, E. W., and Whaley, K. R., 1975, Structure and stratigraphy of the Oak Ridge fault-Santa Susana fault intersection, Ventura basin, California: Athens, Ohio University, M.S. thesis, 81 p.
- Roth, G. H., and Sullwold, H. H., 1958, Cascade oil field, in Higgins, J. W., ed., A guide to the geology and oil fields of the Los Angeles and Ventura regions: Pacific Section, American Association of Petroleum Geologists, p. 166-171.
- Saul, R. B., 1975, Geology of the southeast slope of the Santa Susana Mountains and geologic effects of the San Fernando earthquake: California Division of Mines and Geology Bulletin 196, p. 187-194.
- , 1979, Geology of the SE Oat Mountain quadrangle, Los Angeles County, California: California Division of Mines and Geology Map Sheet 30, scale 1:18,000, text, 19 p.
- Schenck, H. G., 1931, Cephalopods of the genus *Aturia* from western North America: University Publications of California, Department of Geological Sciences Bulletin, v. 19, p. 436-491.
- Schultz, C. H., 1955, Oak Ridge field: California Division of Oil and Gas Summary of Operations, California Oil Fields, v. 41, no. 1, p. 23-31.
- Scott, K. M., and Williams, R. P., 1978, Erosion and sediment yields in the Transverse Ranges, southern California: U.S. Geological Survey Professional Paper 1030, 38 p.
- Seedorf, D. C., 1983, Upper Cretaceous through Eocene subsurface stratigraphy, Simi Valley and adjacent regions, California, in Squires, R. L., and Filewicz, M. V., eds., Cenozoic geology of the Simi Valley area, southern California: Los Angeles, Pacific Section, Society of Economic Paleontologists and Mineralogists, volume and guide book, p. 109-128.
- Seiden, H., 1972, Geology of Las Llajas Canyon, Ventura County, California: Los Angeles, University of California, M.S. thesis, 33 p.
- Shields, K. E., 1977, Structure of the northwestern margin of the San Fernando Valley, Los Angeles County, California: Athens, Ohio University, M.S. thesis, 82 p.
- Simila, G. W., Hagan, J. D., and Eliades, P. G., 1983, Earthquake history of the Simi Valley area, California in Squires, R. L., and Filewicz, M. V., eds., Cenozoic geology of the Simi Valley area, southern California: Los Angeles, Pacific Section, Society of Economic Paleontologists and Mineralogists, volume and guide book, p. 241-246.
- Slosson, J. E., and Barnhart, J. T., 1967, Late Pleistocene deformation in the Limekiln Canyon area, Santa Susana Mountains: Bulletin of the Southern California Academy of Science, v. 66, no. 1, p. 129-134.
- Slosson, J. E., and Associates, 1964, Geologic map of Tract 28648, Porter Ranch, Northridge, California: unpublished map dated December 17, 1964, with accompanying cross sections A-A' through G-G' prepared for Macco Realty Co., scale 1:1,200.
- , 1965, Geologic map of Unit 9, Porter Ranch, Northridge, California: unpublished map dated July 20, 1965, prepared for Macco Realty Co., scale 1:1,200.

- Squires, R. L., 1977, Terebratulid death assemblages, Plio-Pleistocene of Browns Canyon, Santa Susana Mountains, California [abs.]: Geological Society of America Abstracts with Programs, v. 9, no. 4, p. 502.
- \_\_\_\_\_, 1983, Eocene Llajas Formation, Simi Valley, southern California, in Squires, R. L., and Filewicz, M. V., eds., Cenozoic geology of the Simi Valley area, southern California: Los Angeles, Pacific Section, Society of Economic Paleontologists and Mineralogists, volume and guide book, p. 81-95.
- Stewart, R. D., 1952, The Horse Meadows oil field, in Pacific Section, American Association of Petroleum Geologists Field Trip Guidebook, June 1, 1952.
- Tudor, R. B., 1963, Las Llajas oil field: California Division of Oil and Gas Summary of Operations, California Oil Fields, v. 49, no. 2, p. 53-57.
- Turner, D. L., 1970, Potassium-argon dating of Pacific Coast Miocene foraminiferal stages: Geological Society of America Special Paper 124, p. 91-129.
- Watts, W. L., 1897, Oil and gas yielding formations of Los Angeles, Ventura, and Santa Barbara Counties: California State Mining Bureau Bulletin 11, 94 p.
- Weber, F. H., Jr., 1975, Geologic cross-sections of the Sylmar-San Fernando area utilizing data collected in study of San Fernando earthquake: California Division of Mines and Geology Bulletin 196, plate 5, scale 1:18,000.
- \_\_\_\_\_, 1975, Surface effects and related geology of the San Fernando earthquake in the Sylmar area: California Division of Mines and Geology Bulletin 196, p. 71-96.
- Whitcomb, J. H., Allen, C. R., Garmany, J. D., and Hileman, J. A., 1973, San Fernando earthquake series, 1971: Focal mechanisms and tectonics: Review of Geophysics and Space Physics, v. 11, p. 693-730.
- Winterer, E. L., and Durham, D. L., 1958, Geologic map of a part of the Ventura basin, Los Angeles County, California: U.S. Geological Survey Oil and Gas Investigations Map OM-196, scale 1:24,000.
- \_\_\_\_\_, 1962, Geology of southeastern Ventura basin, Los Angeles County, California: U.S. Geological Survey Professional Paper 334-H, p. 275-366.
- Yeats, R. S., 1977, High rates of vertical crustal movement near Ventura, California: Science, v. 196, p. 295-298.
- \_\_\_\_\_, 1978, Neogene acceleration of subsidence rates in southern California: Geology, v. 6, p. 456-460.
- \_\_\_\_\_, 1979, Stratigraphy and paleogeography of the Santa Susana fault zone, Transverse Ranges, California, in Armentrout, J. M., Cole, M. R., and Ter Best, H., eds., Cenozoic paleogeography of the western United States: Pacific Coast Paleogeography Symposium 3: Los Angeles, Pacific Section, Society of Economic Paleontologists and Mineralogists, p. 191-204.
- \_\_\_\_\_, 1981, Quaternary flake tectonics of the California Transverse Ranges: Geology, v. 9, p. 16-20.
- Yeats, R. S., Butler, M. L., and Schlueter, J. C., 1977a, Santa Susana-San Cayetano-Red Mountain fault system: Subsurface geology, mechanical analysis, and displacement rates: Part III. Geology of the central Santa Susana fault area, Ventura and Los Angeles Counties, California: Final Technical Report to U.S. Geological Survey, Contract No. 14-08-0001-15886, 28 p.
- Yeats, R. S., Lant, K. J., and Shields, K. E., 1977b, Subsurface geology of the Santa Susana fault in the aftershock area downstep of the 1971 San Fernando earthquake: Final Technical Report to U.S. Geological Survey, Contract No. 14-08-0001-15271, 26 p.
- Yerkes, R. F., and Campbell, R. H., 1979, Stratigraphic nomenclature of the central Santa Monica Mountains, Los Angeles County, California: U.S. Geological Survey Bulletin 1457-E, 31 p.
- Yerkes, R. F., and Lee, W. H. K., 1979, Maps showing faults and fault activity, and epicenters, focal depths, and focal mechanisms for 1970-1975 earthquakes, western Transverse Ranges, California: U.S. Geological Survey Miscellaneous Field Studies Map MF-1032, scale 1:250,000.

## 10. GEOLOGY AND SEISMICITY OF THE EASTERN RED MOUNTAIN FAULT, VENTURA COUNTY

By ROBERT S. YEATS<sup>1</sup>, W. H. K. LEE, and ROBERT F. YERKES

### ABSTRACT

The Red Mountain fault is a seismically active north-dipping east-trending reverse fault. It marks the south edge of a seknoll that existed during deposition of Pliocene and Pleistocene strata 1 to 3 million years ago. The fault dips about 48° N. at the surface, but oil-well data indicate dips of 60° at depths of 3 km. Near the east end of its trace at the Ventura River, the fault bends sharply northward, and apparent stratigraphic separation diminishes to near zero. Because strata in the footwall are parallel to the fault, actual displacement cannot be determined. Twenty-eight small earthquakes were recorded in the Lake Casitas area northwest of the bend during 1970-75. Two of the earthquakes occurred at apparent depths of 5 km or less; the rest occurred at depths to 12 km, inferred to be within pre-Tertiary rocks. Twenty-six of the events describe a tabular zone, 3 km wide, that projects downward along the dip of the fault; at a depth of 12 km, the zone dips 63° N. Five focal-mechanism solutions verify the observed north dip and reverse displacement and suggest a small component of left slip.

### INTRODUCTION AND GEOLOGIC SETTING

The Red Mountain fault extends from the Ventura River westward 18 km to the coastline at Rincon Point (fig. 10.1) and continues offshore (Weber and others, 1973; Ziony and others, 1974; Jackson and Yeats, 1982). The fault is considered to be active because it offsets a late Pleistocene marine terrace, disrupts a probable Holocene soil zone, and deforms terraces of the Ventura River (Putnam, 1942; Buchanan-Banks and others, 1975; Lajoie and others, 1979; Keller and others, 1982; Rockwell and others, 1984). Along most of its length in hilly terrain south of Red Mountain, the surface trace is poorly exposed and is commonly obscured by landslides (fig. 10.2). Small earthquakes have been recorded north of the surface trace of the eastern segment, and focal mechanisms for some of these events have been determined (fig. 1; Lee and others, 1979). We conclude that these earthquakes are on the Red Mountain fault.

The northern, hanging-wall, block of the eastern segment of the fault consists of Miocene and older sedimentary rocks folded into an east-southeast-trending, doubly plunging anticline—the Red Mountain dome of Putnam (1942). Shale of early Miocene (Saucesian) age is underlain

by 60 m of marine sandstone of Oligocene age, 1,000 m of the nonmarine Sespe Formation of Oligocene and Eocene age, and 580 m of the Coldwater Sandstone, 800 m of the Cozy Dell Shale, and at least 100 m of the Matilija Sandstone, all of Eocene age. These thicknesses are based on well control in the Conoco-Casitas 1 and 2 wells, (cross section, fig. 10.3). The usage of Matilija Sandstone, Cozy Dell Shale and Coldwater Sandstone is that of Vedder (1972), and the usage of Sespe Formation is that of Kew (1924). The thicknesses at Red Mountain are less than those for equivalent formations cropping out to the north (2,130 m for the Sespe, 850 m for the Coldwater, and 1,200 m for the Cozy Dell, as shown on an unpublished map by T. L. Bailey; see also Nagle and Parker, 1971). Based upon outcrop thickness, at least 2,100 m of Tertiary sedimentary rocks underlies the Cozy Dell at the Red Mountain dome; these rocks are assumed to rest on Upper Cretaceous sedimentary rocks.

The southern, footwall, block consists of Pliocene and Pleistocene deep-water sedimentary rocks. The Bailey ash, 1.2 m.y. old (Izett and others, 1974), has been mapped by A. M. Sarna-Wojcicki (written commun., 1976) near the surface trace of the fault. About 3,600 m of Pleistocene and Pliocene beds lies between the ash bed and the base of the Pliocene (Repettian) in the central Ventura Avenue oil field, 3,300 m southeast of the Red Mountain fault (Hacker, 1969; Yeats, 1976, 1980, 1983). In the oil field, the Shell-Taylor 653 well (Yeats, 1980), a 6,553-m-deep test well, penetrated the Pliocene and bottomed in marine Miocene strata without reaching Oligocene marine sandstone (Yeats, 1983). The thickness of the Pliocene and Pleistocene sequence is about the same as in the section that crops out east of the Red Mountain fault, where Pliocene strata overlie beds with microfossils correlated with the Delmontian Stage of Kleinpell (1938) (See cross section C-C' of fig. 2 in Yeats, 1976).

Deep-water Pliocene and Pleistocene sandstone in the Ventura Avenue anticline changes northward to mudstone near the Red Mountain fault. This facies change is observed in the "middle Pico" between the anticline and the Conoco Grubb 173 and Conoco Casitas 2 wells (fig. 10.3); for the "lower Pico" and Repettian the change lies between the oil-producing sandstone in the anticline and

<sup>1</sup>Department of Geology, Oregon State University, Corvallis, Oregon 97331.

Manuscript received for publication on October 1, 1980.

the sliver of siltstone between the lower and upper strands of the Red Mountain fault in these same wells. A change of facies from sandstone westward to mudstone occurs in the homoclinal section that crops out in the north flank of the Cañada Larga syncline (see cross section C-C' of fig. 2 in Yeats, 1976 and the Conoco Grubb 173 and Casitas 2 wells). The northern edge of the sandstone-dominated Pliocene and Pleistocene sequence curves to the southwest parallel to the Red Mountain fault, controlled in part by an ancestral south-flowing drainage parallel to the Ventura River and in part by greater subsidence on the downthrown side of the Red Mountain fault. The hanging-wall block of the fault may have been a seaknoll during the time of deposition of Pliocene and Pleistocene sediments, analogous to the South Mountain seaknoll of Yeats (1965).

#### ACKNOWLEDGMENTS

Support for Yeats was provided by Contracts No. 14-08-0001-15886, 14-08-0001-17730, and 14-08-0001-19173 of the Earthquake Hazards Reduction Program, U.S. Geological Survey. James C. Schlueter prepared the subsurface cross section and a preliminary version of the fault contour map. The Javon Canyon fault trace on figure 10.2 is based on mapping by A. Sarna-Wojcicki (Sarna-Wojcicki and others, this volume). The traces of the Red Mountain fault west of the Conoco Grubb 173 well are based on unpublished mapping by T. W. Dibblee, Jr., and modified

by F. B. Grigsby based on subsurface data. The California Division of Oil and Gas and the petroleum industry released well data essential to the study. Laboratory facilities at Ohio University and Oregon State University were used in reducing the data.

#### GEOLOGIC INVESTIGATION

The surface trace of the Red Mountain fault is modified from Weber and others (1973) on the basis of unpublished oil-company field mapping by T. W. Dibblee, Jr. and F. B. Grigsby (figs. 10.1 and 10.2). The fault zone itself is 300-400 m thick and consists of shale and mudstone of Miocene and Pliocene age dipping mainly to the north (fig. 10.3). The structure contours of figure 10.2 are on the faulted boundary between Pliocene and Pleistocene strata in the footwall block and Miocene and older strata in the hanging-wall block.

Cañada Larga syncline of Putnam (1942), called the Ventura syncline by Weber and others (1973), is truncated by the Red Mountain fault at the Ventura River (fig. 10.2; Weber and others, 1973). Farther west, the fault is in contact with the south flank of this syncline; the north flank is cut out at the outcrop and in the subsurface.

The south-dipping Javon Canyon reverse fault of Sarna-Wojcicki and others (1979; this volume) west of the Conoco Grubb 173 well (fig. 10.2) is the surface trace of the Padre Juan fault of adjacent oil fields. The south dip of the Padre Juan fault is based upon well data from the Rincon oil field (cross section C-D, Rincon Field, California Division of Oil and Gas, 1974; F. B. Grigsby, oral commun., 1984) and the San Miguelito oil field (Hacker, 1969; F. B. Grigsby, oral commun., 1984). We assume that the Padre Juan fault loses separation eastward and dies out west of cross section A-A' (fig. 10.3).

Subsurface control on the Red Mountain fault is based mainly on the Conoco Grubb 173, Conoco Casitas 2, Conoco Hobson 3, Shell Wood 1, and Shell Hoffman 1 wells. The Shell Hoffman well-control point on the Red Mountain fault is from a hole directionally drilled from the surface location shown on figure 10.2. The fault dips 56° N. as shown by data from the Conoco Hobson 3 and Shell Hoffman 1 wells. Farther east, the dip is 55°-60° N., as shown by data from the Conoco Grubb 173, Conoco Casitas 2 (fig. 10.3), and Shell Wood 1 wells. There is only a slight decrease in dip near the surface, in contrast to the San Cayetano and Santa Susana faults to the east (Yeats, 1976; 1983; this volume).

Maximum apparent stratigraphic separation of the fault zone occurs in the vicinity of cross section A-A' (fig. 10.3). The Conoco Casitas 2 well penetrates the marine Eocene strata in the hanging wall and Pliocene and Pleistocene strata ("upper Pico") in the footwall of the Red Mountain fault zone. At the surface, south of the Conoco Grubb

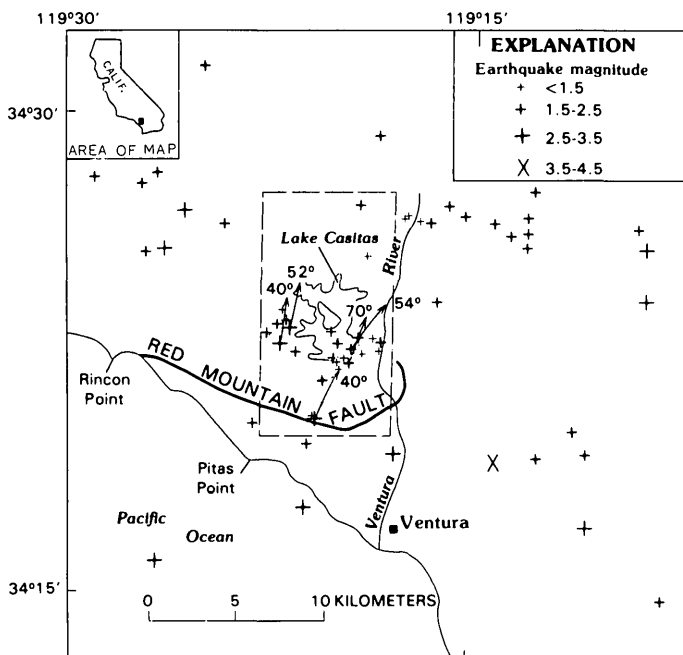


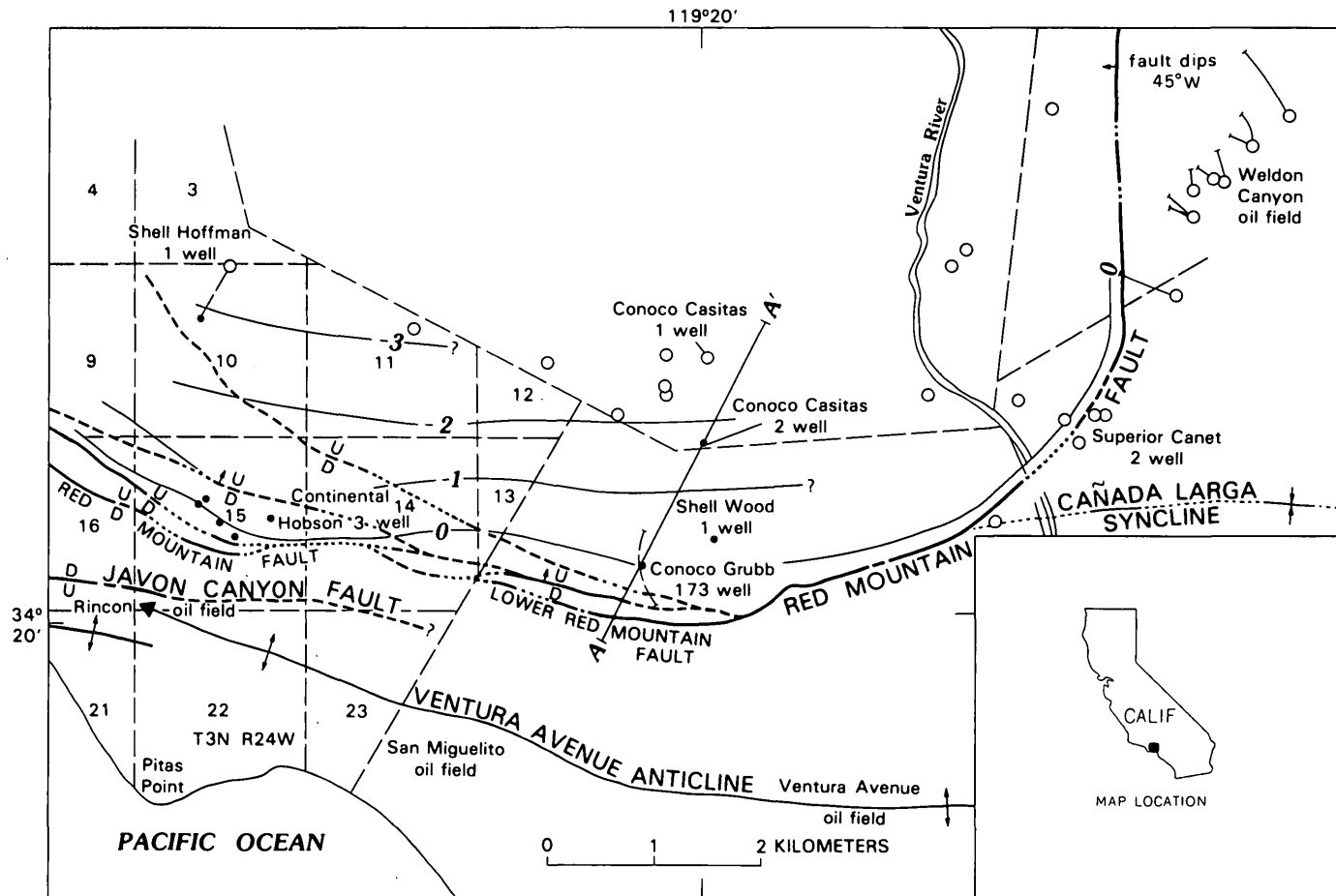
FIGURE 10.1.—Ventura region showing 1970-75 epicenters of earthquakes with magnitudes >1 (Lee and others, 1979), direction (arrows) and plunge of slip vectors, the Red Mountain fault, and outline (dashed line) of area of more detailed study of earthquakes.

173 well, lower Miocene shale in the hanging wall is adjacent to Pliocene and Pleistocene strata in the footwall.

The apparent stratigraphic separation of the top of the Oligocene marine sandstone may be determined by measuring the thickness of strata in the footwall between the Pleistocene bed adjacent to the top of the Oligocene sandstone where it intersects the fault south of the Grubb 173 well and the estimated top of the Oligocene sandstone in the footwall. This sandstone must be more than 6,300 m below sea level in the Ventura Avenue anticline because a deep test well at the crest of the anticline did not reach

it at that depth (Yeats, 1983). The position of this horizon in the footwall, as shown in figure 10.4, is based upon thicknesses of strata of Miocene and Pliocene age exposed east of the Red Mountain fault and in the Ventura River valley north of where it is crossed by the Red Mountain fault (Nagle and Parker, 1971). The apparent stratigraphic separation shown in figure 10.4 is at least 5,500 m and may be more, because the top of the Oligocene sandstone is not controlled by well data.

East of the Conoco Grubb 173 well, the fault changes strike gradually to the northeast, north, and north-



#### EXPLANATION

- Surface trace of fault showing direction of dip—Dashed where inferred, dotted where concealed, queried where uncertain; U, upthrown side; D, downthrown side
- Anticline—Showing direction of plunge
- Syncline—Dotted where concealed
- Oil Wells
- Does not penetrate fault, straight hole
- Map projection of directionally drilled hole
- Penetrates fault, straight hole
- Map projection (approximate) of directionally drilled hole which penetrates fault; circle, surface location; dot, control point on Red Mountain fault
- 2 — Structure contours on fault in kilometers. Zero contour is mean sea level
- A A' Location of section shown in figure 10.3

FIGURE 10.2.—The eastern end of the Red Mountain fault as determined from surface mapping and well data. Traces of the Padre Juan fault and the Ventura Avenue anticline from Weber and others (1973) and unpublished mapping by T. W. Dibblee, Jr., and F. B. Grigsby.

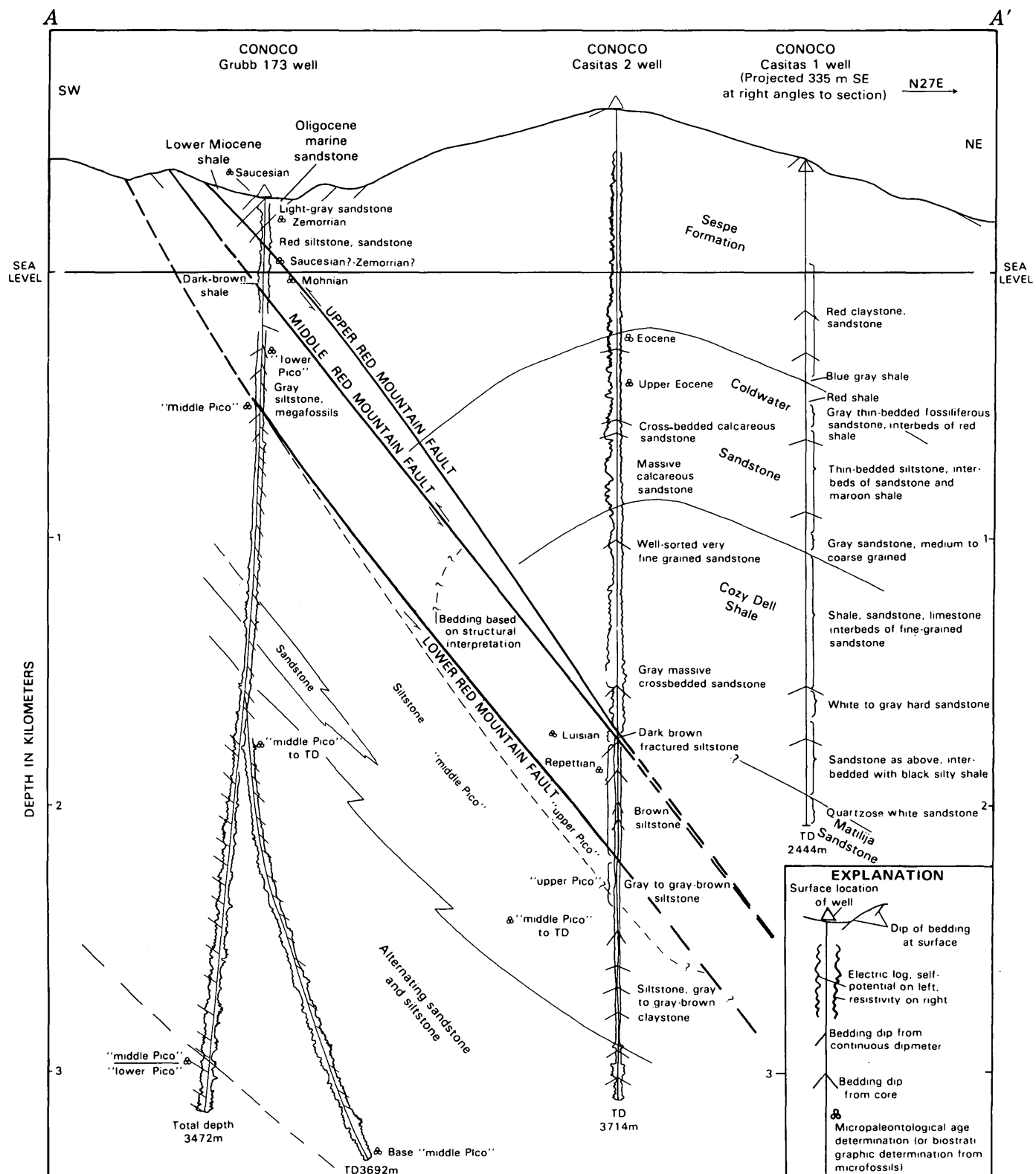


FIGURE 10.3.—Cross section through Red Mountain fault showing well data. The middle Red Mountain fault shown on this figure corresponds to the contoured trace of the Red Mountain fault shown in figure 10.2. No vertical exaggeration. "Upper Pico," "middle Pico," and "lower Pico" are informal descriptive terms used by the petroleum industry for the benthic microfaunal assemblages in the area. See figure 10.2 for section location.

northwest. Wells in the hanging-wall block in this area are too shallow to penetrate the fault, so all control is from the outcrop. Separation diminishes to nearly zero northeast of Ventura River (dotted trace of the fault near the Superior Canet 2 well, fig. 10.2), and the fault cannot be recognized in the subsurface northwest of the Weldon Canyon oil-field wells. Either the Red Mountain changes to a bedding-plane fault in upper Miocene and lower Pliocene strata, or the style of deformation changes from faulting at Red Mountain to folding north of the Cañada Larga syncline. Both folding and faulting may be involved.

### SEISMIC INVESTIGATION

Lee and others (1979) and Yerkes and Lee (1979) relocated 1970–75 earthquakes in the Ventura region, and part of their epicenter map is shown on figure 10.1. Twenty-eight of these epicenters lie within the dashed rectangle shown in figure 10.1 and are sufficiently well located that the radius of statistical uncertainty for the epicenter location is less than 1.5 km and the depth uncertainty is less than 1.8 km. These events are listed in table 10.1. Focal-mechanism solutions for events 8–12 (composite), 14, 16, 19, and 21 are shown in figure 10.5. Trend and plunge of slip vectors based on these focal-mechanism solutions are shown in figure 10.1.

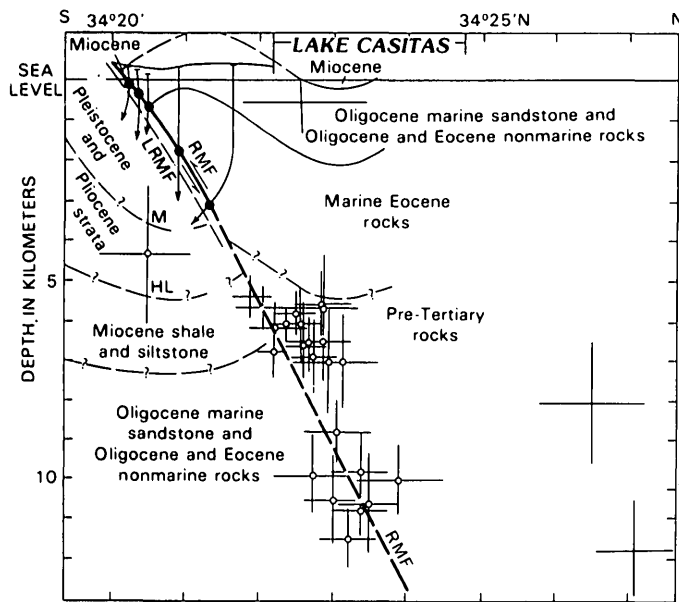


FIGURE 10.4.—Projection of earthquake hypocenters (crosses) located beneath rectangular area shown in figure 10.1 onto a north-south cross section through Red Mountain fault showing surface and well (dots) control. On each hypocenter cross, vertical line indicates depth uncertainty, horizontal line indicates epicenter location uncertainty. Where well trace is terminated by arrow, well continues below arrow into the footwall block. RMF, Red Mountain fault; LRMF, Lower Red Mountain fault. M and HL are electric-log markers from the Ventura oil field (Yeats, 1980). No vertical exaggeration.

As seen in figure 10.1, there is a concentration of epicenters in the vicinity of Lake Casitas, near the east end of the Red Mountain fault where the fault trace changes strike to the north. Within the rectangle, only two earthquakes were at depths shallower than 5 km, and none was deeper than 12 km. Seven events west of the rectangle were at depths of 5 to 8 km (Lee and others, 1979) and may also be related to the Red Mountain fault. Within the rectangle, 12 events occurred in the period September 9–23, 1974, and 8 in the period August 15 to September 7, 1973.

Figure 10.4 is a south-north cross section through the Red Mountain fault, showing earthquake locations within the dashed rectangle and all well-control points projected onto the section. Fault dip is about  $48^\circ$  near the surface, steepening to about  $60^\circ$  at a depth of 3 km, as based on well control. All but two of the 28 earthquakes lie within 1.5 km of a downward extension of the fault as defined by surface and well data if the dip of the extension is steepened to  $63^\circ$  N. Considering the uncertainties in the velocity model used to locate the earthquakes, this agreement between earthquake and oil-well data is excellent.

Nodal planes derived from the five focal-mechanism solutions vary in dip from  $40^\circ$  to  $70^\circ$  (fig. 10.5) and in direction from N.  $7^\circ$  E. to N.  $38^\circ$  E. (fig. 10.1); the average is  $50^\circ$  toward N.  $22^\circ$  E. This dip agrees reasonably well with the fault dip as defined by other means and suggests that the hanging-wall block does not move directly updip but contains a small component of left slip. Discovery of Holocene displacement of the south-dipping Javon Canyon

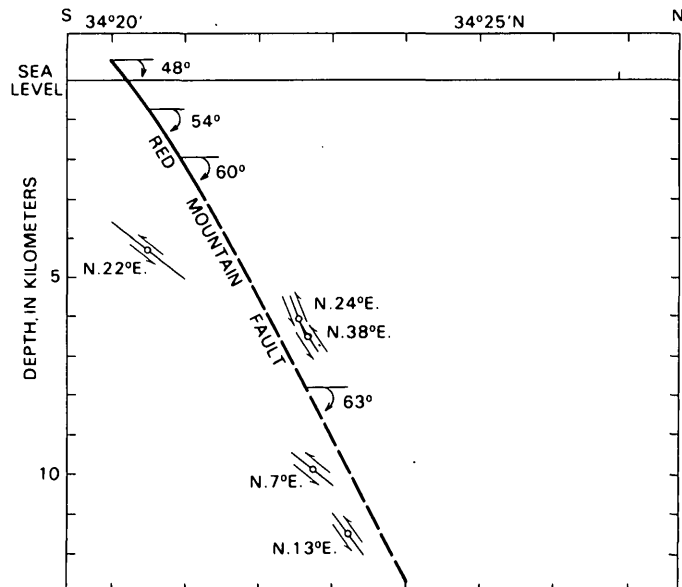


FIGURE 10.5.—Projection of focal-mechanism solutions of selected earthquakes onto a north-south cross section through Red Mountain fault, showing change in fault dip with depth. No vertical exaggeration.

TABLE 10.1.—Earthquakes relocated by Lee and others (1979) and used in this study

[See text for criteria for inclusion]

| Event number | Year | Month | Day | Hour | Minute | Second | Latitude N. | Longitude W. | Depth (km) | Depth error (km) | Epicenter radius (km) | Magnitude |
|--------------|------|-------|-----|------|--------|--------|-------------|--------------|------------|------------------|-----------------------|-----------|
| 1            | 1975 | 01    | 29  | 6    | 8      | 56.26  | 34°25.52'   | 119°19.06'   | 11.10      | 0.9              | 0.6                   | 1.24      |
| 2            | 1975 | 04    | 11  | 3    | 31     | 40.07  | 34°27.12'   | 119°19.25'   | 11.76      | 1.2              | 1.0                   | 1.62      |
| 3            | 1970 | 04    | 23  | 10   | 42     | 53.30  | 34°26.48'   | 119°24.37'   | 8.00       | 1.6              | 1.4                   | 2.46      |
| 4            | 1971 | 12    | 14  | 21   | 21     | 11.91  | 34°22.86'   | 119°18.49'   | 5.49       | .8               | .6                    | 1.96      |
| 5            | 1971 | 12    | 15  | 18   | 47     | 44.42  | 34°22.63'   | 119°18.52'   | 6.59       | .9               | .5                    | 1.37      |
| 6            | 1971 | 12    | 19  | 2    | 13     | 36.32  | 34°23.07'   | 119°19.23'   | 8.77       | .8               | .8                    | 2.49      |
| 7            | 1974 | 09    | 09  | 1    | 28     | 22.92  | 34°22.05'   | 119°19.86'   | 5.59       | .7               | .7                    | 1.33      |
| 8            | 1974 | 09    | 09  | 3    | 41     | 46.81  | 34°22.56'   | 119°19.15'   | 6.02       | 1.0              | .7                    | 1.43      |
| 9            | 1974 | 09    | 09  | 4    | 42     | 55.45  | 34°22.75'   | 119°19.63'   | 6.90       | .9               | .6                    | 1.74      |
| 10           | 1974 | 09    | 09  | 2    | 25     | 50.67  | 34°22.22'   | 119°19.72'   | 6.09       | .7               | .7                    | 1.44      |
| 11           | 1974 | 09    | 10  | 1    | 42     | 33.24  | 34°22.52'   | 119°19.52'   | 5.75       | .8               | .5                    | 1.85      |
| 12           | 1974 | 09    | 10  | 3    | 54     | 39.67  | 34°22.22'   | 119°19.50'   | 6.73       | .6               | .3                    | 1.52      |
| 13           | 1974 | 09    | 17  | 7    | 10     | 54.33  | 34°22.96'   | 119°19.20'   | 7.02       | 1.3              | .9                    | 1.61      |
| 14           | 1974 | 09    | 23  | 2    | 22     | 59.57  | 34°22.72'   | 119°19.42'   | 6.47       | .9               | .6                    | 2.04      |
| 15           | 1975 | 11    | 02  | 2    | 27     | 43.87  | 34°22.91'   | 119°18.70'   | 5.57       | 1.4              | .9                    | 1.42      |
| 16           | 1973 | 08    | 15  | 2    | 16     | 21.88  | 34°20.47'   | 119°20.73'   | 4.30       | 1.8              | 1.3                   | 3.02      |
| 17           | 1973 | 08    | 31  | 1    | 24     | 33.67  | 34°23.46'   | 119°22.16'   | 10.82      | .6               | .7                    | 2.19      |
| 18           | 1973 | 08    | 31  | 5    | 42     | 32.33  | 34°23.42'   | 119°22.18'   | 9.75       | 1.0              | .6                    | 1.93      |
| 19           | 1973 | 09    | 04  | 9    | 11     | 25.92  | 34°23.28'   | 119°21.82'   | 11.51      | .7               | .7                    | 3.40      |
| 20           | 1973 | 09    | 04  | 9    | 28     | 29.52  | 34°23.03'   | 119°22.61'   | 10.51      | 1.2              | .9                    | 1.78      |
| 21           | 1973 | 09    | 07  | 15   | 18     | 10.77  | 34°22.75'   | 119°22.12'   | 9.87       | 1.1              | 1.0                   | 2.59      |
| 22           | 1973 | 09    | 07  | 15   | 18     | 58.35  | 34°22.54'   | 119°21.55'   | .53        | .5               | 1.5                   | 1.96      |
| 23           | 1973 | 09    | 07  | 15   | 19     | 56.80  | 34°23.53'   | 119°21.94'   | 10.59      | 1.3              | .8                    | 1.86      |
| 24           | 1974 | 09    | 10  | 10   | 01     | 18.10  | 34°23.16'   | 119°20.30'   | 7.16       | 1.1              | .7                    | 1.69      |
| 25           | 1974 | 09    | 13  | 3    | 55     | 2.63   | 34°21.91'   | 119°20.00'   | 5.31       | .5               | .5                    | 1.47      |
| 26           | 1974 | 09    | 13  | 3    | 56     | 24.86  | 34°22.39'   | 119°20.02'   | 6.03       | .5               | .4                    | 1.63      |
| 27           | 1974 | 09    | 23  | 2    | 28     | 6.67   | 34°22.90'   | 119°20.11'   | 6.44       | 1.0              | .7                    | 1.84      |
| 28           | 1975 | 01    | 19  | 2    | 35     | 9.41   | 34°23.92'   | 119°22.05'   | 10.31      | .9               | 1.1                   | 1.13      |

fault (Sarna-Wojcicki and others, 1979; this volume) raises the possibility that the south-dipping fault-plane solutions may define the fault rather than the north-dipping ones as shown in figure 10.5. The zone of hypocenters dips north, however, favoring the interpretation of figure 10.5.

## CONCLUSIONS

1. At the east end of the Red Mountain fault, the change in strike from east to north may represent a lateral ramp somewhat reminiscent of that defined by the western limb of the aftershock series of the 1971 San Fernando earthquake (Whitcomb and others, 1973). Although there is a concentration of minor earthquakes near the lateral ramp, focal mechanisms indicate mainly dip slip, in contrast to the left-slip characteristic of earthquakes at the San Fernando lateral ramp.

2. The Red Mountain fault, as defined by 1970–75 earthquakes, is very near the downward projection of the fault as defined by well control. This is seismic confirmation of published evidence (Buchanan-Banks and others, 1975; Lajoie and others, 1979) that the fault is active. However we know of no evidence for historic surface rupture.

3. The fault maintains a dip of about 60°–63° from 3 to 12 km depth.

4. Focal-mechanism solutions are in agreement with geologic evidence that the northern, hanging-wall, block is faulted over the southern, footwall, block. Geodetic evidence (Buchanan-Banks and others, 1975) also suggests the northern block moves upward with respect to the southern block. The slip vectors plunge north-northeast, predominantly reverse with a minor left-slip component.

5. Facies changes in Pliocene and Pleistocene strata suggest that the hanging-wall block of the Red Mountain fault, including its curved eastern end, coincides with a positive region, possibly a seaknoll during the time of deposition.

6. The distribution of earthquakes in the cross section indicates that most of the earthquakes occurred in pre-Tertiary rocks.

## REFERENCES CITED

- Buchanan-Banks, J. M., Castle, R. O., and Ziony, J. I., 1975, Elevation changes in the central Transverse Ranges near Ventura, California: Tectonophysics, v. 24, p. 113–125.
- California Division of Oil and Gas, 1974, California Oil and Gas Fields: Report no. TR 12, v. 2, South, Central Coastal and Offshore California.
- Hacker, R. N., 1969, Geology and oilfields of coastal areas, Ventura and Los Angeles basins, California: Pacific Section, American Association of Petroleum Geologists, Los Angeles, 60 p.

- Izett, G. A., Naeser, C. W., and Obradovich, J. D., 1974, Fission track age of zircon from an ash bed in the Pico Formation (Pliocene and Pleistocene) near Ventura, California [abs.]: Geological Society of America, Abstracts with Programs, v. 6, p. 197.
- Jackson, P. A., and Yeats, R. S., 1982, Structural evolution of Carpinteria basin, western Transverse Ranges, California: American Association of Petroleum Geologists Bulletin, v. 66, p. 805-829.
- Keller, E. A., Rockwell, T. K., Clark, M. N., Dembroff, G. R., and Johnson, D. L., 1982, Tectonic geomorphology of the Ventura, Ojai and Santa Paula areas, western Transverse Ranges, California, in Cooper, J. D., compiler, Guidebook, Neotectonics in southern California, prepared for the 78th Annual Meeting of the Cordilleran Section of the Geological Society of America, Anaheim, California, April 19-21, 1982, p. 25-42.
- Kew, W. S. W., 1924, Geology and oil resources of Los Angeles and Ventura Counties, California: U.S. Geological Survey Bulletin 753, 202 p.
- Kleinpell, R. M., 1938, Miocene stratigraphy of California: Tulsa, American Association of Petroleum Geologists, 450 p.
- Lajoie, K. R., Kern, J. P., Wehmiller, J. F., Kennedy, G. L., Mathieson, S. A., Sarna-Wojcicki, A. M., Yerkes, R. F., and McCrory, P. F., 1979, Quaternary marine shorelines and crustal deformation, San Diego to Santa Barbara, California, in Abbott, P. L., ed., Geological excursions in the southern California area: p. 1-15.
- Lee, W. H. K., Yerkes, R. F., and Simirenko, M., 1979, Earthquake activity and Quaternary deformation of the western Transverse Ranges, California: U.S. Geological Survey Circular 799-A, p. 1-26.
- Nagle, H. E., and Parker, E. S., 1971, Future oil and gas potential of onshore Ventura basin, California, in Cram, I. H., ed., Future petroleum provinces of the United States—their geology and potential: American Association of Petroleum Geologists Memoir 15, v. 1, p. 254-297.
- Putnam, W. C., 1942, Geomorphology of the Ventura region, California: Geological Society of America Bulletin, v. 53, p. 691-754.
- Rockwell, T. K., Keller, E. A., Clark, M. N., and Johnson, D. L., 1984, Chronology and rates of faulting of Ventura River terraces, California: Geological Society of America Bulletin, v. 91, p. 1466-1474.
- Sarna-Wojcicki, A. M., Lajoie, K. R., Robinson, S. W., and Yerkes, R. F., 1979, Recurrent Holocene displacement of the Javon Canyon fault, rates of faulting, and regional uplift, western Transverse Ranges, California [abs.]: Geological Society of America Abstracts with Programs, v. 11, p. 125.
- Vedder, J. G., 1972, Revision of stratigraphic names for some Eocene formations in Santa Barbara and Ventura Counties, California: U.S. Geological Survey Bulletin 1354-D, 12 p.
- Weber, F. H., Jr., Cleveland, G. B., Kahle, J. E., Kiessling, E. F., Miller, R. V., Mills, M. F., Morton, D. M., and Cilweck, Blase, 1973, Geology and mineral resources study of southern Ventura County, California: California Division of Mines and Geology Preliminary Report 14, 102 p.
- Whitcomb, J. H., Allen, C. R., Garmany, J. D., and Hileman, J. A., 1973, San Fernando earthquake series, 1971: Focal mechanisms and tectonics: Reviews of Geophysics and Space Physics, v. 11, p. 693-730.
- Yeats, R. S., 1965, Pliocene seaknoll at South Mountain, Ventura basin, California: American Association of Petroleum Geologists Bulletin, v. 49, p. 526-546.
- \_\_\_\_\_, 1976, Neogene tectonics of the central Ventura Basin, California, in Fritsche, A. E., Ter Best, H., Jr., and Wornardt, W. W., eds., The Neogene Symposium: Pacific Section, Society of Economic Paleontologists and Mineralogists, San Francisco, p. 19-32.
- \_\_\_\_\_, 1980, Neotectonics of the Ventura Avenue anticline: Semi-annual Technical Report to the U.S. Geological Survey, Contract No. 14-08-0001-17730, 28 p.
- \_\_\_\_\_, 1983, Large-scale Quaternary detachments in Ventura basin, southern California: Journal of Geophysical Research, v. 88, no. B1, p. 569-583.
- Yerkes, R. F., and Lee, W. H. K., 1979, Maps showing faults and fault activity, and epicenters, focal depths, and focal mechanisms for 1970-1975 earthquakes, western Transverse Ranges, California: U.S. Geological Survey Miscellaneous Field Studies Map MF-1032, 2 sheets, scale 1:250,000.
- Ziony, J. I., Wentworth, C. M., Buchanan-Banks, J. M., and Wagner, H. C., 1974, Preliminary map showing recency of faulting in coastal southern California: U.S. Geological Survey Miscellaneous Field Studies Map MF-585, scale 1:250,000.



# 11. GEOLOGY AND QUATERNARY DEFORMATION OF THE VENTURA AREA

By R. F. YERKES, A. M. SARNA-WOJCICKI, and K. R. LAJOIE

## ABSTRACT

The seismically active, north-dipping Pitas Point-Ventura fault extends eastward more than 75 km through the northeast Santa Barbara channel into the Ventura area. Geologic and seismic evidence indicate reverse-left-oblique displacement. The onshore segment, the Ventura fault, has been active in Holocene time and forms the boundary between the rising Ventura Avenue anticline on the north and the subsiding Ventura syncline on the south. The eroded anticline exposes about 2.5 km of folded Pleistocene marine strata with an age range estimated at 1.2 to 0.2 m.y. B.P. by tephrochronology and stereochemistry on numerous ash and mollusk collections whose stratigraphic positions are known. Included in the strata are the type Hallian Microfaunal Stage, the base of which is about 0.7 m.y. B.P., and the Wheelerian stage, which in Hall Canyon ranges from about 1.8 to 0.7 m.y. B.P.

These and other data yield a quantitative model of deformation that began about 550,000 yr B.P. and attained average uplift rates of 16 mm/yr over the last 200,000 yr for the axial part of the anticline, a tilt rate of about  $5.6 \times 10^{-6}$  rad/yr over 200,000–80,000 yr B.P. for the steeply dipping upper Pleistocene strata along the south margin of the anticline, and a tilt rate of about  $1.5 \times 10^{-6}$  rad/yr over the past 80,000 yr for the marine terrace platform that transgresses the bedrock there.

## INTRODUCTION

The intensity and relative youth of regional deformation in the Transverse Ranges have been emphasized in comparative or qualitative terms for more than 30 years. Gilluly's advocacy is both long standing (1949, 1962, 1979) and emphatic (1979, p. 475): "there is no escape from the fact that this orogeny is active and active at a rate comparable to that of the formation of any mountain chain we know about."

## PURPOSE

This report supplements the detailed surface geologic map of the Ventura fault by Sarna-Wojcicki and others (1976); it integrates and correlates available surface and subsurface data bearing on the history of the fault and associated structures, together with estimates of absolute ages for the Pleistocene sequence and the rates of its deformation. These data permit tentative dating of the middle Pleistocene Pasadenan orogeny of Stille (1936) in a part of its type area where a large number of age

estimates are available for a great thickness of bracketing marine strata. This report is based on work completed before July 30, 1979.

## PREVIOUS WORK

Published geologic work consists chiefly of regional planimetric geologic or structural maps and brief summaries of stratigraphy and structure. Notable are those of Cartwright (1928), Kew (1932), Reed and Hollister (1936), and Bailey and Jahns (1954). Putnam (1942) mapped and described deformed marine and nonmarine terraces in the Ventura-Carpinteria area and described the geomorphic history. He also reported the uplifted, tilted, and faulted marine terraces in the foothills north of Ventura, noting that to the south (south of the Ventura fault) they are buried beneath dissected alluvial fans.

Natland (1953, 1967) and Natland and Rothwell (1954) defined and correlated the Pliocene and Pleistocene microfaunal stages of the Los Angeles and Ventura Basins, especially the type Hallian Stage from exposures in Hall Canyon near Ventura. This stage is bracketed by estimates of absolute age documented in this report. Holman (1958) presented comprehensive faunal-stratigraphic correlations of the Cenozoic sequence of the Ventura basin based chiefly on subsurface data from oil fields.

Ogle and Hacker (1969) published the first recognition of the Ventura fault (their Pitas Point fault) on a north-south structure section; however, they did not extend the fault to the surface. Quick (1973) cited the evidence of uplifted marine terraces in the hanging wall and an inferred ground-water barrier at the mouth of the Ventura River as evidence for his north-dipping Ventura Foothills reverse fault. Weber and others (1973) published the first detailed compilation of the geology of southern Ventura County on a topographic base (1:48,000) and identified aerial photographic evidence of the Ventura fault. Their stratigraphic nomenclature is adopted for this report.

Cilweck (1975) described trench and borehole evidence of faulting along the trend of the Ventura fault on the grounds of Ventura County General Hospital. Sarna-Wojcicki and others (1976) prepared a detailed (1:6,000) map of surficial geology along the fault, correlated it with the Pitas Point fault offshore to the west, and summarized the evidence for considering it active.

Yerkes and Lee (1979) identified the Pitas Point-Ventura fault as one of several east-trending, active reverse faults in the western Transverse Ranges, for which they derived sense of slip and attitude on the basis of geometric association with earthquake hypocenters and fault-plane solutions.

#### SETTING

Ventura is on the coast at the seaward margin of the Ventura basin, an alluviated lowland remnant of a much

larger late Cenozoic basin of deposition (fig. 11.1). The basin trends east-northeast more than 65 km from the shoreline to the western San Gabriel Mountains; westward, it merges with the Santa Barbara Channel. The north margin of the basin in the present map area is greatly deformed by anticlinal uplift, faulting, and erosion, whereas the synclinal trough to the south is still subsiding. The city of Ventura is bounded on the west by the south-draining Ventura River and on the north by the south flank of the east-trending Ventura Avenue anticline. The

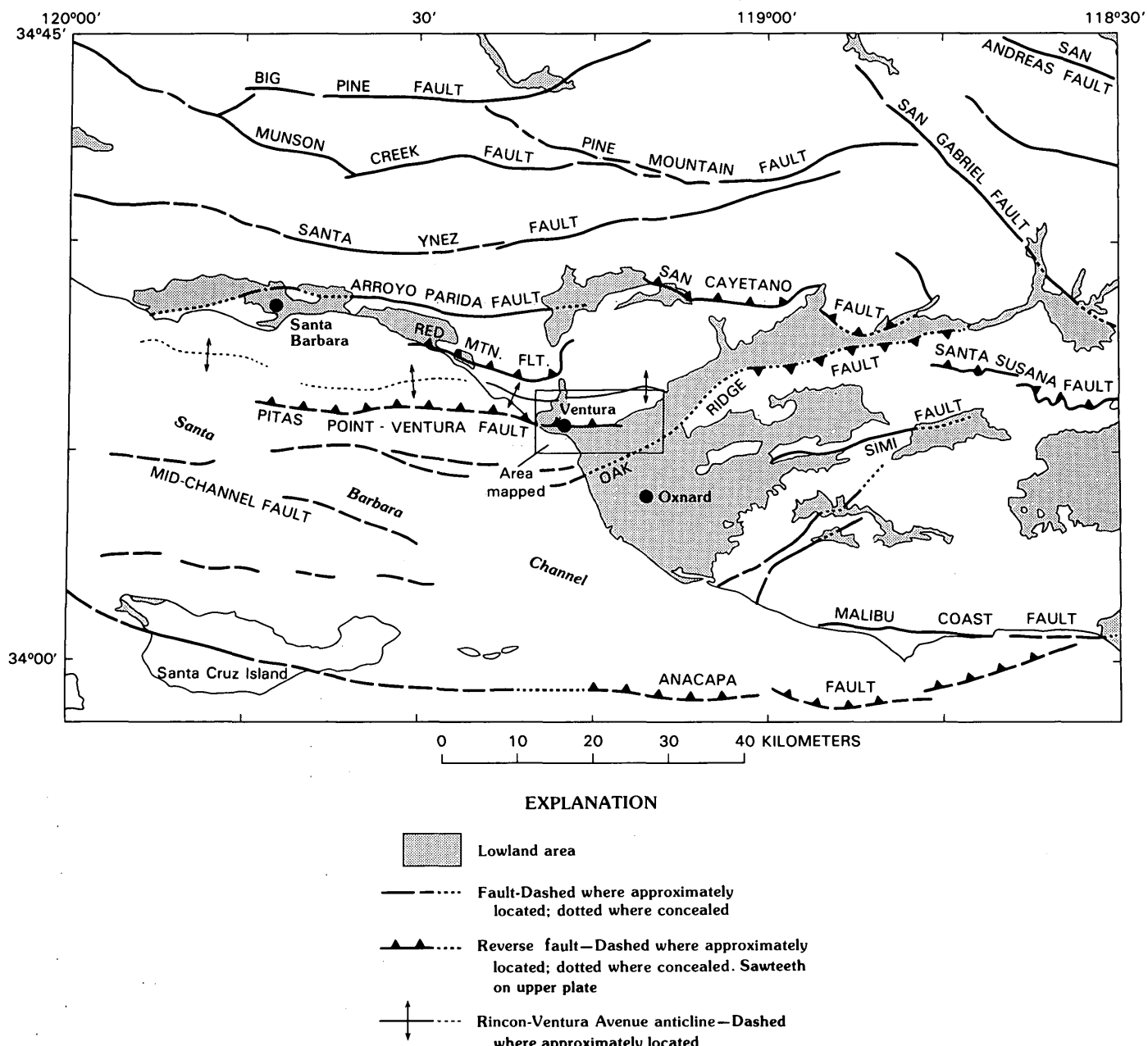


FIGURE 11.1.—Index map of western Transverse Ranges (area bounded by Anacapa and Santa Ynez faults) showing area mapped, extent of modern Ventura basin, and other lowland areas.

city extends eastward along fans built by south-draining streams and rivers cut into the anticline; to the south, these fans merge with and impinge on flood-plain deposits of the large, west-flowing Santa Clara River, which drains most of the basin.

The Ventura Avenue anticline is sharply truncated on the south by the Ventura fault, the onshore segment of the Pitas Point-Ventura fault, a feature more than 75 km long and one of several seismically active fault zones that characterize the western Transverse Ranges. The lowland area south of the Ventura fault includes the flood plain of the Santa Clara River (southeast corner of pl. 11.1). These surficial deposits bury the axis of the east-northeast-trending Ventura syncline, 1–2 km south of the Ventura fault, and the trace of the Oak Ridge fault, a south-dipping reverse fault that parallels the syncline 2 km to the south. Immediately south of the concealed Oak Ridge fault are two isolated northwest-trending, elongate structural domes, the Montalvo mounds.

### STRATIGRAPHIC SEQUENCE

For surface geologic units we follow the stratigraphic nomenclature used by Weber and others (1973); equivalent subsurface units are adapted from Ogle and Hacker (1969) and correlated by means of electric logs of wells. The oldest strata exposed in the core of the Ventura Avenue anticline are siltstone and shale of the upper part of the Pico Formation, here referred to the lower Pleistocene (Wheelerian Stage of Natland and Rothwell, 1954). Approximately 1,000 m of Pico strata is exposed and an additional 1,980 m is known from subsurface data, of which the lower 1,830 m is Pliocene.

The Santa Barbara Formation of Weber and others (1973) overlies the Pico Formation and consists of a shale, siltstone and mudstone sequence on the south flank of the anticline. Exposures thin uniformly westward from about 1,220 m on the east nose of the anticline (section D-D') to about 550 m near the Ventura River. The thinning appears to be related to growth of the anticline and resultant erosion prior to deposition of the San Pedro Formation.

A maximum of about 1,200 m of silty to pebbly sandstone of the San Pedro Formation of Weber and others (1973) are preserved on the south flank of the anticline as the youngest unit of the bedrock sequence. The upper part in Hall Canyon (east of section C-C') is nonmarine (Bailey, 1935) and presumably equivalent to the Saugus Formation of the eastern Ventura basin; the marine-nonmarine boundary has not been traced from Hall Canyon. The upper part of the San Pedro is missing as a result of uplift along the anticline and the Ventura fault. Estimates based on extrapolating the deposition rate and comparisons with the thickness preserved in the Ventura

syncline (fig. 11.2, section C-C') suggest that the total thickness of the unit could have been about 1,400 m.

### AGE ESTIMATES

#### VOLCANIC ASH

Three volcanic ashes exposed in the mapped area (pl. 11.1) provide age control for deformed lower and middle Pleistocene strata and also serve as a check on ages determined by the amino-acid racemization method on mollusks from the upper part of the section. The ashes have been correlated by means of chemical "fingerprints" with localities where their isotopic ages have been determined. A number of trace and minor elements in volcanic glass separated from the ashes are identified by neutron activation analyses (Sarna-Wojcicki and others, 1979), enabling unique identification. The three ashes were erupted from the general vicinity of Long Valley and Mono Glass Mountain north of the town of Bishop in east-central California, as determined by their chemical characteristics as well as by specific site-to-site correlations for two of the ashes. The characteristics are distinctive and cannot be confused with those of tephra erupted from other volcanic provinces. Correlations based on glass chemistry are supported by stratigraphic and paleomagnetic data, both in the vicinity of the town of Ventura and in the volcanic source area.

#### THE BAILEY ASH

The oldest of the three ashes, referred to informally as the Bailey ash (Izett and others, 1974), has been found at a number of locations in the study area (sample locs. 57, 30, A, and B) in the upper part of the Pico Formation near its contact with the Santa Barbara Formation. The ash is exposed intermittently from near Sea Cliff on the west, about 2 km west of the mapped area (pl. 11.1), to the vicinity of Sexton Canyon in the east, a distance of about 18 km. At exposures near the Ventura River, near the structural culmination of the Ventura Avenue anticline, this ash is about 20 cm thick but thins to both the west and the east. The Bailey ash also has been identified in the South Mountain-Balcom Canyon area, about 14 to 26 km east of the area shown in plate 11.1 (Sarna-Wojcicki and others, 1979). A sample of this ash obtained from Balcom Canyon has been dated by Izett and others (1974) at  $1.2 \pm 0.2$  m.y. B.P. by means of fission-track analyses of zircon crystals (table 11.1).

#### THE GRAY ASH

East and west of the Ventura River (pl. 11.1) a 2.5-cm-thick, light-gray ash, here informally designated the gray ash (sample locs. 64 and 129; pl. 11.1, sections A-A' and

TABLE 11.1.—Data on samples from mapped units of tephra

| Map No. | Name       | Locality description <sup>1</sup><br>(feet from reference point) | Elevation<br>(ft.) | Stratigraphic<br>position                 | Estimated<br>age (m.y. B.P.) <sup>2</sup> |
|---------|------------|------------------------------------------------------------------|--------------------|-------------------------------------------|-------------------------------------------|
| 58      | Bishop ash | Ref. 17.5°N. 17.5°W.<br>2850 N. 2600 E.                          | 500                | Middle part of Santa<br>Barbara Formation | 0.7 ± 0.4                                 |
| 69      | Bishop ash | Ref. 17.5°N. 15°W.<br>2700 N. 4100 W.                            | 660                | Middle part of Santa<br>Barbara Formation | 0.7 ± 0.4                                 |
| 64      | Gray ash   | Ref. 17.5°N. 17.5°W.<br>3325 N. 3850 W.                          | 140                | Basal part of Santa<br>Barbara Formation  | Approx. 1.0                               |
| 129     | Gray ash   | Ref. 17.5°N. 17.5°W.<br>4025 N. 3840 W.                          | 600                | Lower part of Santa<br>Barbara Formation  | Do                                        |
| 57      | Bailey ash | Ref. 17.5°N. 17.5°W.<br>4000 N. 3900 W.                          | 200                | Uppermost part of<br>Pico Formation       | 1.2 ± 0.2                                 |
| A       | Bailey ash | Ref. 17.5°N. 17.5°W.<br>4675 N. 6140 E.                          | 600                | Uppermost part of<br>Pico Formation       | Not analyzed                              |
| B       | Bailey ash | Ref. 17.5°N. 15°W.<br>5000 N. 4300 W.                            | 900                | Uppermost part of<br>Pico Formation       | Do.                                       |
| 30      | Bailey ash | Ref. 17.5°N. 12.5°W.<br>9500 N. 5680 W.                          | 1,060              | Basal part of Santa<br>Barbara Formation  | Do.                                       |

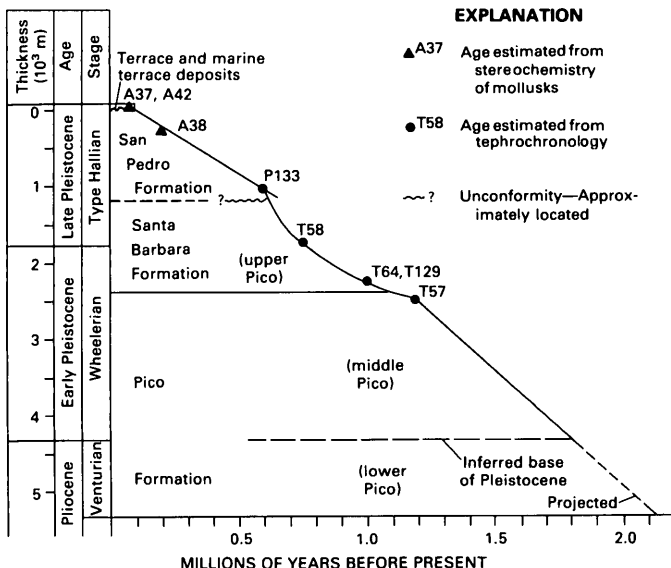
<sup>1</sup> Reference points in minutes north of lat 34° N. and west of long 119° W.<sup>2</sup> From Sarna-Wojcicki and others (1984).

FIGURE 11.2.—Stratigraphic thickness and estimated ages, Pleistocene sequence, south limb of Ventura anticline. Samples A37 and A42 represent mollusks from marine terrace deposits, estimated at 80,000–100,000 yr B.P.; sample A38 represents mollusks from San Pedro Formation, estimated at approximately 200,000 yr B.P. (Lajoie and others, 1979). Sample P133 represents Lava Creek ash (600,000 yr B.P.); T58 represents Bishop ash (730,000 yr B.P.); T64 and T129 represent Glass Mountain-D ash (800,000–900,000 yr B.P.); T57 represents Bailey ash (1.2 m.y. B.P.); age estimates and ash correlations from Sarna-Wojcicki and others, 1984). Other correlations from Natland (1952, 1953) and Holman (1958). Ages of stage boundaries from Van Eysinga (1975). Stratigraphic nomenclature from Weber and others (1973) except for informal terms (in parentheses) applied to subsurface units.

*B-B'*), is in the lower part of the Santa Barbara Formation about 100 m stratigraphically above the Bailey ash. The gray ash is chemically correlated with a gray ash that underlies the Bishop Tuff north of the town of Bishop in east-central California. On the basis of its stratigraphic position, the isotopic ages of overlying and underlying tephra units, and paleomagnetic data, this ash is estimated at about 1 m.y. old (Sarna-Wojcicki and others, 1979).

#### THE BISHOP ASH

The youngest ash in the mapped area (pl. 11.1) overlies the gray ash east of the Ventura River and is exposed intermittently for about 3 km to the east (sample locs. 58 and 69). It occurs in the middle part of the Santa Barbara Formation. The stratigraphic section between this ash and the gray ash is about 180 m thick. This uppermost ash, about 10 cm thick at exposures just east of the Ventura River (sample loc. 58), is correlated generally with the type Bishop Tuff and specifically with the Friant Pumice Member of the Turlock Lake Formation, a chemical type recognized on the basis of its trace- and minor-element chemistry and stratigraphic criteria (Sarna-Wojcicki and others, 1979). The Bishop Tuff has been dated at about 0.7 m.y. B.P. by the potassium-argon method (Dalrymple and others, 1965).

#### MOLLUSKS

Recent developments in the use of amino-acid racemization in fossil mollusks for correlation and age estimates

TABLE 11.2.—*Data on mollusk collections*

| Map No. | Locality description <sup>1</sup><br>(feet from ref. point) | Elevation<br>(feet) (m) | Stratigraphic<br>position            | Estimated age<br>( $10^3$ yr B.P.) <sup>2</sup> |
|---------|-------------------------------------------------------------|-------------------------|--------------------------------------|-------------------------------------------------|
| 37      | Ref. 17°N., 17°W.<br>600°N., 1475°W.                        | 289 88                  | Marine terrace                       | 80-100                                          |
| 41      | Ref. 17°N., 17°W.<br>750°N., 985°W.                         | 361 110                 | --do--                               | 80-100                                          |
| 42      | Ref. 17°N., 17°W.<br>1060°N., 950°W.                        | 384 117                 | --do--                               | 80-100                                          |
| 38      | Ref. 17°N., 17°W.<br>600°N., 1475°W.                        | 285 87                  | Upper part of San<br>Pedro Formation | Approx. 200                                     |

<sup>1</sup> Reference points in minutes north of latitude 34° N. and west of long 119° W.<sup>2</sup> From Wehmiller and others (1978).

have yielded abundant geologically consistent data on Pleistocene marine terrace deposits along the California coast (Table 11.2; Kennedy and Lajoie, 1982). Analyses of fossil mollusks from marine deposits on several isolated remnants of a tilted (8°) terrace platform that truncates the San Pedro Formation at elevations of 53 to 128 m on the south limb of Ventura Avenue anticline just north of Ventura yield a consistent and reasonable estimate of 80,000–100,000 yr B.P., indicating that only one deposit is represented. Analyses of samples from the uppermost San Pedro Formation just below the tilted terrace area yield an age estimate of about 200,000 yr B.P. Fossil mollusks from isolated remnants of a deformed marine terrace at elevations of 5–354 m along the Santa Barbara-Pitas Point segment of the coast (west of map area) yield U-series and amino-acid data that imply an age of 40,000–60,000 yr B.P. (Yerkes and Lee, 1979, table 2, fig. 5; Kaufman and others, 1971; Kennedy and Lajoie, 1982; Lajoie and others, 1982). This mid-Wisconsin age estimate agrees with the cool-water aspect of the molluscan fauna (Putnam, 1942). Finally, fossil mollusks from several localities on three or four separate marine platforms between 2 and 20 m elevation along the coast 10 to 16 km west of the Ventura River yield carbon-14 ages of 1,800 to 5,500 yr B.P., which are consistent with U-series and amino-acid data (Lajoie and others, 1979).

#### AGE AND STRATIGRAPHIC RELATIONS

Figure 11.2 plots maximum thickness of the units on the south flank of the Ventura Avenue anticline against estimated absolute ages of mollusk and ash samples. At least 4,400 m of chiefly to entirely Pleistocene strata is present. The age estimates bracket the type Hallian Stage of Natland (1953) and verify Van Eysinga's (1975) range of 0.7 m.y. to less than 0.1 m.y. for that stage. Our data also support Van Eysinga's assignment of the Wheelerian Stage of Natland (1953) to the early Pleistocene rather than to the late Pliocene.

#### STRUCTURE

##### VENTURA AVENUE ANTICLINE

The Ventura Avenue anticline is the easternmost of several oil-producing structures along the Rincon-Ventura trend, which extends for about 42 km along the north margin of the basin; the western 25 km is submerged in the northeast Santa Barbara Channel. The Ventura Avenue anticline is doubly plunging with an exposed axis about 17 km long in upper Pleistocene strata. Structural closure at the surface is about 1,065 m in basal Pleistocene strata. The core of the structure is cut by opposing, gently dipping thrust faults that have been folded; they are not known to extend to the surface (Yeats, 1976, fig. 6). On the south flank, late Pliocene to late Pleistocene strata dip 30°–55°, and strata as young as about 200,000 years are deformed to the same degree as late Pliocene strata. Only terrace deposits younger than about 80,000 years are not so deformed, although locally they have been tilted to as much as 15° to the south. The fine-grained strata of the Santa Barbara Formation appear to be conformable with the underlying, lithologically similar Pico strata in all respects, whereas the outcrop relations of the much coarser grained San Pedro Formation indicate that it transgresses the Santa Barbara along the south flank of the anticline, especially opposite its structural culmination near the Ventura River. These relations suggest that folding affected this part of the sequence beginning about 550,000 yr B.P. (see fig. 11.2). Deformation of marine terrace deposits dated at 80,000 yr B.P. (fig. 11.3, table 11.1) indicates that uplift along the south flank of the anticline probably still continues.

The Ventura oil field and associated fields along the structural trend are widely noted for reservoir pressures greatly in excess of hydrostatic for subsea depths below about 900 m. In the Ventura oil field, the excess pressure is about 8,250 lb/in<sup>2</sup> (27.6 MPa (megapascals) at –2,745 m) (or 0.9 of assumed lithostatic) at a subsea depth of

9,000 ft (McCulloh, 1969, p. 38). Present evidence indicates that the degree of overpressure increases with depth and that overpressure is confined to the overthrust core of the anticline. Such overpressures may be due to deformation of the reservoir by compressive stresses (Levorsen, 1954, p. 393). The Ventura oil field is an excellent example of this effect, in that the regional structure is dominated by reverse faulting, *P* axes of earthquake fault-plane solutions (generally assumed to reflect the maximum principal compressive stress) trend generally normal to the fold axes and faults, and these structures are known to be active.

#### VENTURA FAULT

Surface evidence bearing on the presence and activity of the Ventura fault has been fully documented (Sarna-Wojcicki and others, 1976). Evidence of the fault includes a long, linear, south-facing topographic scarp as high as 12 m with abrupt crest and toe; its alignment with the

previously mapped east-trending, north-dipping Pitas Point reverse fault that cuts Holocene deposits in the northeast Santa Barbara Channel (Greene, 1976); its consistent juxtaposition of deformed older soils and geologic units on the north with younger soils and undeformed units on the south; the abrupt change of the gradients of all but the largest streams where they cross the scarp; progressively steeper dips downward in upper Pleistocene strata penetrated by auger holes on and north of the escarpment, indicating recurrent uplift of the north block over time; the geometric association with the focal mechanism of at least one well-located earthquake indicating reverse-left-oblique displacement, and the fact that the scarp and its associated features cannot be attributed to present-day erosion. The youngest deposits cut by the fault are those of the Holocene Harmon fan, 10 km east of the Ventura River. The fan is graded to present-day sea level and is unmodified by erosion except for incision by the main drainage of Harmon Canyon. Rodent skeletons taken from trenched burrows 3.5–4 m below

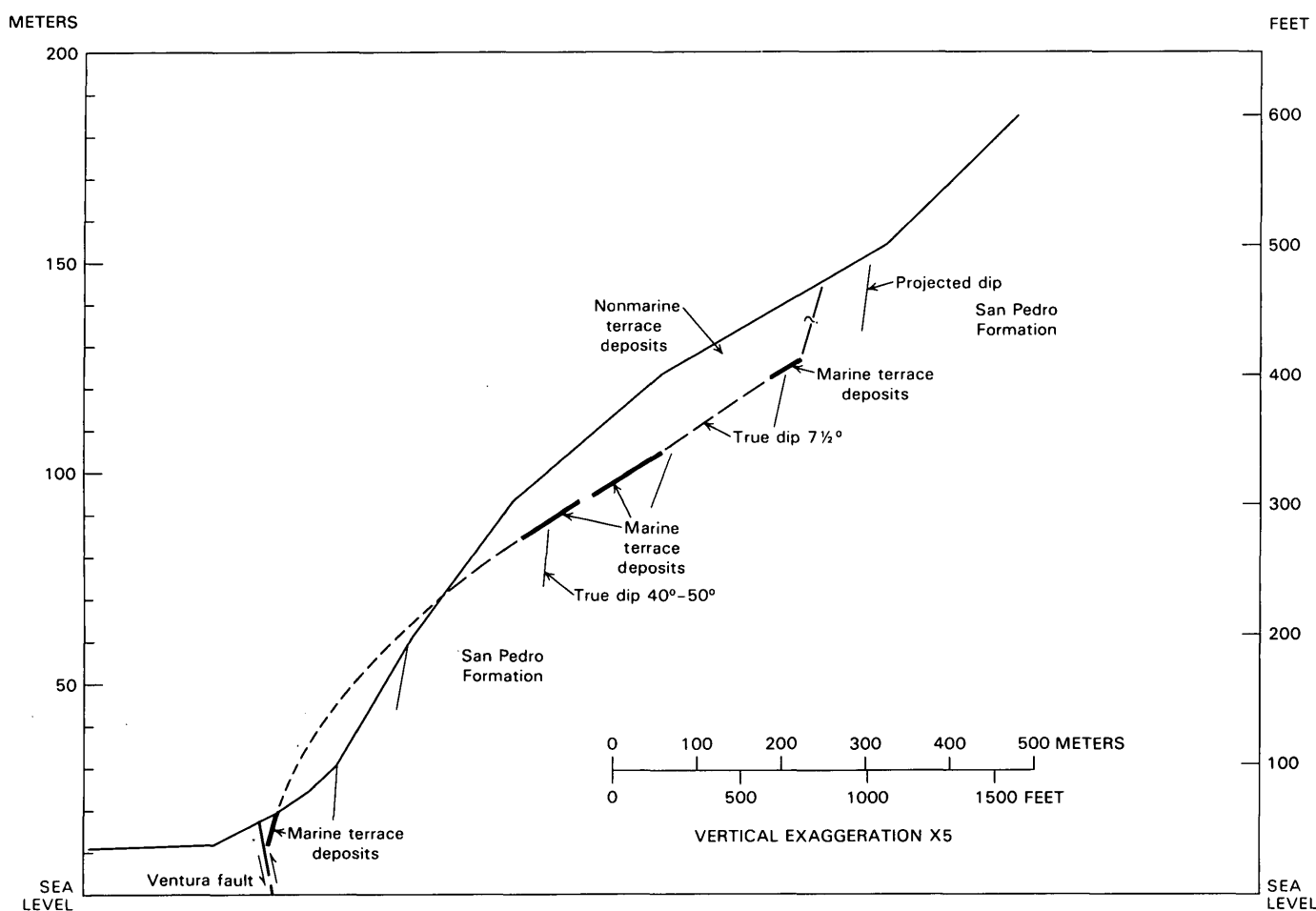


FIGURE 11.3.—Generalized profile of 80,000-yr-B.P. marine terrace platform just north of Ventura showing deformation of platform and relative positions of exposures beneath platform. Control from Sarna-Wojcicki and others (1976).

ground surface of the lower part of the fan are estimated to date from about 6,000 yr B.P. (Sarna-Wojcicki and others, 1976).

The 10-km-long surface trace of the fault represents a north-dipping reverse fault that trends eastward along the south flank of the Ventura Avenue anticline generally opposite its structural culmination. The 1:48,000-scale structure section of Ogle and Hacker (1969) in this area shows the fault to have a north dip of  $60^\circ$  and stratigraphic separation along the fault of about 245 m. Our data indicate a north dip of  $55^\circ$ – $65^\circ$  and a maximum apparent separation of about 200 m at the base of the San Pedro Formation that decreases both eastward and westward from the structural culmination of the anticline. The fault also marks an abrupt change in dip of the stratigraphic sequence from  $35^\circ$  to  $55^\circ$  S. in the hanging wall to very gentle in the footwall. The fault is known to cut and displace marine terrace deposits dated at about 80,000 yr B.P. and nonmarine cover and soils; it is buried locally only by the youngest fan and stream deposits, and it can be related geometrically to at least one well-located earthquake and its focal mechanism. On the basis of these criteria, the fault is considered active.

Projection of the uplifted terrace platform to the Ventura fault (fig. 3) indicates a minimum vertical separation of 30 m, up on the north, for an average rate of at least 0.4 m/1,000 yr; rates derived from offset of the base of the San Pedro Formation average about 0.5 m/1,000 yr during the interval 500,000 to 100,000 yr B.P.

Although most of the smaller stream courses are deflected left laterally as much as 0.3 km (for example, Hall Canyon) or distorted at the fault, quantitative estimates of deflection are unreliable because of great variations in stream size and history. The one reliable earthquake fault-plane solution (N. lat  $34^\circ 19.2'$ , W. long  $119^\circ 14.1'$ —north edge of map on section D-D', depth 7.9 km; event 40 of Yerkes and Lee, 1979) has a primary focal plane with azimuth  $112^\circ$ , dip  $60^\circ$  N. and slip vector with azimuth  $70^\circ$ , plunge  $52^\circ$ . This solution indicates a ratio of about 3.2 parts reverse displacement to one part left lateral. The horizontal components are 1.2 left lateral parallel to the fault and 1.0 normal to the fault trace; the vertical component is 2.2.

#### VENTURA SYNCLINE

The lowland area south of the Ventura fault is underlain by the Ventura syncline, the axis of which trends east-northeast for about 13 km east of the shoreline and west into the Santa Barbara Channel for at least 20 km (Greene, 1976). The syncline involves more than 6,000 m of Pliocene and younger strata; the base of the marine Pleistocene is now about 4,500 m below sea level and that of the marine upper Pleistocene about 2,000 m below sea

level in the Ventura area (section C-C'). The north and south flanks of the syncline are not nearly so tightly compressed in this area as in areas to the east (see Hall and Curran, 1972, section B-B').

#### OAK RIDGE FAULT

The Oak Ridge is a zone of one or more faults that form the south boundary of the Ventura synclinal trough in the western Ventura basin. Although the faults in this area are buried and known only from subsurface data, segments are traceable for more than 100 km from the eastern Santa Barbara Channel to the Santa Susana Mountains. In the map area, the zone trends east-northeast, subparallel to the synclinal axis, for about 10 km east of the shoreline, where displacement locally dies out on the steep south flank of the syncline. East of the map area, the faults form the boundary between the steep north slope of South Mountain and the Santa Clara River valley for a distance of about 30 km. The Oak Ridge is a steeply south-dipping reverse fault, with stratigraphic separation of about 350 m at the base of the San Pedro Formation; it is generally symmetrical in mirror image to the Ventura fault.

The Oak Ridge fault forms the north boundary of a long east- to northeast-trending structural high that extended more than 100 km through the east Santa Barbara Channel-South Mountain-Santa Susana Mountains area in middle Miocene time, when it formed the northwest boundary of the region over the Conejo Volcanics accumulated to thicknesses greater than 2,400 m (Fischer, 1976). The Oak Ridge fault evidently was active in Pliocene time, as the Pico Formation is more than twice as thick north of the fault than it is south of it (Yeats, 1976, fig. 2). Movement along the Oak Ridge continued into Pleistocene time, because the base of the San Pedro Formation is offset, and associated left-lateral slip apparently contributed to uplift of the structures that underlie the Montalvo mounds.

#### MONTALVO MOUNDS

Two isolated, elongate, northwest-trending structural uplifts, the Montalvo mounds, are present in the lowland area near the Santa Clara River. The largest is about 1 km long by 300 m wide and rises about 20 m above the surrounding plain; a quarry at the west end exposes steeply south-dipping strata of the San Pedro Formation. The mounds are compressional features, perhaps underlain by shallow thrust faults, and are compatible with left-lateral slip along the adjacent Oak Ridge fault, as well as with the north-northeast orientation of the regional compressional stress suggested by fault-plane solutions of earthquakes (Yerkes and Lee, 1979).

TABLE 11.3.—*Model of late Quaternary deformation*

| Phase <sup>1</sup> | Unit                          | Thickness or elevation (m) | Time interval (m.y. B.P.) | Time span ( $10^3$ yr) | Vertical component (mm/yr) |
|--------------------|-------------------------------|----------------------------|---------------------------|------------------------|----------------------------|
| 1. S-D             | Middle part of Pico Formation | 2,100                      | 1.8 - ~1.05               | 750                    | 2.8                        |
| 2. S-D             | Santa Barbara Formation       | 1,750                      | 1.05 - 0.55               | 700                    | 2.5                        |
| 4. S-D             | San Pedro Formation           | 1,400                      | 0.5 - 0.2                 | 300                    | 4.7                        |
| 5. U-E             | do                            | 1,400                      |                           |                        |                            |
|                    | Santa Barbara Formation       | 1,150                      |                           |                        |                            |
|                    | Pico Formation                | 940                        |                           |                        |                            |
|                    |                               | <b>3,090</b>               | <b>0.2 - 0</b>            | <b>200</b>             | <b>15.5</b>                |

<sup>1</sup>S-D, subsidence and deposition, ignoring effects of compaction; U-E, uplift and erosion, ignoring effects of faulting.

## QUATERNARY DEFORMATION

The city of Ventura is sited along and near the active Ventura fault, which forms the boundary between the rapidly rising Ventura Avenue anticline on the immediate north and the rapidly subsiding Ventura syncline on the south, in the western Transverse Ranges, a region that has undergone profound compressive deformation in the last 0.5–1 m.y. Although the Ventura fault is not now so active seismically as the north Santa Barbara Channel-Red Mountain areas to the northwest and the Point Mugu area to the southeast (Yerkes and Lee, 1979), it is coextensive with the seismically active Pitas Point fault, and both the Pitas Point and Ventura faults show geologic evidence of Holocene activity. In addition, the Pitas Point-Ventura fault is sandwiched structurally between the seismically active Red Mountain reverse fault to the northwest and the Anacapa reverse fault to the south (source of the 1973  $M_L$  6 Point Mugu earthquake).

The age constraints and stratigraphic-structural relations presented above enable estimation of rates of deformation derived from vertical components of uplift or from tilt on an inferred hinge. Reconstruction of the core area of the Ventura Avenue anticline suggests the sequence of subsidence-deposition and uplift-erosion phases shown in table 11.3.

Phase 5 (table 11.3) assumes no pre-San Pedro erosion of the upper part of the Santa Barbara Formation; this assumption seems unlikely because it does not explain the systematic thinning of the Santa Barbara and implies that deformation began much too recently in terms of the local and regional setting.

Another indication of the degree of deformation, the Wheelerian-Hallian Stage boundary, is exposed at elevations of 240 m on the eroded south flank of the anticline, and its reconstructed elevation over the eroded crest of the anticline is about 1,000 m; approximately the same horizon is buried at depths of about 2 km in the syncline to the south. The average rate of increase of structural

relief due to uplift of the anticline, faulting, and subsidence of the syncline is thus about 15 mm/yr over the past 200,000 years. Reconstruction of the anticline also indicates horizontal north-south shortening of about 30 percent during its formation.

The marine terrace platform along the south flank of the anticline is uplifted locally to elevations of about 128 m, tilted to at least  $7\frac{1}{2}$ ° (fig. 11.3), and faulted. Detailed sections across the areas of best control and numerous age estimates indicate that only one platform is present; its tilt rate over the last 80,000 years is about  $1.5 \times 10^{-6}$  rad/yr, assuming an original slope of 1° but ignoring effects of offset on the Ventura fault. Comparison of average tilt rates for the steeply dipping San Pedro Formation along the south margin of the anticline (about  $5.6 \times 10^{-6}$  rad/yr over 200,000–80,000 yr B.P.) and the unconformably overlying marine terrace platform (about  $1.5 \times 10^{-6}$  rad/yr since 80,000 yr B.P.) indicates that the rate of tilting here decreased significantly since 80,000 yr B.P. Had the earlier rate been maintained over the past 80,000 years, the terrace platform now should dip about 26° instead of about 8°. Vertical offset on the Ventura fault compensated for the tilting; without the fault offset, the tilt rate would have averaged at least  $2.5 \times 10^{-6}$  rad/yr, but still significantly less than the pre-80,000-year rate.

The apparent average uplift rate for the 80,000-yr-B.P. terrace is at least 1.6 mm/yr, which includes offset of at least 0.5 mm/yr on the Ventura fault. For comparison, apparent average rates for several localities from younger terraces (45,000 and 1,800–5,500 yr B.P.) along the Pitas Point-Punta Gorda coast, 10–16 km west of the Ventura River along the Rincon anticlinal trend, range from 1 to 10 mm/yr, depending chiefly on their distance from the anticlinal axis (Sarna-Wojcicki and others, 1979).

The exposure of terrace deposits about 2 km west of the Ventura River between 600 ft and 900 ft elevation (pl. 1) is similar in degree of deformation to the 80,000-year-old terrace; their base has been tilted to about

$7^\circ$ , for an apparent average rate of about  $1.5 \times 10^{-6}$  rad/yr over the past 80,000 years. Other stream terrace deposits exposed at lower elevations in this area are much less deformed and presumably are younger.

To summarize, our data suggest that late Quaternary deformation in the Ventura area began about 550,000 yr B.P. with moderate uplift and erosion, followed by subsidence and deposition until about 200,000 yr B.P. The most vigorous uplift and erosion in the core area of the anticline began about 200,000 yr B.P. (Stille's 1936 estimate: 250,000 yr B.P.), while the marine platform and its 80,000-year-old marine deposits were forming along the south margin of the anticline. Even with compensating offset on the Ventura fault, this platform has since been tilted to about  $8^\circ$  by continued uplift of the anticline, but the apparent average rate was less than half the earlier rate.

The formation, orientation, and rates of deformation of the structures in the Ventura area—the deep, actively subsiding Ventura syncline with flanks overthrust by young reverse faults; the actively rising, deeply eroded Ventura Avenue anticline and the greatly overpressured petroleum reservoirs in its core; the uplifted, tilted, and faulted marine terrace platform and deposits less than about 80,000 years old; and abundant seismic evidence—are all consistent with north-northeast—south-southwest regional compression that has dominated the western Transverse Ranges over the past 0.5 to 1 m.y.

## REFERENCES CITED

- Bailey, T. L., 1935, Lateral changes of fauna in the lower Pleistocene: Geological Society of America Bulletin, v. 46, p. 489–502.
- Bailey, T. L., and Jahns, R. H., 1954, Geology of the Transverse Range province, southern California, in Jahns, R. H., ed., Geology of southern California: California Division of Mines Bulletin 170, v. 1, chap. 2, p. 83–106.
- Cartwright, L. D., Jr., 1928, Sedimentation of the Pico Formation in the Ventura quadrangle, California: American Association of Petroleum Geologists Bulletin, v. 12–3, p. 235–269.
- Cilweck, B. A., 1975, Geologic/fault investigation, General Hospital complex: Unpublished Ventura County Public Works Agency Planning Study, Project no. 9674, 12 p.
- Cousineau, R. P., and Martin, R. A., 1975, Report on East Main Street distress investigation: Los Angeles, Calif., Soils International, Unpublished report to City of San Buenaventura, 14 p.
- Dalrymple, G. B., Cox, Allan, and Doell, R. R., 1965, Potassium-argon age and paleomagnetism of the Bishop Tuff, California: Geological Society of America Bulletin, v. 76, p. 665–674.
- Fischer, P. J., 1976, Late Neogene-Quaternary tectonics and depositional environments of the Santa Barbara Basin, California, in Fritsche, A. E., Ter Best, Harry, and Wornardt, W. W., eds., The Neogene Symposium: Society of Economic Paleontologists and Mineralogists, Pacific Section, Annual Meeting, San Francisco, Calif., 1976, p. 33–52.
- Gilluly, James, 1949, Distribution of mountain building in geologic time: Geological Society of America Bulletin, v. 60, p. 561–590.
- \_\_\_\_\_, 1962, The tectonic evolution of the western United States: Geological Society of London Quarterly Journal, v. 119, p. 133–174.
- \_\_\_\_\_, 1979, Cenozoic tectonics and regional geophysics of the western Cordillera (Review), by R. E. Smith and G. P. Eaton, Geological Society of America Memoir 152, 1978: Eos, American Geophysical Union Transactions, v. 60–22, p. 475.
- Greene, H. G., 1976, Late Cenozoic geology of the Ventura basin, California, in Howell, D. G., ed., Aspects of the geologic history of California Continental Borderland: American Association of Petroleum Geologists, Pacific Section, Miscellaneous Publication 24, p. 499–529.
- Hall, K. B., and Curran, J. F., 1972, Geology and future petroleum potential—Ventura basin, California, in Morrison, R. R., chairman, American Association of Petroleum Geologists-Society of Exploration Geophysicists, Pacific Section, Annual Meeting, 47th, Bakersfield, Calif., 1972, Technical Program Preprints: 18 p.
- Holman, W. J., 1958, Correlation of producing zones of Ventura basin oil fields, in Higgins, J. W., ed., A guide to the geology and oil fields of the Los Angeles and Ventura regions: Los Angeles, Calif., American Association of Petroleum Geologists, Pacific Section, p. 191–199.
- Izett, G. A., Naeser, C. W., and Obradovich, J. D., 1974, Fission-track age of zircons from an ash bed in the Pico Formation (Pliocene and Pleistocene) near Ventura, California [abs.]: Geological Society of America, Annual Meeting, Cordilleran Section, Program with Abstracts, p. 197.
- Kaufman, A., Broecker, W. S., Ku, T. L., and Thurber, D. L., 1971, The status of U-series methods of mollusk dating: Geochimica et Cosmochimica Acta, v. 35, p. 1155–1183.
- Kennedy, G. L., and Lajoie, K. R., 1982, Aminostratigraphy and faunal correlations of late Quaternary marine terraces, Pacific Coast, USA: Nature, v. 299, no. 5883, p. 545–547.
- Kew, W. S. W., 1932, Los Angeles to Santa Barbara, in Gale, H. S., ed., Southern California: International Geological Congress, 16th, Washington, D. C., 1933, Guidebook 15, p. 48–68.
- Lajoie, K. R., Kern, J. P., Wehmiller, J. F., Kennedy, G. L., Mathieson, S. A., Sarna-Wojcicki, A. M., Yerkes, R. F., and McCrory, P. A., 1979, Quaternary shorelines and crustal deformation, San Diego to Santa Barbara, in Abbott, P. L., ed., Geological excursions in the southern California area, original papers and field trip roadlogs prepared for the Geological Society of America Annual Meeting, November, 1979: Department of Geological Sciences, San Diego State University, San Diego, California, p. 3–15.
- Lajoie, K. R., Sarna-Wojcicki, A. M., and Yerkes, R. F., 1982, Quaternary chronology and rates of crustal deformation in the Ventura area, California, in Cooper, J. D. compiler, Neotectonics in southern California: Volume and Guidebook prepared for the 78th Annual Meeting of the Cordilleran Section, Geological Society of America, p. 43–51.
- Levorsen, A. I., 1954, Geology of petroleum, San Francisco, Calif., W. H. Freeman, 703 p.
- McCulloh, T. H., 1969, Geologic characteristics of the Dos Cuadras offshore oil field, chap. C of Geology, petroleum development, and seismicity of the Santa Barbara Channel region, California: U.S. Geological Survey Professional Paper 679, p. 29–46.
- Natland, M. L., 1952, Pleistocene and Pliocene stratigraphy of southern California: California University, Los Angeles, Ph.D. thesis, 165 p.
- \_\_\_\_\_, 1953, Correlation of Pleistocene and Pliocene stages in southern California: Pacific Petroleum Geologist, v. 7, no. 2, p. 2.
- \_\_\_\_\_, 1967, Ventura Basin stratigraphic field trip: American Association of Petroleum Geologists, Pacific Section, Guide Book, Field Trip Routes, 4 p.
- Natland, M. L., and Rothwell, W. T., Jr., 1954, Fossil Foraminifera of the Los Angeles and Ventura regions, California, in Jahns, R. H., ed., Geology of southern California: California Division of Mines Bulletin 170, v. 1, chap. 3, p. 33–42.

- Ogle, B. A., and Hacker, R. N., 1969, Cross section, coastal area, Ventura County, in Geology and oil fields of coastal areas, Ventura and Los Angeles basins, California, American Association of Petroleum Geologists, Society of Exploration Geophysicists, and Society of Economic Paleontologists and Mineralogists, Pacific Sections, Annual Meeting, 44th, Los Angeles, Calif., 1969, Guidebook, scale 1:48,000.
- Putnam, W. C., 1942, Geomorphology of the Ventura region, California: Geological Society of America Bulletin, v. 53, no. 5, p. 691-754.
- Quick, G. L., 1973, Preliminary microzonation for surface faulting in the Ventura, California area, in Moran, D. E., Slosson, J. E., Stone, R. O., and Yelverton, C. A., eds., Association of geology, seismicity, and environmental impact: Engineering Geologists Special Publication 1973, p. 257-262.
- Reed, R. D., and Hollister, J. S., 1936, Structural evolution of southern California: Tulsa, Okla., American Association of Petroleum Geologists, 157 p.
- Sarna-Wojcicki, A. M., Bowman, H. W., Meyer, C. E., Russell, P. C., Asaro, Frank, Michael, Helen, Rowe, J. J., Baedecker, P. A., and McCoy, Gail, 1979, Chemical analyses, correlations, and ages of late Cenozoic tephra units of east-central and southern California: U.S. Geological Survey Open-File Report 80-231, 53 p., 1 pl.
- Sarna-Wojcicki, A. M., Bowman, H. R., Meyer, C. E., Russell, P. C., Woodward, M. J., McCoy, Gail, Rowe, J. J., Jr., Baedecker, P. A., Asaro, Frank, and Michael, Helen, 1984, Chemical analyses, correlations, and ages of upper Pliocene and Pleistocene ash layers of east-central and southern California: U.S. Geological Survey Professional Paper 1293, 40 p.
- Sarna-Wojcicki, A. M., Williams, K. M., and Yerkes, R. F., 1976, Geology of the Ventura fault, Ventura County, California: U.S. Geological Survey Miscellaneous Field Studies Map MF-781, 3 sheets, scale 1:6,000.
- Stille, Hans, 1936, The present tectonic state of the earth: American Association of Petroleum Geologists Bulletin, v. 20, p. 849-880.
- Van Eysinga, F. W. B., 1975, Geological time table (3d ed.): Amsterdam, Elsevier, 1 sheet.
- Weber, F. J., Jr., Cleveland, G. B., Kahle, J. F., Kiessling, E. F., Miller, R. V., Mills, M. F., Morton, D. M., and Cilweck, B. A., 1973, Geology and mineral resources study of southern Ventura County, California: California Division of Mines and Geology Preliminary Report 14, 102 p.
- Wehmiller, J. F., and Belknap, D. F., 1978, Alternative kinetic models for the interpretation of amino acid entiomic ratios in Pleistocene mollusks: examples from California, Washington, and Florida: Quaternary Research, v. 9, p. 330-398.
- Wehmiller, J. F., Lajoie, K. R., Kvenvolden, K. A., Peterson, Etta, Belknap, D. F., Kennedy, G. L., Addicott, W. O., Vedder, J. G., and Wright, R. W., 1977, Correlation and chronology of Pacific Coast marine terrace deposits of continental United States by fossil amino acid stereo-chemistry—technique evaluation, relative ages, kinetic model ages, and geologic implications: U.S. Geological Survey Open-File Report 77-680, 106 p.
- Wehmiller, J. F., Lajoie, K. R., Sarna-Wojcicki, A. M., Yerkes, R. F., Kennedy, G. L., Stephans, T. A., and Kohl, R. F., 1978, Amino-acid racemization dating of Quaternary mollusks, Pacific Coast United States, in Zartman, R. E., ed., Short papers of the Fourth International Conference, Geochronology, Cosmochronology, Isotope Geology, 1978: U.S. Geological Survey Open-File Report 78-701, p. 445-448.
- Yeats, R. S., 1976, Neogene tectonics of the central Ventura basin, California, in Fritsche, A. E., Ter Best, Harry, and Wornardt, W. W., eds., The Neogene Symposium: Society of Economic Paleontologists and Mineralogists, Pacific Section, Annual Meeting, San Francisco, Calif., 1976, p. 19-32.
- Yerkes, R. F., and Lee, W. H. K., 1979, Late Quaternary deformation in the western Transverse Ranges, California: U.S. Geological Survey Circular 799-B, 10 p.

## 12. THE CUCAMONGA FAULT ZONE: GEOLOGIC SETTING AND QUATERNARY HISTORY

By DOUGLAS M. MORTON and JONATHAN C. MATTI

### ABSTRACT

The Cucamonga fault zone is a 1-km-wide east-striking thrust-fault complex that forms the south front of the eastern San Gabriel Mountains. The fault separates crystalline rocks of the mountains from Quaternary alluvium of the upper Santa Ana River valley and thus forms an important geologic and geomorphic boundary in this part of southern California.

A wide variety of Precambrian to Mesozoic crystalline rocks is exposed in the mountain block north of the Cucamonga fault zone. A petrologically and structurally complex assemblage of metamorphic rocks occurs within and immediately north of the thrust zone. Originally meta-sedimentary and plutonic in origin, these rocks have undergone prograde metamorphism to granulite and (or) upper amphibolite facies followed by retrograde metamorphism to amphibolite and lower facies. The retrograde episode was accompanied by intense penetrative deformation. This brittle and ductile deformation created a wide variety of penetrative fabrics whose layering is oriented predominantly east-northeast. Lineations, consisting of parallel minor-fold axes and mineral streaking, trend east-northeast and plunge at small angles to both east and west. The intensity of cataclasis progressively increases toward the mountain front and the Cucamonga fault zone, where the layering is parallel or subparallel to strands of the fault zone. It is not known whether all or part of the cataclastic deformation is genetically related to the Cucamonga fault zone, or whether the cataclastic rocks merely provided zones of structural weakness along which subsequent fault movement occurred.

North of the granulitic and cataclastic rocks is an east-oriented foliated to cataastically deformed body of Mesozoic quartz diorite. Cataclastic layering in the quartz diorite parallels that in rocks to the south, and deformation is most intense in the southern part of the body. North of the quartz diorite are a variety of metasedimentary and granitic rocks that also display cataclastic textures.

Within the Cucamonga fault zone we recognize two major groups of Quaternary alluvial units. Older alluvial units are Pleistocene and, from oldest to youngest, include units  $df_1$ ,  $df_2$ ,  $of_1$ ,  $of_2$ , and  $of_3$ . Younger alluvial units are latest Pleistocene and Holocene and, from oldest to youngest, include units  $yf_1$  through  $yf_4$  and various units of inactive and active alluvium of channel washes and alluvial-fan surfaces.

Faulting within the Cucamonga fault zone has recurred episodically throughout most of Quaternary and, probably, latest Tertiary time. The oldest faults are in the north part of the fault zone, where some faults cut crystalline basement rock but do not break even the oldest Quaternary alluvial units. Younger faults, Cucamonga strands A, B, and C, occur farther south at the mountain front. Here, strand A breaks older Quaternary alluvial units but is concealed beneath younger Quaternary alluvial units. Strands B and C occur south of strand A and form conspicuous scarps in young Quaternary alluvial fans. These relations sug-

gest that faulting within the Cucamonga fault zone may have migrated southward during late Pleistocene and Holocene time.

The alluvial units record the movement history of fault strands. Confirmed displacements on strand A, the oldest structure, occurred after deposition of unit  $df_2$  and again after accumulation of the youngest deposits of unit  $yf_1$ , but not since that time. Strands B and C both evolved during the deposition of unit  $yf_1$ , and recurrent displacements on these two strands disrupted the evolving alluvial deposits of units  $yf_1$  through  $yf_3$ . Displacements on strand B apparently ended during early stages of the deposition of unit  $yf_3$ , whereas displacements have continued on strand C. The latest movement on strand C occurred before the deposition of unit  $yf_4$  which overlaps the fault on Day Canyon fan; this unit may be as old as 1,750 to 1,000 years.

Quaternary faulting within the Cucamonga fault zone has generated a complicated pattern of fault strands where individual strands merge and diverge locally; all strands apparently merge along a single trace in the western part of the fault zone. Thus, although strands A, B, and C form individual faults in the eastern part of the zone, to the west strands B and C merge to form strand B/C and strands A and B/C ultimately merge to form strand A/B/C. The latest episodes of faulting may have occurred mainly on strand C in the eastern 15 km of the Cucamonga fault zone, rather than throughout the entire 25-km length of the fault zone. The more complicated pattern of faulting in the eastern part of the zone may reflect interaction between the Cucamonga and San Jacinto fault zones: northwestward migration of the Perris block and the Peninsular Ranges by Quaternary right-lateral slip on the San Jacinto fault zone may have been taken up partly by reverse- and thrust-fault displacements along the Cucamonga fault zone.

### INTRODUCTION

#### REGIONAL SETTING

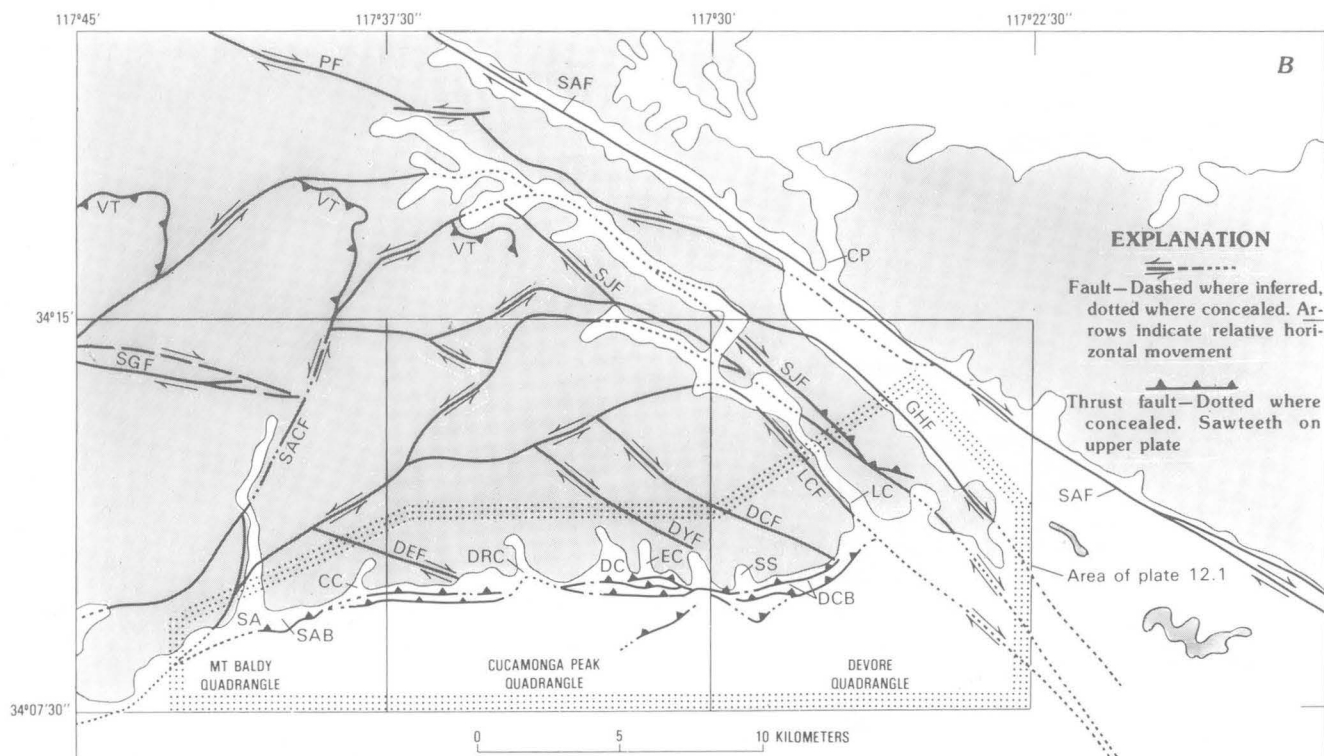
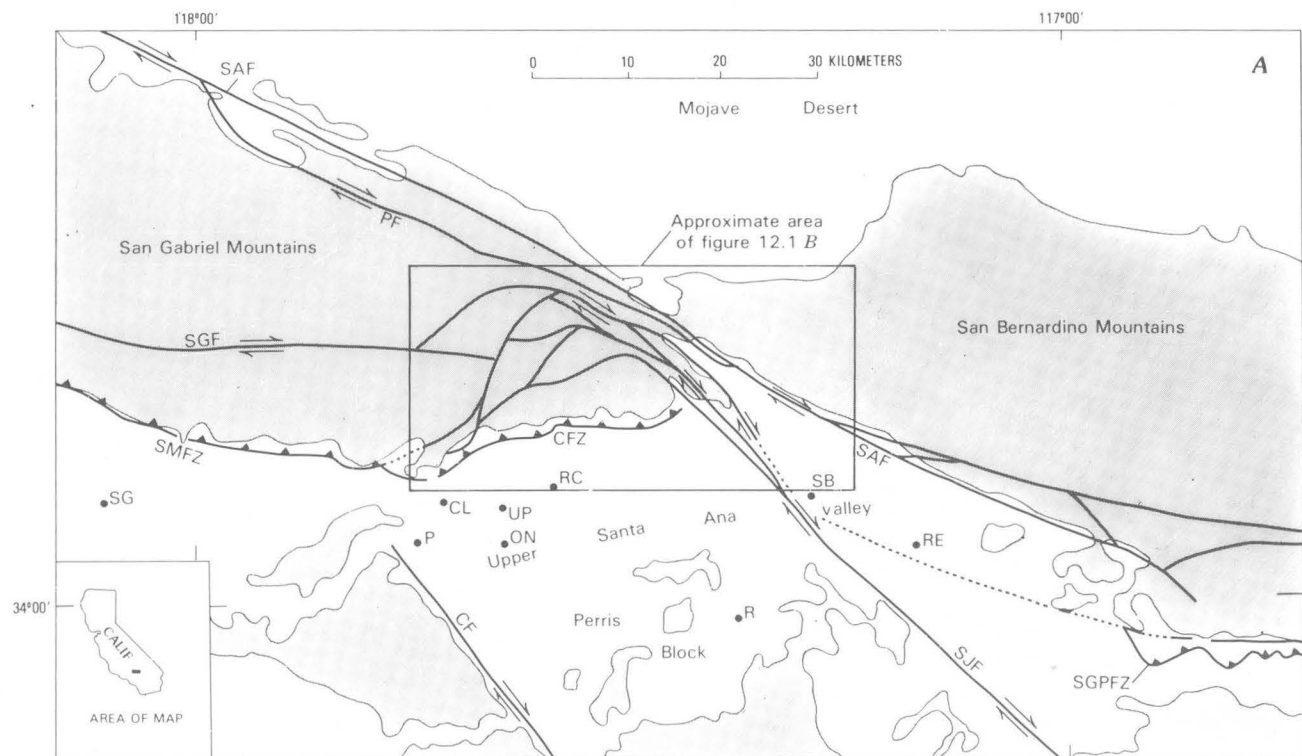
The name "Cucamonga fault" generally is applied to the eastern part of the frontal-fault zone that bounds the south margin of the San Gabriel Mountains (Lamar and others, 1973; Morton and Yerkes, 1974; Ehlig, 1981). In our usage, the Cucamonga fault extends from the San Antonio Canyon area eastward to the Lytle Creek area (fig. 12.1). Along this reach, the frontal-fault zone separates the upper Santa Ana River valley to the south from the most prominent peaks of the eastern San Gabriel Mountains (figs. 12.2, 12.3).

The east and west terminations of the Cucamonga fault zone are unclear. On the east, in the Lytle Creek area, the Cucamonga fault interacts in some unknown way with northwest-oriented right-lateral strike-slip faults of the San Jacinto fault zone (fig. 12.4). These faults include the

Duncan Canyon, Lytle Creek, Meyer Canyon, San Jacinto, and Glen Helen faults. We are uncertain how the Cucamonga fault zone interacts geometrically and kine-

matically with these right-lateral faults or how far eastward the frontal-fault zone extends.

Structural relations at the west end of the Cucamonga



fault zone also are obscure. Of possible relevance here are structures of the San Jacinto fault complex that enter the mountains some 25 km to the east. Where they intersect the southeast margin of the San Gabriel Mountains, right-lateral faults of the San Jacinto fault zone strike northwest. As summarized by Morton (1975a, fig. 2, p. 175), within the interior of the mountains these structures veer westward and diverge or splay into a series of east- to northeast-oriented and north-dipping faults that converge in lower San Antonio Canyon at the west end of the Cucamonga fault zone (fig. 12.1). Here, three discrete fault complexes come together: (1) The Cucamonga fault zone, (2) the converging faults of the interior San Gabriel Mountains, and (3) the Sierra Madre fault zone, an east-trending fault complex that represents the frontal-fault system west of San Antonio Canyon. Relations between these three structural elements are unclear, although the simplest model interprets the Cucamonga and Sierra Madre faults as temporally and structurally related segments of a throughgoing frontal-fault zone. By this interpretation, the Cucamonga fault zone probably passes westward into the Sierra Madre fault zone.

Along its 25-km extent, movement on the Cucamonga fault zone has created prominent fault scarps that disrupt Quaternary alluvial fans flanking the south margin of the mountains (fig. 12.5). These scarps attest to ongoing faulting at the south margin of the eastern Transverse Ranges (Morton and Yerkes, 1974). This part of the upper Santa Ana valley is not yet covered completely by suburban development and thus affords unexcelled views of the surface morphology of young thrust faults that are developed in alluvium.

#### PURPOSE

This preliminary interpretation of the geology of the Cucamonga fault zone is motivated by two factors. First, the fault zone is a youthful and relatively well exposed element of the Transverse Ranges family of thrust faults; data derived from the fault zone thus can increase our understanding of the origin and history of this family of faults. Second, the upper Santa Ana valley area adjacent to the Cucamonga fault zone is undergoing rapid urbanization, especially in communities of Upland and Rancho

Cucamonga. Accordingly, information concerning the Cucamonga fault should be useful for seismic-safety planning in these communities. Within these contexts, the goals of this report are threefold: (1) to describe the general geologic setting of the Cucamonga fault zone; (2) to record the positions of faults and fault scarps within this zone; and (3) to provide a preliminary summary of late Pleistocene and Holocene fault-movement history as recorded by the Quaternary alluvial stratigraphy and by fault-scarp morphology.

This report stems from a project conceived and initiated by D. M. Morton; the junior author joined the project during its tenure. Morton mapped the crystalline rocks (Morton, 1976) and is responsible for interpreting the origin of fabrics and structures within these rocks. Matti refined Morton's (1976) original mapping of Quaternary alluvial units and reinterpreted the distribution of fault scarps in some areas.

#### OTHER INVESTIGATIONS

The unusual basement rocks of the eastern San Gabriel Mountains have received repeated attention since Alf (1948) first described the occurrence of cataclastic rocks. Alf (1948) later amplified his earlier work and gave a generalized account of the geology of the eastern San Gabriel Mountains. Hsu (1955) described in detail the mineralogy of the cataclastic rocks along the range front. Later, Baird (1956) and Ehlig (1958) described basement rocks and structure interior to the range.

Eckis (1928) provided an account of the alluvial-fan sequence flanking the mountains and also described the fault scarps. Later, Eckis (1934) gave a comprehensive account of the general geology in his study of the geology of the southern California coastal plain. In a discussion of ground water in the Fontana-Etiwanda area, Burnham (1953) gave a succinct description of the Cucamonga fault zone. Morton (1975a, b) provided a synoptic discussion of the eastern San Gabriel Mountains and later (Morton, 1976) a preliminary geologic map of the Cucamonga fault zone. Ehlig (1981) briefly discussed rocks in the eastern San Gabriel Mountains. Matti and others (1982) and Morton and others (1982) summarized the faulting history at Day

FIGURE 12.1.—Location and structural setting of the Cucamonga fault zone. Shaded areas indicate bedrock outcrops. A, Index map showing location of the Cucamonga fault zone (CFZ). Major physiographic features include the San Gabriel and San Bernardino Mountains of the Transverse Ranges province, and lowlands of the upper Santa Ana River valley. Major faults include: CF, Chino fault; PF, Punchbowl fault; SAF, San Andreas fault; SGF, San Gabriel fault; SGPFZ, San Gorgonio Pass fault zone; SMFZ, Sierra Madre fault zone; SJF, San Jacinto fault. Cities include: CL, Claremont; ON, Ontario; P, Pomona; R, Riverside; RC, Rancho Cucamonga; RE, Redlands; SB, San Bernardino; SG, San Gabriel; UP, Upland. B, Structural setting of

the eastern San Gabriel Mountains and areas referred to in the text. Stippled line indicates boundaries of plate 12.1. Selected faults include: DCF, Duncan Canyon fault; DEF, Demens Canyon fault; DYF, Day Canyon fault; GHF, Glen Helen fault; LCF, Lytle Creek fault; PF, Punchbowl fault; SAF, San Andreas fault; SACF, San Antonio Canyon fault; SGF, San Gabriel fault; SJF, San Jacinto fault; VT, Vincent thrust. Physiographic features include: CC, Cucamonga Canyon; CP, Cajon Pass area; DC, Day Canyon; DCB, Duncan Canyon Bench area; DRC, Deer Canyon; EC, East Etiwanda Canyon; LC, Lytle Creek; SS, San Sevaine Canyon; SA, San Antonio Canyon; SAB, San Antonio Heights Bench.

Canyon and East Etiwanda Canyon, where we have detailed data derived from fault-scarp profiles, trenching investigations, and soil-profile studies (J. C. Matti, D. M. Morton, J. C. Tinsley, and L. D. McFadden, unpub. data, 1980–84). Later, Metzger and Weldon (1983) summarized their tectonogeomorphic studies of alluvial units in Lytle Creek, near the junction between the San Jacinto and Cucamonga fault zones. Morton and others (1983) briefly described basement rocks of the southeastern San

Gabriel Mountains and provided a simplified geologic map showing the regional distribution of major rock units and fault zones.

#### GEOLOGIC SETTING OF THE CUCAMONGA FAULT ZONE

In this section we describe the petrology and structure of crystalline basement units and Tertiary and Quaternary sedimentary units that crop out within and adjacent



FIGURE 12.2.—Southeastern San Gabriel Mountains and vicinity; oblique aerial photograph looking northeast. Alluviated lowlands of the upper Santa Ana River valley (center and right) are south of the mountain front, and the city of Claremont is in the foreground. The Mojave Desert province is in the far-left background; the San Bernardino Mountains in the far-right background are separated from the San Gabriel Mountains by the San Andreas fault. The Cucamonga fault zone at the base of the San Gabriel Mountains extends from San

Antonio Canyon (SC) east to the Lytle Creek alluvial fan (LC). Note the entrenched fanheads of Cucamonga Canyon (CC; also see fig. 12.11) and Day Canyon (DC; also see fig. 12.5). Note the benchlike topography at the base of the mountains between the Cucamonga Canyon and Day Canyon fanheads; these benches locally are capped by old Pleistocene alluvium, and they probably represent bedrock pediments. Photograph by Robert C. Frampton (photograph No. 64-938B, dated Nov. 21, 1964).

to the Cucamonga fault zone. The basement rocks are discussed in geographic sequence from south to north.

#### CRYSTALLINE BASEMENT ROCK

##### PRECAMBRIAN(?) GRANULITE AND CATACLASITE COMPLEX

Crystalline basement rock exposed within and immediately north of the Cucamonga fault zone forms an east-northeast-striking metamorphic complex (pCgc, pCc) that consists of schist, gneiss, granulite, charnockitic rock, and pods of marble (pl. 12.1). Although undated, the protolith of this complex is considered by most workers to be Precambrian in age. These rocks now are mainly cataclastic and mylonitic; however, brittle and ductile shearing are only the latest penetrative deformation recorded in the rocks, which have had a complicated metamorphic and structural history.

The earliest recognizable structural event included widespread slip folding of a protolith that probably was sedimentary rock. These slip-folding events produced well-defined transposed layering. Metamorphism to granulite and (or) upper amphibolite facies accompanied or followed this deformation. Common prograde mineral assemblages include garnet-biotite-plagioclase-K-feldspar-quartz, orthopyroxene(hypersthene)-biotite-plagioclase, clinopyroxene(diopsidic)-biotite-plagioclase, and sillimanite-garnet-biotite-quartz; less common prograde assemblages include those of diopside- and phlogopite-bearing marble and uncommon massive olivine-orthopyroxene-amphibole-spinel-calcic-plagioclase rock.

Within this gneissic complex, charnockitic rock\* locally occurs as irregular to tabular lenticular masses as much

\* After this chapter had been completed, this charnockite was shown to be Cretaceous in age by Walker and May (1986).



FIGURE 12.3.—Southeastern San Gabriel Mountains and vicinity; oblique aerial photograph looking west. Alluviated lowlands of the upper Santa Ana River valley are south of the mountain front, U.S. Interstate Highway 15 is in the foreground. Note the bedrock-floored benches (pediments) between San Sevaine Canyon (SS) and Day Canyon (DC); strands A, B, and C of the Cucamonga fault zone are located at the toes of these benches, which locally are capped by old Pleistocene alluvium. EC, East Etiwanda Canyon. Photograph by D. M. Morton (Nov. 1976).

ments) between San Sevaine Canyon (SS) and Day Canyon (DC); strands A, B, and C of the Cucamonga fault zone are located at the toes of these benches, which locally are capped by old Pleistocene alluvium. EC, East Etiwanda Canyon. Photograph by D. M. Morton (Nov. 1976).

as 2 km long. The charnockitic rock is medium to coarse grained, is texturally massive to foliated, and has a mineralogy like that of some of the granulite—mainly hypersthene, biotite, and plagioclase, with some quartz and garnet.

Most of the granulitic and charnockitic rocks were affected by a second metamorphism of amphibolite and lower grade. This retrograde metamorphic event was accompanied by nearly complete destruction of olivine, orthopyroxene, and most garnet, and by the generation of widespread amphibole. In general, the charnockitic rock appears to be less affected by retrograde metamorphism than the granulite. Relict granulite is common only west of Deer Canyon.

Retrograde metamorphism from granulite facies to amphibolite and lower facies was accompanied and followed by intense penetrative cataclastic deformation involving both brittle and ductile processes. Cataclasis transposed

much of the layered granulite-amphibolite gneiss into a thinly layered rock containing various cataclastic textures. Intersection between cataclastic slip surfaces and the earlier prograde (granulitic) metamorphic layering produced mesoscopic-scale fold axes and lineations ("b" geometric), the orientation of which was determined by the geometric relations of the two sets of planar structures. West of Deer Canyon, much of this cataclastic layering developed at a high angle to the granulitic layering, whereas east of Deer Canyon the granulitic and cataclastic layering commonly are subparallel. East of San Sevaine Canyon, especially, much of the cataclastic layering appears to have formed subparallel to the older granulitic layering, and here many of the granulite-facies garnets are preserved. The occurrence of cataastically deformed amphibolite-grade rock indicates that cataclasis continued after the rocks had recrystallized to amphibolite facies during retrograde metamorphism.



FIGURE 12.4.—Easternmost San Gabriel Mountains; oblique aerial photograph looking north into Lytle Creek drainage. The Lytle Creek alluvial fan (LC) is in the foreground; Cajon Creek (CC) is between Lytle Creek Ridge (LR) and the base of the San Bernardino Mountains at far right; Cajon Pass region is in the far-right background, and the Duncan

Canyon Bench area (DC) is at the mountain front directly west (left) of Lytle Creek. Strands of the San Jacinto fault zone enter the Lytle Creek drainage from the south, then curve westward into the San Gabriel Mountains without joining the San Andreas fault (see Morton, 1975a, fig. 3). Photograph by D. M. Morton (Feb. 1976).

The predominant orientation of the cataclastic layering is east-northeast, paralleling the overall orientation of this metamorphic belt. Most of the layering dips northward at low to moderate angles. Linear structures trend east-northeast and plunge at small angles to the east and west. These linear structures include minor-fold axes, oriented elongate minerals, and mineral streaking, all of which are parallel on a mesoscopic scale. With progressive cataclastic deformation, the "b"-geometric linear structures were deformed into a consistent orientation ("a" kinematic?) within the plane of cataclastic slip. At the present erosional level, the intensity of cataclastic deformation progressively increases southward toward the mountain front and the Cucamonga fault zone, where rock resembling pseudotachylite occurs locally. This spatial variation in cataclastic texture apparently prompted earlier workers (Alf, 1948; Hsu, 1955) to subdivide the cataclastic granulite unit into multiple formations.

Locally, in the southernmost extent of the cataclastic rock, the cataclastic layering and lineation are deformed into complicated folds whose geometry combines flexural slip and slip folding.

#### CRETACEOUS(?) QUARTZ DIORITE

Foliated to cataclastic quartz diorite (Kqd and Kqdc) occurs north of the Precambrian(?) granulite and cataclasite complex (pl. 12.1). Most of the noncataclastic rock is equigranular, medium-grained, incipiently to intensely foliated biotite-hornblende quartz diorite (Kqd) that grades into subporphyritic biotite-hornblende granodioritic rock containing K-feldspar phenocrysts. The foliation strikes east to northeast and dips northward. Mesocratic ellipsoidal inclusions are common. Between Cucamonga Canyon and San Sevaine Canyon, discontinuous lenticular bodies of coarse-grained hornblende diorite (Kd) occur along the south margin of the quartz



FIGURE 12.5.—Alluvial fans of Day Canyon (DC) and East Etiwanda Canyon (EC), with fault scarps of the Cucamonga fault zone traversing late Quaternary alluvium; oblique aerial photograph looking north. Fault scarps mark the traces of thrust-fault strands A, B, and C. Note the deeply entrenched active washes on the Day Canyon and East Etiwanda Canyon fanheads. Photograph by D. M. Morton (July 1973).

diorite mass. The probable age of both the noncataclastic quartz diorite and the protolith for the cataastically deformed quartz diorite is Cretaceous.

Like the granulite and cataclasite complex, the quartz dioritic rocks have had a complicated structural history. In most places, original textures in the plutonic rocks have been obliterated by later cataclastic deformation. The cataclastic layering strikes east-northeast and is subparallel to the preexisting foliation. The degree of cataclastic deformation generally increases southward. For example, east of San Sevaine Canyon, a discrete 200- to 400-m-thick zone of pervasively deformed mylonitic quartz diorite (Kqdm) occurs between the granulite and cataclasite complex. North of this discrete zone, cataclasis of the quartz diorite is variable. In much of the cataclasite, hornblende appears to have recrystallized during cataclasis to form fine-grained foliated cataclasite that is studded with large (1- to 2-cm-long) hornblende crystals. After hornblende recrystallized, continued cataclasis produced a well-lineated rock having oriented and fragmented hornblende. Subrounded ellipsoidal mesocratic inclusions that occur within the noncataclastic quartz diorite have been flattened parallel to the foliation in the cataclastic quartz diorite. Throughout the outcrop belt of the quartz diorite complex, local intense cataclastic deformation has produced thin (1- to 10-cm-thick) layers of flintlike pseudotachylitic cataclasite.

#### PALEOZOIC(?) AND MESOZOIC PLUTONIC AND METAMORPHIC COMPLEX

An east-striking plutonic-metamorphic complex crops out north of the granulite and cataclastic complex and the quartz diorite complex (pl. 12.1). The metamorphic rocks (Pzs) are of amphibolite grade and consist of quartz-rich garnet-sillimanite-biotite schist and gneiss, quartzite, and marble. Schistosity and layering generally strike east and dip north. East of San Antonio Canyon, these rocks occur as xenoliths, septa, and pods incorporated in plutonic rock of mainly quartz dioritic composition (Kqd); eastward toward Lytle Creek, the amphibolite-grade rocks progressively become more mingled with the quartz diorite. These metamorphic pods and septa east of San Antonio Canyon correlate lithologically with thick sequences of highly deformed metasedimentary rock along the mountain front at Potatoe Mountain, west of San Antonio Canyon. All these rocks probably are correlative with rocks farther to the north outside the map area on the east side of San Antonio Canyon (schist, marble, and quartzite unit of Morton, 1975a, fig. 1).

On the basis of their lithology—thick marble and quartzite sequences associated with schist and gneiss—the amphibolite-grade metasedimentary rocks probably are early Paleozoic in age. The quartz diorite intruding these

metamorphic rocks probably represents the same Cretaceous(?) plutonic body or intrusive series as the quartz diorite in the plutonic complex to the south.

#### MISCELLANEOUS CRETACEOUS(?) GRANITOID ROCKS

Quartz monzonite to granodiorite dikes and small irregular bodies (Kqm), of probable Cretaceous age and in part cataastically deformed, cut both of the metamorphic complexes as well as the quartz diorite complex. The dikes are foliated and strike east-west.

A body of intensely cataastically deformed leucogranite (Kgc) occurs east of Lytle Creek. This rock has a well-defined lineation produced by streaked-out quartz and feldspar. Nearby, a fault-bounded sliver of medium-to coarse-grained leucocratic muscovite granite (Kg) is present within the San Jacinto fault zone at the mountain front. Both these units probably are Cretaceous in age.

#### PELONA SCHIST

The Pelona Schist (ps) occurs in small masses within and east of the San Jacinto fault zone (pl. 12.1). This schist is a major unit in the interior of the eastern San Gabriel Mountains, where it constitutes a thick sequence of well-layered greenschist-facies rock. The Pelona Schist underlies the Vincent thrust, a regional-scale feature that may represent a late Mesozoic or early Tertiary subduction zone. The base of the Pelona is nowhere exposed and its basement is speculative (Ehlig, 1981). The age of the protolith for the schist is Mesozoic, probably Cretaceous or older. The age of metamorphism may be earliest Tertiary (Ehlig and others, 1975; Evans, 1982). The unit is not intruded by Mesozoic plutonic rocks, but it is intruded by dikes, irregular small bodies, and one sizable granodiorite pluton of Miocene age. Within the study area, the Pelona Schist consists of well-layered, siliceous, white-mica-albite schist and slightly foliated, crudely layered greenstone.

#### TERTIARY INTRUSIVE ROCKS MIOCENE GRANODIORITE

A fault-bounded mass of Miocene biotite granodiorite (Tgd) occurs east of Lytle Creek (pl. 12.1). Unlike the Mesozoic plutonic rocks, this granodiorite is a uniform-appearing texturally massive medium- to coarse-grained rock. The K-Ar age on biotite from samples of this unit is  $14.0 \pm 0.4$  m.y. B.P. (Miller and Morton, 1977). Similar ages were obtained for other parts of the unit farther northwest in the San Gabriel Mountains (Hsu and others, 1963; Miller and Morton, 1977).

## MISCELLANEOUS INTRUSIVE ROCKS

A few leucocratic quartz porphyry dikes (Tq) intrude quartz diorite on the east side of San Antonio Canyon. We believe that these dikes are Tertiary (Miocene?) in age. A small fault-bounded mass of porphyritic biotite dacite (Td) occurs within the Cucamonga fault zone between Cucamonga and Demens Canyons. This rock is similar lithologically to the Mountain Meadows Dacite Porphyry as mapped by Shelton (1955) west of the study area. Biotite from a similar-appearing dike rock collected in the Glendora area, 11 km west of San Antonio Canyon, yielded a K-Ar age of  $27.5 \pm 2.5$  m.y. B.P. (Rogers, 1967).

Fine-grained andesitic to basaltic dikes (Ta) have intruded the Miocene granodiorite and other basement-rock units in the southeastern San Gabriel Mountains. A single differentiated body of diabase to gabbro, whose fine-grained marginal parts resemble the andesitic-basaltic dike rock, is well exposed in a freeway cut on Interstate Highway 15 east of Lytle Creek. Although these bodies are undated, they postdate the 14-m.y.-old Miocene granodiorite.

## CENOZOIC SEDIMENTARY ROCKS

## TERTIARY CONGLOMERATE

A sequence of poorly bedded nonmarine conglomerate is exposed discontinuously for 4 km along the mountain front between Morse Canyon and the mouth of Lytle Creek (pl. 12.1). On the basis of regional considerations, we believe that this unit is late Tertiary in age. The conglomerate consists primarily of gneissic cobbles that are unlike any of the basement rocks exposed today in the eastern San Gabriel Mountains. At all localities, the conglomerate is overlain in thrust contact by the granulite and cataclasite complex. The attitude of bedding, which dips vertically or is overturned steeply to the north, suggests that the conglomerate constitutes the north limb of an overturned syncline that was produced by reverse displacements on the Cucamonga fault. Farther west along the frontal-fault zone, similar structures exist in late Tertiary sedimentary rocks in the Azusa area (Shelton, 1955; Morton, 1977) and in the San Fernando Valley area (Barrows and others, 1977).

QUATERNARY ALLUVIAL DEPOSITS  
IDENTIFICATION AND CORRELATION

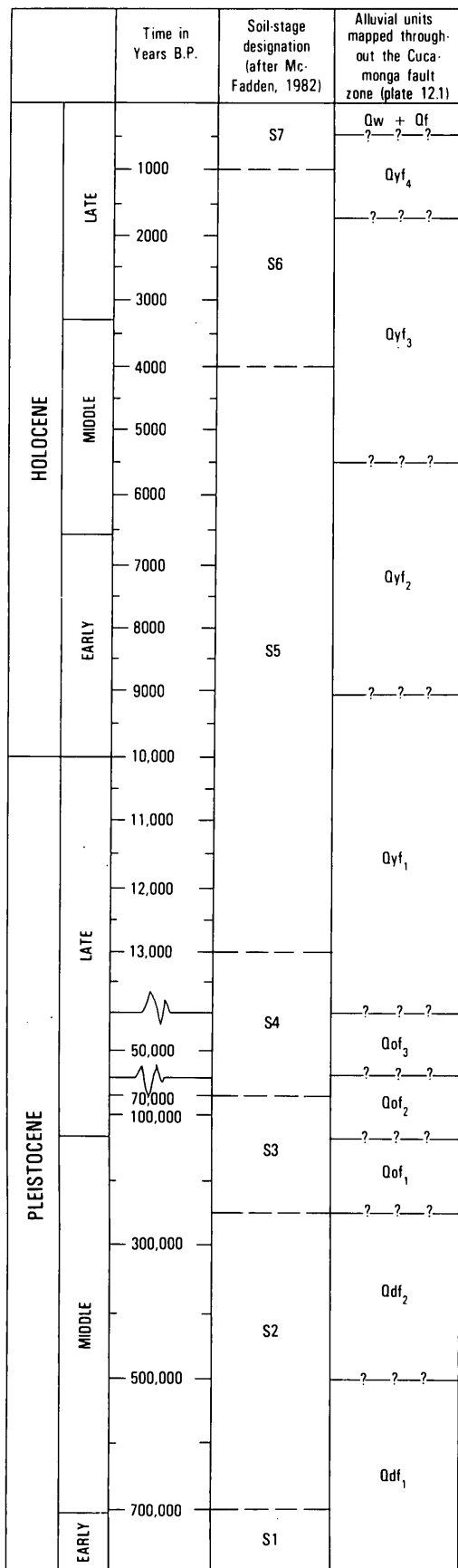
We recognize 11 Quaternary alluvial units within the Cucamonga fault zone, and we use six criteria to identify these units: (1) topographic position within flights of stream terraces; (2) degree of erosional dissection; (3) preservation of primary depositional features such as channel-and-bar morphology; (4) structural and temporal

relations to various fault strands of the Cucamonga fault zone; (5) differences in lithology and physical stratigraphy between some alluvial units; and (6) differences in soil-profile characteristics. On the basis of these criteria we recognize four major groups of alluvial units (fig. 12.6): (1) sediment in washes and on alluvial-fan surfaces that is actively transported by modern stream flows, or that presently is inactive (Qw and various categories of Qf on the geologic map); (2) latest Pleistocene and Holocene alluvial-fan deposits that are slightly to moderately dissected and that have pedogenic soil profiles lacking significant argillitic horizons (various categories of Qyf on the geologic map); (3) late Pleistocene alluvial-fan deposits that are well dissected and that have pedogenic soil profiles containing moderately developed argillitic horizons (various categories of Qof on the geologic map); and (4) Pleistocene alluvial-fan deposits that are extremely dissected and that have pedogenic soil profiles containing well-developed argillitic horizons (various categories of Qdf on the geologic map).

Nearly every alluvial fan within the Cucamonga fault zone displays a nested series of fluvial terraces. On each fan it is relatively easy to work out relative age relations and to subdivide the alluvial-terrace succession according to the six criteria cited above. However, it is not so easy to correlate individual alluvial units from one alluvial fan to another or from the alluvial-fan surface to the remnant flights of terraces clinging to the walls of upstream bedrock canyons. This correlation problem exists because the individual alluvial units cannot be identified and correlated simply on the basis of lithology or some striking aspect of geomorphology. For example, units identified on the geologic map as Qyf<sub>1</sub> through Qyf<sub>4</sub> generally look the same in terms of their color, bedding characteristics, grain-size distribution, sand-gravel ratios, and degree of consolidation. In the absence of radiometric age determinations, the only reliable means of correlating the alluvial units is by subtle to pronounced differences in their soil-profile characteristics and by subtle differences in the weathering characteristics of bedrock cobbles and boulders on the alluvial-fan surfaces. Correlation by these techniques would require detailed soil-profile investigations from all alluvial units within the Cucamonga fault zone, and this level of study was beyond the scope of our preliminary investigation.

Although we identified and correlated alluvial units mainly on the basis of alluvial and tectonic geomorphology, we supplemented our geomorphic interpretations with soils data where possible. Most published soil-profile descriptions are from the east half of the Cucamonga fault zone, where soils have been described in the Lytle Creek and Duncan Canyon bench areas and in the vicinity of the East Etiwanda and Day Canyon alluvial fans (McFadden, 1982, p. 276-296; McFadden, in Matti and others, 1982).

## RECENT REVERSE FAULTING IN THE TRANSVERSE RANGES, CALIFORNIA



Supplemental soils information comes from two sources: (1) soil profiles we examined at several localities in the western half of the Cucamonga fault zone (indicated on the geologic map); and (2) generalized soil maps available for the entire study area (U.S. Soil Conservation Service, 1980). In the absence of comprehensive soil-profile studies, we used aerial photographs to subdivide the alluvial units mainly on the basis of geomorphology and relative position within terrace sequences (the appendix summarizes technical information concerning the flight series, scale, and vintage of aerial photographs used in this study).

These geomorphic criteria do not always permit accurate correlation between drainage basins. Therefore, our classification and correlation of alluvial units is preliminary, and the age assignment for some units may require modification as their soil profiles are studied more carefully and as the soil chronosequence for this district is tested and modified. We have correlated individual alluvial units throughout the Cucamonga fault zone; however, because we only have limited control on the relative ages of these units, a unit at one locality may not be exactly time correlative with the same labeled unit at another locality. Our alluvial units are general stratigraphic categories only, and in places they may include two or more localized subsidiary units. The units in each category evolved during the same general time interval, but the timing of degradational and aggradational events on each alluvial fan probably was unique.

#### OLDER ALLUVIAL UNITS (UNITS QOF AND ODF ON THE GEOLOGIC MAP)

Older alluvial units consist of highly dissected deposits that occur in isolated outcrops scattered along the mountain front (pl. 12.1). The units occur as elevated stream-terrace deposits along major drainages, as isolated patches on ridgecrests, and as thin wedges perched on basement-floored benches along the mountain front. These wedges represent alluvial materials that accumulated on a former pediment surface. The older alluvial deposits are Pleistocene in age.

The older deposits are reddish brown, vary from consolidated to well indurated, and range in composition from cobble-boulder gravel to cobby-pebbly sand and sandy

FIGURE 12.6.—Diagram illustrating approximate stratigraphic relations between Quaternary alluvial units mapped throughout the Cucamonga fault zone and pedogenic soil stages recognized by McFadden (1982). The numerical ages of the alluvial units are not known; time scale is included at left to show our best estimate of the approximate age for each unit. Subdivisions of the Holocene arbitrarily separate the epoch into three equal parts; subdivisions of the Pleistocene from G. M. Richmond, U.S. Geological Survey (written commun. to J. I. Ziony, U.S. Geological Survey, 1984).

gravel. Stratification generally dips a few degrees south, except for localized deposits perched on piedmont benches within or immediately north of the Cucamonga fault zone, where deposits affected by faulting have been rotated backward to the north. Here, the beds commonly are horizontal, and northward dips as steep as 30° occur locally.

We recognize two categories of older alluvial units (fig. 12.6). On the geologic map (pl. 12.1) the extremely dissected alluvial units are identified as Qdf<sub>1</sub> and Qdf<sub>2</sub>; the moderately to well dissected units are identified as Qof<sub>1</sub>, Qof<sub>2</sub>, and Qof<sub>3</sub>. For convenience, in the text we refer to these as units od<sub>1</sub>, od<sub>2</sub>, of<sub>1</sub>, of<sub>2</sub>, and of<sub>3</sub>.

The older alluvial units are thin to thick sedimentary fills that are distinguished from younger alluvial units by their extensive erosional dissection, by their high-standing terrace positions, and by their well-developed soil profiles that have conspicuous argillic B horizons. The B horizons are reddish (hues ranging from 5YR to 10R, determined from Munsell soil-color charts; Munsell, 1975) and contain mafic and mesocratic basement clasts that generally are decomposed. Although the older alluvial units all have similar sedimentary textures and structures and have similar clast compositions and sand-gravel ratios, with increasing age their argillic horizons are thicker and better developed, the hues are increasingly red, and the mafic and mesocratic clasts are more thoroughly degraded and disaggregated.

**YOUNGER ALLUVIAL UNITS**  
(UNITS QYF, QF, AND QW ON THE GEOLOGIC MAP)

Younger Quaternary alluvium forms extensive Holocene and latest Pleistocene alluvial-fan deposits that flank the mountain front (pl. 12.1). Locally, some younger alluvial units were deposited directly on rock-floored surfaces, but this relationship occurs only near the mountain front. Most younger alluvial units accumulated on top of terrace surfaces cut into underlying alluvial units. The younger alluvial units typically consist of thin sedimentary fills 1 to 3 m thick that are yellowish gray, are unconsolidated to moderately consolidated, and consist of sandy cobble-boulder gravel that fines to pebbly-cobbly sand and sandy gravel southward away from the mountain front. Crude stratification in these units dips gently southward. Some younger alluvial units are so thin that they constitute only patchy veneers deposited discontinuously on top of erosional surfaces cut into underlying alluvial units. Units such as these could be viewed as geomorphic surfaces, but we map them as geologic units.

We recognize six younger alluvial units (fig. 12.6) and several subdivisions of these units. On the geologic map (pl. 12.1) these units are identified as units Qyf<sub>1</sub> through Qyf<sub>4</sub>, and units Qfio, Qfiy, and Qw. For convenience, in

the text we refer to these as units yf<sub>1</sub> through yf<sub>4</sub>, and as various units of inactive and active alluvium. Most of the younger alluvial units occur on the head of every alluvial fan in the Cucamonga fault zone except the Deer Canyon fan, whose entire surface is mantled by a continuous veneer of active wash and inactive alluvium.

The youngest alluvial units consist of sediment of washes and alluvial-fan surfaces that either is worked actively by modern streamflows, or presently is inactive but could be re-trained during channel-switching events. Progressively older alluvial units (yf<sub>4</sub>, yf<sub>3</sub>, yf<sub>2</sub>, yf<sub>1</sub>) are similar to each other in terms of sedimentary textures and structures, and they have similar clast compositions and sand-gravel ratios. However, they can be distinguished from each other because they have increasingly dissected surfaces and increasingly degraded channel-and-bar morphologies, their basement clasts are increasingly weathered, and their soil profiles are increasingly mature and better developed (fig. 12.6).

The younger alluvial units occur as a nested sequence of alluvial fills and cut terraces that are incised successively into each other. This nested-fan stratigraphy is displayed best on the fanheads, where stream-cut terraces and their associated fills have been created by cycles of degradation and aggradation. During degradational phases, streamflows carved out erosional terraces on older alluvial units. During aggradational phases, sediment was deposited on the cut terraces and buttressed unconformably against confining stream-cut terrace walls or against other paleotopography. In some cases, aggrading fills exceeded the height of confining stream-cut terrace walls; the streamflows then could migrate laterally beyond the confining walls and distribute alluvium over adjacent fanhead surfaces. Meanwhile, as these events occurred on proximal parts of the alluvial fans, on distal surfaces the aggrading veneers presumably feathered out laterally and downfan on underlying alluvial units.

At least two factors have been responsible for the nested stratigraphy displayed by the late Pleistocene and Holocene alluvial succession: (1) changes in climate and changes in drainage-basin-dependent factors, and (2) fault- or flexure-induced changes in ground elevation on portions of the alluvial-fan surface. Studies in the San Gabriel Mountains (Bull and others, 1979; McFadden and others, 1980; McFadden, 1982) have attempted to discriminate between alluvial events induced by tectonism and those events induced by other factors. We have not attempted to evaluate the impact of climatic change or drainage-basin evolution on the stratigraphic development of late Pleistocene and Holocene alluvial units within the Cucamonga fault zone. However, our studies suggest that tectonism along various strands of the fault zone contributed significantly to the evolution of some of these units.

## GEOMETRY AND HISTORY OF THE CUCAMONGA FAULT ZONE

### GENERAL FEATURES

The Cucamonga fault is an east-striking thrust-fault complex. Although commonly referred to as the Cucamonga fault, the mountain-front area is best considered as a fault zone. The surface expression of this fault zone in most places is about 1 km wide. At Day Canyon, this width is doubled if the Etiwanda Avenue scarp is considered as the south margin of the zone. Within the Cucamonga fault zone, we have identified many individual faults, many of which do not extend very far laterally on the geologic map (pl. 12.1) because the faults are discontinuous or poorly exposed. Temporal and structural relations between these faults and Quaternary alluvial units suggest that faulting has occurred intermittently on the various strands of the zone and may have shifted from one part of the zone to another during different episodes of the Quaternary. In this way, faulting has been distributed throughout a relatively wide fault zone rather than being confined to a single fault strand.

Individual faults occur in three different geologic settings. (1) In the mountains, faults and shear zones occur in crystalline basement rock. The number of faults and the pervasiveness of fracturing and crushing generally increase southward toward the mountain front. (2) Within a 500-m-wide zone at the mountain front itself the cataclasite progressively is more fractured and sheared by numerous discontinuous or discontinuously exposed faults; here, some of the reverse and thrust faults have placed basement rock over older Quaternary alluvial units. (3) The most conspicuous evidence for tectonism within the Cucamonga fault zone is a series of fault scarps that occur on the aprons and heads of most of the Quaternary alluvial fans which flank the eastern San Gabriel Mountains (fig. 12.5).

### FAULTING WITHIN CRYSTALLINE ROCK

Within crystalline rock, the faults are exposed best in canyon walls because poor exposures obscure many faults on hillslopes. Fault-gouge layers in crystalline rock generally range in thickness from 1 cm to several tens of centimeters. The faults and shears commonly undulate and splay in a complex fashion both downdip and along strike, and the structures commonly anastomose. With few exceptions, individual faults dip north into the mountains at moderate angles. The mean of 49 measured dips is  $43^\circ$ , and the range is  $0^\circ$  to  $80^\circ$ . The nearly consistent downdip plunge of slickensides in gouge indicates that latest movements were dip-slip. The fact that some of these structures do not break even the oldest Quaternary

alluvial units indicates early Quaternary or pre-Quaternary tectonism within the Cucamonga fault zone.

In the eastern part of the Cucamonga fault zone in Morse Canyon, 400 m north of the mountain front, late Tertiary conglomerate is faulted against crystalline basement rock along reverse faults. Here, the faults do not appear to break nearby older alluvial deposits. East of San Sevaine Canyon, in the Duncan Canyon bench area, the same conglomerate unit is overlain by cataclasite along a thrust fault that appears to be older than strand A to the south. Here, we are not certain whether this older strand breaks older alluvial deposits.

At several localities along the mountain front, cataclasite is thrust over older alluvium (figs. 12.7 to 12.9), a relation that we observed at nine separate localities. Most of these are at the south edge of the mountains, spectacular examples occurring on the east margin of the Deer Canyon fanhead embayment (fig. 12.7) and at East Etiwanda Canyon (fig. 12.8). Two additional localities occur farther north toward the interior of the mountains. Between Deer Canyon and Day Canyon, 500 m north of the mountain front, a patch of ridge-capping older gravel is in thrust contact with cataclasite (fig. 12.9). At Demens Canyon a similar distance north of the mountain front, cataclasite again is thrust over older alluvium. These isolated examples indicate that Quaternary displacements within the Cucamonga fault zone occurred not only at the mountain front but also within basement rocks at distances as far as 500 m north of the mountain front.

These relations within the mountain front indicate that tectonism within the Cucamonga fault zone has been prolonged and intermittent. Reverse-fault and thrust-fault activity occurred (1) after the deposition of late Tertiary sediments, (2) before the deposition of older Quaternary alluvial deposits, and (3) after the deposition of older Quaternary alluvial deposits.

### FAULTING WITHIN QUATERNARY ALLUVIAL MATERIALS

#### GENERAL DESCRIPTION AND NOMENCLATURE

Fault scarps that offset alluvial fans south of the mountain front occur fairly continuously between the San Antonio Heights bench on the west and the Duncan Canyon bench on the east (fig. 12.5). These fault scarps disrupt all but the youngest Holocene alluvial units and occur on every alluvial fan within the Cucamonga fault zone except the San Antonio Canyon and Deer Canyon fans.

Most scarps have surface offsets ranging between 2 m and 20 m, although some offsets are greater; on the upper fanhead of Day Canyon, one scarp segment has a surface offset of 40 m. Scarp morphologies vary throughout the Cucamonga fault zone: some scarps appear youthful, whereas other scarps are variably degraded. An apron of

gravely alluvium occurs along the base of many of the higher scarps; this apron, which is as much as 1 m thick and extends a few tens of meters downfan, was derived from alluvial materials exposed in the scarp face.

Although the 1971 San Fernando earthquake produced complex patterns of discontinuous ground rupture and scarp formation where thrust faults disrupted young alluvium (Kamb and others, 1971; U.S. Geological Survey Staff, 1971), Quaternary faulting of alluvial deposits within the Cucamonga fault zone generally created a more straightforward pattern represented by three major fault strands. These three discrete but locally discontinuous fault strands can be traced throughout much of the fault zone, and we believe a distinctive fault-movement history can be reconstructed for each of the strands. Our fault nomenclature for the late Quaternary part of the Cucamonga fault zone reflects these interpretations.

We designate the three major fault strands that disrupt Quaternary alluvium as Cucamonga strands A, B, and C (fig. 12.1; pl. 12.1). We distinguish these three strands on the basis of their structural and temporal relations to the various Quaternary alluvial units and the morphology, height, and preservation of their fault scarps. Strand A scarps, though preserved locally in older alluvial units, mainly have been destroyed or concealed by younger alluvial units. Strands B and C both have created scarps in younger alluvial units, but strand C scarps look fresher and appear to have offset younger deposits than have strand B scarps. These distinctions hold throughout the Cucamonga fault zone, although they are complicated by complete mergence of the strands in the western part of the fault zone and by local mergence elsewhere (fig. 12.1). Where two structures coalesce into a single trace, our nomenclature reflects this interpretation—for example,

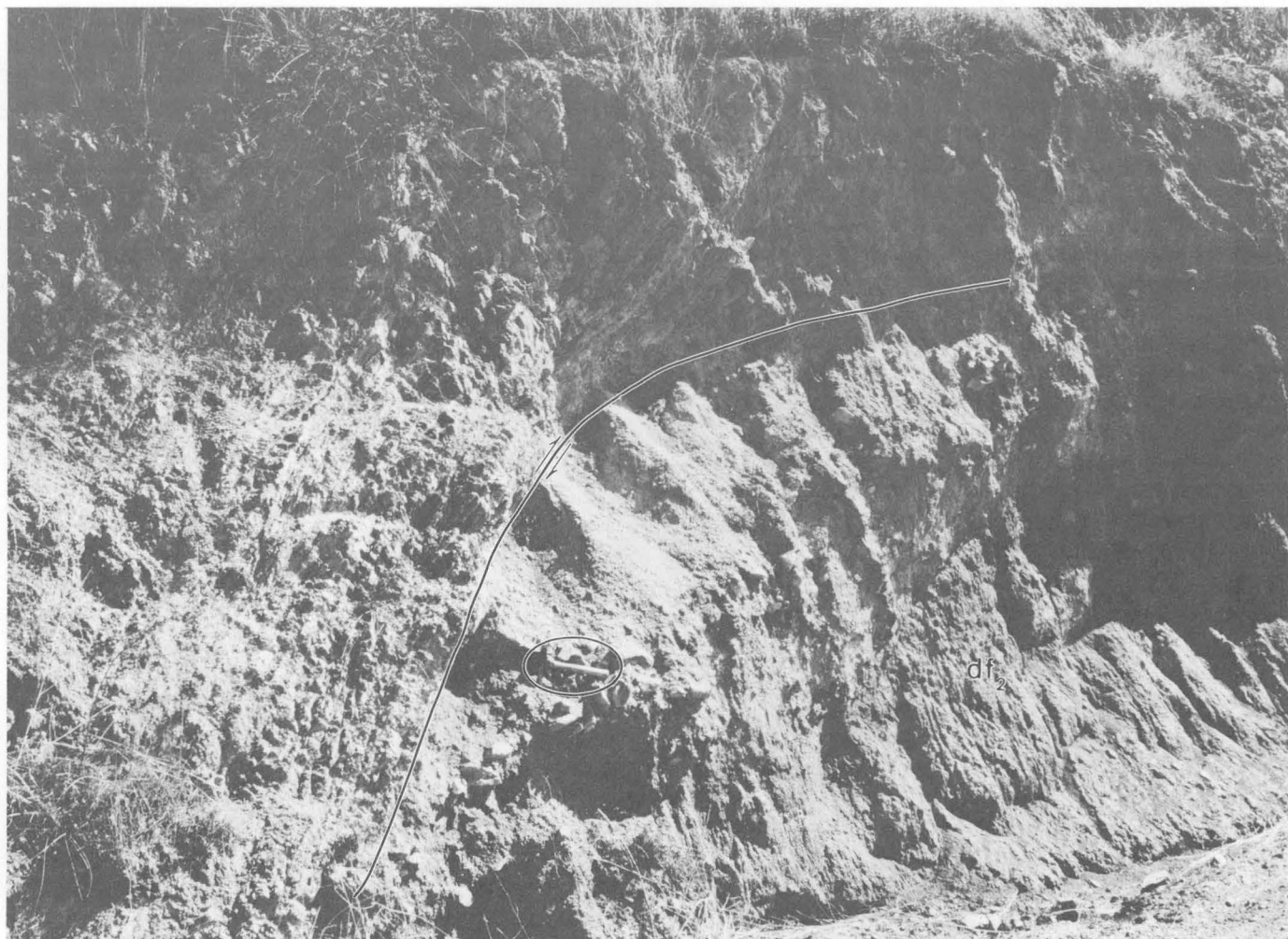


FIGURE 12.7.—Crystalline basement rock thrust southward over alluvium of unit  $df_2$  along north-dipping strand A of the Cucamonga fault zone; view looking east at a locality on the east margin of the Deer Canyon fanhead embayment, several hundred meters east of the center of sec.

13, T. 1 N., R. 6 W. The crystalline rocks consist of layered cataclasites of the granulite and cataclasite unit; the alluvium consists of angular cobbles and pebbles in a clay-rich reddish matrix of sand and granules. Photograph by D. M. Morton (March 1974).

strand A/B indicates the mergence of strands A and B and strand B/C indicates the mergence of strands B and C.

Strands A, B, and C occur as three discrete faults only in the east-central segment of the Cucamonga fault zone, between Deer Canyon and the Duncan Canyon bench (pl. 12.1; fig. 12.1). Even here the strands locally merge to form only one or two discrete structures. Relations are displayed best on the Day Canyon fan, where the three strands occur in sequence from north to south (pl. 12.1; figs. 12.1, 12.5). Farthest north, strand A is a single tectonic break or an anastomosing series of related breaks that is exposed intermittently along the mountain front and that forms discontinuous scarps. Farther south, strands B and C both form discrete nearly continuous scarps in Holocene and latest Pleistocene alluvium.

Westward from Deer Canyon, we recognize progressively fewer discrete fault strands (pl. 12.1; fig. 12.1).

Between Deer and Cucamonga Canyons, apparently only two discrete late Pleistocene and Holocene structures occur—strands A and B/C. In this part of the fault zone, strand A has no scarps but continues to hug the mountain front as a single tectonic break or as an anastomosing series of related breaks. Along this stretch, strand B/C forms a conspicuous scarp in Holocene and late Pleistocene alluvium. Farther west, between Cucamonga and San Antonio Canyons, we recognize only one discrete late Pleistocene and Holocene structure—strand A/B/C, which forms a conspicuous scarp in Pleistocene and Holocene alluvium.

The easternmost exposures of fault strands in the Cucamonga fault zone occur in the Duncan Canyon bench area (pl. 12.1; fig. 12.1). There, we recognize two discrete late Pleistocene and Holocene structures—strands A and B/C. Strand A is a single tectonic break that curves north-

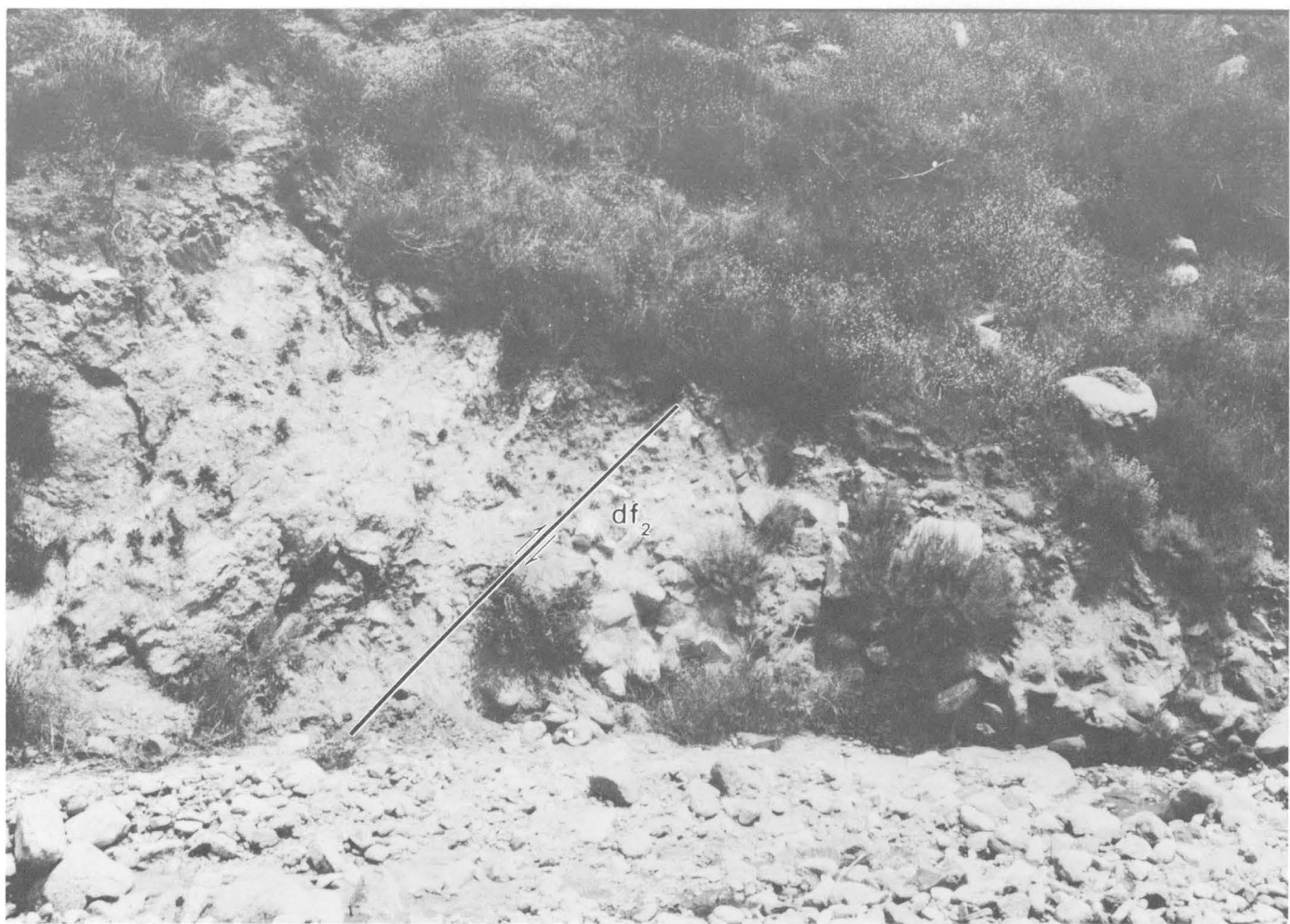


FIGURE 12.8.—Crystalline basement rock thrust southward over alluvium of unit  $df_2$  along north-dipping strand A of the Cucamonga fault zone; view looking east at the east wall of East Etiwanda Canyon Wash, at about the 2,200-ft elevation (pl. 12.1). The crystalline rocks consist

of layered cataclasite of the granulite and cataclasite unit; alluvium consists of rounded and highly weathered cobbles and boulders enclosed by coarse sand and granules. Largest boulders are about 1 m. Photograph by D. M. Morton (May 1973).

eastward toward the mountain front and there coalesces with Cucamonga strand I, a discrete fault strand that produced faulting probably before deposition of the oldest Quaternary alluvium. Strand B/C follows a conspicuous 2-km-long escarpment that fronts the Duncan Canyon bench and separates the bench from young alluvium of the Lytle Creek fan (fig. 12.4). Although the origin of this escarpment is equivocal (Metzger and Weldon, 1983), we tentatively attribute it to faulting on strand B/C. This interpretation is supported by seismic-refraction studies conducted by Bull and others (1979, p. B-6), who concluded that a fault coincides with the steep terrace front of the Duncan Canyon bench. Although Bull and others (1979) rule out a fluvial origin for this topographic scarp, the possibility of fluvial modification of a tectonic scarp cannot be ruled out. East of Duncan Canyon bench, the geometry and complexity of the Cucamonga fault zone are unknown because young Holocene deposits of Lytle

Creek fan conceal any fault strands of the zone that may be present there (fig. 12.4).

#### DISTRIBUTION, MORPHOLOGY, AND HISTORY OF STRANDS A, B, AND C

##### STRAND A

Strand A is exposed intermittently throughout the entire length of the Cucamonga fault zone and forms a single tectonic break or an anastomosing series of related breaks. We identify strand A at the following localities: (1) at the southwest end of the Duncan Canyon bench, where strand A forms degraded faceted scarps in Tertiary sedimentary rocks; (2) questionably on the San Sevaine Canyon eastern fanhead, where degraded and poorly developed scarps in unit  $yf_1$  probably represent strand A; (3) along the mountain front between the East

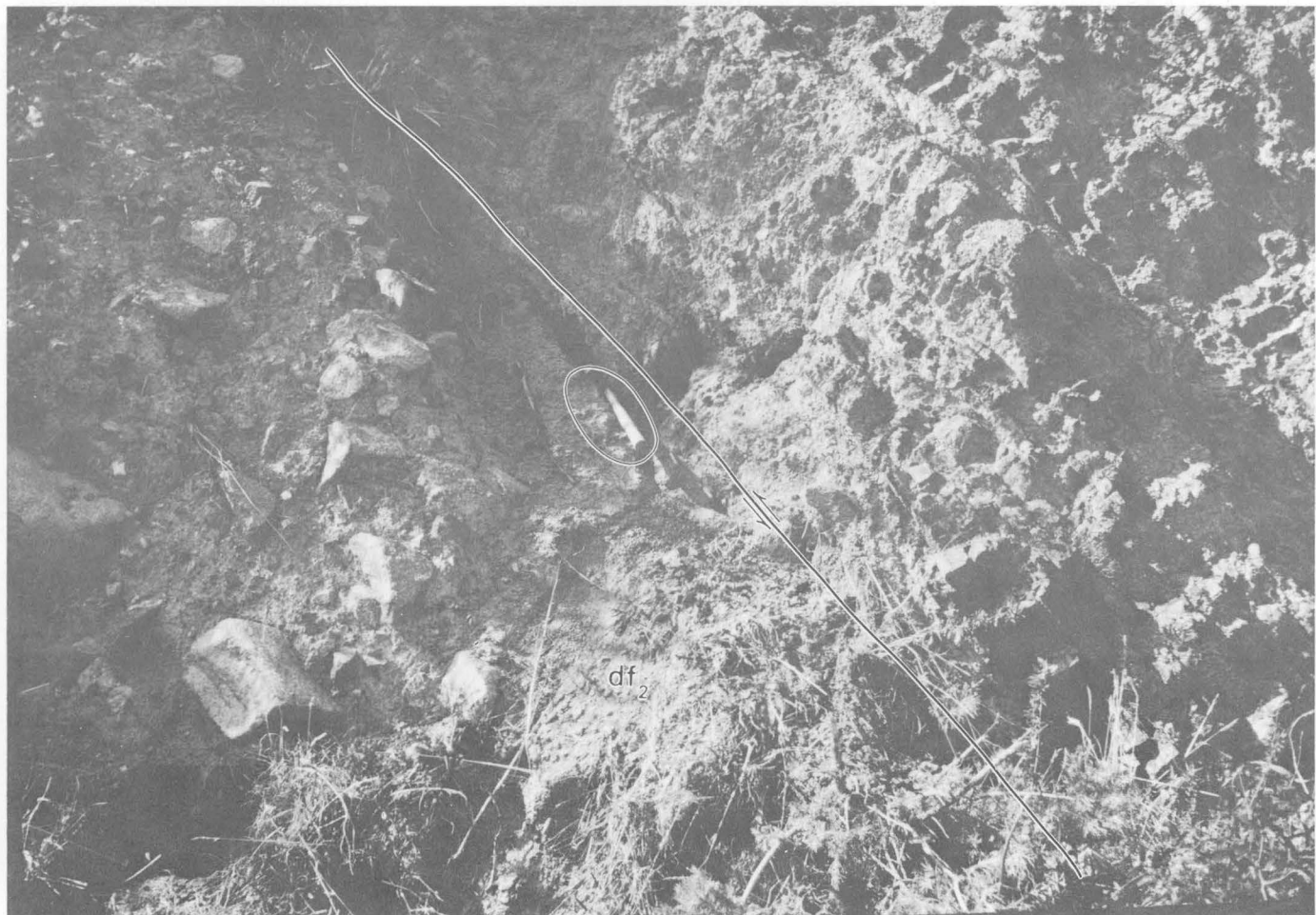


FIGURE 12.9.—Crystalline basement rock (cataclasite) thrust southward over alluvium of unit  $df_2$  along north-dipping thrust fault that occurs north of strand A of the Cucamonga fault zone; view looking west, 400 m north of the mountain front between Day and Deer Canyons.

Locality is on a ridge crest at elevation 2,520 ft in NW $\frac{1}{4}$  sec. 18, about 150 m east of the boundary between sec. 13 and 18, T. 1 N., R. 6 W. (pl. 12.1). Photograph by D. M. Morton (Feb. 1974).

Etiwanda Canyon and Day Canyon fanhead embayments, where strand A forms well-preserved scarps in unit  $df_2$ ; (4) on the Day Canyon fanhead, where we believe strand A partly is responsible for the scarp that bounds the south side of the hill underlying the Day Canyon station (fig. 12.10); (5) within the mountain front between Deer Canyon and Demens Canyon fanhead embayments; (6) within the mountain front between Demens and Angalls Canyons; (7) along the mountain front in the SE $\frac{1}{4}$  and SW $\frac{1}{4}$  sec. 16, T. 1 N., R. 6 W.; (8) questionably on the Cucamonga Canyon eastern fanhead where a degraded and modified scarp in  $yf_1$  may represent strand A; and (9) at the southwest end of the San Antonio Heights bench, where strand A partly is responsible for the strand A/B/C scarp that bounds the topographic bench.

Strand A locally is joined by younger fault strands. For example: (1) At the southwest end of the Duncan Canyon bench, in sec. 14, T. 1 N., R. 6 W., strand A locally merges with strand C to form strand A/C; (2) on the western fanhead of East Etiwanda Canyon, strand A locally merges with strand B' to form strand A/B'; (3) on the Day Canyon fanhead, strand A locally merges with strand B to form strand A/B; and (4) on the San Antonio Heights bench, strand A merges with strand B/C to form strand A/B/C. Where strand A is joined by a younger strand, the fault scarps that disrupt alluvium younger than unit  $yf_1$  were created by strand B or C ground ruptures that reactivated strand A. In these places, our fault nomenclature (A/B, A/B', A/B/C) is designed to show that the older strand (strand A) has been reactivated by a younger strand of faulting (strand B, B', or B/C) that locally merges with the older structure, and it does not indicate that strand A has continued to function as a discrete strand. Continued activity of strand A can be ruled out because along strike, where the younger strands diverge from strand A and the older structure continues as an entirely independent fault, strand A shows no evidence of movement since the accumulation of earlier deposits of unit  $yf_1$ .

The antiquity of strand A is emphasized by the relation between paleotopography created by the fault and sediment of younger alluvial units: Locally, the younger sediments buttress unconformably against old degraded fault scarps created by earlier ground ruptures on strand A. This relationship is illustrated clearly at five localities: (1) at the southwest end of the Duncan Canyon bench, in sec. 13; (2) along the mountain front between East Etiwanda and Day Canyons; (3) on the Day Canyon fanhead south of the Day Canyon station, where unit  $yf_1$  was deposited with buttress unconformity against high ground of unit  $df_2$  that was rotated backward to the north as a result of displacements on strand A (fig. 12.10); (4) west of Angalls Canyon, in the SE $\frac{1}{4}$  sec. 16, T. 1 N., R. 6 W.; and (5) at the extreme southwest end of the San

Antonio Heights bench, where units  $df_2$  and  $yf_1$  were deposited with buttress unconformity against high ground of unit  $df_2$  that is fronted on the south by a scarp created during strand A displacements.

Available evidence indicates that strand A generated displacements mainly during Pleistocene time, before the deposition of unit  $yf_1$ . However, the strand appears to have been still active during the deposition of early phases of this unit. For example, on the eastern fanheads of Cucamonga and San Sevaine Canyons, unit  $yf_1$  locally is disrupted by discontinuous scarps that are aligned with the inferred trace of strand A projected from adjacent outcrops. Moreover, evidence on Day Canyon fanhead (discussed below) suggests that there, also, strand A ruptured earliest deposits of unit  $yf_1$ . Strand A does not appear to have produced ground ruptures since the accumulation of younger deposits of unit  $yf_1$ , because the strand is buried by these deposits and by all other younger alluvial units.

#### STRAND B

Strand B extends throughout the entire length of the Cucamonga fault zone, and scarps attributable to this strand occur on the heads of most late Quaternary alluvial fans. In the east-central part of the fault zone, strand B typically is a discrete structure separate from other strands; however, east and west from this sector, strand B merges with strand C to form strand B/C and ultimately merges with strand A to form strand A/B/C (pl. 12.1; fig. 12.1). Where strand B scarps are discontinuous and are separated by extensive alluviated gaps lacking fault features, we correlate the scarps and assign them to strand B on the basis of their unique morphology and unique relation to young alluvial units.

In the east-central part of the fault zone, where strand B occurs as a discrete fault (fig. 12.5), the strand is characterized by the following features: (1) Scarps associated with the fault are destroyed or concealed where the fault is traversed by units  $yf_3$  and  $yf_4$  and by active and inactive alluvium. (2) The scarps generally are degraded in appearance—embayed by headward-eroding gullies, with slopes laid back by erosion. (3) The scarps consistently are higher where they disrupt unit  $yf_1$  and older units than where they disrupt unit  $yf_2$ .

Wherever we have identified strand B, the alluvial stratigraphy and scarp morphology suggest the following fault-movement history. (1) Strand B probably did not exist before the deposition of unit  $yf_1$ . (2) Late in the deposition of unit  $yf_1$ , ground rupture on strand B initiated the formation of scarps. (3) Base-level fall at these scarps caused incision of degradational terraces upstream in the fanhead embayments and promoted local aggradation on downfan surfaces of unit  $yf_1$ . (4) Subsequently,

thin discontinuous veneers of unit  $yf_2$  were deposited locally both on the cut terraces upstream from the evolving scarps and on top of the  $yf_1$  terrace surfaces downstream from the scarps. (5) Episodic ground rupture and scarp formation on strand B recurred during the evolution of unit  $yf_2$ , and streamflows intermittently cascaded over the scarps and contributed to their degradation. (6) As unit  $yf_2$  alluviation came to a close, ground rupture on strand B created low-standing scarps now seen to break unit  $yf_2$ . (7) The last ground rupture on strand B apparently occurred before or during earliest deposition of unit  $yf_3$ , as indicated by the apparent absence of scarps in units  $yf_3$  and  $yf_4$  and in inactive and active sediment.

#### STRAND C

Strand C occurs as a discrete structure only in the east-central part of the Cucamonga fault zone (pl. 12.1; fig. 12.1). Between the Deer Canyon fanhead embayment and

the Duncan Canyon bench, the fault forms prominent scarps on most of the late Quaternary alluvial fans (fig. 12.5). Where these scarps are discontinuous and are separated by extensive alluviated gaps lacking fault features, we correlate the scarp segments and assign them to strand C on the basis of their unique morphology and their unique relation to the younger alluvial units.

Between Deer and Henderson Canyons, strand C occurs south of strand B. However, east of Henderson Canyon, the two structures apparently cross each other, and we suggest that between Henderson Canyon and the Duncan Canyon bench strand C lies north of strand B. The two structures apparently merge along the front of the Duncan Canyon bench, where they form the high escarpment that separates the topographic bench from younger alluvium of Lytle Creek fan.

Throughout its extent, strand C is characterized by the following features: (1) Strand C does not offset unit  $yf_4$  and youngest deposits of unit  $yf_3$ , or active and inactive



FIGURE 12.10.—Low-altitude oblique aerial photograph looking west across the upper fanhead of Day Canyon. The alluvial fan surface in the foreground and middleground slopes about  $5^\circ$  to the south and consists of a 3- to 5-m-thick alluvial fill of unit  $yf_1$  which has had several degradational terraces incised into its upper surface. The isolated knoll in the background consists of unit  $df_2$  that was deposited nonconformably on bedrock; the bedrock and gravel units both have been backtilted by displacements on Cucamonga strand A/B that forms the prominent scarp (A/B) at the south margin of the knoll. The scarp has a surface offset of about 40 m. Fluvial erosion follow-

ing deposition of unit  $df_2$  created the isolated knoll, and unit  $yf_1$  was deposited with buttress unconformity against this paleogeographic feature. In the middle ground Cucamonga strand A locally forms a low scarp in unit  $yf_1$  (A, arrow), but the fault largely is concealed by degradational terrace surfaces that have been incised into unit  $yf_1$  (dots indicate the concealed trace of strand A). Cucamonga strand B forms a degraded scarp along the left margin of the photograph (solid line indicates the position of the thrust fault and sawteeth identify the upper plate). Photograph by D. M. Morton, June 1979.

alluvium; (2) strand C scarps generally are youthful in appearance, especially on the fanheads of Day and San Sevaine Canyons; (3) strand C scarps are not deeply embayed by young headward-eroding gullies, and the scarp profiles are relatively steep; (4) the scarps consistently are relatively high where they cut units  $yf_1$  or  $yf_2$ .

Evidence on the Day Canyon and East Etiwanda Canyon fanheads suggests that strand C caused ground rupture more recently than strand B. We base this interpretation on two facts: (1) Where the two strands form separate scarps, strand C scarps appear fresher than strand B scarps; and (2) strand C has formed scarps in oldest deposits of unit  $yf_3$ , but strand B does not appear to form scarps in these or in any younger deposits. Strand C apparently has not produced ground ruptures since the deposition of the youngest alluvial deposits (unit  $yf_4$  or possibly the youngest deposits of unit  $yf_3$ ); throughout the eastern part of the Cucamonga fault zone, strand C scarps are completely destroyed and buried by these young deposits. These relationships occur on the eastern fanhead of San Sevaine Canyon, on Morse Canyon fanhead, on unnamed fans between Morse Canyon and Henderson Canyon, on East Etiwanda Canyon fanhead, and on the Day Canyon fanhead. Latest ground rupture on strand C thus occurred before the deposition of unit  $yf_4$ .

#### STRANDS B/C AND A/B/C IN THE WESTERN PART OF THE CUCAMONGA FAULT ZONE

Only one youthful scarp series disrupts the late Pleistocene and Holocene alluvium in the western part of the Cucamonga fault zone. Between the Deer Canyon and Cucamonga Canyon fanheads, we assign this scarp series to strand B/C; west of the Cucamonga Canyon fanhead, we assign it to strand A/B/C.

#### STRAND B/C

Geomorphic and stratigraphic relations on the Cucamonga Canyon fanhead suggest that strands B and C have merged between Deer Canyon and Cucamonga Canyon. An oblique aerial photograph of the Cucamonga Canyon fanhead (fig. 12.11) shows one major set of scarps that occurs south of strand A. No direct evidence indicates whether this scarp represents strand B or C alone or whether it represents mergence of the two strands along a single fault trace. We must assign the scarp series to one strand or the other, or both, on the basis of scarp morphology, amount of surface offset, and relationship between the fault scarps and various alluvial units.

*Scarp morphology.*—West of the Deer Canyon fanhead, the strand B/C scarp series locally is embayed by headward-eroding gullies, and scarp morphologies generally are degraded and appear mature. These geomor-

phic characteristics also are displayed by strand B where it occurs as a discrete scarp in the east-central part of the fault zone. By contrast, scarps of strand C in the east-central sector are fresher appearing and are not embayed as much by headward-eroding gullies. Based on geomorphic evidence alone, the strand B/C scarp in the western part of the Cucamonga fault zone has more features in common with strand B than with strand C.

*Surface offsets.*—Profiles across the strand B/C scarp (fig. 12.12) show that it has a surface offset of about 20 m in alluvium of unit  $yf_1$  (profile 12-1) and a surface offset of about 4 to 5 m in alluvium of unit  $yf_2$  (profile 12-2). A comparison between these scarp profiles and those we measured for strands B and C on the Day Canyon and East Etiwanda Canyon fanheads (Matti and others, 1982, figs. 13 and 14; J. C. Matti, D. M. Morton, J. C. Tinsley, and L. D. McFadden, unpub. data 1980-84) shows a significant difference in surface offset between scarps in equivalent stratigraphic units: cumulative surface offset for strands B and C in unit  $yf_1$  is about 28 m (16 m on strand C and 12 m on strand B), in contrast to only 20 m for strand B/C in the same unit on the Cucamonga Canyon fanhead. These relations indicate that strand B/C has not generated the same amount of vertical displacement as the combined strands B and C to the east. One possible faulting scenario is suggested by geomorphic relations between the three strands: The more degraded and embayed aspect of strand B/C, in comparison with the fresher appearance of strand C in the east-central part of the fault zone, suggests that strand B/C represents strand B displacements and older displacements on strand C but may not represent more recent displacements on strand C. Thus, strand B/C may have generated the full 12 m of vertical displacement represented by strand B but only half of the 16 m represented by strand C.

*Relation to alluvial units.*—West of the Deer Canyon fanhead, the strand B/C scarp series in all cases is completely degraded and destroyed by deposits of unit  $yf_3$  (for example, on the fanheads of San Antonio Canyon, Cucamonga Canyon, and Angalls Canyon). East of Deer Canyon, scarps of strand B display a similar relationship to unit  $yf_3$ . By contrast, although scarps of strand C east of Deer Canyon locally are degraded and destroyed by youngest deposits of unit  $yf_3$ , the fault has created 2- to 6-m scarps in older deposits of unit  $yf_3$  and locally has created a 2-m scarp in unit  $yf_4$  (Matti and others, 1982, fig. 14, profiles 14-7 through 14-10). If unit  $yf_3$  in the western part of the Cucamonga fault zone is approximately time correlative with unit  $yf_3$  in the east-central part of the zone, then strand B/C shares the movement history of strand B and older phases of strand C history but does not share younger phases of strand C history. This interpretation is compatible with arguments based on surface-offset comparisons for the three fault strands.

On the basis of these three indirect arguments, we believe that strand B/C in the western part of the Cucamonga fault zone represents the mergence of strands B and C into a single fault zone. This single fault probably represents the full history of strand B where that fault forms a discrete scarp in the east-central part of the fault zone, as well as the older history of faulting on strand C where it forms a discrete scarp to the east; however, latest displacements on strand C in the east-central part of the fault zone may not have occurred on strand B/C in the western part of the fault zone. We discuss the implications of this interpretation below.

#### STRAND A/B/C

We infer that strands A, B, and C merge into a single fault trace west of the Cucamonga Canyon fanhead because, in this vicinity, we can find evidence of only one scarp series that breaks the late Quaternary alluvium. Thus, ground ruptures that occurred on separate strands A, B, and C in the east-central part of the Cucamonga fault zone occurred on a single fault trace in the westernmost part of the fault zone, near its mergence with the Sierra Madre fault zone. However, as with strand B/C, strand A/B/C does not appear to have generated the same amount of cumulative vertical displacement as was generated by strands A, B, and C where those faults form discrete strands; moreover, the strand may not have moved during the latest ground ruptures on strand C. These tentative conclusions are based on the observation that the strand A/B/C scarp does not appear to be as high as the combined heights of scarps of strands A, B, and C in the east-central part of the fault zone and on the fact that the fault does not form a scarp in alluvium that we assign to unit  $yf_3$  on the San Antonio Canyon fanhead.

#### SLIP RATES AND FAULTING RECURRENCE: A PRELIMINARY STATEMENT

In the east-central part of the Cucamonga fault zone, two alluvial fans that emanate from Day and East Etiwanda Canyons form a 3-km-wide apron that is traversed by fault strands A, B, and C (fig. 12.1). This alluvial apron provides an ideal opportunity to examine the detailed history of these faults during late Pleistocene and Holocene time because the fanhead areas have not been modified extensively by agricultural or urban development and because the alluvial succession on the two fanheads is cut by spectacular fault scarps (fig. 12.5) that provide an opportunity to link the history of faulting to the history of alluvial sedimentation. We have conducted detailed stratigraphic and scarp-profiling studies on the two fanheads, and we have trenched the strand C scarp in an

effort to obtain information on rates of slip, recurrence of faulting, and the amount of ground rupture during a typical earthquake (Matti and others, 1982; Morton and others, 1982; Matti and Tinsley in Clark and others, 1984; J. C. Matti, D. M. Morton, J. C. Tinsley, and L. D. McFadden, unpubl. data 1980–84). In this report we summarize data and preliminary interpretations that will be presented elsewhere.

Alluvial deposits on the Day Canyon and East Etiwanda Canyon fanheads are traversed by thrust-fault strands A, B, and C, which form conspicuous scarps that were created by recurring ground-rupturing displacements. In trenches across strand C, the fault zone is about 2 m wide, dips about  $35^\circ$  N., and projects near the middle of the scarp face; elongate cobbles within the fault zone have been rotated and aligned parallel to the plane of movement. Profiles across the fault scarps show that strand C has surface offsets ranging from 2 to 16 m (Matti and others, 1982, fig. 13); where strands A and B merge to form strand A/B, the scarp has offsets ranging from 8 to 40 m (Matti and others, 1982, fig. 14). The scarp heights vary systematically with the age of the alluvial units that they disrupt: The scarps are highest in the oldest units and are progressively lower in progressively younger units, indicating that strands A, B, and C generated recurring ground ruptures throughout the evolution of the latest Pleistocene and Holocene alluvial succession. Since the deposition of oldest sediment of unit  $yf_1$ , the faults have generated about 36 m of cumulative surface offset (Matti and others, 1982).

Our reconstruction of alluvial and faulting history on the Day Canyon and East Etiwanda Canyon alluvial fans leads to a fault-movement model in which a typical ground-rupturing earthquake generates a surface offset of about 2 m (Matti and others, 1982; Morton and others, 1982). This figure is suggested by fault-scarp profiles which show that surface offsets in alluvial units of different ages differ by multiples of about 2 m. We suggest that during latest Pleistocene and Holocene time, earthquakes having vertical displacements of about 2 m had an average recurrence of about 625 yr. This recurrence estimate is approximate and depends upon three factors: (1) a well-constrained measurement of 36 m of cumulative surface offset on strands A, B, and C since the accumulation of unit  $yf_1$ ; (2) our inference that the 36 m of cumulative offset represents 18 2-m ground-rupture events; and (3) our interpretation that the first recognizable scarp-forming event occurred about 13,000 yr ago and the last recognizable event occurred 1,000 to 1,750 yr ago. The 13,000-year estimate is a maximum age for undated sediment of unit  $yf_1$  based on a comparison of its soil profiles with alluvial soil profiles in the Cajon Pass region that have yielded radiometric ages of about 12,400 yr B.P. (Weldon, 1983; J. C. Tinsley and J. C. Matti,

unpub. data 1984). The 1,000–1,750-yr figure is our best estimate for the age of unit  $yf_4$  that depositionally overlaps strand C and in trench exposures appears to be unfaulted; the numerical age is based on a mean-residence-time soil-carbon date of  $2,230 \pm 80$  yr from the soil profile of an older unit buried by the unfaulted deposits (Matti and others, 1982, p. 41), and on a comparison of soil profiles in the unfaulted unit with soil profiles elsewhere in the region that have yielded radiometric ages of about 1,000 to 2,000 yr. If 36 m of cumulative surface offset on strands A, B, and C represent 18 ground ruptures of about 2 m each, then the average recurrence interval for the 11,250-yr period between the first recognizable ground-rupture event 13,000 yr ago and the last recognizable event 1,750 yr ago is about 625 yr. If the next 2-m ground rupture event occurred tomorrow, then 19 events in 13,000 yr would yield an average recurrence of 684 yr—close to the 700-yr average recurrence we proposed earlier (Matti and others, 1982; Morton and others, 1982).

Measurements of fault-plane dips and determinations of surface offsets for thrust-fault scarps suggest minimum slip rates of 4.5 mm/yr for the 13,000-yr period between the first recognizable faulting event and the present, and 5.5 mm/yr for the 11,250-yr period between the first and last recognizable faulting events (J. C. Matti and J. C. Tinsley, unpub. data 1984; compare with Morton and others, 1982, and Matti and Tinsley in Clark and others, 1984). Estimates of seismic moment indicate expectable surface-wave magnitudes of 6.5 to 7.2 for fault-rupture lengths of 10 to 25 km, assuming an average stress drop of 60 bars, an average seismogenic crustal thickness of about 10 to 15 km, a maximum seismogenic crustal thickness of about 20 km, and crustal materials having average properties of elasticity and rigidity (J. C. Tinsley and J. C. Matti, unpub. data 1984).

#### PATTERNS OF FAULTING WITHIN THE CUCAMONGA FAULT ZONE: SOME SPECULATIONS AND QUESTIONS

Throughout late Cenozoic time the Cucamonga fault zone has played varying tectonic roles. For example, various workers have suggested that the ancestral Cucamonga fault zone was the eastern segment of a middle Miocene fault (the Malibu Coast-Cucamonga fault) that may have generated as much as 90 km of left-lateral offset (Barbat, 1958; Jahns, 1973; Campbell and Yerkes, 1976). Subsequently, the ancestral Cucamonga fault may have been associated with a late Miocene strike-slip fault system formed by a southern strand of the San Gabriel fault, which various workers have interpreted as a right-lateral fault that is obscured by or interacts with the frontal-fault system of the Sierra Madre and Cucamonga fault zones (see various interpretations by Dibblee, 1968,

fig. 1; Ehlig, 1973, fig. 1, and 1981, fig. 10-2; Crowell, 1975a, fig. 1, 1975b, p. 208–209, 1982, fig. 1). However, the course of the southern strand of the San Gabriel fault is not well documented, and its possible relation to the ancestral Cucamonga fault is not obvious.

Our investigations focused on the Pleistocene and Holocene history of the Cucamonga fault, during which time tectonism within the zone has been expressed by reverse and thrust displacements along fault strands that break both crystalline rocks and Quaternary alluvial units. This pattern of faulting probably extends back to the early Pleistocene and perhaps the latest Tertiary, but evidence for this earlier compressional history is sketchy. Pre-Quaternary reverse displacements within the fault zone can be seen in the Duncan Canyon bench area, where reverse faults of strand I (pl. 12.1) have juxtaposed crystalline basement rock against overturned beds of upper Tertiary sedimentary rock. These faults do not disrupt even the oldest Pleistocene alluvial units, indicating pre-Quaternary compressional deformation here. This early tectonism apparently was followed by a prolonged period of tectonic quiescence during the Pleistocene, as evidenced by the presence of alluvium-covered bedrock pediment surfaces along the southern base of the eastern San Gabriel Mountains (figs. 12.2, 12.3). This period of stability lasted long enough to allow the pediment surfaces to evolve and then to receive Pleistocene older alluvial deposits that have well-developed argillic horizons (unit  $df_2$ ). Since that time, the pediment surfaces and their Pleistocene alluvial covers have been disrupted and backtilted by late Quaternary faulting along Cucamonga strands A, B, and C (fig. 12.10).

Throughout Pleistocene and Holocene time, compressional strain release appears to have followed distinct time-space patterns. For example, the youngest faults within the zone, strands B and C, are those that form scarps in the young Quaternary alluvial fans. Farther north, at the mountain front, a second series of faults, strand A, breaks Pleistocene alluvial units but is concealed beneath most of the Holocene alluvial units. Northward for a kilometer or so, another series of structures is represented by some faults and shear zones that cut crystalline basement rocks but that do not break even the oldest Quaternary alluvial units. These observations suggest that, during Pleistocene and Holocene time, faulting within the Cucamonga fault zone may have migrated southward.

This southward-younging pattern of faulting is complicated by two additional time-space patterns: (1) The late Pleistocene and Holocene fault strands are not distributed uniformly throughout the length of the Cucamonga fault zone; and (2) the latest ground ruptures recognizable in the east-central part of the fault zone may not have occurred in the western part of the zone. These two factors

are related to each other, and together they raise questions about past and future patterns of ground rupture within the Cucamonga fault zone and about the neotectonic role of the zone.

#### IS THE CUCAMONGA FAULT ZONE SEGMENTED?

A conservative viewpoint argues that ground rupture associated with a large seismic event most likely would extend throughout the entire Cucamonga fault zone. Thus, one estimate for seismic moment and surface-wave magnitude could be predicated on a 25-km fault-rupture length that incorporates significant ground rupture throughout the entire extent of the fault zone. However, some seismic events may not have generated significant scarp formation throughout the entire fault zone. Specifically, the most recent ground ruptures on the youthful-appearing strand C in the Day Canyon-East Etiwanda Canyon area may not have been recorded by strands B/C and A/B/C in the western part of the fault zone. This interpretation follows when the scarp morphology and movement history of strands B/C and A/B/C are compared with those of strands A, B, and C:

(1) The strand B/C and A/B/C scarps are more degraded in appearance than the strand B and C scarps in the vicinity of Day Canyon and East Etiwanda Canyon, and they are embayed by headward-eroding arroyos that have deposited considerable amounts of young unfaulted alluvium on the downthrown blocks of the faults (fig. 12.11 and pl. 12.1).

(2) The strand B/C and A/B/C scarps in all cases are completely degraded and buried by alluvium of unit  $yf_3$  (for example, on the fanheads of San Antonio, Cucamonga, and Angalls Canyons; see fig. 12.11).

(3) Surface offsets for scarps of strands B/C and A/B/C are not as great as surface offsets on strands A, B, and C in the Day Canyon-East Etiwanda Canyon area. This observation applies not only to cumulative-offset comparisons, but also to comparisons of offset since the deposition of unit  $yf_2$ . On the Cucamonga Canyon fanhead, strand B/C has a cumulative offset of about 20 m (fig. 12.12, profiles 12.1 and 12.2); by contrast, on the Day Canyon and East Etiwanda Canyon fanheads, strands B and C together have generated about 28 m of cumulative surface offset (12 m on strand B and 16 m on strand C). In addition, the strand B/C scarp in unit  $yf_2$  on the Cucamonga Canyon fanhead has a surface offset of only about 4 or 5 m (fig. 12.12, profile 12.2); by contrast, on the Day Canyon and East Etiwanda Canyon fanheads, the strand B and C scarps in broadly equivalent units have surface offsets that could be as great as 12 m, depending upon the exact correlation between alluvial units in the two areas.

Thus, three arguments lead to the hypothesis that patterns of ground rupture within the Cucamonga fault zone may reflect a segmented fault system; that is, different segments of the fault zone may have behaved independently from each other throughout the late Quaternary history of faulting. Thus, where strands A, B, and C form separate discrete faults in the eastern segment of the fault zone, this segment may have had a different history of ground rupture than segments occupied by strands A and B/C or strand A/B/C to the west. The Deer Canyon and Cucamonga Canyon fanhead embayments appear to be critical junctures within this segmented system, because each fanhead marks the boundary between segments of the Cucamonga fault zone that have different numbers of discrete fault strands and that may have had different faulting histories.

These speculations lead to several questions:

(1) Is the Cucamonga fault zone a segmented fault system today?

(2) In view of the fact that the most recent scarp-forming ground ruptures may have been confined to strand C in the east-central part of the fault zone, is it reasonable to expect future scarp-forming ruptures throughout the entire length of the zone? Or would significant ground rupture and scarp formation occur only in the eastern segment?

(3) Has ground rupture leading to scarp formation ever occurred throughout the entire 25-km length of the Cucamonga fault zone?

(4) Do the recurrence-interval and slip-rate estimates for the Day Canyon-East Etiwanda Canyon area apply to other segments of the Cucamonga fault zone?

(5) If the Cucamonga fault zone now is a segmented fault system, has it always been? Or has a segmented configuration evolved from one in which the frequency and amount of ground rupture and scarp formation were more uniform throughout the entire fault zone? Has the character of the fault zone alternated cyclically between segmented and nonsegmented behavior?

(6) Does segmented behavior of the fault zone imply that compressional tectonism in the zone reflects interactions between small crustal blocks rather than large blocks the scale of the Peninsular Ranges and Transverse Ranges provinces?

These questions have bearing not only on the long-term history of the Cucamonga fault zone, but also on assessments of seismic potential and seismic hazards related to ground rupture and seismic shaking.

#### WHAT IS THE NEOTECTONIC ROLE OF THE CUCAMONGA FAULT ZONE?

Throughout latest Pleistocene and Holocene time the Cucamonga fault zone has responded to north-south compression. Strain release at the extreme western end of

the fault zone has occurred episodically by multiple thrust-fault displacements that have been generated cumulatively along a single strand, A/B/C. Eastward, strain release has been spread out among progressively larger numbers of fault strands—by the advent of strand B/C east of the

San Antonio Heights area and strands B and C east of Deer Canyon. Locally within the eastern part of the Cucamonga fault zone, additional discrete Holocene fault segments also may have evolved; the Etiwanda Avenue scarp on the distal part of the Day Canyon fan may repre-



FIGURE 12.11.—Oblique aerial photograph looking northeast into the Cucamonga Canyon drainage, showing late Quaternary alluvium disrupted by the fault scarp of strand B/C of the Cucamonga fault zone. The high strand B/C scarp disrupts unit  $yf_1$  and has a surface offset of about 20 m determined from a profile measured across the scarp a few hundred meters east of the conspicuous stand of trees in the center of the photograph (fig. 12.12, profile 12-1). Note the weathered and embayed morphology of the high scarp. A lower scarp segment of strand B/C is obscured by a stand of trees; this scarp disrupts unit  $yf_2$  and has a surface offset of about 4 or 5 m determined from profile measurements (fig. 12.12, profile 12-2). Note that unit  $yf_2$  is deeply incised into unit  $yf_1$ , in the same way as the channel wash  $Q_w$  of the active channel is deeply entrenched into units  $yf_2$  and  $yf_3$ . On the west lobe of the Cucamonga Canyon fanhead, strand B/C

is joined by strand A to form strand A/B/C; at the left margin of the photograph, strand A/B/C forms a high scarp in unit  $yf_1$  that is comparable in height to the strand B/C scarp in unit  $yf_1$  on the eastern fanhead. Neither strand B/C nor A/B/C disrupts alluvium of unit  $yf_3$ . Where the east end of the strand A/B/C scarp is truncated by this unit, the faceted scarps that trend northeast parallel to the broad dirt road are fluvial features created by streamflows from Cucamonga Canyon. Note that, on both east and west lobes of the Cucamonga Canyon fanhead, units  $yf_2$  and  $yf_3$  are overlain by alluvial-fan deposits of unit  $Q_f$  that have prograded southward on top of the upper surfaces of both units; this relation indicates the antiquity of units  $yf_2$  and  $yf_3$ . Photograph by Robert C. Frampton and John S. Shelton (Frampton photograph No. 4-9071C, dated Dec. 5, 1953).

sent such a segment. These distribution patterns lead to the hypothesis that the Cucamonga fault zone may be a segmented fault system in which the timing and distribution of Quaternary ground rupture become more complex as the zone is traced from San Antonio Canyon eastward toward the San Jacinto fault zone. These patterns may reflect the complex nature of geometric and kinematic interactions between the Cucamonga fault zone and the San Jacinto family of right-lateral faults.

We speculate that northwestward migration of the Perris block and Peninsular Ranges by right-lateral displacements on the San Jacinto fault zone partly has been taken up by late Pleistocene and Holocene thrust-fault displacements within the Cucamonga fault zone. Thus, the Cucamonga fault zone may represent a zone of convergence between the Peninsular Ranges and Transverse Ranges Provinces: South of the Cucamonga fault zone, the Perris block and Peninsular Ranges are slipping northwestward along traces of the San Jacinto fault zone; however, this right-lateral migration apparently is impeded by the eastern Transverse Ranges, and the Perris block and alluviated upper Santa Ana River valley apparently are being thrust beneath the eastern San Gabriel Mountains.

Convergence rates across the Cucamonga fault within this zone must be factored into the overall strain budget of the region. Here, the neotectonic San Andreas and San Jacinto faults have late Quaternary slip rates of 25 mm/yr and 8 to 12 mm/yr, respectively (Weldon and Sieh, 1981; Sharp, 1981). Our studies suggest a minimum convergence rate of about 5 mm/yr for the Cucamonga fault

zone during latest Pleistocene and Holocene time—a rate that could double to 10 mm/yr if the alluvial succession proves to be younger than we believe. Thus, if the Cucamonga fault zone represents convergence between the Peninsular Ranges and Transverse Ranges Provinces, then half to nearly all of the 8 to 12 mm annual slip on the San Jacinto fault could have been taken up by latest Pleistocene and Holocene convergence within the Cucamonga fault zone. Such a model would imply that part or all of the slip on the San Jacinto fault has not contributed to slip on the San Andreas fault during latest Quaternary time. Viewed in this way, the Cucamonga fault zone may represent a major zone of convergence between large crustal blocks.

This short-term model may have implications for long-term interaction between the San Jacinto and San Andreas fault zones. Morton (1975a) indicates that right-lateral faults of the San Jacinto zone do not have mappable connections with the San Andreas fault (see fig. 12.1 of this report). This suggests that long-term slip on the San Jacinto fault may not have contributed to slip on the San Andreas but instead may have been taken up within the plexus of north-dipping reverse and left-lateral faults within the interior of the southeastern San Gabriel Mountains (Morton, 1975b). Thus, convergence within the modern Cucamonga fault zone may be a neotectonic analog for long-term interactions between crustal blocks in this region.

By contrast, Weldon (1984) suggests that, even though the San Jacinto fault zone may not have a mappable connection with the San Andreas fault, the 8 to 12 mm of annual slip on the San Jacinto nevertheless feeds into the San Andreas and contributes to slip on that fault. If this interpretation is correct, then the 5 mm convergence rate within the Cucamonga fault zone may not reflect wholesale convergence between major crustal blocks of the Peninsular and Transverse Ranges but instead may simply reflect interactions between local small blocks in a region where the San Jacinto and San Andreas faults merge in a complicated manner. This interpretation might also account for the segmented behavior that appears to have characterized the Cucamonga fault zone during latest Pleistocene and Holocene time.

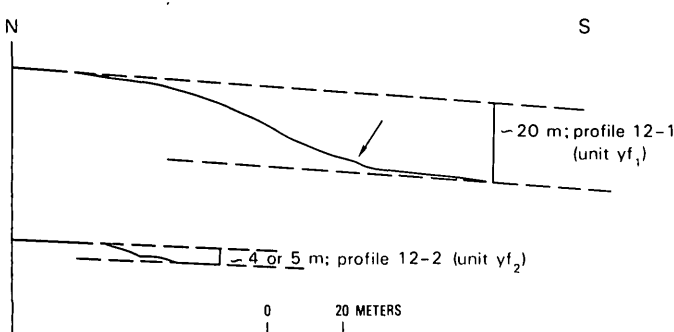


FIGURE 12.12.—Profiles across the strand B/C scarp on the east fanhead of Cucamonga Canyon; location of profiles is shown on pl. 12.1. Profile 12-1 illustrates a scarp in alluvium of unit  $yf_1$ . The scarp has a surface offset of about 20 m, and the main segment has a smoothly curving face with a maximum slope of about  $30^\circ$ . A lower break in slope (arrow) may represent a secondary fault scarp developed on the toe of the main scarp. Profile 12-2 illustrates a scarp in alluvium of unit  $yf_2$ . The scarp has a surface offset of about 4 to 5 m and has a smoothly curving main face with a maximum slope of about  $20^\circ$ . As on the Day Canyon and East Etiwanda Canyon fanheads, variation in scarp height and surface offset on strand B/C here correlate with alluvial stratigraphy: The scarp is higher and has greater surface offset in unit  $yf_1$  than in unit  $yf_2$ .

## CONCLUSIONS

The Cucamonga fault zone experienced episodic thrust faulting throughout the late Quaternary, giving rise to a complex but decipherable tectonic history. Overall, the surface pattern of faulting is one of mergence and splaying of scarp segments that appear to be discontinuous and unrelated but that we have traced as discrete strands throughout the fault zone. At the west end of the zone, multiple scarps merge into a single scarp series—strand

A/B/C. In the central part of the zone, strand A diverges from strand B/C. In the eastern part of the fault zone, strands A, B, and C form three principle scarps that merge locally. The eastern segment of the fault zone is geometrically complicated, perhaps reflecting interaction with the San Jacinto fault zone. Fault-scarp morphology and relations with alluvial units suggest that the eastern 15 km of the Cucamonga fault zone may have been seismically more active for the last 4,000 yr than the western part of the fault zone.

The fault strands have had distinctive movement histories. Strand A disrupted early deposits of alluvial unit  $yf_1$  but has not generated ground ruptures since that time (except where locally reactivated by strand B or strand C). Strand B evolved late in the history of unit  $yf_1$  and continued to generate ground ruptures during the evolution of unit  $yf_2$  but has not generated ruptures since that time. Strand C also evolved late in the history of unit  $yf_1$  and has continued to generate displacements that have ruptured all alluvial deposits except unit  $yf_4$  and younger deposits of unit  $yf_3$ . The youngest deposits disrupted by strand C are about 1,750 to 1,000 yr old (J. C. Matti, D. M. Morton, J. C. Tinsley, and L. D. McFadden, unpub. data 1980-84).

## REFERENCES CITED

- Alf, R. M., 1943, Mylonites in the eastern San Gabriel Mountains: California Journal of Mines and Geology, v. 39, no. 2, p. 144-151.
- , 1948, A mylonite belt in the southeastern San Gabriel Mountains, California: Geological Society of America Bulletin, v. 59 no. 11, p. 1101-1119.
- Baird, A. K., 1956, Geology of a portion of the San Gabriel Mountains: Claremont, Calif., Claremont Graduate School, M. A. thesis, 96 p.
- Barbat, W. F., 1958, The Los Angeles Basin area, California, in Weeks, L. G., ed., Habitat of oil—a symposium: Tulsa, Oklahoma, American Association of Petroleum Geologists, p. 62-77.
- Bull, W. B., Menges, C. D., and McFadden, L. D., 1979, Stream terraces of the San Gabriel Mountains: Final technical report to the earthquake hazards reduction program under contract 14-08-0001-G-394, U.S. Geological Survey, 138 p.
- Burnham, W. L., 1953, The geology and ground water conditions of the Etiwanda-Fontana area, California: Claremont, Calif., Pomona College, M.A. thesis, 136 p.
- Campbell, R. H., and Yerkes, R. F., 1976, Cenozoic evolution of the Los Angeles Basin area—relation to plate tectonics, in Howell, David G., ed., Aspects of the geologic history of the California continental borderland: Pacific Section, American Association of Petroleum Geologists, Miscellaneous Publication 24, p. 541-558.
- Clark, M. M., Harms, K. K., Lienkaemper, J. J., Harwood, D. S., Lajoie, K. R., Matti, J. C., Perkins, J. A., Rymer, M. J., Sarna-Wojcicki, A. M., Sharp, R. V., Sims, J. D., Tinsley, J. C., and Ziony, J. I., 1984, Preliminary slip-rate table and map of late Quaternary faults of California: U.S. Geological Survey Open-File Report 84-106, 12, p., scale 1:750,000.
- Crowell, J. C., 1975a, The San Andreas fault in southern California, in Crowell, J. C., ed., San Andreas fault in southern California: California Division of Mines and Geology Special Report 118, p. 7-27.
- , 1975b, The San Gabriel fault and Ridge Basin, southern California, in Crowell, J. C., ed., San Andreas fault in southern California: California Division of Mines and Geology Special Report 118, p. 208-219.
- , 1982, The tectonics of Ridge Basin, southern California, in Crowell, J. C., and Link, M. H., eds., Geologic history of Ridge Basin, southern California: Pacific Section, Society of Economic Paleontologists and Mineralogists, p. 25-42.
- Dibblee, T. W., Jr., 1968, Displacements on San Andreas fault system in San Gabriel, San Bernardino, and San Jacinto Mountains, southern California, in Dickinson, William R., and Grantz, Arthur, eds., Proceedings of conference on geologic problems of the San Andreas fault system: Stanford University Publications in Geological Sciences, v. XI, p. 260-278.
- Eckis, Rollin, 1928, Alluvial fans of the Cucamonga District, southern California: Journal of Geology, v. 36, no. 3 p. 225-247.
- , 1934, South coastal-basin investigation; geology and ground-water storage capacity of valley fill: California Division of Water Resources Bulletin 45, 279 p.
- Ehlig, P. L., 1958, Geology of the Mount Baldy region of the San Gabriel Mountains, California: Los Angeles, University of California, Ph.D. thesis, 153 p.
- , 1973, History, seismicity, and engineering geology of the San Gabriel fault, in Moran, D. E., Slosson, J. E., Stone, R. O., and Yelverton, C. A., eds., Geology, seismicity, and environmental impact: Los Angeles, Association of Engineering Geologists Special Publication, p. 247-251.
- , 1981, Origin and tectonic history of the basement terrain of the San Gabriel Mountains, central Transverse Ranges, in Ernst, W. G., ed., Geotectonic development of California (Rubey volume 1): Englewood Cliffs, N. J., Prentice-Hall, Inc., p. 253-283.
- Ehlig, P. L., Davis, T. E., and Conrad, R. L., 1975, Tectonic implications of the cooling age of the Pelona Schist: Geological Society of America Abstracts with Programs, v. 7, no. 3, p. 91-96.
- Evans, J. G., 1982, The Vincent thrust, eastern San Gabriel Mountains, California: U.S. Geological Survey Bulletin 1507, 15 p.
- Hsu, K. J., 1955, Granulites and mylonites of the region about Cucamonga and San Antonio Canyons, San Gabriel Mountains, California: University of California Publications in Geological Sciences, v. 30, no. 4, p. 223-352.
- Hsu, K. J., Edwards, George, and McLaughlin, W. A., 1963, Age of the intrusive rocks of the southeastern San Gabriel Mountains, California: Geological Society of America Bulletin, v. 74, no. 4, p. 507-512.
- Jahns, R. H., 1973, Tectonic evolution of the Transverse Ranges Province as related to the San Andreas fault system, in Kovach, R. L., and Nur, Amos, eds., Proceedings of the conference on tectonic problems of the San Andreas fault system: Stanford University Publications in Geological Sciences, v. XIII, p. 149-170f.
- Kamb, Barclay, Silver, L. T., Abrams, M. J., Carter, B. A., Jordan, T. H., and Minster, J. B., 1971, Pattern of faulting and nature of fault movement in the San Fernando Valley earthquake, in the San Fernando, California, Earthquake of February 9, 1971: U.S. Geological Survey Professional Paper 733, p. 41-54.
- Lamar, D. L., Merifield, P. M., and Proctor, R. J., 1973, Earthquake recurrence intervals on major faults in Southern California, in Moran, D. E., Slosson, J. E., Stone, R. O., and Yelverton, C. A., eds., Geology, seismicity, and environmental impact: Los Angeles, Association of Engineering Geologists Special Publication, p. 265-276.
- Matti, J. C., Tinsley, J. C., McFadden, L. D., and Morton, D. M., 1982, Holocene faulting history as recorded by alluvial history within the Cucamonga fault zone: a preliminary view, in Tinsley, J. C., McFadden, L. D., and Matti, J. C., eds., Late Quaternary pedogenesis and alluvial chronologies of the Los Angeles and San Gabriel Mountain areas, southern California: Field trip 12, Geological Society of America, Cordilleran Section, 78th Annual Meeting, Anaheim, Calif., Guidebook, p. 21-44.

- McFadden, L. D., 1982, The impacts of temporal and spatial climatic changes on alluvial soils genesis in southern California: Tucson, University of Arizona, Ph. D. thesis, 430 p.
- Metzger, LiLi, and Weldon, R. J., 1983, Tectonic implications of the Quaternary history of lower Lytle Creek, southeast San Gabriel Mountains: Geological Society of America Abstracts with Programs, v. 15, no. 5, p. 418.
- Miller, F. K., and Morton, D. M., 1977, Comparison of granitic intrusions in the Pelona and Orocopia Schists, southern California: U.S. Geological Survey Journal of Research, v. 5, no. 5, p. 63-69.
- Morton, D. M., 1975a, Synopsis of the geology of the eastern San Gabriel Mountains, southern California: California Division of Mines and Geology Special Report 118, p. 170-176.
- , 1975b, Relations between major faults, eastern San Gabriel Mountains, southern California: Geological Society of America Abstracts with Programs, v. 7, no. 3, p. 352-353.
- , 1976, Geologic map of the Cucamonga fault zone between San Antonio Canyon and Cajon Creek, southern California: U.S. Geological Survey Open-File Report 76-726, scale 1:24,000.
- Morton, D. M., Matti, J. C., and Tinsley, J. C., 1982, Quaternary history of the Cucamonga fault zone, southern California: Geological Society of America Abstracts with Programs, v. 14, no. 4, p. 218.
- Morton, D. M., Rodriguez, E. A., Obi, C. M., Simpson, R. W., and Peters, T. J., 1983, Mineral resource potential map of the Cucamonga Roadless Areas, San Bernardino County, California: U.S. Geological Survey Miscellaneous Field Studies Map MF-1646-A, scale 1:31,680.
- Morton, D. M., and Yerkes, R. F., 1974, Spectacular scarps of the frontal fault system, eastern San Gabriel Mountains, southern California (abstract): Geological Society of America Abstracts with Programs, v. 6, no. 8, p. 223-224.
- Munsell Soil Color Charts, 1975 edition: Baltimore, Maryland, Munsell Color, Macbeth Division of Kollmorgen Corporation.
- Proctor, R. J., and Payne, C. M., 1972, Evidence for, and engineering consequences of, recent activity along the Sierra Madre Fault zone, southern California: Geological Society of America Abstracts with Programs, v. 4, no. 3, p. 220-221.
- Rogers, T. H., compiler, 1967, San Bernardino sheet of Geological map of California: California Division of Mines and Geology, scale 1:250,000.
- Sharp, R. V., 1981, Variable rates of late Quaternary strike slip on the San Jacinto fault zone, southern California: Journal of Geophysical Research, v. 86, no. B3, p. 1754-1762.
- Shelton, J. S., 1955, Glendora volcanic rocks, Los Angeles Basin, California: Geological Society of America Bulletin, v. 66, no. 1, p. 45-90.
- U.S. Geological Survey Staff, 1971, Surface faulting, in The San Fernando, California, earthquake of February 9, 1971: U.S. Geological Survey Professional Paper 733, p. 55-79.
- U.S. Soil Conservation Service, 1980, Soil Survey of San Bernardino County, southwestern part, California: U.S. Department of Agriculture publication, 65 p., 12 maps (scale 1:24,000).
- Walker, N.W., and May, D.J., 1986, U-Pb Zircon ages from the SE San Gabriel Mts., CA: Evidence for Cretaceous metamorphism, plutonism, and mylonitic deformation predating the Vincent thrust: Geological Society of America Abstracts with Programs, v. 18, p. 195.
- Weldon, R. J., 1983, Climatic control for the formation of terraces in Cajon Creek, southern California: Geological Society of America Abstracts with Programs, v. 15, no. 5, p. 429.
- , 1984, Quaternary deformation due to the junction of the San Andreas and San Jacinto faults, southern California: Geological Society of America Abstracts with Programs, v. 16, no. 6, p. 689.
- Weldon, R. J., and Sieh, K. E., 1981, Offset rate and possible timing of recent earthquakes on the San Andreas fault in Cajon Pass, California: EOS, American Geophysical Union Transactions, v. 62, no. 45, p. 1048.

## APPENDIX

### TECHNICAL DATA FOR AERIAL PHOTOGRAPHS

The following aerial photographs were used to map the fault scarps and Quaternary alluvial units identified throughout the Cucamonga fault zone (pl. 12.1):

(1) Black-and-white photographs, series GSJ, frames 2-102 through 2-108 and 2-228 through 2-238, scale 1:24,000, dated 1/15/78 (flown for this project by I. K. Curtis Services, Inc.).

(2) Black-and-white photographs (scale 1:20,000) flown for the U.S. Department of Agriculture, Soil Conservation Service:

|                 |         |          |
|-----------------|---------|----------|
| AXL-35K, frames | 118-130 | 2/02/53  |
| AXL-36K, frames | 135-140 | 2/02/53  |
| AXL-39K, frames | 94-113  | 2/11/53  |
| AXL-39K, frames | 153-170 | 2/11/53  |
| AXL-51K, frames | 82-95   | 3/08/53  |
| AXL-51K, frames | 103-119 | 3/08/53  |
| AXL-15W, frames | 56-65   | 10/15/59 |
| AXL-15W, frames | 70-79   | 10/15/59 |
| AXL-15W, frames | 122-135 | 10/15/59 |
| AXL-15W, frames | 143-158 | 10/15/59 |
| AXL-18W, frames | 29-36   | 11/06/59 |
| AXL-18W, frames | 39-47   | 11/06/59 |
| AXL-18W, frames | 50-57   | 11/06/59 |

(3) Black-and-white photographs flown for the U.S. Geological Survey, series GS-VBNF, scale 1:24,000, flown 4/16/66: frames 1-168 through 1-185; frames 1-204 through 1-219; frames 1-228 through 1-242; and frames 1-257 through 1-266.

(4) Black-and-white aerial photographs flown for the U.S. Geological Survey, series GS-VR, scale 1:23,600, frames 8-17 through 8-32 (7/13/52) and frames 26-1 through 26-12 (8/26/52).

(5) Black-and-white aerial photographs flown for the U.S. Department of Agriculture, Soil Conservation Service, scale 1:20,000: AXL-60, frames 63 through 91 (04/38); AXL-42, frames 15 through 41 (6/03/38); and AXL-63, frames 62 through 80 (04/38).